R-10-68

Äspö Hard Rock Laboratory

Long Term Sorption Diffusion Experiment (LTDE-SD)

Results from rock sample analyses and modelling

Kersti Nilsson, Johan Byegård, Eva Selnert,
Henrik Widestrand, Sanne Höglund, Erik Gustafsson

Geosigma AB

December 2010

Svensk Kärnbränslehantering AB
Swedish Nuclear Fuel
and Waste Management Co

Box 250, SE-101 24 Stockholm
Phone +46 8 459 84 00

ISSN 1402-3091
SKB R-10-68

Äspö Hard Rock Laboratory

Long Term Sorption Diffusion Experiment (LTDE-SD)

Results from rock sample analyses and modelling

Kersti Nilsson, Johan Byegård, Eva Selnert,
Henrik Widestrand, Sanne Höglund, Erik Gustafsson

Geosigma AB

December 2010

Keywords: Diffusion, Sorption, Radionuclides, Matrix rock, Natural fracture, Crystalline rock, *In situ*, Tracers, Experiment.

Abstract

Rock material that has been exposed to a cocktail of radioactive tracers during the Long Term Sorption Diffusion Experiment (LTDE-SD) has been analyzed using both radionuclide specific methods and non-radionuclide specific autoradiography. This report contains the measured penetration profiles, a qualitative interpretation as well as modelling of the results using a matrix diffusion sorption model.

Measured penetration profiles have been obtained both for the rock material in the near vicinity to a natural facture and to rock material assumed to represent a less disturbed matrix rock.

Penetration depths of at least 2–3 cm have been obtained for the non-sorbing or very weakly sorbing tracers (e.g. ^{36}Cl and ^{22}Na, respectively) after 200 days of contact time between the tracer cocktail solution and the rock. For the more strongly sorbing tracers (e.g. ^{63}Ni, ^{133}Ba and ^{137}Cs) high enrichment (due to sorption) could be found in the samples located closest to the water-rock interface. Nevertheless, penetration profiles could be measured also for these tracers; strongly declining concentrations for the samples located 0–5 mm into the rock were observed. A number of presumed strongly sorbing tracers (e.g. ^{57}Co, ^{153}Gd and ^{110m}Ag) were found to be absent in the inner part the rock, an observation that to some extent is caused by the somewhat higher detection limits for these tracers in the inner part the rock. Altogether the general pattern of sorption behaviour was found to, qualitatively, be consistent with the assumed matrix diffusion model. Strongly sorbing tracers were enriched on the fracture surfaces with restricted or minimal matrix diffusion while pronounced penetration due to matrix diffusion was noted for non-sorbing and weakly sorbing tracers. Since the *in situ* experiment was performed in absence of hydraulic gradients, the penetration into the rock matrix is considered as being a result of diffusion alone and it is concluded that no advection was involved. The combined result of visualised rock penetration by autoradiography (detection limit of ~1 cm) and the penetration depth for ^{22}Na and ^{36}Cl confirms that a connected porosity exists in the rock matrix.

Quantitative model calculations using a homogenous sorption/matrix diffusion model and employing independently determined laboratory sorption and diffusion properties show that the penetration into the rock is deeper than predicted by the model. Also, the shape of the penetration profiles deviates from that predicted which is proposed to be caused by a heterogeneous porosity distribution in the rock; an explanation that is supported by autoradiography analyses as well as ^{14}C-PMMA (Polymethylmethacrylate impregnation) analyses.

An attempt has also been made to fit model parameters to experimental data, with values for the diffusivity, the porosity and the sorption distribution coefficient (K_d) as fitting parameters. The results of this indicate lower K_d values and/or larger diffusivity compared with laboratory determined values. However, due to difficulties in simulating the measured penetration profiles with the applied sorption/matrix diffusion model, quantitative results should be used with care.

The amount of ^{36}Cl (anionic species) in the rock is approximately one order of magnitude lower than what was expected from the porosity data. The modelling indicated that an anion exclusion effect corresponding to an effective decrease of the diffusivity by a factor of 3 to 7 may provide good conceptual agreement with the anion exclusion theory, for the combination of the ^{36}Cl and the ^{22}Na results.

A robust concept for K_d data extraction to be used in safety assessment is presented by combining the measured concentrations in the aqueous phase and the measured concentration in the rock sample closest to the water-rock interface.

The K_d results were compared to those from laboratory experiments and from the aqueous phase measurements during the *in situ* phase of the experiment. The conclusive summary of the exercise of the K_d comparison is that there is a risk of overestimation using the techniques employing only study of the tracer loss in the aqueous phase, irrespectively if the aqueous phase data are from *in situ* or laboratory conditions. It is also indicated that the aqueous phase result and the penetration profile cannot be modelled simultaneously with satisfactory results by using a single-rate homogeneous porosity model.

Sammanfattning

Bergmaterial, som har exponerats för en cocktail av radioaktiva spårämnen under försöket "Long Term Sorption Diffusion Experiment (LTDE-SD)" har i detta arbete analyserats, både med radionuklidspecifika metoder och med icke-radionuklidspecifik autoradiografi. Rapporten innehåller uppmätta penetrationsprofiler, kvalitativ tolkning samt modellering av resultaten enligt en matrisdiffusions-/sorptionsmodell.

Uppmätta penetrationsprofiler har erhållits för både bergmaterial närmast en naturlig spricka och för bergmaterial som förväntats bestå av mindre påverkat matrisberg.

Penetrationsdjup på minst 2–3 cm har erhållits för de förväntat icke- eller mycket svagsorberande spårämnena (dvs ^{36}Cl respektive ^{22}Na) som ingick i studien, detta som resultat av 200 dagars kontakttid mellan cocktailen av spårämnen och berget. För de mer starksorberande spårämnena (dvs ^{63}Ni, ^{133}Ba och ^{137}Cs) syntes en hög anrikning på grund av sorption vid ytan. Icke desto mindre kunde penetrationsprofiler uppmätas för dessa spårämnen; starkt avtagande koncentrationer observerades för prov belägna 0–5 mm från bergytan. För ett antal förmodat starksorberande spårämnen (dvs ^{57}Co, ^{153}Gd och ^{110m}Ag) fanns inga uppmätbara halter i den inre delen av bergmatrisen. Sammantaget befanns den generella sorptionsbilden stämma kvalitativt överens med en antagen matrisdiffusionsmodell; starkt sorberande spårämnen anrikade på sprickytorna med en begränsad eller minimal matrisdiffusion medan en tydlig inträngning orsakad av matrisdiffusion kunde noteras för icke- samt svagsorberande spårämnen. Eftersom *in situ*-experimentet utfördes i frånvaro av hydrauliska gradienter, kan inträngningen i matrisberget betraktas som ett resultat av enbart diffusion och slutsatsen är att ingen advektion var inblandad. Det kombinerade resultatet av inträngning i matrisberg visualiserat med autoradiografi (detektionsgräns ~1 cm) och penetrationsdjup för ^{22}Na och ^{36}Cl bekräftar att konnekterad porositet förekommer i matrisberget.

Kvantitativa modellberäkningar med en matrisdiffusions-/sorptionsmodell där oberoende bestämda laboratorievärden använts för sorption och diffusion visar att inträngningen i bergmatrisen är längre än vad modellen förutsäger. Det måste dock påpekas att formen på den uppmätta penetrationsprofilen i många fall avviker signifikant från vad en homogen matrisdiffusionsmodell förutsäger. Det föreslås att detta är orsakat av heterogen porositetsfördelning i bergmatrisen; en förklaring som stöds av autoradiografianalyser samt utförda ^{14}C-PMMA (Polymetylmetakrylat-impregnerings)-analyser.

Försök att modellera passningsberäkningar har också utförts, dvs att variera de numeriska värdena för diffusivitet, porositet och sorptionsfördelningskoefficienten (K_d) för att kunna anpassa den beräknade modellen till de experimentella resultaten. Utfallet kan sammanfattas till att det krävs en minskning av K_d och/eller en ökning av diffusiviteten jämfört med bestämda värden från laboratorieanalyser. Dessa resultat måste dock ses som osäkra på grund av svårigheten att simulera de uppmätta resultaten med den använda homogena matrisdiffusionsmodellen.

Mängden ^{36}Cl (anjon) i bergmaterialet är ungefär en tiondel av förväntat utifrån porositetsdata. Modelleringen indikerade att en påverkan av anjonexklusion motsvarande en effektiv minskning av diffusiviteten med en faktor 3 till 7 kan ge en bra begreppsmässig överensstämmelse med anjonexklusionsteorin, för kombinationen av ^{36}Cl- och ^{22}Na-resultaten.

För extraktion av K_d-data som kan användas i säkerhetsanalyser presenteras ett robust koncept, genom att kombinera den uppmätta koncentrationen i vattenfasen och den uppmätta koncentrationen i bergprovet närmast gränsskiktet vatten/berg.

De framtagna K_d-värdena jämförs med värden från laboratorieexperiment och från mätningarna av vattenfasen under *in situ*-fasen av experimentet. Den slutliga sammanfattningen av K_d-jämförelserna är att det finns en risk med överskattning då tekniker som endast omfattar studier av spårämnesförluster i vattenfasen används, oberoende av om vattendata härrör från försök *in situ* eller i laboratoriemiljö. Resultaten tyder också på att vattenfasdata och penetrationsprofilerna inte kan modelleras simultant med tillfredsställande resultat om en enkel homogen porositets- och diffusionsmodell används.

Acknowledgements

We gratefully acknowledge the collaboration with Prof. Marja Siitari-Kauppi and colleagues at the Laboratory of Radiochemistry, University of Helsinki, in the material preparation and analysis work, and Henrik Ramebäck and colleagues at the Swedish Defence and Research Institute in Umeå regarding method development and analysis work.

Johan Harrström and Sofia Winell, Geosigma AB are gratefully acknowledged for their contribution to the modelling work and Magnus Kronberg, SKB is gratefully acknowledged for help with method development and analysis work at Baslab.

Finally we are very grateful for the in depth and constructive review that was provided by James Crawford, Kemakta Konsult AB, Anders Winberg, Conterra AB and Martin Löfgren, Niressa AB.

Contents

1 Introduction

The Long Term Sorption Diffusion Experiment (LTDE-SD) is one of the experiments within the Natural Barriers research programme at the SKB Äspö Hard Rock Laboratory (HRL), the goal of which is to increase the scientific knowledge of the safety margins of the final repository for spent nuclear fuel and to provide data for performance and safety assessment calculations.

Transport of radionuclides in water-conducting rock fractures over 5–50 m distances has been studied within the Tracer Retention and Understanding Experiments (TRUE) experimental programme since the late 90's /Winberg et al. 2000, Andersson et al. 2002/. Advection, dispersion, sorption and diffusive mass transfer are relevant processes of which dispersion and diffusive mass transfer can be difficult to distinguish by modelling alone of concentration-time curves.

Because the evaluation of the results of the TRUE experiment /Winberg et al. 2003a/ identified diffusion processes as an important retention mechanism, a demand for extended knowledge of diffusion and sorption processes over longer time scales in a controlled rock volume was identified. A sorption-diffusion experiment without advection and dispersion effects, LTDE-SD, was consequently set up. The LTDE-SD experiment aims at increasing knowledge of sorption and diffusion under *in situ* conditions and to provide data for performance and safety assessment calculations, i.e.:

- To obtain data on sorption properties and processes of individual radionuclides on natural fracture surfaces and inner surfaces in the rock matrix.
- To investigate the magnitude and extent of diffusion into matrix rock from a natural fracture *in situ* under natural rock stress and hydraulic pressure and groundwater chemical conditions.
- To compare laboratory derived diffusion constants and sorption coefficients for the investigated rock with the sorption behaviour observed *in situ* at natural conditions, and to evaluate if laboratory scale sorption results are representative also for *in situ* conditions.

The main *in situ* experiment was performed from September 2006 through April 2007. During this time period of ~7 months, radionuclide tracers were circulated, sampled and monitored in the test section of borehole KA3065A03 (see Section 1.3). Following the termination of the *in situ* experiment, the target rock volume was over-cored by drilling of a 300 mm diameter borehole which was subsequently sampled, geologically characterised and analysed for trace element concentration profiles within the rock.

A laboratory program was performed in parallel to the *in situ* experiment and the subsequent analysis of the in rock material. The aim of the laboratory experiments was to produce site-specific laboratory derived retention parameters (e.g. diffusivity and sorption distribution coefficients) for which the applicability to the actual *in situ* experiment results later can be tested. The laboratory experiments were performed with material from the exploration borehole KA3065A02, the core of the 36 mm extension borehole and fracture material from the opposite side of the stub surface in KA3065A03. A common tracer solution was prepared and divided for use *in situ* and in the laboratory experiments.

1.1 Scope

One important task of the LTDE-SD programme was therefore to, after the circulation phase had been completed and rock samples extracted, measure radionuclide concentrations at different positions in the rock matrix and consequently use these data for determination of sorption and diffusion properties.

This report is focused on the data from analysis of radionuclides in the rock material as well as the distribution of the radionuclides between fracture minerals and matrix rock and comparison with laboratory determined transport parameters.

1.2 LTDE-SD-reports

This particular report, R-10-68, constitutes one in a suit of three SKB R-reports presenting the performance, results and conclusions of the LTDE-SD laboratory and *in situ* experiment.

- R-10-66 /Widestrand et al. 2010a/. The report covers the performance and results of laboratory sorption and diffusion experiments and porosity investigations, using geologically and mineralogical characterised site-specific crushed and intact rock materials.
- R-10-67 /Widestrand et al. 2010b/. The report covers the performance of the main *in situ* experiment and results from water phase measurements. Sorption coefficients were determined from tracer declining concentration time curves by applying a surface sorption model and a one-dimensional diffusion-sorption model.
- R-10-68, i.e. this report, covers the performance and results of over-core drilling of the *in situ* experiment target rock volume, subsequent sampling, geological characterisation and analysis of radionuclide penetration and distribution in the rock. The report is focused on evaluation and modelling of the penetration profiles as well as the distribution of the radionuclides between fracture minerals and matrix rock. Results are compared to sorption and diffusion coefficients determined in the supporting laboratory experiments (R-10-66) and from the water phase measurements (R-10-67) of the *in situ* experiment.

The preparations for the LTDE-SD experiments included geological and hydrogeological characterisation of the site at Äspö HRL, as well as supporting laboratory tests and a functionality test with short lived radionuclides. These preparatory activities are presented in a set of reports.

/Winberg et al. 2003b/ describes in detail the geologic features of the rock matrix in the vicinity of the test area. Borehole imaging by BIPS (Borehole Image Processing System) and core logging in the two boreholes were used to correlate fractures in the two holes. The correlation was substantiated by mineralogical and geochemical studies including stable isotopes.

Within the framework of collaboration between SKB and Ontario Power Generation's (OPG) Nuclear Waste Management Division, supporting laboratory experiments on core samples from the LTDE-SD borehole KA3065A03 were performed by /Vilks et al. 2005/. The experimental programme consisted of porosity measurements, diffusion cell experiments, radial diffusion experiments and permeability measurements.

During 2004, pre-tests including hydraulic testing (flow logging, interference and pressure build-up tests) and non radioactive tracer tests (dilution test and leakage testing) were performed by /Wass 2005/.

Installation and installation tests of the experimental set up at LTDE-SD were finalized during 2005.

During September to October 2005 a functionality test with short lived radionuclides was conducted /Widestrand et al. 2006/. The functionality test was the final preparation for the main experiment and it showed that concentration-time curves based on sampling and on-line measurements of the radioactivity in the test section could be produced with the experimental set-up used. The successively decreasing concentrations with time for the sorbing tracers showed that sorption processes in the test section could be studied at the LTDE-SD site. Only minor sorption on tubings could be measured for the most strongly sorbing tracers, which indicated that the sorption mainly occurred on the stub and 36 mm section rock surfaces. It was concluded that sampling and on-line measurements complement each other and that both should be used in the main experiment.

1.3 Overview of the LTDE-SD *in situ* experiment

A brief overview of the LTDE-SD site, experiment and sample locations is given in this section. A more detailed description of the experiment is given in /Widestrand et al. 2010b/.

The site is located in the niche at tunnel section 3,065 m at a level of –410 m.a.s.l. in the Äspö HRL. KA3065A03 is the experimental borehole and KA3065A02 has served as an exploration pilot borehole to find a suitable target structure on which to perform the experiment, see Figure 1-1 and Figure 1-2.

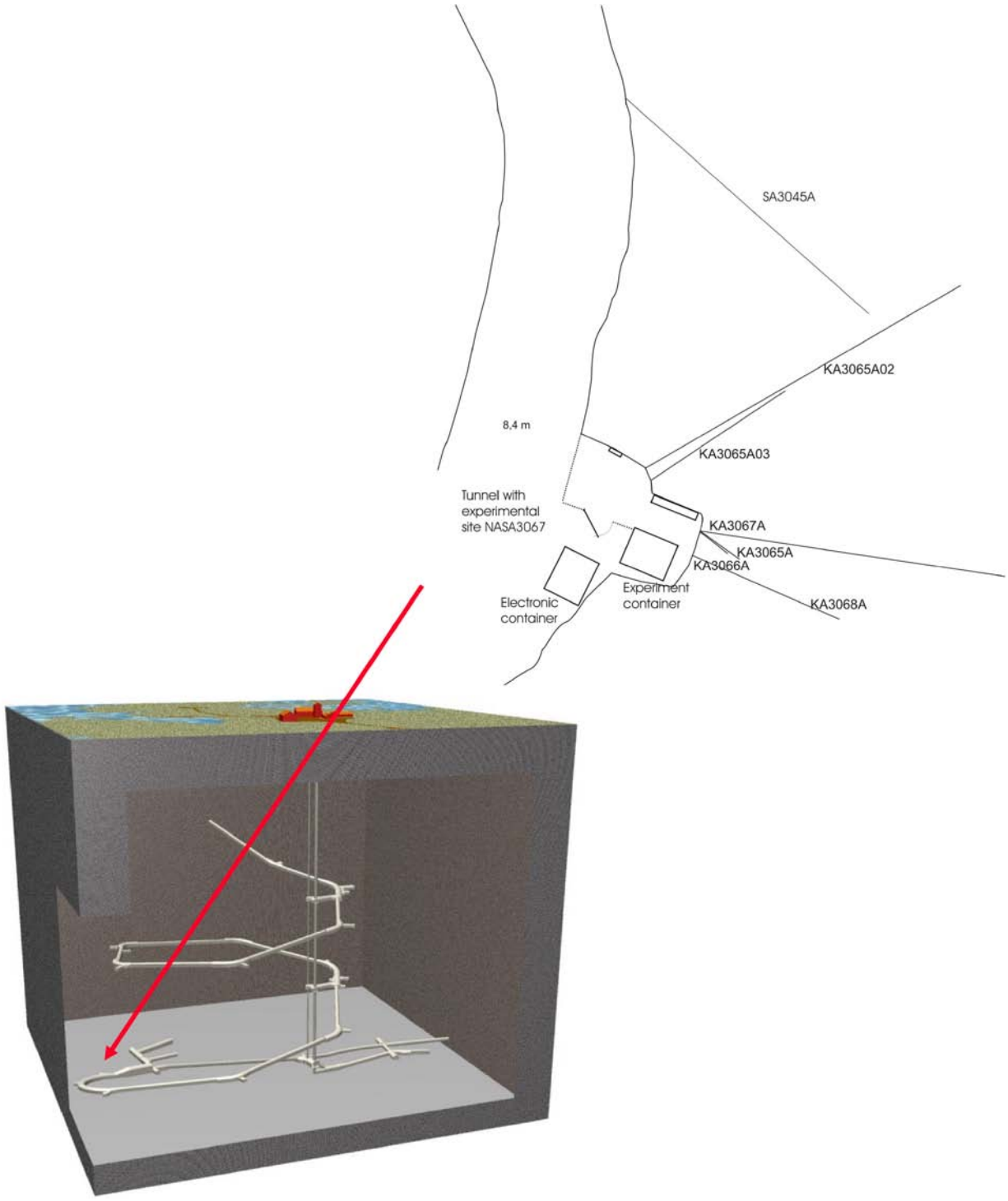

Figure 1-1. *Location of the LTDE-SD experimental site and borehole layout at NASA 3067A in Äspö HRL.*

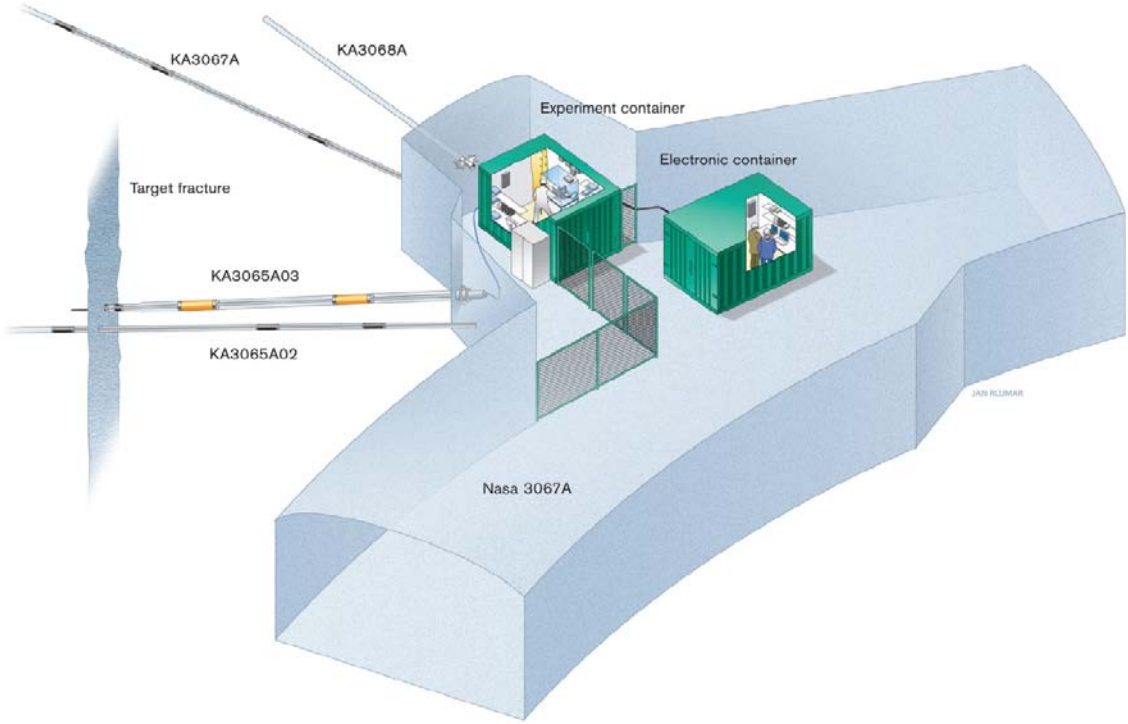

Figure 1-2. *LTDE-SD experimental site and borehole layout at NASA 3067A in Äspö HRL. The experimental borehole KA3065A03 is shown beside the pilot borehole KA3065A02.*

For the *in situ* study of diffusion and sorption of different tracers, two borehole sections were isolated by packers in the experimental borehole KA3065A03:

- The natural fracture on the surface of the stub (#10a, b) of the 197 mm wide borehole was sealed off with a polyurethane cylinder and a PEEK (PolyEther Ether Ketone) lid, which constituted a "cup-like" packer. This gave an isolated fracture surface with a diameter of 177 mm. This experimental section was used in order to obtain information of the tracer interaction with a natural fracture surface of an open water conducting fracture.
- The small diameter (36 mm) extension borehole was packed off using a double packer system leaving a 300 mm long section in contact with non-fractured rock. This part was used in order to address tracer interaction with the rock matrix without any influences of the fracture environment.

Further, the borehole outside the stub was packed off with a system of one mechanical and two inflatable packers. The system of packers and an elaborate pressure regulating system was used to eliminate the hydraulic gradient along the borehole during the *in situ* tests. The experimental set up in borehole KA3065A03 is illustrated in Figure 1-3 and a more detailed view of the test sections is illustrated in Figure 1-4.

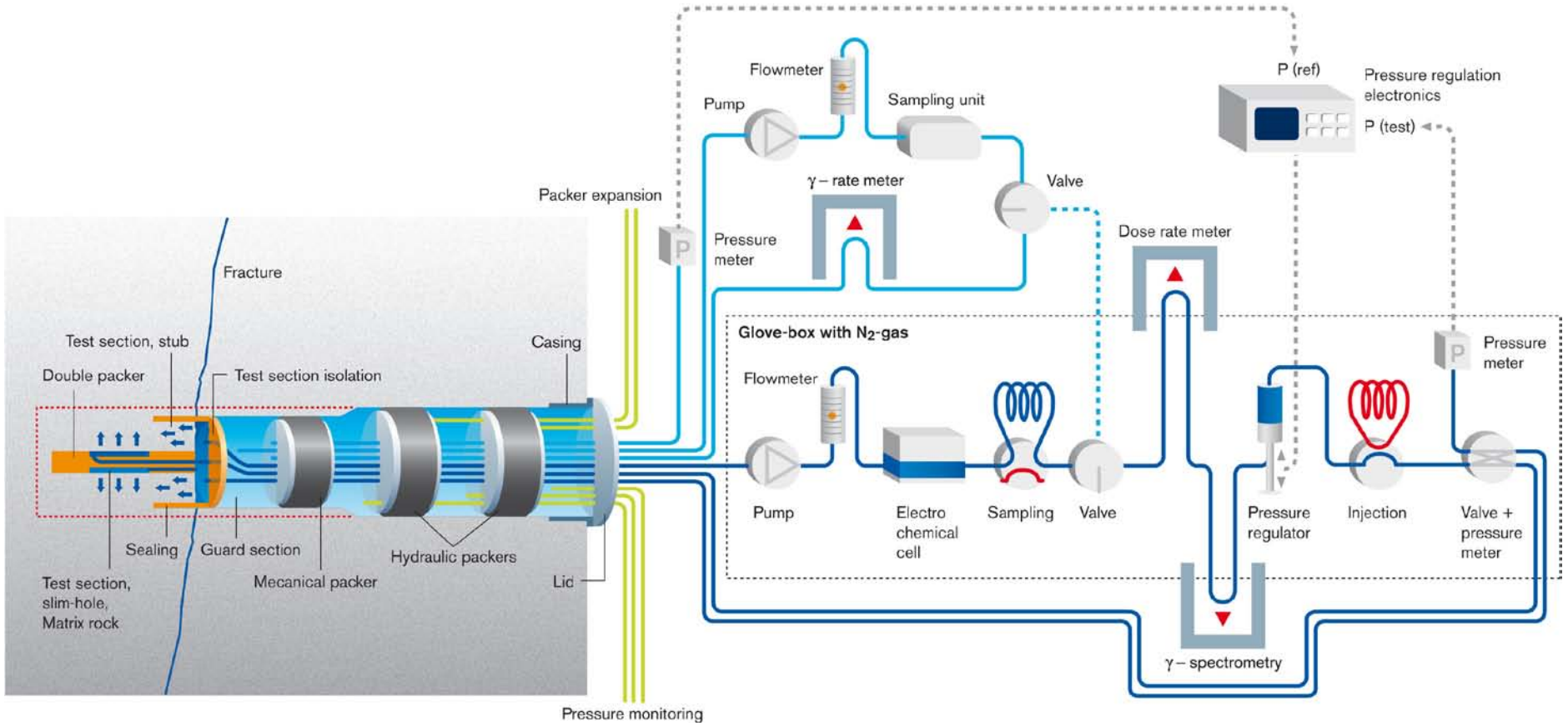

Figure 1-3. *Experimental design in borehole KA3065A03, including packers, pressure regulation and measurement and injection/sampling possibilities. A more detailed view of the test sections in front of the natural fracture (Test section stub) and in matrix rock (Test section slim-hole) is illustrated in Figure 1-4.*

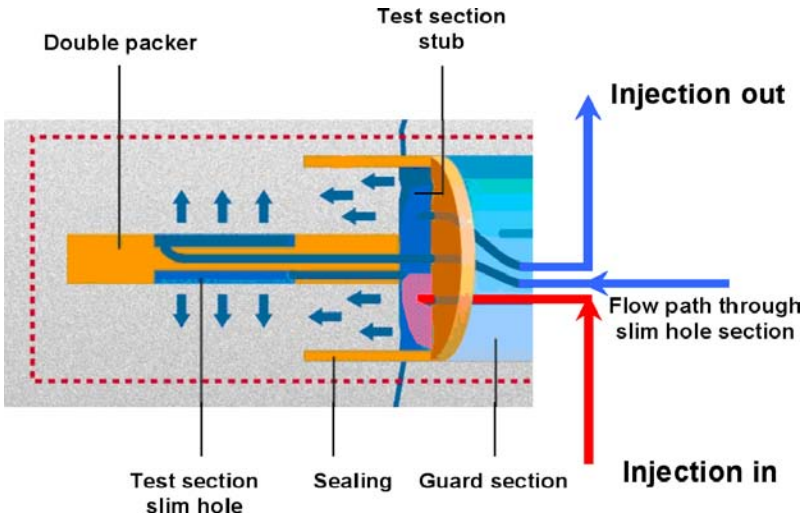

Figure 1-4. *Schematic of view of the test sections in borehole KA3065A03. The stub section by the natural fracture and the slim hole section in matrix rock (in blue; red colour is representing acidic stock solution at the injection moment).*

The *in situ* experiment comprised injection and seven months of monitoring and sampling of 22 trace elements (Table 1-1) representing a variety of chemical species and sorption behaviour. The majority of the tracers are homologues and/or analogues to long-lived radionuclides present in spent nuclear fuel. The events following the *in situ* experimental phase of the LTDE-SD are reported in Appendix 1. The results from the *in situ* experimental phase, including water chemistry data, are reported in /Widestrand et al. 2010b/.

The injection of radionuclides was performed on September 28, 2006 and the experiment was terminated on April 12, 2007. Following the *in situ* experiment, the experimental section was emptied from trace elements by rinsing the system with isopropyl alcohol. Thereafter an epoxy resin was injected in order to increase the mechanical strength of the rock prior to over-coring and to protect the stub and borehole water-rock interface from flushing water used for drilling. The target rock volume (enclosed by a red dotted line in Figure 1-3 and 1-4) was over-cored by drilling a 300 mm diameter cored borehole during April 27 to May 2, 2007. The resulting 278 mm diameter core was subsequently sampled and analysed for trace element concentration profiles within the rock, see Section 2.2. The analyses of the water samples were performed during February 2007 to July 2008. The results of the radionuclide tracer analyses in rock material, performed from October 2008 through April 2010 and results from associated modelling are presented in this report.

Table 1-1. Information on the radionuclide tracers used in the LTDE-SD experiment. The acronym ICP-SFMS stands for: Inductively Coupled Plasma – Sector Field Mass Spectrometry.

Tracer	Half-life	Presumed sorption mechanism	Analysis method
$^{22}Na^{+}$	2.6 y	Cation exchange	γ-spectrometry
$^{36}Cl^{-}$	3.0E5 y	Non-sorbing (possible subject to anion exclusion)	Liquid scintillation counting after chemical separation
$^{57}Co^{2+}$	272 d	Surface complexation	γ-spectrometry
$^{63}Ni^{2+}$	100 y	Surface complexation	Liquid scintillation counting after chemical separation
$^{99}TcO_4^{-}$	2.1E5 y	Non-sorbing, Tc(IV) under reuducing conditions	ICP-SFMS
$^{102}Pd^{2+}$	Stable	Surface complexation	ICP-SFMS
$^{109}Cd^{2+}$	463 d	Surface complexation	γ-spectrometry
$^{110m}Ag^{+}$	250 d	Surface complexation	γ-spectrometry
$^{133}Ba^{2+}$	10.5 y	Cation exchange	γ-spectrometry
$^{137}Cs^{+}$	30 y	Cation exchange	γ-spectrometry
$^{153}Gd(III)$	240 d	Surface complexation	γ-spectrometry
$^{226}Ra^{2+}$	1,600 y	Cation exchange	γ-spectrometry (measured from its daughter radionuclide Bi-214)
$^{236}UO_2^{-}$	2.3E7 y	Surface complexation, U(IV) under reducing conditions	ICP-SFMS
$^{237}NpO_2^{+}$	2.1E6 y	Surface complexation, Np(IV) under reducing conditions	ICP-SFMS
Tracers that were used during the circulation phase of the LTDE-SD experiment, but could only be analyzed to a very limited extent in the rock samples, because of their short half-lives.			
$^{35}SO_4^{2-}$	*87.5 d*	*Non-sorbing, possibly reduced to S(-II)*	*Liquid scintillation counting after chemical separation*
$^{75}SeO_4^{2-}$	*120 d*	*Non-sorbing, possibly reduced to Se(-II)*	*γ-spectrometry*
$^{85}Sr^{2+}$	*65 d*	*Cation exchange*	*γ-spectrometry*
$^{95}Zr(IV)$	*64 d*	*Surface complexation*	*γ-spectrometry*
$^{95}NbO_2^{+}$	*35 d*	*Surface complexation*	*γ-spectrometry*
$^{113}Sn(IV)$	*115 d*	*Surface complexation*	*γ-spectrometry*
$^{175}Hf(IV)$	*70 d*	*Surface complexation*	*γ-spectrometry*
$^{233}PaO(OH)_3$	*27 d*	*Surface complexation*	*γ-spectrometry*

2 Performance

The tasks presented in this section comprise over-core drilling, extraction of rock core samples, sectioning and crushing of core samples. Over-core drilling was required for the possibility of extracting core samples for analysis of the distribution of the radioactive tracers in the rock after the circulation phase of the LTDE-SD experiment. Most of the extracted core samples were sectioned into slices of different thickness prior to analysis and about half of the sliced core samples were crushed. Furthermore, the selection process of core samples for analysis is described in this section as well as the geological characterisation which was performed before as well as after the selection of core samples for analysis. Sample handling, sample preparation processes and analysis methods as well as modelling approaches are also described.

2.1 Over-core drilling

The main events during the over-core drilling (see also Figure 2-1) are described in Appendix 1.

During the dismantling of the borehole equipment and the over-core drilling, measurements of potential losses/desorption of tracers was performed both by on-line measurement of the drilling fluid and by combined sampling/measurement of the fluid. Activity losses during the initial drilling were very low and only small concentrations, near the detection limits for ^{57}Co, ^{85}Sr, ^{133}Ba, ^{137}Cs and ^{22}Na, could be detected in a few samples, see Appendix 2.

Figure 2-1. *Drilling machine is prepared for 300 mm diameter over-core drilling at experimental borehole KA3065A03.Drill bit with core barrel in centre of photo. Open vessel for collecting drilling fluid beneath borehole collar.*

A critical incident during the drilling was when the PEEK lid packer and epoxy resin accidently loosened from the core and the fracture surface was exposed to flushing water, causing desorption of tracers. Some of the water samples showed very low concentrations of ^{57}Co, ^{85}Sr, ^{133}Ba, ^{137}Cs and ^{22}Na. The highest concentration was found for ^{137}Cs for which up to 0.9 MBq was leached over the whole period that the stub was flushed. This corresponds to about 8.5% of the injected radioactivity. However, this is likely an over-estimation since the highest concentration measured during each time period was used for the estimation, see Appendix 2.

2.2 Extraction of rock core samples

2.2.1 Cutting of the core

The core, with a diameter of 278 mm and length of 1.1 m was cut before drilling for core sampling was made. Prior to the cutting and core sampling, the core was coated with clear epoxy resin (1–2 mm layer) in order to avoid contamination, see Figure 2-2. The cutting was made at one position, perpendicular to the length axis, see Figure 2-3.

Figure 2-2. *Epoxy resin coating on the 278 mm diameter core, shielding the rock in order to avoid leakage or contamination of tracers. In front is the fracture surface, where the 177 mm diameter stub is, sealed off by the PU rubber. The 36 mm diameter extension borehole can be seen in the middle. For a view of the scheme for drilling of core samples, see Figure 2-6, which shows a projection from another angle.*

Figure 2-3. *Cutting of the core.*

2.2.2 Drilling of core samples

Drilling water and drilling debris were collected in order to enable an investigation of any potential contamination during the core sample extraction phase, see Figure 2-4 and Figure 2-5. After one hole had been drilled, it was plugged with rubber plugs in order to prevent contamination. For the same reason, the drill bits and core barrel were carefully cleaned with water between each drilled core, first using a brush for the outside of the drill bit/core barrel and a bottle brush for the inside of the drill bit/core barrel. Thereafter the same procedure was repeated using ethanol, followed by rinsing with ethanol. This procedure was followed for all of the core sample drillings.

Core samples from the stub

The stub has a diameter of 177 mm and was confined by a polyurethane cylinder. Before drilling for extraction of core samples, the stub surface was coated with clear epoxy resin to prevent contamination from sample to sample. 18 cylindrical core samples (labelled A1–A18) at different positions (each with a diameter of 24 cm and length of 17 mm) were drilled out, perpendicular to the stub surface, cf. Figure 2-4 and Figure 2-6. Additionally, three blank core samples located outside the cup-like packer (therefore expected to not have been in contact with the tracer solution) were sampled and were labelled A19–A21.

Figure 2-4. *Drilling of a D core sample.*

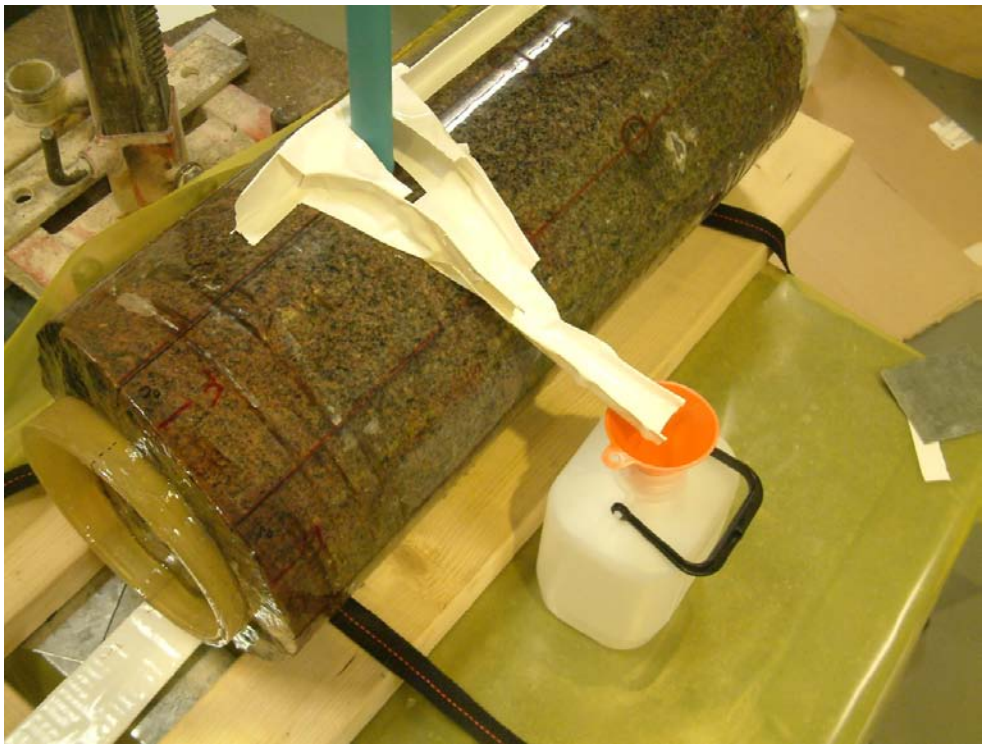

Figure 2-5. *Drill water and drilling debris collection and sampling.*

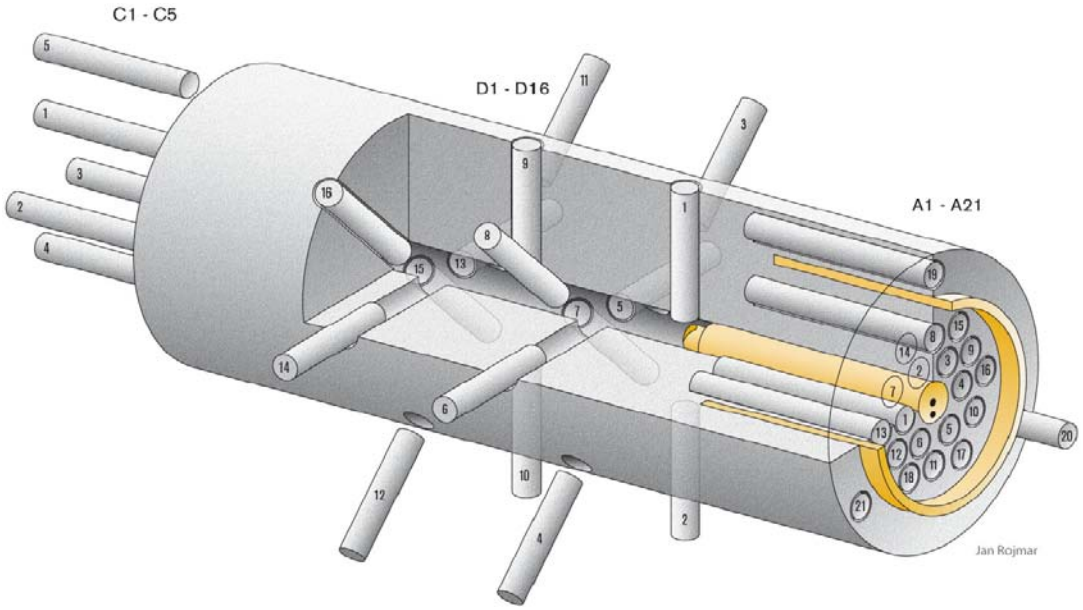

Figure 2-6. *Cutaway drawing of the 278 mm diameter over-coring used in the experimental borehole KA3065A03. The test section at the target fracture (the stub; diameter of 177 mm) is confined by a polyurethane cylinder (yellow). The test section (small hole in the middle of the over-core stub; diameter of 36 mm) in the matrix rock away from the fracture is confined using a specially designed packer. The system also contains a PEEK dummy but not shown in the figure, see Figure 1-3.*

Core samples perpendicular to the small centered hole

In the part of the 278 mm core that surrounds the test section in the small centred hole (36 mm diameter), 16 core samples with 24 mm diameter were drilled. The drillings were performed diametrically, perpendicular to the length axis of the core. This was carried out by drilling 8 core holes with a 28 mm drill through the core. Every core was split into two, one from each side of the test section in the small hole. The core holes were fixed in a relation of 45° to each other. The core samples were labelled D1–D16 and their positions are displayed in Figure 2-6. Besides this, 5 blank core samples (representing the matrix rock) were sampled by drilling parallel to the length axis of the core. The core samples were labelled C1–C5 and their positions are displayed in Figure 2-6.

Core samples from the PEEK lid covered with epoxy resin

As described in Section 2.1 the post-experimentally injected epoxy resin and the PEEK lid (Figure 2-7) accidently loosened from the fracture surface during the over core drilling.

In total 18 PEEK/epoxy core samples with 24 mm diameter were drilled from the epoxy coated lid. These core samples were drilled at exactly the same positions as the A core samples from the stub. The drilling was performed in the direction from the epoxy side straight into the PEEK disc. The core samples were designated identification numbers B1–B18.

The drilling was mainly performed because of two aspects:

- It was observed that parts of fracture coatings were attached to the epoxy surface after the PEEK-epoxy lid loosened from the stub during the drilling (Figure 2-8). These fracture coatings could presumably be identified as having been attached to the fracture surface during the circulation phase of the experiment. Analyses of the tracer content in the B-cores, (each one located exactly opposite to an A-core with the same number, see Figure 2-9) in combination of the results of the A-cores, could therefore provide a correct estimate of the tracer content of that particular part of the fracture.

- Besides the adsorption of tracers on the rock fracture, some tracer sorption on the PEEK lid during the circulation phase of the experiment was suspected; this is motivated e.g. by the observation of tracer adsorption on the PEEK tubes in the circulation equipment /Widestrand et al. 2010b/. It could therefore be of interest to at least obtain some preliminary quantification of this effect.

Consequently, the B-samples were sawn in various directions to enable visualisation with auto-radiography as well as surface samples suitable for activity measurements.

Figure 2-7. *The post-experimentally injected epoxy surface covering the PEEK-disc that accidently loosened from the fracture surface.*

Figure 2-8. *Visible fracture coatings on the epoxy surface.*

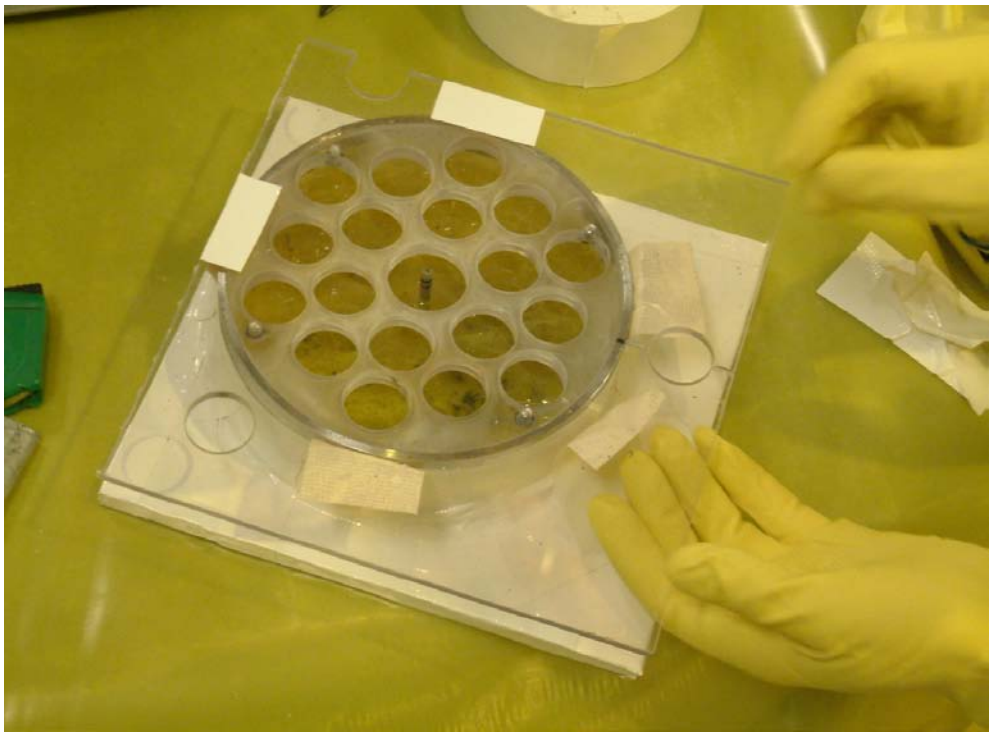

Figure 2-9. *Preparations before drilling of the B-core samples using a jig attached to the epoxy coated PEEK lid for achieving their appropriate positions. At this stage a protective coating of clear epoxy resin had been applied on the first yellow coloured layer of epoxy.*

2.3 Sectioning and crushing of cores

With the purpose of enabling tracer sampling and analysis at varying depth in the core, all the A and D core samples (except for two core samples from the inactive outside of the polyurethane cylinder, cores A19 and A21) were divided into a number of smaller sub-samples by sawing into thin slices.

Due to the risk of contamination during the initial drilling of the core samples, i.e. tracers on the outer surfaces of the rock cores that may have been spread during the drilling e.g. by the flushing water, a large majority of the initially cylindrical rock cores were cut into rods before cutting into slices, cf. Figure 2-10. In this way, the potentially contaminated surfaces of the cylindrical drill cores were removed and only the presumably not contaminated inner rock was used for the subsequent slicing procedure.

A low speed saw, Isomet (Buehler), with an Isocut diamond blade was used to saw each core sample into 15 slices (for an example see Figure 2-10). The speed of rotation was about 250–300 rpm which was effective enough to obtain the slices within reasonable times while minimizing the damage to the cores. The thickness of the blade was 0.25 mm which gave a loss of rock matrix of about 0.3 mm. In order to minimize the risks of desorption of radionuclides during the sawing procedure, ethanol was used as a cooling agent. The ethanol was collected individually after each cut and 11 samples (all of them from the slice 1 cut) was thereafter measured using γ-spectrometry measurements. The results showed that for two samples an average of 7% of the ^{22}Na (the weakest sorbing of the γ-emitting tracer) had been leached; for all other samples the activity was below the detection limit. For the stronger sorbing tracer ^{137}Cs and ^{133}Ba, an average of approximately 1% leaching was indicated.

Since it was expected that several of the sorbing tracers would have accumulated at extremely small penetration depth (in A-core samples as well as in D-core samples), efforts were made to obtain as thin slices as possible in the rock in the vicinity of the water-rock interface. For the weakly and non-sorbing tracers, it was instead anticipated that the amount of the tracers in the rock would be quite low and that the measurement condition would be favored using larger samples. Based on this,

the first three slices close to the water-rock interface were cut into ~1 mm thickness, next set of three slices were cut into ~3 mm and the third set of slices were cut into ~5 mm each. The slice thickness was thereafter increased to 10 and 20 mm thickness (also sets of three slices). However, due to the irregularity of the surface samples (due to the shape of the stub surface and the small diameter extension borehole, respectively), the sample closest to the water-rock interface often had to be expanded to a larger thickness than 1 mm.

Figure 2-10 shows an outline diagram of the sawing procedure for core sample A1. The system used for labelling of the rock slices is shown in the partition diagram. The rock slices were thereafter weighed and the depth from the stub surface was measured. An example of the actual slice thickness and the corresponding distance from the stub surface is presented in Table 2-1 for core sample A1.

Subsequently, half of the batch of slices from core samples of type A and D was crushed and some of these were selected for dissolution followed by ICP-SFMS and/or liquid scintillation measurements. The first 9 slices of each of the selected core samples were crushed slightly with a mortar (porcelain) and thereafter crushed by a mill (Retsch). The thicker slices, number 10 to 15 (10 mm and 20 mm) were pressed into smaller pieces and thereafter crushed with the mill.

Concerning sawing of the PEEK-epoxy samples (B samples, B5 shown in Figure 2-11), a separate blade suitable for plastics was used. These B-samples constituted of PEEK material and two layers of epoxy resin; the first yellow-coloured layer was injected after the termination of the circulation phase of the *in situ* experiment and the second clear layer was applied as a protection prior to the drilling of the B-cores, see Figure 2-9.

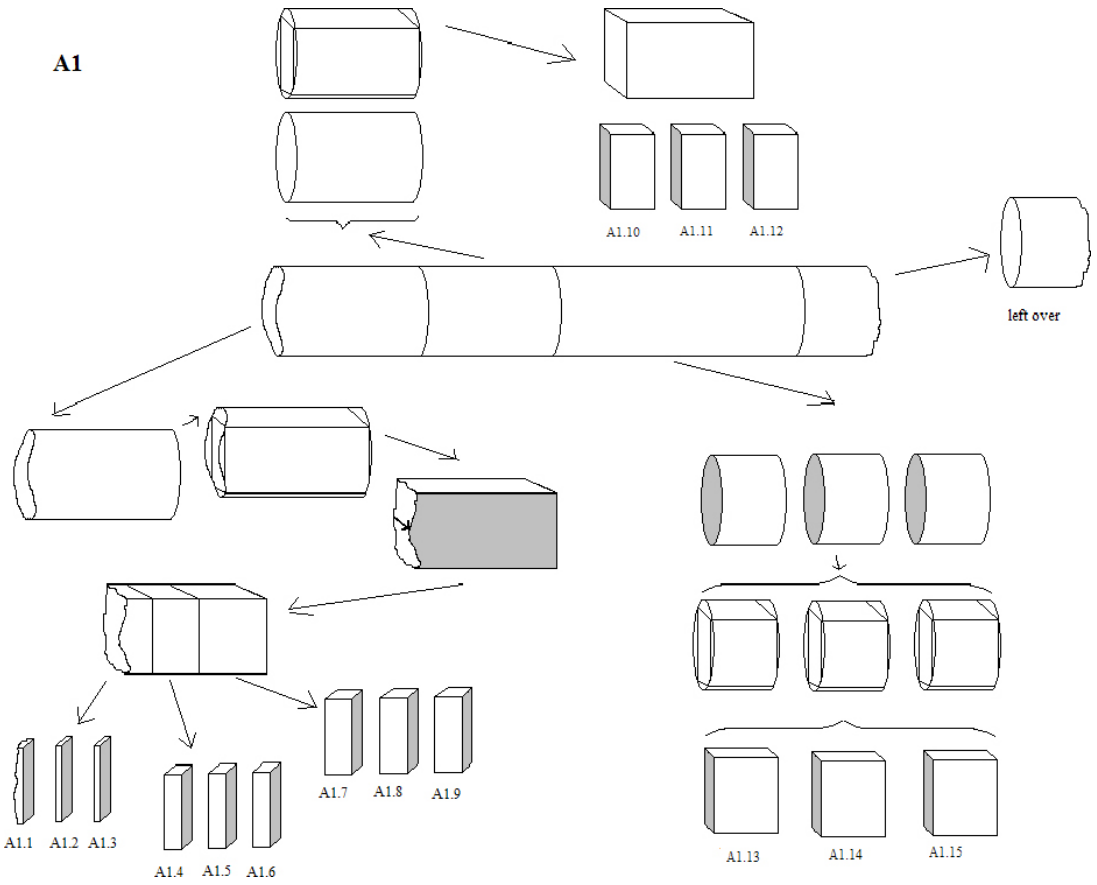

Figure 2-10. *Partition diagram of the sawing procedure of a core sample (in this example A.1) into subsamples and thereafter into cuboid shape (c. 16×16 mm) and finally thin slices (c. 3×1, 3×3, 3×5, 3×10 and 3×20 mm, see text above). The shaded areas represent surfaces exposed to autoradiographic imaging plates.*

Table 2-1. Thickness measurements and an illustration of a corresponding calculation of the distance from stub surface, exemplified by the core sample A1, cf. the lower part of Figure 2-7.

Sample	Thickness of the slice (mm)	Depth at end of slice (mm)[1)]	Depth in middle of slice (mm)
A1.1	5.0	5.0	2.5
A1.2	0.7	6.0	5.7
A1.3	0.8	7.1	6.7
A1.4	3.1	10.6	9.0
A1.5	2.7	13.5	12.2
A1.6	3.0	16.9	15.4
A1.7	6.4	23.6	20.4
A1.8	5.3	29.2	26.6
A1.9	5.3	34.9	32.2
A1.10	10	45.2	40.2
A1.11	10	55.5	50.5
A1.12	10	65.8	60.8
A1.13	20	86.1	76.1
A1.14	20	106.4	96.4
A1.15	20	126.7	116.7

[1)] (assuming 0.3 mm loss in cutting).

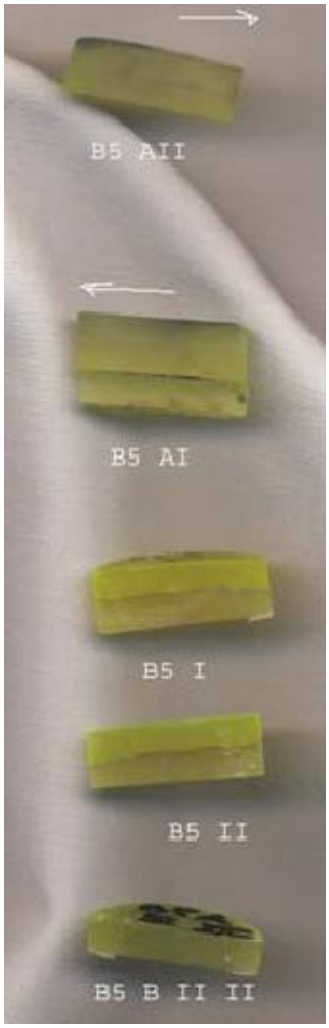

Figure 2-11. *Sawn B-samples prepared for autoradiography. The yellow epoxy layer (on top) and the clear epoxy layer (below) can be seen for the first four samples. The tracer activity is located in the interface between the two layers, i.e. at the surface that has been in contact with the natural fracture at the core stub.*

2.4 Selection of core samples for analysis

As were discussed in the previous section, 21 small diameter core samples were extracted axially from the over-cored fracture surface (the "stub") and 16 rock cores radially from the test section in the 36 mm borehole according to Figure 2-6. These rock cores, named A- and D-cores respectively, were thereafter sawn into thin slices (cf. Section 2.3). However, due to project budget constraints, only 18 of the 37 extracted rock core samples were analyzed for tracer concentration profiles by laboratory analysis methods; nine as crushed rock material and nine as sawn slices. A selection procedure was therefore applied in order to prioritize a suitable set of cores for analysis of tracer content. With the comparative low number of samples, it was considered important to obtain samples representing the variation of properties that could have different impact of the diffusion and sorption behaviour, i.e. to cover potential extremes that could occur. Factors considered during the selection process were:

- geological variations at the stub and in the 36 mm borehole section,
- tracer activity; i.e. preliminary γ-spectrometry measurements combined with measurements performed with a handheld contamination monitor (plastic scintillation) of the whole cores after extraction,
- preliminary estimations of the penetration depths; the estimated tracer penetration into the rock after studying autoradiographs of the first 3 cm and/or 6 slices of each rock core.

The result of the selection process was that 12 A-cores (among them, 2 samples intended as blank samples) and 8 D-cores were selected for tracer analysis, see Table 2-2. Both core samples that, according to the autoradiographs, displayed indications of evenly distributed matrix diffusion, penetration influenced by microfractures as well as variable penetration depth were included. In Figure 2-12, an A-core sample with tracer activity associated with fracture minerals and micro-fractures is illustrated as well as a D-core sample with relatively deep and evenly distributed tracer penetration. Concerning activity, the core samples represent variable amounts of both γ- and β-radiation when measuring on the entire core. Among the A-cores selected, 7 of the core samples were on their end surfaces (representing the stub) covered by fracture minerals and three had no fracture coating.

The selection of PEEK/epoxy cores (B-cores) was made as ^{99}Tc and ^{236}U had not been detected in the A-core samples and thus the chosen B-core samples were the ones corresponding to the A-core samples that previously had been dissolved and analyzed for ^{236}U and ^{99}Tc. However, only a qualitative estimation of the tracer activities in the PEEK/epoxy cores was possible to make. A description of the selected rock- and PEEK/epoxy samples, the performed sample preparations and laboratory analyses, is presented in Table 2-2.

2.5 Geological characterisation of core samples

An overall geological characterisation of the fracture surface (i.e. the stub) and the rock matrix has been presented by /Winberg et al. 2003b/. Nevertheless, after the *in situ* phase of the LTDE-SD experiment, supplementary documentation was produced;

- A general description of the rock type as well as mapping of fractures after the over-core drilling.
- Geological characterisation of mineralogy, alteration, microfractures and fracture coatings after the extraction of the small rock core samples.

In addition, laboratory measurements of corresponding rock material that were not exposed to radioactive solutions (e.g. the core of the slim-hole and mate of the stub) have also been performed /Widestrand et al. 2010a/. The results from the geological characterisation with examples are presented in Section 3.1, and the complete set of information is presented in Appendix 3.

Table 2-2. Overview of the selected rock and PEEK/epoxy core samples, performed sample preparation and laboratory analyses.

Core sample ID	Rock core geometry	Sample state	Sample preparation	Laboratory analyses
A-cores				
A1	cube	sliced+crushed	dissolved	HPGe[1], ICP-SFMS[2], LSC[3] (Ni-63)
A5	cube	sliced		HPGe
A6	cube	sliced+crushed	leached, dissolved	HPGe, ICP-SFMS, LSC (Cl-36 and Ni-63)
A8	cube	sliced+crushed	dissolved	HPGe, ICP-SFMS, LSC (Ni-63)
A9	cube	sliced+crushed	leached, dissolved	HPGe, ICP-SFMS, LSC (Cl-36 and Ni-63)
A10	cylinder	sliced		HPGe
A12	cube	sliced	leached	HPGe, LSC (Cl-36)
A15	cube	sliced		HPGe
A16	cube	sliced	leached	HPGe, LSC (Cl-36)
A17	cube	sliced+crushed	leached, dissolved	HPGe, ICP-SFMS, LSC (Cl-36 and Ni-63)
Reference core samples from the outside of the stub, i.e. surface not exposed for the tracer cocktail				
A19	cylinder			HPGe, ^{14}C-PMMA[4)] /Widestrand et al. 2010a/
A20	cube	sliced+crushed	leached	HPGe, LSC (Cl-36)
D-cores				
D1	cube	sliced+crushed	leached, dissolved	HPGe, ICP-SFMS, LSC(Cl-36 and Ni-63)
D5	cube	sliced		HPGe
D6	cube	sliced+crushed	dissolved	HPGe, ICP-SFMS, LSC (Ni-63)
D7	cube	sliced	leached	HPGe, LSC(Cl-36)
D8	cube	sliced		HPGe
D12	cube	sliced+crushed	dissolved	HPGe, LSC(Ni-63)
D13	cube	sliced+crushed	leached, dissolved	HPGe, ICP-SFMS, LSC (Cl-36 and Ni-63)
D14	cube	sliced	leached	HPGe, LSC(Cl-36)
B-cores, i.e. PEEK-epoxy				
B1/B1 II	cylinder	sawn	dissolved	HPGe, ICP-SFMS
B6	cylinder	sawn	dissolved	HPGe, ICP-SFMS
B8	cylinder	sawn	dissolved	HPGe, ICP-SFMS
B9	cylinder	sawn	dissolved	HPGe, ICP-SFMS
B17	cylinder	sawn	dissolved	HPGe, ICP-SFMS

[1] High-Purity Germanium detector.

[2] Inductively Coupled Plasma – Sector Field Mass Spectrometry.

[3] Liquid Scintillation Counter.

[4] ^{14}C-PMMA was performed also on inactive samples from experimental borehole KA3065A03, as well as water saturation porosity measurements, also performed on inactive samples from pilot borehole KA3065A02.

Geological characterisation performed within the present work, i.e. after slicing of the cores into thin rock samples, consisted of characterisation primarily focused on documentation of visible microfractures, other features that might influence the diffusion and sorption processes and observations of mineral phases that correspond to areas containing high concentrations of tracers (blackening at the AR-films). The samples were also photographed and/or documented with magnified scanned images of the surfaces of the slices. The documentation is displayed in Appendix 3.

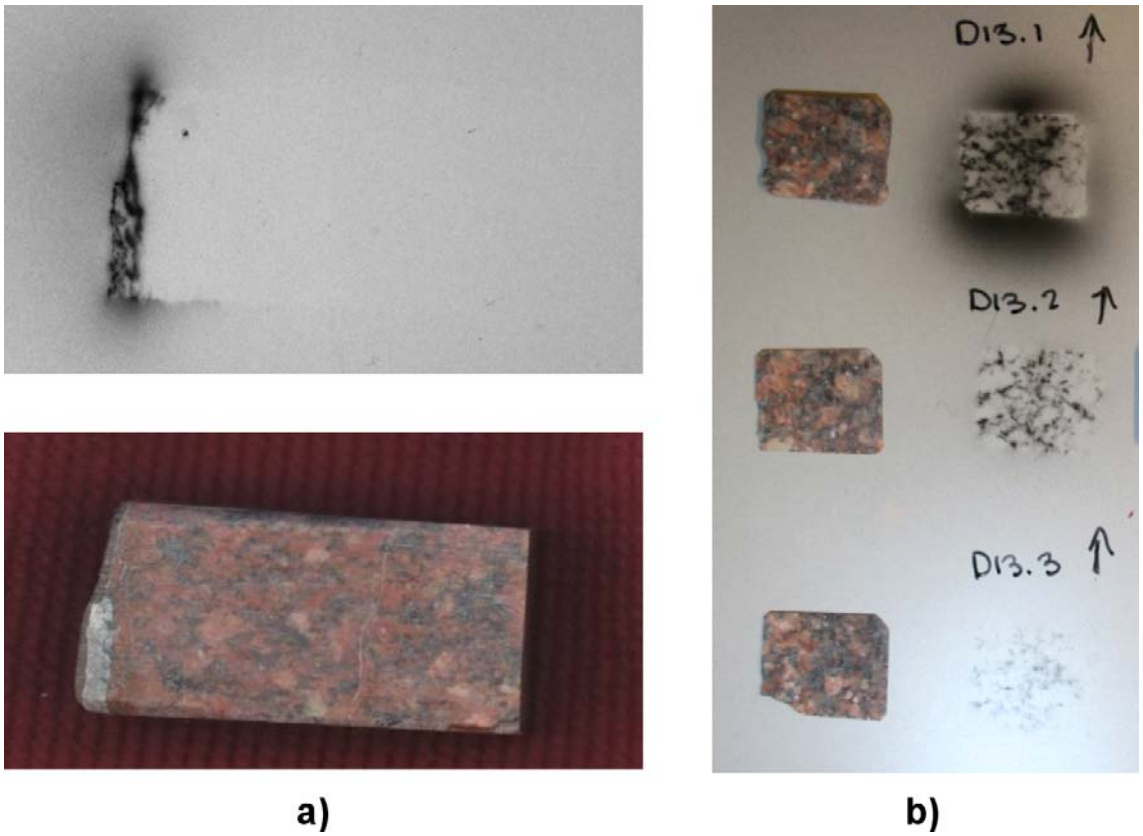

Figure 2-12. *Examples of autoradiographs, and their corresponding photographs, that were used during the selection and prioritization of cores. a) Core sample A17 (first 30 mm cube, surface parallel with the diffusion direction) which indicate near surface tracer activity that to a large degree is associated with the fracture minerals and with microfractures parallel to the fracture surface; b) Core sample D13 (first 3 slices i.e. ~3.6 mm, fracture surface parallel to the pictures) indicating a distribution of tracer activity (dark areas in autoradiographs) into the rock matrix mainly associated with the dark minerals of the rock.*

No characterisation has been made of the geological material stuck onto the PEEK lid and the material sampled as B-cores, as the priority was to perform tracer analyses. In this case, before drilling the B-core samples, it was necessary to apply a protecting epoxy resin layer on top of the material (i.e. the surface that had been the interface to the stub). After that, it was not possible to characterise the geological material.

2.6 Logistics scheme for sample handling

The core samples were initially treated and analyzed according to Table 2-2 and a scheme showing the subsequent sample handling analysis is shown in Figure 2-13. The tasks performed at FOI (Swedish Defence Research Agency) comprise pre-treatment of core samples and ICP-SFMS analyses, while geological characterisation, leaching of core samples, chemical separations and gamma- and liquid scintillation measurements were performed at Baslab, Clab (a facility run by SKB).

2.7 Sample preparation

2.7.1 Gamma spectrometry measurements (HPGe)

Gamma spectrometry measurements were performed using both crushed samples and sliced rock samples. Crushed rock samples were transferred into 20 mL plastic bottles and sliced samples were attached with double-sided tape in a fixed position in Petri-dishes prior to measurement. Entire cores were analyzed aligned vertically with the active side closest to the detector.

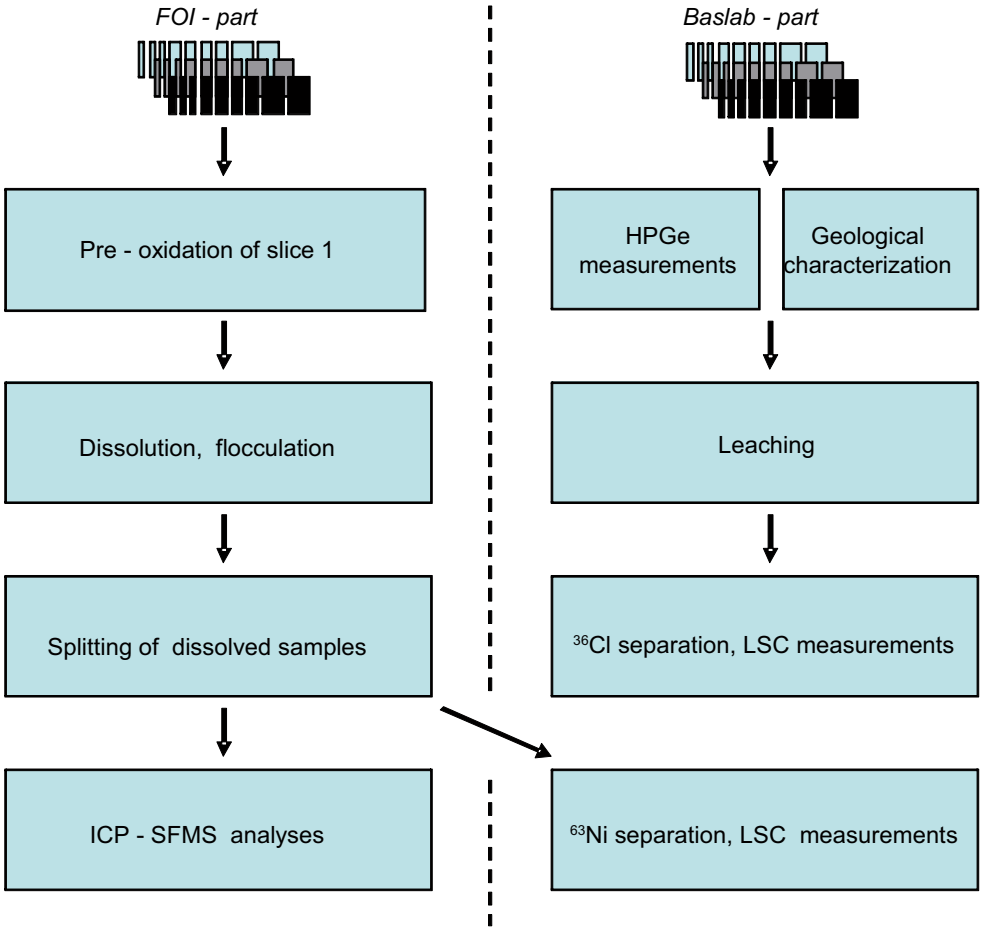

Figure 2-13. *Sample handling.*

2.7.2 Analysis of ^{63}Ni (LSC), ^{99}Tc, ^{236}U and ^{237}Np (ICP-SFMS)

Contrary to the gamma spectrometry measurements, the LSC analyses of ^{63}Ni and the ICP-SFMS analyses required that the tracer content of the rock was transferred to an aqueous sample. The crushed rock samples were therefore dissolved as a lithium borate melt and then dissolved in 1.4 M HNO_3.

In order to be able to analyze ^{63}Ni by LSC, separation of ^{63}Ni from all the other β-emitting radionuclides in the aqueous phase was performed. The separation procedure is based on a dimethylglyoxime complexation of Ni^{2+}.

2.7.3 Analysis of ^{36}Cl (LSC)

Analyses of ^{36}Cl performed on dissolved rock samples were considered as inappropriate; this since the lithium borate melt method was suspected to cause losses due to evaporation of Cl_2(g). Instead a leaching method was applied which was considered appropriate for this presumed non-sorbing tracer. The crushed or intact rock slices were weighed and placed in plastic bottles with 10 mL of 0.16 M $NaNO_3$ for leaching during 4 weeks (crushed slices) or 8 weeks (intact slices) before the sampling of the leachate was performed. The contact times were based on calculations using diffusivity data /Vilks et al. 2005/ and should according to diffusion calculations allow more than 99% diffusion leaching of ^{36}Cl for the slices as well as for the crushed samples.

Furthermore, in order to enable analysis of ^{36}Cl by LSC, separation of ^{36}Cl from the other β-emitting radionuclides in the leachate was performed. This procedure includes precipitation of Cl^- with Ag^+ and re-dissolution in NH_3.

2.8 Analysis methods

2.8.1 Autoradiography

Two techniques of autoradiography were used during the current work; digital autoradiography, which uses Imaging Plates and fluorescence scanning by FLA 5100 scanner (Fluorescence & Radioluminography Laser Scanner) and film autoradiography which uses conventional X-ray films for radioactive element detection.

Imaging Plates are flexible image sensors in which very small crystals of photo-stimulable phosphor of barium fluorobromide containing a trace amount of bivalent europium as a luminescence centre are uniformly coated on a polyester support film. Exposure of samples on an imaging plate is similar to that of photo-film but it can be re-used after erasing the latent image from the plate with uniform white light. Thereafter, FLA scanning is performed to get digital autoradiographs from which the penetration of adsorbed radionuclides can be evaluated. Digital autoradiography is 50 to 100 times more sensitive than the film autoradiography, which allows shorter exposure times /Penttinen et al. 2006/.

Before cutting into slices, a selection of 16 cuboid samples (from the water-rock interface to ~3 cm depth) were exposed on x-ray film and/or imaging plates to reveal the "profile" autoradiograph showing the penetration depths of the adsorbed radionuclides.

After cutting, the surfaces of the newly sawn rock slices were exposed on Imaging Plates with two different exposure times; 1 and 3 days.

For the first 9 rock slices of each core, film autoradiography was performed as a complement to the digital autoradiography. This was motivated by the fact that the resolution of film autoradiographs is better than the resolution of digital autoradiographs and therefore improves the interpretation of mineral specific sorption. The exposure time for film autoradiography was 3 days for Biomax MR (Kodak) X ray films (a high performance autoradiography film for ^{14}C and other low-energy β-emitting nuclides). The film autoradiographs were also scanned with CanoScan 9900 table scanner.

2.8.2 ICP-SFMS

The ICP-SFMS instrument was an Element2 ICP-SFMS with a "Twister" spray chamber and a "conical nebulizer". The analyses were performed at FOI, Umeå, Sweden.

2.8.3 HPGe

The HPGe measurements were performed at Baslab, Clab. The compressor-cooled HPGe detector was a (GEM35190P, ORTEC) of 37% relative efficiency and for data evaluation, the computer program GammaVision (6.07) was used. Due to a rather bad energy resolution obtained for some of the measurements, it was concluded that the automated peak search fit within the GammaVision program did not give satisfying results. For this reason some of the spectra were extracted as numerical datafiles in Microsoft Excel where the peak identification and quantification was performed manually. The detection limits for these measurements are 2σ.

Calibration samples with suitable geometries for analysis of sliced and crushed rock samples were produced by adding appropriate amounts of the mixed radionuclide gamma-ray reference solution (QCY44) to square concrete casts (16×16 mm) in Petri dishes or to crushed rock material in plastic bottles. Prior to hardening of the concrete, the reference solution was distributed evenly in the rock material by stirring with a spoon. The heights of the reference samples were adjusted to suite the rock sample heights. The thinnest samples (1 mm) were in both cases difficult to produce and were instead made by adding calibration solution to a paper (viscose and polyester) of appropriate thickness and geometry and allowing it to dry.

In order to assure that no contamination of the detector had occurred, a measurement of a blank sample (an empty sample holder; air) was performed within each series of 10 sample measurements. Besides that, one calibration sample was also included in the series to assure that the calculation efficiency was maintained.

The concentration of the ^{226}Ra radioisotope was measured from the presence of its γ-emitting daughter isotope ^{214}Bi. However, a background correction had to be made because of ^{214}Bi being present in ~75% of the blank samples, probably a result of varying radon concentrations in the air in the laboratory. Therefore, based on the observed variation of the background count rate, the detection limit of ^{226}Ra was raised from ~ 0.7 Bq/sample to 1.4 Bq/sample.

It should also be mentioned that HPGe spectroscopy was applied in the preliminary estimations of the activity of the different cores after the extraction, cf. Section 2.4.

2.8.4 LSC

The LSC instrument was a Wallac 1414 Guardian, with the computer program Wallac Winspectral for data evaluation. The analyses were performed at Baslab, Clab with background measurements made in connection with each sample batch. Emulsifier-Safe™ and OptiPhase HiSafe 3 were used as scintillation liquids. The detection limits for ^{36}Cl and ^{63}Ni are reported as 3σ and 5σ, respectively. The latter higher detection limit was due to the more complex sample matrix consisting of dissolved rock material.

2.9 Modelling

The experimentally determined penetration curves (also, for one case, in combination with data for the aqueous phase) in this work have been analysed using a diffusion-sorption model in order to evaluate porosity, sorption and diffusion characteristics of the material. This basic modelling attempt was intentionally aimed to address sorption/diffusion using as simple model as possible and therefore minimizing the number of parameters needed for description of the process. A constraint is therefore that all modelling has been done using an approach assuming a homogeneously distributed porosity combined with a single diffusion rate; a condition which is highly questionable when observing the ^{14}C-PMMA measurements of the porosity distributions (performed on inactive samples from pilot borehole KA3065A02 and experimental borehole KA3065A03) /Widestrand et al. 2010a/. Nevertheless, it has been considered beyond the scope of this report to fully include approaches of heterogeneous diffusion, a technique that earlier has demonstrated to give a good conceptual agreement for laboratory diffusion studies of sorbing tracers, e.g. /Johansson et al. 2000/. This latter work, however still addressed heterogeneity using a very simplified one-dimensional model. For obtaining a realistic addressing of the porosity heterogeneity observed in the ^{14}C-PMMA measurement, sophisticated models with an extended number of modelling parameters would probably be necessary.

The sorption has only been addressed using an approach of a linear equilibrium distribution of the tracer between the aqueous and the rock phase, i.e. chemical kinetic constraints and/or non-linear sorption effects has not been included. Furthermore, no address of a mechanism of mobility of the ions associated with the rock phase (e.g. so called surface diffusion) has been included.

2.9.1 One-dimensional diffusion model

The sorption-diffusion *in situ* experiments performed in this work were mainly aimed to quantify the diffusion and sorption parameters of the rock. In this work, the diffusion process is described by the formation factor, F_f (–) which describes how much smaller the effective diffusivity, D_e (m^2/s), in the rock is compared with the diffusion rate in pure water, D_w (m^2/s), i.e.:

$$D_e = D_w \cdot F_f \qquad (2.1)$$

The advantage of applying a formation factor is that it conceptually should only be dependent of the rock conditions and therefore, presuming that a basic sorption/diffusion model is applied, be equal for all different tracers studied although the water diffusivities of them may vary.

The apparent diffusivity, i.e. the actual diffusion rate when taking e.g. sorption into account is defined as

$$D_a = \frac{D_e}{\varepsilon + K_d \rho} \tag{2.2}$$

where ε is the porosity of the rock, K_d (m^3/kg) is the sorption distribution coefficient (i.e. tracer concentration in the rock phase divided by the tracer concentration in the aqueous phase) and ρ is the rock density (2,700 kg/m^3 used throughout this work). For the vast majority of the sorbing tracers, the ε term is negligible compared to the $K_d \rho$ term.

The water diffusivities of the different tracers used in this work have been obtained from /Li and Gregory 1974/. For the cases where the formation factor has been obtained from laboratory diffusion experiments using tritiated water as tracer, a water diffusivity of $2.1 \cdot 10^{-9}$ m^2/s has been used for calculation of the formation factor from the experimentally measured effective diffusivities (D_e) for tritiated water according to:

$$F_f = \frac{D_e}{2.1 \cdot 10^{-9}} \tag{2.3}$$

The $2.1 \cdot 10^{-9}$ m^2/s value used refers to the work of /Mills and Lobo 1989/ and has been compensated for elevated temperatures in the laboratory environment.

The general one-dimensional diffusion equation is expressed by;

$$\frac{\partial C}{\partial t} = D \frac{\partial^2 C}{\partial x^2} \tag{2.4}$$

In the present situation the interaction can be regarded as diffusion from a stirred solution of limited volume into a plane sheet. In order to benefit from the analytical solution of this case given by /Crank 1975/, a case where diffusion from both sides of the sheet occurs will be considered, cf. Figure 2-14. The sheet occupies the space $-l \le x \le l$, while the solution is of limited extent and occupies the spaces $-l-a \le x \le -l$ and $l \le x \le l+a$. The occupation length of the water phase, a, is set to:

$$a = V / A + K_a \tag{2.5}$$

where V [m^3] corresponds to the volume in the test section and A [m^2] is the surface area exposed to the volume. The K_a [m] term is included in the cases when a surface sorption (additionally to the sorption in the rock matrix) is addressed.

The length of the sheet (l) has no influence of the rate of the loss of tracer in the water phase as long as the contribution of tracer diffusing from one side to the other can be neglected. The length can therefore be set arbitrarily and in this particular case l has been set in order to obtain a tracer concentration in the middle of the sheet (x = 0) that is at least 10^8 times lower than the tracer concentration in surface layer of the sheet (i.e. $x = l$ or $x = -l$).

The concentration of the solute in the solution is always uniform and is initially C_0, while the sheet initially is free from solute. The following boundary conditions therefore apply:

$$C=0, \qquad a\frac{\partial C}{\partial t} = \pm D \frac{\partial C}{\partial x} \qquad -l \le x \le l, \qquad t = 0 \tag{2.6}$$

and

$$a\frac{\partial C}{\partial t} = \pm D \frac{\partial C}{\partial x}, \qquad x = \pm l, \qquad t > 0 \tag{2.7}$$

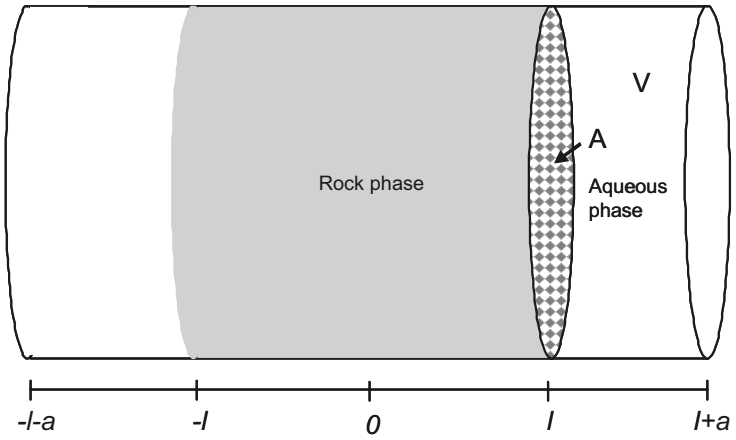

Figure 2-14. *Conceptual model applied in the diffusion calculations.*

The analytical solution to this problem has been given by /Crank 1975/. The total concentration within the sheet, C_x, (including both the pore water concentration and the mass sorbed on the rock) at the distance x at a given diffusion time of t is given by the expression:

$$C_x = C_\infty \left\{ 1 + \sum_{j=1}^{\infty} \frac{2(1+\alpha_r)\exp\left(-\frac{D_a q_j^2 t}{l^2}\right)}{1+\alpha_r+\alpha_r{}^2 q_j^2} \frac{\cos\left(\frac{q_j x}{l}\right)}{\cos q_j} \right\} \tag{2.8}$$

where C_∞ is the concentration in the sheet at infinite time and the q_j values are the non-zero positive roots of:

$$\tan q_j = -\alpha_r q_j \tag{2.9}$$

and α_r is the ratio of the capacities of the rock and water phase, defined by;

$$\alpha_r = \frac{a}{l(\varepsilon + K_d \rho)} \tag{2.10}$$

Furthermore, the decrease of the concentration of tracer in the start cell, C_1, can be calculated according to:

$$C_1 = C_{1(0)} - \frac{C_\infty m}{V_1 \rho} \left\{ 1 - \sum_{j=1}^{\infty} \frac{2\alpha_r(1+\alpha_r)\exp\left(\frac{-D_a q_j^2 t}{l^2}\right)}{1+\alpha_r+\alpha_r{}^2 q_j^2} \right\} \tag{2.11}$$

where $C_{1(0)}$ corresponds to the initial concentration in the start cell.

By applying mass balance, C_∞ can be calculated according to:

$$C_\infty = \frac{C_0 a}{l + a/(\varepsilon + K_d \rho)} \tag{2.12}$$

The program Solver in Microsoft Office Excel uses a non-linear optimization code to search for an optimal value, *i.e.* a min or max value. In this work the program was used to minimize the sum of squared errors (weighted by the uncertainty of each measurement) by varying one, two or all three of the parameters D_e, K_d and ε in the diffusion model. Those of the parameters not varied, were held constant (fixed) during the calculation, applying laboratory derived numerical values of these parameters.

2.9.2 Overview of modelling cases

Five different cases of modelling have been included in this work: different cases were investigated, in which one, two or all of the parameters were varied, respectively.

- Case 1 involves predictions of the penetration profile and the loss of tracer in the aqueous phase using only independently determined laboratory values for D_e (through diffusion experiment) K_d (batch sorption experiment) and ε (water saturation measurement). This means a calculation of the expected outcome of the *in situ* experiment; the results of the calculation are then qualitatively compared to the results of the experiment. No parameter estimation by model fitting is thus performed for this case.
- For Case 2, the sorption coefficient K_d parameter is used as the fitting parameter (D_e and ε fixed to laboratory-derived values) to obtain as good fit as possible to the measured penetration profile. The tracer losses in the aqueous phase during the circulation phase are not addressed in this modelling case.
- Case 3 is the opposite of Case 2, i.e. F_f and ε were used as fitting parameters while K_d was kept constant using the laboratory values.
- In Case 4, all the three parameters mentioned (K_d, F_f and ε) were used as fitting parameters simultaneously, however still using only the measured penetration profile data to fit the model.
- Finally, an estimation was performed, Case 5, in which experimental data from both the penetration profile and from the time dependence of the losses of tracers in the aqueous phase were used. As in Case 4, all the three parameters (K_d, F_f and ε) were used as fitting parameters simultaneously.

It should also be mentioned that for all tracers studied (except the non-sorbing ^{36}Cl and possibly the very weakly sorbing ^{22}Na) the ε term is negligible compared to the $K_d \rho$ term in Equation (2.2) and therefore has no influence in the calculations within the intervals given by the physical constraints, $0 < \varepsilon < 1$. Consequently, the Case 3 and the Cases 4–5 effectively become cases with 1 and 2 fitting parameters, respectively.

In Table 2-3 a summary of the investigated cases is presented.

The uncertainties in the parameters (D_e, K_d and ε) were estimated with the use of the Goal Seek program in Microsoft Office Excel. The uncertainty levels were estimated to the limit of where an increase or decrease of a single parameter causes the best-fit criterion (i.e. lowest sum of the squared sum of errors) to be increased by a factor of the square root of 2, according to the concept described by /Meinrath et al. 2000/.

Table 2-3. Summary of the modelling cases (1–5) performed within this work. For the fixed parameters, independently determined laboratory data was used and the estimated parameters were varied in order to fit the experimentally obtained data (data from the penetration profile and from the water phase measurements).

	Fixed K_d	Fixed F_f	Fixed ε	Estimated K_d	Estimated F_f	Estimated ε	Fitted to penetration profile data	Fitted to water phase data
Case 1	X	X	X					
Case 2		X	X	X			X	
Case 3	X				X	(X)[A]	X	
Case 4				X	X	(X)[A]	X	
Case 5				X	X	X[A]	X	X

[A] Except for ^{36}Cl, the porosity (ε) is always negligible compared with the $K_d \cdot \rho$ term (cf. Section 4.6) and is therefore in the vast majority of the cases a very non-sensitive estimation parameter.

3 Results

3.1 Geological characterisation

The Äspö HRL is according to /Rhén et al. 1997/ dominated by four major rock types; fine-grained greenstone, Äspö diorite, Småland (Ävrö) granite and fine-grained granite. The nomenclature of these rock types have previously been updated (Hultgren P (SKB), pers. comm.) in order to get correspondence between the Äspö rock types and the Site investigations rock types. The Småland (Ävrö) granite has been updated to Ävrö granodiorite, the Äspö diorite to Ävrö granodiorite or Ävrö quartzmonzodiorite when mineralogical, chemical or density data is available. The investigated rock material in the current report is interpreted to be of Ävrö granodiorite composition, based on density data /Widestrand et al. 2010a/.

The geological materials characterised consist of rock slices from the fracture surface (stub) core samples (A-cores) and, rock slices from the matrix rock core samples (D-cores) from the matrix rock surrounding the 36 mm diameter borehole. As was discussed in Section 2.5, the current report focuses on geological features that might influence the diffusion and sorption processes (exemplified in Table 3-1). The subsequent work included identification of:

1) Fracture minerals (A-cores, slice 1)
2) Microfractures
3) Deviations from the general mineralogy (e.g. porous mineral grains with cavities)

In addition, the slices were photographed and other conditions that might influence on the analyses (e.g. remaining epoxy resin) were documented. Documentation of areas at the rock slice that correspond to areas containing high concentrations of tracers (blackening at the AR-films) was also performed.

A complete set of the geological characterisations performed is presented in Appendix 3 and the results from the small diameter rock core (corresponding to the 36 mm borehole in the *in situ* experiment) is presented in /Widestrand et al. 2010a/.

Fracture minerals (A-cores)

The occurrence and distribution of fracture minerals on each rock core were difficult to determine due to the protective epoxy layer) covering the fracture surface, and that the fracture coatings were thin (range 0 to 2 mm, but for most samples about 0.5 mm). In order to get an improved determination of the fracture mineral coating a photograph taken before the surface was covered by epoxy resin was used as well (Figure 3-1).

Calcite and chlorite were found to be the dominating fracture minerals, although quartz, epidote and chalcopyrite were visible to a minor extent as well. The fracture minerals were however not evenly distributed over the fracture surface and consequently, the different A-cores exhibit variable mineralogy; from relatively thick coating of calcite (overlying a thin layer of chlorite) to thin chlorite, and to no fracture coating at all. Further on, the uneven distribution of fracture minerals were also reflected in the separate cores which means that the A-cores were not always totally covered/uncovered with fracture minerals, see Table 3-2.

Compared with the initial characterisation of the target structure /Winberg et al. 2003b/, the occurrence of calcite was somewhat less than the expected. One possible explanation for that might be that thin layers of fracture minerals were fixed on the PEEK-epoxy cores (Figure 3-1). No characterisation of the PEEK-epoxy cores (B-cores) was performed and therefore, neither the amounts of minerals nor the mineral phases on this material were determined. The layers of chlorite were found to be very thin and somewhat underestimated during the previous geological characterisation of the whole cores. The wall rock close to the fracture surface was altered, i.e. mainly red-stained and/or microfractured, although porous mineral grains with cavities were visible as well.

Table 3-1. Example from the geological characterisation of the two first rock core slices from sample A1.

	**A1.1** Uneven slice, average thickness is 5 mm. Several sealed microfractures near the fracture surface area A, i.e. the uppermost area in the picture. (The fracture surface is covered with epoxy resin to a large extent.)
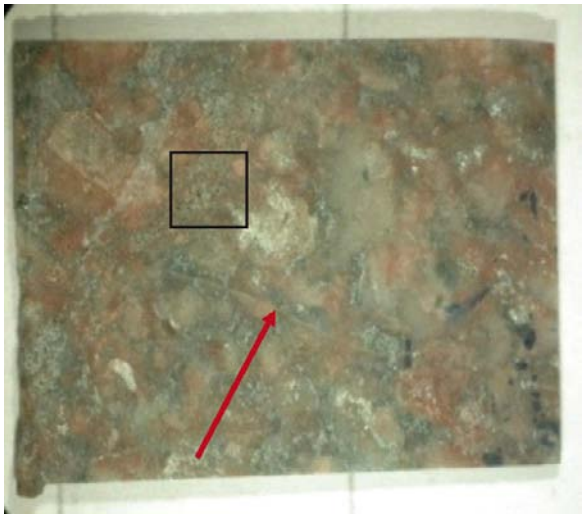	**A1.2** **a)** Picture through stereomicroscope (8×). Partly open or sealed microfracture, perpendicular to the red arrow. The black square represents the approximate area of A1.2b.
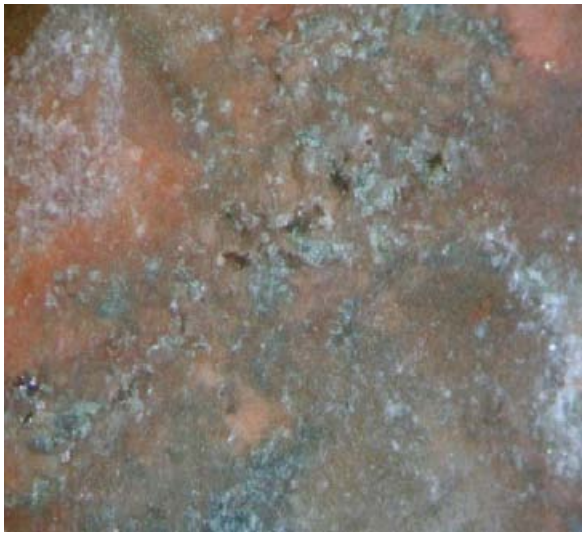	**A1.2** **b)** Picture through stereomicroscope (50×). Porous mineral grains with cavities.

As were discussed above, the A-cores were found to be heterogeneous with respect to fracture mineralization and one single core (slice 1) may have parts that were covered with fracture minerals as well as parts without. Therefore, a simplification was performed and the A-cores were divided into two groups of samples; with or without fracture minerals on the surface area. This means that all rock samples with documented fracture minerals that covered more than 50% of the surface were judged as fracture mineral coated. Samples with less than 50% fracture minerals were considered as non-covered i.e. equal to the rock matrix see Table 3-2. This subdivision was thereafter used during the later analytical and modelling work.

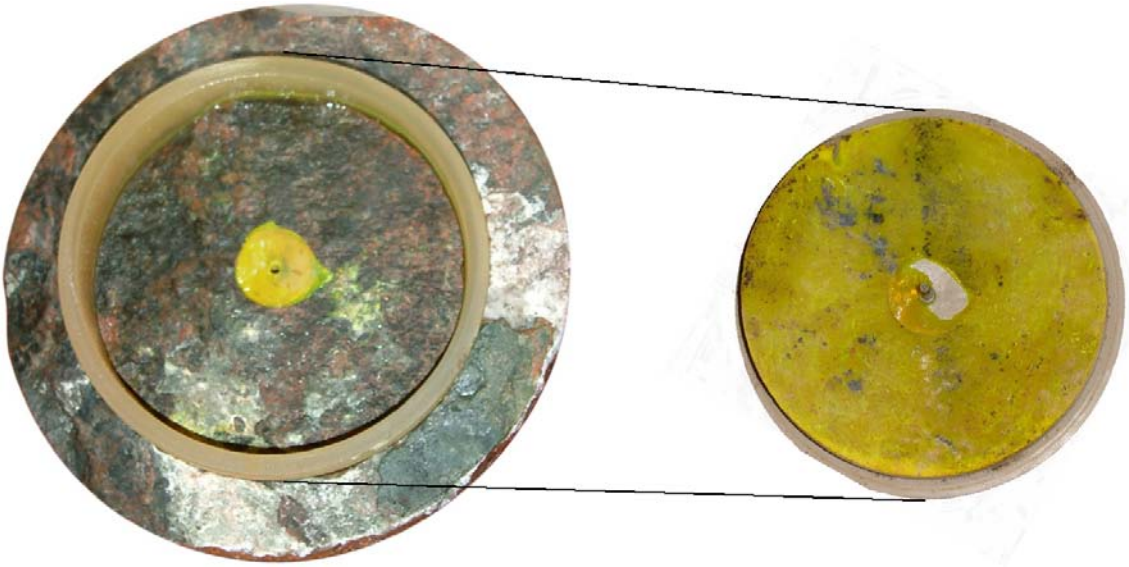

Figure 3-1. *Photograph of the stub to the left and the PEEK-epoxy plate to the right. It is the area inside the polyurethane cylinder that has been exposed to the tracer solution. The PEEK-epoxy plate has been reversed in order to simplify the comparison with the stub surface (/fracture plane). Most of the grey spots visible at the yellow surface are remaining rock material, primarily fracture minerals.*

Table 3-2. Rock core samples, with the division into fracture mineral coated rock core samples or matrix rock. The estimated percentages and dominating fracture mineral is given as well. For the samples that were sliced and penetration profiles were measured (normal style) a reference to the data set used for the modelling is given. The samples given in italic style were only measured as whole core and were consequently not selected for further laboratory analyzes or modelling. Detailed characterisation of each core is given in Appendix 3.

Core sample ID	Percentage of surface covered by fracture minerals	Dominant fracture minerals	Judged as fracture mineral coated	Retention data set used for modelling, cf. Table 4-1
Stub samples (drilled normal to the exposed fracture surface)				
A1	50%	Chlorite	Yes	Fracture mineral coated
A2	*20%*	*Calcite*	*No*	
A3	*50%*	*Chlorite*	*Yes*	
A4	*75%*	*Calcite that is overlaying chlorite*	*Yes*	
A5	50%	Calcite	Yes	Fracture mineral coated
A6	95%	Calcite that is overlaying chlorite	Yes	Fracture mineral coated
A7	*75%*	*Chlorite*	*Yes*	
A8	70%	Chlorite	Yes	Fracture mineral coated
A9	50%	Calcite that is overlaying chlorite	Yes	Fracture mineral coated
A10	90%	Calcite that is overlaying chlorite	Yes	Fracture mineral coated
A11	*60%*	*Calcite and chlorite*	*Yes*	
A12	25%	Calcite that is overlaying chlorite	No	Matrix rock
A13	*45%*	*Chlorite*	*No*	
A14	*15%*	*Chlorite*	*No*	
A15	35%	Chlorite	No	Matrix rock
A16	0%	None	No	Matrix rock
A17	100%	Calcite that is overlaying chlorite	Yes	Fracture mineral coated
A18	*100%*	*Calcite that is overlaying chlorite*	*Yes*	
Slim hole samples (no fracture minerals (drilled normal to the axis of the 36 mm cored hole)				
D1, D5, D6, D7, D8, D12, D13, D14			No	Matrix rock
D2, D3, D4, D9, D10, D11, D15, D16			*No*	

3.1.1 Microfractures

Microfractures were documented in the A-cores, as well as the D-cores. When studying the separate slices, 50% of the analyzed A-cores (ten) had visible microfractures from slice 1 to 6 (i.e. 0–15 mm from the stub) and 50% of the analyzed D-cores (eight) had visible microfractures at the first 15 mm (Table 3-3). Several of the investigated D-core slices had microfractures that were fresh and consequently they were supposed to be newly formed (i.e. induced by drilling or stress release), something that was noticed during the documentation of whole cores as well, see Appendix 3. However, no specific rock-mechanical analyses in order to investigate these fresh fractures were performed during the current work. A general discussion of sample disturbances are thus presented in /Winberg et al. 2003b/ and in /Li 2001/). Fresh microfractures were only sparsely documented in the A-cores.

Studying the rock core slices in a stereomicroscope, the microfractures were found to be open, partly opened or sealed. Although it is the open and partly opened microfractures will have the greatest influence on the tracer penetration, sealed fractures might have an increased porosity /Penttinen et al. 2006/ and may therefore act as a transport path as well.

3.1.2 Autoradiographs (AR)

The average tracer concentration in the rock roughly corresponds to black areas in the autoradiographs (the blackening depends on the radiation properties of individual tracers). The black areas might however be larger than the actual radioactive area due to various radiation energies of the tracers and the penetration depth visible from the AR is not as deep as for the corresponding analyzes with e.g. HPGe.

Generally, the autoradiographs from the stub (A-cores) show patterns of blackening that are heterogeneous with clearly observed microfractures and plane-parallel fractures as well as areas similar to those seen in the slimhole (D-cores). The autoradiographs associated with the slimhole on the other hand (D-cores), have a distribution of the black areas that to a great extent corresponds to areas with dark minerals (e.g. biotite and chlorite, titanite and amphibole, as seen in Figure 3-2). The black areas generally correspond to the interpretation of a relatively homogeneous porosity pattern available for diffusion in the Ävrö-granodiorite matrix /Widestrand et al. 2010a/.

AR profiles from cores that are dominated by calcite at the fracture surface (A-cores) show blackening (sorption) at the outermost layer as well as in layers inside the fracture mineralization, sub-parallel to the surface (Figure 3-3). These internal black layers are interpreted to be pore spaces between several different generations of calcite, or boundaries between chlorite and calcite. The weak blackening in the calcite matrix indicates that sorption in calcite is weak. Autoradiographs for samples without fracture minerals show different distribution patterns, which indicate diffusion into the matrix.

Table 3-3. List of rock core samples where microfractures were found from 0 to 15 mm (slice 1 to 6). The microfractures were mainly identified as partly opened.

A-cores		D-cores	
ID	Comments	ID	Comments
A1	Single microfracture	D1	Several microfractures in slice 1, single microfracture in slice 2 and 3, respectively
A9	Single microfracture in slice 1–3, respectively, several in slice 4–6	D7	Single microfracture in slice 1–3, respectively
A10	Single microfracture	D8	Single microfracture in slice 1–3, respectively
A16	Single microfracture, but several in slice 3 and 4	D13	Single microfracture in slice 1–6, respectively, with the exception of slice 4 which contains several microfractures.
A17	Single microfracture		

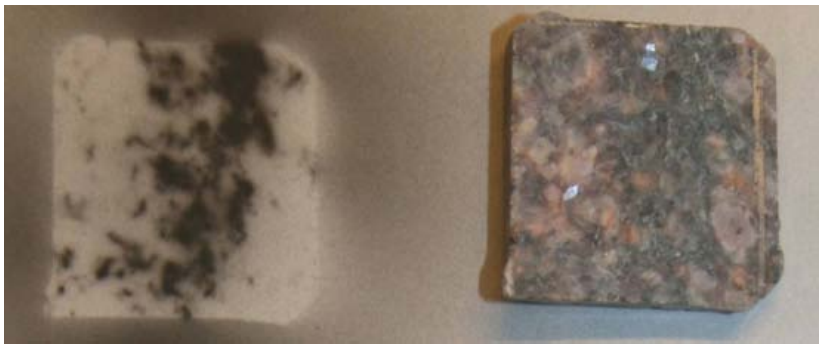

Figure 3-2. *Autoradiograph of slice D7.1, cf. Figure 2-6. The blackening is interpreted to correspond primarily to the dark minerals and a single microfracture. The base of the slice is approximately 16 mm.*

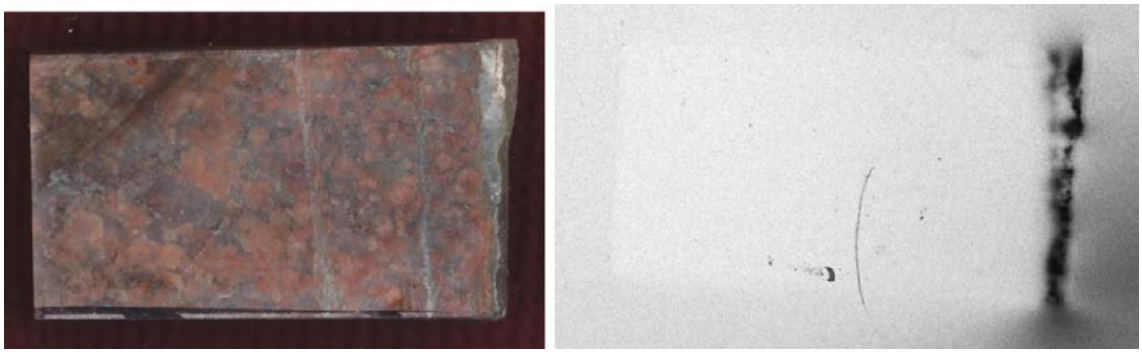

Figure 3-3. *a) Profile of the slice A6, sawn into a cuboid (before cutting into slices). A calcite/chlorite fracture coating is visible to the right in the picture. The size of the rock sample is c. 27×16 mm. Slice 1, which is a part of this rock piece, is uneven and between 1 and 2 mm (mean = 0.97 mm). b) the corresponding autoradiograph showing black layers inside the calcite and at the boundary of calcite/chlorite.*

3.2 Tracer surface distribution on stub and slimhole surfaces

3.2.1 A-cores

The natural fracture surface (the stub), which is sampled by the A-cores, was found to be partially coated with fracture minerals with a thickness variation within 0 to 2 mm (cf. Section 3.1). Due to the heterogeneous distribution of these fracture minerals, analyses were performed in order to find possible indications of the influence of fracture coatings and/or effects of the flow pattern of the circulated tracer-spiked groundwater.

Immediately after drilling, the extracted non-sectioned A- and D-core samples were measured with γ-spectrometry in order to obtain a general view of the tracer distribution on the stub fracture surface, cf. Section 2.4. The activity per drillcore for ^{137}Cs is illustrated in Figure 3-4 where the light green color respresents the lowest activities and the dark green the highest ones. According to this figure, the distribution of activity appears to be random, but somewhat lower at the lower right side of the fracture surface (as viewed *en face*). Compared with the fracture coatings on the surface (cf. Figure 3-1, Section 3.1 and Appendix 3), there are no clear indications that the high/low activities of ^{137}Cs correspond to a specific mineral phase. Comparisons of the distribution of other tracers (e.g ^{22}Na, ^{133}Ba and ^{57}Co) measured at the same time, indicate a random pattern as well.

The measured activities in the laboratory of the first slice of the 10 analyzed A-cores and 8 D-cores have been summarized as well (D-cores are presented in Section 3.2.2). Several of these first slices were irregular, i.e. have varying thicknesses, (cf. A1, Table 3-1) and consequently, the fracture mineral coated A-core slices may, besides fracture minerals, consist of ordinary Ävrö granodiorite as well. However, most of the tracer activity is supposedly restricted to the surface that have been in contact to the tracer-spiked groundwater, and consequently with fracture minerals in fracture mineral coated slices.

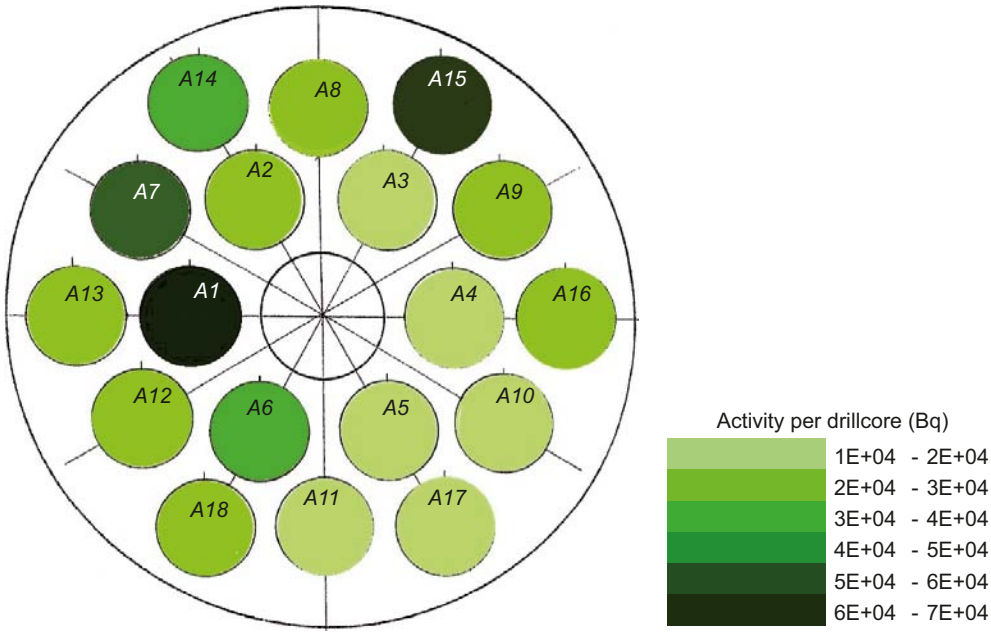

Figure 3-4. *Tracer surface distribution of ^{137}Cs on the stub surface, measured with γ-spectrometry on the whole rock cores. The circle in the centre represents the slim-hole.*

The activity of some tracers in the first rock slice of each A-core is presented in Figure 3-5. The results are presented according to the classification of the rock cores described in Section 3.1, i.e. rock core slices with more than 50% surface covered by fracture minerals belongs to the fracture mineral coated group and slices with less than 50% area covered by intact rock. Alternative divisions of the slices are not discussed in the present report.

As can be seen in the diagrams, the group of fracture mineral coated slices has both higher and lower measured activity compared to the rock slices without fracture minerals. There is neither any clear correlation when studying slices with different fracture coatings. For example; rock core A6, which is the only rock core with significant higher activity of ^{137}Cs than the rock itself (represented by A12, A15 and A16) has been documented with relatively thick fracture coatings (≥ 0.5 mm), consisting of relatively thick calcite that is overlaying chlorite (cf. Figure 3-5). However, the rock cores A9, A10, A17, are also dominated by calcite overlaying a thin chlorite layer without having as high activity as A6. Chlorite is the dominating fracture mineral in both A1 and A8, but as the first chlorite coated slice of A8 is not analyzed for Cs, Na and Ba no comparison between these cores is performed. A possible reason for the poor correlations is that the first slices (Slice1) not only consist of fracture coatings but also to a varying extent of matrix rock which contributes to the measured activity.

Other observations made after the evaluation of the analyses of the first slice in A-cores were;

- ^{133}Ba displays a similar distribution as ^{137}Cs, although the activity is lower.
- Concerning the analyzed tracers presented in Figure 3-5 (i.e. ^{22}Na, ^{133}Ba and ^{137}Cs) the fracture mineral coated slices have activities that are approximately in the same range as the ones for samples without any fracture coating.
- Slices with microfractures and/or small cavities (i.e. A1, A9, A10, A16 and A17; Appendix 3) do not show any general increase of tracer activities. For tracer profiles, see Appendices 4 and 5.
- The total measured activities in slice 1 in the A-cores are in the same range as both D-cores and A-cores without fracture minerals although the spread of the ^{137}Cs activity is larger in the A-cores than in the D-cores.

A further description of the tracer abundance in the epoxy resin is given in Section 3.5 of this report.

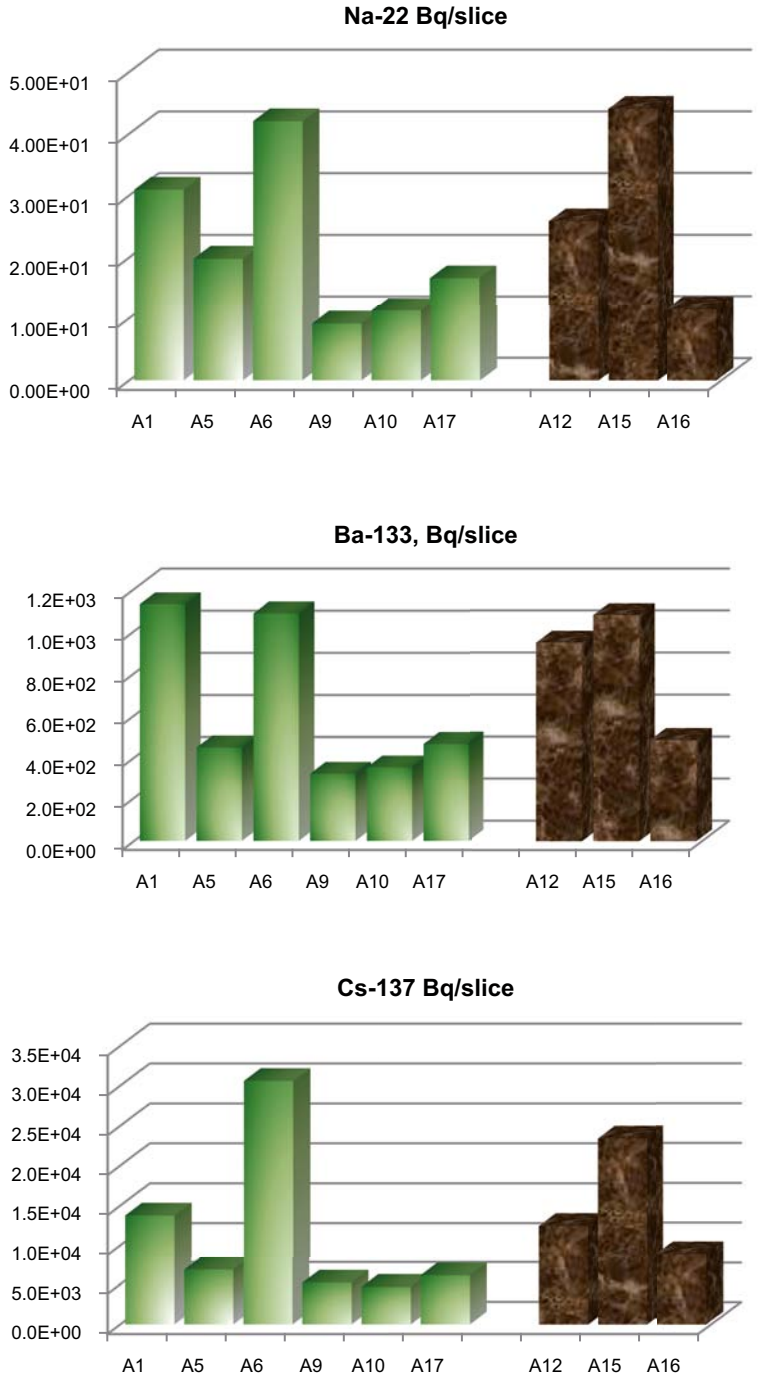

Figure 3-5. *Measured activity of ^{22}Na, ^{133}Ba and ^{137}Cs in the first slice of the rock cores from the stub; i.e. closest to the tracer-spiked water in the experiment. Green bars represent rock core slices with fracture mineralization (>50% covering), brown bars represent rock core slices without fracture minerals (i.e. <50%). Note the different scales. Rock core A8 is excluded as all material from the first slice was not accessible for these analyzes. Also note that the amount of rock material measured differs between the different samples which is suspected to give some misrepresentation of particularly ^{22}Na, see text for discussion*

The representation in Figure 3-5 has been made in order to compare the amount of tracer adsorbed on different parts of stub surface and the results have therefore been normalized as Bq per sample, using the assumption that the surface of the different cores are approximately the same. However, the thickness of these surface samples varies somewhat, this mainly due to the irregularity of the shape. One should therefore acknowledge the limitation in this first slice comparison, especially for non- or weakly sorbing tracers such as ^{22}Na where a significant in-diffusion should have taken place and a misrepresentation could be obtained due to variation of the amount of measured rock material. Nevertheless, for the more strongly sorbing tracers, the results of the measurements show that the first slice normally contains more than 90% of the totally sorbed tracer and the representation is therefore justified.

3.2.2 D-cores

As can be seen in Figure 3-6 and in Section 2.2.2, the D-cores are from the area/volume affected by the small diameter borehole, drilled normal to the cylindrical surface of the 36 mm borehole. The cores are distributed across the mantle surface according to Figure 3-6b. Figure 3-6b shows the distribution of the ^{137}Cs activity in the borehole, when measured on whole cores (i.e. non-sectioned cores). Compared to the A-cores, the distribution is heterogeneous although the ^{137}Cs activities are in a relatively restricted range, i.e. from $1.2 \cdot 10^4$ to $2.8 \cdot 10^4$ Bq.

The measured activities from the laboratory analyzes of slice 1 of the selected D-cores (cf. Section 2.4), are presented in Figure 3-7 and Figure 3-8. As can be seen, the distribution of activities in the core slices does not follow any pronounced pattern except for D14 which has some of the highest activities for several of the tracers. D14 is situated relatively close to the inflow of the tracer-spiked solution. The slices with documented microfractures D1, D6, D8 and D13 show various activities as well. This supports the suggestion that some of the microfractures were newly formed (cf. Section 3.1), i.e. they were not present during the circulation of the tracer-spiked groundwater.

3.2.3 Summary of the tracer distribution studies

The observed heterogeneity in the radionuclide distribution, both with respect to the A-cores and D-cores, can be an effect of several influencing factors such as mineralogical/textural heterogeneity, flow heterogeneity (e.g. incomplete mixing of the tracer labelled groundwater for the first days of experiment due to the rather low circulation flow rate) or the sampling method.

One explanation is that heterogeneity in the mineralogy and/or texture of the different areas sampled has caused the heterogeneous distribution of tracers among the rock samples. Based on the general geological characterisation, one would according to this concept expect stronger heterogeneity in the geologically more heterogeneous fracture core samples (A-samples) and a more homogeneous distribution in the more homogeneous matrix rock samples (D-samples). Such a tendency is indicated by the somewhat larger variability in e.g. the Cs activity in the A-samples compared with the D-samples. The observed co-variation of Na-Ba-Cs levels in the cores presented in Figure 3-5 supports that variations in sorption capacity due to mineralogy and/or texture exist near the fracture surface. The attempts to link the activity of the first slices to the area coverage of fracture mineral coatings gives no support for such a relation for Na-Ba-Cs. Since the coatings are relatively thin, and Na-Ba-Cs has penetrated much deeper than the thickness of the coatings, the cause of variation in sorption capacity may thus also be attributed to the fracture wall rock beyond the thin coatings. It should also be noted that the geological characterisation methods were not primarily attempted to, and do not therefore supply enough detail for quantification of sorption-mineralogy relations on a single slice level.

The variability seen in the D-samples may seem surprisingly high, but the sample size is too small (~16×16×1 mm slice or 24 mm core measurement) for being a fully representative rock type sample relative to the grain size of the Ävrö-granodiorite. Sample variability in mineralogical composition causing variability in the tracer results can consequently not be excluded.

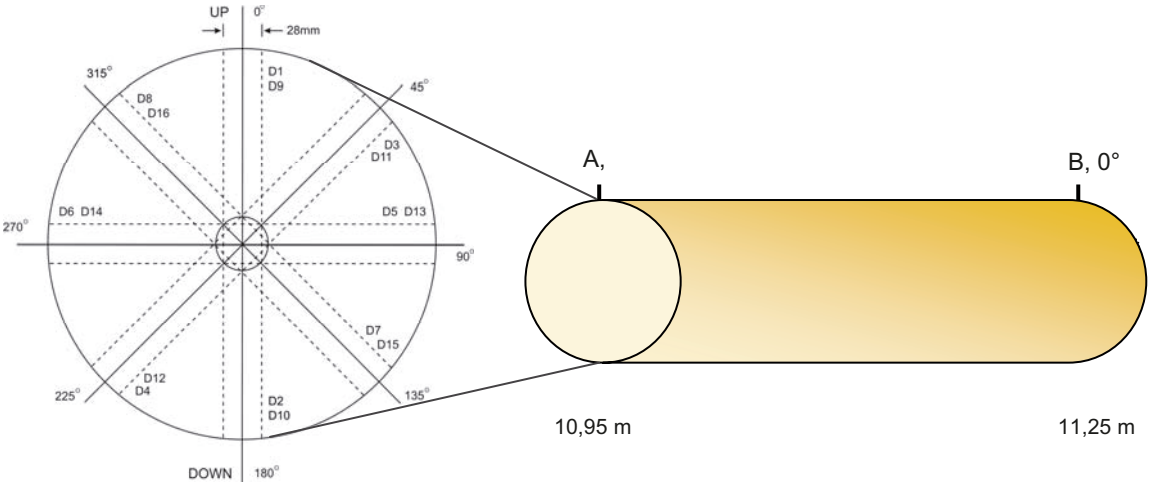

a)

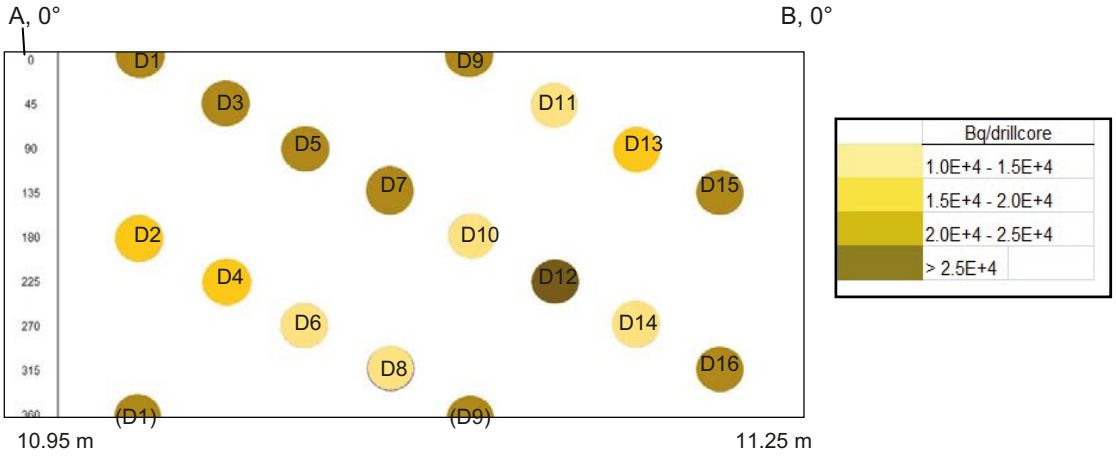

b)

Figure 3-6. *Slimhole test section with an illustration of the various positions of the drill cores. The rock cores are drilled in pairs, with two opposite rock cores at the same distance from the test section boundary (reference A). and; b) Plan view (fold-up A to B,0°) of the surface distribution of ^{137}Cs, measured with γ-spectrometry on whole rock cores, in the test section in the 36 mm borehole. The D1 rock core is to the upper left and D16 to the lower right (bottom part of the figure). The relatively low acitivity in D14 might be due to a remaining epoxy layer during the measurement which in turn gave a longer distance to the detector which would decrease the measurement efficiency.*

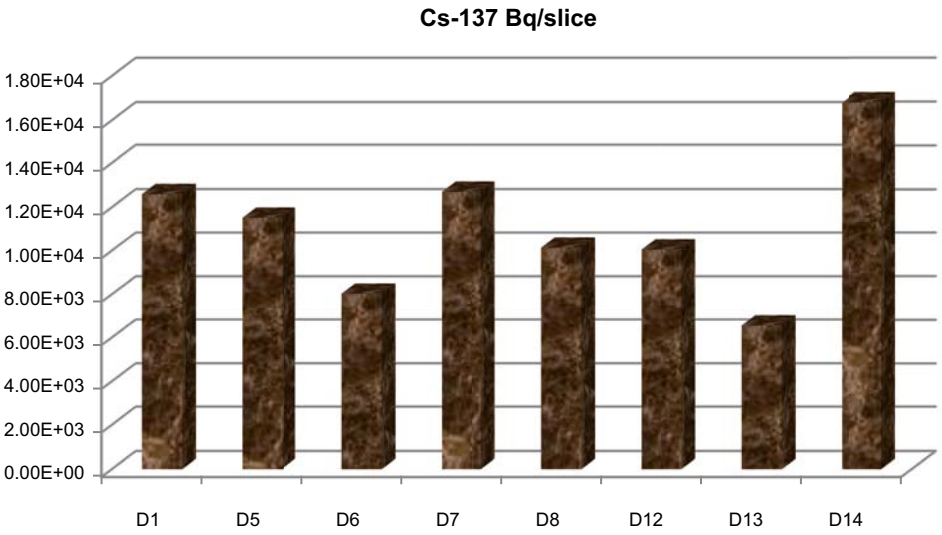

Figure 3-7. *Measured activity of ^{137}Cs in the first slice of the D-cores analyzed on HPGe; i.e. closest to the tracer-spiked groundwater in the slimhole.*

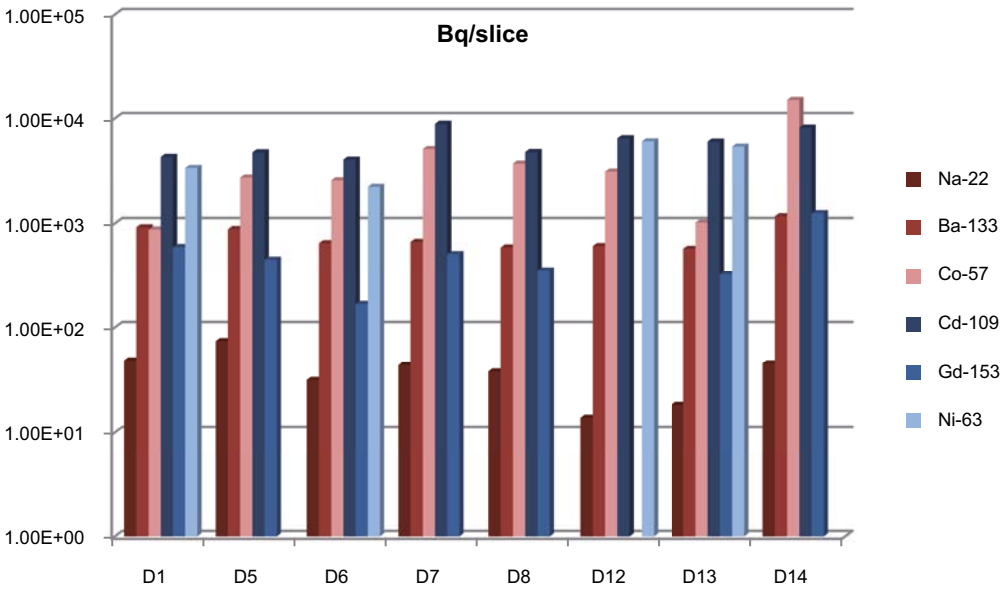

Figure 3-8. *Measured activity of ^{22}Na,^{133}Ba, ^{57}Co, ^{153}Gd, ^{109}Cd and ^{63}Ni in the first slice of the rock core; i.e. closest to the circulated tracer-spiked groundwater in the slimhole (D-cores). For the samples where there is no representation of ^{63}Ni, the tracer was not analyzed for these samples. For the D12 sample, the ^{153}Gd tracer was found to be below 175 Bq.*

A disturbance in the analysis of surface activity is introduced by the removal of the epoxy resin. This led to a removal of large parts of the sorbed activity for the more strongly sorbing tracers with very short penetration depths. The removal of the epoxy resin is likely to have caused some of the observed variability in the remaining core activity for the strongly sorbing tracers. Analyses of selected PEEK/epoxy material (B-core samples) have been performed, and the results are presented in Table 3-4 and discussed in Section 3.5. However, as the results are only qualitative, a summation of A-core and B-samples was not possible.

Another explanation for the heterogeneity in the radionuclide distribution could be heterogeneous flow during the circulation phase of the experiment. A short time period may thus have been required for diffusive mixing before the entire section volume was properly mixed. This could have resulted in tracer adsorption that mainly occurred onto rock surfaces located in or close to these preferential flow paths. This would affect only the few most strongly sorbing tracers that had rapidly decreasing concentrations during the initial circulation phase (hours to a few days). However, one has to acknowledge that such an explanation requires that the sorption is associated with kinetic limitation, i.e. the sorption/desorption kinetics would not be fast enough to establish an equilibrium. Diffusive mixing in the aqueous phase would after some time even out concentration gradients in the aqueous phase so the effect could reasonably not be expected for most of the tracers. The D14 result (highest activity for more strongly sorbing tracers of the D-cores) could be interpreted as such an indication since it was situated close to the flow inlet to the borehole section. However, since this core had its epoxy resin layer intact attached to it, substantially higher activity is expected according to the epoxy resin results presented in Section 3.5. Regarding the surface activity evaluation of the fracture surface (A-samples) it is also affected by the uneven distribution of the surface activity between the first slice and the corresponding epoxy surface. Consequently, flow effects can neither be verified nor excluded for the more strongly sorbing tracers and flow effects are not suspected for other tracers.

The summarized and proposed explanation for the observed heterogeneous spatial distribution of the tracers in this experiment is that a textural and/or mineralogical heterogeneity is influencing the sorption of the tracers in the fracture surface and that sample size and epoxy resin removal contributes to variability in the results.

3.3 Tracer concentrations in core sample profiles

The detailed results of the penetration profile measurements of the different tracers are summarized in the bullets below. Uncertainties and detection limits presented are based on a 2σ confidence level. In Section 3.4, a more elaborate discussion of the results in comparison to the predicted behaviour is presented from a quantitative perspective; this section will only deal with qualitative observations and general conclusions made from visual inspections of the results.

- Regarding the presumed non-sorbing tracer ^{36}Cl, the concentrations in the rock samples are much lower than would be expected from the porosity measurements within the LTDE-SD laboratory program /Widestrand et al. 2010a/. For this reason, a special investigation of these results adressing possible influence of anion exclusion is given in Section 4.6. All discussions and representations of the ^{36}Cl results are therefore referred to that section of the report. However, a full representation of ^{36}Cl data is given in Appendix 4.

- Results from the measurements of γ-emitting tracers with measurable penetration depth in centimeters (i.e. ^{22}Na, ^{133}Ba and ^{137}Cs) are shown as penetration profiles in Figure 3-9 to Figure 3-15 (samples from the stub test section) and in Figure 3-16 to Figure 3-23 (samples from the slim hole section). A general observation for ^{133}Ba and ^{137}Cs is that the penetration profile is very steep in the first 5 mm, then, with increasing depth, a plateau is reached. For the weakly sorbing tracer ^{22}Na, decreasing concentrations are indicated to a depth of approximately 30 mm, thereafter a plateau is indicated for some of the cases. Penetration profiles of γ-emitting tracers in all cores are presented in Appendix 5.

- Autoradiographs were selected to represent two sets of samples for the fracture at the stub test section (Figure 3-15) and two sets from the rock material surrounding the slim hole test section (Figure 3-22). Two of the autoradiograph sets represents sample with somewhat longer penetration depths (A6 and D13) while two sets of samples represents samples with somewhat shorter penetration depths (A12 and D1). The autoradiographs show activity in the center part of the slice and clearly demonstrate that no significant part of the activity is associated with the edges where the sawing occurred. It is therefore obvious that diffusion has taken place during the experiment and therefore any suspicion that the plateaus observed for e.g. ^{137}Cs would be indicative of all tracers observed in inner rock samples should result from contamination during the sample drilling can be discarded.

- Concerning ^{57}Co, a measureable concentration was generally only obtained for the first slice of the penetration profile. However, for three of the D-samples measureable concentrations were found in some of the inner slices and these penetration profiles are shown in Figure 3-23.

- Comparisons of the different tracers with respect to their relative concentrations are given in Figure 3-24 to Figure 3-27.

- Some examples of the results for the measurements of the presumed strongly sorbing γ-emitting tracers (i.e. ^{57}Co, ^{109}Cd, ^{110m}Ag, ^{153}Gd and ^{226}Ra) are given in Figure 3-28 to Figure 3-31, where they are compared to results of e.g. ^{22}Na and ^{137}Cs. For the majority of these strongly sorbing tracers, they have only been possible to quantify in the first slice; for the rest of the samples the activities were below the detection limits (given as 2σ from the counting statistics). However, as can be seen in the figures, several of these tracers have comparatively high detection limits (expressed as relative concentrations in the figures). Hence, the absence of measurable activities in the inner slices of the rock cannot be taken as proof that diffusion to these depths of these strongly sorbing tracers has not occurred. As an example, with the exception of ^{57}Co, a possible decrease in the relative concentrations similar to ^{137}Cs would not have been possible to measure for the majority of the tracers, since they in such a case would be below the detection limits. Analytical data from the mentioned strongly sorbing γ-emitting tracers are reported in Appendix 6.

- Some results of the presumed strongly sorbing tracer ^{63}Ni are included in Figure 3-28, Figure 3-30 and Figure 3-31. A full representation of the ^{63}Ni results is given in Appendix 4. As mentioned, the lack of γ-radiation for the ^{63}Ni radioisotope made it necessary to apply a special elaborate separation method in the measurements which nevertheless resulted in very good measurement conditions with possibilities to measure lower relative concentrations in the rock phase compared to the majority of the γ-emitting tracers. For this reason, measureable concentrations of ^{63}Ni were obtained for all samples studied, i.e. even for some of the inner rock samples where no other presumed sorbing tracers could be quantified. For this reason, the ^{63}Ni is the tracer that offers the best possibilities of studies of diffusion of presumed surface complexation sorbing tracers.

- Some examples of the results for the tracers measured using ICP-SFMS are given in Figure 3-32 to Figure 3-34. The ^{102}Pd tracer is, however, excluded since it was strongly interfered by SrO during the mass spectrometry measurements. As is shown in the figures, no quantification was obtained for ^{99}Tc or ^{236}U in any of the rock phase measurement performed. However, the detection limits shown in the figures (expressed as the relative concentrations) indicates that it is not expected to find any measurable concentrations of these tracers in the rock; this is mainly due to the observation of the non-sorbing behavior in the circulation phase of the experiment for these tracers (probably caused by the absence of low redox potential in the circulation experiment, described in /Widestrand et al. 2010b/). This was explained by the failure of maintaining the reducing conditions in the experiment which caused presence of the oxidized species (Tc(VII) O_4^- and U(VI)O_2^{2+}, respectively) and no formation of the strongly sorbing respective tetravalent species. A concentration corresponding to full saturation of the porosity would correspond to a C/A_{tot} of approximately 10^{-6} g^{-1} which is around 2 orders of magnitudes below the detection limits for ^{99}Tc and ^{236}U. The ^{237}Np tracer was indicated to have a somewhat stronger sorption during the circulation phase and this observation in combination with the better detection limit made it possible to observe a measurable concentration in the first slice of all profiles. However, as for Tc and U, the lack of reducing conditions gave no reduction to the stongly sorbing

tetravalent species and therefore the presumed weakly sorbing $Np(V)O_2^+$ dominated. The C/A_{tot} obtained is in the range of 10^{-4} g^{-1}, indicating a sorption strength somewhere in between the ^{22}Na and ^{137}Cs tracers. The detection limits for all non-detected tracers are presented in Appendix 7.

- Some general qualitative observations regarding the A-cores compared with D-cores and the different tracers can be made:
  - There is no pronounced difference between A-cores and D-cores concerning their penetration profiles for ^{133}Ba and ^{137}Cs. However, concerning ^{22}Na, the penetration depth is indicated to be somewhat larger for some of the A-cores than generally for the D-cores. The A-cores without fracture coating show short to average penetration depth for ^{22}Na.
  - For ^{110m}Ag, the activities in the first slice are below the detection limit in all but one of the D-cores while all of the first slices in the A-cores contain ^{110m}Ag activity. The difference between the A-core and D-cores is even more pronounced when the results of the preliminary γ-spectrometry measurements of the entire cores are considered (Appendix 8); measurements that were performed much earlier than the corresponding slice measurements and therefore not suffering from an advanced decay of the ^{110m}Ag radioisotope. The A-cores indicate activities in the range of 200–1,000 Bq per sample while the vast majority of the D-cores are below 100 Bq per sample.
  - The ^{36}Cl activities in the slices closest to the surface of the cores are approximately 10 times higher in the A cores than in the D cores.
  - The autoradiographs (AR) of the A-cores differ from the AR of the D-cores, where in the latter case the penetration is even and can usually be detected on the three first slices (c. 0–4 mm). In the A-cores, the penetration is often short and might be caused by the fracture mineralizations on the surface and microfractures parallel to the surface.

In Figure 3-24 to Figure 3-27 comparisons are made of the penetration profiles for the different tracers using some selected rock samples. The tracers included in these figures (i.e. ^{22}Na, ^{36}Cl, ^{63}Ni, ^{133}Ba and ^{137}Cs) were the ones for which penetration profiles could be obtained in the vast majority of the cases, i.e. where measurements usually could be obtained in the inner part of the rock samples. On the Y-axis of these figures, the ratio of the measured rock concentration to the measured aqueous concentration at the end of the circulation phase of the *in situ* experiment /Widestrand et al. 2010b/ are given. The dimension of this ratio (m^3/kg) is the same as for the K_d and one can therefore (as is further described in Section 4.4) regard the value obtained for the surface sample as a conservative K_d estimate, i.e. the minimum sorption found in the LTDE-SD experiment. The results shown in the figures are generally qualitatively consistent with what is to be expected from a matrix diffusion concept, i.e.:

- Tracers that were lost in significant amounts during the circulation phase of the experiment (e.g. ^{63}Ni and ^{137}Cs) show a pronounced enrichment in the surface slices, combined with a significant decrease in concentration when moving further into the rock; indicative of a low apparent diffusion rate.
- Tracers for which no sorption could be verified during the circulation phase of the experiment (e.g. ^{22}Na and ^{36}Cl) are present at low concentrations in the surface slices; a concentration that does not decrease very much when moving further into the matrix. This is indicative of a comparatively high apparent diffusion, as should be expected from a non-sorbing tracer.

These figures therefore provide a good qualitative support that a diffusion process has taken place during the *in situ* experiment and that this process is in good qualitative agreement with a matrix diffusion sorption model. Nevertheless, as further investigated in the modelling section of this report Chapter 4, the agreement to predicted diffusion curves using a single rate diffusion model is generally poor. The main reason for this is that a small part of the tracers migrates much further in to the matrix than what a homogenous diffusion model can predict which raises some doubt of the applicability of that model.

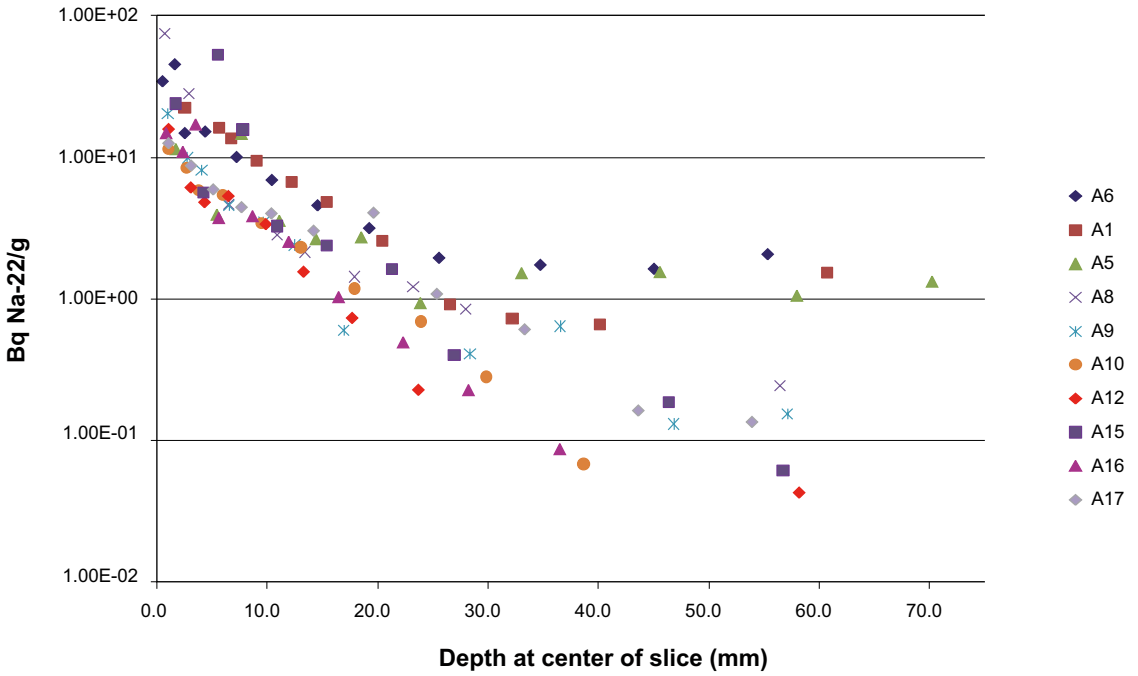

Figure 3-9. *^{22}Na activity versus penetration depth in A-cores, 0–75 mm. No representation of the measurements where the tracer concentration was found to be below the detection limit has been included in the figure. Error bars and detection limits are displayed in Appendix 5.*

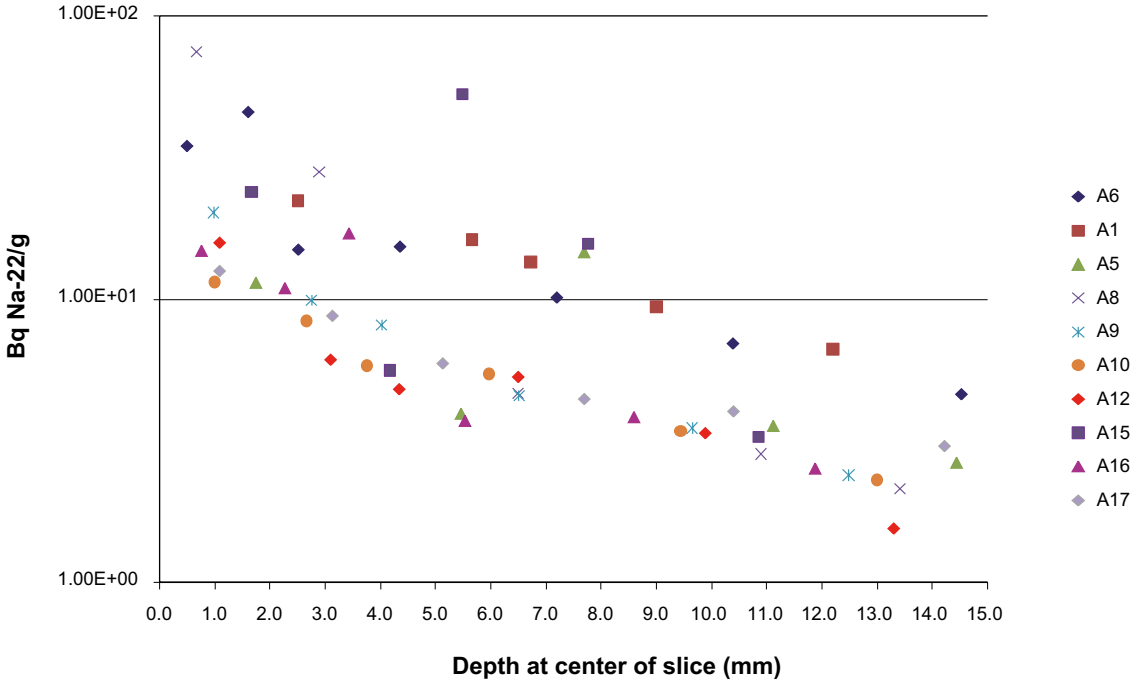

Figure 3-10. *^{22}Na activity versus penetration depth in A-cores, 0–15 mm, same data as for Figure 3-9 except that the short distance penetration (<15 mm) has been expanded. No representation of the measurements where the tracer concentration was found to be below the detection limit has been included in the figure. Error bars and detection limits are displayed in Appendix 5.*

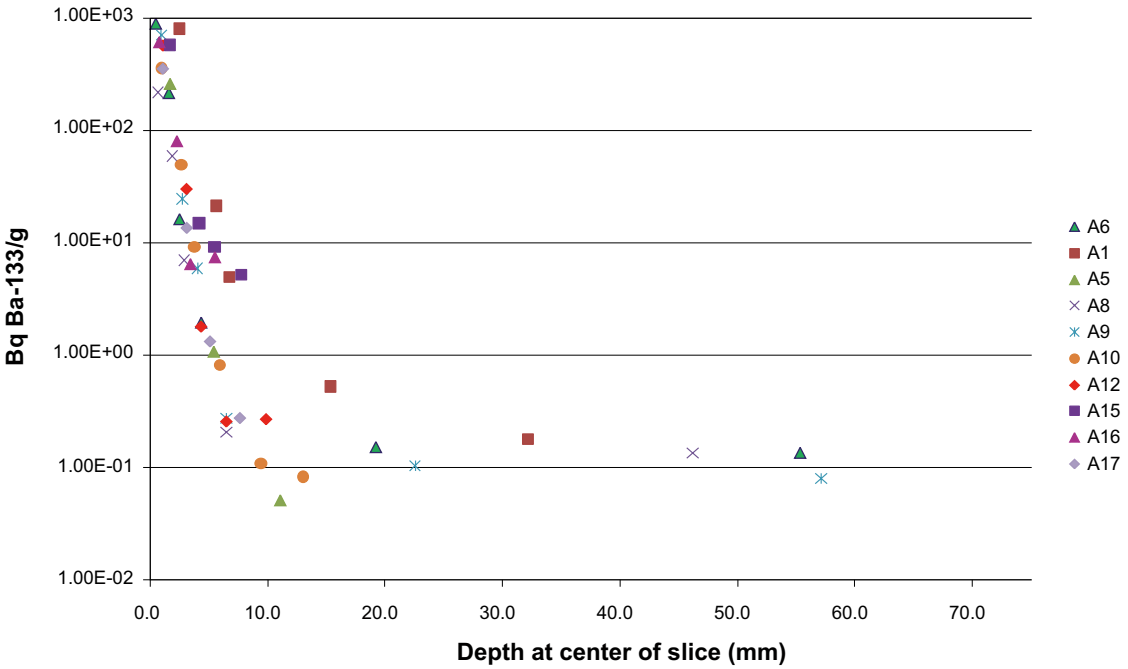

Figure 3-11. *^{133}Ba activity versus penetration depth in A-cores, 0–75 mm. No representation of the measurements where the tracer concentration was found to be below the detection limit has been included in the figure. Error bars and detection limits are displayed in Appendix 5.*

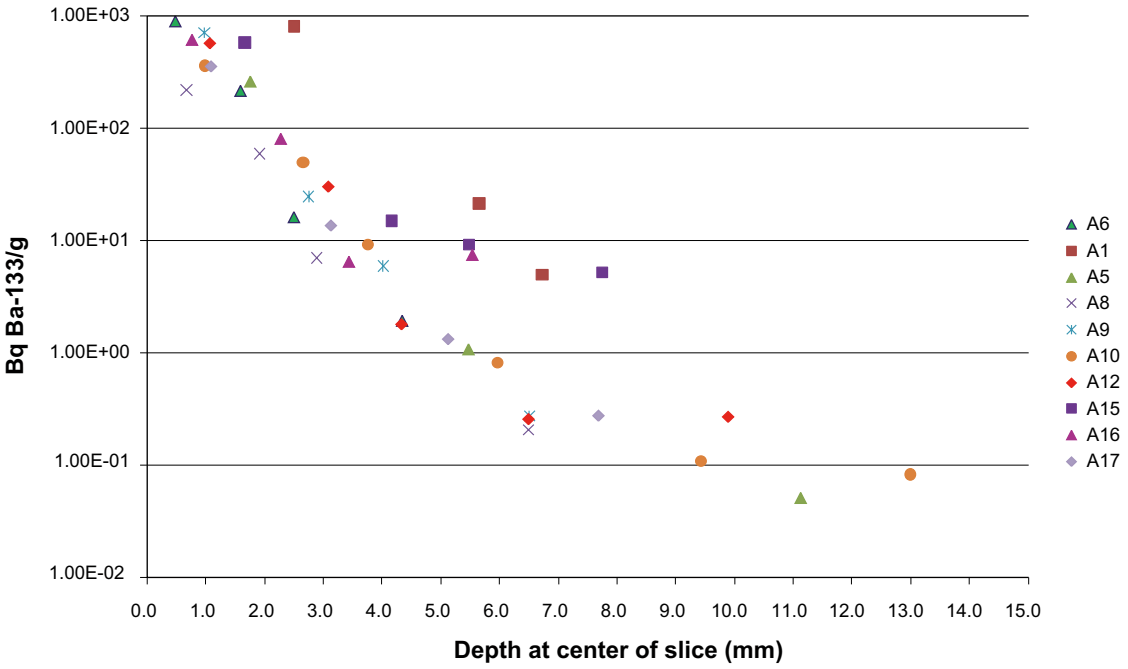

Figure 3-12. *^{133}Ba activity versus penetration depth in A-cores, 0–15 mm, same data as for Figure 3-11 except that the short distance penetration (<15 mm) has been expanded. No representation of the measurements where the tracer concentration was found to be below the detection limit has been included in the figure. Error bars and detection limits are displayed in Appendix 5.*

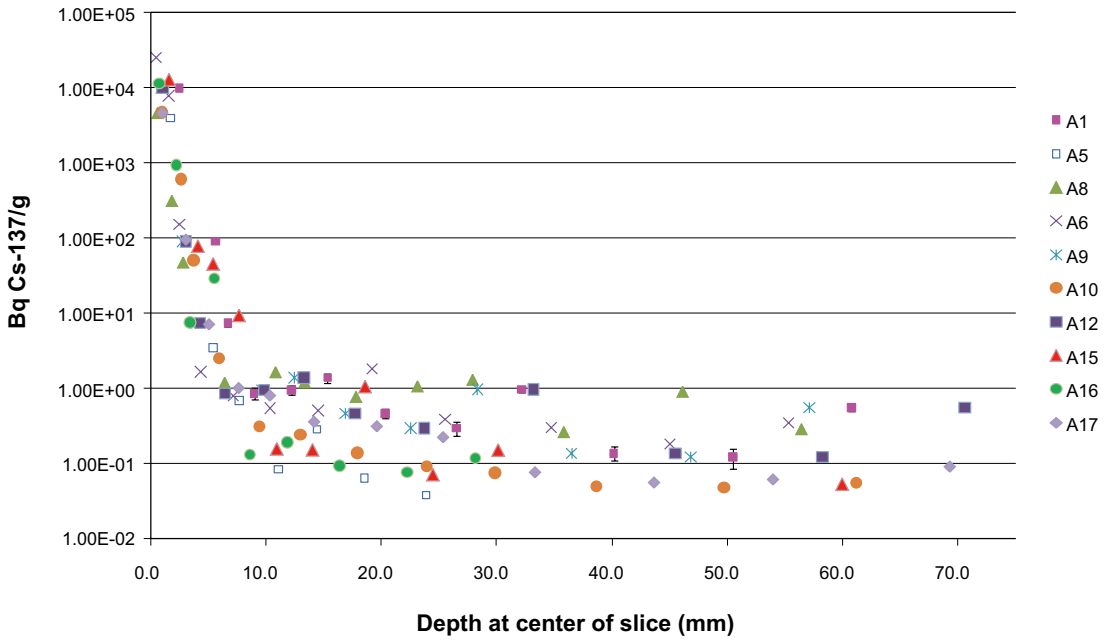

Figure 3-13. *^{137}Cs activity versus penetration depth in A-cores, 0–75 mm. No representation of the measurements where the tracer concentration was found to be below the detection limit has been included in the figure. Error bars and detection limits are displayed in Appendix 5.*

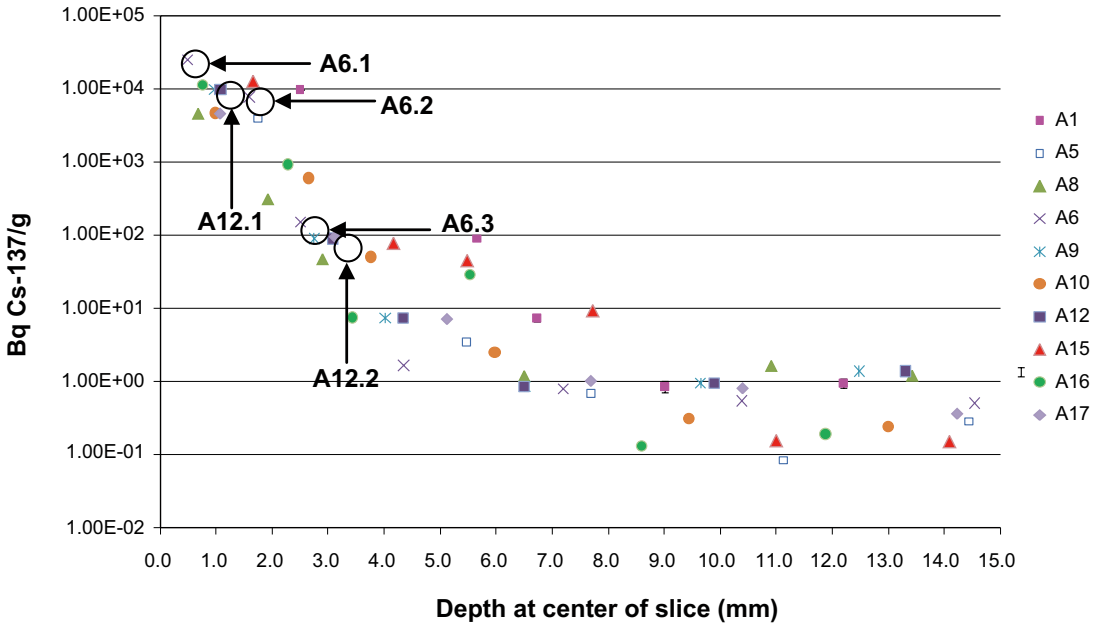

Figure 3-14. *^{137}Cs activity versus penetration depth in A-cores, 0–15 mm, same data as for Figure 3-13 except that the short distance penetration (<15 mm) has been expanded. No representation of the measurements where the tracer concentration was found to be below the detection limit has been included in the figure. Error bars and detection limits are displayed in Appendix 5. The measurements corresponding to the autoradiographs shown in Figure 3-15 are marked in the figure.*

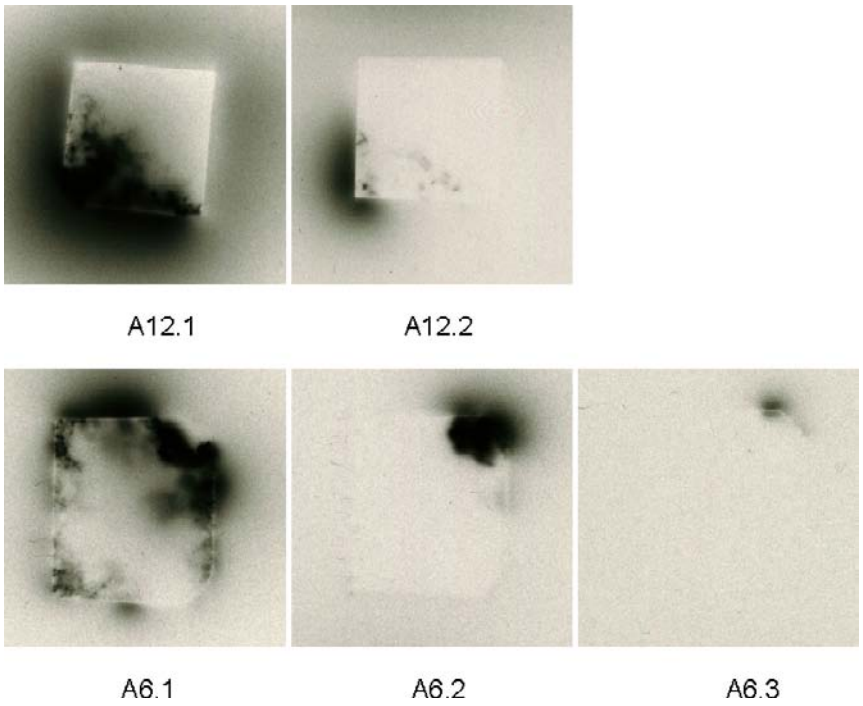

Figure 3-15. *Autoradiography analyses of the selected A-core samples. The size of the sample is 16×16 mm and the corresponding measurements of ^{137}Cs in the same samples are shown in Figure 3-14.*

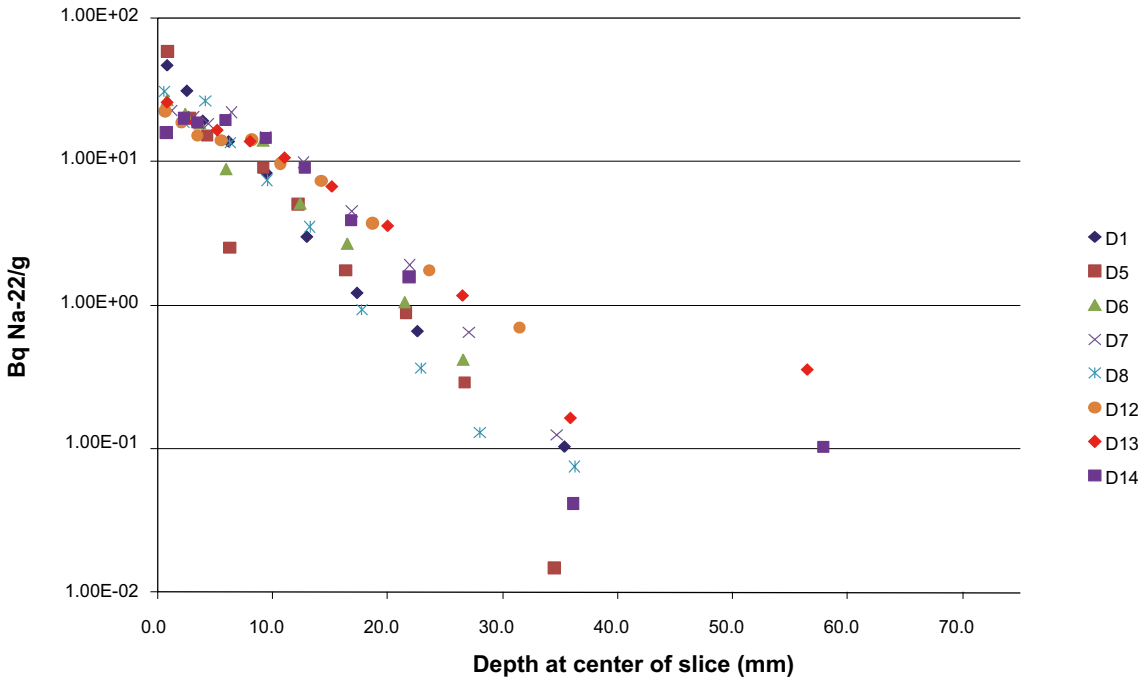

Figure 3-16. *^{22}Na activity versus penetration depth in D-cores, 0–75 mm. No representation of the measurements where the tracer concentration was found to be below the detection limit has been included in the figure. Error bars and detection limits are displayed in Appendix 5.*

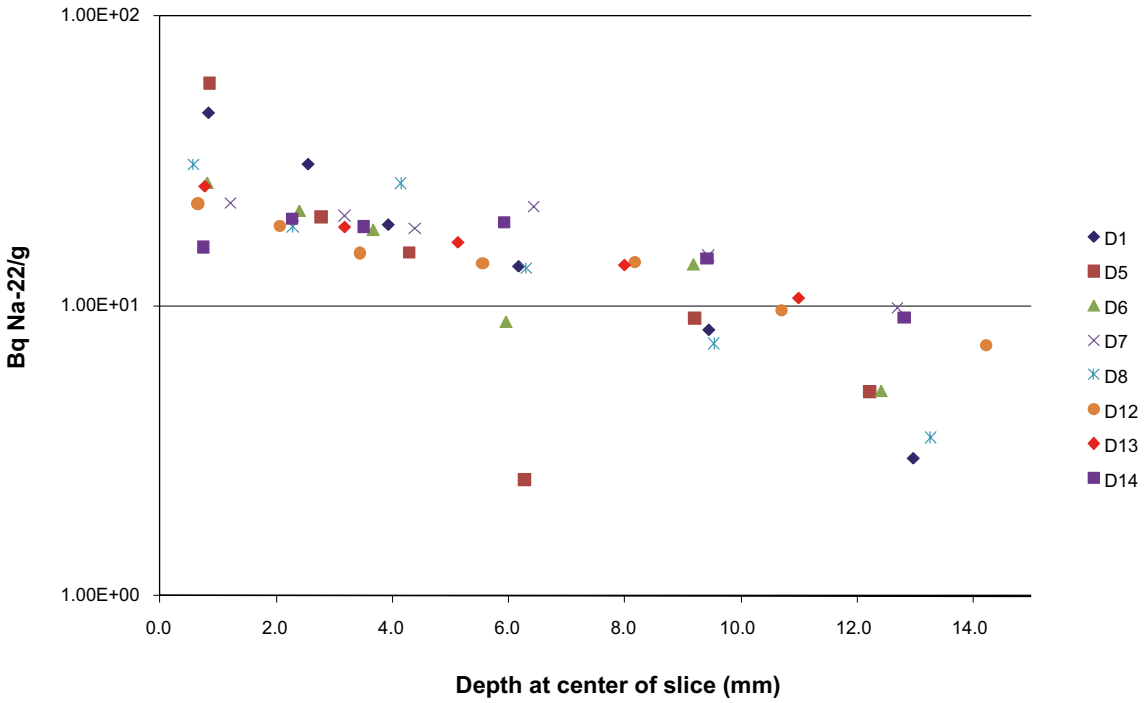

Figure 3-17. *^{22}Na activity versus penetration depth in D-cores, 0–15 mm, same data as for Figure 3-16 except that the short distance penetration (<15 mm) has been expanded. No representation of the measurements where the tracer concentration was found to be below the detection limit has been included in the figure. Error bars and detection limits are displayed in Appendix 5.*

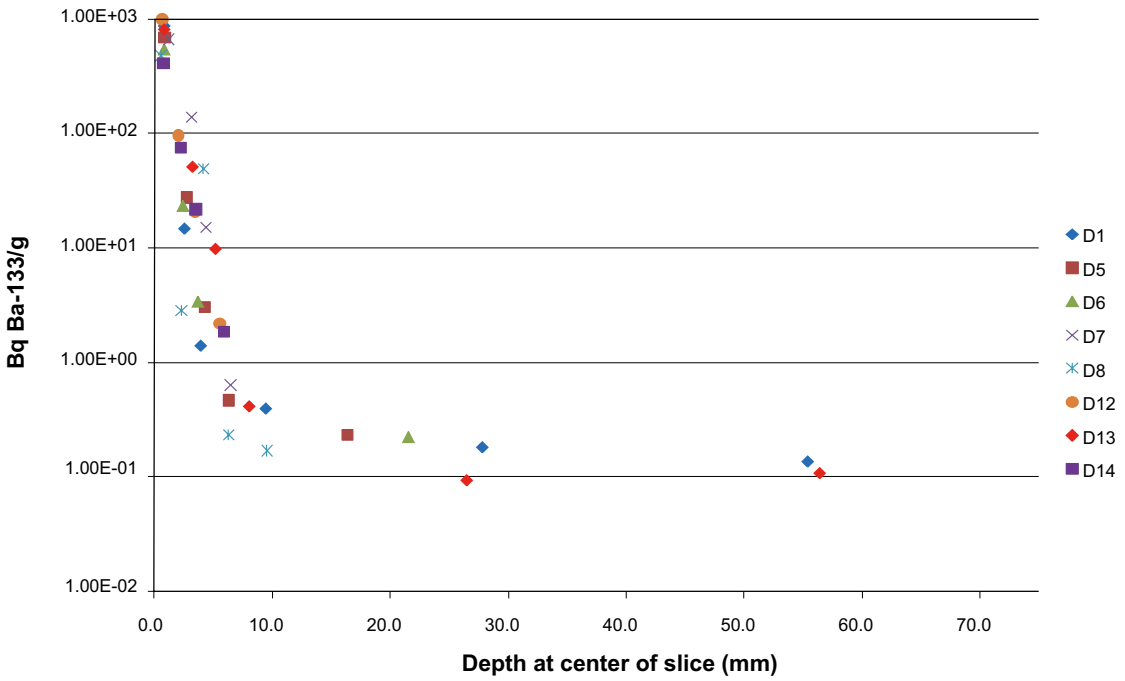

Figure 3-18. *^{133}Ba activity versus penetration depth in D-cores, 0–75 mm. No representation of the measurements where the tracer concentration was found to be below the detection limit has been included in the figure. Error bars and detection limits are displayed in Appendix 5.*

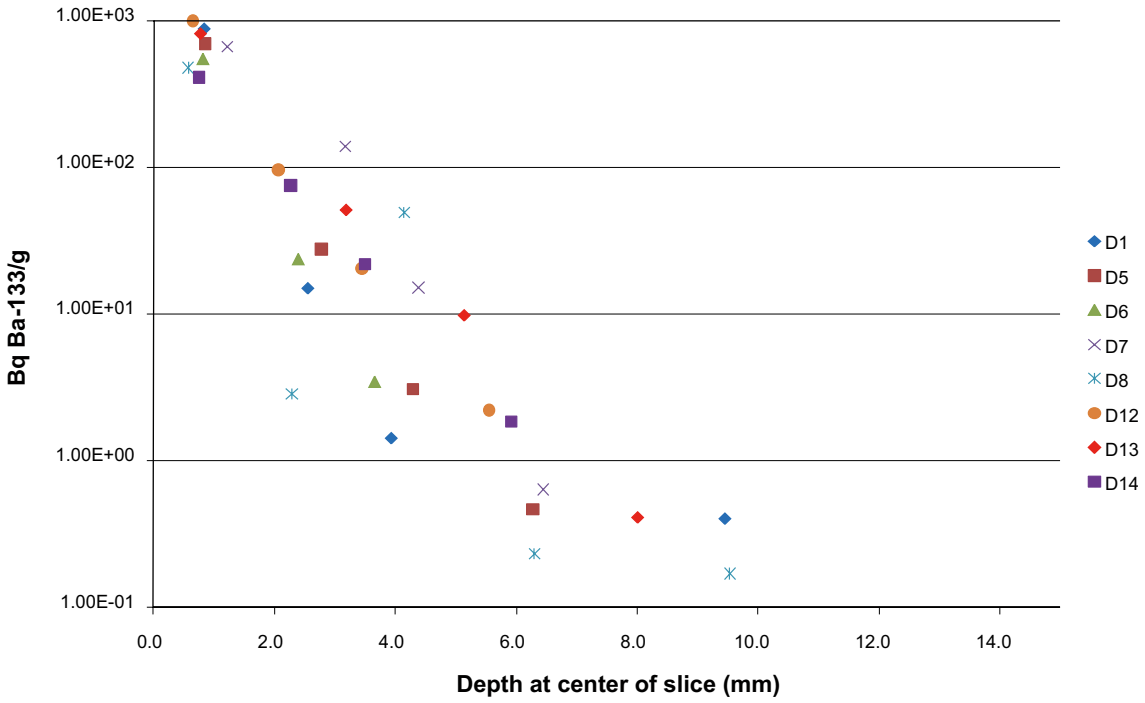

Figure 3-19. *^{133}Ba activity versus penetration depth in D-cores, 0–15 mm, same data as for Figure 3-18 except that the short distance penetration (<15 mm) has been expanded. No representation of the measurements where the tracer concentration was found to be below the detection limit has been included in the figure. Error bars and detection limits are displayed in Appendix 5.*

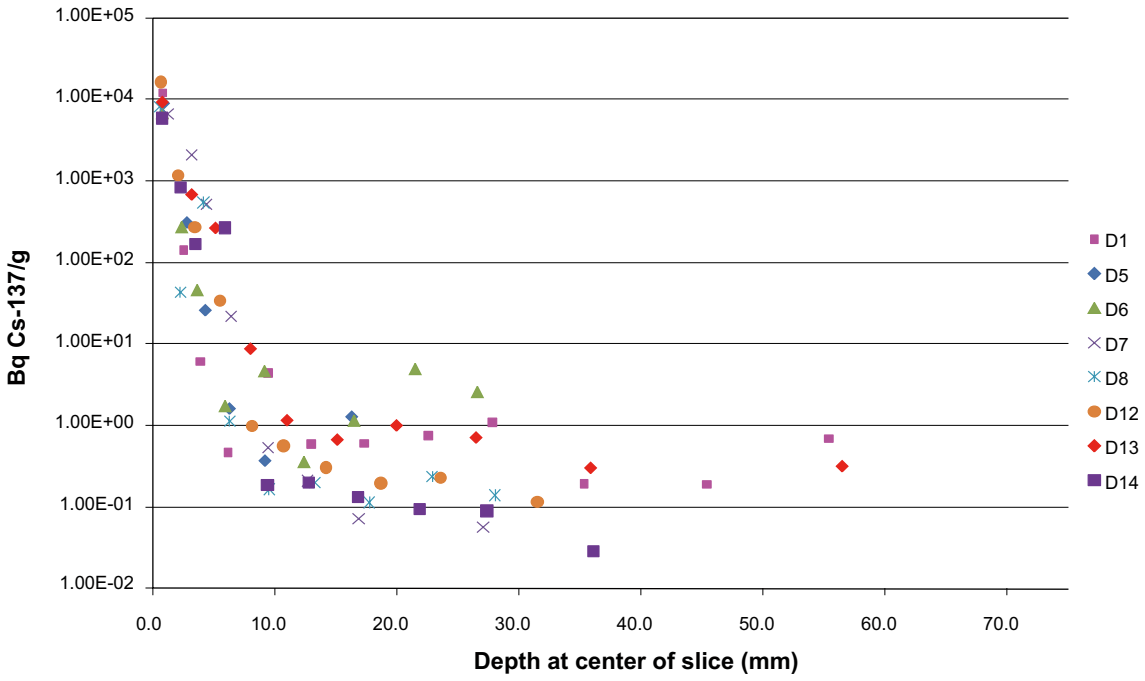

Figure 3-20. *^{137}Cs activity versus penetration depth in D-cores, 0–75 mm. No representation of the measurements where the tracer concentration was found to be below the detection limit has been included in the figure. Error bars and detection limits are displayed in Appendix 5.*

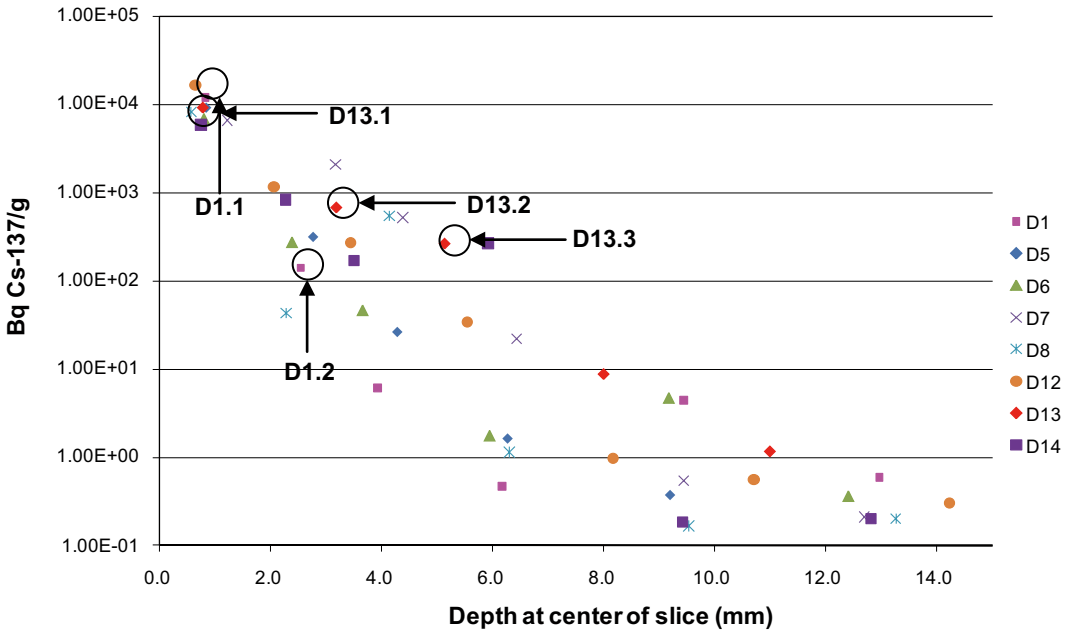

Figure 3-21. *^{137}Cs activity versus penetration depth in D-cores, 0–15 mm, same data as for Figure 3-20 except that the short distance penetration (<15 mm) has been expanded. No representation of the measurements where the tracer concentration was found to be below the detection limit has been included in the figure. Error bars and detection limits are displayed in Appendix 5. The measurements corresponding to the autoradiographs in Figure 3-22 are marked in the figure.*

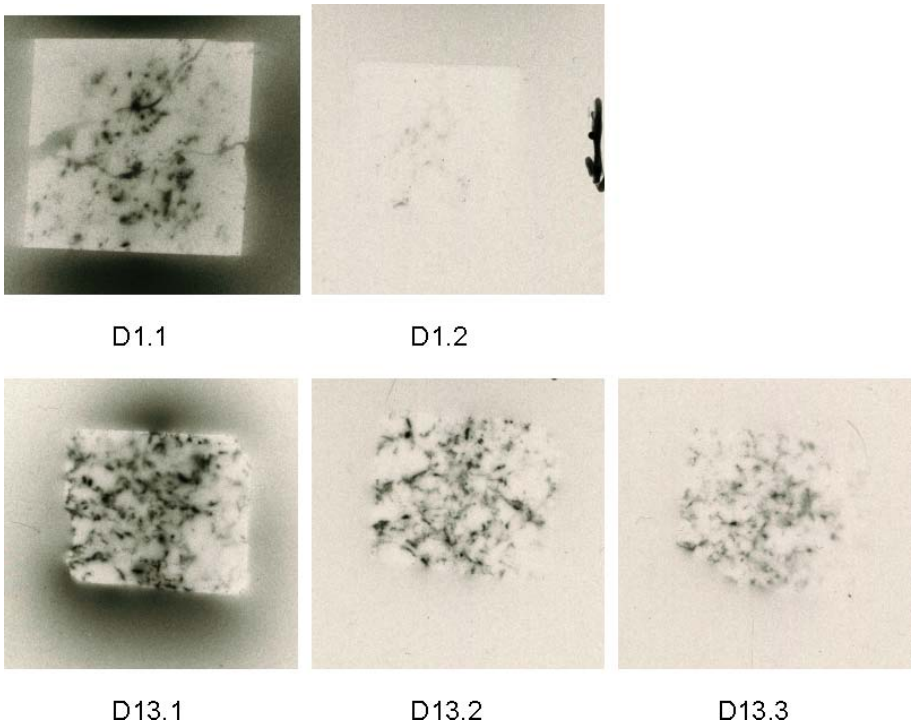

Figure 3-22. *Autoradiography analyses of the selected D-core samples. The size of the samples is 16×16 mm and the corresponding measurements of ^{137}Cs in the same samples are shown in Figure 3-21.*

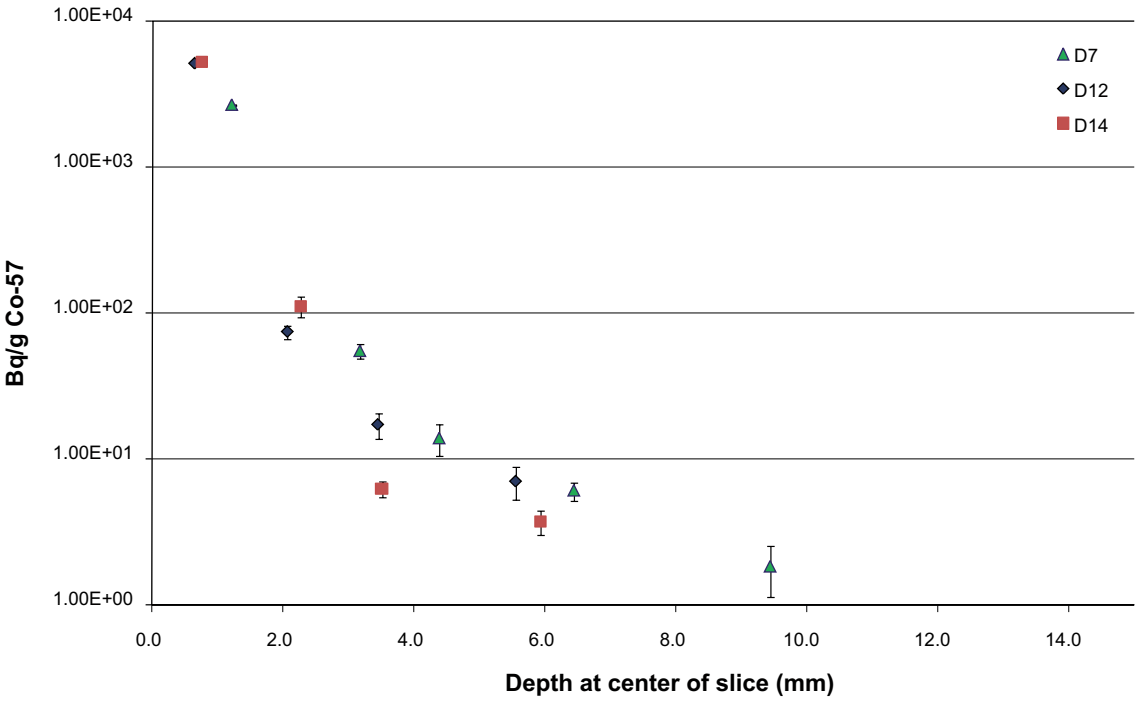

Figure 3-23. *Penetration profiles for ^{57}Co activity in three D-core samples, 0–15 mm. No representation of the measurements where the tracer concentration was found to be below the detection limit has been included in the figure. The detection limits for ^{57}Co are c. 0.3–4 Bq/g.*

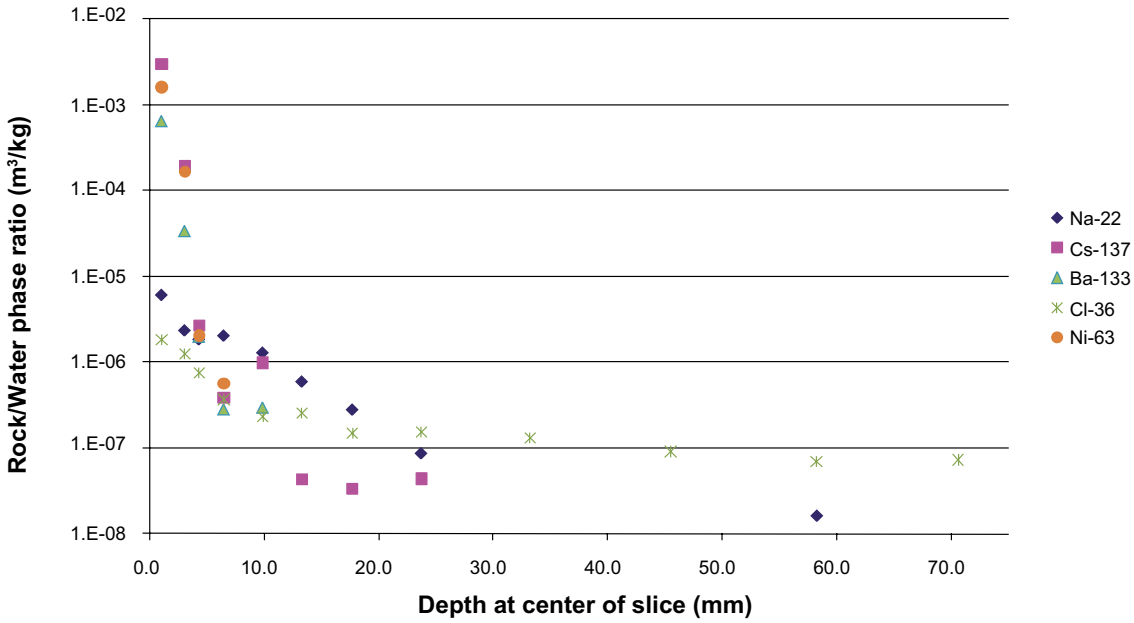

Figure 3-24. *Pentration profiles for core sample A12; an example of a core where a generally short tracer penetration has been measured. The Y-axis refers to the measured tracer concentration in that part of the rock phase (Bq/kg) divided by the tracer concentration in the water phase (Bq/m³) at the time of termination of the experiment. Values where the tracer concentration in the rock were found to be below the detection limit have been omitted in the figure. Error bars and detection limits are displayed in Appendix 5.*

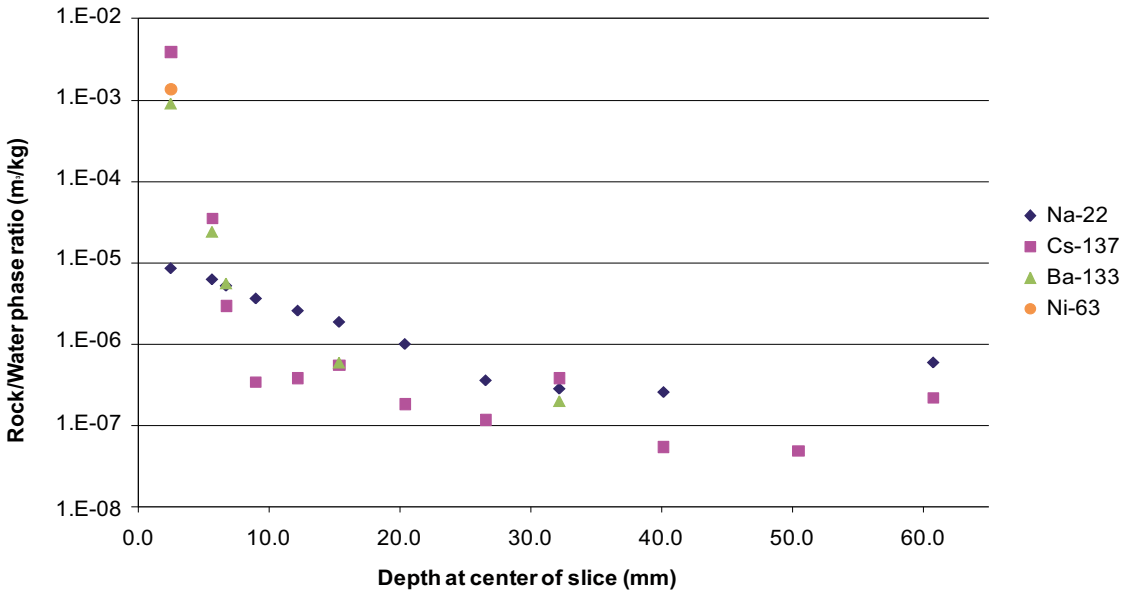

Figure 3-25. *Pentration profiles for core sample A1, an example of a core where a deep tracer penetration has been measured. The Y-axis refers to the measured tracer concentration in that part of the rock phase (Bq/kg) divided by the tracer concentration in the water phase (Bq/m³) at the time of termination of the experiment. Values where the tracer concentration in the rock were found to be below the detection limit have been omitted in the figure. Error bars and detection limits are displayed in Appendix 5.*

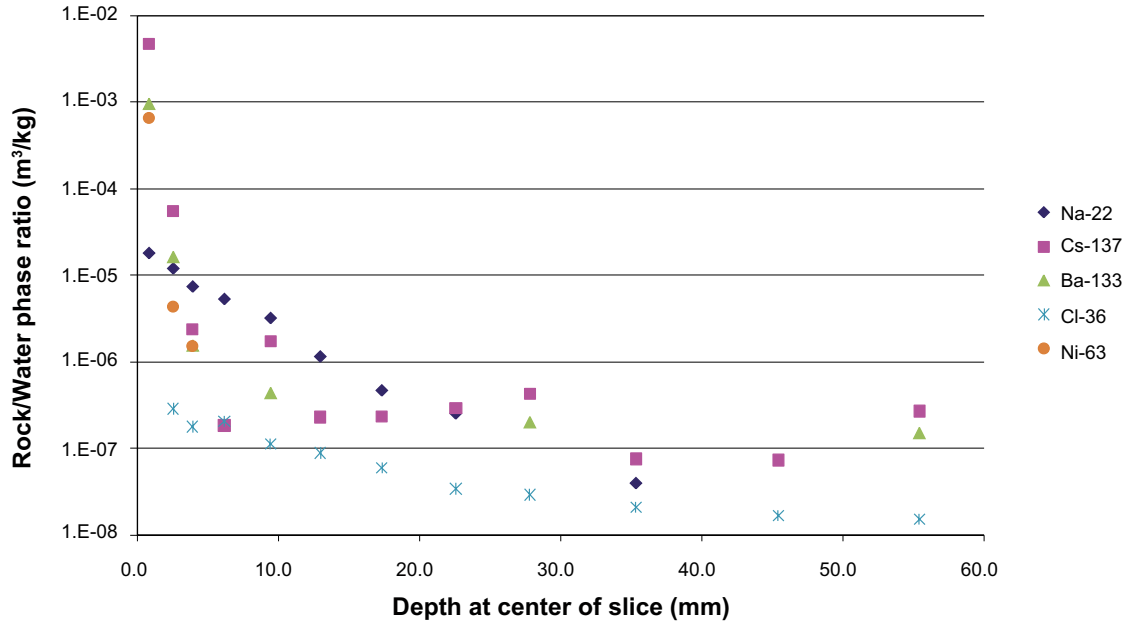

Figure 3-26. *Pentration profiles for core sample D1, an example of a core where a short tracer penetration has been measured. The Y-axis refers to the measured tracer concentration in that part of the rock phase (Bq/kg) divided by the tracer concentration in the water phase (Bq/m³) at the time of termination of the experiment. Values where the tracer concentration in the rock were found to be below the detection limit have been omitted in the figure. Error bars and detection limits are displayed in Appendix 5.*

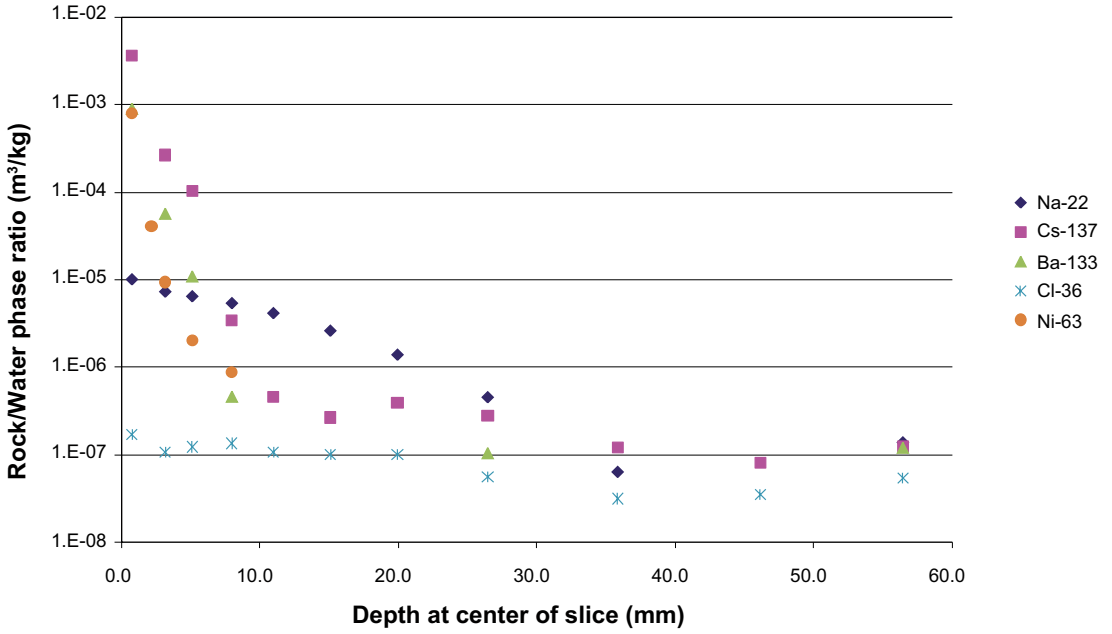

Figure 3-27. *Pentration profiles for core sample D13, an example of a core where a deep tracer penetration has been measured. The Y-axis refers to the measured tracer concentration in that part of the rock phase (Bq/kg) divided by the tracer concentration in the water phase (Bq/m³) at the time of termination of the experiment. Values where the tracer concentration in the rock were found to be below the detection limit have been omitted in the figure.Error bars and detection limits are displayed in Appendix 5.*

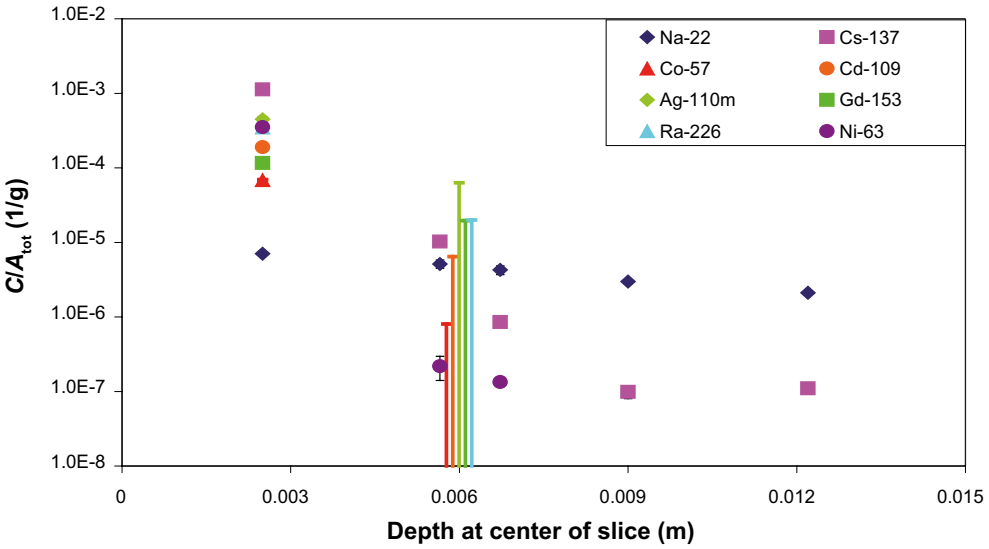

Figure 3-28. *Penetration profiles of different strongly sorbing tracers in drill core A1, given in comparison with the corresponding penetration profiles of ^{22}Na and ^{137}Cs. The detection limits (2σ) for the tracers in the second sample (at 6 mm) are illustrated as error bars with its upper end reaching the value of the detection limit. The relative concentration, C/A_{tot}, refers to the concentration of tracer in the rock sample (Bq/g) divided by the total amount of tracer (Bq) added in the experiment.*

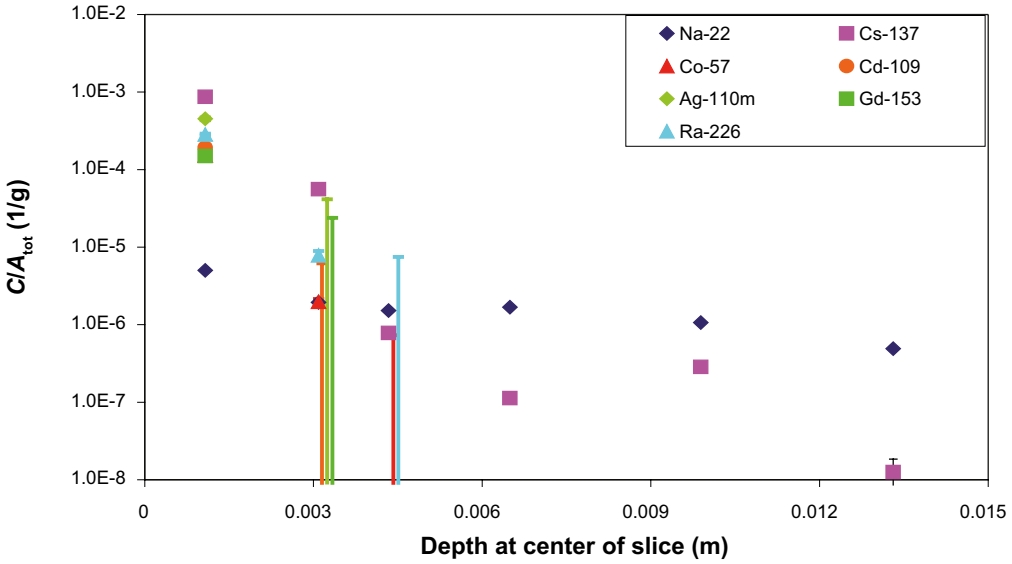

Figure 3-29. *Penetration profiles of different strongly sorbing tracers in drill core A12, given in comparison with the corresponding penetration profiles of ^{22}Na and ^{137}Cs. The detection limits (2σ) for the tracers in the different samples (^{109}Cd, ^{110m}Ag and ^{153}Gd at 3 mm, ^{57}Co and ^{226}Ra at 4.5 mm) are illustrated as error bars with its upper end reaching the value of the detection limit. The relative concentration, C/A_{tot}, refers to the concentration of tracer in the rock sample (Bq/g) divided by the total amount of tracer (Bq) added in the experiment.*

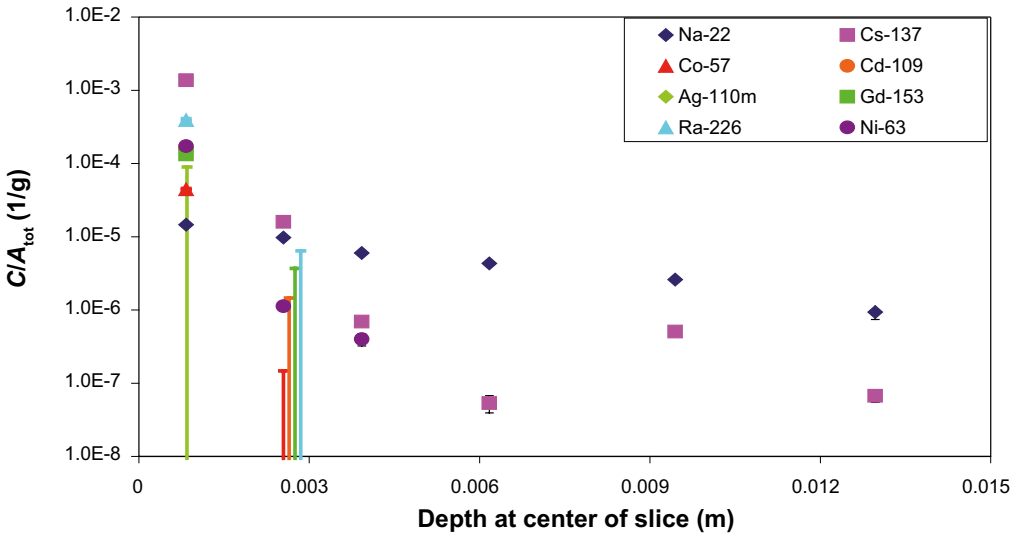

Figure 3-30. *Penetration profiles of different strongly sorbing tracers in drill core D1, given in comparison with the corresponding penetration profiles of ^{22}Na and ^{137}Cs. The detection limits (2σ) for the tracers in the different samples (^{57}Co, ^{109}Cd, ^{153}Gd and ^{226}Ra at 3 mm, ^{110m}Ag at 1 mm) are illustrated as error bars with its upper end reaching the value of the detection limit. The relative concentration, C/A_{tot}, refers to the concentration of tracer in the rock sample (Bq/g) divided by the total amount of tracer (Bq) added in the experiment.*

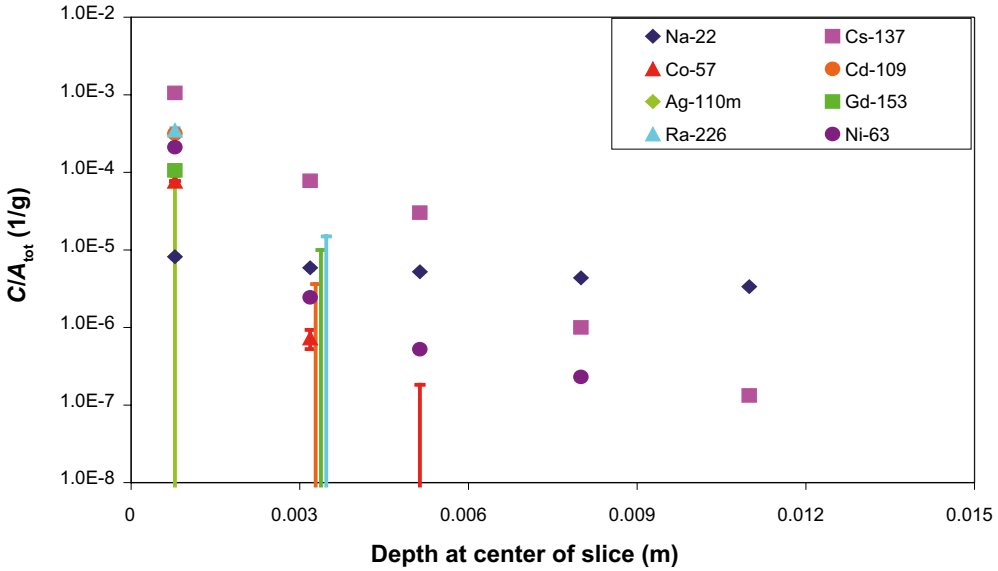

Figure 3-31. *Penetration profiles of different strongly sorbing tracers in drill core D13, given in comparison with the corresponding penetration profiles of ^{22}Na and ^{137}Cs. The detection limits (2σ) for the tracers in the different samples (^{109}Cd, ^{153}Gd and ^{226}Ra at 3 mm, ^{110m}Ag at 1 mm, ^{57}Co at 5 mm) are illustrated as error bars with its upper end reaching the value of the detection limit. The relative concentration, C/A_{tot}, refers to the concentration of tracer in the rock sample (Bq/g) divided by the total amount of tracer (Bq) added in the experiment.*

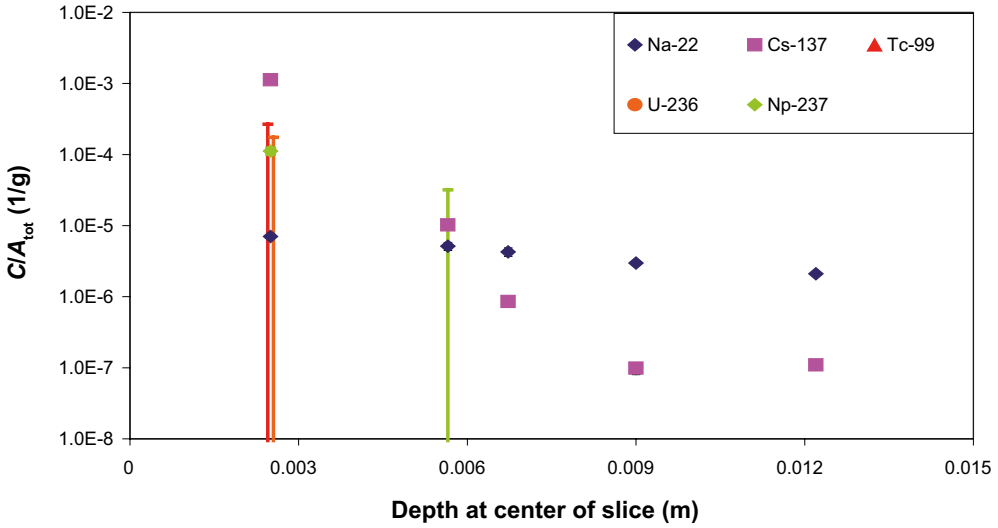

Figure 3-32. *Penetration profiles of different redox sensitive tracers in drill core A1, given in comparison with the corresponding penetration profiles of ^{22}Na and ^{137}Cs. The detection limits (2σ) for the tracers in the different sample (^{99}Tc and ^{236}U at 2.5 mm, ^{237}Np at 6 mm) are illustrated as error bars with its upper end reaching the value of the detection limit. The relative concentration, C/A_{tot}, refers to the concentration of tracer in the rock sample (Bq/g) divided by the total amount of tracer (Bq) added in the experiment.*

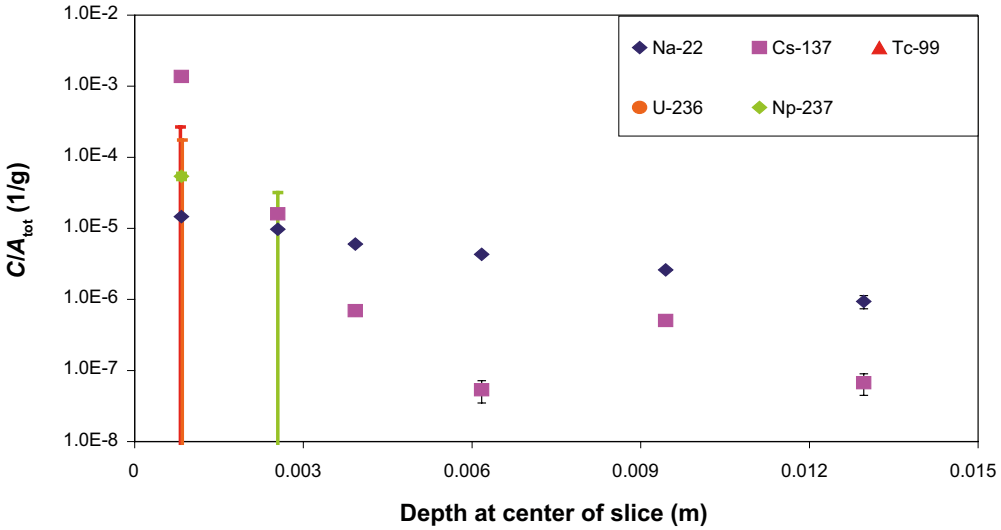

Figure 3-33. *Penetration profiles of different redox sensitive tracers in drill core D1, given in comparison with the corresponding penetration profiles of ^{22}Na and ^{137}Cs. The detection limits (2σ) for the tracers in the different sample (^{99}Tc and ^{236}U at 1 mm, ^{237}Np at 2.5 mm) are illustrated as error bars with its upper end reaching the value of the detection limit. The relative concentration, C/A_{tot}, refers to the concentration of tracer in the rock sample (Bq/g) divided by the total amount of tracer (Bq) added in the experiment.*

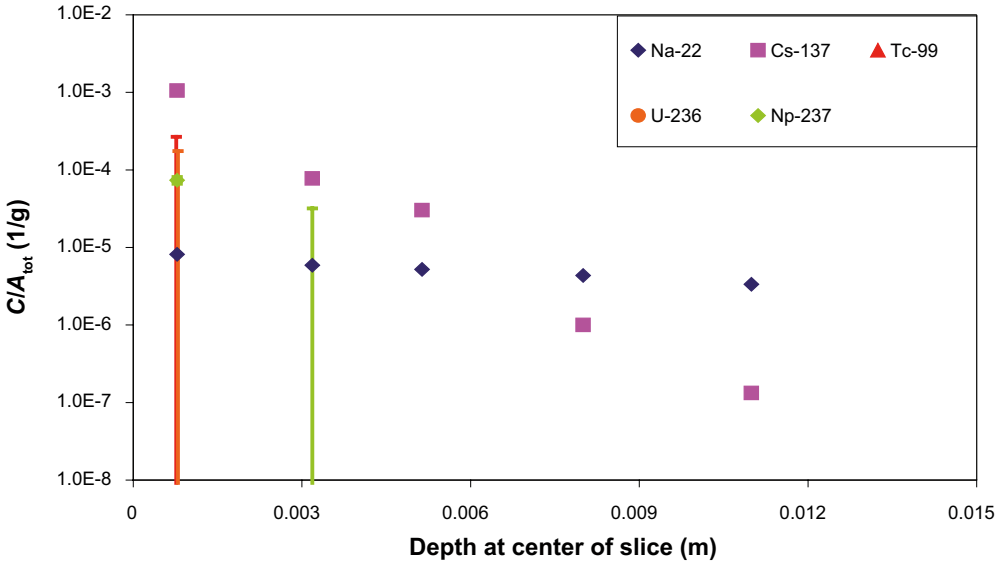

Figure 3-34. *Penetration profiles of different redox sensitive tracers in drill core D13, given in comparison with the corresponding penetration profiles of ^{22}Na and ^{137}Cs. The detection limits (2σ) for the tracers in the different sample (^{99}Tc and ^{236}U at 1 mm, ^{237}Np at 3 mm) are illustrated as error bars with its upper end reaching the value of the detection limit. The relative concentration, C/A_{tot}, refers to the concentration of tracer in the rock sample (Bq/g) divided by the total amount of tracer (Bq) added in the experiment.*

3.4 Interpretation of the results using the mineral/ microfracture analysis

Attempts have been made to match the analytical results with analysis of the fracture minerals (A-samples from the stub surface) and analysis of the microfractures (A-samples from the stub surface and D-samples from the small hole; see Table 3-3 and Appendix 3).

The results can be summarized as:

- In the A12 core (0–15 mm), a sample characterised by generally short tracer penetration depth, no microfractures in the diffusion direction could be found (which does not exclude that there might be some unnoticed microfractures). Fracture coatings were present only on parts the stub surface (<30%). The result of short penetration depth (Figure 3-24) is fairly coherent with the autoradiography results, cf. Figure 3-15. (In core A12, epoxy filaments have been present on some of the slices.)
- In core A1 (0–17 mm), with a generally deeper tracer penetration depth (Figure 3-25), there were mineral aggregates with cavities and 50% of the fracture surface was covered with fracture coatings. The autoradiography feature is uneven due to the asymmetric slice.
- In core D1 (0–15 mm), with a generally short tracer penetration depth (Figure 3-26), there were some microfractures in the first three slices (0–5 mm) and some in slice six. Also the autoradiography results showed short penetration depth (see Figure 3-22).
- In core D13 (0–12 mm) with a generally deeper tracer penetration (Figure 3-27), there were both open and sealed microfractures fairly deep into the core sample. Also in this case, the tracer penetration depth is quite consistent with the autoradiography penetration depth. For the other D core samples with microfractures, several of the fractures are expected to originate from drilling or sawing of the cores. The core samples have mainly shown intermediate penetration depths of most tracers, and the transport is considered as a result of matrix diffusion.
- From the results of the autoradiography, there is an indication that the radionuclides have diffused deeper in most of the D samples compared to the A samples. However, none of the radionuclide specific measurements of the individual tracers show any significant difference between the group of A core samples and the group of D core samples concerning penetration depths.

It should be noted that sample irregularities are likely to be a source of irregular shape of the measured penetration profiles. For some of the tracer penetration profiles there are irregularities from the smooth penetration curve for one or more tracer. As an example, in core A16 (cf. Appendix 4 and Appendix 5), the ^{22}Na and ^{36}Cl concentrations increase at approximately 3 mm from the surface. For ^{133}Ba and ^{137}Cs there are concentration increases at approximately 4 mm. The geological characterisation performed for this particular core sample shows a single sealed microfracture at c. 3 mm from the surface and at 4 mm there is an additional sealed microfracture present. Although sealed, these microfractures can be suspected to constitute comparatively fast pathways for tracer diffusion and therefore be a source of the increased heterogeneity observed. Unfortunately, the levels of radioactivity in these samples are far below what can be measured with autoradiography results and no such visualizations can be obtained for this sample.

The innermost analyzed sample (c. 55–65 mm) in some of the core profiles (A1, A6, A15 and D13, see Appendix 5) shows a concentration increase (for both ^{22}Na and ^{137}Cs) compared with previous samples in the profiles. This is also the case for ^{137}Cs in core A9 and D1. Furthermore, an increase at 55–65 mm of ^{36}Cl was also present in A12, D13 and D14. The activity increases compared with the previous samples in the profiles were in the ranges 0.3–2.1, 0.3–0.7 and 0.2–0.4 Bq/g for ^{22}Na, ^{137}Cs and ^{36}Cl, respectively. There is a possibility that these slices were contaminated in the process of sawing the cores into rock pieces, as one of the major cuts (in all sample cores) was performed at the position between piece number 12 and piece number 13 at c. 65 mm (cf. Figure 2-10).

On the other hand, the cores A1 and A6 are situated next to each other, cf. Figure 3-4. Likewise, the core samples A9 and A15 (with a very small activity increase) are in positions side by side, opposite the first mentioned core samples (see Figure 3-4). Therefore an alternative explanation is that increased tracer concentrations in the samples located in the inner part of the rock may be explained by diffusion taking place along microfractures in directions subparallel to the rock surface, i.e. that these subparallel microfractures act as shortcuts in the diffusion process and therefore outcompete the process of diffusion perpendicular to the fracture surface.

3.5 Tracer activities in PEEK epoxy cores

Studies of the tracer distribution on the epoxy samples were mainly performed because of the reasons mentioned in Section 2.2.2.

A partition diagram of sample B1 is shown in Figure 3-35 and examples of the result of the auto-radiography analyses of this sample are illustrated in Figure 3-36 to Figure 3-38. As a summary, it can be concluded that the major part of the radioactivity in the epoxy samples seem to originate from the rock-epoxy interface. Nevertheless, it can be shown that a considerable tracer adsorption has taken place on the surface of the PEEK lid.

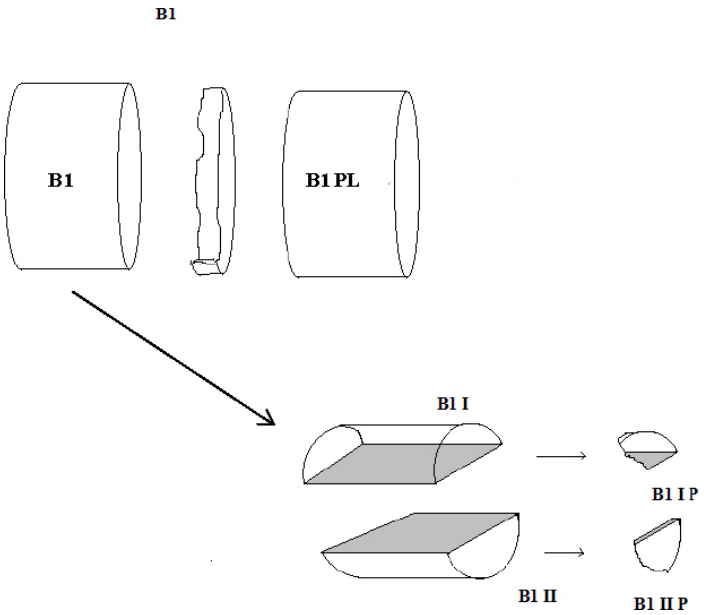

Figure 3-35. *Partition diagram of PEEK/epoxy sample B1 showing the shapes of the pieces and the relation to the core sample. Piece B1 is the second, clear epoxy layer, B1 PL is the PEEK lid and the disc in-between is the first yellow epoxy layer. The left side (closest to the clear epoxy layer) of the latter is the part that has been in contact with the natural fracture on the stub section.*

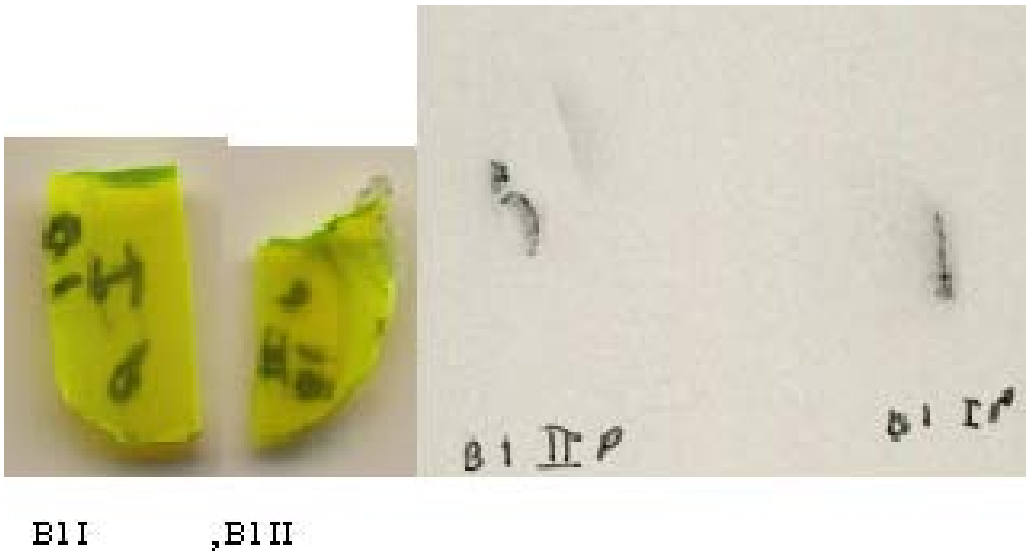

Figure 3-36. *Pictures (left) and corresponding autoradiograhs (right) of the epoxy sample of the B1-core (i.e. the part of the experimental epoxy resin injection covering the A1 core sample). As can be seen, strong blackening is obtained on the side of the epoxy that had been in contact with the rock surface, while the blackening of the part that had been in contact with the PEEK lid was hardly visible.*

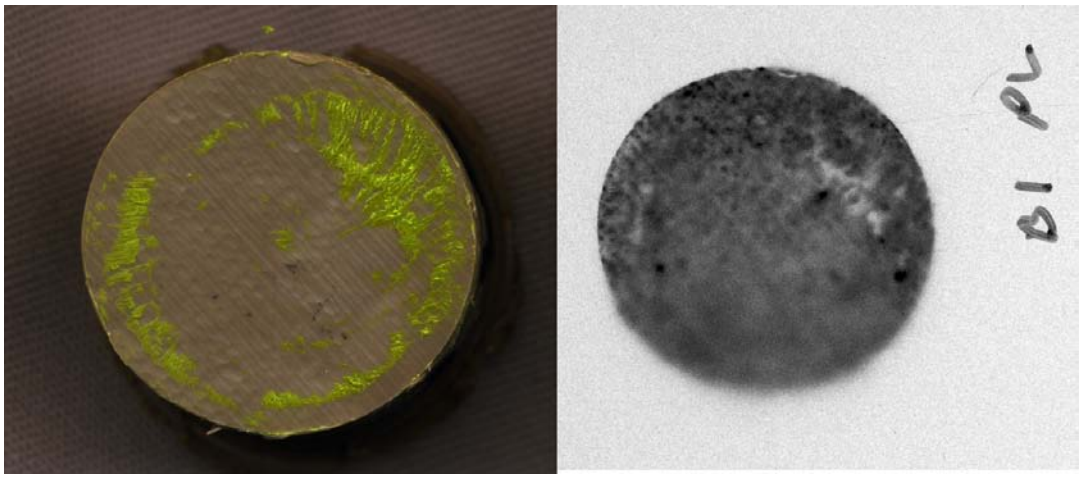

Figure 3-37. *Photograph and corresponding autoradiograph of the B1 sample which was cut in the interface of the PEEK lid and the injected epoxy resin. The photograph shows the PEEK lid after cutting off the epoxy resin; yellow resin traces are visible on the PEEK surface. It is easily seen that a considerable part of the blackening originates from a part where no epoxy resin is present, i.e. tracer adsorption on the PEEK lid took place during the experiment.*

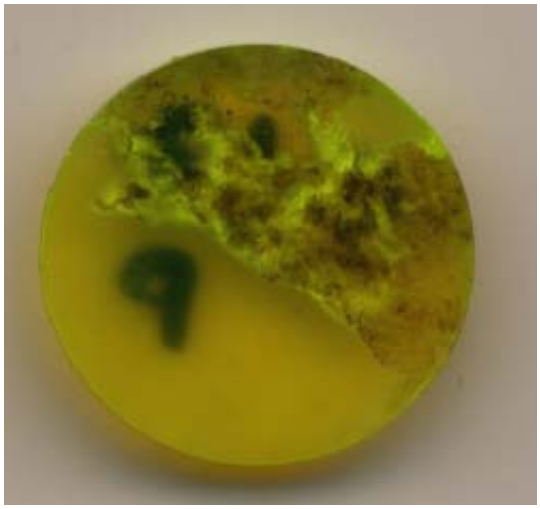

Figure 3-38. *A photograph of the B17 sample (i.e. the epoxy sample covering the A17 rock fracture sample), As can be seen, a significant part of the rock material has stuck on the surface and it is presumed that the measurement of the surface sample of A17 will underestimate the actual amount of tracer that has adsorbed during the experiment.*

Some of the epoxy samples (B1, B6, B8, B9 and B17; corresponding to the A-core samples that were dissolved and analyzed for ^{236}U and ^{99}Tc.) were measured with HPGe and ICP-SFMS (Table 3-4 and Table 3-5). The reason was initially that ^{99}Tc and ^{236}U had not been detected in the A-core samples, but they were below the detection limit (250 and 100 ng/sample, respectively) also in all analysed PEEK epoxy samples.

The results of the HPGe measurements (Table 3-4) show that for the tracers expected to sorb strongly by surface complexation (e.g. ^{57}Co, ^{109}Cd, ^{110m}Ag and ^{153}Gd), a very large part (30–100%) of the tracer adhered to the fracture surface or fracture coatings in the circulation phase of the *in situ* experiment and is now attached to the epoxy surface that previously was in contact with the fracture surface or fracture coatings. An obvious contrast to this observation is the results for e.g. the presumed sorbing (by cation exchange) ^{137}Cs, which only to a minor extent (<13%) is associated with the epoxy phase. A possible explanation for this might be that surface complexation may take place

at e.g. iron oxides at the absolute rock-water interface; iron oxides that are less consolidated with the rock and could easily be removed due to attachment to the epoxy resin. Cs would, according to this explanation, interact with the rock material that is more consolidated with the (wall) rock phase and therefore not subjected to removal due to the epoxy injection.

Table 3-4. Estimation of tracer distribution between Epoxy (B-samples) and the first A-core slice, results from γ-measurements. The sum of the tracer activity in Slice 1 and the tracer activity measured in Epoxy piece/pieces with adhered rock material is presented as the total surface activity. The part of that total activity which was found in the Epoxy is also given in the table.

Sample		^{22}Na	^{57}Co	^{109}Cd	^{110m}Ag	^{133}Ba	^{137}Cs	^{153}Gd
A1/B1	Sum activity, rock slice 1 + Epoxy (Bq)	62	27,000	16,000	3,800	1,400	14,600	3,800
	Part in the epoxy	50%	93%	55%	92%	21%	6%	82%
A6/B6	Sum activity, rock slice 1 + Epoxy (Bq)	94	13,000	11,000	3,600	1,200	31,600	2,100
	Part in the epoxy	55%	78%	29%	93%	12%	3%	49%
A8/B8	Sum activity, rock slice 1 + Epoxy (Bq)	47	15,000	4,000	625	190	2,400	1,170
	Part in the epoxy	26%	99.5%	90%	<100% [1)]	47%	13%	<100% [1)]
A9/B9	Sum activity, rock slice 1 + Epoxy (Bq)	37	10,000	5,900	870	400	5,300	1,200
	Part in the epoxy	76%	89%	52%	79%	19%	2%	57%
A17/B17	Sum activity, rock slice 1 + Epoxy (Bq)	98	14,000	16,000	6,700	570	6,300	2,200
	Part in the epoxy	83%	89%	30%	95%	19%	3%	62%
Concentration in the solution containing the excess of epoxy obtained at the epoxy injection (Bq/mL)		480	80	470	<2	100	480	<4

[1)] No tracer found in the surface sample of the rock, tracer only measured in the epoxy sample.

Table 3-5. Estimation of ^{237}Np tracer distribution between Epoxy (B-samples) and the first A-core slice, results from ICP-SFMS measurements. The sum of the tracer amount in Slice 1 and the tracer amount measured in Epoxy piece/pieces with adhered rock material is presented as the total surface amount. The part of that total amount which was found in the Epoxy is also given in the table.

Sample		^{237}Np
A1/B1	Sum amount, rock slice 1 + Epoxy (ng)	137
	Part in the epoxy	86%
A6/B6	Sum amount, rock slice 1 + Epoxy (ng)	31
	Part in the epoxy	69%
A8/B8	Sum amount, rock slice 1 + Epoxy (ng)	10
	Part in the epoxy	14%
A9/B9	Sum amount, rock slice 1 + Epoxy (ng)	17.8
	Part in the epoxy	<77%
A17/B17	Sum amount, rock slice 1 + Epoxy (ng)	30.8
	Part in the epoxy	<63%

The issue of the distribution of tracer of the surface samples between the rock and the epoxy layer raises a general question of how much of the tracer loss in the experimental section that should be considered sorption due to interaction with the rock surfaces. In the proceeding modelling chapter, it has been chosen to only include the tracer amount measured on the rock surfaces and consequently not address the amount of tracer found in the Epoxy layer as a result of sorption on the rock. However, this approximation must be acknowledged as a potential source to an underestimation of the sorption distribution coefficients (K_d) evaluated in that chapter.

The results of the ^{22}Na tracer (expected to sorb by cation exchange) deviates from the proposed explanation, showing high amounts (26–83%) of its surface tracer content in the epoxy phase. However, one should for this case consider the results of the measurement of the excess solution of the liquid epoxy resin during the epoxy injection /Widestrand et al. 2010b/; i.e. the epoxy solution that was injected in excess and discharged from the borehole. This solution contained 480 Bq/mL of ^{22}Na, which is very high compared to the activities found in the surface samples. It is therefore likely that the ^{22}Na measured in the epoxy samples is to the major extent explained by ^{22}Na dissolved in the liquid epoxy resin during the epoxy injection and is not a result of ^{22}Na sorption on rock material attached to the epoxy resin. In /Widestrand et al. 2010b/ it is proposed that a cation exchange desorption occurs which could be initiated by the TETA amine present in the epoxy resin.

4 Modelling

The results of the modelling are given according to the different Cases (1–5) specified in Section 2.9.2 and the outcome of the exercise is presented specified to the different cases.

4.1 Prediction (Case 1)

Predictions of concentration time curves, showing the loss of tracer from the aqueous phase as a function of time and predictions of penetration depth curves have been performed with the diffusion model, Case 1. This exercise aimed to calculate penetration profiles based on independently determined retention parameters (i.e. sorption distribution coefficient from batch laboratory experiments, diffusivities from through-diffusion experiments and porosity from water saturation measurements). Afterwards, a qualitative comparison was made of the calculated penetration profiles with those obtained in this work from measured *in situ* results. The independently determined laboratory values for D_e (F_f), K_d and ε are presented in Table 4-1. Hence, no parameter estimation by model fitting was performed for this case.

Predictions were made for elements showing different sorption behaviour; Na (cation exchange), Cl (non-sorbing), Ni (surface complexation) and Cs (cation exchange).

The *in situ* measured results originated from solid material that had been divided into two groups; fracture mineral coated A-cores (most of the A-cores) and matrix rock cores (all of the D-cores and some of the A-cores; cf. Table 3-2. To reflect the different characteristics of the two solid materials, sorption and diffusion data have been selected according to the division described in Table 3-2 /Widestrand et al. 2010a, Vilks et al. 2005/.

- For the material considered as fracture mineral coated cores, diffusion characteristics (porosity and diffusivity) have been selected as the maximum measured values for the repective parameters obtained from the elaborate investigation of /Vilks et al. 2005/. The K_d-values given originate from laboratory batch sorption experiment measurements /Widestrand et al. 2010a/ using materials sampled from the same fracture as where the *in situ* experiment was performed. One may argue that the this selection will obtain values that may only be representative to the rock material in the absolute vicinity of the water-rock interface; nevertheless, this selection seems appropriate for the sorbing tracer where the penetration depth is very short.
- For the material considered as matrix rock cores, the sources for the diffusion charactristics is the average values for the matrix rock samples /Widestrand et al. 2010a/. Similarily, the K_d-values have been obtained as average from the results of the batch laboratory experiment using non-altered matrix rock sampled from the core of the slim hole.

Table 4-1. Selected K_d, F_f and ε values for the tracers (elements) used in the prediction of the penetration depth curves and concentration-time curves for the fracture mineral coated A-cores and the matrix rock. Discussion of the selected values for K_d, F_f and ε is given in the text above.

	K_d (m³/kg)				F_f	ε
	Na-22	Cl-36	Ni-63	Cs-137		
Fracture mineral coated	1.2E–4	1.0E–8	1.6E–1	4.8E–1	4.8E–4	5.0E–2
Matrix rock	2.9E–4	1.6E–4	1.5E–2	2.2E–2	2.2E–5	2.1E–3

The results of the predictions are shown in Figures 4-1 to Figure 4-4 together with measured *in situ* results obtained in this work. The aqueous phase error bars only represent counting statistics (2σ), and not the total error including e.g. sampling /Widestrand et al. 2010b/.

The most striking general observation is that the measured penetration profiles show very limited resemblance with the predictions using the single rate homogeneous diffusion model. There is a marked tendency that the a tailing is obtained with a small part of the tracer migrating far much longer in to the rock than what can be predicted from the diffusion model applied. There is also a strong variation in the tracer concentrations that indicate that the results are influenced by a heterogeneity, both with respect to diffusivity and porosity. This observation is supported by the results of the PMMA porosity distribution studies /Widestrand et al. 2010b/ and the results of the radioactive tracer distributions studies (Section 3.1.2).

^{22}Na: The predictions of more or less no decrease for the aqueous concentration are verified by the experimental data. The predicted penetration depth indicates that by applying a detection limit of around 0.1 Bq/g, it should be possible to find ^{22}Na in the order of centimetres into the fracture mineral coated material and not longer than one centimetre for the rock matrix (Figures 4-1a and 4-1b, right). However, the experimental results show that the actual penetration depth of ^{22}Na has been much larger than predicted and the shape of the curve deviates considerably compared with the model prediction.

^{36}Cl: As for ^{22}Na, the model calculation indicates that more or less no decrease of the aqueous concentration should be obtained; a fact that is verified by the experimental observations, see Figure 4-2a and 4-2b, left. The two samples selected for comparison of the experimentally measured penetration profile with the calculated profile show that the measured amount of ^{36}Cl tracer in the rock is much lower compared to the predictions (cf. Figure 4-2a and 4-2b, right). The shape of the measured penetration profiles does not show very much resemblance to the predicted profiles. A possible explanation for the low amount of ^{36}Cl is that an anion exclusion effect has occurred; a topic that is further investigated in Section 4.6.

^{63}Ni: There is a good agreement between predicted aqueous concentration and measured data in the case where the retention data for the fracture mineral coated material is used (Figure 4-3a left). However, in the case where the aqueous concentration of ^{63}Ni is calculated using the retention data selected for the matrix rock, the calculated sorption model underestimates the sorption obtained in the experiment (Figure 4-3b left). Thus, the K_d and diffusivity selected to represent the matrix rock are clearly too low to describe the loss of nickel from the aqueous phase in the *in situ* experiment. The penetration depth predicted for the two material types is within the range of one mm, cf. Figure 4-3a and b (left). However, these results are contradicted by the experimentally obtained results which shows that presence of ^{63}Ni tracer could be measured ~8 mm into the matrix.

^{137}Cs: Use of the retention data assumed to represent fracture mineral coated A-cores gives a sorption loss in the aqueous phase that is stronger than actually measured sorption (Figure 4-4a left). On the other hand, using the retention data aimed to represent the matrix rock gives a sorption loss that is below what is observed in the experiment. (Figure 4-4b left). Regarding the penetration depth, both predict depths just below one mm. This prediction is strongly contradicted by the observation of measurable concentration of ^{137}Cs several cm into the rock matrix.

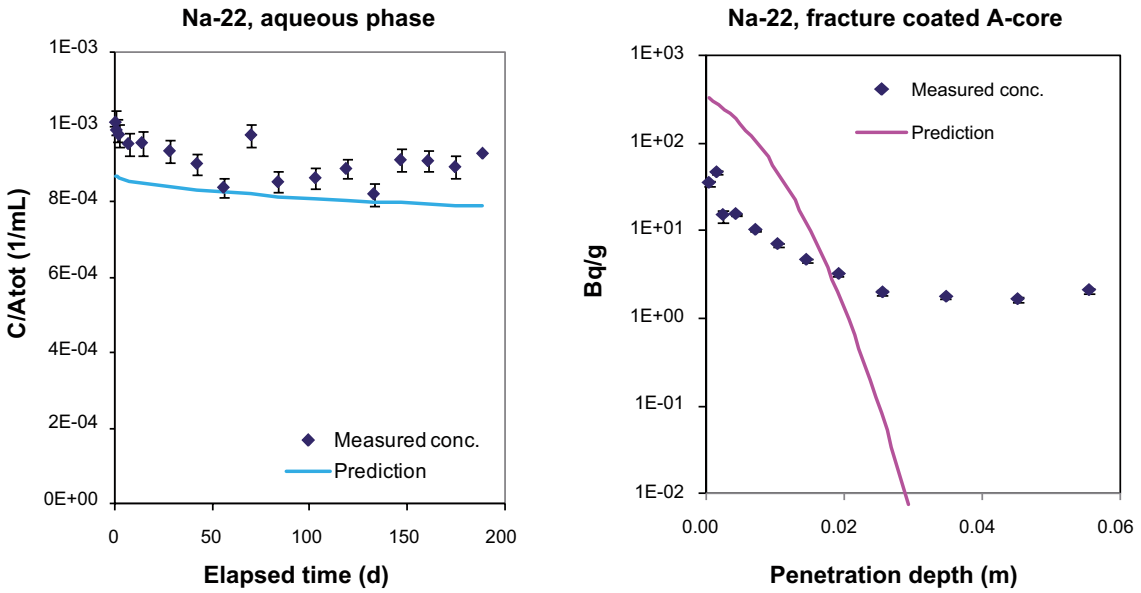

Figure 4-1a. *Prediction of ^{22}Na aqueous concentration-time curve (left) together with the measured aqueous concentration during the* in situ *experiment. To the right, the predicted penetration profile for fracture mineral coated A-core is given, in comparison with the measured A6 sample profile.*

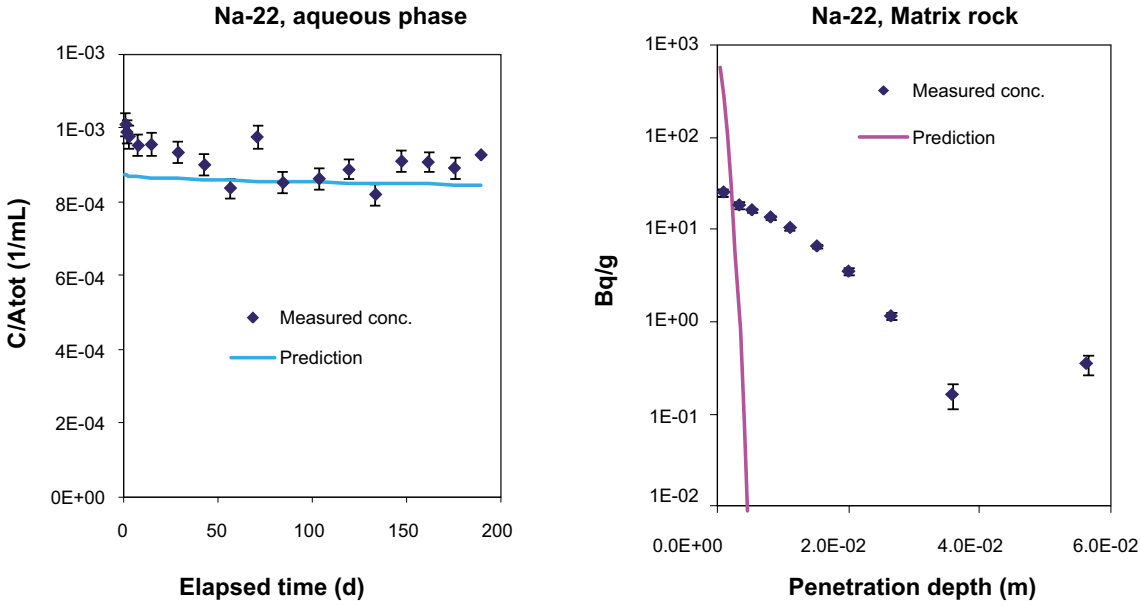

Figure 4-1b. *Prediction of ^{22}Na aqueous concentration-time curve (left) together with the measured aqueous concentration during the* in situ *experiment. To the right, the predicted penetration profile for matrix rock is given, in comparison with the measured D13 sample profile.*

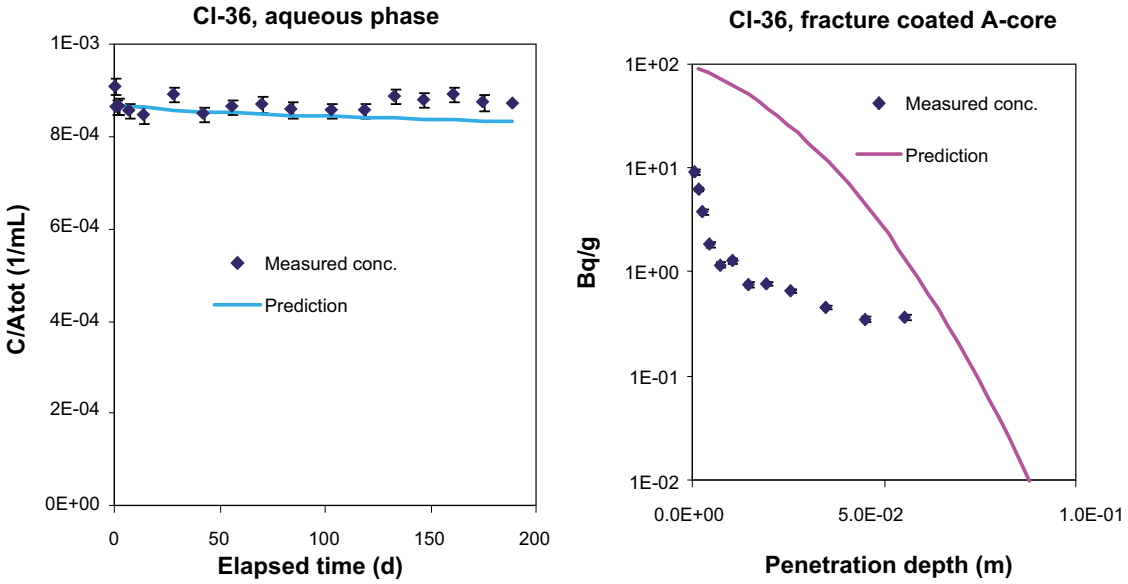

Figure 4-2a. *Prediction of ^{36}Cl aqueous concentration-time curve (left) together with the measured aqueous concentration during the* in situ *experiment. To the right, the predicted penetration profile for fracture mineral coated A-core is given, in comparison with the measured A6 sample profile.*

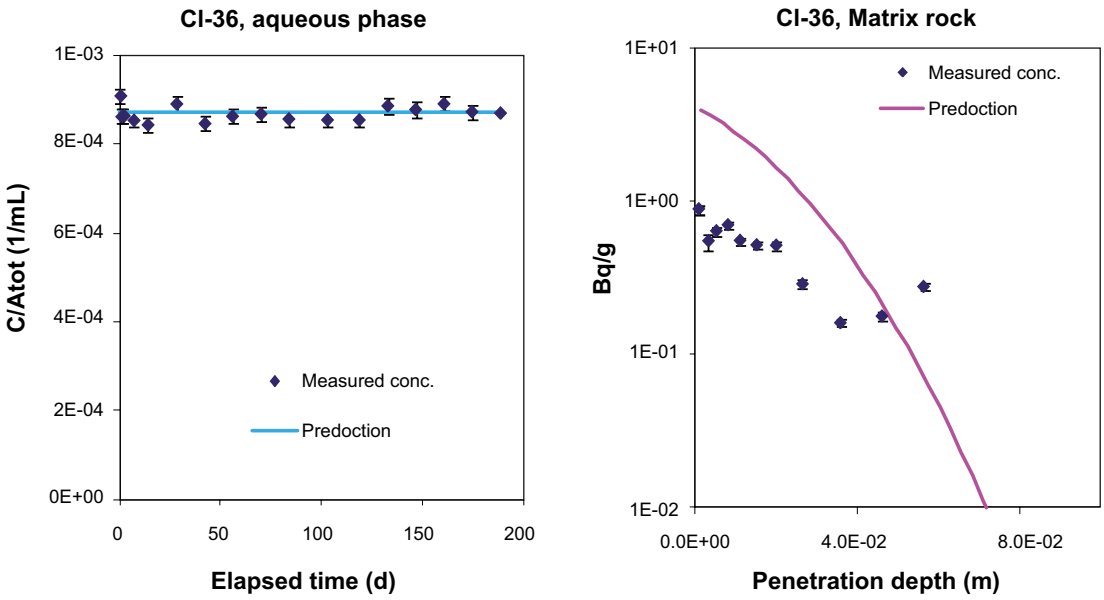

Figure 4-2b. *Prediction of ^{36}Cl aqueous concentration-time curve (left) together with the measured aqueous concentration during the* in situ *experiment. To the right, the predicted penetration profile for matrix rock is given, in comparison with the measured D13 sample profile.*

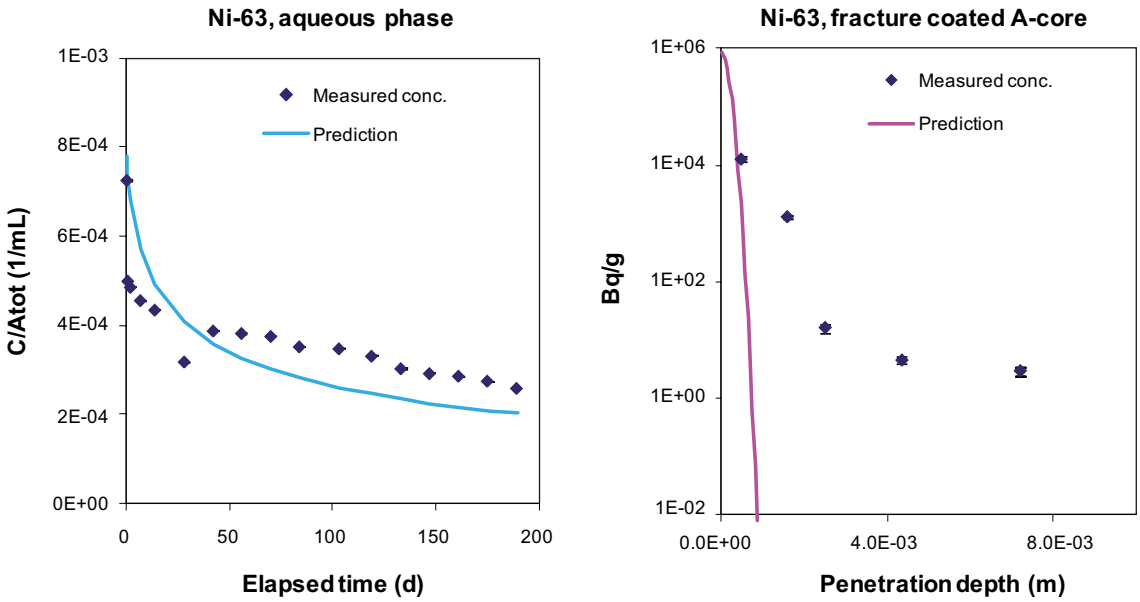

Figure 4-3a. *Prediction of ^{63}Ni aqueous concentration-time curve (left) together with the measured aqueous concentration during the* in situ *experiment. To the right, the predicted penetration profile for fracture mineral coated A-core is given, in comparison with the measured A6 sample profile.*

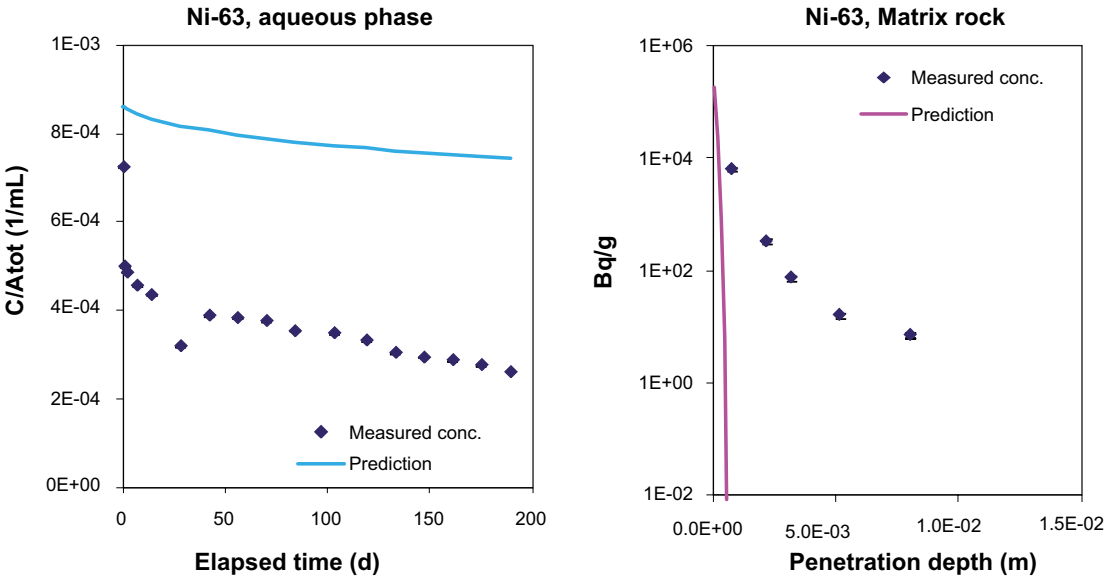

Figure 4-3b. *Prediction of ^{63}Ni aqueous concentration-time curve (left) together with the measured aqueous concentration during the* in situ *experiment. To the right, the predicted penetration profile for matrix rock is given, in comparison with the measured D13 sample profile.*

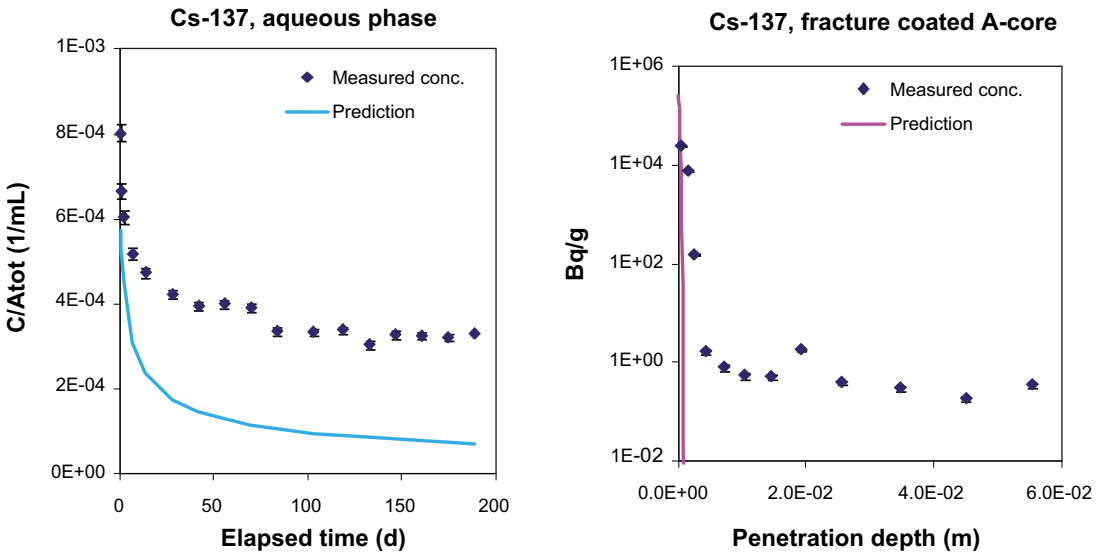

***Figure 4-4a**. Prediction of ^{137}Cs aqueous concentration-time curve (left) together with the measured aqueous concentration during the* in situ *experiment. To the right, the predicted penetration profile for fracture mineral coated A-core is given, in comparison with the measured A6 sample profile.*

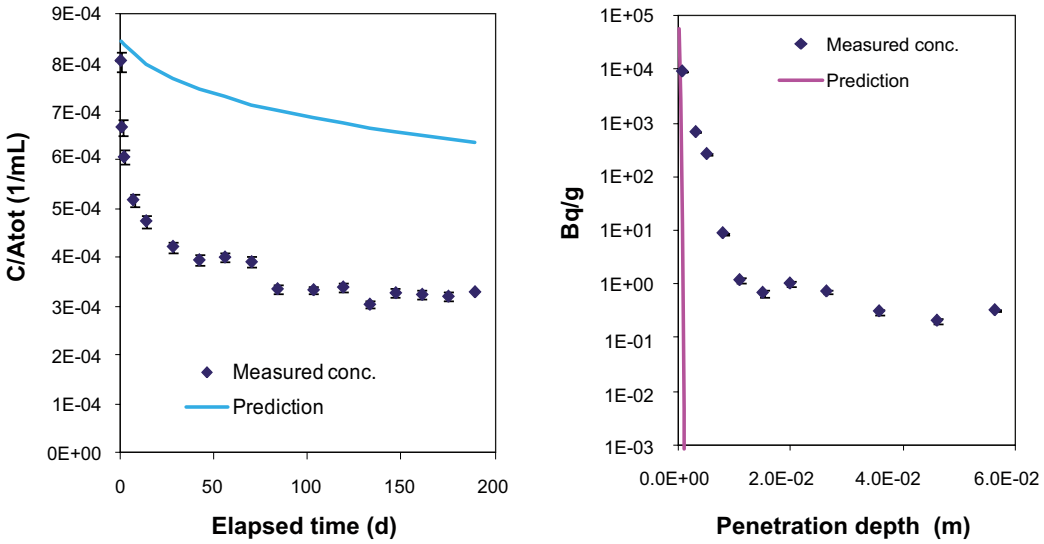

***Figure 4-4b.** Prediction of ^{137}Cs aqueous concentration-time curve (left) together with the measured aqueous concentration during the in situ experiment. To the right, the predicted penetration profile for matrix rock is given, in comparison with the measured D13 sample profile.*

4.2 Parameter estimation (Case 2–Case 5)

Four different cases of modelling have been investigated, in which one, two or all of the parameters were varied in order to obtain the best fit of the calculated results to the experimental data. Those of the parameters not varied, were held constant (fixed) in the calculation, applying laboratory-derived numerical values of these parameters, cf. Table 4-1. Measurements of the tracer loss in the aqueous phase during the circulation phase of the *in situ* experiment were not addressed in the fitting procedure, except for Case 5.

As mentioned in previous sections, a general trend seen in the penetration profile results is that a forward tailing is obtained for most tracers. After reaching distances of typically 1–3 cm in to the rock, a low and constant level of tracer concentration is obtained, this due to reasons that are not fully understood. It is easily realised (e.g. by comparing the predictions and the experimental results given in Section 4.1) that this trend can not be reproduced by modelling using a fully homogeneous diffusion model. Applying a modelling with equal relative weight of all data points, would therefore not have produced any meaningful results. It was therefore decided to perform the modelling calculation under the condition that one only aim to address the tracer interaction in the vicinity of the rock/water boundary, i.e. not including the tailing part that is assumed to be severely influenced by sample heterogeneity. One must of course be aware of that such an operation causes exclusion of the part of the tracer that has been retarded to a minor degree in the rock, i.e. one may suspect a potential overestimation of the K_d compared to a concept of including all data without any exclusion. However, in all cases studied, the data points removed never consists of more than 0.1% of the total amount of the tracer found in the rock. It is foreseen that a future modelling which addresses different aspects of sample heterogeneity (or other alternative processes) will be necessary to explain the entire penetration profile data.

For this reason, a mathematical calculation module was developed that was aimed to exclude data points from the forward tailing part of the penetration profile. This was performed by searching for a point on the curve where a drastic decrease of the slope was obtained (i.e. the “start” of the forward tailing part of the curve) and exclude the data points obtained hereafter. One must of course be aware of that such an operation causes exclusion of the part of the tracer that has been retarded to a minor degree in the rock, i.e. one may suspect a potential overestimation of the K_d compared to a concept of including all data without any exclusion. However, in all cases studied, the data points removed never contribute more than 0.1% of the total amount of the tracer found in the sample.

The low amount of ^{36}Cl (presumed non-sorbing) found in the samples and the suspicion that anion exclusion has occurred has called for a special investigation of the results for this tracer, cf. Section 4.6. The results of the modelling for ^{36}Cl are therefore only presented in that section and not included in the presentation of modelling Case 2–Case 5.

4.2.1 Case 2

In Case 2, the sorption coefficient, K_d, was used as the fitting parameter (D_e and ε were fixed to laboratory values) to obtain as good fit as possible to the measured *in situ* penetration profiles. Measurements of the tracer loss in the aqueous phase during the circulation phase of the *in situ* experiment were not addressed in this fitting procedure.

Some examples of the modelled penetration profile curves in comparison to the measured concentrations are shown in Figure 4-5 to Figure 4-11. For information purposes the resulting calculated aqueous concentration vs. time curves together with *in situ* measured aqueous concentrations are also shown although one must have in mind that no address of this information was made in the fitting calculations. The error bars appearing in the figures for Co, Cd, Ba and Gd represent the detection limits for the γ-spectrometry measurements of these tracers in the measurements where the activity of these tracers were too low to be quantified,

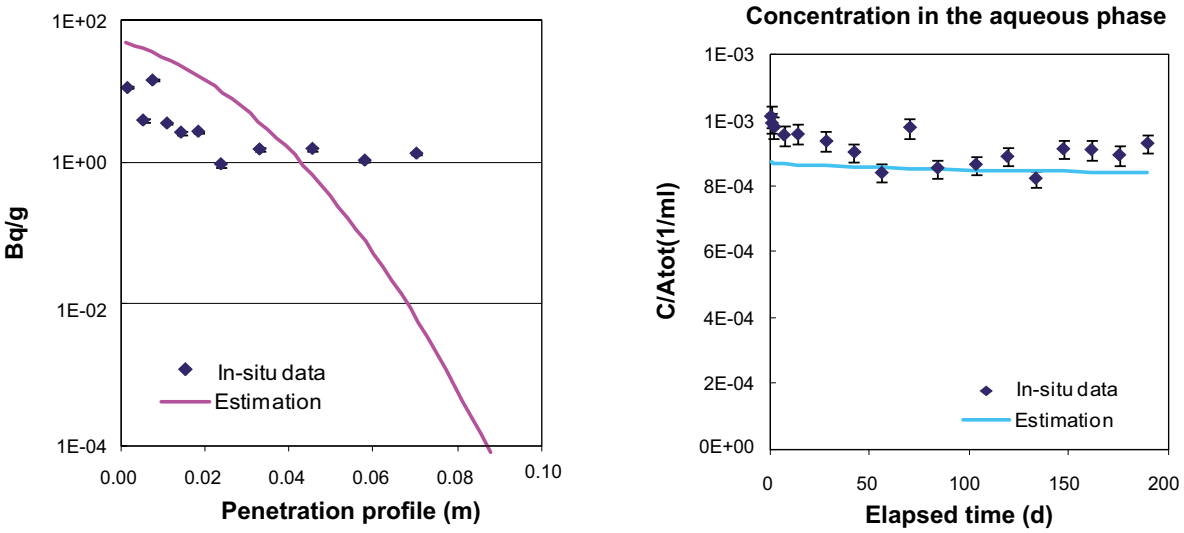

Figure 4-5. Illustration of the outcome of a Case 2 modelling, ^{22}Na diffusion in A5 core. The left figure illustrates the fit of the calculated penetration profile to the experimentally measured data. The right figure illustrates the corresponding loss of tracers in the aqueous phase obtained with the model applied. However, it is important to consider that the Case 2 modelling did not include any attempt to fit the model to the aqueous data.

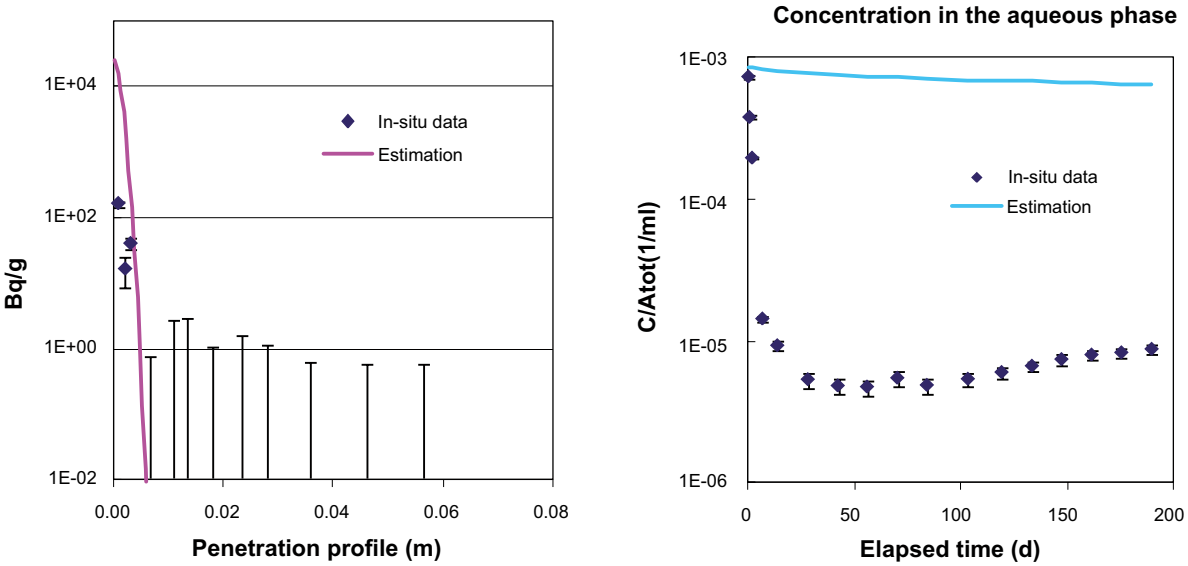

Figure 4-6. Illustration of the outcome of a Case 2 modelling, ^{57}Co diffusion in A8 core. The left figure illustrates the fit of the calculated penetration profile to the experimentally measured data. The right figure illustrates the corresponding loss of tracers in the aqueous phase obtained with the model applied. However, it is important to consider that the Case 2 modelling did not include any attempt to fit the model to the aqueous data.

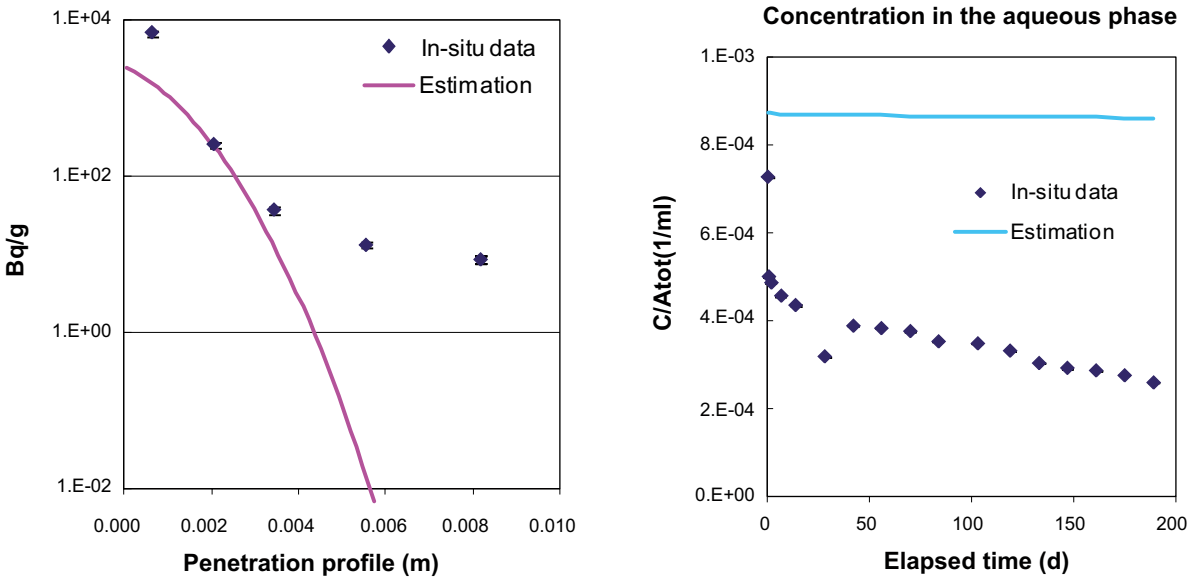

Figure 4-7. *Illustration of the outcome of a Case 2 modelling, ^{63}Ni diffusion in D12 core. The left figure illustrates the fit of the calculated penetration profile to the experimentally measured data. The right figure illustrates the corresponding loss of tracers in the aqueous phase obtained with the model applied. However, it is important to consider that the Case 2 modelling did not include any attempt to fit the model to the aqueous data.*

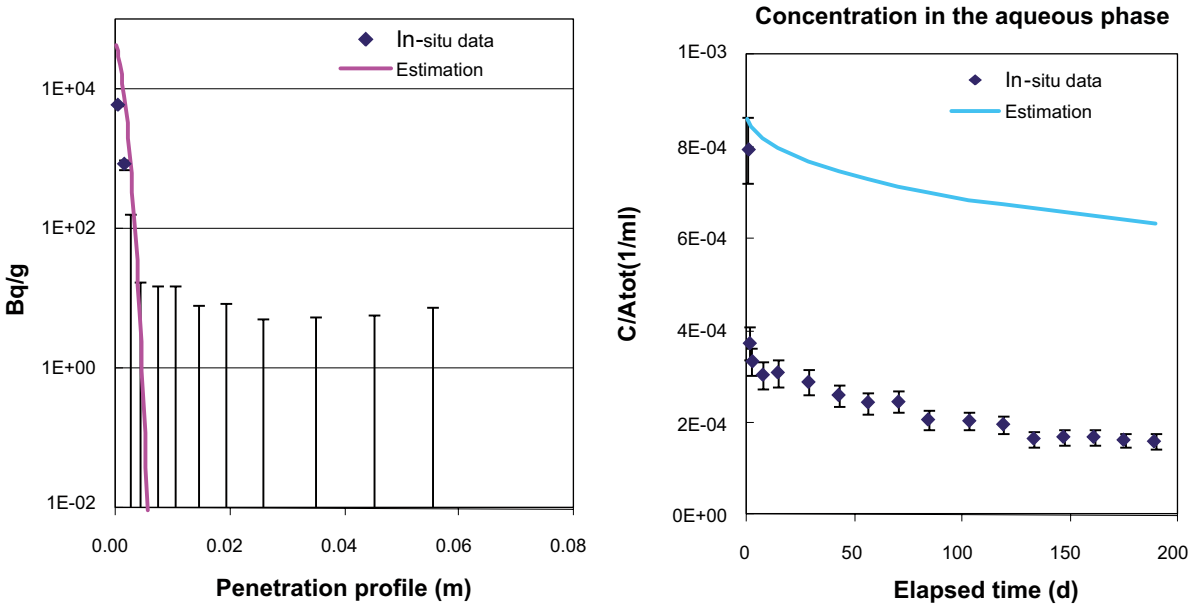

Figure 4-8. *Illustration of the outcome of a Case 2 modelling, ^{109}Cd diffusion in A6 core. The left figure illustrates the fit of the calculated penetration profile to the experimentally measured data. The right figure illustrates the corresponding loss of tracers in the aqueous phase obtained with the model applied. However, it is important to consider that the Case 2 modelling did not include any attempt to fit the model to the aqueous data.*

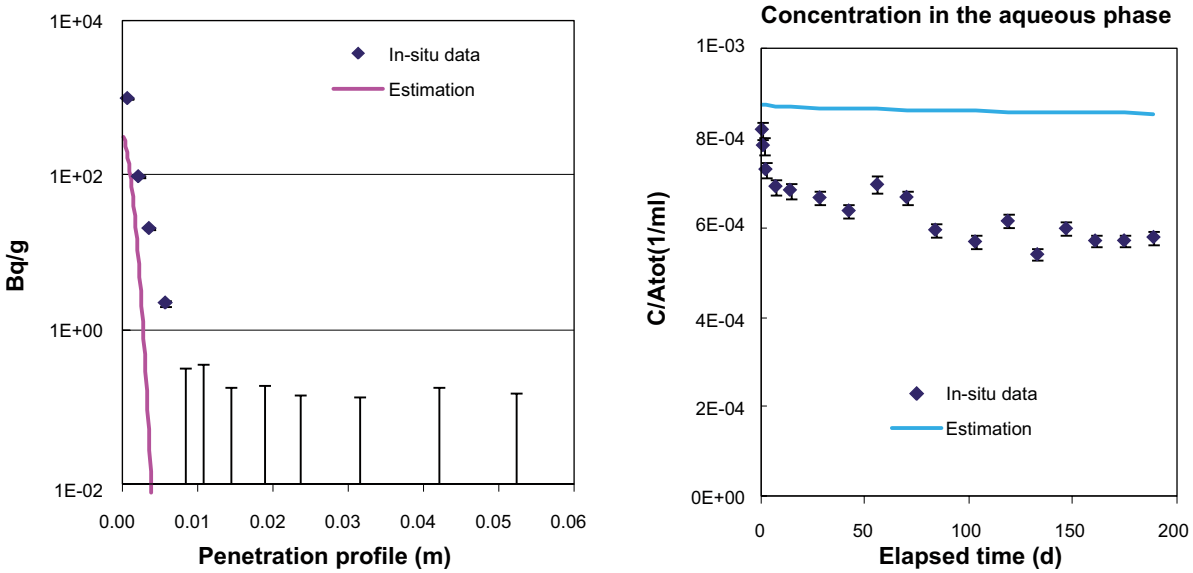

Figure 4-9. *Illustration of the outcome of a Case 2 modelling, ^{133}Ba diffusion in D12 core. The left figure illustrates the fit of the calculated penetration profile to the experimentally measured data. The right figure illustrates the corresponding loss of tracers in the aqueous phase obtained with the model applied. However, it is important to consider that the Case 2 modelling did not include any attempt to fit the model to the aqueous data.*

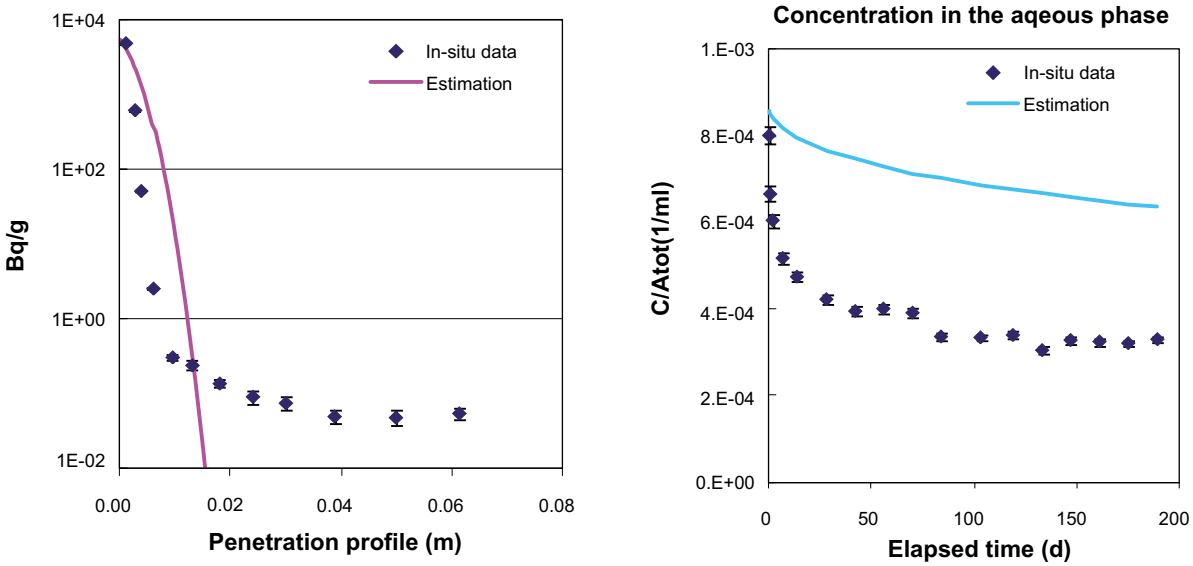

Figure 4-10. *Illustration of the outcome of a Case 2 modelling, ^{137}Cs diffusion in A10 core. The left figure illustrates the fit of the calculated penetration profile to the experimentally measured data. The right figure illustrates the corresponding loss of tracers in the aqueous phase obtained with the model applied. However, it is important to consider that the Case 2 modelling did not include any attempt to fit the model to the aqueous data.*

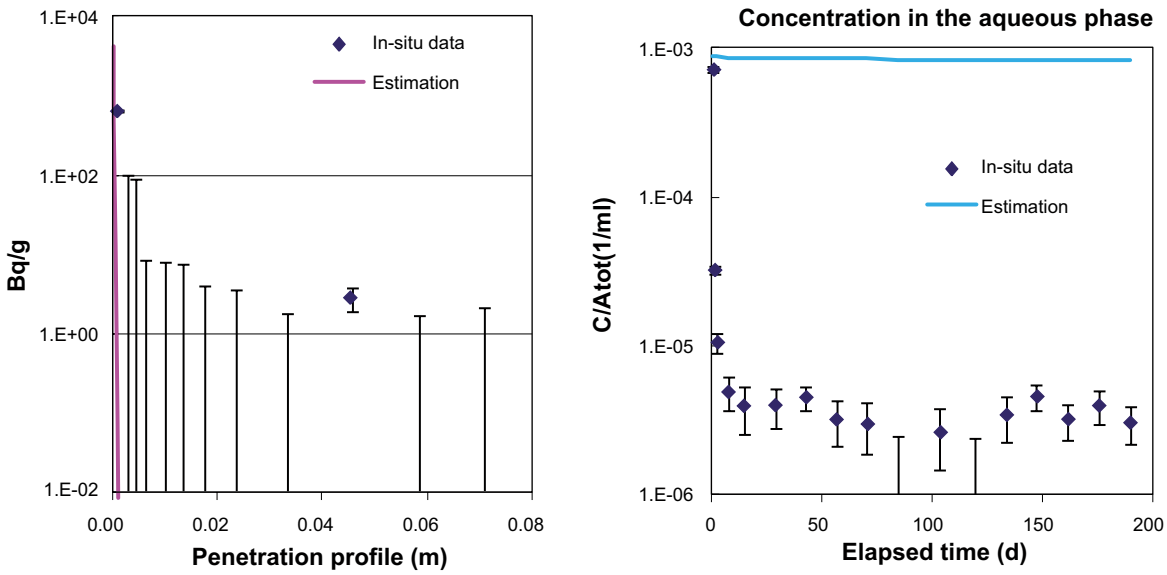

Figure 4-11. *Illustration of the outcome of a Case 2 modelling, ^{153}Gd diffusion in A12 core. The left figure illustrates the fit of the calculated penetration profile to the experimentally measured data. The right figure illustrates the corresponding loss of tracers in the aqueous phase obtained with the model applied. However, it is important to consider that the Case 2 modelling did not include any attempt to fit the model to the aqueous data.*

The full set of modelled data, given as penetration profiles combined with the corresponding aqueous concentrations, is presented in Appendix 9. The estimated K_d (m^3/kg) values obtained from the modelling are summarised in Table 4-2, given in comparison to the batch sorption determined K_d values. Graphical representations of the comparisons are given in Figure 4-12 to Figure 4-16.

A general conclusion from the Case 2 modelling is that the K_d:s determined from the modelling are generally lower than the K_d:s determined from laboratory batch experiments. This fact could already be indicated by the outcome of the predictions presented for Case 1 where it was shown (using a homogeneous matrix diffusion model) that the observation of sorbing tracers having diffused centimetres in to the matrix was not compatible with the high K_d obtained in the batch laboratory experiment. However, an important observation from this modelling exercise is that the use of a reduced K_d in order to obtain a good fit of the penetration profile data is accompanied by a significant underestimation of the sorption loss in the aqueous phase. This observation raises doubts of the correctness of the low K_d:s modelled. A possible explanation for this is that structural heterogeneity of the rock causes fast diffusion channels, which need a reduced K_d (when applying the homogeneous diffusion model), to explain the locally increased penetration depth caused by microfractures, cavities, etc.

Table 4-2. Case 2. Estimated K_d (m^3/kg) for various tracers based on *in situ* experimental data from the core penetration profiles. Average values combined with the minimum and maximum values are provided for the different tracers and solid sample groups, n refers to the number of sample cores where the radioactivity measurement gave values above the detection limits. F_f and ε were held fixed in the calculations. The fixed laboratory obtained values for the formation factor (F_f) and the porosity (ε) used for the different cases are also included in the table.

Tracer		K_d (m^3/kg), estimated from the *in situ* core penetration profile, modelling results			K_d (m^3/kg) from batch sorption laboratory measurements, for comparison [1]	
		A-cores		D-cores		
		Fracture mineral coated cores	Matrix rock	Matrix rock	Crushed rock from fracture mineral coated cores	Crushed rock from matrix rock
		F_f=4.8E–4 ε=0.003	F_f=2.2E–4 ε=0.003	F_f=2.2E–4 ε=0.003		
Na-22	average	Not defined [2]	3.9E–6	3.5E–6	<1E–3 [3]	2.9E–4
	Min	<9.7E–6	3.0E–6	1.8E–6		1.7E–4
	max	1.0E–3	5.2E–6	6.4E–6		4.2E–4
	n	7	3	8		3
Ni-63	average	4.8E–3		1.1E–4	1.6E–1	1.5E–2
	Min	1.5E–3		4.9E–5	4.6E–2	8.2E–3
	max	9.8E–3		1.9E–4	2.7E–1	2.5E–2
	n	5	0	4	2	3
Ba-133	average	5.4E–4	1.6E–4	1.4E–4	1.2E–2	2.1E–3
	Min	1.3E–4	1.6E–4	9.9E–5	9.8E–3	2.0E–3
	max	9.5E–4	1.6E–4	2.3E–4	1.5E–2	2.3E–3
	n	2	1	3	2	3
Cs-137	average	3.8E–3	2.2E–4	1.8E–4	4.8E–1	2.2E–2
	Min	7.1E–4	1.6E–4	4.0E–5	1.0E–1	1.2E–2
	max	9.4E–3	2.5E–4	3.8E–4	8.6E–1	3.2E–2
	n	7	3	8	2	3
Co-57	average	3.4E–3	4.9E–4	1.4E–3	4.0E–1	5.0E–2
	Min	2.6E–3	4.9E–4	1.8E–5	2.7E–1	3.6E–2
	max	4.2E–3	4.9E–4	4.0E–3	5.3E–1	6.1E–2
	n	2	1	3	2	3
Cd-109	average	3.1E–3			5.9E–2	5.1E–3
	Min	3.0E–3			2.6E–2	4.0E–3
	max	3.2E–3			9.2E–2	5.9E–3
	n	2	0	0	2	3
Gd-153	average	1.6E–5	2.7E–3		>0.4 [4]	>0.4 [4]
	Min	1.6E–5	2.7E–3			
	max	1.6E–5	2.7E–3			
	n	1	1	0		

[1] Batch sorption studies were performed on material from pilot borehole KA3065A02 and experimental borehole KA3065A03 /Widestrand et al. 2010a/.

[2] 5 out of 7 modelling gave only “lower than” values, an average value was therefore not possible to calculate. The corresponding min-value refers to the lowest “lower than” value.

[3] It was not possible by counting statistics of the measurement in the batch sorption experiment to verify any decrease of tracer concentration in the aqueous phase (batch sorption sample in comparison to blank sample). Hence, only a detection limit is given which has been calculated from the highest possible tracer concentration decrease that is within the counting statistics (2σ).

[4] All tracer added in the experiment was found to sorb on the rock material. The value is based on the detection limit in the aqueous phase measurement.

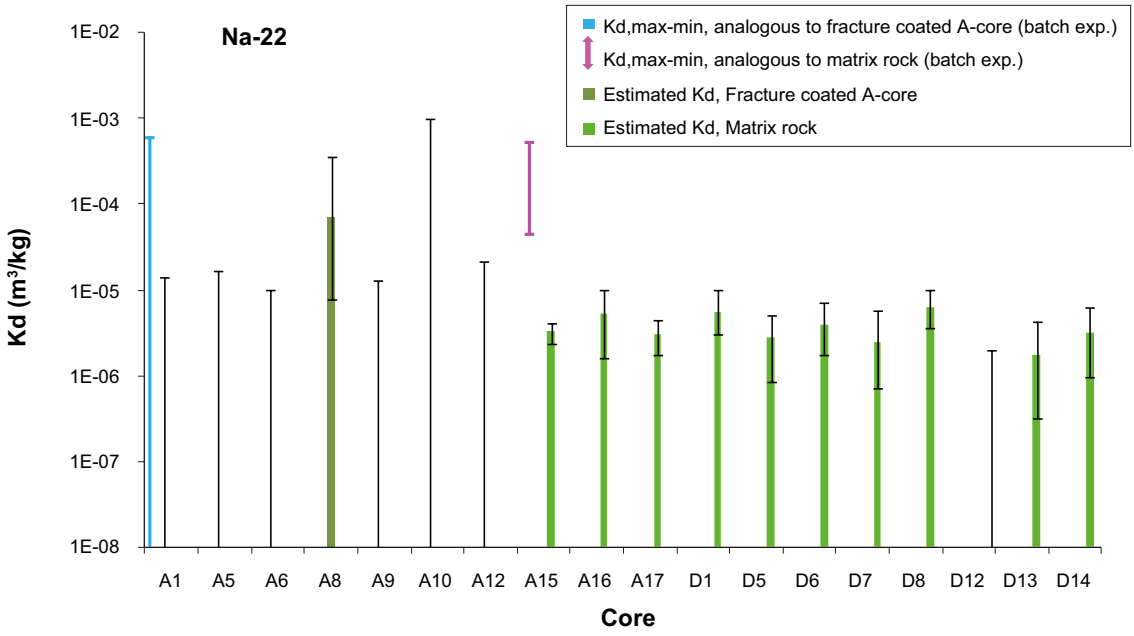

Figure 4-12. *K_d-values (m^3/kg) obtained from the curve fitting procedure using fixed ε and F_f, i.e. Case 2. For samples characterized as fracture mineral coated rock, calculated values are represented by dark green bars and for the matrix rock, clear green bars are used. For samples where only a "lower than" K_d value could be calculated, the value is represented by a black error bar, otherwise the error bars are used to represent the uncertainty of the calculated values. Comparisons are also made to K_d values determined from laboratory batch experiment where the blue error bar represents the interval of the measured values for fracture coated rock and the pink error bar represents the interval for the matrix rock.*

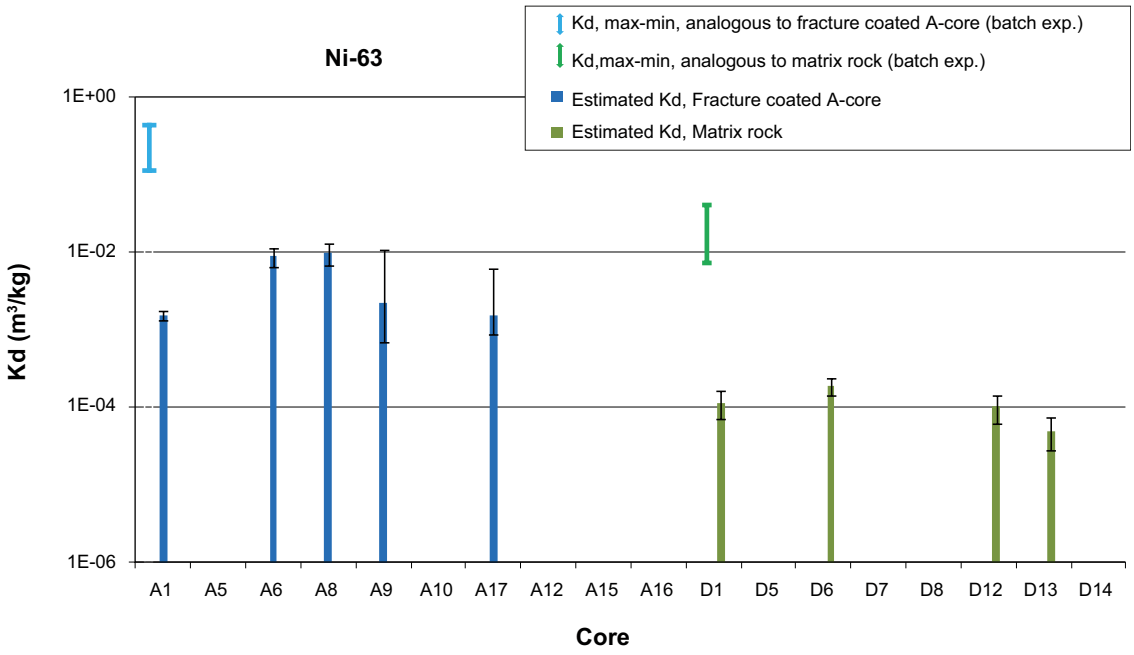

Figure 4-13. *K_d-values (m^3/kg) obtained from the curve fitting procedure using fixed ε and F_f, i.e. Case 2. For samples characterized as fracture mineral coated rock, calculated values are represented by dark blue bars and for the matrix rock, dark green bars are used. The black error bars are used to represent the uncertainty of the calculated value. Comparisons are also made to K_d values determined from laboratory batch experiment where the light blue error bar represents the interval of the measured values for fracture coated rock and the clear green error bar represents the interval for the matrix rock.*

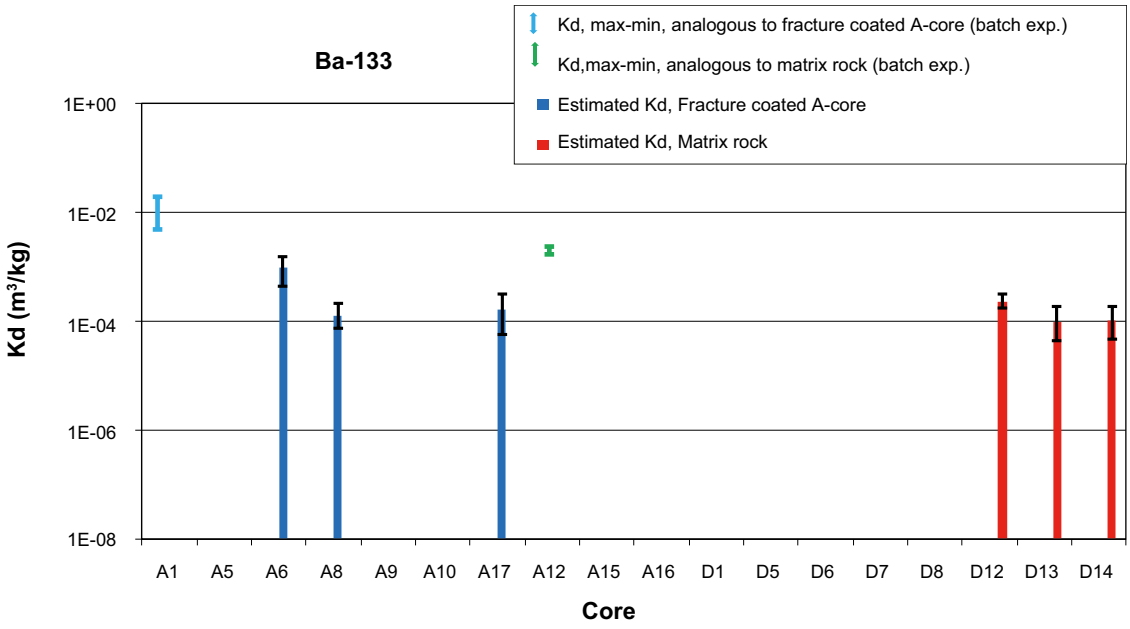

Figure 4-14. *K_d values (m^3/kg) obtained from the curve fitting procedure using fixed ε and F_f, i.e. Case 2. For samples characterized as fracture mineral coated rock, calculated values are represented by dark blue bars and for the matrix rock, red bars are used. The black error bars are used to represent the uncertainty of the calculated value. Comparisons are also made to K_d values determined from laboratory batch experiment where the light blue error bar represents the interval of the measured values for fracture coated rock and the clear green error bar represents the interval for the matrix rock.*

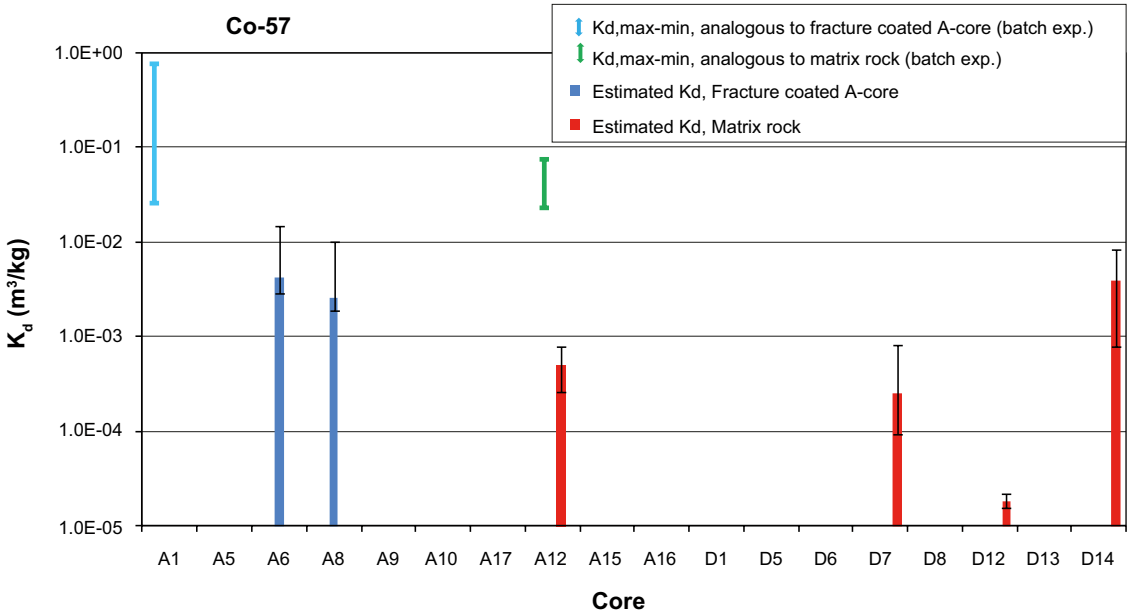

Figure 4-15. *K_d values (m^3/kg) obtained from the curve fitting procedure using fixed ε and F_f, i.e. Case 2. For samples characterized as fracture mineral coated rock, calculated values are represented by dark blue bars and for the matrix rock, red bars are used. The black error bars are used to represent the uncertainty of the calculated value. Comparisons are also made to K_d values determined from laboratory batch experiment where the light blue error bar represents the interval of the measured values for fracture coated rock and the clear green error bar represents the interval for the matrix rock.*

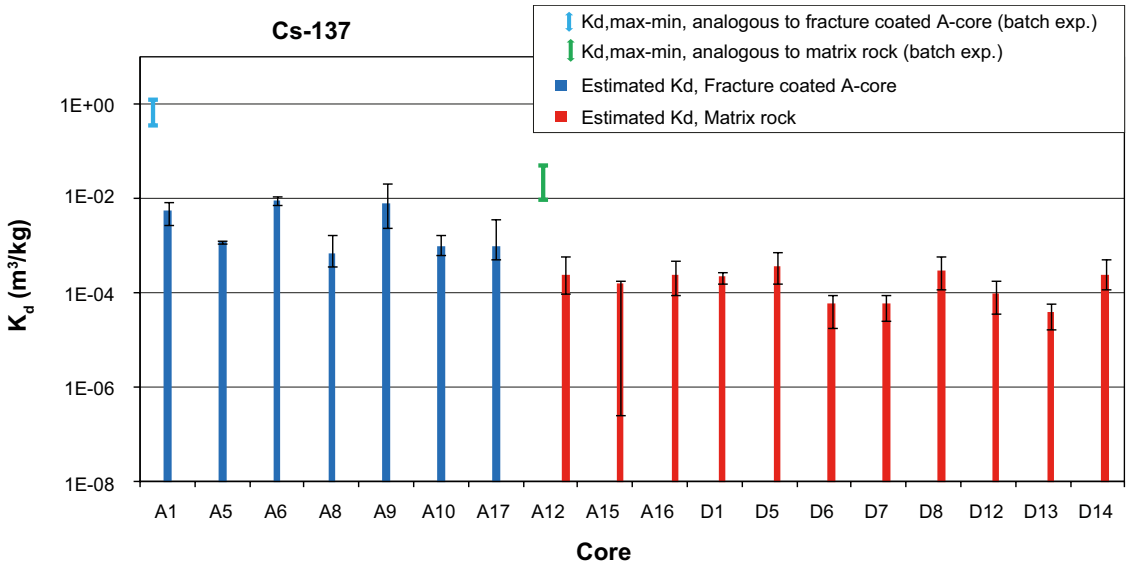

Figure 4-16. *K_d values (m^3/kg) obtained from the curve fitting procedure using fixed ε and F_f, i.e. Case 2. For samples characterized as fracture mineral coated rock, calculated values are represented by dark blue bars and for the matrix rock, red bars are used. The black error bars are used to represent the uncertainty of the calculated value. Comparisons are also made to K_d values determined from laboratory batch experiment where the light blue error bar represents the interval of the measured values for fracture coated rock and the clear green error bar represents the interval for the matrix rock.*

4.2.2 Case 3

For Case 3, the diffusivity (represented by the formation factor, F_f = De/Dw) and the porosity, ε, were used as the fitting parameters to obtain the best fit to the measured *in situ* penetration profile. The sorption coefficients K_d (m^3/kg) used in this case were kept constant during the calculations and were obtained from the LTDE-SD batch laboratory experiment program (batch sorption studies were performed on material from pilot borehole KA3065A02 and experimental borehole KA3065A03). /Widestrand et al. 2010a./ As for Case 2, only the penetration profile data was used for fitting the model to the experimental data; the data for the concentration of the tracers in the aqueous phase was thus omitted in the calculations.

The results from the calculations can be seen in Appendix 9 where the modelled penetration profiles are shown together with the *in situ* measured data. The figures below (Figure 4-17 to Figure 4-20) exemplify the results for Na and Cs with comparison of the calculated penetration profiles to the corresponding measured data. Besides the penetration profiles, the corresponding calculations of the losses in the aqueous phase are also presented; however, one should have in mind that no attempt to fit the calculated model to these measured data has been performed.

The numerical results of the modelling, i.e. the formation factors that produce the best fit of the calculation to the measured penetration profiles, are summarised in Table 4-3. One conclusion of the modelling of Case 3 is that the porosity term, ε, has in every studied case a very limited influence on the results of the calculation. This can easily be realised from the description of the one-dimension diffusion model (Section 2.9.1) where it is shown (Equation 2.10 and 2.12) that the application of ε is as a part of the ($\varepsilon + K_d\rho$) term. Since the lowest K_d used in these calculation is $1.2 \cdot 10^{-4}$ m^3/kg (^{22}Na for fracture mineral coated cores), the minimum value of the $K_d\rho$ term (provided a rock density, ρ, of 2,700 kg/m^3) will be in the range of 0.3. This means that using realistic porosity values (e.g. 0.1–1%) ε will be negligible compared to the $K_d\rho$ term, even for the slightly sorbing ^{22}Na tracer. Accordingly, as presented in Appendix 10, only "lower than" values are therefore obtained for ε in the modelling; in the case of ^{22}Na, values in the range of < 0.1–< 0.4 are obtained. Modelling of the sorbing tracers is thus totally insensitive to the ε and no representation of this parameter is therefore included in Table 4-3.

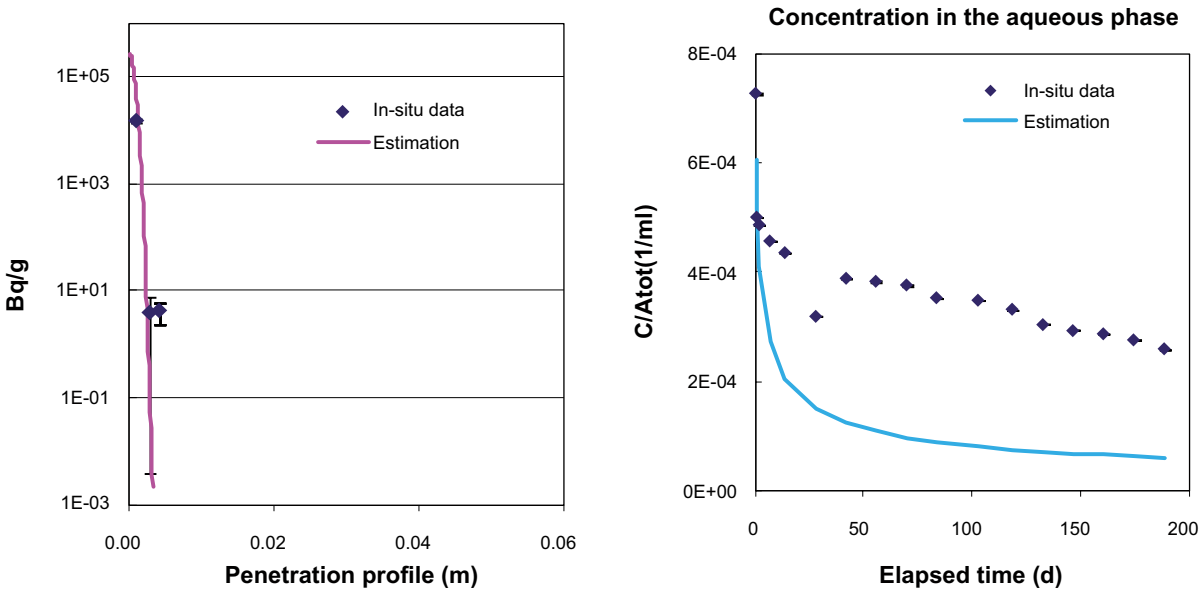

Figure 4-17. *Illustration of the outcome of a Case 3 modelling, ^{63}Ni diffusion in A9 core. The left figure illustrates the fit of the calculated penetration profile the experimentally measured data. The right figure illustrates the corresponding loss of tracers in the aqueous obtained with the model applied. However, it is important to consider that the Case 3 modelling did not include any attempt to fit the model to the aqueous data.*

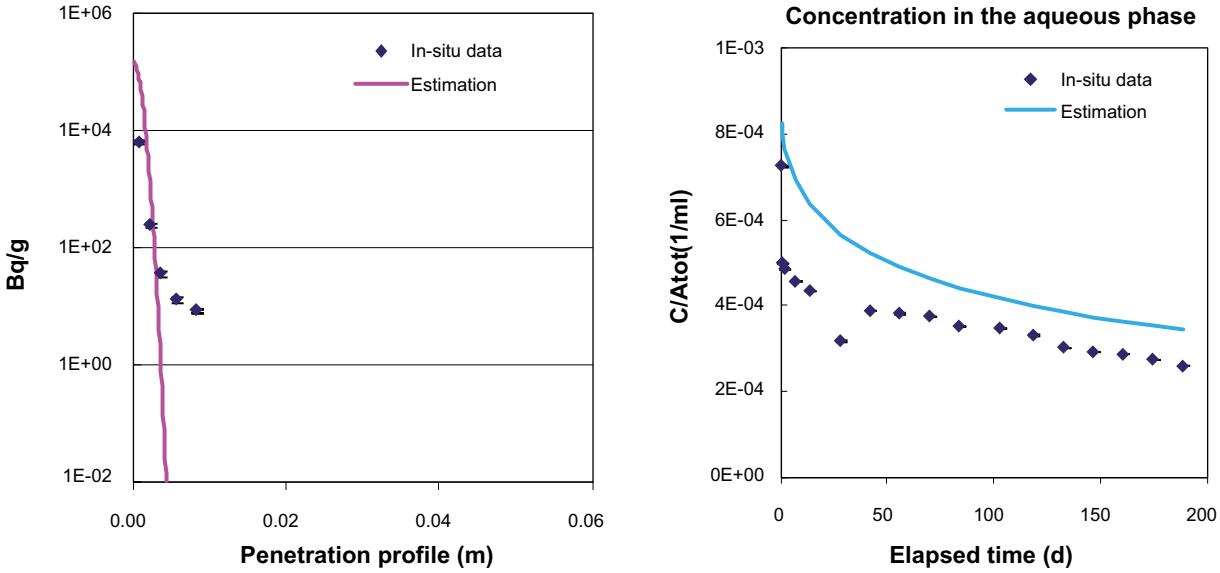

Figure 4-18. *Illustration of the outcome of a Case 3 modelling, ^{63}Ni diffusion in D12 core. The left figure illustrates the fit of the calculated penetration profile the experimentally measured data. The right figure illustrates the corresponding loss of tracers in the aqueous phase obtained with the model applied. However, it is important to consider that the Case 3 modelling did not include any attempt to fit the model to the aqueous data.*

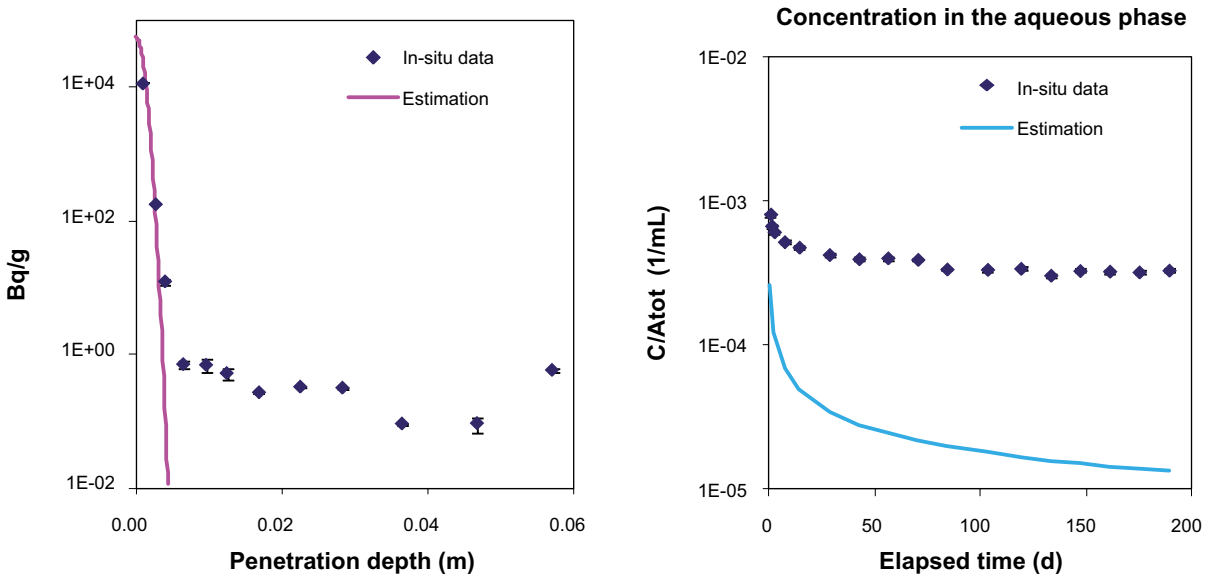

Figure 4-19. *Illustration of the outcome of a Case 3 modelling, ^{137}Cs diffusion in A9 core. The left figure illustrates the fit of the calculated penetration profile the experimentally measured data. The right figure illustrates the corresponding loss of tracers in the aqueous phase obtained with the model applied. However, it is important to consider that the Case 3 modelling did not include any attempt to fit the model to the aqueous data.*

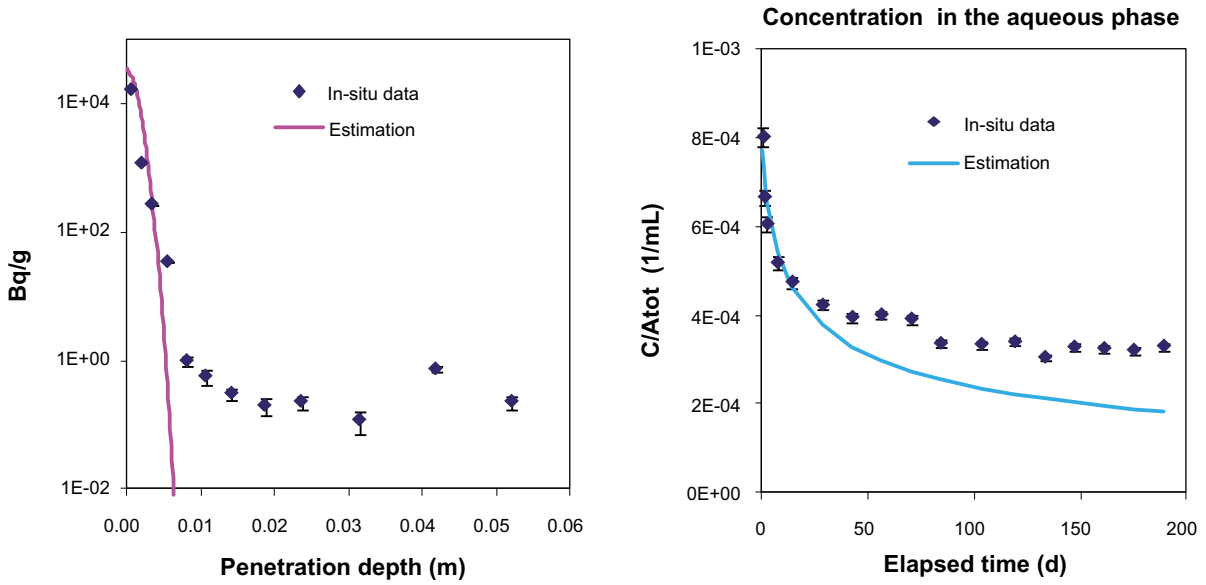

Figure 4-20. *Illustration of the outcome of a Case 3 modelling, ^{137}Cs diffusion in D12 core. The left figure illustrates the fit of the calculated penetration profile the experimentally measured data. The right figure illustrates the corresponding loss of tracers in the aqueous phase obtained with the model applied. However, it is important to consider that the Case 3 modelling did not include any attempt to fit the model to the aqueous data.*

Table 4-3. Case 3. Results from estimation of F_f for various tracers based on *in situ* experimental data from the penetration profiles. Estimated average values combined with the minimum and maximum values are provided for the different core sample groups. n refers to the number of sample cores used in the modelling. K_d (m^3/kg) was fixed during each fitting procedure and the values used are presented in the table. A: Fracture mineral coated cores, B: Matrix rock.

Tracer	K_d (Fixed to batch laboratory sorption values) m^3/kg		F_f, estimated from modelling of the core penetration profile		
			A-samples		D-samples
			Fracture mineral coated cores (A)	Matrix rock (B)	Matrix rock (B)
Na-22		average	4.2E–4	5.4E–4	6.4E–4
	A: 1.2E-4	min	6.0E–5	3.4E–4	4.2E–4
		max	9.2E–4	7.5E–4	8.4E–4
	B: 2.9E-4	n	7	3	8
Ni-63		average	1.6E–2		1.4E–3
	A: 1.6E-1	min	6.3E–3		8.8E–4
		max	3.7E–2		2.2E–3
	B: 1.5E-2	n	4		4
Ba-133		average	3.0E–3	2.9E–4	3.9E–4
	A: 1.2E-2	min	1.1E–3		3.0E–4
		max	4.9E–3		5.5E–4
	B: 2.1E-3	n	2	1	3
Cs-137		average	3.8E–2	1.6E–3	7.1E–3
	A: 4.8E-1	min	1.4E–2	1.0E–3	5.2E–4
		max	6.3E–2	2.5E–3	4.3E–2
	B: 2.2E-2	n	2	3	8
Co-57		average	2.7E–2	3.8E–3	6.2E–3
	A: 4.0E-1	min	2.7E–2		2.4E–3
		max	2.8E–2		1.1E–2
	B: 5.0E-2	n	2	1	3
Cd-109		average	1.9E–3		
	A: 5.9E-2	min	1.6E–3		
		max	2.2E–3		
	B: 5.1E-3	n	2		
Comparison, F_f obtained by separate diffusion measurements					
Matrix rock, LTDE-SD, /Widestrand et al. 2010a/				2.2E–5	2.2E–5
Maximum value, /Vilks et al. 2005/			4.8E–4		

When comparing the formation factors obtained from the modelling of the different tracers, two important observations can be made:

- The values are much higher (typically 1–3 orders of magnitudes) than the values obtained from the different independently performed diffusion measurements, e.g. through diffusion experiment with tritiated water /Widestand et al. 2010b/ and uranine/iodide diffusion on intact core /Vilks et al. 2005/. It is obvious that one has to allow a higher diffusivity (i.e. higher formation factor) than the laboratory determined values in order to explain the experimentally obtained diffusion profiles.
- A clear trend of increasing modelled formation factor with increasing sorption strength is observed. This must be regarded as a conceptual inconsistency as the formation factor should, with application of a homogenous matrix diffusion/sorption model, be independent of the sorption strength, i.e. the same for every tracer studied.

4.2.3 Case 4

In this modelling calculation, denoted Case 4, all three parameters, K_d (m^3/kg), F_f and ε, were varied simultaneously to obtain as good a fit as possible to the measured *in situ* penetration profiles. As for Case 2 and Case 3, only the measured penetration profile data were used in the model fitting and no address of the corresponding measured aqueous phase data was made. The results are summarised in Table 4-4.

As was realized at an early stage (an analogy to the discussion presented for Case 3) ε and K_d only influence the model calculation in terms of their respective contribution to the $(\varepsilon + K_d\rho)$. It is therefore not possible in the fitting calculation to identify individual values of both these parameters, i.e. only a lumped value of the capacity factor $(\varepsilon + K_d\rho)$ can be identified. However, due to the physical restrictions of the porosity $(0 < \varepsilon < 1)$ one can for the majority of the tracers studied neglect the contribution of ε to the $(\varepsilon + K_d\rho)$ term and thereby calculate the K_d value; this procedure has been applied to the values presented in Table 4-4. However, as is the case for ^{22}Na, with very low values of the $(\varepsilon + K_d\rho)$ term (i.e. low sorption), this assumption is somewhat questionable and may cause an overestimation of the K_d presented for Na. However, the $(\varepsilon + K_d\rho)$ term values obtained in the modelling for ^{22}Na are presented in Appendix 10.

Table 4-4. Case 4. Results from simultaneous estimation of K_d (m^3/kg) and F_f for various tracers based on *in situ* experimental data from the core penetration profiles. In all calculations, it has been assumed that the porosity contribution to the capacity factor is negligible. Estimated average values combined with minimum and maximum values are provided for the different core sample groups, n refers to the number of core samples used in the modelling of that particular rock sample type.

Tracer		K_d (m^3/kg), estimated from the core penetration profile			K_d (m^3/kg), batch lab. exp. for comp.	F_f, estimated from the core penetration profile		
		A-samples		D-samples		A-samples		D-samples
		Fracture mineral coated cores	Matrix rock	Matrix rock	A-Fracture mineral coated rock, B-Matrix rock	Fracture mineral coated cores	Matrix rock	Matrix rock
Na-22	average	5.5E–5	1.6E–5	9.2E–6	A:1.2E–4	7.5E–5	8.7E–5	9.0E–5
	Min	2.9E–6	4.4E–6	4.8E–6		3.7E–5	2.5E–5	3.5E–5
	Max	3.5E–4	3.7E–5	1.3E–5	B: 2.9E–4	1.0E–4	2.0E–4	1.4E–4
	n	7	3	8		7	3	8
Ni-63	average	1.4E–3		6.2E–4	A:1.6E–1	2.6E–4		8.2E–5
	Min	5.1E–4		1.9E–4		6.5E–5		4.1E–5
	Max	2.7E–3		1.1E–3	B:1.5E–2	7.1E–4		1.4E–4
	n	4		4		4		4
Ba-133	average	4.9E–4	9.3E–4	7.8E–4	A:1.2E–2	9.5E–5	1.9E–4	2.1E–4
	Min	9.4E–5	9.3E–4	3.8E–4		5.1E–5	1.9E–4	1.2E–4
	Max	8.9E–4	9.3E–4	1.2E–3	B:2.1E–3	1.4E–4	1.9E–4	2.9E–4
	n	2	1	3		2	1	3
Cs-137	average	6.7E–2	3.8E–3	4.0E–3	A:4.8E–1	8.6E–3	5.3E–4	3.7E–4
	Min	8.5E–4	2.2E–3	1.4E–3		5.6E–5	2.0E–4	1.3E–4
	Max	4.4E–1	6.8E–3	1.5E–2	B:2.2E–2	5.9E–2	1.2E–3	1.1E–3
	n	7	3	8		7	3	8
Co-57	average	1.5E–4	5.2E–4	4.1E–4	A:4.0E–1	1.3E–5	8.1E–5	8.4E–5
	Min	1.5E–5	5.2E–4	2.4E–5		7.2E–6	8.1E–5	5.6E–6
	Max	2.9E–4	5.2E–4	8.6E–4	B:5.0E–2	1.9E–5	8.1E–5	1.6E–4
	n	2	1	3		2	1	3
Cd-109	average	2.6E–4			A:5.9E–2	3.6E–5		
	Min	4.3E–5				1.9E–5		
	Max	4.8E–4			B:5.1E–3	5.3E–5		
	n	2				2		
Comparison, F_f obtained by separate diffusion measurements								
Matrix rock, LTDE-SD, /Widestrand et al. 2010a/							2.2E–5	2.2E–5
Maximum value, /Vilks et al. 2005/						4.8E–4		

The figures below (Figure 4-21 and Figure 4-22) exemplify the results for Na and Cs. In figures in Appendix 9 the entire results can be found.

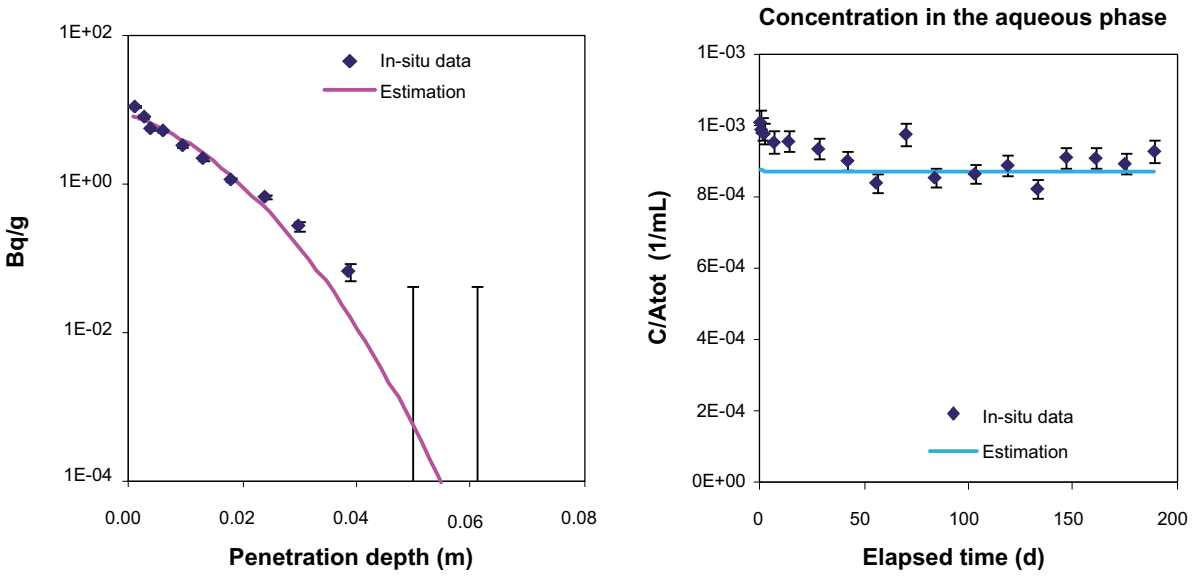

Figure 4-21. *Illustration of the outcome of a Case 4 modelling, ^{22}Na diffusion in A10 core. The left figure illustrates the fit of the calculated penetration profile to the experimentally measured data. The right figure illustrates the corresponding loss of tracers in the aqueous phase obtained with the model applied. However, it is important to consider that the Case 4 modelling did not include any attempt to fit the model to the aqueous data.*

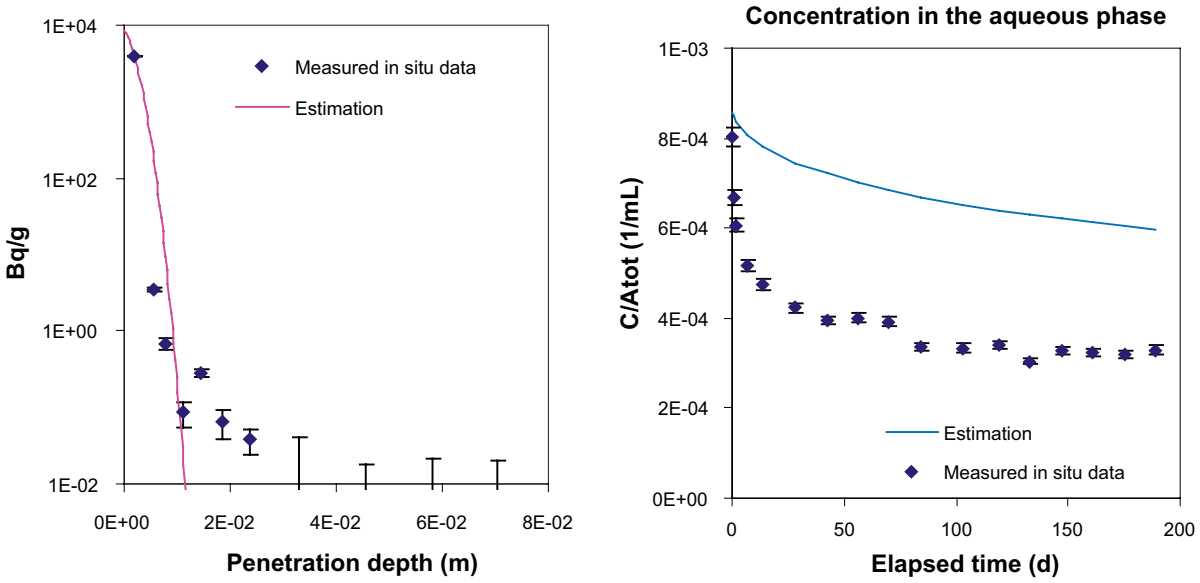

Figure 4-22. *Illustration of the outcome of a Case 4 modelling, ^{137}Cs diffusion in D7 core. The left figure illustrates the fit of the calculated penetration profile to the experimentally measured data. The right figure illustrates the corresponding loss of tracers in the aqueous phase obtained with the model applied. However, it is important to consider that the Case 4 modelling did not include any attempt to fit the model to the aqueous data.*

4.2.4 Case 5

A further modelling attempt, denoted Case 5 in Table 2-3, was performed in which all the retention parameters, i.e. K_d, F_f and ε were varied simultaneously in order to fit the experimental data. However, in this case the concentration of the tracers in the aqueous phase was also incorporated in the modelling, i.e. the data sets of the aqueous concentration and the penetration profiles were both used for fitting calculation of the retention parameters. Further information concerning the measurements of the water phase concentrations can be found in /Widestrand et al. 2010b/.

This modelling attempt was considered meaningful only for the tracers where the sorption was high enough to enable an observable loss in the aqueous phase, but still low enough to allow diffusion reaching some of the inner slices of the penetration profiles. For this reason, the ^{137}Cs and the ^{63}Ni data were exclusively selected for performing this Case 5 exercise. As for Case 4, no unique values of ε and K_d could be identified from the modelling; this since they both influence the diffusion calculation only by their contribution to the ($\varepsilon + K_d \rho$). However, particularly in the present case, when only using the relatively strongly sorbing tracers ^{63}Ni and ^{137}Cs, the neglect of the ε versus the $K_d \cdot \rho$ can be very well motivated and K_d for this case is therefore calculated using the assumption that $\varepsilon << K_d \rho$. The results are presented in Table 4-5 and in Appendix 9 and 10.

Table 4-5. Case 5. Results from simultaneous estimation of K_d (m³/kg), F_f and ε for various tracers based on *in situ* experimental data from both the core penetration profiles and the aqueous concentration-time curves. Estimated average values combined with minimum and maximum values are provided for the different core sample groups, n refers to the number of core samples, where the radioactivity measurement gave values above the detection limits.

Tracer		K_d (m³/kg), estimated from both the core penetration profile and the aqueous concentration-time curve			F_f, estimated from both the core penetration profile and the aqueous concentration-time curve		
		A-samples		D-samples	A-samples		D-samples
		Fracture mineral coated cores	Matrix rock	Matrix rock	Fracture mineral coated cores	Matrix rock	Matrix rock
Ni-63	average	5.3E–3		4.6E–4	2.5E–3		7.6E–5
	min	2.8E–4		2.5E–4	2.7E–5		7.2E–5
	max	1.3E–2		6.5E–4	4.1E–3		8.1E–5
	n	3		3	3		3
Cs-137	average	8.4E–3		4.1E–3	1.7E–3		3.5E–4
	min	2.4E–3		2.4E–3	4.5E–4		1.7E–4
	max	1.8E–2		5.9E–3	2.6E–3		4.5E–4
	n	3		3	3		3

4.3 Summary of modelling results

A general condition applicable to the modelling performed within this work is that in almost every case, some measured values located at distance into the rock matrix have been omitted in the fitting calculations (further described in Section 4.2). One can from the results easily realize that a homogeneous diffusion process cannot explain the low concentration plateau most often seen several cm into the rock matrix. It was thus realized that modelling using all data with equal weighing of all measurement data would not be tractable. A general concept was therefore set up in which data points where the calculated slope (concentration v/s distance) is lower than –5 for this point and all points at longer distance are excluded from the calculation. Using this approximation, the modelling would include >99% of the adsorbed tracers but nevertheless it has to be acknowledged that a readily identifiable fast (but not yet determined) minor migration process has been omitted in the modelling.

4.3.1 Estimation of K_d with fixed diffusivity (Case 2)

The result of the modelling using the results of the penetration profiles with fixed laboratory values of diffusivity and variation of the K_d is shown in Table 4-2. It is obvious that the K_d:s have to be set comparatively low (typically 1–2 orders of magnitudes lower than the corresponding batch laboratory sorption values) in order to obtain a better agreement with the measured penetration profiles. The reason for this is probably the comparatively high concentrations of sorbing tracers found in the second and third slice (~4–8 mm penetration depth) which cannot be explained using the laboratory batch sorption measured K_d:s.

Comparing the K_d values from this modelling to the "conservative" estimates made from simple measurements of solid and aqueous phase presented in Section 4.4, it is somewhat unexpectedly observed that the presumably conservative method yields higher K_d:s than the modelling. The reason for this is that the modelling presented in Section 4.2.1 does not include the results measured for water phase tracer concentrations. For sorbing tracers like Cs and Ni, the model approach used is thus given the freedom to apply low K_d:s to explain the tracer penetration several mm into the rock matrix. The mismatch in the water phase (low K_d modelling giving almost no decrease in the water phase while experimental data is showing ~50% loss of tracer in the aqueous phase) is not addressed in this modelling which thus favors solutions of low K_d:s. The conservative estimate method addresses the actually measured concentration of the aqueous phase and this is probably the reason for obtaining higher K_d:s from this estimate compared with the modelling.

This interpretation is in line with the modelling presented in the LTDE-SD laboratory report /Widestrand et al. 2010a/ where diffusion modelling was performed in a reversed mode; including only the aqueous data. In this work, the sorption coefficients obtained from modelling were generally much higher than what was obtained from corresponding batch laboratory experiment.

4.3.2 Estimation of diffusivity (formation factor) with fixed K_d (Case 3)

The results of the estimation of diffusivities (i.e. the formation factor) using the experimental results of the penetration profiles together with a fixed value of the K_d:s from the batch laboratory experiment, are presented in Table 4-3. One can compare this to the results of the through diffusion results which gave formation factors of 2E–5 for intact rock and 5E–4 for surface material. It is obvious that one has to increase the diffusivity 1–2 orders of magnitudes to explain the tracer content of sorbing tracer several mm in to the rock matrix (cf. the predictions in Section 4.1). It is possible that the increased diffusivity could be a result of an increased porosity or connectivity in the immediate first mm of the rock closest to the water-rock interface, this since the majority of the interaction of sorbing tracers in this study is restricted to this interface. The through diffusion experiments address diffusion in scales of several cm and it is possible that theses values have not been influenced by increased connectivity in the rock closest to the water-rock interface. /Widestrand et al. 2010a/

One should, as mentioned earlier, acknowledge that the shape of the penetration profiles give rather poor agreement with a theoretical model of homogeneous diffusion; there is obviously an influence of heterogeneity in the diffusion.

Estimation of porosity has also been made but, as expected, this parameter is in almost every case totally insensitive to the results. This since the $K_d \cdot \rho$ parameter is orders of magnitude higher than the porosity when dealing with cations and therefore always dominate in the capacity factor. For the case of the anions, it is referred to the Section 4.6 where a similar exercise is performed and compared to the possibility of anion exclusion influencing the results

4.3.3 Estimation of both the diffusivity and the K_d (Case 4 and Case 5)

For the majority of the tracers, the modelling using two estimation parameters (cf. Table 4-4) gives somewhat lower K_d:s and also somewhat lower formation factors compared with the cases when they are calculated individually using fixed F_f (Case 2) and fixed K_d (Case 3). However, the modelling using two estimation parameters on the relatively few number of data points (typically 3–6) is suspected to give too large degree of freedom to the fitting procedure, which can be the reason for the comparatively high variation of the values obtained.

For the sorbing tracers like ^{57}Co and ^{109}Cd, comparatively low K_d-values were obtained which at first glance is quite unexpected. However, samples with more than one data point have selectively been chosen for the modelling. If the corresponding water phase data is checked, the prediction using such low K_d predicts that there should be almost no loss of tracer from the aqueous phase, an observation that is clearly contradicted by the measured results.

The modelling performed in Case 5 (cf. Section 4.2.4) differs from Case 4 in that this case also addresses the data for the time dependence of the tracer loss in the aqueous phase. In most cases, it is difficult to obtain a reasonable fit for both data sets. This can be regarded as an illustration of the general outcome of comparing the modelling of the results of the rock phase (this report) with the results of the modelling of the results of the aqueous phase /Widestrand et al. 2010b/; one has to apply low K_d values to explain the rather long penetration distance in to the rock and has to apply high K_d values to explain the rather high losses from the aqueous phase.

4.4 Conservative K_d-estimations

The K_d factor (e.g. the equilibrium ratio of the tracer concentration in the rock phase and the water phase) is an important entity used for safety analysis calculations. Since it requires that equilibrium has been reached and since the diffusion rates in the rock matrix are very low, the present LTDE-SD *in situ* experiment is not very well designed for a direct measurement of the *in situ*-derived K_d (i.e. combined measurement of the rock and water concentration of the tracers). A better methodology for determining the K_d in this experiment requires modelling of the combined diffusion and sorption processes (cf. Section 4.2 and 4.3).

As an alternative to the modelling approaches described in previous sections, attempts will be presented describing methods using measured data of the tracer concentrations in the rock and the water phase to make conservative estimates of the K_d. These methods are aimed to make simplified use of the obtained data from the LTDE-SD experiment as an estimate of the "minimum amount of sorption that can be proven" in the experiment, without having to make any modelling assumptions.

1. The conservative K_d estimates in this report are obtained using three different concepts: In the cases where the drill core has been sliced, the tracer concentration (Bq/kg) in the slice closest to the surface is divided by the concentration in the water phase (Bq/m^3) at the end of the circulation phase of the LTDE-SD to give the K_d (m^3/kg).
2. Based on the results of the slice measurements, one can generally conclude that the vast majority of the adsorbed tracers can be found <5 mm into the matrix (possibly with ^{22}Na as an exception). Based on this observation a conservative estimate of K_d can be approximated by dividing the measured amount of tracer in the first 5 mm of the 24 mm diameter core (6 g); this divided by the last measured tracer concentration in the water phase. In the cases where only measurements of the entire non-sliced core are available (process described below), the measured tracer amount has conservatively been assumed to be homogeneously distributed in the 5 mm of the drill core to obtain the tracer concentration in the rock. This concentration has been divided by the water phase concentration, as described in the preceding bullet.

The latter method is based on data from measurements on the entire core (Appendix 8) for the cases where no measurements of the sliced core were available. Since these measurements were performed long before the slice measurements were done, results from some comparatively short-lived radio-isotopes (e.g. the tetravalent ^{175}Hf) could be used in these measurements.

The results of the two methods for using the analysis of the rock material for conservative K_d estimation are presented in Table 4-6 and Table 4-7, respectively.

Table 4-6. Conservative estimates of the K_d using the analyses of the rock material in combination with the analyses of the water phase at the end of the circulation part of the LTDE-SD experiment. In this table, K_d are calculated using tracer concentration (Bq/kg) in the first slice of the sample profile divided by the tracer concentration in the water phase (Bq/m³) at the end of the experiment. n refers to the number of samples included in the modelling. Comparisons are made with the K_d:s determined by the batch sorption experiments /Widestrand et al. 2010a/.

Tracer		K_d (m³/kg), estimated from the *in situ* core penetration profile, modelling results.			K_d (m³/kg) from batch sorption laboratory measurements, for comparison.	
		A-cores		D-cores		
		Fracture mineral coated cores	Matrix rock	Matrix rock	Crushed rock from fracture mineral coated cores	Crushed matrix rock
Na-22	average	9.1E–6	6.2E–6	1.1E–5	<1E–3[1)]	2.9E–4
	min	3.9E–6	5.1E–6	5.4E–6		1.7E–4
	max	2.5E–5	8.1E–6	2.0E–5		4.2E–4
	n	7	3	8		3
Ni-63	average	1.4E–3		7.0E–4	1.6E–1	1.5E–2
	min	8.7E–4		4.6E–4	4.6E–2	8.2E–3
	max	2.0E–3		8.5E–4	2.7E–1	2.5E–2
	n	5		4	2	3
Ba-133	average	5.0E–4	5.8E–4	6.7E–4	1.2E–2	2.1E–3
	min	2.1E–4	5.7E–4	4.0E–5	9.8E–3	2.0E–3
	max	8.7E–4	6.1E–4	9.7E–8	1.5E–2	2.3E–3
	n	7	3	3	2	3
Cs-137	average	3.2E–3	3.6E–3	3.2E–3	4.8E–1	2.2E–2
	min	1.4E–3	2.6E–3	2.0E–3	1.0E–1	1.2E–2
	max	8.7E–3	4.4E–3	5.7E–3	8.6E–1	3.2E–2
	n	7	3	8	2	3
Co-57	average	1.0E–2	2.6E–2	1.4E–2	4.0E–1	5.0E–2
	min	9.7E–4	9.3E–3	1.4E–3	2.7E–1	3.6E–2
	max	1.5E–2	3.8E–2	3.2E–2	5.3E–1	6.1E–2
	n	7	3	8	2	3
Cd-109	average	1.3E–3	8.1E–4	1.2E–3	5.9E–2	5.1E–3
	min	2.1E–4	5.8E–9	6.6E–4	2.6E–2	4.0E–3
	max	2.0E–3	1.2E–3	2.5E–3	9.2E–2	5.9E–3
	n	7	3	8	2	3
Gd-153	average	5.3E–2	7.7E–2	2.7E–2	>4E–1[2)]	>4E–1[2)]
	min	<2.6E–2	4.9E–2	1.1E–2		
	max	8.7E–2	1.2E–1	4.4E–2		
	n	7	3	8		
Ag-110m	average	1.2E–1	1.6E–1	1.9E–2	>1E–2[2)]	>1E–2[2)]
	min	<3.3E–2	1.2E–1	<6.4E–3		
	max	2.3E–1	2.5E–1	2.9E–2		
	n	7	3	8		
Ra-226	average	1.7E–3	2.5E–3	2.3E–3	5.6E–2	7.5E–3
	min	6.3E–4	2.1E–3	1.6E–3	3.7E–2	6.7E–3
	max	3.0E–3	3.0E–3	3.8E–3	7.5E–2	8.3E–3
	n	7	3	8	2	3

[1)] It was not possible to statistically verify any decrease of tracer concentration in the aqueous phase. Hence, a value of K_d could not be calculated as if the counting statistics were below the detection limit.

[2)] All tracer added in the experiment was found to sorb on the rock material. The value is based on the detection limit in the aqueous phase measurement.

Table 4-7. Conservative estimates of the K_d using the analyses of the rock material in combination with the analyses of the water phase at the end of the circulation part of the LTDE-SD experiment. In this table, K_d are calculated by assuming that all tracer measured in the rock material is homogenously distributed in the first 5 mm of the rock samples. The obtained tracer concentration (Bq/kg) was then divided by the tracer concentration in the water phase (Bq/m³) at the end of the experiment.

		A-cores		D-cores
		Fracture mineral coated cores	Matrix rock	Matrix rock
Na-22	average	1.2E–5	1.1E–5	1.4E–5
	min	5.7E–6	5.7E–6	1.1E–5
	max	2.6E–5	1.6E–5	1.9E–5
Co-57	average	4.7E–3	5.4E–3	1.1E–2
	min	3.1E–4	1.8E–3	2.3E–3
	max	1.1E–2	7.5E–3	2.9E–2
Se-75	average	1.1E–4	1.2E–4	4.6E–5
	min	6.9E–5	<7.4E–5	2.4E–5
	max	1.4E–4	1.5E–4	1.2E–4
Sr-85		<3.2E–5	<3.1E–5	<6.7E–5
Cd-109	average	6.2E–4	5.8E–4	5.2E–4
	min	6.2E–5	4.1E–4	2.1E–4
	Max	1.2E–3	8.2E–4	1.1E–3
Ag-110m	average	5.3E–2	4.4E–2	<4.2E–2
	Min	2.0E–2	1.5E–2	
	Max	1.1E–1	7.1E–2	
Ba-133	average	3.0E–4	3.1E–4	2.3E–4
	Min	6.7E–5	2.0E–4	1.2E–4
	Max	8.5E–4	4.9E–4	3.4E–4
Cs-137	average	1.3E–3	1.6E–3	1.1E–3
	Min	4.4E–4	1.1E–3	6.8E–4
	max	3.4E–3	2.9E–3	1.6E–3
Gd-153	average	2.8E–2	2.7E–2	1.4E–2
	min	1.3E–2	1.6E–2	3.5E–3
	max	4.2E–2	4.4E–2	3.5E–2
Hf-175	max	<3.3E–2	<2.5E–2	<2.2E–2
Ra-226	average	9.3E–4	1.1E–3	9.4E–4
	min	2.0E–4	6.4E–4	4.6E–4
	max	2.6E–3	1.7E–3	1.4E–3
	n	12	6	16

4.5 Summary of the retention parameter estimation

As a general conclusion, there is an agreement of the results to the sorption behaviour predicted from the LTDE-SD laboratory program and also to the general knowledge of tracer behavior, i.e. the sorption strength observed in laboratory experiment is the same as approximated from the different penetration distances observed in the diffusion results. Nevertheless, one must acknowledge the obvious problem to model the results with a single diffusion rate. For the very weakly-sorbing and non-sorbing tracers (e.g. ^{22}Na and ^{36}Cl) very low concentrations of the tracers were found in the first slices closest to the water-rock interface. The concentrations decrease comparatively slowly from the rock surface and into the rock. The moderately sorbing tracers (e.g. ^{137}Cs, ^{63}Ni and ^{133}Ba) are present at quite high concentrations in the first slices and, for most cases, decrease to a level 3–4 orders of magnitudes lower than the surface concentration already after 3–4 slices. For the very strongly sorbing tracer, e.g. ^{153}Gd, activities can only be measured in the first slices. The results can therefore be regarded as confirmation of a combined sorption/diffusion process taking place in the rock; a process that is dependent on the retention parameters (diffusivity and sorption) that can be determined in independently performed laboratory experiments.

4.5.1 Predictions using the laboratory values for diffusivity, porosity and K_d

For the very weakly sorbing or non-sorbing tracers (e.g. ^{36}Cl and ^{22}Na), measured tracer concentrations in the rock phase are ~1 order of magnitude lower than what is predicted from the laboratory measurements of the porosity, diffusivity and the sorption. One can speculate that the isopropanol rinsing and/or the accidental exposure of the stub surface to the drilling water during the extraction process might have caused back-diffusion and/or desorption of the tracers present at the water-rock interface.

An additional general observation concerning the non- or weakly-sorbing tracers is that the shape of the penetration profiles deviates strongly from the diffusion process predicted by modelling. This is particularly pronounced for the A6-sample. In the modelling of the diffusion of non-altered matrix rock of Äspö diorite and fine-grained granite /Johansson et al. 2000/ it was shown that an introduction of the effect of heterogeneously distributed porosity gave penetration profiles with straight lines in lin-log space; in the present case it is indicated that the effect of heterogeneity could be even more pronounced. This is not surprising since the fracture samples are probably more influenced by microfractures etc than the intact rock that was used in the work of /Johansson et al. 2000/. No numerical modelling addressing heterogeneous diffusion has been performed for the LTDE-SD results but the qualitative results of the PMMA porosity measurements /Widestrand et al. 2010b/ and the radioactive tracer distribution studies using autoradiography support the hypothesis of heterogeneity playing an important role.

Concerning the more strongly sorbing tracers (here exemplified by ^{63}Ni and ^{137}Cs) the predicted penetration profiles show that one should expect penetration depths only parts of mm and that already at the second slice there should be no measurable tracer concentration. However, as for the other tracers, a plot in the log scale shows that there is a small part of the tracer reaching much longer into the matrix than what is expected from a homogeneous diffusion/sorption-model. A plausible explanation for the general heterogeneous pattern could be a heterogeneous distribution of porosity, e.g. existence of microfractures combined with an increased number of dead-end pores in the rock closest to the water-rock interface.

One also has to consider the possibility that contamination during the drilling might have caused the e.g. Cs concentration plateau that is abundant in almost every measured drill core. (This topic is further discussed in Section 3.3 /Appendix 11).

A very premature modelling attempt addressing a heterogeneous approach is presented below in Figure 4-23. In this exercise the tailing part of the ^{137}Cs diffusion in sample A6 has been selectively used for fitting diffusion parameters (i.e. K_d, F_f and ε) to describe an additional diffusion which can explain the tracer found several cm in to the matrix. In the presentation in Figure 4-23, the results of this process is given in addition to the results of the similar exercise performed for this sample in case 5, i.e. varying K_d, F_f and ε in order to obtain a fit of the first part of the penetration profile. As can be seen, in order to obtain a fit of the tailing of the penetration profile curve, it is necessary to apply a process with more or less no sorption is occurring i.e. where (opposite to the case 5) the $K_d\rho$ term is negligible to the ε term. Nevertheless, the diffusivity obtained when fitting this tailing process shows a value that is in agreement with what has been observed in laboratory experiment, an observation that supports the explanation of the tailing being a result of diffusion.

It must be emphasized that this modelling attempt utilizes 6 fitting parameters (however, two of them shown to be insensitive) and that there is no independent data determining that the diffusion should be described as a two pathway process. Hence, the relatively good agreement between the model and the experimental results should be treated with care and should only be interpreted that the experimental results are possible to explain by diffusion processes.

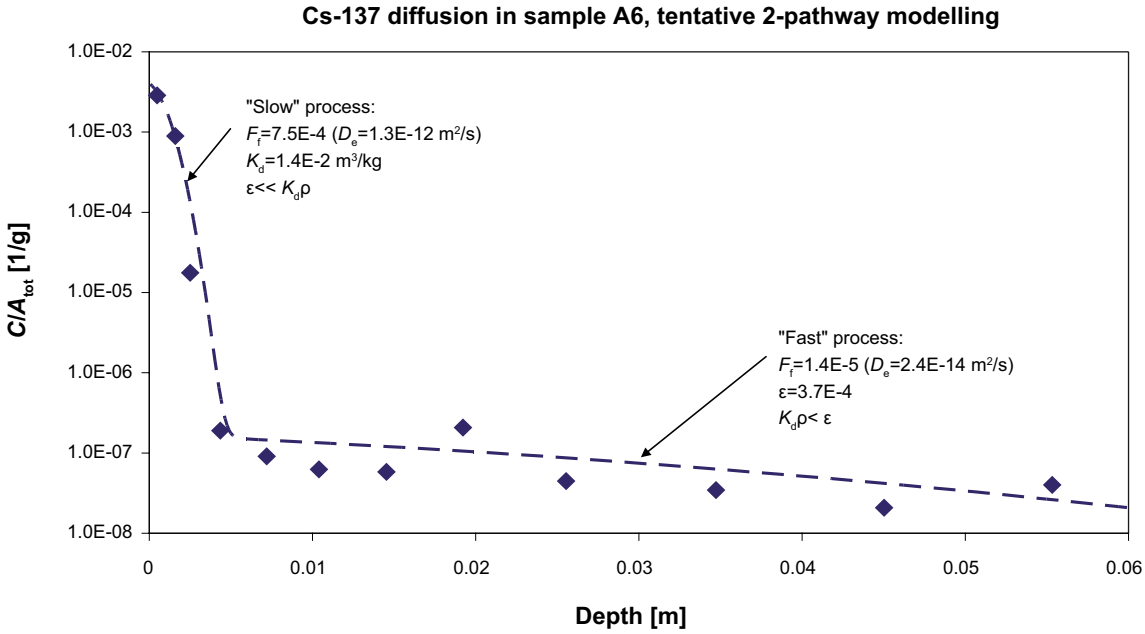

Figure 4-23. *Results of a tentative modelling using a two pathway model. The modelling is performed only in order to investigate to what extent the tailing observed can be explained with realistic diffusion rates using a heterogeneous multi-rate model. No actual justification of the existence of a double pathway diffusion with the given parameter values is thus claimed by the presentation of the figure.*

4.5.2 K_d comparisons

A general comparison of the results of the different K_d estimations performed within the LTDE-SD project is presented in Figure 4-24; given as the minimum and maximum range obtained using different techniques. For comparison, a selection has been made including only a few number of the tracers studied; a selection made in order to obtain a representation of tracers with different characteristics (e.g. oxidation states, sorption mechanisms and/or sorption strength).

For the diffusion techniques where no individual values of K_d and F_f can be identified (i.e. where the tracer loss in the aqueous phase is dependent of the lumped $K_d \cdot F_f$ product), a complementary data representation (Figure 4-25) is also given where the $K_d \cdot F_f$ product is used for comparison between the different methods. The numerical values of the comparisons are given in Table 4-8 and Table 4-9.

It has been pointed out earlier that a general trend is that the modelling case where only the measurements of the aqueous phase are used give the highest K_d values of the different methods in the comparison. It has been indicated that, especially for strongly sorbing tracers, there is an influence of losses in the aqueous phase not directly proven to be rock-water interactions, which could be identified as a source of overestimations. Examples of such potential processes are sorption on equipment parts, interactions with small particles e.g. ferric oxides formed due to not maintaining sufficient reducing conditions during the experiment, etc. The laboratory sorption experiments give results in the same range which is not surprising since this technique also is restricted to studies of the loss in the aqueous phase.

As a comparison, K_d obtained from modelling knowing only the rate of loss of tracer from the aqueous phase /Widestrand et al. 2010b/ (i.e. excluding all information from the solid phase measurements) has also been calculated.

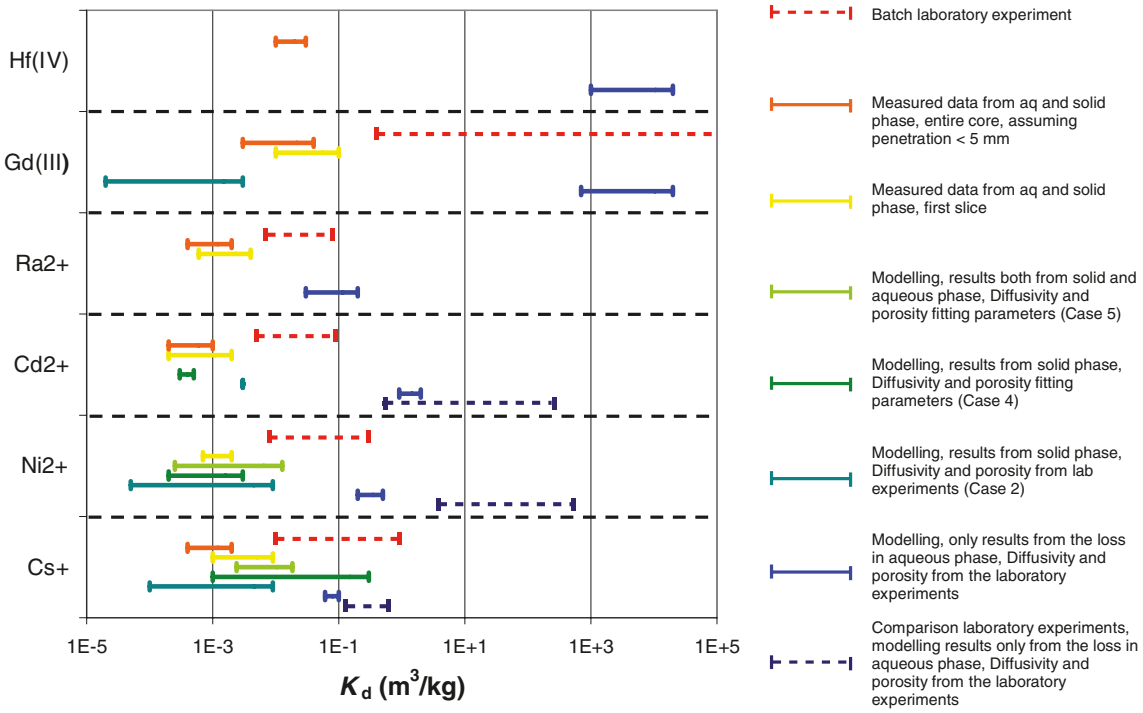

Figure 4-24. *Comparison of the K_d value intervals determined by the different techniques applied within the LTDE-SD experiment, cf. text for details. Besides the evaluation performed for the results of the* in situ *experiments, a comparison is also made to batch laboratory experiments and laboratory experiments with sorption on entire drill cores /Widestrand et al. 2010a/.*

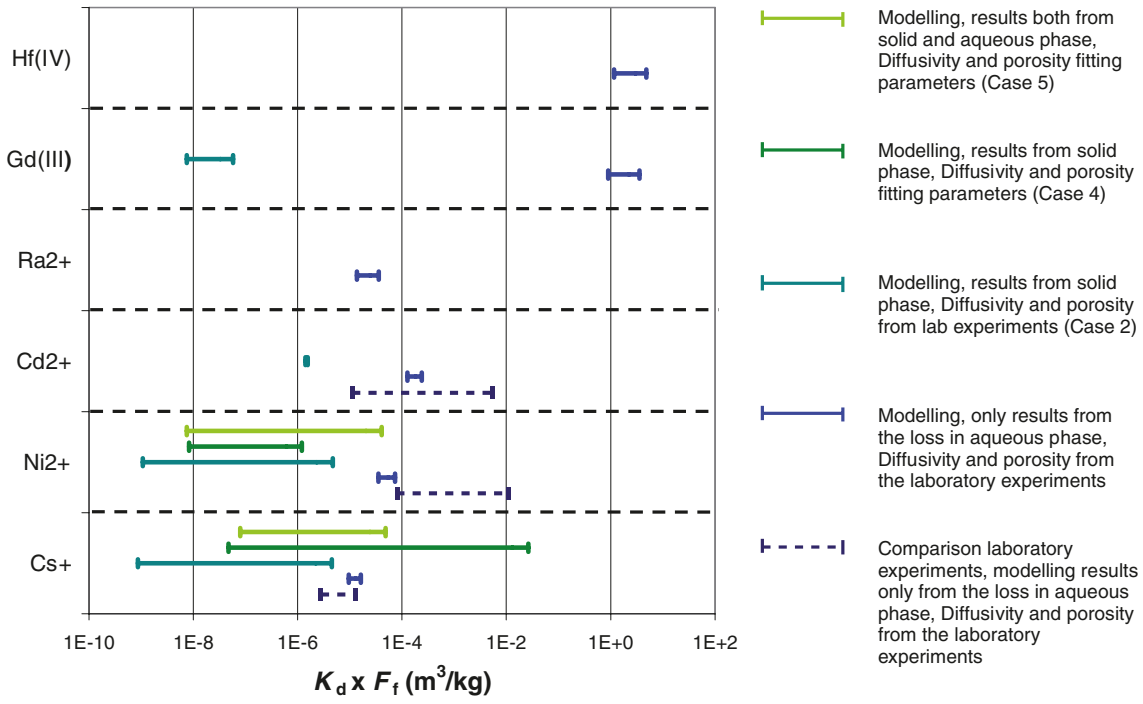

Figure 4-25. *Comparison of the intervals $K_d \cdot F_f$ (m3/kg) values determined by the different techniques applied within the LTDE-SD experiment, cf. text for details. Besides the evaluation performed for the results of the* in situ *experiments, a comparison is also made to laboratory experiments with sorption on entire drill cores /Widestrand et al. 2010a/.*

Table 4-8. Comparison of maximum and minimum K_d (m^3/kg) for selected tracers obtained by the different methods applied within the LTDE-SD experiments.

	Modelling, only results from the loss in aqueous phase /Widestrand et al. 2010b/, D_e and ε from the laboratory experiment		Comparison laboratory experiments /Widestrand et al. 2010a/, modelling results only from the loss in aqueous phase, D_e and ε from the laboratory experiment		Modelling, results from solid phase, D_e and ε from lab experiment (Case 2)		Modelling, results from solid phase, D_e and ε fitting parameter (Case 4)	
	Min	Max	Min	Max	Min	Max	Min	Max
Cs^+	6.0E–2	1.0E–1	1.3E–1	6.2E–1	1.0E–4	9.0E–3	1.0E–3	3.0E–1
Ni^{2+}	2.0E–1	5.0E–1	3.8E+0	5.3E+2	5.0E–5	9.0E–3	2.0E–4	3.0E–3
Cd^{2+}	9.0E–1	2.0E+0	5.4E–1	2.6E+2	3.0E–3	3.0E–3	3.0E–4	5.0E–4
Ra^{2+}	3.0E–2	2.0E–1						
Gd(III)	7.0E+2	2.0E+4			2.0E–5	3.0E–3		
Hf(IV)	1.0E+3	2.0E+4						
	Modelling, results from solid phase and aqueous phase, *D*e and ε fitting parameter (Case 5)		**Measured data from aqueous and solid phase, first slice**		**Measured data from aqueous and solid phase, entire core, assuming penetration < 5 mm**		**Batch laboratory experiment /Widestrand et al. 2010a/**	
Cs^+	2.4E–3	1.8E–2	1.0E–3	9.0E–3	4.0E–4	2.0E–3	1.0E–2	9.0E–1
Ni^{2+}	2.5E–4	1.3E–2	7.0E–4	2.0E–3	Not measured		8.0E–3	3.0E–1
Cd^{2+}			2.0E–4	2.0E–3	2.0E–4	1.0E–3	5.0E–3	9.0E–2
Ra^{2+}			6.0E–4	4.0E–3	4.0E–4	2.0E–3	7.0E–3	8.0E–2
Gd(III)			1.0E–2	1.0E–1	3.0E–3	4.0E–2	4.0E–1	1.0E+6
Hf(IV)					1.0E–2	3.0E–2		

Table 4-9. Comparison of maximum and minimum $K_d \cdot F_f$ (m^3/kg) for selected tracers obtained by the different methods applied within the LTDE-SD experiments.

	Modelling, only results from the loss in aqueous phase, D_e and ε from the laboratory experiment		Comparison laboratory experiments, modelling results only from the loss in aqueous phase, D_e and ε from the laboratory experiment		Modelling, results from solid phase, D_e and ε from lab experiment (Case 2)		Modelling, results from solid phase, D_e and ε fitting parameter (Case 4)		Modelling, results from aqueous phase and solid phase, D_e and ε fitting parameter (Case 5)	
	Min	Max	Min	Max	Min	Max	Min	Max	Min	Max
Cs^+	9.5E–6	1.6E–5	2.7E–6	1.3E–5	8.7E–10	4.5E–6	4.7E–8	2.6E–2	7.9E–8	4.9E–5
Ni^{2+}	3.5E–5	7.3E–5	8.0E–5	1.1E–2	1.1E–9	4.7E–6	8.3E–9	1.2E–6	7.4E–9	4.1E–5
Cd^{2+}	1.3E–4	2.4E–4	1.1E–5	5.5E–3	1.4E–6	1.5E–6				
Ra^{2+}	1.4E–5	3.6E–5								
Gd(III)	9.0E–1	3.6E+0			7.5E–9	5.8E–8				
Hf(IV)	1.2E+0	4.8E+0								

The technique that is associated with the lowest K_d-values is the modelling using only the penetration profile data. The fact that the penetration depth is much larger than what should be expected from homogeneous sorption (in most cases shorter than mm) makes it necessary to apply a low K_d in order to explain the penetration curves, e.g. Cs reaching up to ~1 cm into the rock. These low K_d-values cannot reproduce the actual loss of tracer observed in the aqueous phase which is an indication that this technique is suspected to underestimate the real K_d. Combining this observation with the results of the modelling using only the water phase results, it is thus quite obvious that there exists a conceptual uncertainty when applying a homogeneous matrix diffusion sorption concept.

A possible explanation to this could be the presence of heterogeneously distributed porosity, i.e. presence of microfractures and voids closest to the water-rock interface which increases the diffusivity in minor parts of the rock. This means that the apparent diffusion profiles are to a very high extent a reflection of the heterogeneous porosity in the water-rock interface and not basically a penetration profile in a homogenous medium. The 14C-PMMA porosity distribution studies /Widestrand et al. 2010a/ showed strongly heterogeneous porosity distributions for the fracture samples (A-samples) which thus are in agreement with the experimental results. However, the 14C-PMMA results for the rock matrix samples (D-samples) indicated a more homogeneous porosity distribution dominated by grain boundary porosity. The experimental observation of obtaining more or less the same degree of heterogeneity in the penetration profiles for the D-samples is thus somewhat contradictory. One possible explanation to this could be that this is caused by the heterogeneity in the mineralogy, an explanation which to some extent is supported by indication of the correlation between adsorption and dark minerals (e.g. biotite) given in Figure 3-2.

The largest deviation of the different methods of determining K_d is observed for the Gd(III) tracer where the maximum of the results from the modelling of the penetration profiles is more than two orders of magnitudes lower than the corresponding K_d from batch sorption experiment. However, the results of the penetration profiles are based on a few numbers of samples where the Gd tracer actually could be found in the second slice of the profile. For the absolute majority of the profiles measured, Gd was only found in the first slice which therefore not was appropriate for modelling. It is therefore obvious that the range given for measurements of the Gd profiles suffers from a sample bias and should be treated and used with care.

The techniques of combining measurements of the aqueous phase and solid phase (preferentially the slice closest to the water-rock interface) to a K_d-value, give values in the lower range of the different techniques compared. This value can be argued as being conservative since diffusive equilibrium is not expected to have been obtained due to the comparatively short contact times. Furthermore, this approach addresses both the aqueous and rock measurement and it is also advantageous that it is not needed to address any diffusion process at all. A possible source for overestimation is that the surface core samples (i.e. the slices located closest to the water-rock interface) could be influenced by presence of higher amount of surface sorption sites than ordinary matrix rock, but this possible overestimation is most likely much minor than the underestimation due to the diffusive non-equilibrium. Another source of underestimation is the observed large losses of tracer from the surface to the epoxy disc.

The conclusive summary of the exercise of the K_d comparison is that there is a serious risk of overestimation using the techniques employing only study of the tracer loss in the aqueous phase. It is also indicated that heterogeneity in the porosity distribution /Widestrand et al. 2010a/ makes it difficult to use the penetration profile data for the rock sample to model a K_d. Because of this conceptual uncertainty, the most robust concept seems to be to combine the measured concentrations in the aqueous phase and measured concentration in the rock sample closest to the water-rock interface. Based on the assumption that full diffusion equilibrium has not been obtained for the contact times used, one can easily argue that these values therefore should be considered as conservative. Nevertheless, the observation of penetration profiles indicative of diffusion can be observed for e.g. ^{36}Cl and ^{22}Na at least one cm into the rock matrix, the LTDE-SD experiment confirms that connected porosity available for diffusion exists further into the rock matrix.

4.6 Anion exclusion

4.6.1 Background

The rather low amount of the presumably non-sorbing tracer ^{36}Cl found in the sliced drill cores samples can be regarded as indication of a process or a rock material property that restricts diffusion, in relation to what is expected from a homogeneous diffusion model for a non-sorbing and non ionic tracer. As can be seen in Figure 4-26 the C/C_0-values (pore concentration of ^{36}Cl in the rock samples divided by the concentration in the bulk water phase) is about 1 closest to the water-rock interface in six out of nine penetration profiles, but significantly lower in the subsequent points of measurement, with a slope change around 5 mm penetration depth.

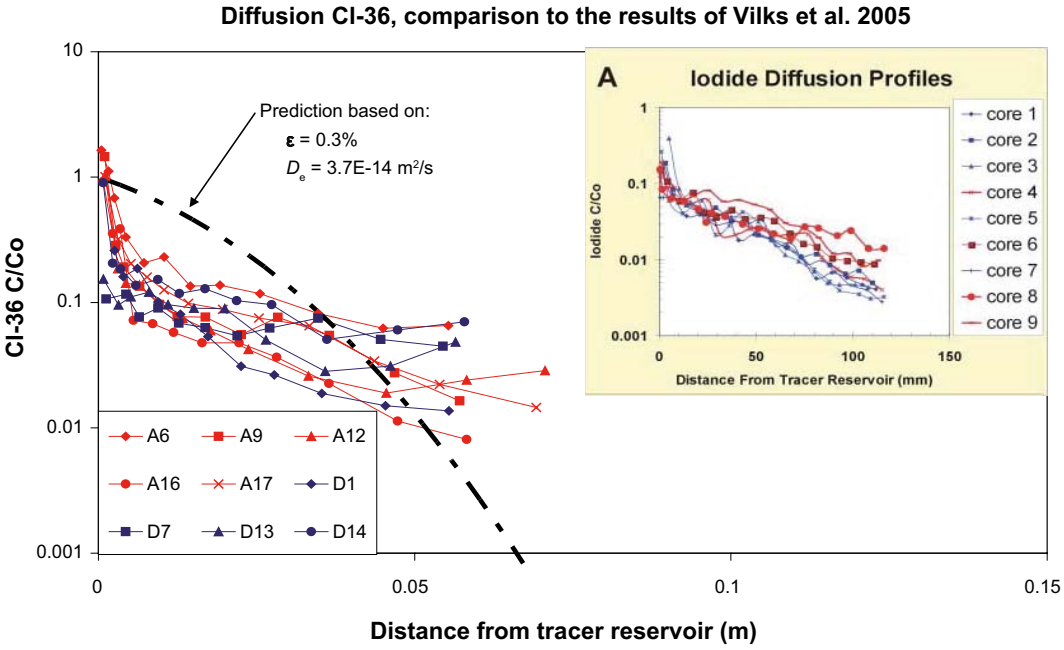

Figure 4-26. *Penetration profiles of ^{36}Cl in five fracture samples (red dots) and four matrix rock samples (blue dots). The C/C_0 refers to the pore water concentration (assuming 0.3% porosity, the same value is assumed in /Vilks et al. 2005/) divided by the bulk water concentration. For comparative purposes, similar results of the LTDE-SD laboratory investigation of iodide diffusion of /Vilks et al. 2005/ are presented. In this investigation, the results from samples considered influenced by an intersecting fracture is marked in red and samples without such influence are marked in blue.*

Furthermore, there is very little resemblance of the theoretical predicted penetration profile and the measured penetration profiles; this observation is valid both for the *in situ* experiments with ^{36}Cl and for the laboratory experiments with iodide. This deviation has called for an extended evaluation of the ^{36}Cl penetration profiles in which the possibility of influence of anion exclusion is investigated, i.e. anion exclusion defined as a mechanism in which negatively charged anions are repelled from the negatively charged pore surfaces of the rock and therefore obtaining reduced storage capacity and/or reduced mobility in the rock.

4.6.2 Best fit of the ^{36}Cl penetration profiles

The first series of modelling has been performed by using the porosity and the formation factor (i.e. the diffusivity) as fitting parameters and using a K_d of 0, i.e. no sorption. The results of this exercise are given in Figure 4-27 and Table 4-10 and low porosities and diffusivities are obtained. Especially the porosity is low (0.04±0.03%), which, however, is to be expected from the observation of the low concentrations in the rock material closest to the water-rock interface, cf. discussion above. The average formation factor evaluated from the ^{36}Cl penetration profiles for the matrix rock samples $(1.5\pm1.2)\cdot10^{-5}$ which can be compared with the evaluation of the laboratory through diffusion experiments using H^3HO /Widestrand et al. 2010a/ for which an average value of $(2.2\pm1.2)\cdot10^{-5}$ was obtained. Based on this singular observation, there is consequently no strong indication of any anion exclusion effect giving a reduced diffusivity for negatively charged substances. The most pronounced deviation from the homogenous matrix diffusion model is nevertheless the low porosity that has to be assigned to adjust the calculated penetration profiles to the experimentally measured values; 0.04% to be compared to the results of the 0.2–5% (cf. Table 4-1) determined by the water saturation measurements /Widestrand et al. 2010b/. This can be interpreted as an indication that a large amount of the porosity is not available for diffusion of ^{36}Cl; a tentative conclusion based on the low amount of ^{36}Cl found in the rock samples.

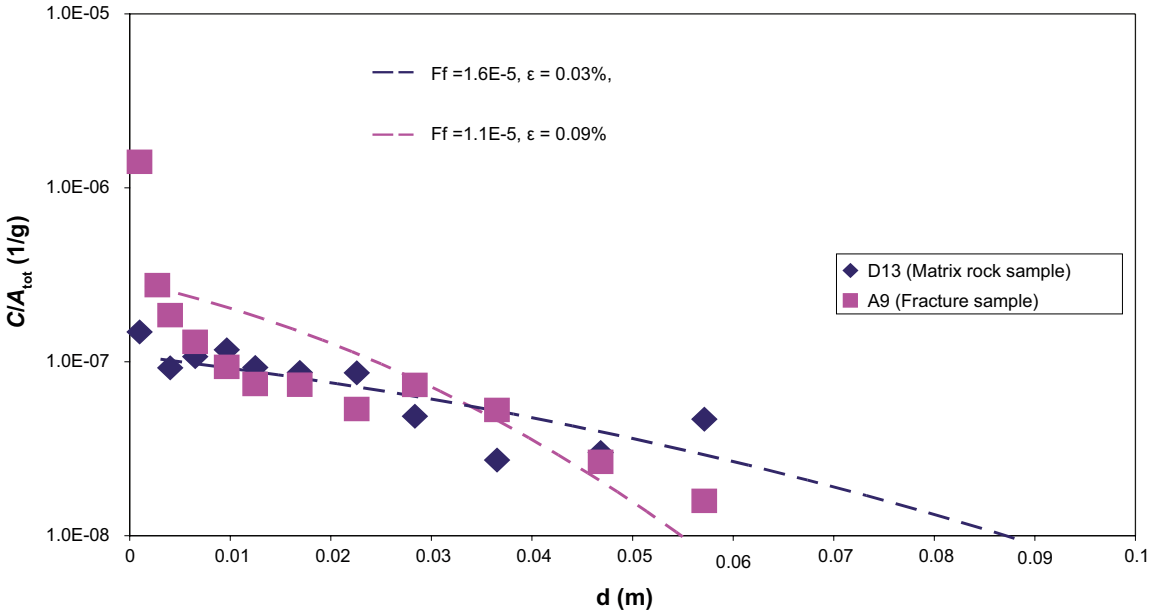

Figure 4-27. Best fit of a matrix diffusion model to the experimentally obtained penetration profiles of ^{36}Cl, exemplified by a rock matrix sample (D13, in blue) and a fracture sample (A9, in red)

Table 4-10. Formation factors (and the corresponding effective diffusivities) together with the porosities obtained for the fitting of a homogenous diffusion model to the experimental data of the ^{36}Cl penetration profile.

Sample	F_f	D_e	ε	Sample	F_f	D_e	ε
A6	2.4E–5	4.2E–14	1.3E–3	D1	5.6E–6	9.6E–15	4.3E–4
A9	1.1E–5	1.8E–14	9.0E–4	D7	1.5E–5	2.5E–14	2.9E–4
A12	1.3E–5	2.3E–14	4.2E–4	D13	1.6E–5	2.7E–14	3.4E–4
A16	6.4E–6	1.1E–14	4.9E–4	D14	2.2E–5	3.7E–14	6.5E–4
A17	1.6E–5	2.7E–14	7.3E–4				
Average	1.4E–5	2.4E–14	7.6E–4	Average	1.5E–5	2.5E–14	4.3E–4
+/–	1.3E–5	2.3E–14	6.8E–4	+/–	1.2E–5	2.0E–14	2.8E–4

4.6.3 Comparison with ^{22}Na diffusion

It is interesting to compare the ^{36}Cl results to the results of the least sorbing of the slightly sorbing cations, i.e. the ^{22}Na tracer. A quick glance of comparison on the penetration profiles (Appendix 4 and 5) shows that the relative concentration of ^{22}Na is 10–100 times higher compared with ^{36}Cl in the rock material closest to the water-rock interface. Using a homogenous matrix diffusion sorption model, this would result in a capacity factor ($\alpha = \varepsilon + K_d\rho$) 10–100 times higher for ^{22}Na than for ^{36}Cl. Since a $K_d = 0$ is assumed for the presumed non-sorbing tracer ^{36}Cl, the $K_d\rho$-term should be in the range of 0.004–0.04; with a rock density of 2,700 kg/m^3 a K_d in the range of $1.5 \cdot 10^{-5}$–$1.5 \cdot 10^{-6}$ m^3/kg would have been obtained.

As can be seen in Figure 4-28, this given range of K_d-values fails to reproduce the ^{22}Na penetration profile curve. It is obvious that it is necessary to use a higher diffusion rate for ^{22}Na than for ^{36}Cl to obtain a model that reasonably fits the experimental data. The anion exclusion mechanism, i.e. electrostatic repulsion of the negatively charged surface of the pores and the negatively charged anions, therefore offers a possibility of assigning a lower diffusivity for anions such as ^{36}Cl compared with cations and/or non-charged compounds and could therefore tentatively explain the characteristics of the obtained data.

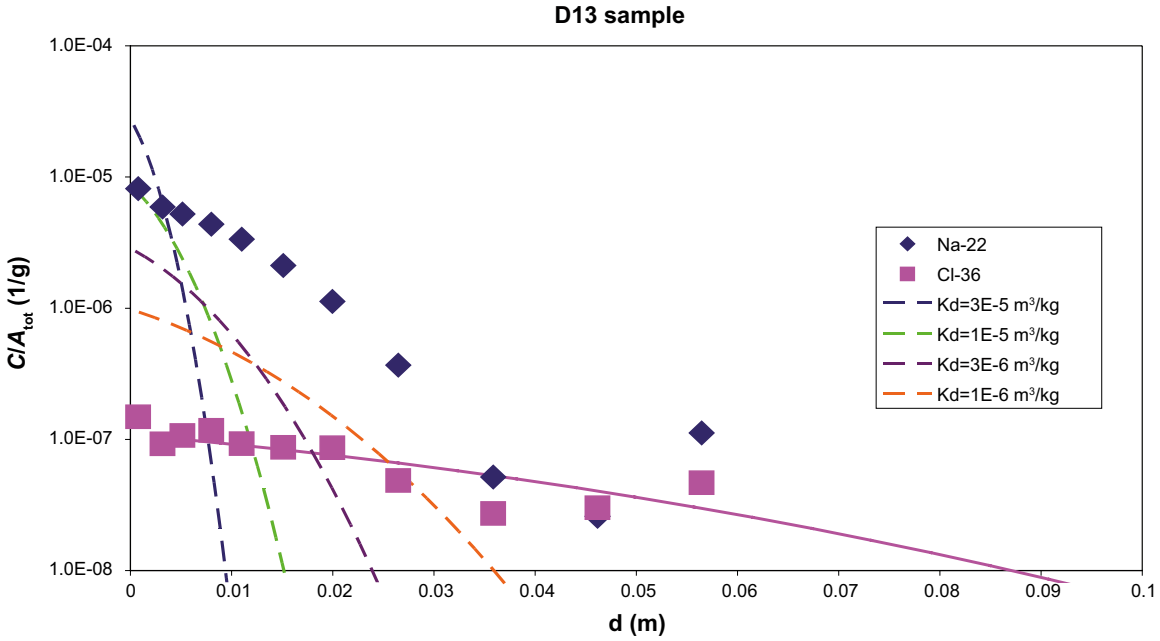

Figure 4-28. *Experimentally obtained penetration profile of ^{36}Cl and ^{22}Na, together with the best fit of matrix diffusion model (non-sorbing) to the ^{36}Cl data, pink solid line. The different dashed lines refers to the calculated penetration profiles for ^{22}Na obtained by using the same diffusion characteristics (diffusion rate and porosity) as for ^{36}Cl, however, with varying K_d.*

Using the anion exclusion modelling approach, a reasonably good fit to the experimental data can be obtained, cf. Figure 4-29 and Table 4-11 for the numerical results. Using this approach to all the samples which has been analyzed for ^{36}Cl and ^{22}Na, an anion exclusion factor ($F_{f,Na}/F_{f,Cl}$) is obtained with a value of 4±3 for fracture samples and 8±4 for matrix sorption samples. However, the following lack of consistency with other experimental data must be acknowledged:

- Based on this anion exclusion modelling attempt, the formation factor for substances that are not influenced by anion exclusion (e.g. H^3HO and the cations) should according to the evaluation using the *in situ* results be in the range of $(2–9)\cdot10^{-5}$ for fracture samples and $(6–12)\cdot10^{-5}$ for matrix rock samples. This can be compared with the results of the laboratory through diffusion experiments using H^3HO where the corresponding range (only matrix rock samples used) was $(1.4–3.1)\cdot10^{-5}$, i.e. significantly lower. However, one must be aware of that the differences in diffusion experiment method (in-diffusion in the former case, through-diffusion in the latter case) may have an impact of this difference.
- For the two laboratory through diffusion experiments samples where, besides the mainly used tracer H^3HO also the diffusion of ^{36}Cl was addressed, one sample showed a breakthrough without any lower diffusion of ^{36}Cl compared to H^3HO. For the other sample, no breakthrough of ^{36}Cl was obtained at all, and one order of magnitude lower diffusivity was estimated for this sample.
- As mentioned, the amount of ^{36}Cl in the rock surface samples is much lower than what should be expected from the predictions using the laboratory determined porosity and diffusivity, cf. Figure 4-2a and 4-2b. It should be emphasized that the porosity obtained in the calculation is applied both for ^{36}Cl and ^{22}Na, i.e. no reduction of the pore space due to electrostatic repulsion between the anions and the pore surfaces is addressed in the calculations. However, it is theoretically possible to calculate using the higher porosity for ^{22}Na combined with the reduced porosity for ^{36}Cl and still obtaining the same results, this since the porosity term is negligible compared to the $K_d\rho$ for ^{22}Na and therefore in itself having no sensitivity for the penetration profile calculation for that tracer. Such a concept would thereby explain the reduced porosity indicated for ^{36}Cl (and for Uranine in the investigation of /Vilks et al. 2005/) as caused by anionic exclusion repulsion.

However, the very low thickness that is normally assumed for the electrostatic double layer strongly contradicts that the reduction of the effective pore space due to anionic repulsion should be as high as a factor in the order of 10 (i.e. the difference of the water saturation porosity and the porosity obtained from the curve fitting of ^{36}Cl penetration profiles). It seems therefore more likely to assume that only a part of the connected porosity has been utilized for storage of the tracers, and that this should apply also for the sorbing tracers. The low degree of utilization may be due to a heterogeneous and highly tortuous system, where the transport paths to part of the pore space are long in the perspective of the relatively short experimental time.

- The shapes of the penetration profile curves (^{36}Cl for the *in situ* experiments, iodide and Uranine in the laboratory experiments, /Vilks et al. 2005/) show very little resemblance to the predicted curve using a homogenous matrix diffusion model.
- A possible explanation of all deviations of the experimental data to the predicted homogeneous matrix diffusion model could be the presence of heterogeneously distributed porosity. Such a concept was dealt with by e.g. /Johansson et al. 2000/ which addressed the results of PMMA studies of the porosity distribution in calculation of diffusion in Äspö diorite and fine-grained granite. The hypothesis of heterogeneous diffusion is supported by the studies of the spatial distribution of the porosity using the ^{14}C-PMMA-technique presented in /Widestrand et al. 2010a/. Nevertheless, the much lower amount of the non-sorbing anionic tracers in the rock material compared to what should be expected from the porosity measurement cannot be explained by the heterogeneously distributed porosity and therefore indicates another process, e.g. anion exclusion, or a rock material property that restricts diffusion of a non-sorbing anionic tracer.

Table 4-11. Data obtained from the evaluation of the penetration profile data of ^{36}Cl and ^{22}Na according to an anion exclusion model, see text for details.

	D_w Cl 1.7E–9	**D_w Na 1.1E–9**		**Possible anion exclusion factor (F_f,Na / F_f,Cl)**			
Fracture samples							
	D_e Cl	D_e Na	ε				+/–
A6	4.2E–14	8.3E–14	1.3E–3	3.0	average	3.8	3.4
A9	1.8E–14	3.6E–14	9.0E–4	3.0	min	1.8	
A12	2.3E–14	2.7E–14	4.2E–4	1.8	max	5.8	
A16	1.1E–14	3.8E–14	4.9E–4	5.2			
A17	2.7E–14	1.0E–13	7.3E–4	5.8			
Matrix rock samples							
	D_e Cl	D_e Na	ε				
D1	9.6E–15	6.9E–14	4.3E–4	10.9	average	7.8	4.5
D7	2.5E–14	1.3E–13	2.9E–4	7.5	min	5.5	
D13	2.7E–14	1.3E–13	3.4E–4	7.4	max	10.9	
D14	3.7E–14	1.4E–13	6.5E–4	5.5			

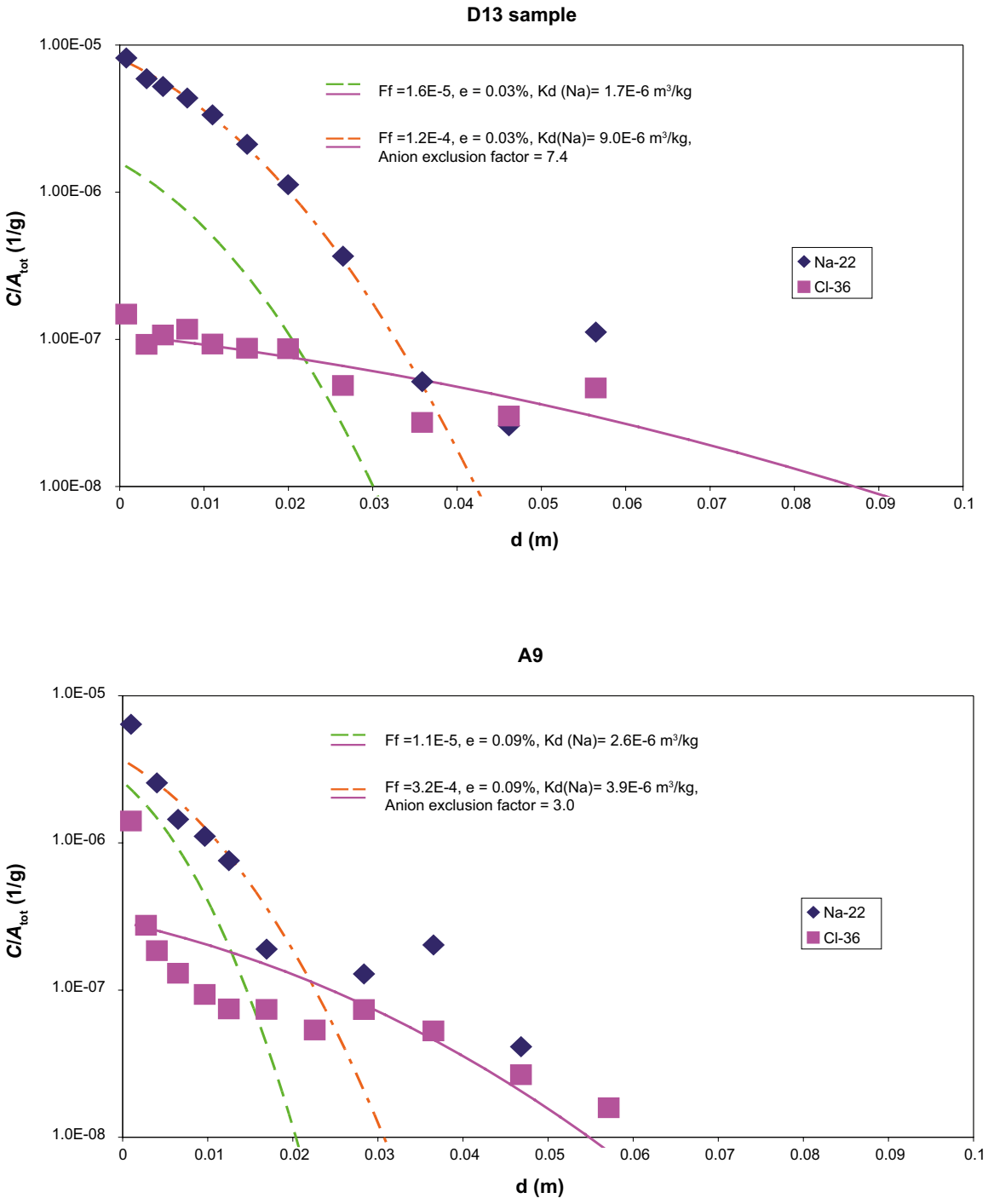

Figure 4-29. *Illustration of the effect of including an anion exclusion mechanism to the fitting of a matrix diffusion sorption model to the experimentally obtained penetration profiles of ^{36}Cl and ^{22}Na, see text for details. Matrix rock sample D13 is illustrated in the top and the fracture sample A9 is illustrated in the bottom.*

5 Discussion and conclusions

In this chapter general conclusive remarks from the evaluation and modelling on data from the analysis of the rock samples, originating from the *in situ* experiment, are presented in Section 5.1 and 5.2. Some conclusions concerning the general performance of the *in situ* experiment and the general outcome of the LTDE-SD experiment are given in Section 5.3.

5.1 Radionuclide penetration and distribution

Autoradiograph analyses of the sliced rock samples indicate that the radionuclides diffuse in a heterogeneous pattern. The migration paths can visually be associated with microfractures and with the biotite part of the rock.

There is an indication of a heterogeneous distribution of tracers on the different surfaces in the *in situ* experiment (natural fracture and unaltered matrix rock) that cannot easily be explained, although impact of mineralogy heterogeneity on the sorption has been obtained. The impact of the epoxy that loosened from the natural fracture surface of the stub has furthermore complicated this situation. However, there is an indication that tracers expected to adsorb by surface complexation were adsorbed by minerals loosely attached to the fracture surface, since they to a major part were attached to the epoxy after the accidental separation of the epoxy from the natural fracture at the stub, during the over core drilling. In contrast, the cation exchange sorbing ^{137}Cs has been bound to material strongly associated with the matrix rock (no fracture minerals present) since only very minor parts of this tracer were found in the epoxy.

Penetration depths of at least 2–3 cm have been found for the very weakly sorbing tracer ^{22}Na and typically in the range of 0.5 cm for the more strongly sorbing tracer ^{137}Cs. For the presumed non-sorbing tracer ^{36}Cl, the penetration depth is about the same as for ^{22}Na, although with significantly lower total amounts than what was to be expected, based on the laboratory determined porosity and diffusivity. It must also be mentioned that the shape of the penetration profiles indicates a significant influence of a heterogeneous distribution of the porosity (and hence diffusivity). However, no elaborate modelling attempt using heterogeneous diffusion has so far been performed within this project.

Diffusion profiles have been registered for many of the tracers involved in the study. Qualitative inspection of the data yields that the slope of the different diffusion profiles follows the trend of the presumed strength of sorption, i.e. ^{36}Cl < ^{22}Na < ^{63}Ni ≈ ^{133}Ba ≈ ^{137}Cs. Given their tabulated K_d-values, one would, expect some difference in their respective diffusion characteristics (e.g. between ^{137}Cs and ^{133}Ba), but it seems reasonable to assume that the resolution of the experimental technique used is not high enough to capture such differences. Observations of the relative concentrations of tracers in the rock slice closest to the water-rock interface follow the trend of ^{137}Cs > ^{63}Ni > ^{133}Ba > ^{22}Na > ^{36}Cl, i.e. as expected from the tabulated K_d values. Combining these observations provides good qualitative proof that a combined diffusion/sorption process has taken place during the experiment.

The combination of the batch sorption experiment determined K_d and the through diffusion determined diffusivities on rock samples from the LTDE-SD site /Widestrand et al. 2010a/ has been used for predicting the penetration profile curves for tracers used in the present *in situ* experiment. In the prediction, a single-rate matrix-diffusion model was used. Comparison of these predictions to the *in situ* experimental results shows:

- Much lower amounts of the non-sorbing tracer ^{36}Cl can be observed in the rock samples than what was predicted.
- Very low penetration depths of the different sorbing tracers were predicted, typically < 3 cm for ^{22}Na and < 2 mm for ^{137}Cs. However, the measured penetration profiles show that in the vast majority of the sample cores, tracers could be found much further into the matrix than what was predicted.

5.2 Radionuclide sorption and diffusion

The modelling using a single-rate matrix-diffusion model to fit the penetration profile results has yielded the following results:

- Using a diffusivity determined in an independent through diffusion experiment on samples from the LTDE-SD site /Widestrand et al. 2010a/, a K_d was varied in order to fit the experimentally obtained penetration profile. The K_d obtained in this process is typically 1–2 orders of magnitude lower than the corresponding K_d determined by batch sorption experiments on LTDE-SD site specific samples.
- For the opposite approach (i.e. using the batch sorption determined K_d as a fixed parameter and varying the diffusivity to fit the *in situ* experimental data), diffusivity values (i.e. illustrated by the formation factor) need to be increased 1–2 orders of magnitudes compared to laboratory-derived parameters to fit the *in situ* experimental data.
- Using an approach in which both the diffusivity and the sorption coefficients are allowed to vary in order to fit the *in situ* experimental data (i.e. no address of any independently measured laboratory data) indicates that a somewhat lower K_d in combination with a somewhat higher diffusivity, both in comparison with laboratory measurements, is needed to fit the *in situ* experimental data. It should be noted that modelling of penetration profile data can give unique values of K_d and diffusivity. This is contrary to the technique using only the time dependence of the loss in the aqueous phase which only is sensitive to the combined product of the diffusivity and the K_d /Widestrand et al. 2010b/. However, it is worth noting that the present technique involves variation of two parameters to a very low number of data points which introduces considerable conceptual uncertainty to this modelling approach.

An illustration of the three modelling concepts is given in Figure 5-1 which shows the results of modelling using the ^{137}Cs tracer (A16 core sample) in comparison to the experimentally obtained results.

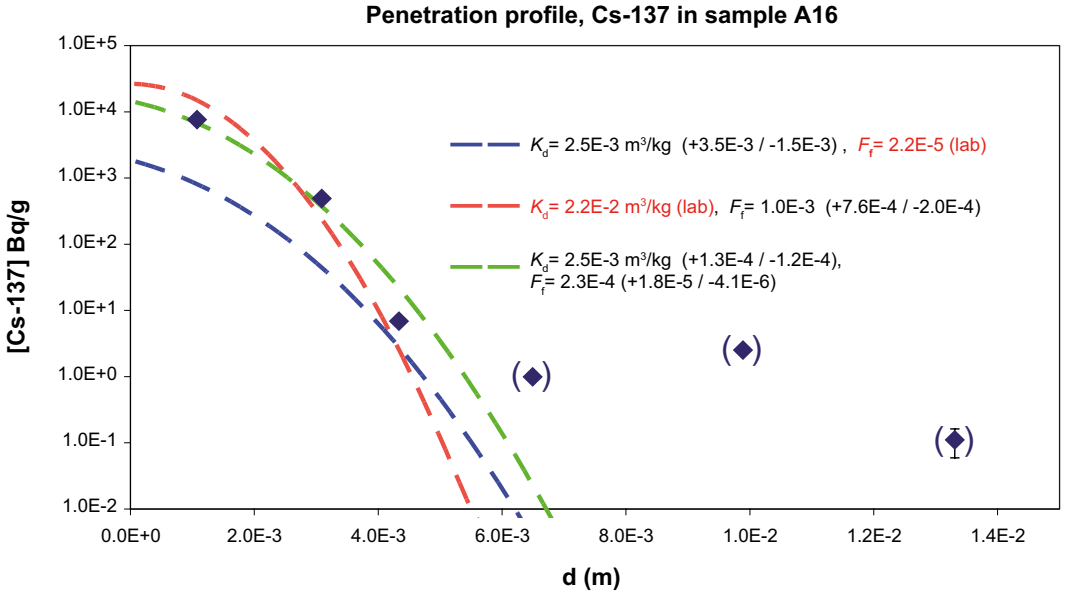

Figure 5-1. *Exemplification of how successively progressed fitting of the single-rate diffusion model to the* in situ *experimental results can be obtained by the different cases: Case 2 – fixed diffusivity, K_d varied (blue line), Case 3 – fixed K_d, diffusivity varied (red line), Case 4 – both K_d and diffusivity varied (green line). As mentioned in the text the modelling has been focused on the slow penetration profile process (which constitutes >99% of the sorbed tracer, therefore the datapoints representing the very minor but fast penetration process have been excluded.*

A conclusive summary of the modelling is that the interaction observed in this experiment (occurring mainly in the rock material less than 5 mm from the water-rock interface) seems to be influenced by a somewhat decreased K_d compared to batch sorption experiments and with an increased diffusivity compared to the results obtained by through diffusion experiments.

A forward tailing can be seen for all the tracers that have been subject to modelling (i.e. ^{36}Cl, ^{22}Na, ^{133}Ba, ^{63}Ni and ^{137}Cs). This result is proposed to be caused by porosity heterogeneity, e.g. fracture associated migration paths where comparatively fast diffusion could take place. However, the possibility of a contamination had taken place during the sampling can not fully be excluded; likewise an impact of other transport mechanisms must probably be further explored. The data points considered as associated to this tailing have not been included in the modelling which has to be taken into consideration regarding the modelling values obtained from curve fitting. This exclusion has been justified by the fact that the tailing part of the penetration curve only constitutes a very minor part of the total amount of the tracer added, but one must be aware that the modelling interpretation of this report is made under the conditions of not addressing the very minor but fast migration process.

In addition to the tailing observed for the penetration profiles, the general shape of the curves deviates significantly from the shape yielded by the homogeneous diffusion-sorption model. Given the observation in the ^{14}C-PMMA studies of a heterogeneously distributed porosity (/Widestrand et al. 2010a/), the difficulty to fit a single-rate based diffusion model to the measured results does not come as a surprise.

The amount of ^{36}Cl (anionic species) in the rock is approximately one order of magnitude lower than what should be expected from the porosity data /Widestrand et al. 2010a/. A modelling attempt has indicated that an anion exclusion effect corresponding to an effective decrease of the diffusivity by a factor of 3 to 7 may provide good conceptual agreement with the anion exclusion theory, for the combination of the ^{36}Cl and the ^{22}Na results. However, it should be noted that this concept demands a decrease of the porosity with approximately a factor of 10 compared to the porosity measured using water saturation technique.

As a complement to the modelling, K_d values have been calculated by simply applying the ratio of the aqueous concentration of the tracer at the end of the circulation phase of the *in situ* experiment and the tracer concentration in the rock closest to the water-rock interface boundary. This technique produces K_d values higher than the ones obtained by the modelling of the penetration profiles but lower than what are obtained from corresponding modelling using only the results of the tracer loss in the aqueous phase.

5.3 Concluding remarks on the LTDE-SD experiment

The LTDE-SD experiment aims at increasing knowledge of sorption and diffusion under *in situ* conditions and to provide data for performance and safety assessment calculations. In the current report a first modelling attempt using a single-rate based homogeneous diffusion-sorption model is presented and results are compared to results obtained in the supporting laboratory experiments /Widestrand et al. 2010a/ and to results from the aqueous phase of the *in situ* experiment /Widestrand et al. 2010b/. However, a fully integrated interpretation of all LTDE-SD reports with generalized conclusions e.g. with regards to the possibility to expand the LTDE-SD results (in Ävrö granodiorite) to other sites or geological situations, to consider the general guiltiness of laboratory data, consideration of rock mechanical aspects etc has not been possible to include in the evaluation at this stage. Nevertheless, some concluding remarks can be drawn from the LTDE-SD project.

In situ sorption and diffusion have been demonstrated for a series of elements exclusively present in the LTDE-SD experiment, and also for some tracers which have been used in earlier performed dynamic *in situ* tracer experiments performed at the Äspö HRL. The amounts lost from the aqueous phase of the different tracers follow very well the general knowledge of the relative sorption strengths of the tracers; as established from previous laboratory batch sorption experiments and *in situ* dynamic tracer experiments at the Äspö HRL.

Visualization techniques show that penetration into grain boundary porosity and micro fractures dominate the diffusion pathways and extends at least one cm into the rock matrix. The observation of penetration profiles indicative of diffusion can be observed for e.g. ^{36}Cl and ^{22}Na several cm into the rock matrix, thus the LTDE-SD experiment confirms that connected porosity available for diffusion exists further into the rock matrix.

The experimental set-up and experimental and analysis procedures developed and adopted enabled to produce results from aqueous phase analysis as a function of time and from analysis of rock samples as a function of positions in the rock. The obtained results were utilized to determine *in situ* sorption coefficients (K_d) and diffusion constants (D_e) for groups of tracers with different sorption processes and sorption strength. The *in situ* results regarding sorption processes are in good agreement with the behaviour observed in laboratory experiments. The redox sensitive tracers show the largest variations depending on the actual conditions in each separate experiment. The chemical speciation calculations in combination with ion exchange speciation sampling supports the evaluations.

It has been indicated that, especially for strongly sorbing tracers, there is an influence of losses in the aqueous phase not directly proven to be rock-water interactions, which could be identified as a source of overestimations using only aqueous phase measurements for K_d determinations. Examples of such potential processes are sorption on equipment parts, interactions with small particles e.g. ferric oxides formed due to not maintaining sufficient reducing conditions during the experiment.

Supporting pressure monitoring data, in combination with the general setup of the experiment with a strict pressure control relative to the surrounding rock pressure, show that the *in situ* experiment was performed in absence of hydraulic gradients. Consequently, penetration into the rock matrix must be considered as being a result of diffusion alone, and that no advection was involved. The ambient chemical conditions were practically unchanged for most tracers by the use of radionuclide trace elements.

The conclusive summary of the exercise of the K_d comparison is that there is a risk of overestimation using the techniques employing only study of the tracer loss in the aqueous phase, irrespectively if the aqueous phase data are from *in situ* or laboratory conditions. It is also indicated that the aqueous phase result and the penetration profile cannot be modelled simultaneously with satisfactory results by using a single-rate homogeneous porosity model. A combined modelling using aqueous phase and penetration profile data may require a model capable of heterogeneous porosity distribution. Such a modelling may also give more conclusive data regarding the *in situ* diffusivity.

A robust concept for data extraction to be used in safety assessment is to combine the measured concentrations in the aqueous phase and measured concentration in the rock sample closest to the water-rock interface. Based on the assumption that full diffusion equilibrium has not been obtained for the contact times used, one can easily argue that these values therefore should be considered as conservative.

6 References

SKB's (Svensk Kärnbränslehantering AB) publications can be found at www.skb.se/publications.

Andersson P, Byegård J, Dershowitz B, Doe T, Hermanson J, Meier P, Tullborg E-L, Winberg A (ed), 2002. Final report of the TRUE Block Scale project. 1. Characterisation and model development. SKB TR-02-13, Svensk Kärnbränslehantering AB.

Crank J, 1975. The mathematics of diffusion. 2nd ed. Oxford: Clarendon.

Johansson H, Byegard J, Skalberg M, 2000. Impact of porosity heterogeneity in the diffusion of some alkali- and alkaline earth-metals in crystalline rock. In: Smith R W, Shoesmith D W (eds). Scientific basis for nuclear waste management XXIII: symposium held in Boston, Massachusetts, USA, 29 November–2 December 1999. Warrendale, PA: Materials Research Society. (Materials Research Society Symposium Proceedings 608), pp 191–198.

Li Y-H, Gregory S, 1974. Diffusion of ions in sea water and in deep sea sediments. Geochimica et Cosmochimica Acta, 38, pp 703–714.

Li C, 2001. Äspö Hard Rock Laboratory. Long Term Diffusion Experiment. Microscopic observation of disturbance in drillcore samples from KA3065A02 and KA3065A03. SKB IPR-01-03, Svensk Kärnbränslehantering AB.

Mills R, Lobo V M M, 1989. Self-diffusion in electrolyte solutions: a critical examination of data compiled from the literature. Amsterdam: Elsevier. (Physical Sciences Data 36)

Meinrath G, Ekberg C, Landgren A, Liljenzin J O, 2000. Assessment of uncertainty in parameter evaluation and prediction, Talanta 51, pp 231–246.

Penttinen L, Siitari-Kauppi M, Ikonen J, 2006. Oskarshamn site investigation. Determination of porosity and micro fracturing using the ^{14}C-PMMA technique in samples taken from Oskarshamn area. SKB P-06-62, Svensk Kärnbränslehantering AB.

Rhén I (ed), Gustafson G, Stanfors R, Wikberg P, 1997. Äspö HRL – Geoscientific evaluation 1997/5. Models based on site characterization 1986–1995. SKB TR 97-06, Svensk Kärnbränslehantering AB.

Vilks P, Miller N H, Stanchell F W, 2005. Laboratory program supporting SKB's Long Term Diffusion Experiment. Report 06819-REP-01300-10111-R00, Atomic Energy of Canada Limited.

Wass E, 2005. LTDE Long-Term Diffusion Experiment. Hydraulic conditions of the LTDE experimental volume – results from Pre-Tests 0.1–6. SKB IPR-05-25, Svensk Kärnbränslehantering AB.

Widestrand H, Byegård J, Börjesson S, Bergelin A, Wass E, 2006. LTDE Long-Term Diffusion Experiment. Functionality tests with short-lived radionuclides 2005. SKB IPR-06-05, Svensk Kärnbränslehantering AB.

Widestrand H, Byegård J, Selnert E, Skålberg M, Höglund S, Gustafsson E, 2010a. Äspö Hard Rock Laboratory. Long Term Sorption Diffusion Experiment (LTDE-SD). Supporting laboratory program – Sorption diffusion experiments and rock material characterisation. With supplement of adsorption studies on intact rock samples from the Forsmark and Laxemar site investigations. SKB R-10-66, Svensk Kärnbränslehantering AB.

Widestrand H, Byegård J, Kronberg M, Nilsson K, Höglund S, Gustafsson E, 2010b. Äspö Hard Rock Laboratory. Long Term Sorption Diffusion Experiment (LTDE-SD). Performance of main in-situ experiment and results from water phase measurements. SKB R-10-67, Svensk Kärnbränslehantering AB.

Winberg A, Andersson P, Hermanson J, Byegård J, Cvetkovic V, Birgersson L, 2000. Äspö hard rock laboratory. Final report of the first stage of the tracer retention understanding experiments. SKB TR-00-07, Svensk Kärnbränslehantering AB.

Winberg A, Andersson P, Byegård J, Poteri A, Cvetkovic V, Dershowitz W, Doe T, Hermanson J, Jaime Gómez-Hernández J, Hautojärvi A, Billaux D, Tullborg E-L, Holton D, Meier P, Medina A, 2003a. Final report of the TRUE Block Scale project. 4. Synthesis of flow, transport and retention in the block scale. SKB TR-02-16, Svensk Kärnbränslehantering AB.

Winberg A, Hermansson J, Tullborg E-L, Staub I, 2003b. Äspö Hard Rock Laboratory. Long-Term Diffusion Experiment. Structural model of the LTDE site and detailed description of the characteristics of the experimental volume including target structure and intact rock section. SKB IPR-03-51, Svensk Kärnbränslehantering AB.

Appendix 1

Major events following the experimental phase

Table A1-1. Major events.

Date	Event
2007-04-12	Termination of the experiment, exchange of groundwater to isopropyl alcohol.
2007-04-12	Epoxy injection.
2007-04-17	Removal and dismantling of borehole equipment is started. Circulation in the guard section and pilot hole is shut off. The borehole is closed for a short while due to trouble with the drainage.
2007-04-18	The borehole equipment has been removed and the borehole is sealed.
2007-04-24	The borehole is opened for over-core drilling. The drill water is taken from HD0025A.
2007-04-27	Larger core segment removed. When using a camera, it is found that the peek-plate has come off. Peek plate is fished out with the drill. Borehole left open with stub exposed, pump left inside the borehole to keep stub dry.
2007-04-30	The pump does not keep the borehole dry and one has to assume that this may have been the case throughout the weekend. The Drilling equipment has been anchored to the bedrock and everything is ready for drilling. Drilling stopped at 11.75 m. Drill core doesn't come off, special equipment needed.
2007-05-02	Borehole is opened. Attempts are made to use the drill bit to get the core out. Further drilling. Breaking the core using special equipment. Core finally taken out, it broke at a perfect place behind the last packer. Borehole plugged.
2007-05-04	The borehole is closed and the core is transported to Clab.
2007-06-08	Orientation and scaling of the core.
2007-08-03	Decision of detailed performance of the core sampling (stub surface, external stub surface small hole section, beyond small hole section and PEEK lid).
2007-08-06	Cutting of the core.
2007-08-08 to 2007-08-13	Rock core sampling.
2007-08-14 to 2007-09-05	PEEK lid sampling.
2007-08-27	Scintillation measurements of the core samples.
2007-10-03 to 2007-10-04	Short HPGe-measurements of the core samples.
2007-10-10	Core samples arrived at University of Helsinki.
2008-08-27 to 2008-08-28	Geological characterisation of the core samples at UH. Photographing of the core samples.
2007-12 to 2008-01	Slicing and square-cutting of rock cores.
2008-10-08 to 2008-10-30	Preparation of HPGe calibration samples.
2008-10-15 to 2009-10-09	Method test and LSC analyses (^{36}Cl).
2008-10-24	Start of HPGe analyses of core samples.
2008-11-20	Start for leach tests for LSC analyses (^{36}Cl).
2009-01-19 to 2009-09-11	Method test and LSC analyses (^{63}Ni).
2009-01-20 to 2009-01-21 and 2009-06-22 to 2009-06-23	Geological characterisation of the sliced core samples at UH. Photographing of the sliced core samples.
2010-04-16	Stop of HPGe analyses of core samples.

Appendix 2

Handling of radionuclides in the LTDE-SD main *in situ* experiment

A2.1 Main *in situ* experiment

The LTDE-SD main *in situ* experiment commenced September 27, 2006 when the stock solution was injected in the test section at the experimental site.

In connection with the injection and during the course of the experiment water samples were taken out of the test section (KA3065A03: 1), the guard section (KA3065A03: 2), i.e. the section in the experimental borehole bound to the test section, and in the pilot borehole (KA3065A02: 3). In addition, a number of environmental samples were taken prior to radionuclide tracer injection. These samples were supplemented with a sample from tunnel drainage system gauging box MA3411G, 2007-01-22. To ensure that the area had not been contaminated during the experiment the environmental sampling was done once again after the experiment was terminated.

Before the samples were transported to Baslab for subsequent analysis they were checked for any possible external contamination of Clab's radiation protection organization. In connection with some of the transports Clab's staff also took smear tests in and outside the containers and on the concrete slab outside the experimental borehole KA3065A03. None of these measurements led to any action.

The experiment was carried out according to plan. On 12 April 2007 the experiment was terminated and the radionuclide labelled groundwater in the test section was replaced with isopropyl alcohol. Initially the isopropyl alcohol was circulated by the 36-mm hole, i.e. the part of the test section containing matrix rock. To ensure good mixing the flow path was thereafter shifted between 36-mm hole and the part of the test section at core stub, i.e the natural fracture.

The exchange was followed with both HPGe detector and RNI-instruments. HPGe results for Co-57, Sr-85, Cs-137 and Na-22 are presented in Figure A2-1. The last HPGe measurement before the exchange was used to calculate the initial concentrations.

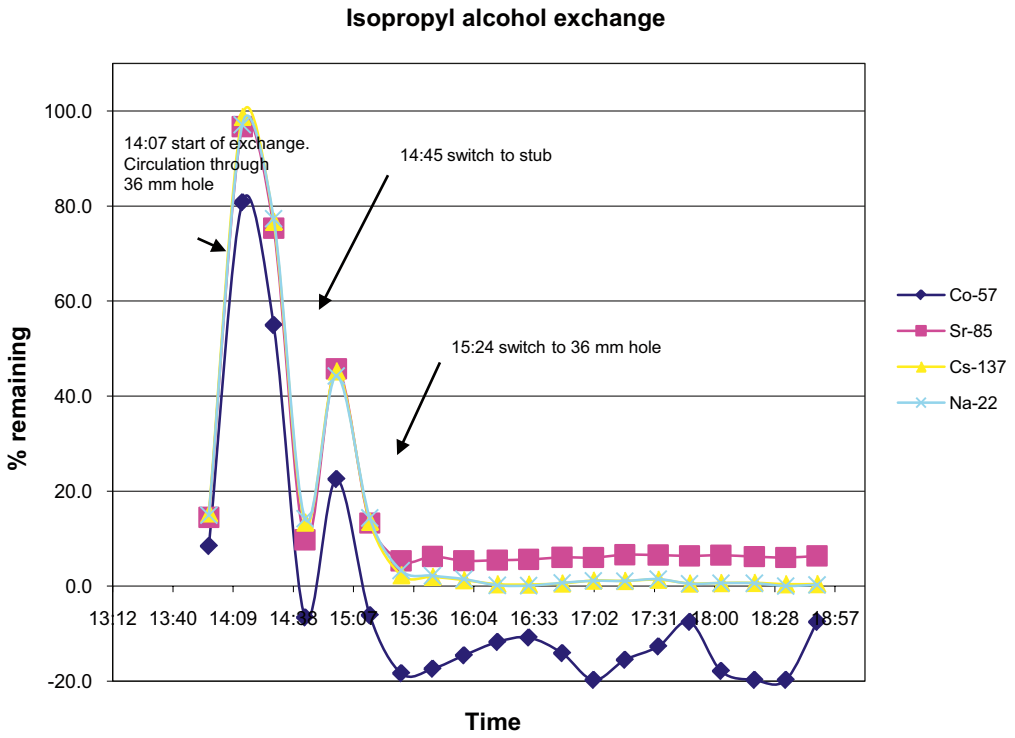

Figure A2-1. *Remaining Co-57, Sr-85, Cs-137 and Na-22 relative to the concentrations just before the exchange began. Activity resulting from Co-57 adsorbed on the tubes has been subtracted.*

In total about 5 litres of isopropyl alcohol was injected at the exchange, that's approximately five experimental volumes. The corresponding volume was drawn off and collected in a series of samples for later analysis.

After 2.5 litres of isopropyl alcohol were injected Na 22 and Cs-137 stabilized below the stop criterion with concentrations <1% of their original concentrations. At that moment, Sr-85 concentration is still around 6%. After a further 2.5 litres of injected isopropyl alcohol Sr-85 seemed to have stabilized at about 6% so it was decided to break based on sodium and cesium concentrations. The risk was too great to strontium desorbed from the test section surfaces. Negative Co-57 values can be explained by small amounts desorbed from the tube in front of the detector.

Evaluations of the samples show that Na-22 and Cs-137 reached <1% of their original concentrations, as is the case for Sr-85 which means that the 6% which was measured online at the exchange to isopropyl alcohol originate from a contamination of the tubing.

When the exchange to isopropyl alcohol was completed, epoxy resin was injected to protect the test sections during the forthcoming dismantling of borehole instrumentation and over core drilling. After the epoxy injection is considered the absolute majority of the nuclides in liquid phase have been removed from the experimental setup and collected in bottles for transportation, analysis and disposal of at Baslab.

During dismantling of borehole equipment water samples was taken for HPGe analysis. Low concentrations of Co-57, Sr-85, B-133, Cs-137 and Na-22 were detectable but largely dominated by naturally occurring Rn-daughters. The equipment was also measured with a scintillation detector. Only the large hydraulic packers and the supporting steel plate for the test section Peek lid gave increases of 20–25 cps (counts per second) compared with the background of 10–15 cps. This may be a result of extra Rn daughters accumulating on the borehole walls sticking to these larger objects as they were slowly hauled out of the borehole. Smaller tubes that were mounted as far into the hole but was not in contact with the borehole walls showed no elevated count rates.

Clab's radiation protection staff took smear tests and measured the equipment for contamination after dismantling. The whole borehole equipment was then released for unrestricted use.

The next step in the experiment was over core drilling the experimental borehole KA3065A03 to extract the test section rock, i.e. the core stub with the natural fracture and the rock surrounding the small diameter borehole. A core drill of 300 mm was used, see Figure A2-2. The drilling caused large quantities of water flowing out of the borehole, both cooling water to the drill bit and also groundwater from the borehole was washed out. As the test sections were filled with epoxy at the start it protected them effectively from the flushing water.

Drilling was relatively short so there was really no risk that the drill would steer off course and harm test sections which could have exposed them to water with desorption of radionuclides as a result. Unexpectedly, the Peek lid and epoxy resin loosened from the core stub and thus the fracture surface was exposed to the water in the borehole. From an emissions standpoint, this was not particularly serious since only small amounts of radioactivity were available (most adsorbed on the core stub surface or inside the rock matrix) and the nuclides, which slowly began to desorb, were diluted in very large quantities of water. However, it was a bit unfortunate from a purely experimental point of view as ideally a completely unaffected surface is aimed at.

As mentioned above, water samples were taken for HPGe analysis during the dismantling as well as during over core drilling. Some of these showed small concentrations of Co-57, Sr-85, B-133, Cs-137 and Na-22. In Table A2-1 activities of Na-22 and Cs-137 are presented, also a few samples from the dismantling are included.

Of the nuclides which have been detected the Cs-137 nuclide contributed by far the largest during the dismantling and drilling. The other nuclides activity was often below the detection limit. During the dismantling and over core drilling the water flowing out of the borehole contained about 5 Bq/L Cs-137, which would correspond to 0.91 MBq in the whole process. This represents around 8.5% of the injected activity lost during the dismantling and over core drilling process. The calculation is based on 15 samples from dismantling and over core drilling, the highest concentration in each time period has been chosen, implying 8.5% lost is a large overestimation.

Figure A2-2. *The drilling machine is prepared for 300 mm diameter over core drilling at experimental borehole KA3065A03. Drill bit with core barrel in centre of photo. Open vessel for collecting fluid beneath borehole collar.*

Figure A2-3. *The 300 mm diameter core mapped at SKB Clab before sampling. The core stub with natural fracture is enclosed by the yellow poly urethane cylinder (to the right in the photo).*

Table A2-1. Summary of Na-22 and Cs-137 activities. Samples taken at dismantling of borehole equipment and over core drilling in KA3065A03.

Sample	Na22 (Bq/kg)	(+/)	Cs137 (Bq/kg)	(+/)	Comment
Guard section at dismantling 070417 10:54	1.9	0.3	3.1	0.3	Pressure connection between test section (KA3065A03:1) and guard section (KA3065A03:2) quite recently opened. Dismantling.
KA3065A03:2 (guard) 070417 11:23	<1.8		1.8	0.2	Supporting steel plate for the test section lid in KA3065A03 quite recently released from the Peek lid in the borehole. Dismantling.
Mixed water flowing out of borehole 070417 16:27	<2.6		2.5	0.2	Dismantling is ongoing.
Sample from sealed borehole 070418 15:03	<1.8		3.1	0.2	Sample when borehole sealed with lid at borehole collar after dismantling completed.
Sample in vessel beneath borehole collar 070423 11:20	<2.4		9.8	0.3	Valve opened and 75 litres of groundwater discharged from borehole into open vessel. Sampling in the mixed water in the vessel.
Sample from borehole 070424 11:30	<2.4		12.5	0.4	110 litres discharged from borehole followed by sampling of the flowing water at borehole collar. Over core drilling
Flowing open borehole 070425 09:30	<2.2		3.1	0.2	Sampling after drill phase 1, including marking of core in borehole bottom with pinch bar.
After drill stop 070426 18:32	<1.8		<2.1		Sampling after the today drilling.
Before start of drilling 070427 07:24	<2.2		2.8	0.2	Sampling before the today start of drilling.
Sample after drilling 070427 09:39	<5.3		24.6	0.4	Sampling just before large rock segment is retrieved. The Peek lid may have loosened from the core stub.
Peek lid has loosened 070427 13:35	<2.3		5.6	0.3	It is confirmed that Peek lid and adhered epoxy resin has loosened from the core stub.
Sample on discharging water 070428 11:43	<2.0		2.5	0.2	Sample from open flowing borehole, waiting for drilling to continue.
Sample on discharging water 070430 07:39	<2.6		2.6	0.9	Sample from open flowing borehole, prior to the today start of drilling.
Sample on discharging water during drilling 070502 11:54	<2.5		9.3	1.2	Sampling during drill phase 2.
Sample on discharging water during the final drilling 070502 15:55	<2.3		3.9	0.9	Problem to break the core at the expected fractures. Finally the core is retrieved and the borehole sealed with a lid at borehole collar.
KA3065A03 Sealed borehole 070504 10:44	<0.4		0.5	0.2	Valve on lid opened and sample taken from sealed borehole.

A2.2 Radionuclide tracers used in the LTDE-SD experiment

The radionuclide tracers injected in LTDE-SD main *in situ* experiment are summarized in Table A2-2.

Table A2-2. Summary of the radionuclides used in LTDE-SD main *in situ* experiment. Injected activity is calculated from HPGe measurements on the injection solution (decay corrected to the injection date, 2007-09-27).

Tracer	Half life	Decay mode	Oxidation State	Radio-toxicity classfication	Injected activity (MBq)
^{22}Na	2.603a	β+, γ	Na(I)	C	3.86
^{57}Co	271.79d	ε, γ	Co(II)	C	23
^{75}Se	119.64d	ε, γ	Se(-II, IV, VI)	C	5.4
^{85}Sr	64.9d	ε, γ	Sr(II)	C	55.1
^{95}Zr	64.0d	β-, γ	Zr(IV)	C	0.1
^{109}Cd	462.6d	ε, γ	Cd(II)	B	33.1
^{110m}Ag	249.9d	β-, γ	Ag(I)	B	0.57
^{113}Sn	115.1d	ε, γ	Sn(II)	C	0.11
^{133}Ba	10.5a	ε, γ	Ba(II)	C	2.17
^{137}Cs	30.17a	β-, γ	Cs(I)	C	10.7
^{153}Gd	239.47d	ε, γ	Gd(III)	C	5.24
^{175}Hf	70.0d	ε, γ	Hf(IV)	C	2.89
^{233}Pa	27.0d	β-, γ	Pa(IV, V)	C	14.2
^{35}S	87.5d	β-	S(VI)	D	11.5[1)]
^{36}Cl	3.0·10^5a	β-	Cl(-I)	C	6.45[1)]
^{63}Ni	100a	β-	Ni(II)	C	24.9[1)]
^{99}Tc	2.1·10^5a	β-	TC(IV, VII)	C	65.9 kBq[1)]
^{226}Ra	1,600a	α, (γ)	Ra(II)	A	0.28[1)]
^{236}U	2.342·10^7a	α	U(IV, VI)	B	0.16 kBq[1)]
^{237}Np	2.144·10^6a	α	Np(IV, V)	A	6.55 kBq[1)]
Sum:					**200**
(Radio toxicity classified)				A:	0.3
				B:	34
				C:	154
				D:	11

[1)] Activity calculated from purchased amount.

A2.3 Remaining activity

After over core drilling is considered virtually no activity remaining in the experimental borehole, KA3065A03. The groundwater with radionuclides has been collected in the form of samples or at the exchange to isopropyl alcohol and the subsequent epoxy resin injection. The rock material with adsorbed radionuclides has been transported to Clab for sampling (Figure A2-3). No radionuclides must have been diffused out through and past the rock matrix, which was over drilled and retrieved from the experimental site, that are supported by the subsequent analysis of the core material.

A2.4 Control measurements

A2.4.1 Smear tests

The smear tests Clab Radiation organization's staff took at the experimental site showed no surface contamination, and is below the limit 40 kBq/m^2. The results are reported in Table A2-3.

Table A2-3. Measured activity in smear tests taken at the experimental site. All samples are below current detection limits (hence the <values).

Sampling point	2006-10-02	2007-01-24	2007-05-14
Concrete slab	<1 kBq/m^2	<7 kBq/m^2	<1 kBq/mv
Floor in container C1	<1 kBq/m^2	<1 kBq/m^2	
Shoe shift point in C1	<1 kBq/m^2	<1 kBq/m^2	<1 kBq/m^2
Borehole KA3065A03		<1 kBq/m^2	
Wash basin in C1		<1 kBq/m^2	
Tunnel floor after drilling completed			<1 kBq/m^2
Container C2			<1 kBq/m^2

A2.4.2 Guard section and pilot borehole

The water samples collected from the guard section in the experimental borehole KA3065A03 and the pilot borehole KA3065A02 to detect any leakage from the test section did not show any trace of such a leak. The samples were analyzed with a HPGe detector. The γ-spectrum were analyzed for MDA values (Minimum Detectable Activity). Table A2-4 presents the measured MDA values for Na-22 divided by the total injected amount of activity of Na-22. MDA values are time-corrected.

Guard section volume was 8 ± 1 litres and the sample volume that were measured with HPGe-detector was 1 litre.

Table A2-4. Detection limits of Na-22 at sampling in the guard section in the event of leakage from the test section. Values are given as the smallest fraction of the radioactivity in the test section that could be detected in the guard section. This can be considered as the maximum fraction that could leak into the guard section before it could be detected, based on the actual detection limit for the different sampling points of time.

Date and time	Radionuclide	Decay corrected activity/Total injected activity
2006-09-27 14:01	^{22}Na	<7E–07
2006-09-27 23:35	^{22}Na	<9E–07
2006-09-28 09:20	^{22}Na	<3E–06
2006-09-29 13:49	^{22}Na	<5E–07
2006-10-04	^{22}Na	<7E–07
2006-11-08	^{22}Na	<6E–07
2007-02-07	^{22}Na	<8E–07
2007-02-21	^{22}Na	<9E–07
2007-03-07	^{22}Na	<7E–07
2007-03-21	^{22}Na	<2E–06
2007-04-04	^{22}Na	<1E–06
2007-04-13	^{22}Na	<1E–06
2007-04-16	^{22}Na	<1E–06

A2.4.3 Environmental samples

None of the environmental samples taken at the LTDE-SD experimental site after dismantling and over core drilling showed measurable concentrations, estimated detection limit of <0.5 Bq/kg for Na-22.

A2.4.4 Continuous monitoring

In addition to the water samples, continuous monitoring of dose rate (with RNI 10/SR-instrument) was done in the circulating water in the test section (here with an external RNI10/55 GM probe), inside the experiment container, in the circulating water in the guard section (here with a Bicron 1.5”×1.5” plastic scintillation probe linked to RNI10/SR) and at the fence enclosing the experimental site. RNI instruments are dose rate instruments for contiuous monitoring of the effective dose rate in

(µ Sv/h) or pulse counting with external probes for monitoring of the experimental test sections. In Figure A2-4 dose rate at the fence that encloses the experimental site from the tunnel and the dose rate in the experimental container (C1) close to the glovebox are presented. The figure clearly shows the increase in dose rate associated with the injection of radionuclides in the test section circulating groundwater. In the experiment container, it rose to about 3 µSv/h while at the fence it rose to about 0.4 µSv/h. After injection, the dose rate slowly declined in both experimental container and at the fence. When the experiment was finished and the radioactive samples transported to Clab dose rate dropped to almost the same levels as prior to tracer injection. When the tubing for the experimental set up was dismantled in early June, a further slight reduction was noted.

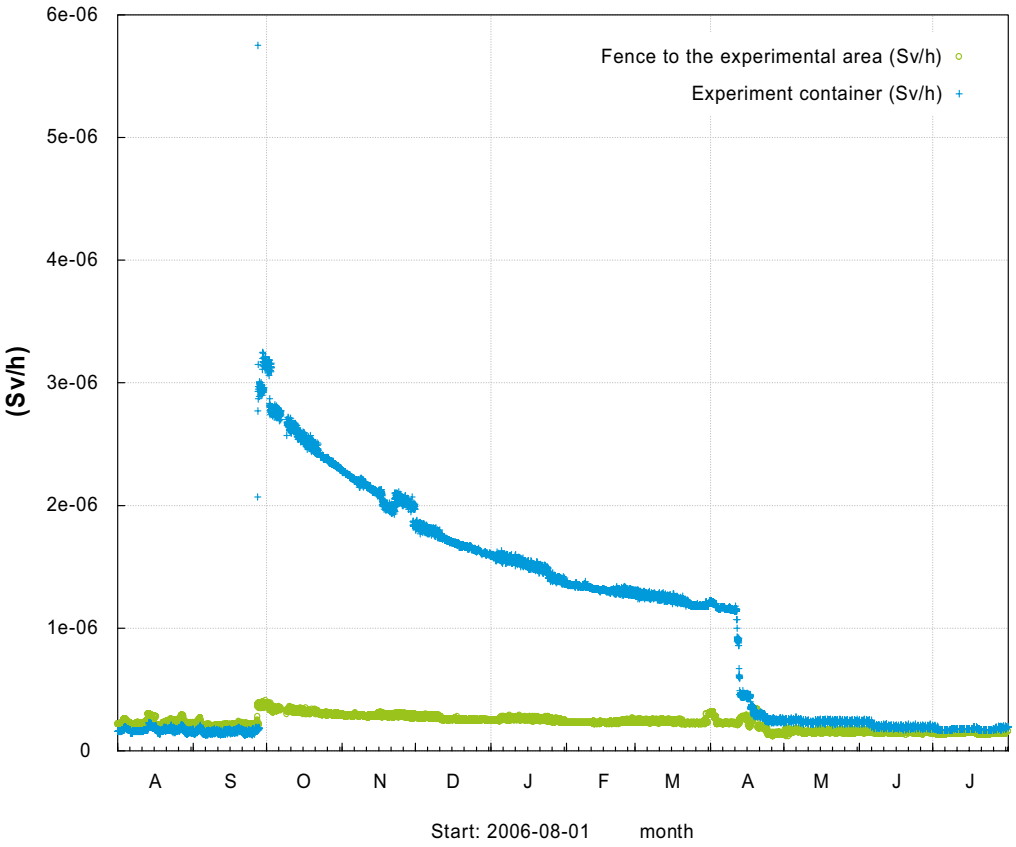

Figure A2-4. *Dose rate monitoring (in Sv/h) in the experimental container (blue) and at the fence enclosing the experimental site (green).*

Appendix 3

Geological characterization

A1

Characterization of whole core

B. *A.*

General:
Remaining epoxy on the fracture surface, c. 80%.

Partially, 0–1 mm width between the epoxy and the fracture surface.

About 50% coverage of fracture minerals, with a thickness of ≤ 0.5 mm.

Mineralogy:
Quartz, k-feldspar, plagioclase, biotite, chlorite, titanite, hematite/magnetite and epidote.

K-feldspar to varying extent albitized, biotite partially altered to chlorite and plagioclase is partially saussuritized, i.e altered to epidote, sericite and albite. Titanite is probably hematite stained, visible as rusty color around some of the mineral grains.

Fracture surface coating (A): Chlorite and possibly calcite.

Fracture fillings, sealed fractures: chlorite and/or calcite.

Fractures:

a) Increasing amount of microfractures, mainly sealed, from about 4 cm and towards the fracture surface (A). The last cm = sealed fine-meshed network of very thin sealed and partly open microfractures.

b) At about 10.5 cm core length, two thin sealed fractures (≤ 1 mm width) with surrounding oxidation at an angle of approximately 45° to the borehole axis.

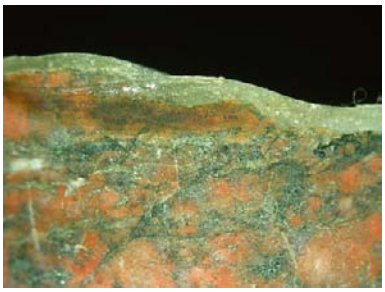

Wall rock alteration:
Red-staining as well as weak albitization, are visible with decreasing intensity from the fracture surface and inwards, about 11.5 cm. In microscope, weak degree of alteration is discernible throughout the whole core.

Characterization of the subdivided rock core

The first 30 mm of the cubic sawn rock core.

The first 3 cm of the rock core, cut into cubic form. Fracture material (primarily chlorite) to the right.

Autoradiogram of the identical rock slice after one day exposure time.

Sliced rock cores (except for A1.1 the photos are from the back side of the slice, i.e. a few mm from the fracture surface).

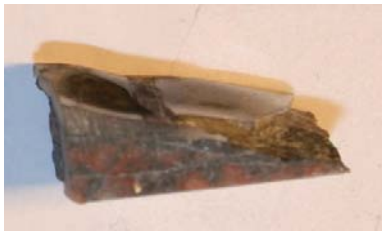

A1.1.

Uneven slice, average thickness is 5 mm. Several sealed microfractures near the fracture surface area A, i.e. the uppermost area at the picture which is also covered with epoxy to a large extent.

Fracture coating is estimated to cover ~50% of the surface.

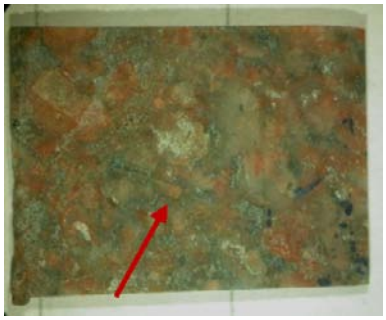

A1.2

a)

Picture through stereomicroscope (8×).

Partly open (or sealed) microfracture, perpendicular to the red arrow.

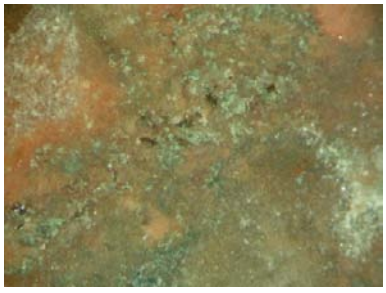

A1.2

b)

Picture through stereomicroscope (50×).

Porous mineral grains with vugs.

Sliced rock cores (except for A1.1 the photos are from the back side of the slice, i.e. a few mm from the fracture surface).

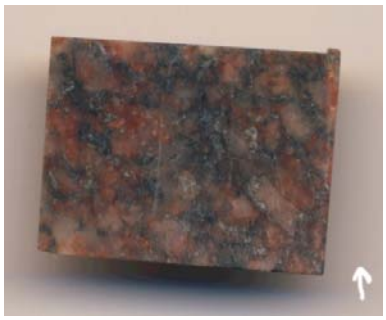

A1.3
Sealed microfracture with calcite and/or quartz.

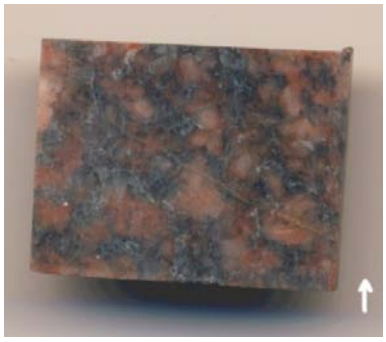

A1.4
Sealed microfracture with calcite and/or quartz.

- Rock slices 5 and 6 have microfractures of the same character as previous slices.
- Slices 6 to 16 have not been characterized with stereomicroscope.

Autoradiographs of the rock slices.

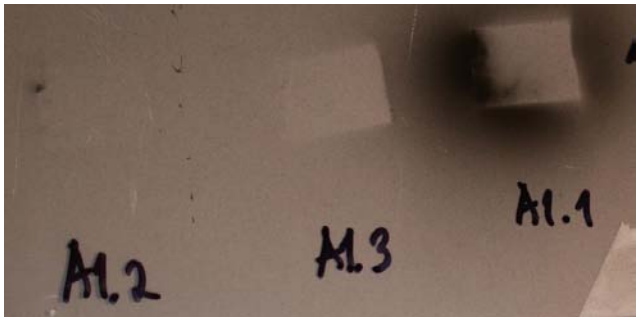

Film autoradiograph of rock slice A1.1 to A1.3 at 1 day exposure time. The blackening on the film represent radioactivity of primarily Cesium (Cs), at the thin end of the slice.

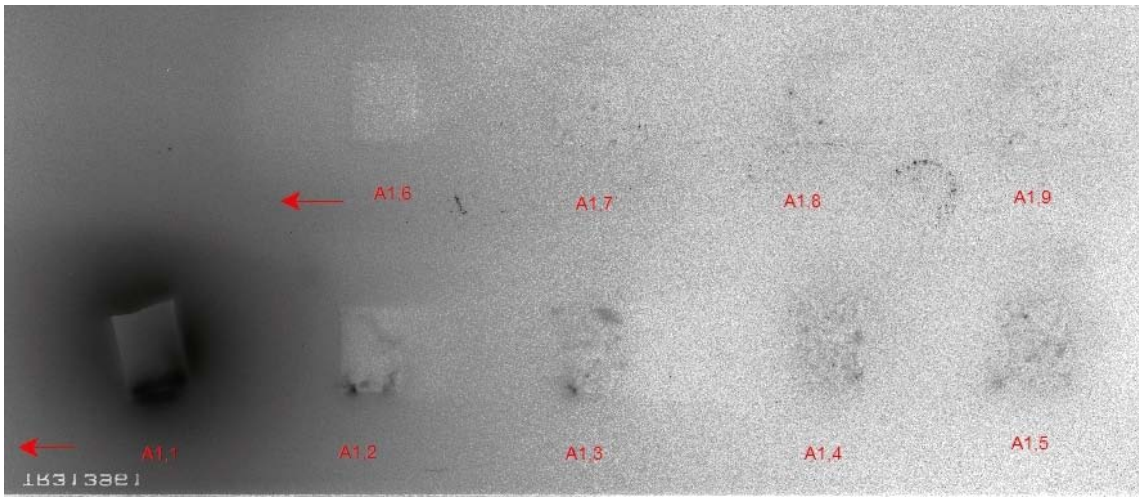

FLA-autoradiograph of rock slices A1.1 to A1.9. Blackening (slice A1.1 to A1.3) is representing the radioactivity in the slice.

A5

Characterization of whole core

B. *A.*

General:
Fracture surface covered with epoxy (100%).

Approximately 50% of the fracture surface has a thin (≤ 0.5 mm) fracture coating.

Mineralogy:
Quartz, k-feldspar, plagioclase, biotite, chlorite, titanite, hematite/magnetite and epidote.

K-feldspar to varying extent albitized, biotite partially altered to chlorite and plagioclase is partially saussuritized, i.e. altered to epidote, sericite and albite. Titanite is probably hematite stained, visible as rusty color around some of the mineral grains.

Fracture surface coating (A): minor amount of chlorite that is overlaid by calcite and/or quartz.

Fracture mineralogy, sealed fractures: calcite, hematite ± laumontite.

Fractures:
a) Sealed fracture 2 cm from and parallel with fracture surface (A). Forms a circle which does not close the ends (as illustrated for rock core A4).
b) Sealed fracture 5.5 cm from (A) but at angle to the borehole axis.
c) Small microfractures close to the fracture surface (A).

Wall rock alteration:
Red-staining, faint to medium. Faint degree, irregular at the second part of the rock core (towards B).

Characterization of the subdivided rock core

Sliced rock cores.

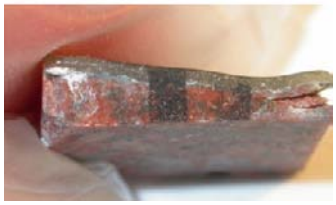

A5.1

Irregular slice.

Visible fracture coating under the epoxy layer (i.e. calcite ± chlorite) in addition to fractured rock, estimated to ~ 50%.

No visible microfractures.

Faint to weak alteration.

Sliced rock cores.

A5.2

Missing rock slice.

A5.3

No microfractures.

Faint alteration.

A5.4

Redstaining in grain boundaries.

- No specific notations for the remaining slices except for A5.9 which have a possible microfracture.

Autoradiographs of the rock slices.

Scanned images of rock slice A5.1 and A5.2, as well as film autoradiogram at 1 day exposure time. The blackening on the film represent radioactivity from sorptive elements, primarily Cesium (Cs).

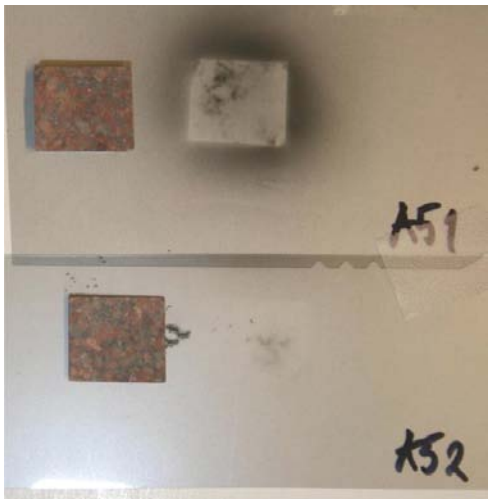

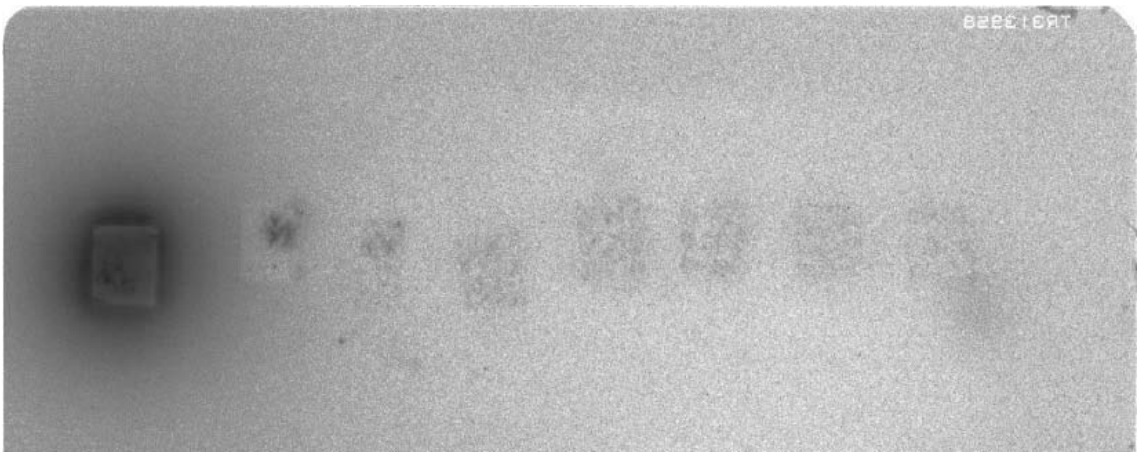

FLA-autoradiograph of rock slice A5.1 (to the left) to A5.8.

A6

Characterization of whole core

B. *A.*

General:
Epoxy cover 100% of the fracture surface.

The fracture surface coating is 0–2 mm thick and cover c. 95% of the surface.

Mineralogy:
Quartz, k-feldspar, plagioclase, biotite, chlorite, titanite, hematite/magnetite and epidote.

K-feldspar to varying extent albitized, biotite partially altered to chlorite and plagioclase is partially saussuritized, i.e. altered to epidote, sericite and albite. Titanite is probably hematite stained, visible as rusty color around some of the mineral grains.

Fracture surface coating: Calcite, chlorite, epidote and minor amount of chalcopyrite, ± quartz.

Fracture fillings, sealed fractures: Calcite.

Fractures:
a) Sealed fractures, 0.5 and 1 cm from fracture surface (A).
b) 2 fractures c. 45° to the borehole axis between the “0.5” and “1 cm fractures” described in a). Not visible round the whole core.
c) Very thin microfractures at c. 8 cm distance from the fracture surface (A). No specific orientation.

Wall rock alteration:
Faint to medium (possibly strong) degree of oxidation, i.e. red-staining.

Characterization of the subdivided rock core

The first 30 mm of the cubic sawn rock core.

Profile of A6, fracture material to the right in the picture.

Autoradiograph (film-AR) of the identical section of the rock at 1 day exposure time.

Sliced rock core.

A6.1

The rock slice is uneven and the protecting epoxy layer (top of the fracture coating A) is visible in the upper left corner. Close to this epoxy is a thin rim of fracture coating, i.e. chlorite/±epidote and calcite.

Fracture coating is estimated to cover ~95% of the surface of the slice.

No microfractures are documented

A6.2

No specific notations

A6.3

No specific notations

- Remaining slices are without any notations.

Autoradiographs of the rock slices.

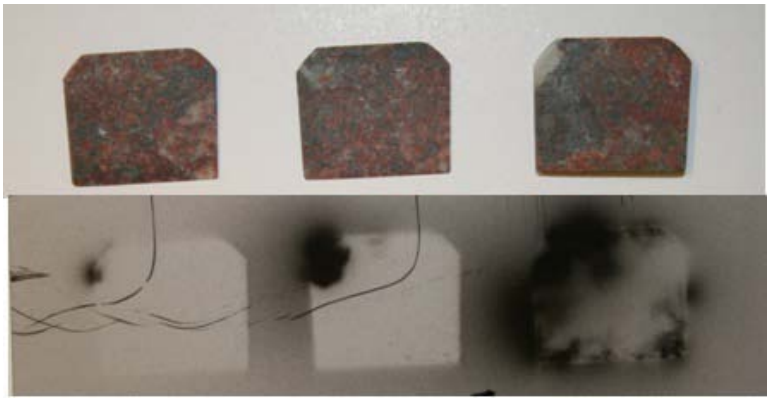

Photoimages of penetration depth in rock slice A6.1 (to the right) to A6.3 on film autoradiogram at 1 day exposure time. A3.1 has uneven thickness, which is not visible at the picture above.

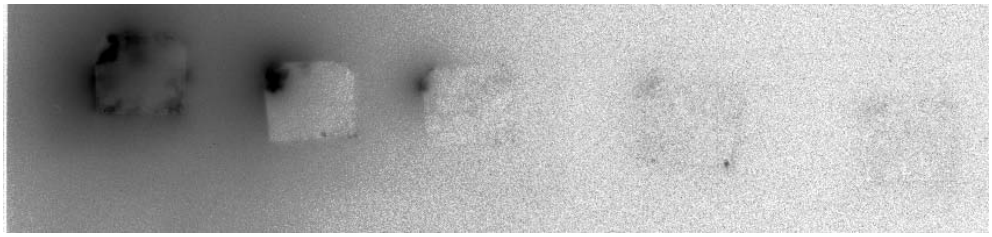

FLA-autoradiograph of rock slice A6.1 to A6.6, where A6.1 is to the left.

A8

Characterization of whole core

B. *A.*

General:
Epoxy cover 100% of the fracture surface.

The fracture coating is thin (≤ 0.2 mm) and cover about 50% of the surface area.

Mineralogy:
Quartz, k-feldspar, plagioclase, biotite, chlorite, titanite, hematite/magnetite and epidote.

K-feldspar to varying extent albitized, biotite partially altered to chlorite and plagioclase is partially saussuritized, i.e. altered to epidote, sericite and albite. Titanite is probably hematite stained, visible as rusty color around some of the mineral grains.

Fracture surface coating (A): Chlorite ± epidote.

Fracture fillings, sealed fractures: Calcite.

Fractures:

a) Sealed fracture at about 2.5 cm distance from fracture surface (A).

b) Thin, sealed microfractures sporadic over the core. No specific orientation although.

Wall rock alteration:
Faint to medium oxidation, i.e. red-staining.

Characterization of the subdivided rock core

The first 30 mm of the cubic sawn rock core.

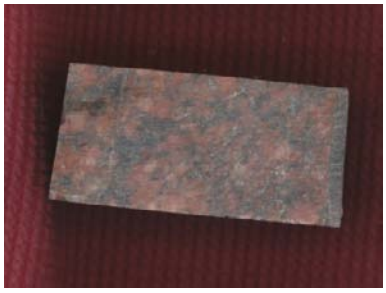

The first 3 cm of the rock core, cut into cubic form. Fracture material to the right in the picture.

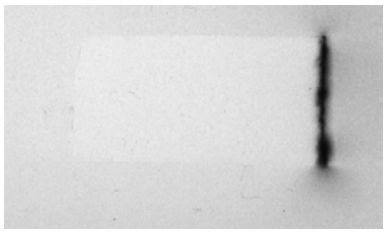

Autoradiogram of the identical section of the rock at 1 day exposure time.

Sliced rock core (photo from the back side of the slice, i.e. a few mm from the fracture surface).

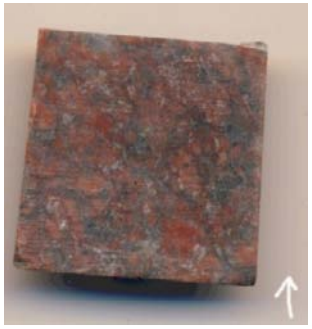

A8.1

Only a very thin layer of chlorite on the fracture surface (not visible on the picture), covering ~70% of the fracture surface

No microfractures

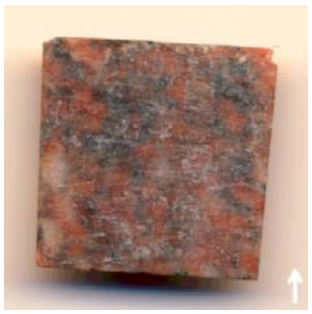

A8.2

No visible microfractures

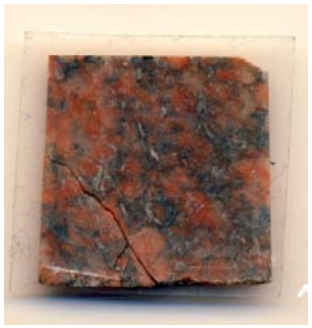

A8.3

Broken during sawing into slices.

- A8.3 – A8.6 No visible microfractures
- A8.6 – A8.15 No geological characterization performed.

Autoradiographs

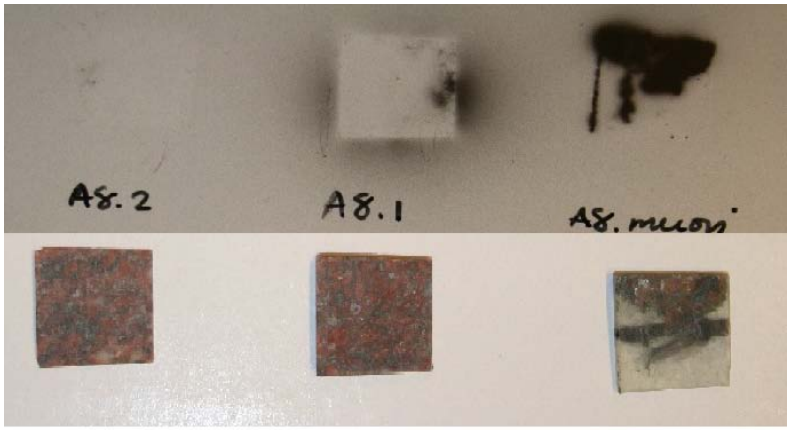

Photo images of profile penetration depth of rock slice A8.1 to A8.2 on film autoradiogram at 1 day exposure time. The slice to the right consists of epoxy and small amounts of rock material and possibly fracture material.

A9

Characterization of whole core

B. *A.*

General:
Epoxy covers 100% of the fracture surface.

50% of the fracture surface has a thin (≤ 0.5 mm) fracture coating.

Mineralogy:
Quartz, k-feldspar, plagioclase, biotite, chlorite, titanite, hematite/magnetite and epidote.

K-feldspar to varying extent albitized, biotite partially altered to chlorite and plagioclase is partially saussuritized, i.e. altered to epidote, sericite and albite. Titanite is probably hematite stained, visible as rusty color around some of the mineral grains.

Fracture surface coating (A): calcite, minor amounts of chlorite ± epidote.

Fractures:
a) Sealed fracture with calcite, red colored due to small hematite grains at a distance of c.3 cm from the fracture surface (A). At 70° to the borehole axis.
b) Several short (0.5 to 1 cm) microfractures parallel with a).

Wall rock alteration:
Red-staining, faint to medium degree, increasing towards fracture surface (A).

Characterization of the subdivided rock core

The first 30 mm of the cubic sawn rock core.

The first 3 cm of the rock core, cut into cubic form. Fracture material (primarily chlorite) to the right.

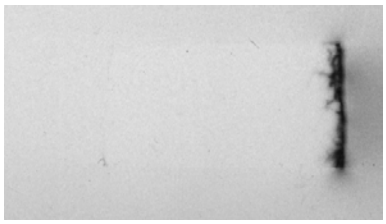

Autoradiogram of the identical rock slice at 1 day exposure time.

Sliced rock cores (photo from the back side of the slice, i.e. a few mm from the fracture surface).

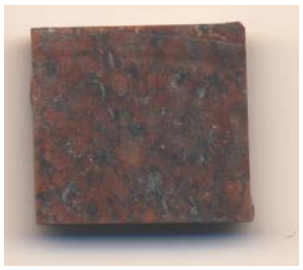

A9.1

Porous grain boundaries as well as single porous mineral grains (e.g. altered titanite, and chlorite).

Single microfractures.

Fracture coating is estimated to cover ~50% of the surface (not visible in the picture).

A9.2

Porous titanite grains. One tiny sealed mickrofracture.

A9.3

One tiny sealed mickrofracture.

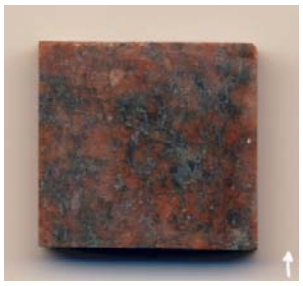

A9.4

Two sealed microfractures and probably one partly opened.

A9.5

Two sealed microfractures and probably one partly opened.

A9.6

Two sealed microfractures and probably one partly opened.

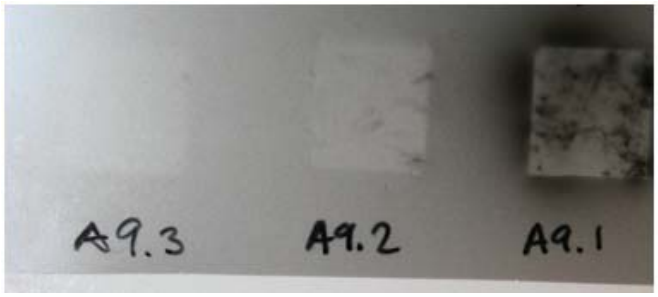

Film autoradiograph of rock slice A9.1 to A9.3 at 1 day exposure time.

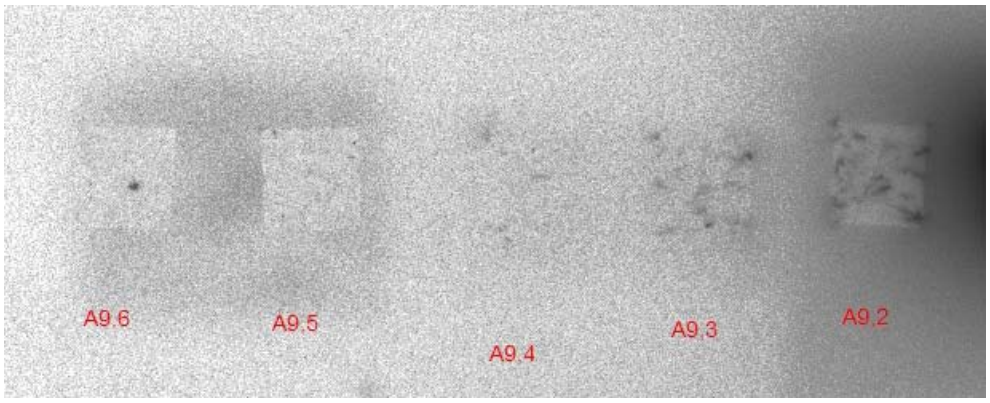

FLA-autoradiograph of rock slice A9.2 to A9.6.

A10

Characterization of whole core

B. *A.*

General:
Epoxy covers 100% of the fracture surface.

The fracture coating covers 100% of the fracture surface and is relatively thick (0.5–2 mm) at c. 75% of the area. At the remaining 25% of the surface the coating is thin (≤ 0.5 mm).

Mineralogy:
Quartz, k-feldspar, plagioclase, biotite, chlorite, titanite, hematite/magnetite and epidote.

K-feldspar to varying extent albitized, biotite partially altered to chlorite and plagioclase is partially saussuritized, i.e altered to epidote, sericite and albite. Titanite is probably hematite stained, visible as rusty color around some of the mineral grains.

Fracture surface coating (A): calcite, chlorite, chalcopyrite, epidote.

Fracture mineralogy, sealed fractures: calcite, quartz, chlorite, chalcopyrite ± oxidized walls.

Fractures:
a) Sealed fracture, 0.5–1 mm thick at 2.7 cm.

b) Several microfractures at 0–3 cm.

c) Diagonal (45°) sealed/partly opened fracture at 7 cm.

Wall rock alteration:
Weak to strong red-staining with increasing intensity towards the fracture surface (A).

Characterization of the subdivided rock core

Sliced rock cores

A10.1

Photographs of both the epoxy covered fracture surface (A), as well as the opposite side of the rock slice showing red-stained bedrock (M-S alteration).

Two small sealed microfractures (< 3 mm length) are visible.

A10.2

Two small microfractures.

Signs of recrystallization.

A10.3

The degree of alteration is less than in rock slice A10.1 (i.e. W-M alteration).

A10.4, A10.5

No divergence from the overall geology. Probably one sealed microfracture in slice A10.4.

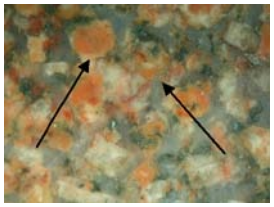

A10.6

Illustration of microfractures (sealed) in the rock slice. Magnified photograph (30×).

A10.6

Sealed microfractures.

A10.7–A10.15

Sealed microfracture in slice 8 and partly open in slice 9. Large amount of hematite in slice A10.10.

Autoradiographs of the rock slices.

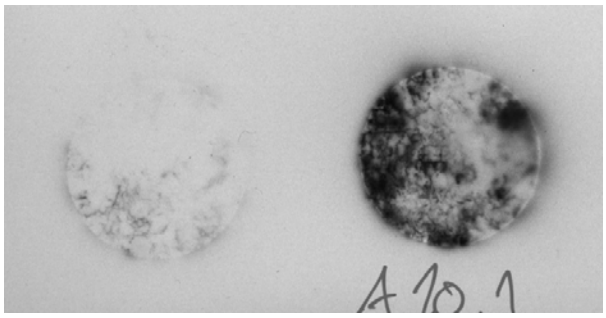

Film autoradiograph of rock slice A10.1 and A10.2 at 1 day exposure time.

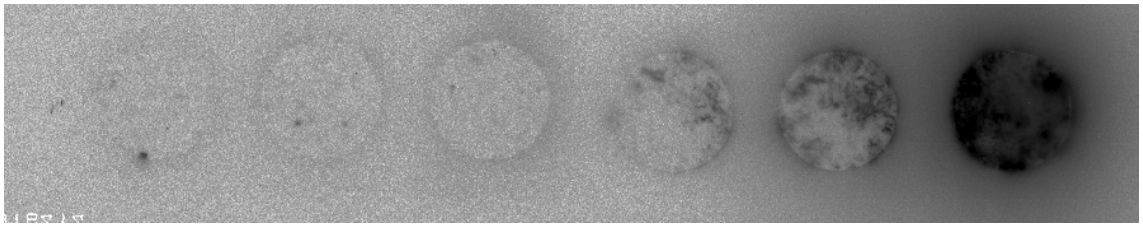

FLA-autoradiograph of rock slice A10.1 to A10.6.

A12

Characterization of whole core

B. A.

General:
Fracture surface covered with epoxy (100%).

The fracture surface coating is very thin and covers about 30%.

The core has been scratched during drilling.

Mineralogy:
Quartz, k-feldspar, plagioclase, biotite, chlorite, titanite, hematite/magnetite and epidote.

K-feldspar to varying extent albitized, biotite partially altered to chlorite and plagioclase is partially saussuritized, i.e. altered to epidote, sericite and albite. Titanite is probably hematite stained, visible as rusty color around some of the mineral grains.

Fracture surface coating (A): chlorite and calcite ± epidote.

Fracture fillings (partly open fractures): chlorite and calcite.

Fractures:
a) Partly opened fracture at 0–1 cm distance from the fracture surface (A), not exactly parallel to the fracture surface but perpendicular to the borehole axis.

b) Partly opened fracture at about 6 to 8 cm from the fracture surface (A). Undulating.

Wall rock alteration:
Red-staining, weak to strong degree, increasing towards fracture surface.

Characterization of the subdivided rock core

Sliced rock cores (photo from the back side of the slice, i.e. a few mm from the fracture surface).

A12.1

Epoxy covered on the opposite side as the photograph shows.

Grainboundaries partly porous.

Calcite in the lower right corner , as well as a thin layer of chlorite, is from a partly opened fracture 0–10 mm from the fracture surface A (described above).

Fracture coating is estimated to cover ~25% of the surface (not visible in this picture).

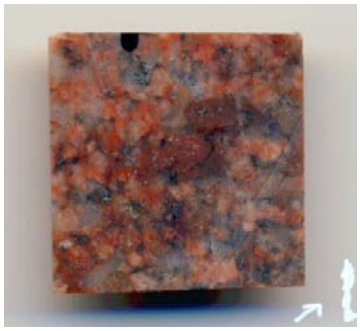

A12.2

Weakly red-stained.

Altered titanite grains, i.e small vugs inside.

A12.3

Broken during sawing.

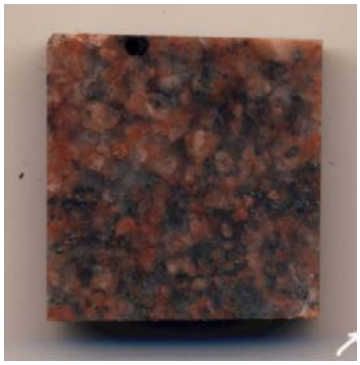

A12.5

Small pore space in a few grainboundaries.

A12.4, A12.6–A12.12

No deviations from the general description of the geology above.

Autoradiographs of the rock slices.

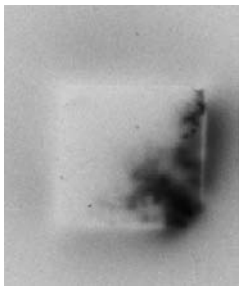

Film autoradiograph of rock slice A12.1 at 1 day exposure time.

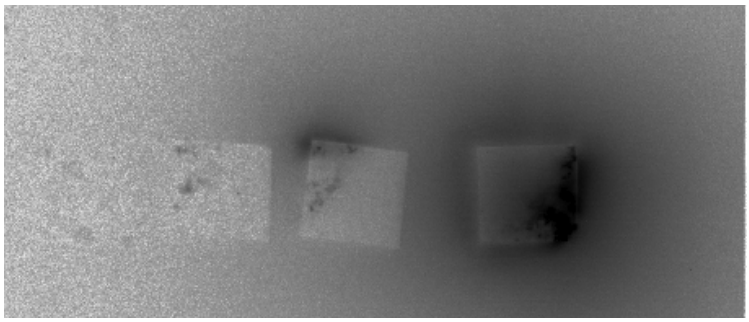

FLA-autoradiograph of rock slice A12.1 (to the right) to A12.4.

A15

Characterization of whole core

B. *A.*

General:
Epoxy covers 100% of the fracture surface.

Mineral coating on approximately 15% of the fracture surface.

Mineralogy:
Quartz, k-feldspar, plagioclase, biotite, chlorite, titanite, hematite/magnetite and epidote.

K-feldspar to varying extent albitized, biotite partially altered to chlorite and plagioclase is partially saussuritized, i.e. altered to epidote, sericite and albite. Titanite is probably hematite stained, visible as rusty color around some of the mineral grains.

Fracture surface coating (A): chlorite ± epidote.

Fracture fillings in partly open fracture: chlorite and calcite.

Fractures:
a) One partly opened fracture (parallel with the fracture surface (A)) at about 4 cm distance from the fracture surface (A).

b) Two thin partly open fractures (with calcite) cuts approximately diagonal to the borehole axis at about 7 to 8 cm distance from the fracture surface (A).

Wall rock alteration:
Faint to weak/medium degree of oxidation (red-staining).

Characterization of the subdivided rock core

Sliced rock cores (photo from the back side of the slice, i.e. a few mm from the fracture surface).

A15.1

No microfractures or vugs.

No divergence from the overall geology described above.

Fracture coating is estimated to cover ~35% of the surface (not visible in this picture).

A15.2

No microfractures or vugs.

No divergence from the overall geology described above.

A15.3

No microfractures or vugs.

No divergence from the overall geology described above.

Autoradiographs of the rock slices.

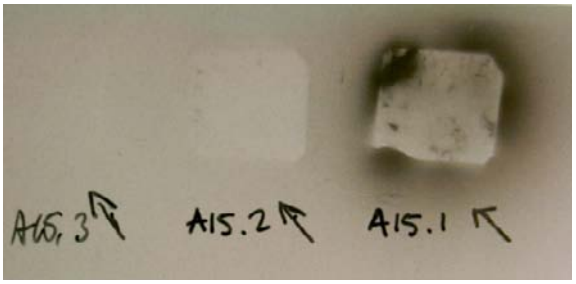

Film autoradiograph of rock slice A15.1 to A15.3 at 1 day exposure time.

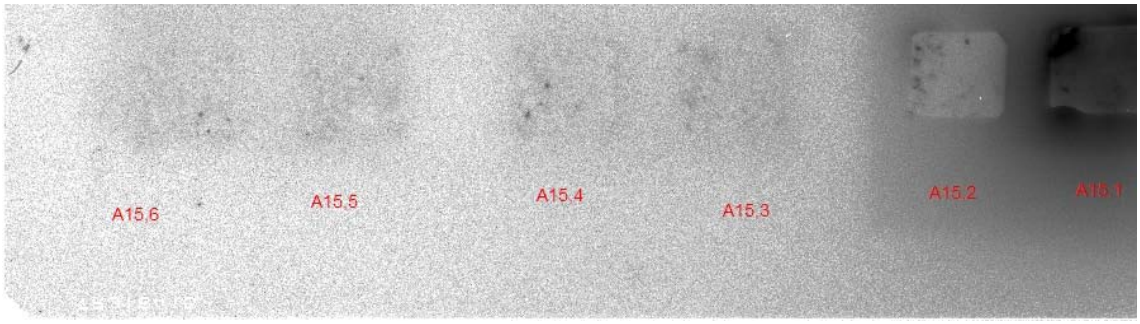

FLA-autoradiograph of rock slice A15.1 to A15.6.

A16

Characterization of whole core

B. *A.*

General:
100% epoxy covers the fracture surface.

No visible fracture coating.

Mineralogy:
Quartz, k-feldspar, plagioclase, biotite, chlorite, titanite, hematite/magnetite and epidote.

K-feldspar to varying extent albitized, biotite partially altered to chlorite and plagioclase is partially saussirized, i.e altered to epidote, sericite and albite. Titanite is probably hematite stained, visible as rusty color around some of the mineral grains.

Fracture surface coating (A): None.

Fracture filling: Calcite, hematite and possibly small amounts of chlorite ± laumontite.

Fractures:
a) One partly open fracture at about 4 cm distance from fracture surface (A).

b) a few microfractures close to and subparallel to the fracture surface.

Wall rock alteration:
Faint to medium degree of oxidation (red-staining).

Characterization of the subdivided rock core

Sliced rock cores (photo from the back side of the slice, i.e. a few mm from the fracture surface).

A16.1
Open microfracture.
Several partly opened microfractures.

Sliced rock cores (photo from the back side of the slice, i.e. a few mm from the fracture surface).

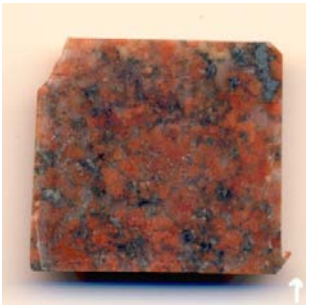

A16.2

Thin microfracture (probably the same as one of the microfractures in A16.1).

A16.3

Thin microfracture (probably the same as one of the microfractures in A16.1).

A16.4

Parly open microfractures, with calcite.

Thin microfracture (probably the same as in A16.1).

A16.5–A16.7 has thin sealed microfractures.

A16.8–A16.12; no divergence from the overall geology described above.

Autoradiographs of the rock slices.

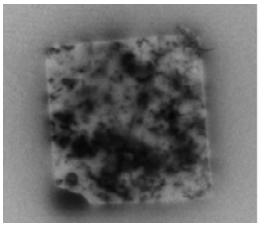

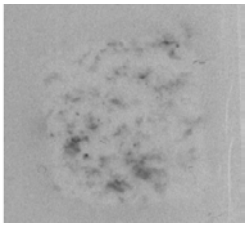

A16.1

Film autoradiograph of rock slices A16.1 (to the left) and A16.2 at 1 day exposure time.

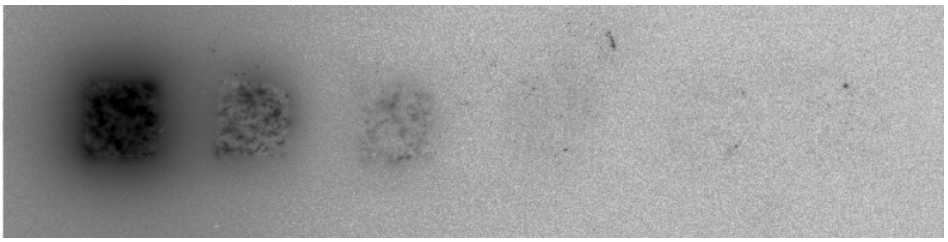

FLA-autoradiograph of rock slice A16.1 (to the left) to A16.6.

A17

Characterization of whole core

B. *A.*

General:
100% epoxy covers the fracture surface.

About 65% of the fracture surface has a thin fracture coating, ≤0.5 mm. Remaining surface area (c.35%) has a thicker coating, 0.5–1.5 mm (at 200°–300°).

Mineralogy:
Quartz, k-feldspar, plagioclase, biotite, chlorite, titanite, hematite/magnetite and epidote.

K-feldspar to varying extent albitized, biotite partially altered to chlorite and plagioclase is partially saussirized, i.e altered to epidote, sericite and albite. Titanite is probably hematite stained, visible as rusty color around some of the mineral grains.

Fracture surface coating (A): calcite.

Fracture filling: Calcite hematite and minor amounts of chlorite.

Fractures:
a) Several small subparallel fractures and microfractures close to the fracture surface (A).
b) 3 parallel sealed fractures at about 2, 2.5 and 4.5 cm distance from fracture surface (A) respectively.

Illustration of thick fracture coating (epoxy covered) as well as small chlorite/calcite filled fractures close to the fracture surface (A).

Wall rock alteration:
Weak to medium degree of oxidation (red-staining) at A, gradually decreasing towards B where no visible alteration is seen.

Characterization of the subdivided rock core

The first 30 mm of the cubic sawn rock core.

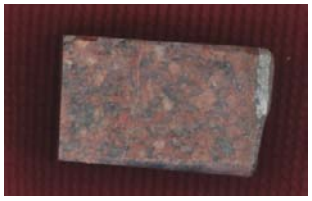

The first 3 cm of the rock core, cut into cubic form. Fracture material (primarily calcite) to the right.

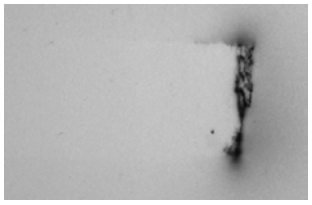

Autoradiogram of the identical rock slice at 1 day exposure time

Sliced rock cores (photo from the back side of the slice, i.e. a few mm from the fracture surface).

A17.1
Sealed microfracture.

A17.piece
Sealed microfracture.

A17.2

A17.3
Partly open microfracture.

A17.4–A17.6. No divergences from the overall geology, described above.
A17.7–A17.15. No geological characterization of the slices was performed.

Autoradiographs of the rock slices.

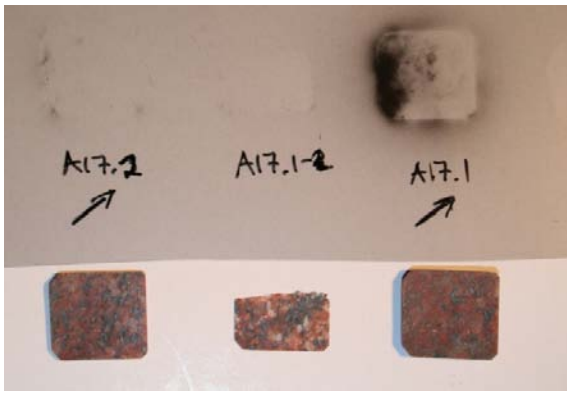

Film autoradiograph of rock slice A17.1, A17.1-2 and A17.2 at 1 day exposure time and the corresponding slices.

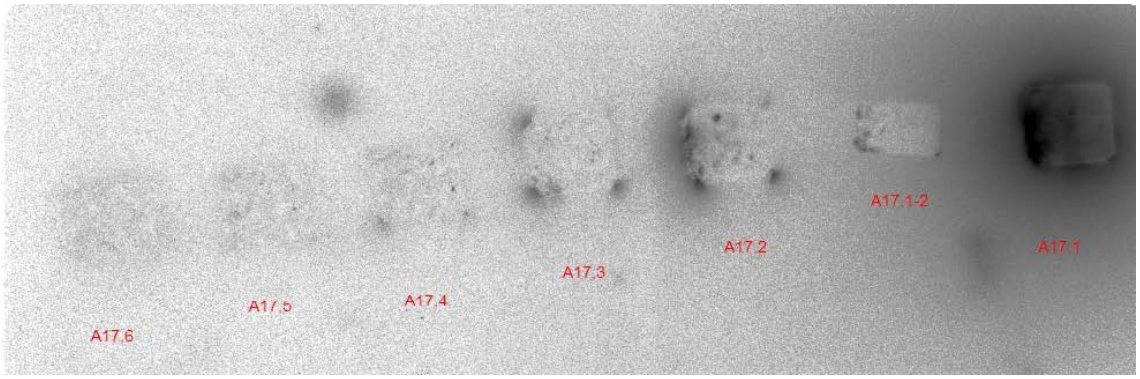

FLA-autoradiograph of rock slices A1.1 to A1.9. Blackening (slice A1.1 to A1.3) is representing the radioactivity in the slice.

D1

Characterization of whole core

B. *A.*

Mineralogy:
Quartz, k-feldspar, plagioclase, biotite, chlorite, titanite, hematite/magnetite and epidote.

K-feldspar to varying extent albitized, biotite partially altered to chlorite and plagioclase is partially saussuritized, i.e. altered to epidote, sericite and albite. Titanite is probably hematite stained, visible as rusty color around some of the mineral grains.

Fracture filling, sealed fracture: no clear visible minerals, probably small amounts quartz or calcite.

Fractures:
Sealed thin fracture (rotation 80° on core), subparallel with the borehole axis.

Signs of old sealed fracture close to B, visible as red-staining.

Wall rock alteration:
Faint degree of oxidation (red-staining) at (B) quickly decreasing to no visible alteration at (A).

Partly rusty color around titanite, hematite/magnetite and chlorite.

Sliced rock cores (the photos are from the back side of the slice, i.e. a few mm from the fracture surface).

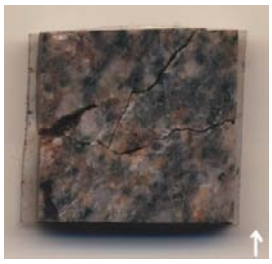

D1.1.

Several open and partly open microfractures, 3 of them were broken during sawing into slices.

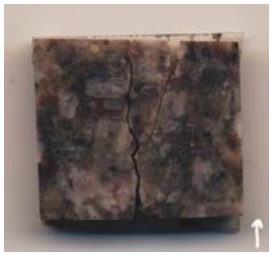

D1.2

Several open and partly open microfractures, some of them were broken during sawing into slices.

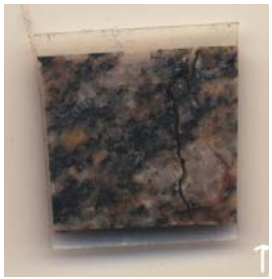

D1.3

Several open and partly open microfractures,1 of them were broken during sawing into slices.

- Rock slice 6 have microfractures of the same character as slice 1–3.
- Slices 7 to 16 have not been characterized with stereomicroscope.

Autoradiographs of the rock slices

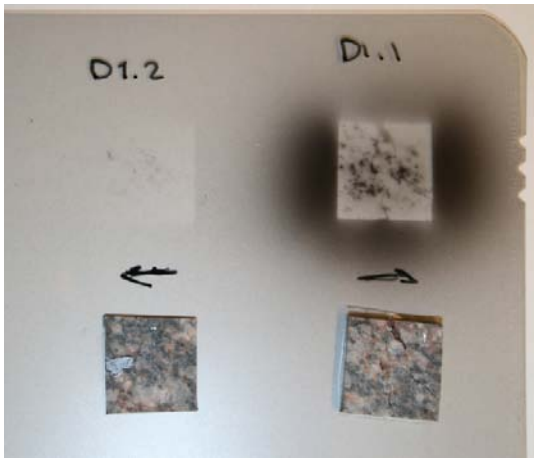

Film autoradiograph of rock slice D1.1 and D1.2 at 1 day exposure time.

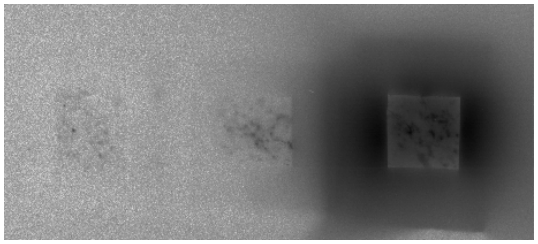

FLA-autoradiograph of rock slice D1.1 to D1.3.

D5

Characterization of whole core

B. A.

Mineralogy:
Quartz, k-feldspar, plagioclase, biotite, chlorite, titanite, hematite/magnetite and epidote.

K-feldspar to varying extent albitized, biotite partially altered to chlorite and plagioclase is partially saussuritized, i.e. altered to epidote, sericite and albite.

Fractures:
No detectable.

Wall rock alteration:
Faint alteration.

Characterization of the subdivided rock core

Sliced rock cores (the photos are from the back side of the slice, i.e. a few mm from the fracture surface).

D5.1.
One open fracture, probably due to drilling.

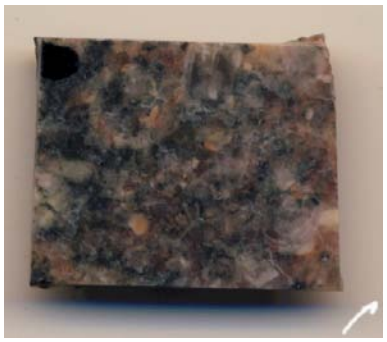

D5.2.
No visible microfractures

D5.3 to D5.6 – No remarks

Autoradiographs of the rock slices.

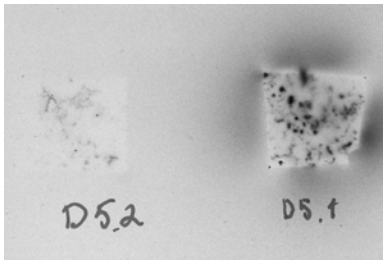

Film autoradiograph of rock slice D5.1 to D5.2 at 1 day exposure time.

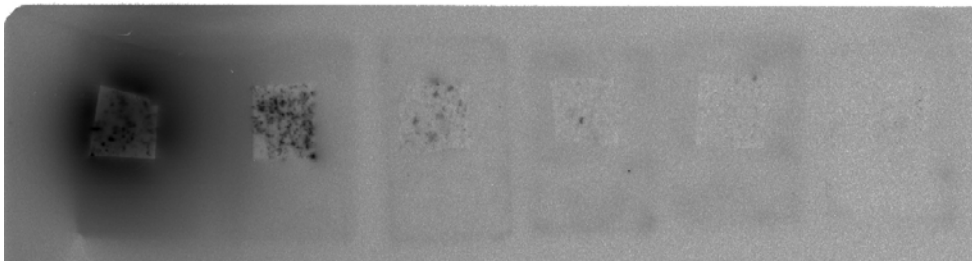

FLA-autoradiograph of rock slice D5.1 to D5.6.

D7

B. *A.*

Mineralogy:
Quartz, k-feldspar, plagioclase, biotite, chlorite, titanite, hematite/magnetite and epidote.

K-feldspar to varying extent albitized, biotite partially altered to chlorite and plagioclase is partially saussuritized, i.e. altered to epidote, sericite and albite.

Fracture filling, sealed fracture: Calcite, hematite ± quartz ± laumontite.

Fractures:
a) Sealed fracture at about 6 cm distance from (A). The angle is approximately 20° to the borehole axis.

b) Small microfractures at 0.5–1 mm from the slimhole (A) when the core is rotated 160°. Possibly drill induced microfractures.

Wall rock alteration:
No clear signs of alteration, except for small areas around old sealed fractures.

Sliced rock cores

D7.1.

Uneven slice. One microfracture.

D7.2.

One microfracture.

Slice 3 is broken during the laboratory work.

Slice 4 has a sealed microfracture.

Slices 5 to 6 have no visible microfractures, although slice Remaining slices, i.e. 7 to 15, have not been characterized with stereomicroscope.

Autoradiographs of the rock slices.

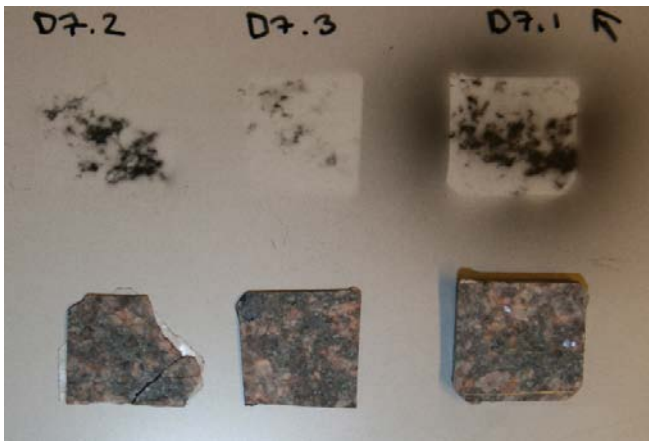

Film autoradiograph of rock slice D7.1 to D7.3 at one day exposure time.

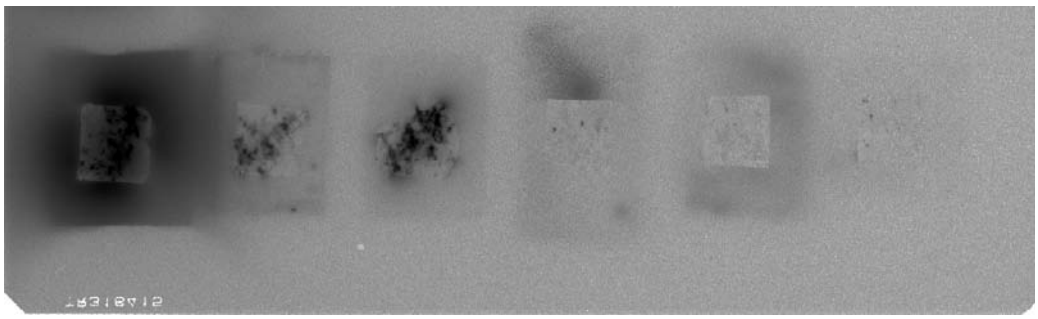

FLA-autoradiograph of rock slice D7.1 (to the left) to D7.6 (to the right). Note that slice D7.2 and D7.3 have switched positions.

D8

Characterization of whole core

Mineralogy:
Quartz, k-feldspar, plagioclase, biotite, chlorite, titanite, hematite/magnetite and epidote.

K-feldspar to varying extent albitized, biotite partially altered to chlorite and plagioclase is partially saussuritized, i.e. altered to epidote, sericite and albite.

Fracture filling, sealed fracture: Calcite ± quartz.

Fractures:
a) Sealed fracture at about 3cm distance from (A). The angle is approximately 20° to the bore-hole axis.

b) Several small microfractures at 0.5–1 mm from the slimhole (A). Possibly drill induced microfractures.

Wall rock alteration:
Faint to weak oxidation (red-staining). Most of the red-staining probably originate from old sealed fractures.

Characterization of the subdivided rock core

The first 30 mm of the cubic sawn rock core.

The first 3 cm of the rock core, cut into cubic form.

Autoradiogram of the identical rock slice after one day exposure time

Sliced rock cores (the photos are from the back side of the slice, i.e. a few mm from the fracture surface).

D8.1

Uneven slice.

Several small (3–4 mm length) microfractures. No visible aperture.

D8.2

The small microfractures that was visible in Slice 1, is documented in Slice 2 as well.

Slices 3 to 5 have microfractures without any visible aperture or fracture filling.

There are no microfractures in slices 6 to 9, but microfracturing is documented in slices 10 to 14.

Autoradiographs of the rock slices.

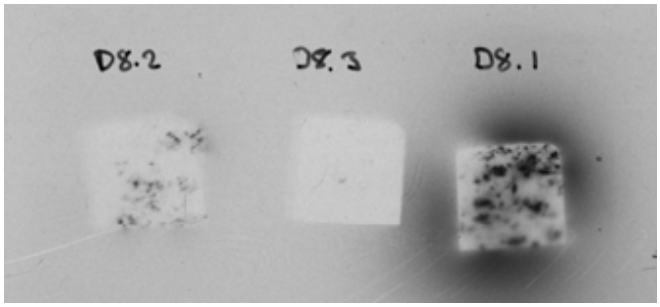

Film autoradiograph of rock slice D8.1 to D8..3 at 1 day exposure time.

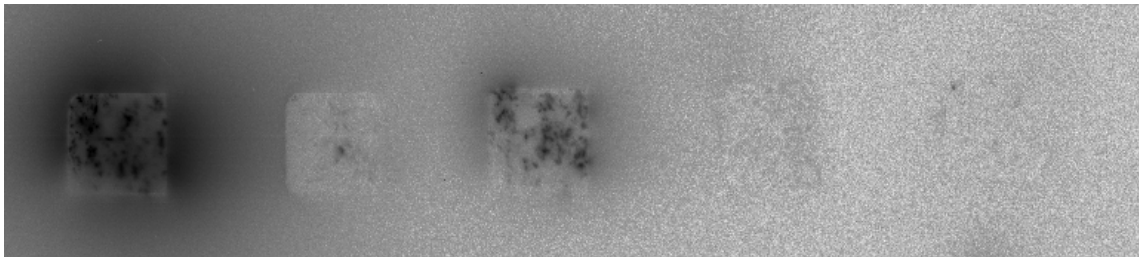

FLA-autoradiograph of rock slices D8.1 (to the left) to D8.6. Note that D8.2 and D8.3 have switched positions.

D12

Characterization of whole core

B. *A.*

General:
Minor amounts of remaining epoxy on the core at the surface towards the slimhole (A).

Mineralogy:
Quartz, k-feldspar, plagioclase, biotite, chlorite, titanite, hematite/magnetite and epidote.

K-feldspar to varying extent albitized, biotite partially altered to chlorite and plagioclase is partially saussuritized, i.e. altered to epidote, sericite and albite.

Fracture filling, sealed fractures: calcite and hematite ± quartz ± laumontite.

Wall rock alteration:
Nearly no signs of alteration. Single mineral grains are slightly red-stained or albitized.

Characterization of the subdivided rock core

The first 30 mm of the cubic sawn rock core.

The first 3 cm of the rock core, cut into cubic form.

Autoradiogram of the identical rock slice after one day exposure time

Sliced rock cores (the photos are from the back side of the slice, i.e. a few mm from the fracture surface).

D12.1

No documented microfractures

D12.2

One documented microfracture

- D12.4 – one micofracture.
- D12.3, D12.5 and D12.6 – no visible microfractures.

Autoradiographs.

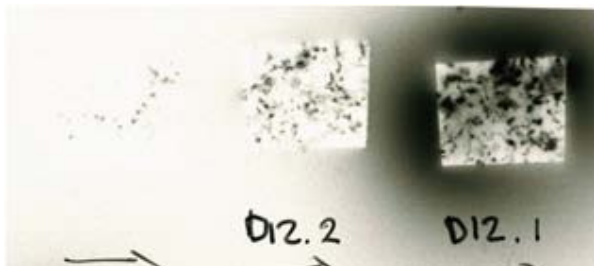

Film autoradiograph of rock slice D12.1 to D12.3 at 1 day exposure time.

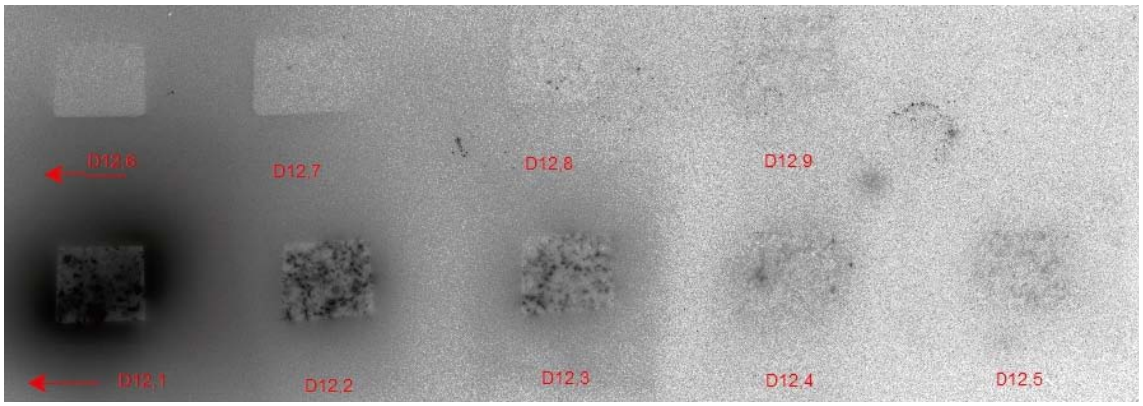

FLA-autoradiograph of rock slices D12.1 to D12.9.

D13

Characterization of whole core

B. *A.*

Mineralogy:
Quartz, k-feldspar, plagioclase, biotite, chlorite, titanite, hematite/magnetite and epidote.

K-feldspar to varying extent albitized, biotite partially altered to chlorite and plagioclase is partially saussuritized, i.e. altered to epidote, sericite and albite.

Fracture filling, sealed fractures: calcite and hematite ± quartz and laumontite.

Fractures:
a) Open (or partly open) microfracture at the slimhole surface (A).

b) 2 sealed fractures with different orientations (cross cutting), visible in the upper part of the core (1–4 cm).

c) Microfractures around the fractures described in b).

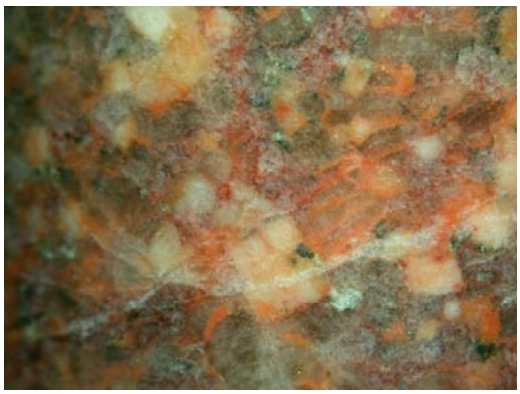

Illustration of the two sealed fractures described in b).

Wall rock alteration:
Red-staining, only around sealed fractures.

Characterization of the subdivided rock core

The first 30 mm of the cubic sawn rock core.

The first 3 cm of the rock core, cut into cubic form. Fracture material (primarily chlorite) to the right.

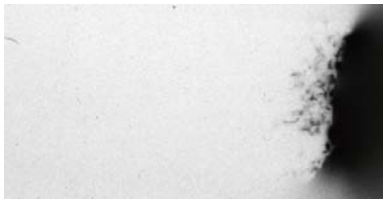

Autoradiogram of the identical rock slice after one day exposure time.

Sliced rock cores

D13.1.

Several sealed, partly open and/or open microfractures.

D13.2.

Sealed or partly open microfracture.

- Slices 3 to 6 contain several microfractures as well.
- Slices 7 to 15 have not been characterized by stereomicroscope.

Autoradiographs of the rock slices.

Film autoradiograph of rock slice D13.1 to D13. at 1 day exposure time.

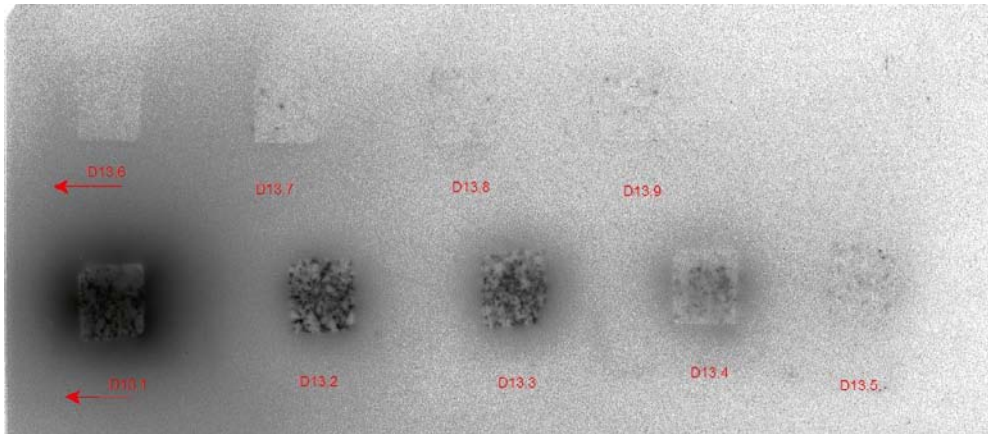

FLA-autoradiograph of rock slices D13.1 to D13.9.

D14

Characterization of whole core

B. *A.*

General:
Epoxy at the surface towards slimhole (yellow).

Mineralogy:
Quartz, k-feldspar, plagioclase, biotite, chlorite, titanite, hematite/magnetite and epidote.

K-feldspar to varying extent albitized, biotite partially altered to chlorite and plagioclase is partially saussuritized, i.e. altered to epidote, sericite and albite.

Fracture filling, sealed fractures: calcite and hematite ± quartz ± laumontite.

Fractures:
2 sealed fractures with different orientations (cross cutting), visible with core rotation 135–315° and 2.3 cm from (A). Both fractures split up and have small forks. α-angle is about 60–70°.

Wall rock alteration:
Faint to weak oxidation (red-staining) in the last part of rock core, from about. 9 to 12 cm (close to B).

Characterization of the subdivided rock core

Sliced rock cores (the photos are from the back side of the slice, i.e. a few mm from the fracture surface).

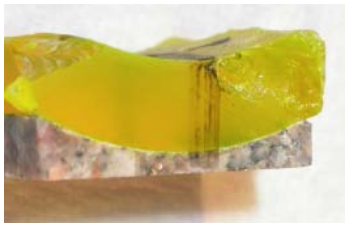

D14.1.
Uneven slice.
No documented microfractures.

D14.2.
No visible microfractures.

- Slice 3 and 4 have no documented microfractures.
- Slice 5 has one microfracture, probably sealed and slice 6 has a few mineral grains with vugs.
- D14.7 – D14.12 have no visible microfractures or other remarks.

Autoradiographs of the rock slices.

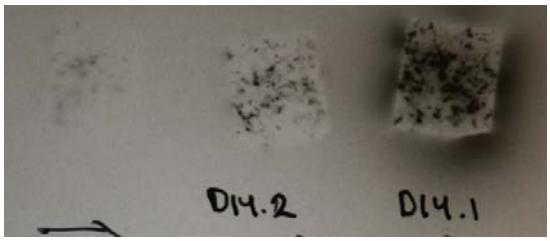

Film autoradiograph of rock slice D14.1 to D14.3 at 1 day exposure time.

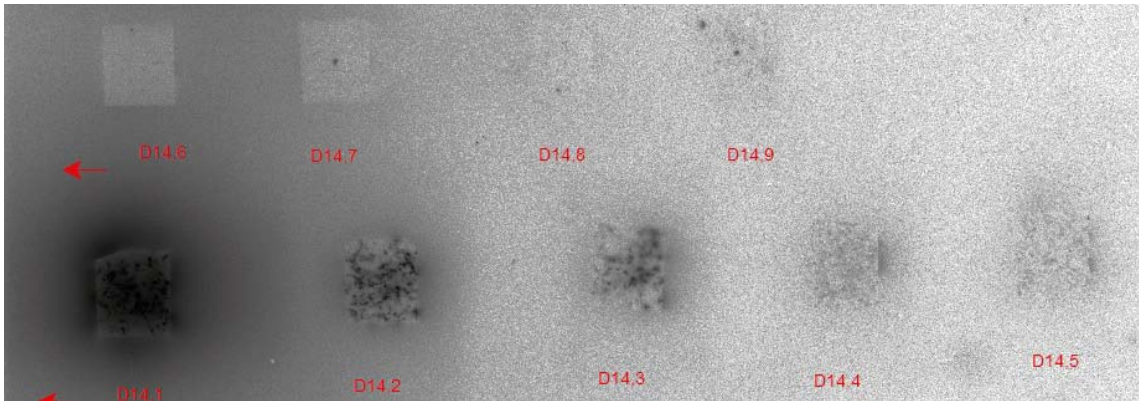

FLA-autoradiograph of rock slices D14.1 to D14.9.

Appendix 4

Tracer activities versus penetration depth (LSC)

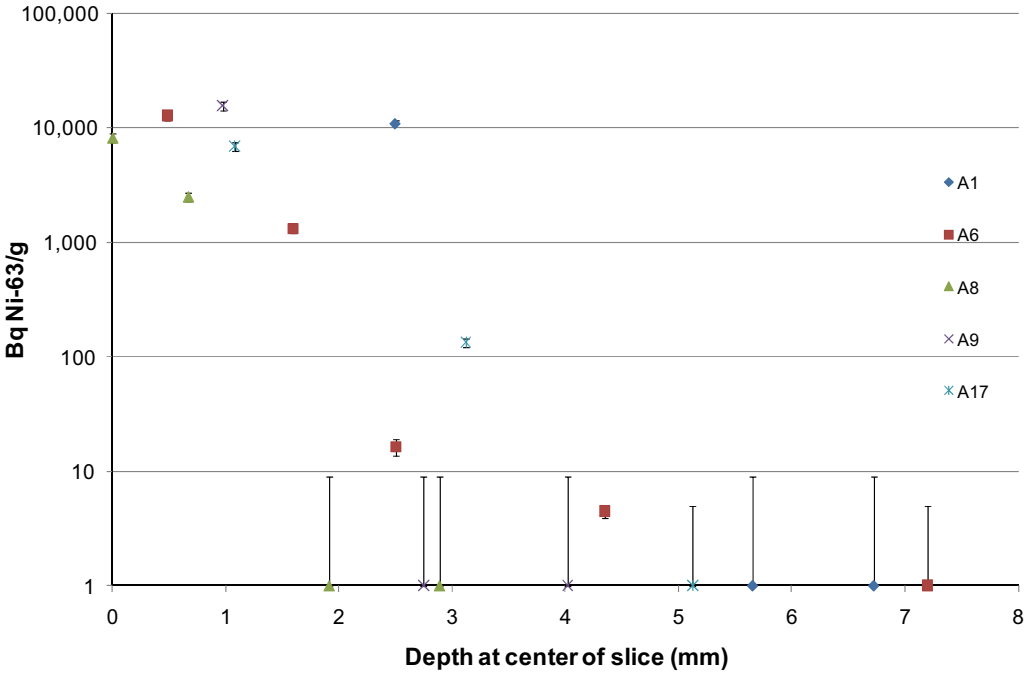

Figure A4-1. *Ni-63, A-cores. A value below the detection limit is shown as a corresponding bar. The activities in the two A8 samples at < 1 mm depth should be added if one wants to compare the activities in the first slices of the A-cores. The A8 core sample at 0 mm consists of 90% epoxy and 10% rock material.*

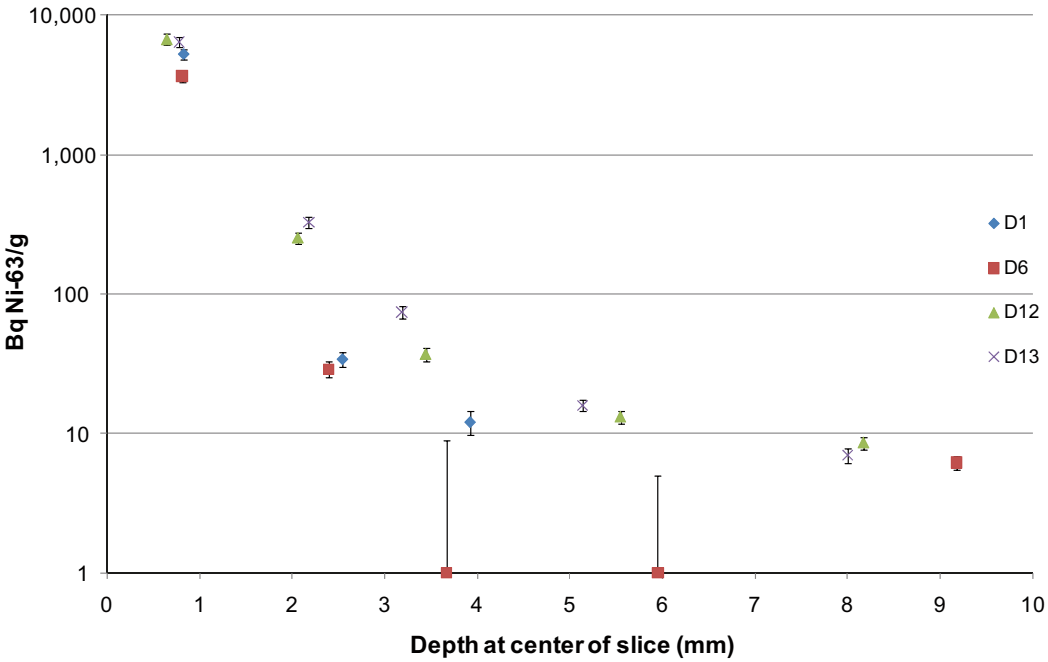

Figure A4-2. *Ni-63, D-cores. A value below the detection limit is shown as a corresponding bar.*

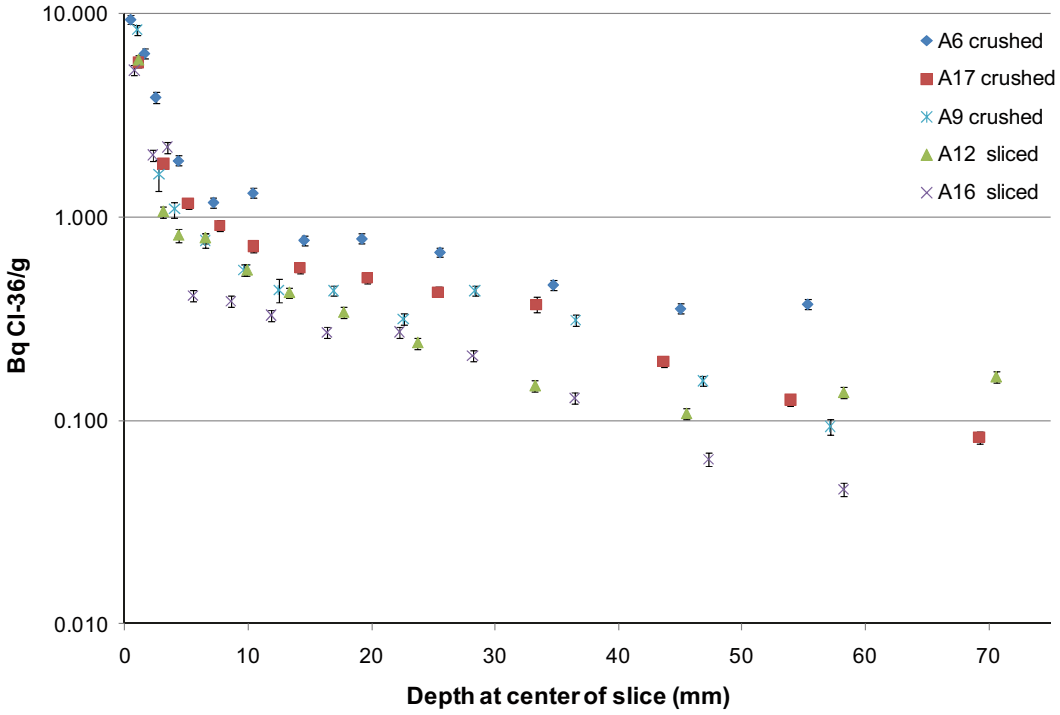

Figure A4-3. *Cl-36, A-cores.*

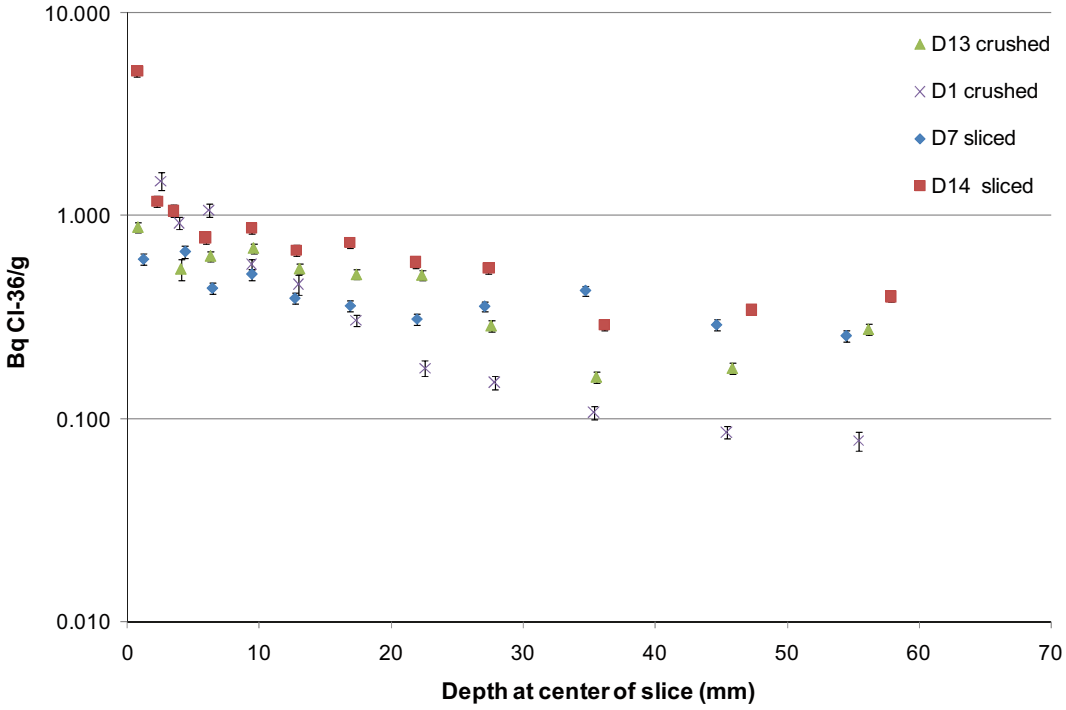

Figure A4-4. *Cl-36, D-cores.*

Appendix 5

Tracer activities versus penetration depth (HPGe)

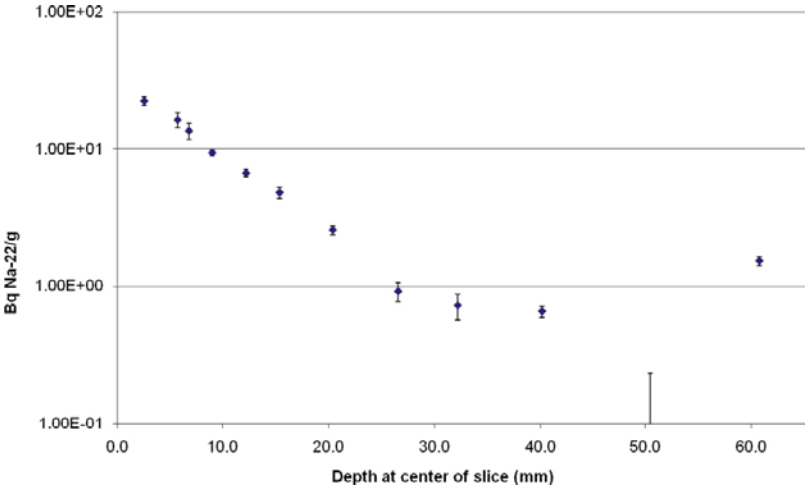

Figure A5-1. *Na-22 activities in core A1 versus length. A value below the detection limit is shown as a corresponding bar.*

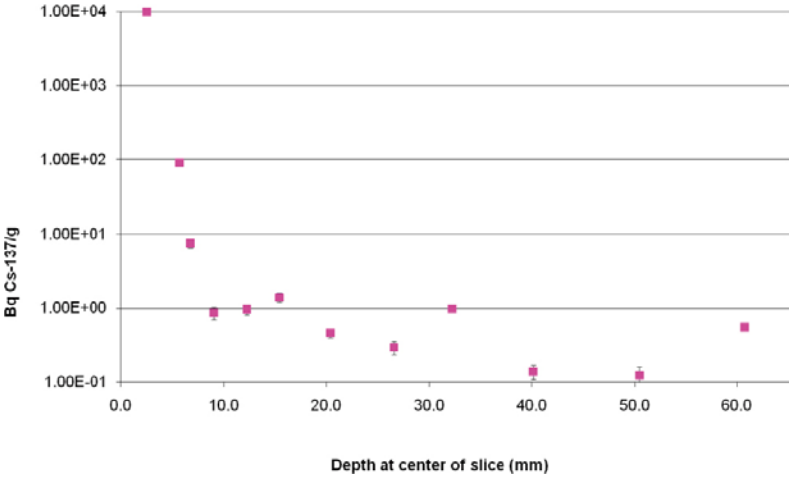

Figure A5-2. *Cs-137 activities in core A1 versus length.*

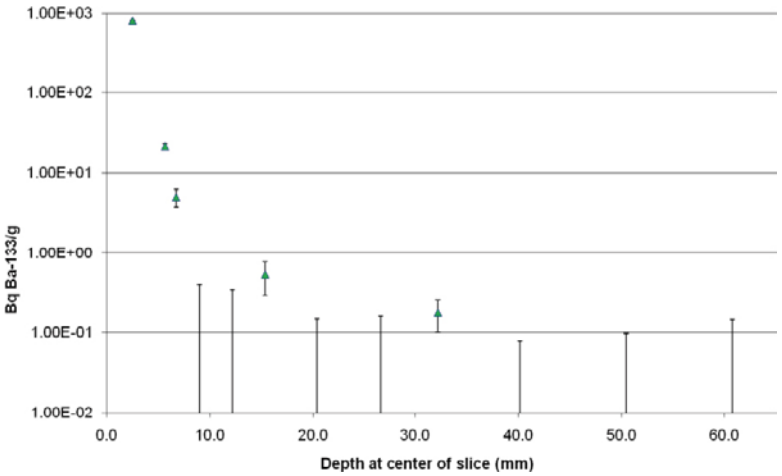

Figure A5-3. *Ba-133 activities in core A1 versus length. A value below the detection limit is shown as a corresponding bar.*

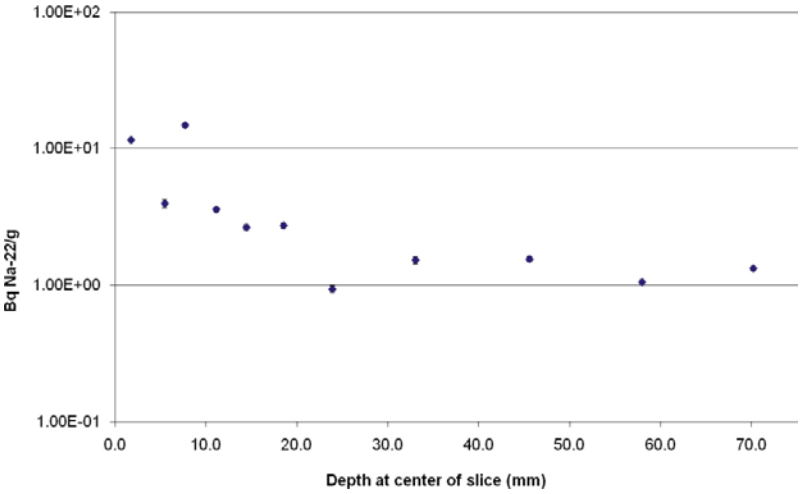

Figure A5-4. *Na-22 activities in core A5 versus length.*

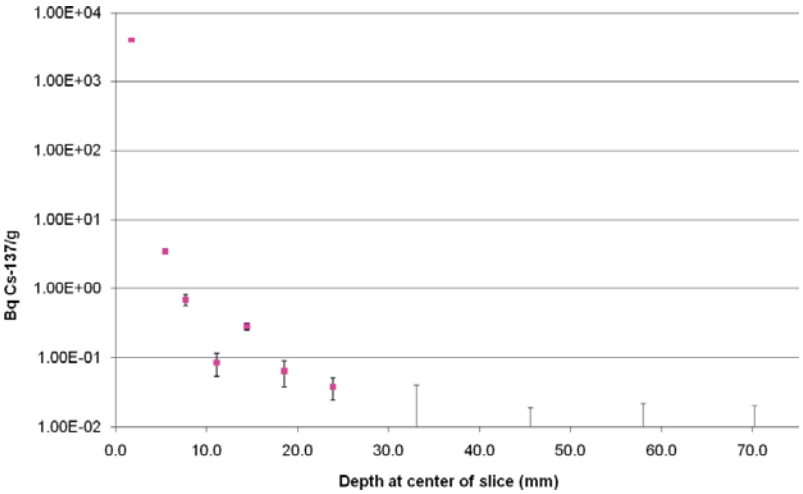

Figure A5-5. *Cs-137 activities in core A5 versus length. A value below the detection limit is shown as a corresponding bar.*

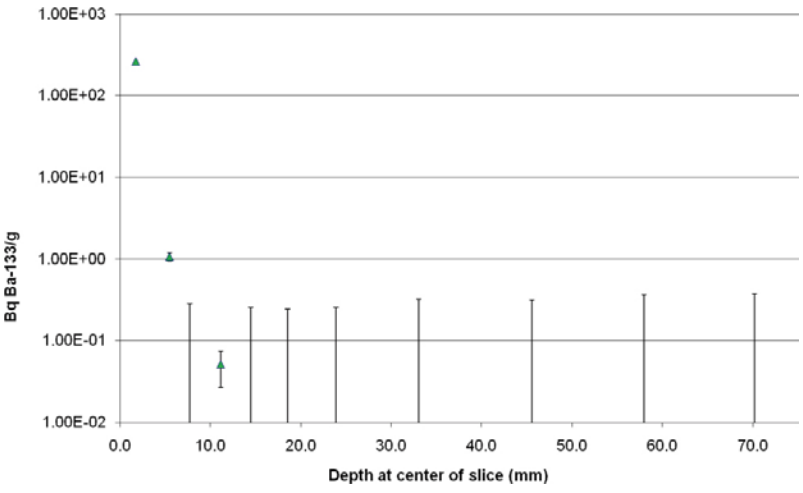

Figure A5-6. *Ba-133 activities in core A5 versus length. A value below the detection limit is shown as a corresponding bar.*

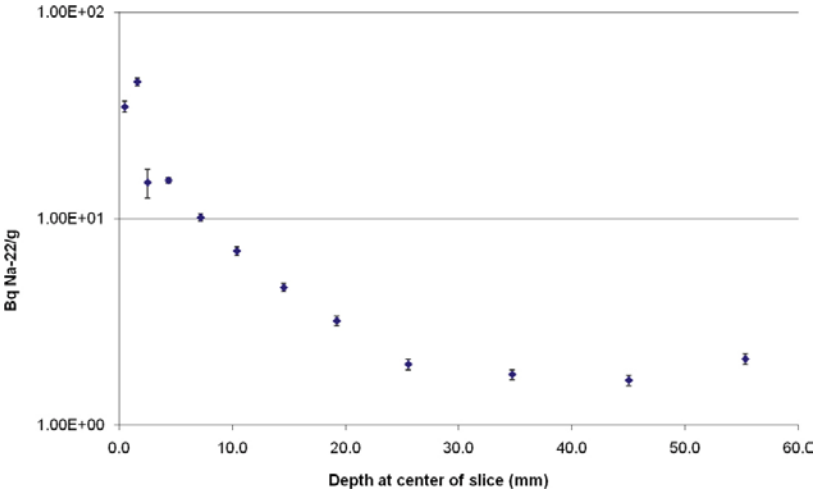

Figure A5-7. *Na-22 activities in core A6 versus length.*

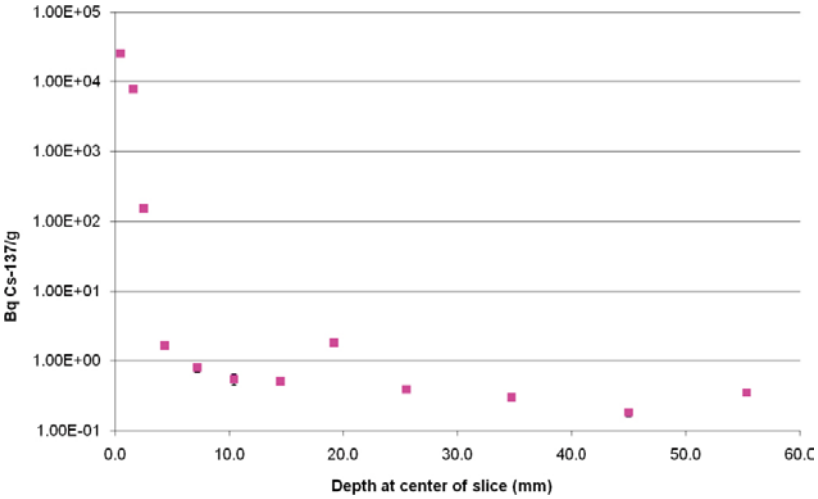

Figure A5-8. *Cs-137 activities in core A6 versus length.*

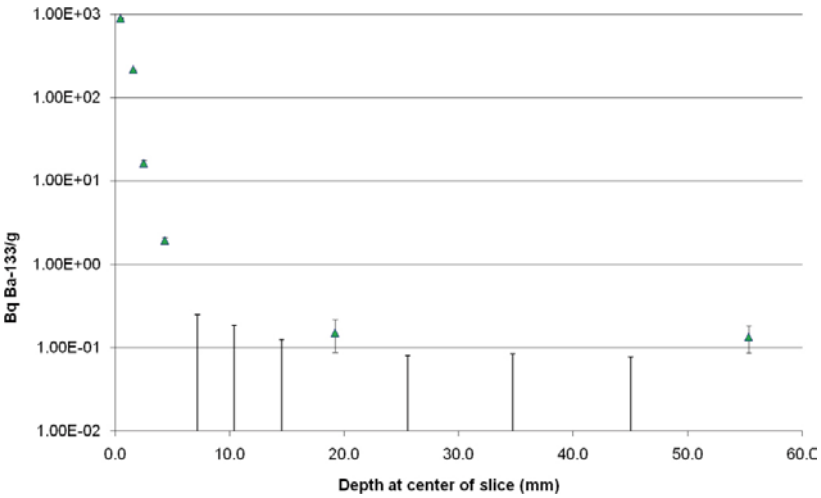

Figure A5-9. *Ba-133 activities in core A6 versus length. A value below the detection limit is shown as a corresponding bar.*

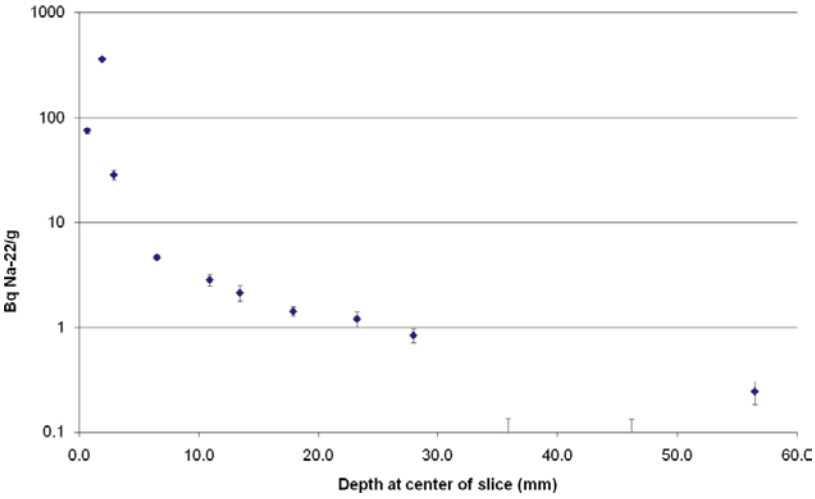

Figure A5-10. *Na-22 activities in core A8 versus length. A value below the detection limit is shown as a corresponding bar. The sample A8P, consisting mainly of Epoxy is not included.*

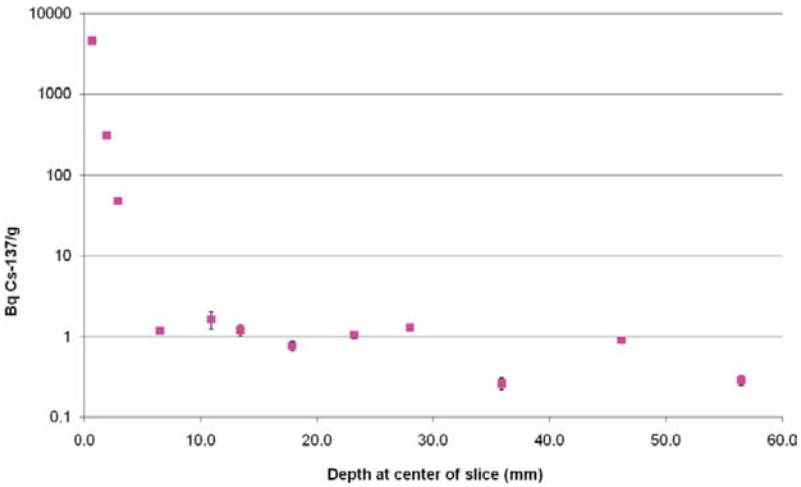

Figure A5-11. *Cs-137 activities in core A8 versus length. The sample A8P, consisting mainly of Epoxy is not included.*

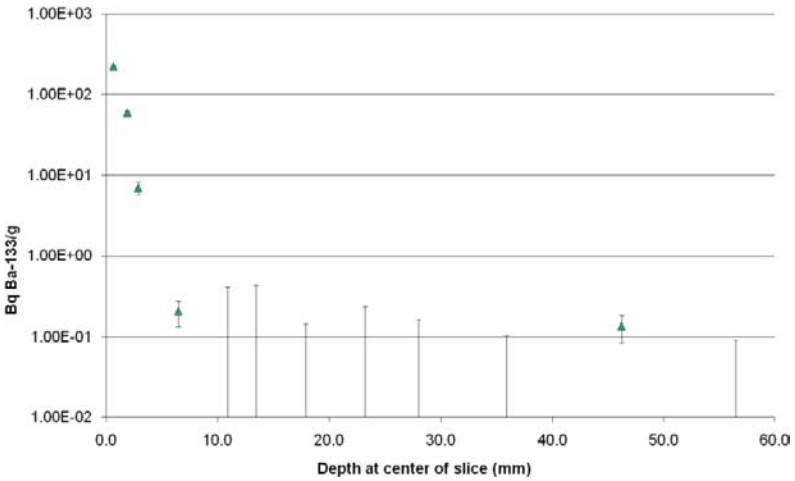

Figure A5-12. *Ba-133 activities in core A8 versus length. A value below the detection limit is shown as a corresponding bar. The sample A8P, consisting mainly of Epoxy is not included.*

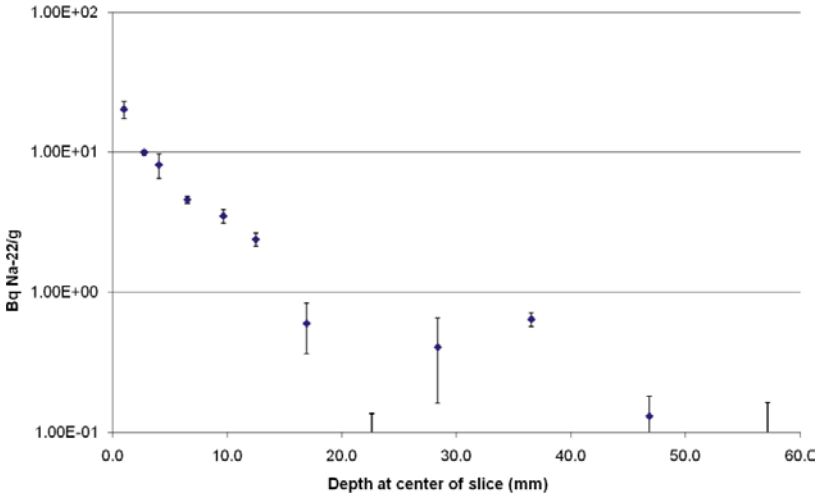

Figure A5-13. *Na-22 activities in core A9 versus length. A value below the detection limit is shown as a corresponding bar.*

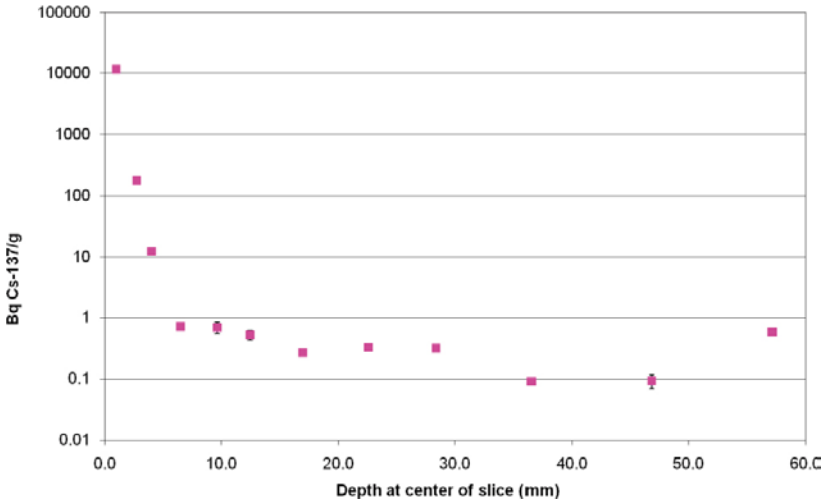

Figure A5-14. *Cs-137 activities in core A9 versus length.*

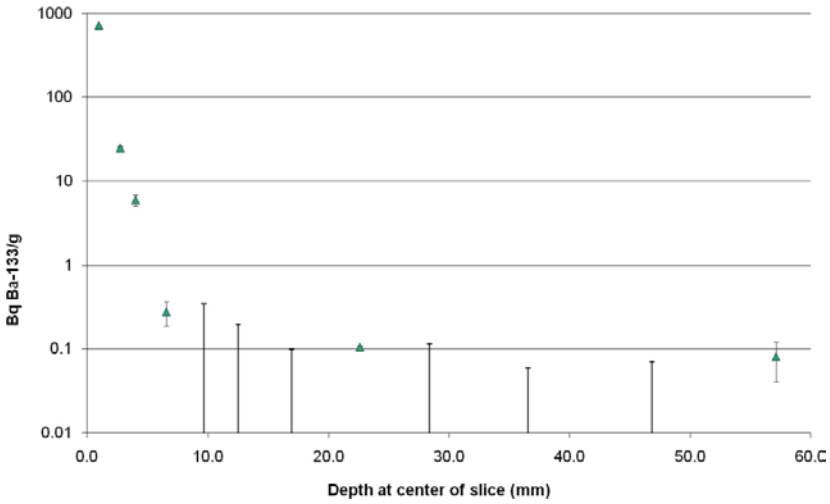

Figure A5-15. *Ba-133 activities in core A9 versus length. A value below the detection limit is shown as a corresponding bar.*

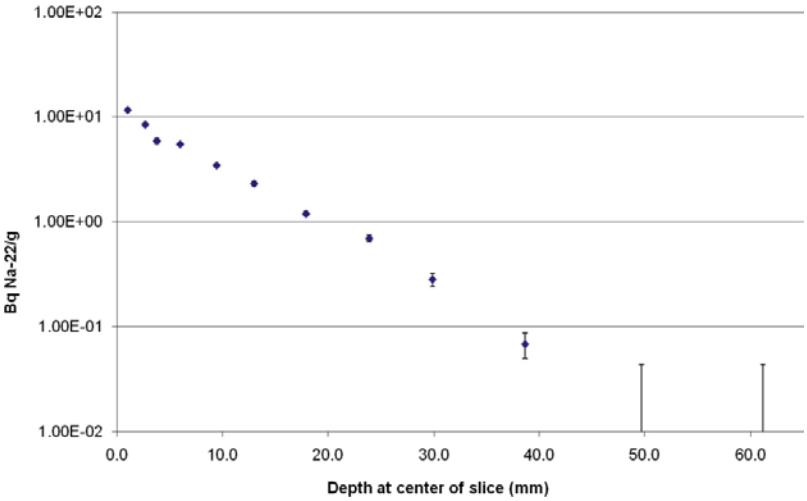

Figure A5-16. *Na-22 activities in core A10 versus length. A value below the detection limit is shown as a corresponding bar.*

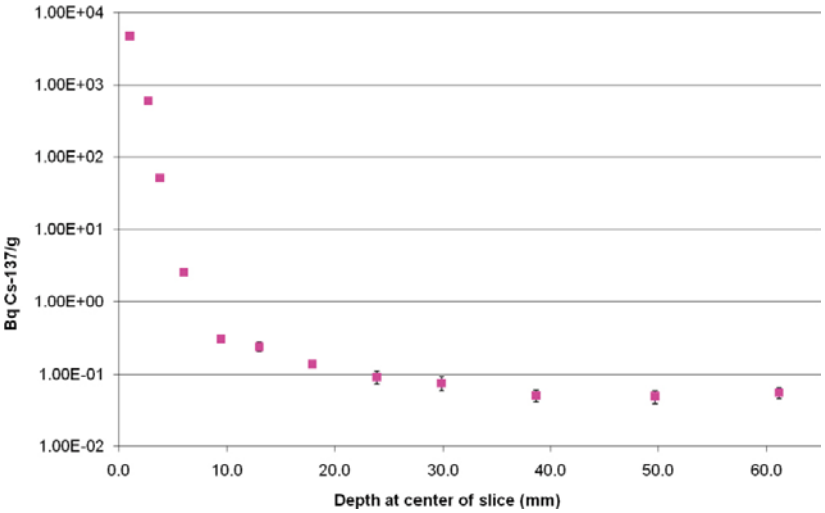

Figure A5-17. *Cs-137 activities in core A10 versus length.*

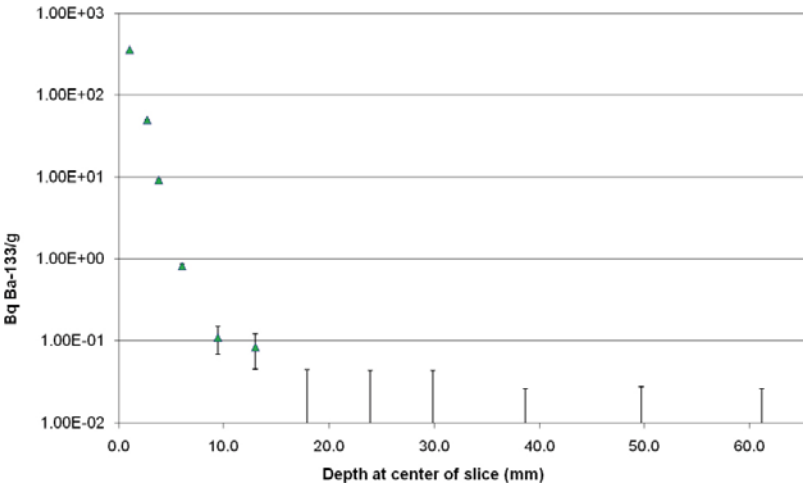

Figure A5-18. *Ba-133 activities in core A10 versus length. A value below the detection limit is shown as a corresponding bar.*

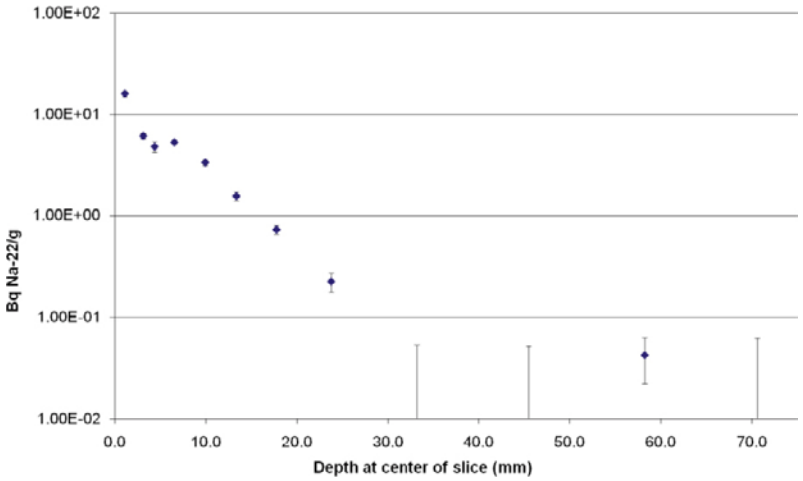

Figure A5-19. *Na-22 activities in core A12 versus length. A value below the detection limit is shown as a corresponding bar.*

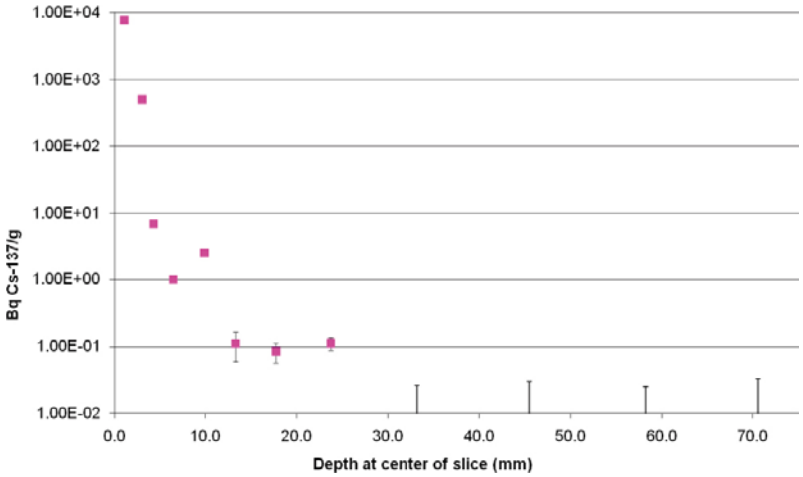

Figure A5-20. *Cs-137 activities in core A12 versus length. A value below the detection limit is shown as a corresponding bar.*

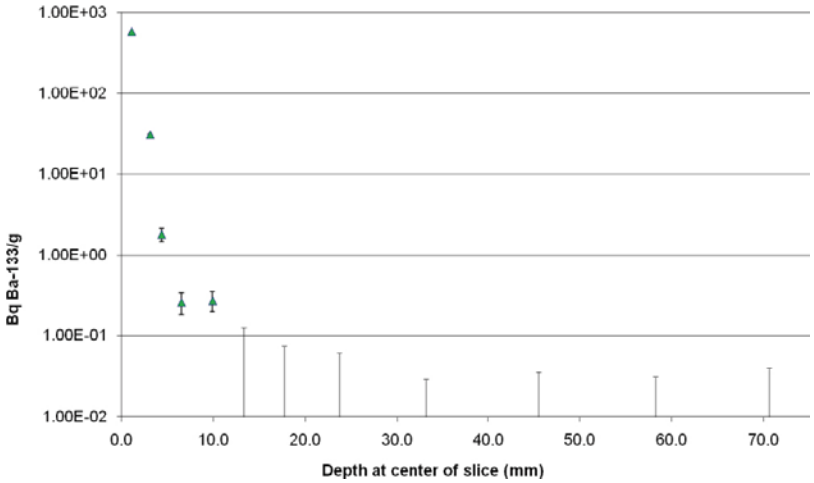

Figure A5-21. *Ba-133 activities in core A12 versus length. A value below the detection limit is shown as a corresponding bar.*

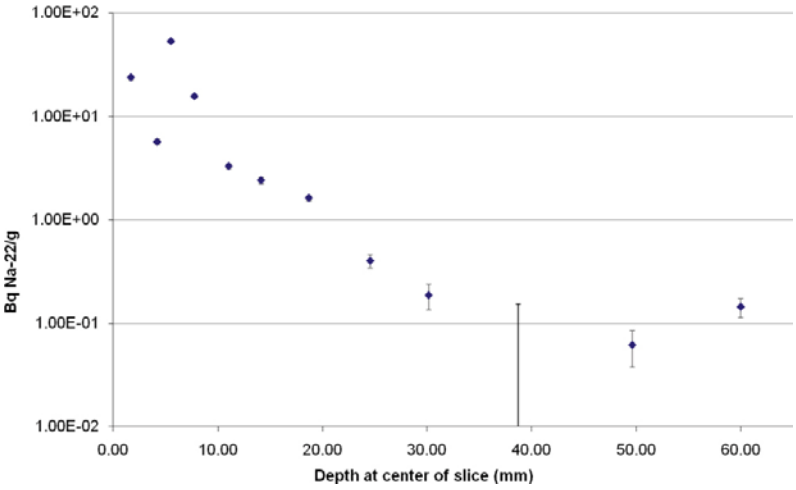

Figure A5-22. *Na-22 activities in core A15 versus length. A value below the detection limit is shown as a corresponding bar.*

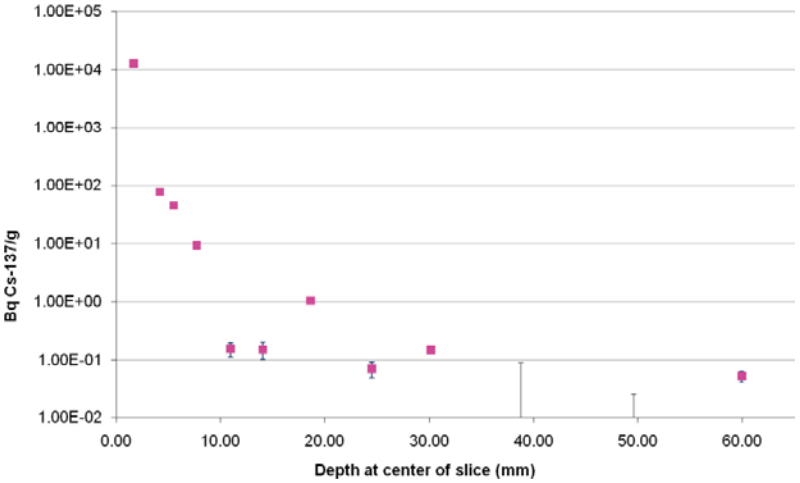

Figure A5-23. *Cs-137 activities in core A15 versus length. A value below the detection limit is shown as a corresponding bar.*

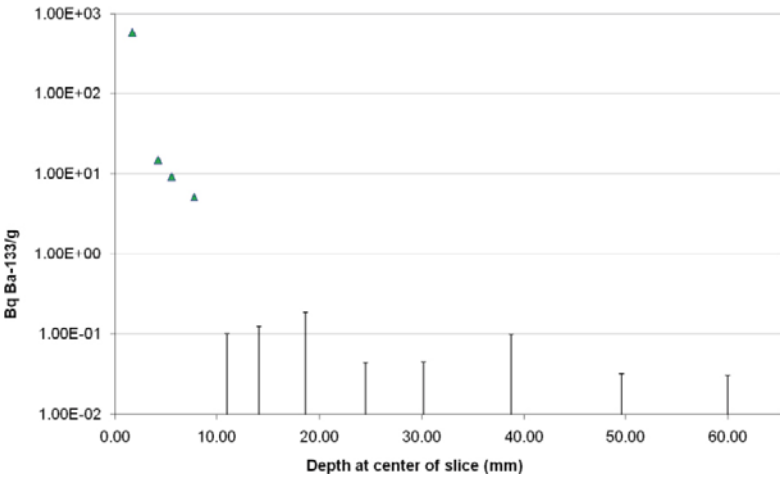

Figure A5-24. *Ba-133 activities in core A15 versus length. A value below the detection limit is shown as a corresponding bar.*

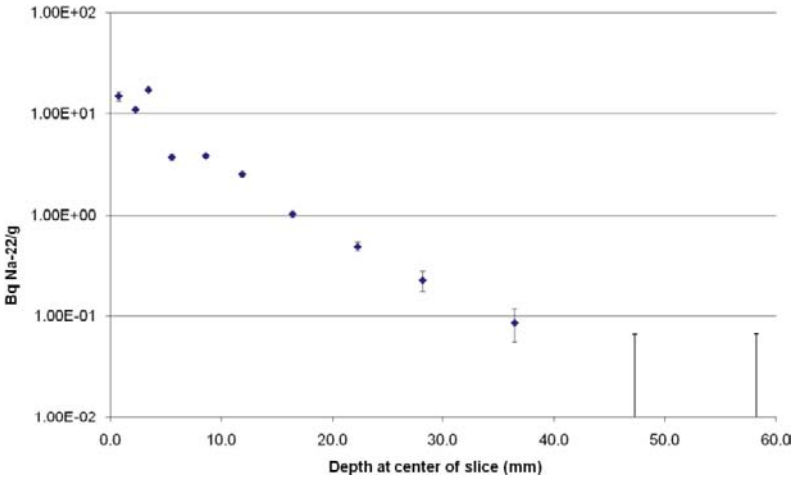

Figure A5-25. *Na-22 activities in core A16 versus length. A value below the detection limit is shown as a corresponding bar.*

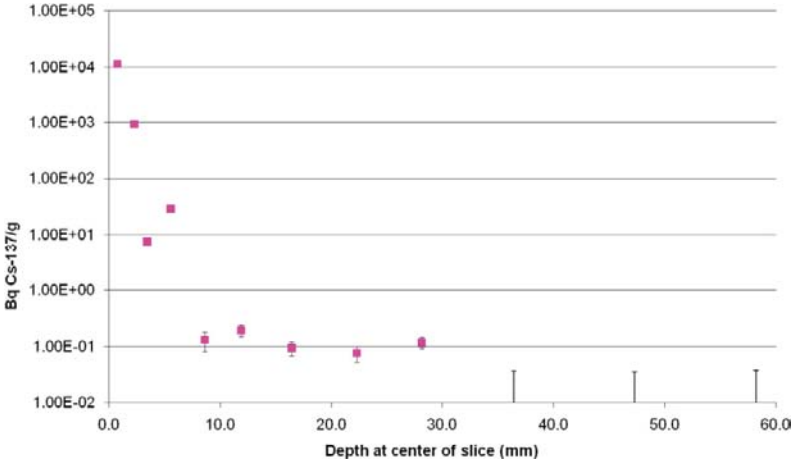

Figure A5-26. *Cs-137 activities in core A16 versus length. A value below the detection limit is shown as a corresponding bar.*

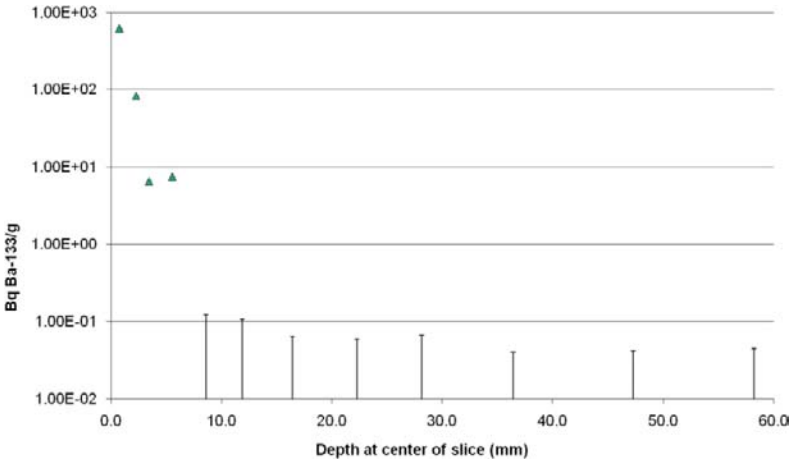

Figure A5-27. *Ba-133 activities in core A16 versus length. A value below the detection limit is shown as a corresponding bar.*

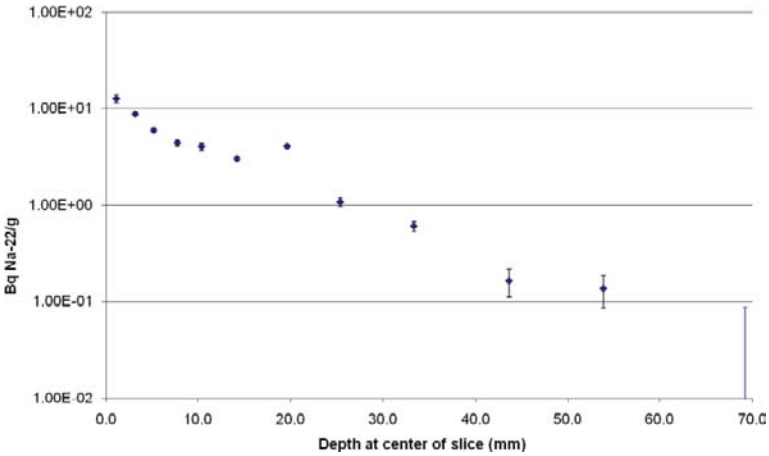

Figure A5-28. *Na-22 activities in core A17 versus length. A value below the detection limit is shown as a corresponding bar. A thin slice (0.33 g) between the first and second sample is not included in the analysis.*

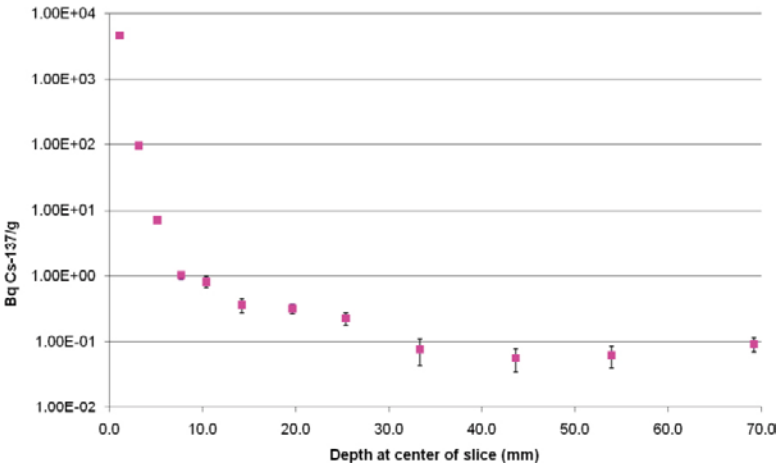

Figure A5-29. *Cs-137 activities in core A17 versus length. A thin slice (0.33 g) between the first and second sample is not included in the analysis.*

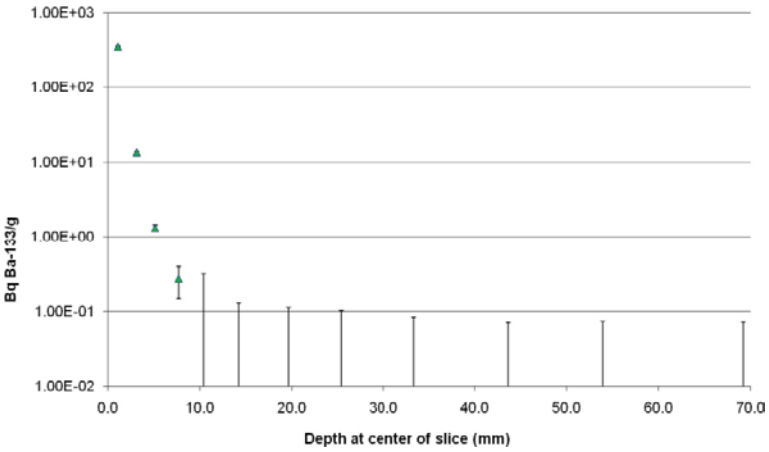

Figure A5-30. *Ba-133 activities in core A17 versus length. A value below the detection limit is shown as a corresponding bar. A thin slice (0.33 g) between the first and second sample is not included in the analysis.*

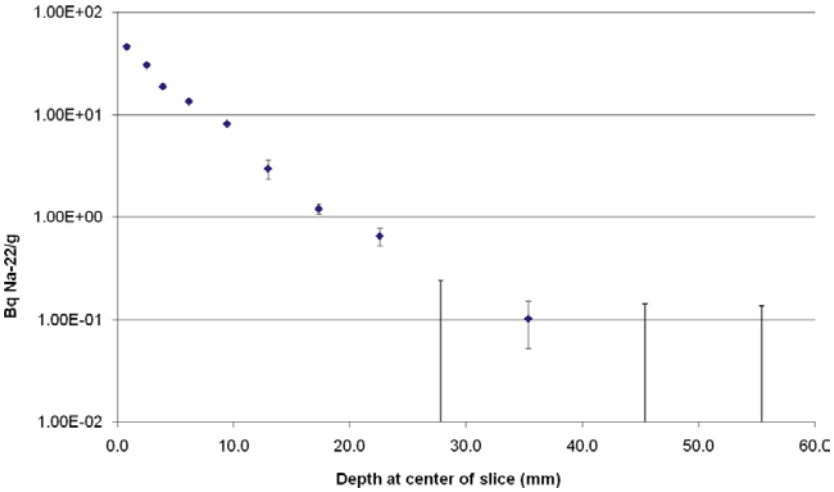

Figure A5-31. *Na-22 activities in core D1 versus length. A value below the detection limit is shown as a corresponding bar.*

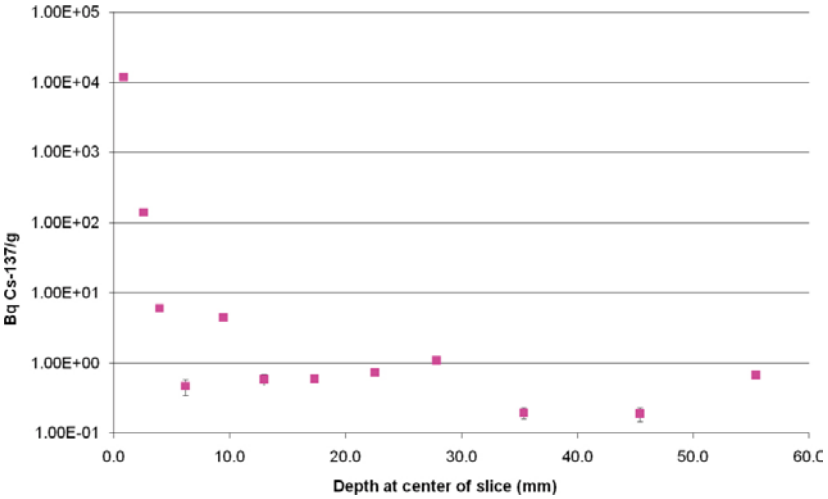

Figure A5-32. *Cs-137 activities in core D1 versus length.*

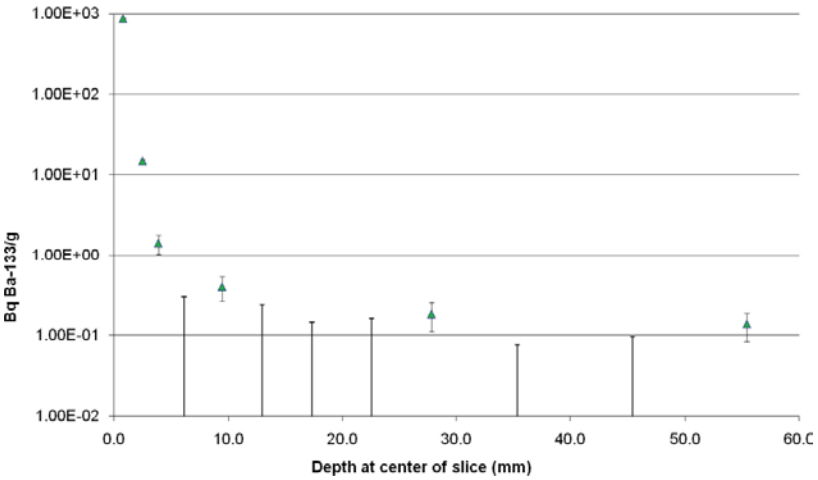

Figure A5-33. *Ba-133 activities in core D1 versus length. A value below the detection limit is shown as a corresponding bar.*

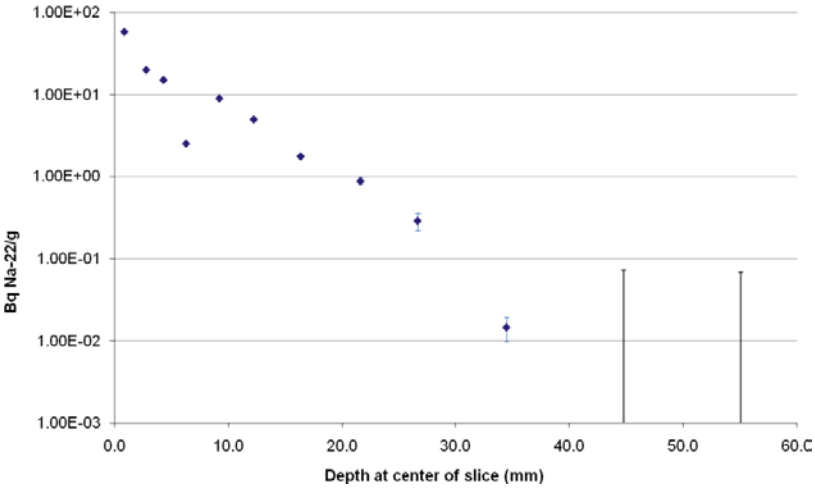

Figure A5-34. *Na-22 activities in core D5 versus length. A value below the detection limit is shown as a corresponding bar.*

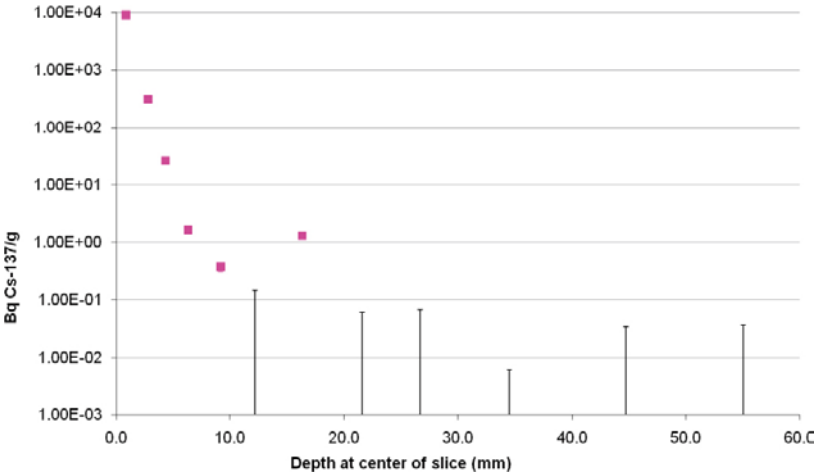

Figure A5-35. *Cs-137 activities in core D5 versus length. A value below the detection limit is shown as a corresponding bar.*

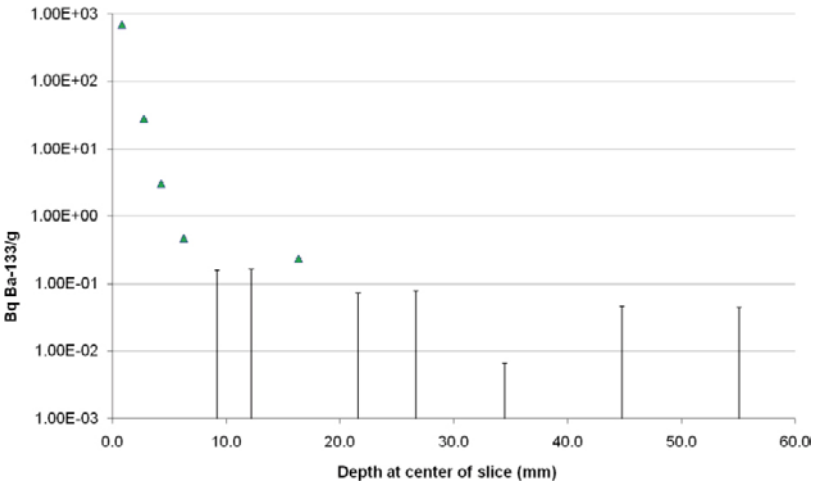

Figure A5-36. *Ba-133 activities in core D5 versus length. A value below the detection limit is shown as a corresponding bar.*

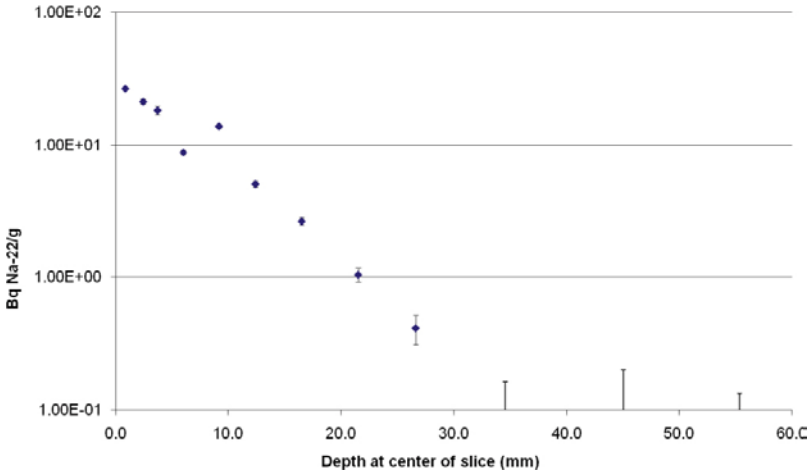

Figure A5-37. *Na-22 activities in core D6 versus length. A value below the detection limit is shown as a corresponding bar.*

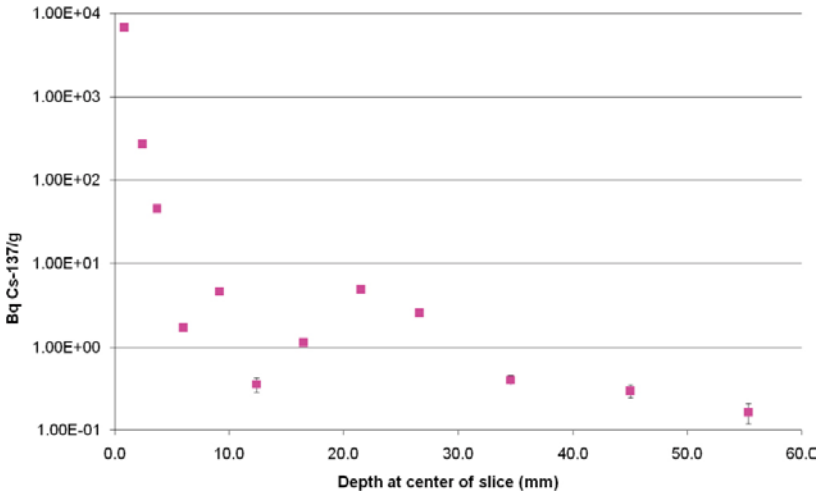

Figure A5-38. *Cs-137 activities in core D6 versus length.*

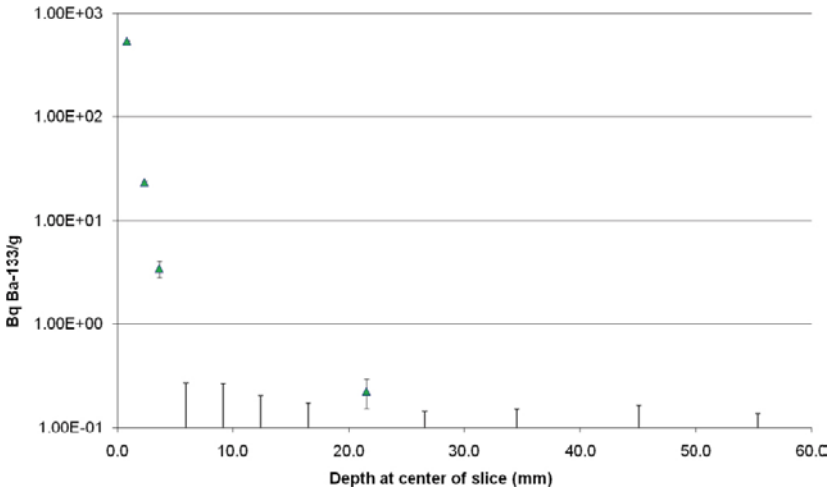

Figure A5-39. *Ba-133 activities in core D6 versus length. A value below the detection limit is shown as a corresponding bar.*

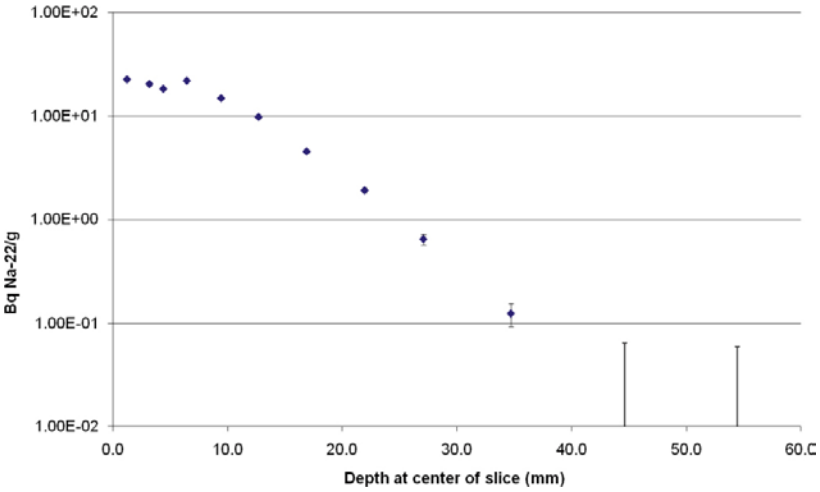

Figure A5-40. *Na-22 activities in core D7 versus length. A value below the detection limit is shown as a corresponding bar.*

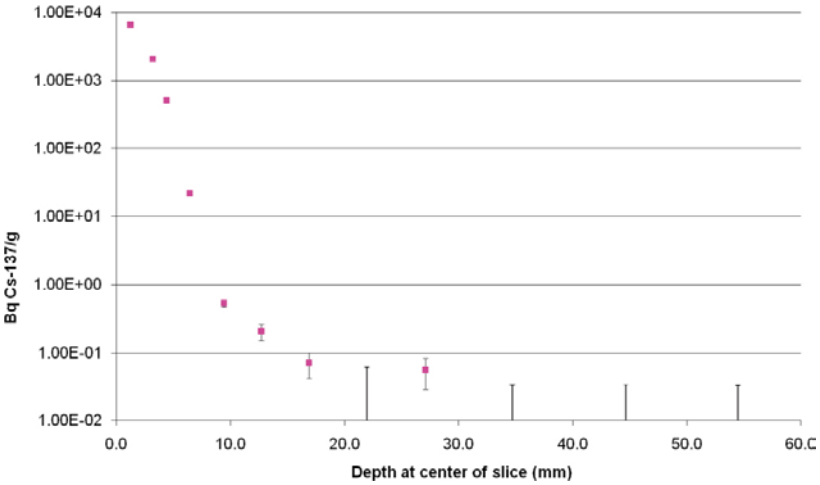

Figure A5-41. *Cs-137 activities in core D7 versus length. A value below the detection limit is shown as a corresponding bar.*

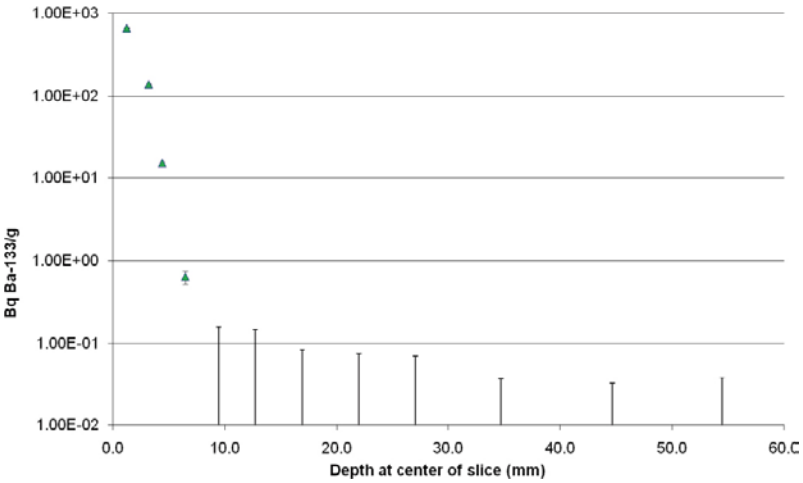

Figure A5-42. *Ba-133 activities in core D7 versus length. A value below the detection limit is shown as a corresponding bar.*

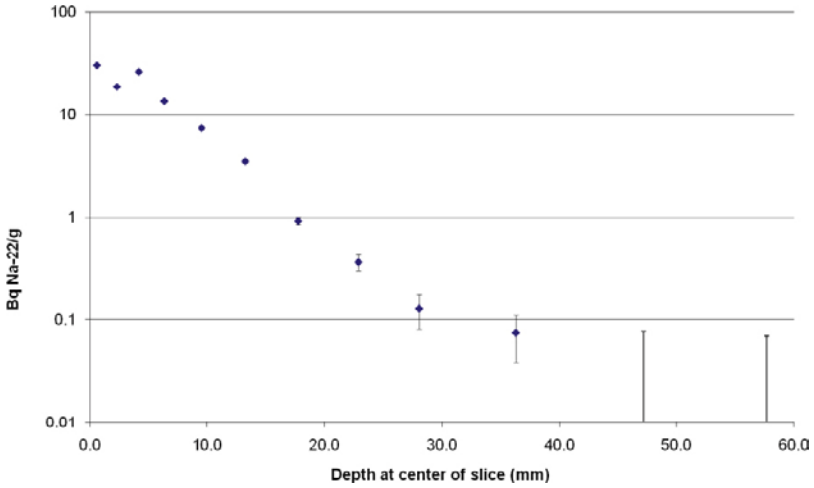

Figure A5-43. *Na-22 activities in core D8 versus length. A value below the detection limit is shown as a corresponding bar.*

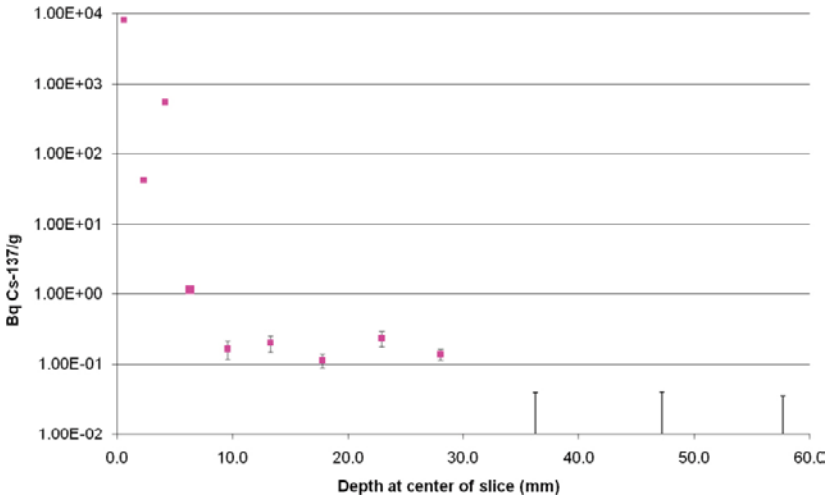

Figure A5-44. *Cs-137 activities in core D8 versus length. A value below the detection limit is shown as a corresponding bar.*

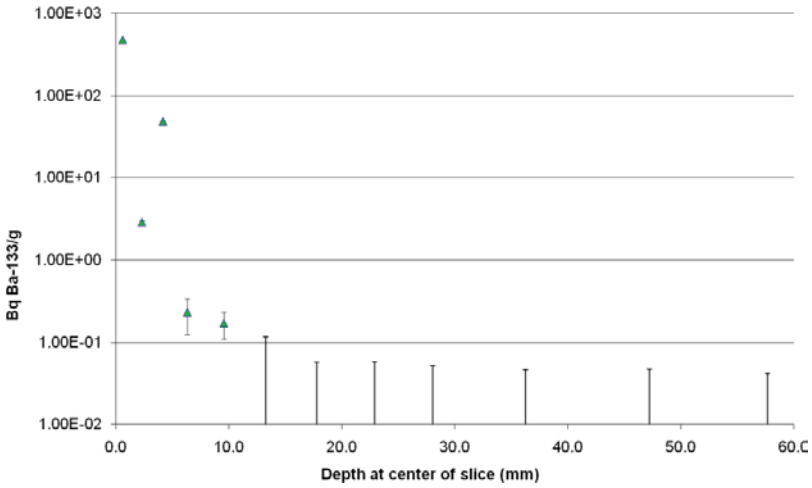

Figure A5-45. *Ba-133 activities in core D8 versus length. A value below the detection limit is shown as a corresponding bar.*

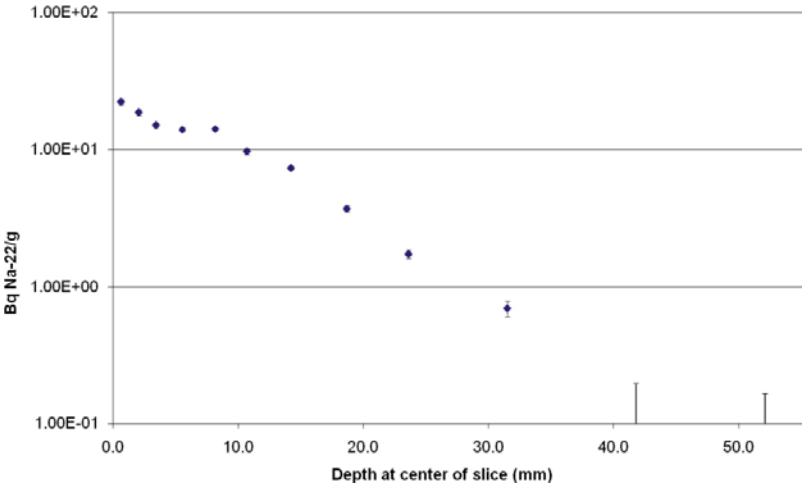

Figure A5-46. *Na-22 activities in core D12 versus length. A value below the detection limit is shown as a corresponding bar.*

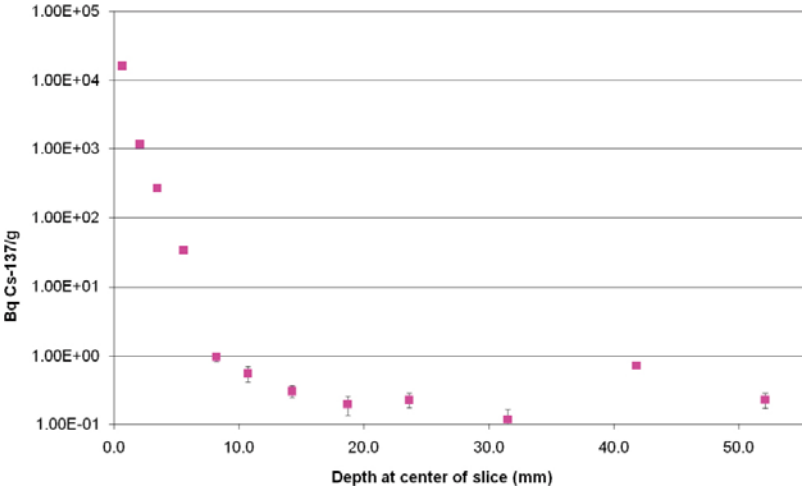

Figure A5-47. *Cs-137 activities in core D12 versus length. A value below the detection limit is shown as a corresponding bar.*

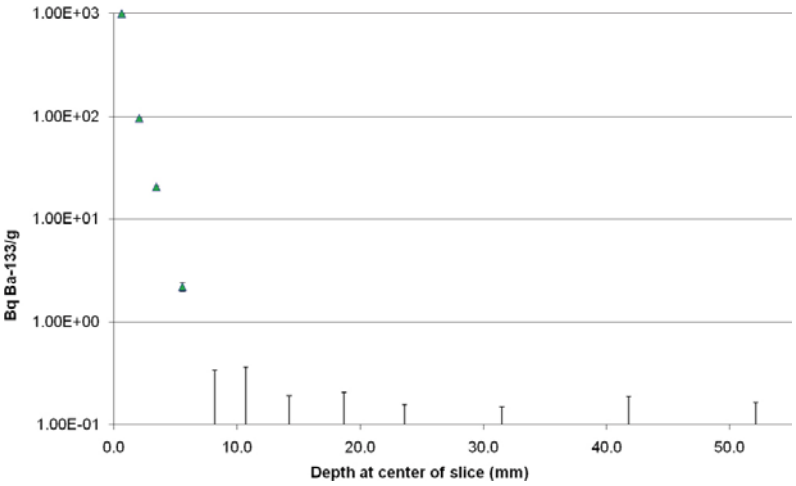

Figure A5-48. *Ba-133 activities in core D12 versus length. A value below the detection limit is shown as a corresponding bar.*

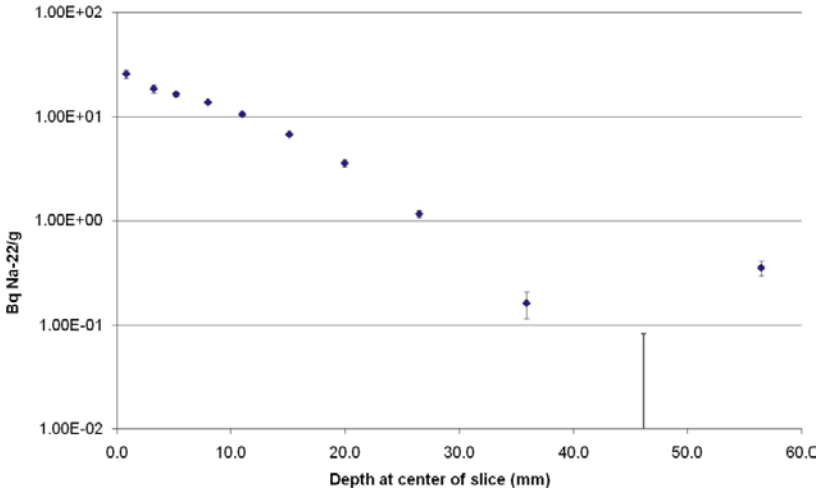

Figure A5-49. *Na-22 activities in core D13 versus length. A value below the detection limit is shown as a corresponding bar.*

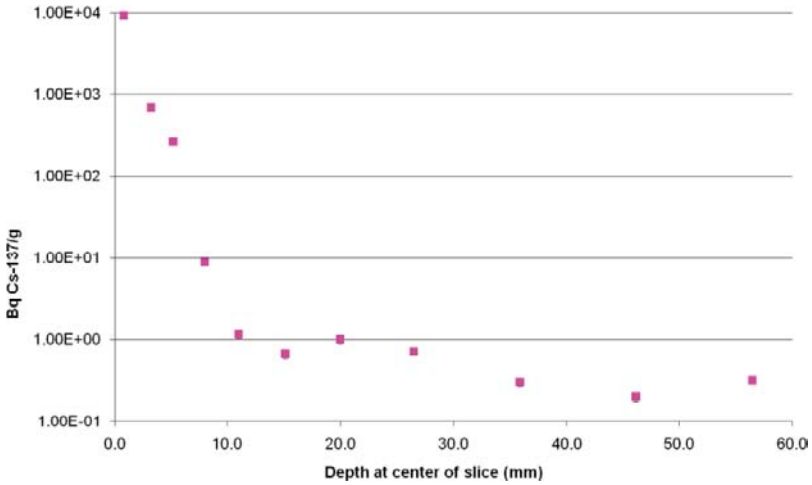

Figure A5-50. *Cs-137 activities in core D13 versus length.*

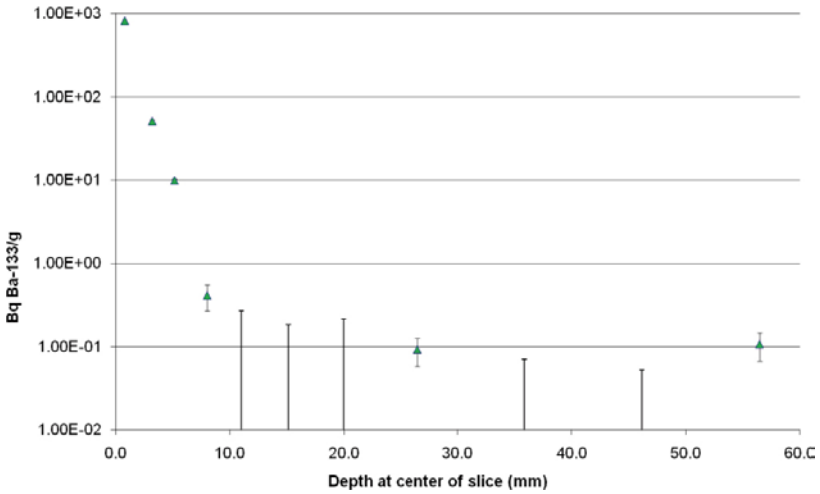

Figure A5-51. *Ba-133 activities in core D13 versus length. A value below the detection limit is shown as a corresponding bar.*

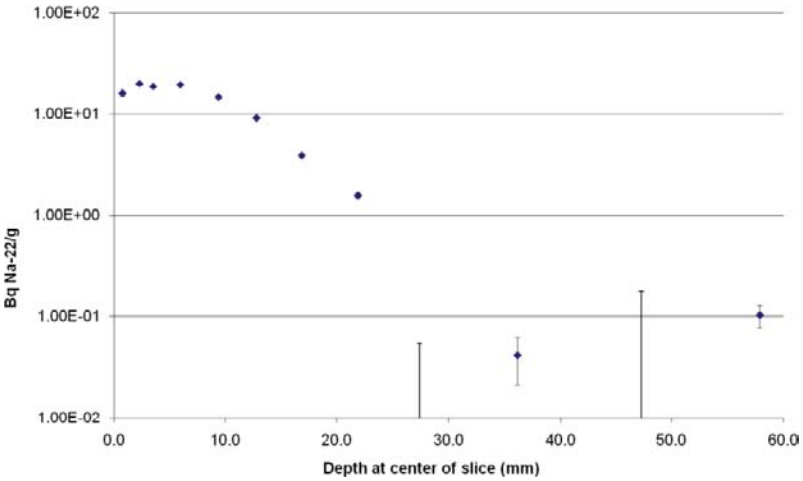

Figure A5-52. *Na-22 activities in core D14 versus length. A value below the detection limit is shown as a corresponding bar.*

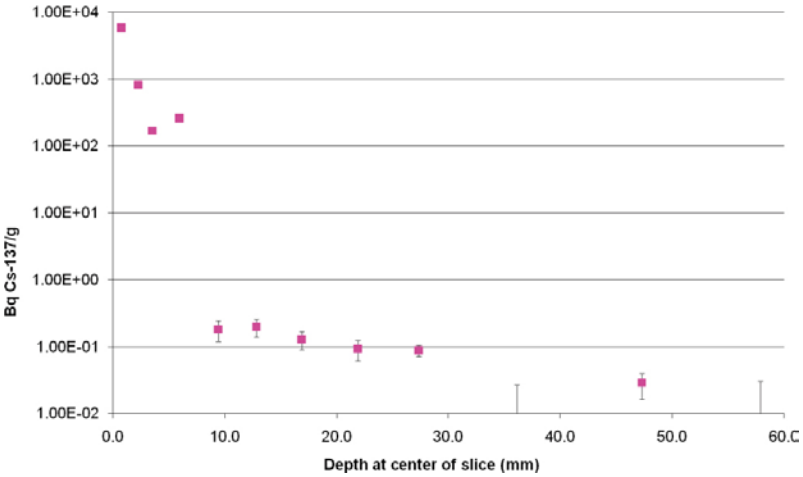

Figure A5-53. *Cs-137 activities in core D14 versus length. A value below the detection limit is shown as a corresponding bar.*

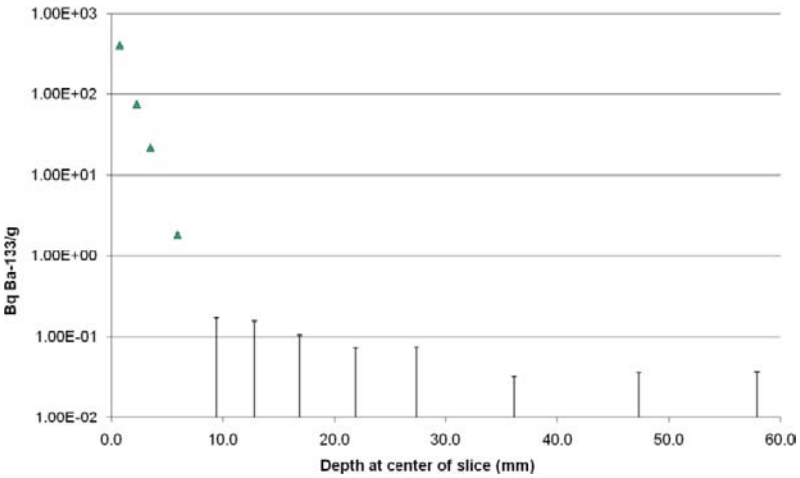

Figure A5-54. *Ba-133 activities in core D14 versus length. A value below the detection limit is shown as a corresponding bar.*

Appendix 6

Tracer penetration 0–3 mm

	Co-57 Bq/g	Co-57 unc./g	Cd-109 Bq/g	Cd-109, unc./g	Ag-110m Bq/g	Ag-110m, unc./g	Gd-153 Bq/g	Gd-153, unc./g	Ra-226 Bq/g	Ra-226, unc./g	Np-237, ng/g	Np-237, unc./g
A1.1	1298	14	5154	165	211	10	499	38	160	12	35	10
A1.2	<15		<22		<30	-	<84	-	<9		<10	
A5.1	2511	8.6	3280		256	5.2	370	27	63	0.92		
A5.2	-	-	-	-	-	-	-	-	-			
A5.3	<2	-	<20		<5	-	<14		<1			
A6.1	2276	21	6181	240	202	11	868	136	186	7	38	10
A6.2	92	9	853	116	<12	-	<96	-	31	4	<10	
A6.3	<13	-	<170	-					<9			
A8.P											39.1	9.5
A8.1	160	13	890	170	<58	-	<338	-	39	4	<10	
A8.2	17	8	278	98					<12			
A8.3	40	8	<169	-								
A8.4	<0.8											
A9.1	2434	29	6230	296	408	25	1144	69	158	8	40	10
A9.2	<5		<79		<9		<39		<6		<10	
A10.1	2125	9	7814	80	133	11	977	30	80	1		
A10.2	<7		<70		<7		<52		3	0.2		
A10.3									<1			
A12.1	2872	14	5216	134	212	8	644	27	130	3		
A12.2	37	3	<168		<19		<103		<0			
A12.3	<14											
A15.1	1534	12	5318	143	212	10	870	30	158	4		
A15.2	<4		<49		<6		<17		<2			
A16.1	6307	30	9680	244	448	21	1526	53	188	0.1		
A16.2	<9		<93		<8		<59		9	0.1		
A16.3									<2			
A17.1	1160	12	8786	141	260	13	647	27	58	3	58	10
A17.2	<2		<33		<5		<14		<3		<10	
A17.3												

	Co-57 Bq/g	Co-57 unc./g	Cd-109 Bq/g	Cd-109, unc./g	Ag-110m Bq/g	Ag-110m, unc./g	Gd-153 Bq/g	Gd-153, unc./g	Ra-226 Bq/g	Ra-226, unc./g	Np-237, ng/g	Np-237, unc./g
D1.1	839	20	4318	197	<42		571	43	180	8	17	10
D1.2	<3		<39				<16		<3		<10	
D5.1	2181	15	3762	150	<31		358	32	141	6		
D5.2	<5		<52				<34		2	0.2		
D6.1	2189	13	3437	116	<15		141	68	114	2	38	10
D6.2	<9		<97				<56		<4		<10	
D7.1	2664	13	4615	116	<30	-	266	24	108	4		
D7.2	55	6	<133				<85		7	0.8		
D7.3	14	3							<2			
D7.4	6	1										
D7.5	2	1										
D7.6	<1											
D8.1	3024	13	3888	112	<11		290	70	120	2		
D8.2	<4		<29				<20		<1			
D12.1	5130	27	10606	247	<34		<286		237	3	24.5	10
D12.2	74	8	<170						9	2	<10	
D12.3	17	3							<2			
D12.4	7	2										
D12.5	<4											
D13.1	1448	19	8549	231	<50	-	454	46	159	10	23	10
D13.2	-	-	-	-			-	-	-	-	<10	
D13.3	14	4	<98				<43		<7			
D13.4	<3											
D14.1	5251	14	2872	93	52	5	440	21	97	2		
D14.2	111	18	<24		<13		<188		7	1.0		
D14.3	<19	-							<2			
D14.4	6	1										
D14.5	4	1										
D14.6	<3											

Appendix 7

Tracers below the detection limit

	Se-75 Bq/g	Tc-99 ng/g	Sn-113 Bq/g	Hf-175 Bq/g	U-236 ng/g
A1.1	<1373	<25	<1996	<29055	<10
A5.1	<844	-	<1505	Decayed	-
A6.1	<1756	<25	<2474	<34163	<10
A8.P	-	<25	-	-	<10
A8.1	<1582	-	<1556	<31288	-
A9.1	<1829	<25	<3015	<33373	<10
A10.1	<949	-	<1714	Decayed	-
A12.1	<721	-	<1035	<14371	-
A15.1	<936	-	<1574	<18996	-
A16.1	<1608	-	<2545	<41890	-
A17.1	<717	<25	<1146	<14546	<10
D1.1	<1287	<25	<1837	<23044	<10
D5.1	<1039	-	<1172	<19526	-
D6.1	<1498	<25	<2619	Decayed	<10
D7.1	<796	-	<1391	<16894	-
D8.1	<1421	-	<2633	Decayed	-
D12.1	<3234	<25	<5637	Decayed	<10
D13.1	<1440	<25	<2103	<27501	<10
D14.1	<651	-	<972	<13996	-

Appendix 8

Tracers in entire cores [1]

	Na-22 Bq/core	Na-22 +/-	Co-57 Bq/core	Co-57 +/-	Se-75 Bq/core	Se-75 +/-	Sr-85 Bq/core	Sr-85 +/-	Zr-95 Bq/core	Zr-95 +/-	Cd-109 Bq/core	Cd-109 +/-
A1	223	116	7354	4432	1821	888	<5559		<2372		27508	17558
A2	220	111	1859	1121	1524	657	6072	3013	<1181		13458	8596
A3	143	74	2332	1406	1778	783	<1997		<824		8227	5261
A4	123	66	4299	2591	1659	748	<2671		<1368		15456	9869
A5	198	101	8520	5134	1572	701	<2420		<1945		11233	7180
A6	293	149	4453	2685	1265	731	<6294		<1211		13959	8931
A7	147	79	4076	2457	1920	911	<5190		<2267		18987	12129
A8	104	55	2506	1511	1914	860	<2770		<1723		10038	6417
A9	105	58	5633	3395	1777	812	<2713		<2293		15985	10206
A10	114	60	4813	2901	1411	624	<2128		<987		16411	10475
A11	135	71	5314	3202	1176	521	<2399		<1636		16598	10594
A12	166	88	12402	7474	1879	858	<3892		<2311		24083	15374
A13	106	59	7539	4543	2129	911	<2456		<2703		21064	13444
A14	237	119	2225	1342	1031	545	<3432		<1557		10929	6986
A15	88	51	4211	2538	2098	962	<4333		<1721		13837	8843
A16	130	68	8013	4829	1768	787	<2505		<2289		11783	7530
A17	134	70	3227	1945	967	463	<2567		<1409		24878	15874
A18	166	90	5092	3069	1443	686	<3177		<2563		25607	16344
A20	<19		<6.5		<24						<87	
D1	320	137	3359	1510	606	339	7477	3568	<1615		11930	6579
D2	258	111	22126	9942	447	271	<2746		<1968		7625	4249
D3	259	112	2568	1154	<432		<3307		<1524		9347	5160
D4	303	130	13808	6205	453	280	<2993		<1820		9604	5313
D5	278	119	4624	2078	446	277	6790	3202	<1664		9282	5124
D6	243	105	4320	1941	423	257	<3116		<1885		8117	4485
D7	277	119	7125	3202	515	284	<2950		<2023		9675	5343
D8	314	133	3475	1562	<334		<2679		<1572		8766	4838
D9	348	148	4631	2081	565	329	<3567		<2239		12411	6844
D10	205	91	10690	4804	572	276	7303	3328	<1881		22652	12469
D11	239	103	25628	11516	920	425	<2415		<1865		17439	9614
D12	266	114	9161	4117	557	304	<3214		<2138		17112	9427
D13	201	88	3880	1744	516	238	5764	2751	<1521		15707	8648
D14	247	107	22732	10214	1058	485	<3061		<1835		13246	7312
D15	195	86	6292	2828	620	332	<2817		<1763		27867	15335
D15b	217	95	5997	2695	408	261	4685	2498	1981	844	28447	15655
D16	195	87	29392	13207	1664	720	11223	4985	<1517		17331	9563

[1] γ-spectrometry measurements (not performed under well calibrated conditions) of entire drill cores performed > 1 year before the measurements of the sliced rock material containing information of short-lived tracers.

Tracers in entire cores [2]

	Ag-110m Bq/core	Ag-110m +/-	Sn-113 Bq/core	Sn-113 +/-	Ba-133 Bq/core	Ba-133 +/-	Hf-175 Bq/core	Hf-175 +/-
A1	1156	835	<1301		3879	188	<3519	
A2	185	140	<687		1823	99	<1854	
A3	272	199	<599		1022	64	<1555	
A4	602	435	<612		996	64	<1830	
A5	581	420	<635		1149	64	<1802	
A6	477	353	<1534		2131	131	<4145	
A7	486	358	<1164		2675	142	<3319	
A8	284	212	<776		1231	77	<2323	
A9	718	521	<829		1604	90	<2244	
A10	307	224	<610		930	58	<1431	
A11	646	468	<556		973	60	1969	1086
A12	946	683	<1019		2656	135	3111	2016
A13	795	574	<776		3063	144	2701	1494
A14	288	212	<845		1537	90	<2316	
A15	680	495	<999		1735	101	<3017	
A16	550	399	<690		1070	67	1866	1184
A17	670	484	<638		1137	69	<1725	
A18	1035	746	1015	589	5323	238	<2448	
A20	<21				<7			
D1	<88		<780		1845	1096	<1357	
D2	104	87	<729		1131	672	<1426	
D3	<83		<802		1544	917	<1707	
D4	58	50	<748		1335	793	<1600	
D5	<79		<779		1486	883	<1466	
D6	<80		<741		1319	784	<1436	
D7	<82		<736		1441	856	<1327	
D8	<63		<617		1100	654	<1189	
D9	<86		<815		1544	917	<1735	
D10	84	70	<644		1533	910	<1277	
D11	328	239	<672		1355	805	<1470	
D12	71	60	<844		1617	961	<1717	
D13	<58		<627		1282	762	<1048	
D14	305	223	<686		1477	877	<1542	
D15	<82		<780		1314	781	<1189	
D15b	102	82	828	342	1346	800	<1729	
D16	381	278	<801		2161	1283	<1638	

[2] γ-spectrometry measurements (not performed under well calibrated conditions) of entire drill cores performed > 1 year before the measurements of the sliced rock material containing information of short-lived tracers.

Appendix 9

Modelling diagrams

Case 2

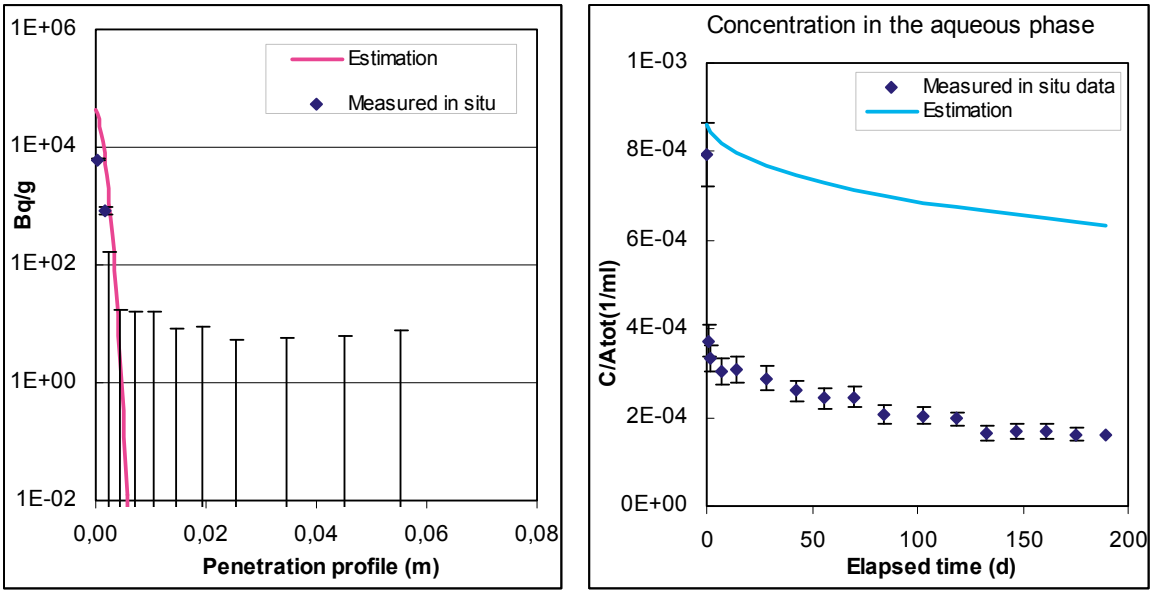

Figure Case 2. *Tracer: Cd-109. Core: A6.*

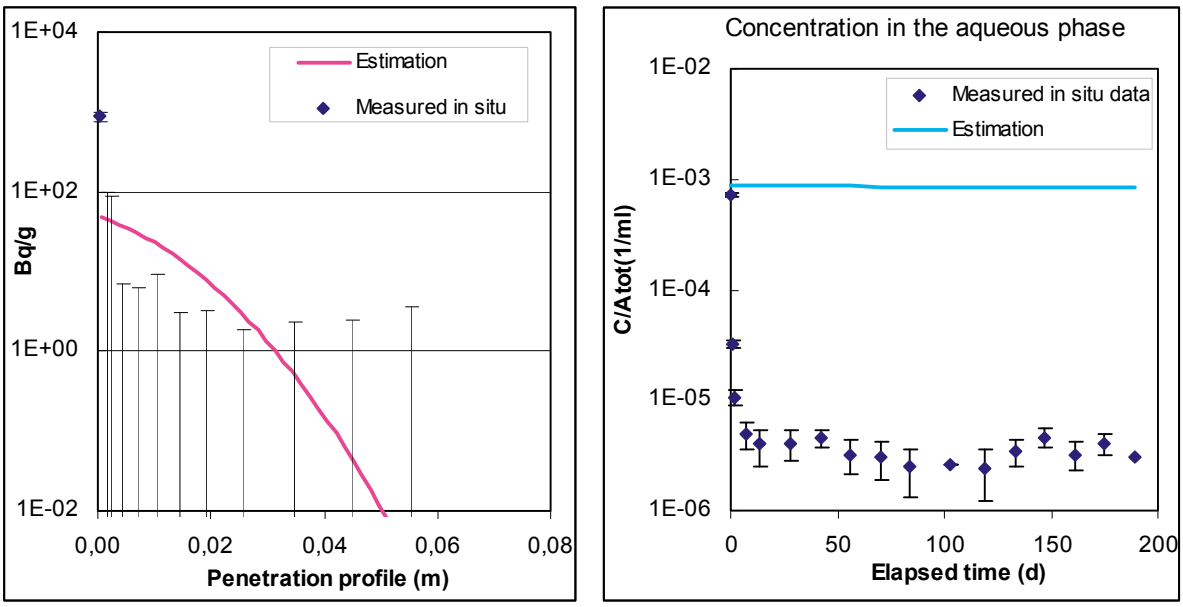

Figure Case 2. *Tracer: Gd-153. Core: A6.*

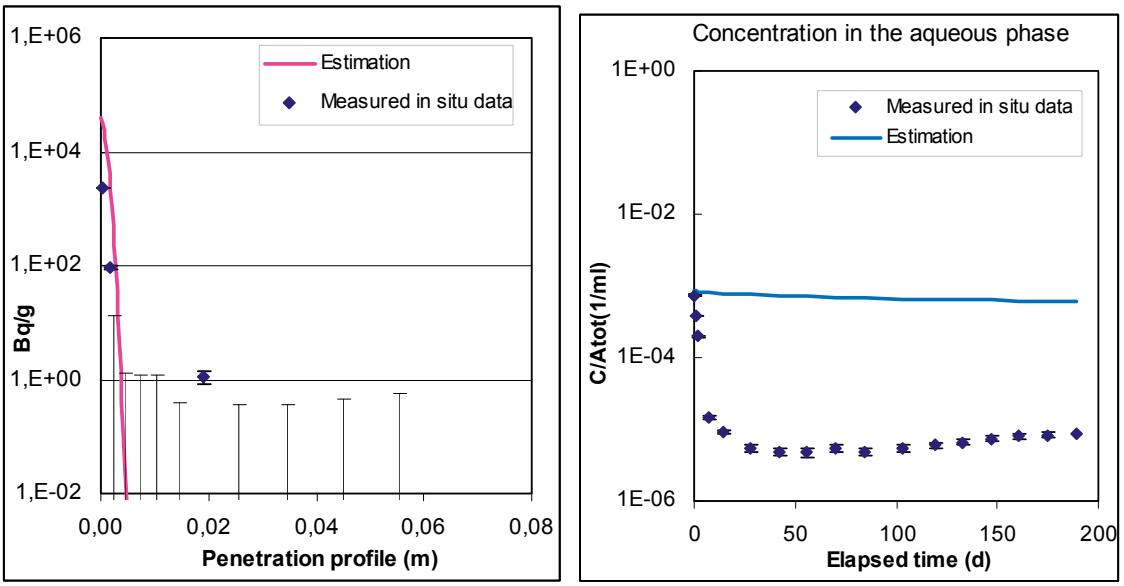

Figure Case 2. *Tracer: Co-57. Core: A6.*

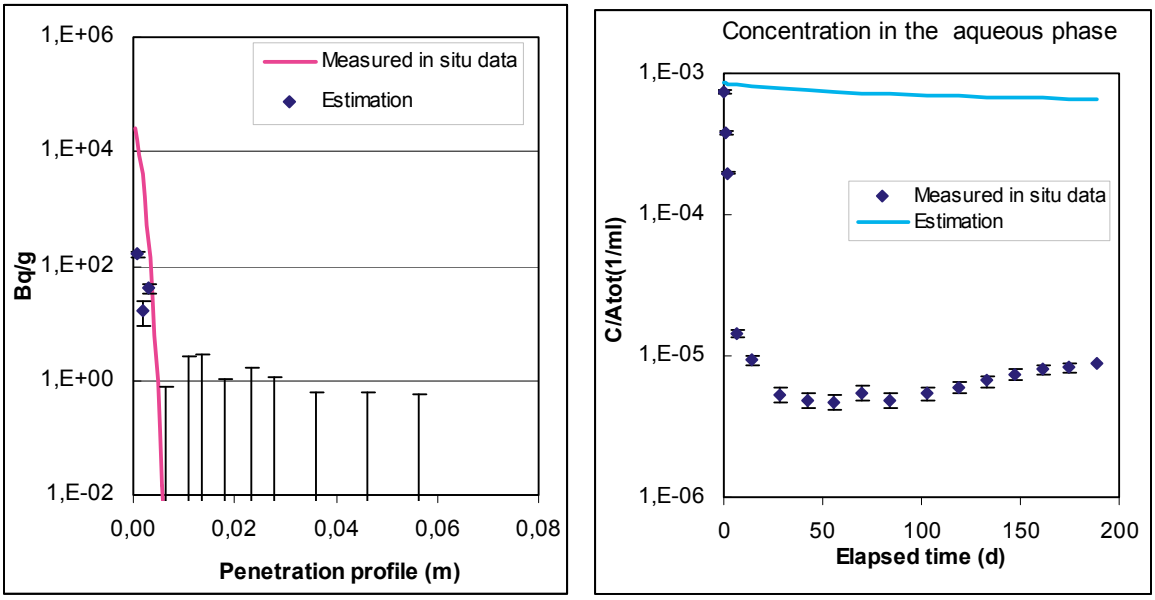

Figure Case 2. *Tracer: Co-57. Core: A8.*

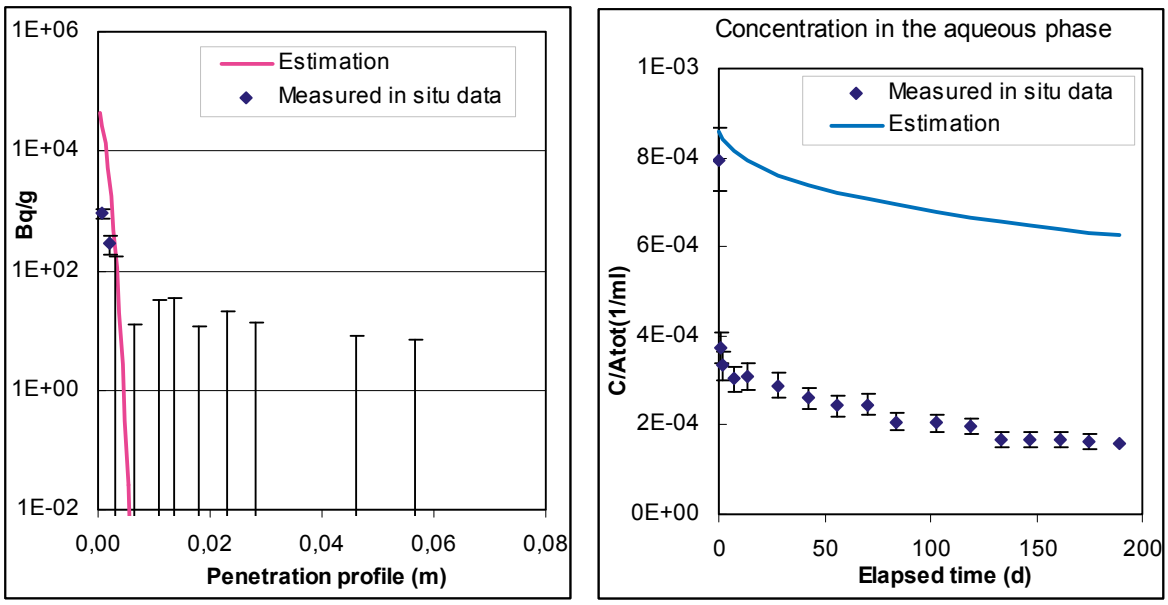

Figure Case 2. *Tracer: Cd-109. Core: A8.*

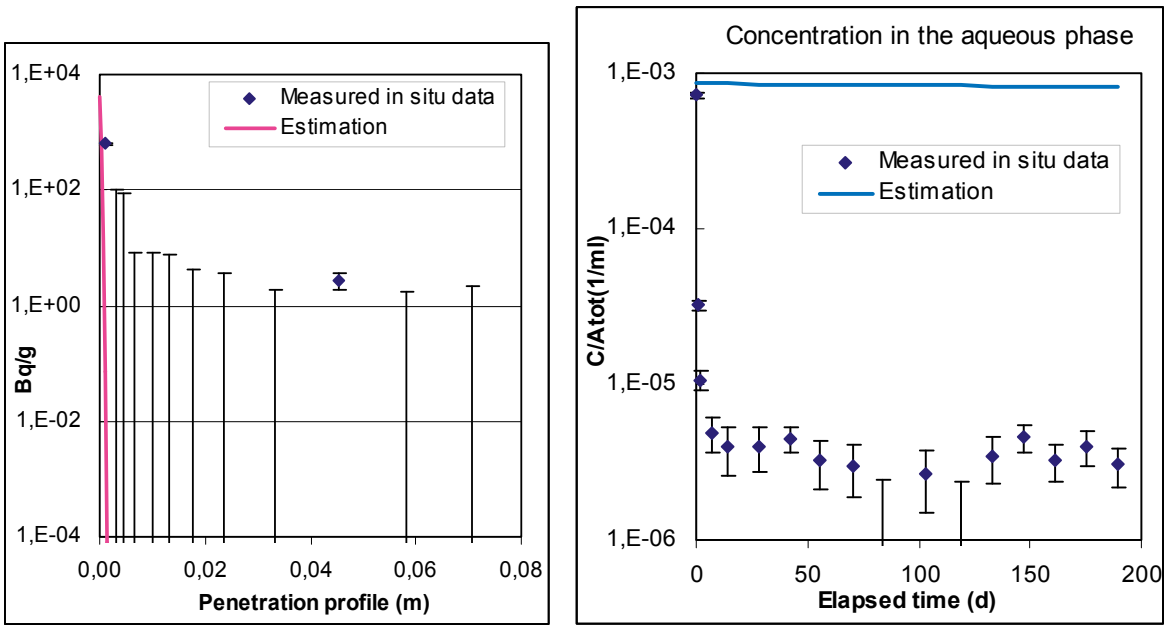

Figure Case 2. *Tracer: Gd-153. Core: A12.*

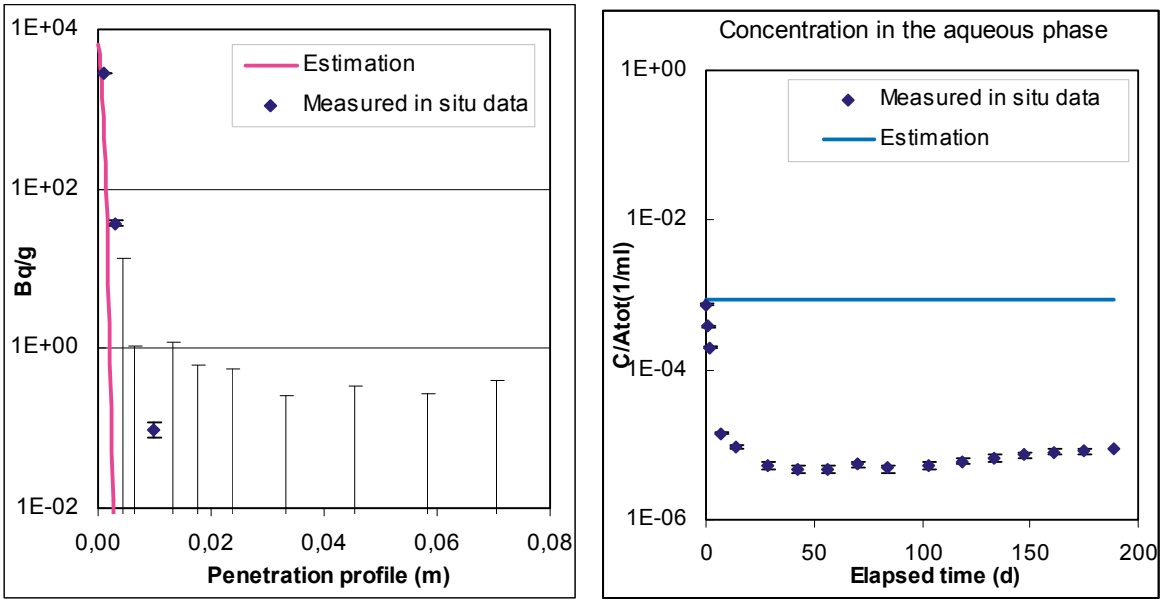

Figure Case 2. *Tracer: Co-57. Core: A12.*

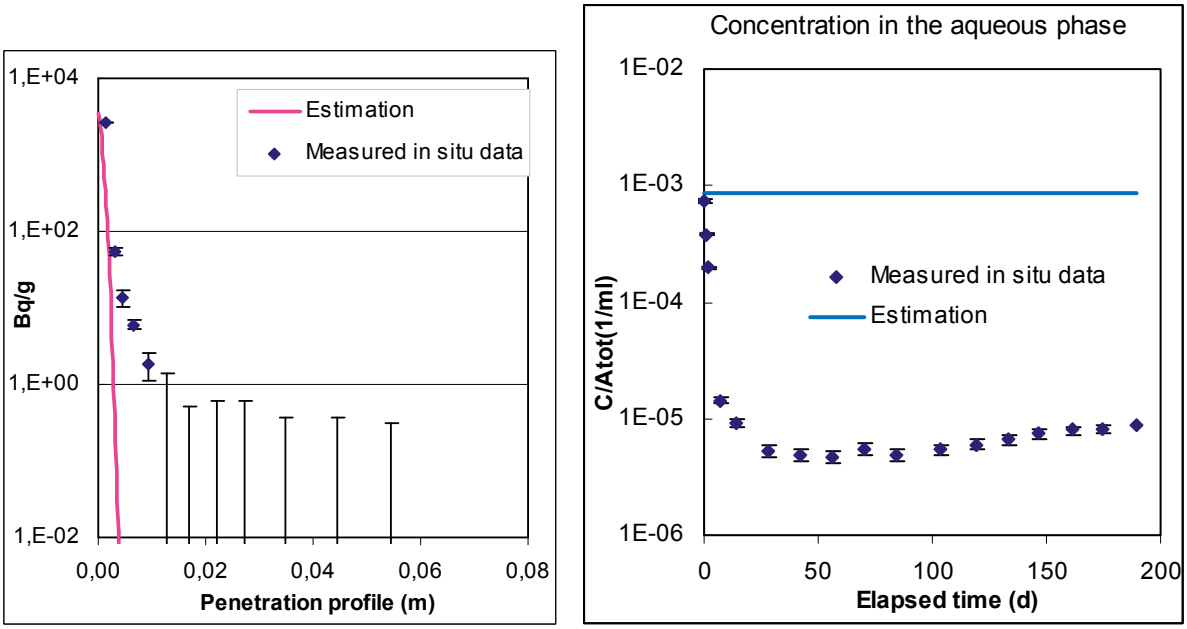

Figure Case 2. *Tracer: Co-57. Core: D7.*

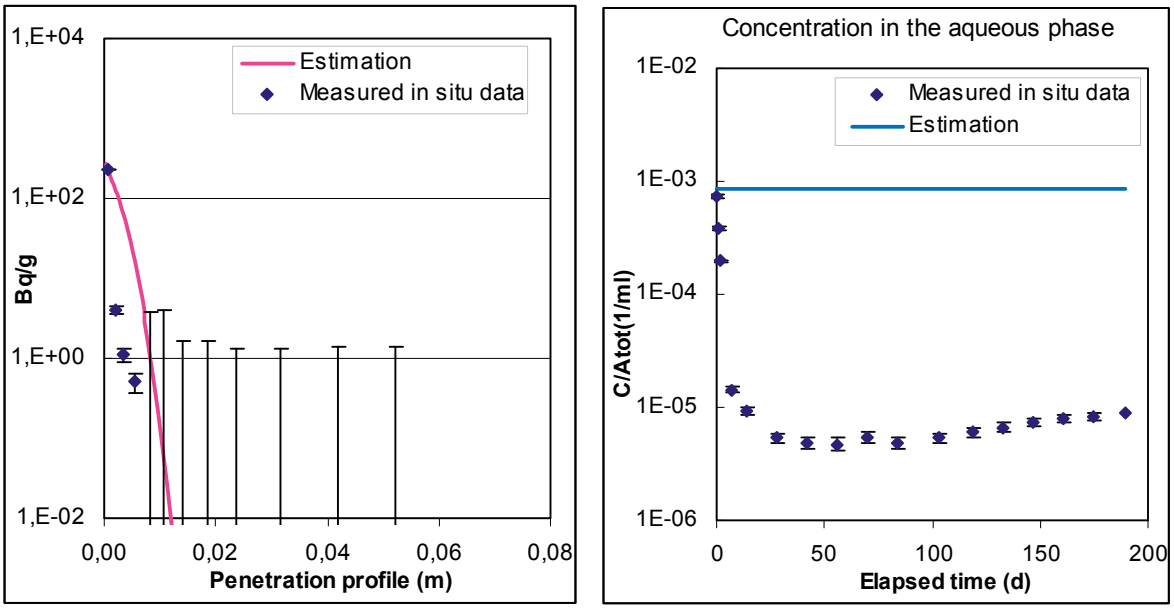

Figure Case 2. *Tracer: Co-57. Core: D12.*

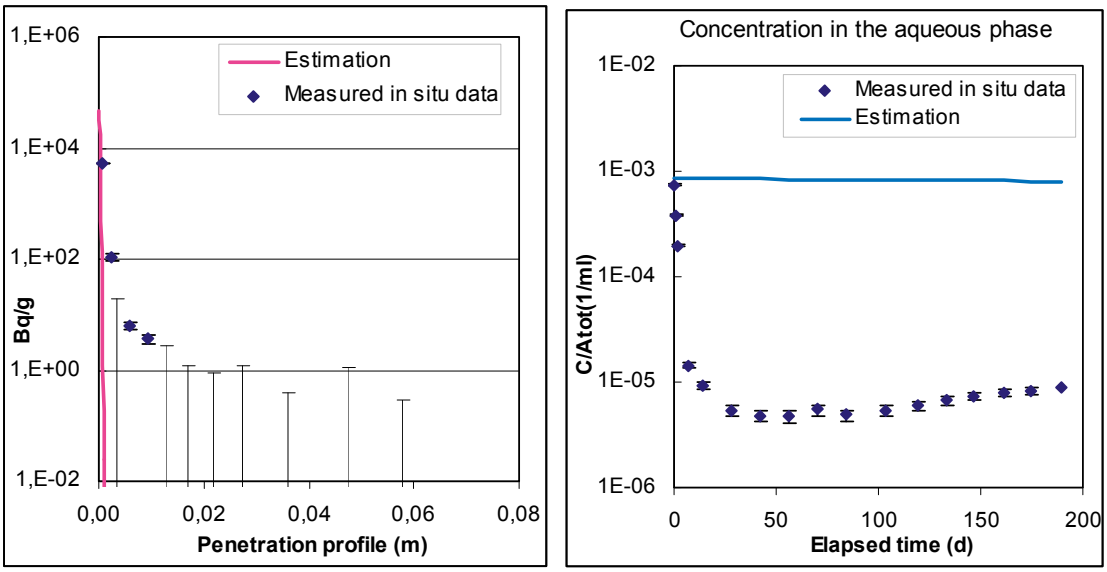

Figure Case 2. *Tracer: Co-57. Core: D14.*

Ba-133

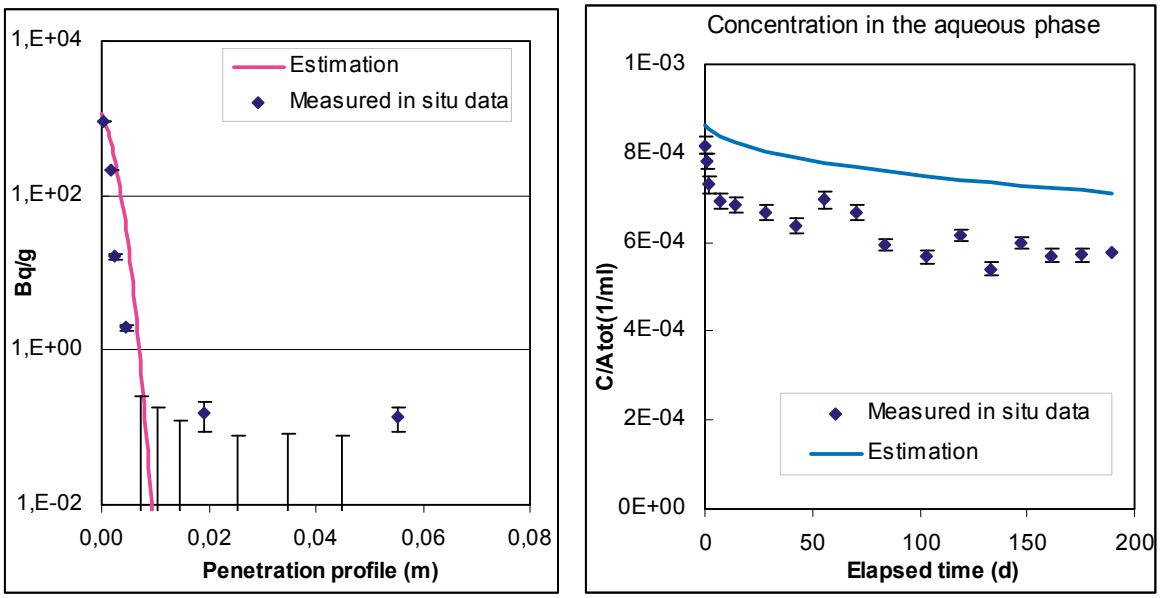

Figure Case 2. *Tracer: Ba-133. Core: A6.*

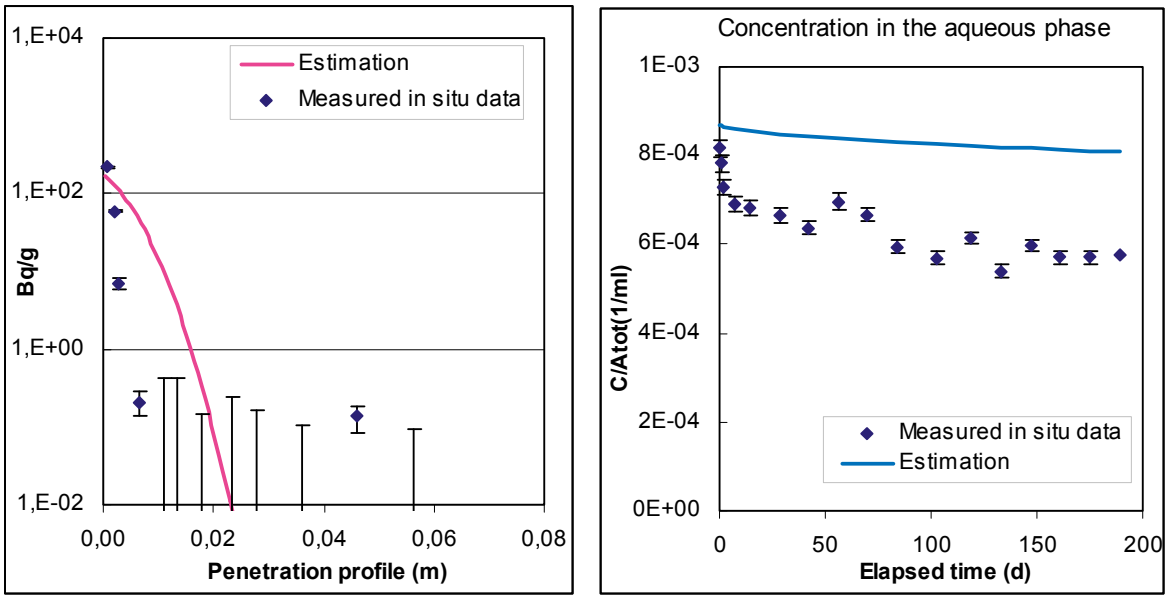

Figure Case 2. *Tracer: Ba-133. Core: A8.*

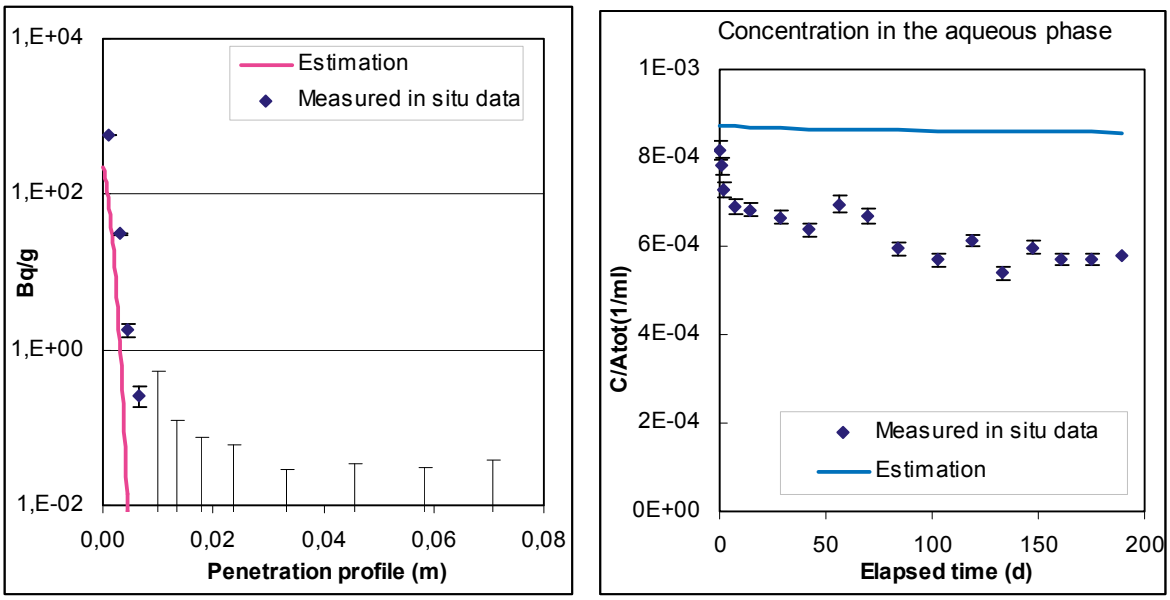

Figure Case 2. *Tracer: Ba-133. Core: A12.*

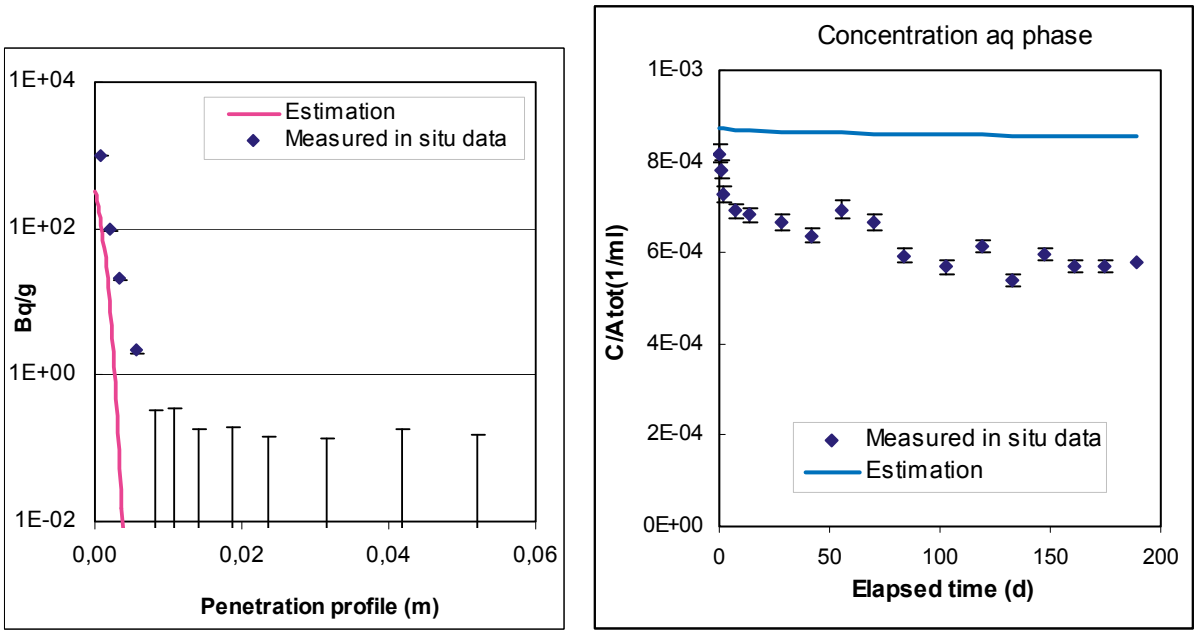

Figure Case 2. *Tracer: Ba-133. Core: D12.*

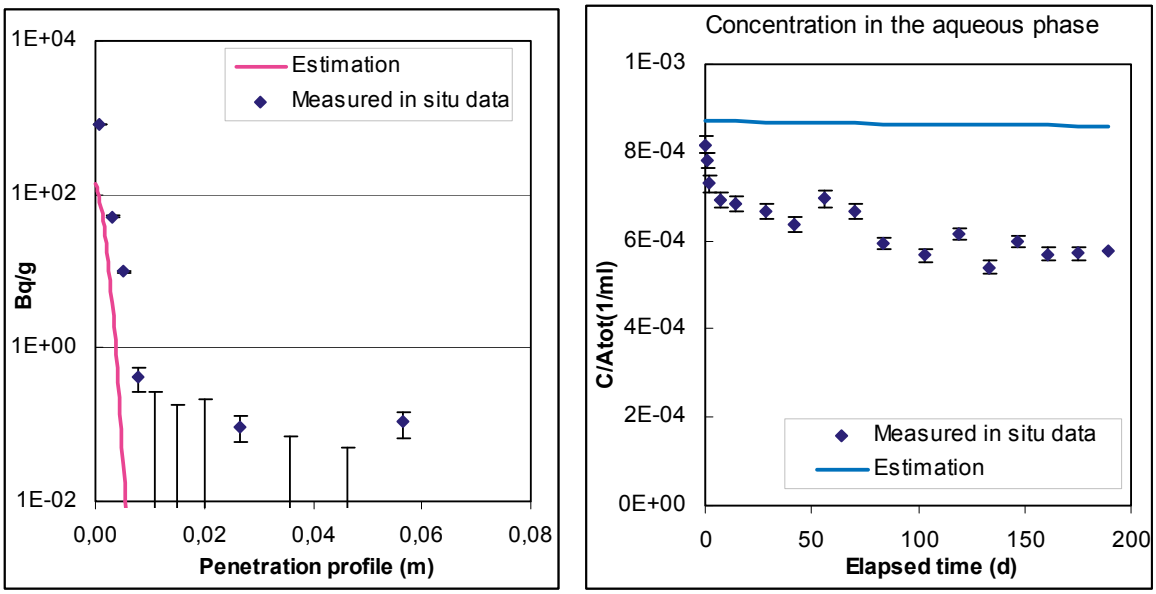

Figure Case 2. *Tracer: Ba-133. Core: D13.*

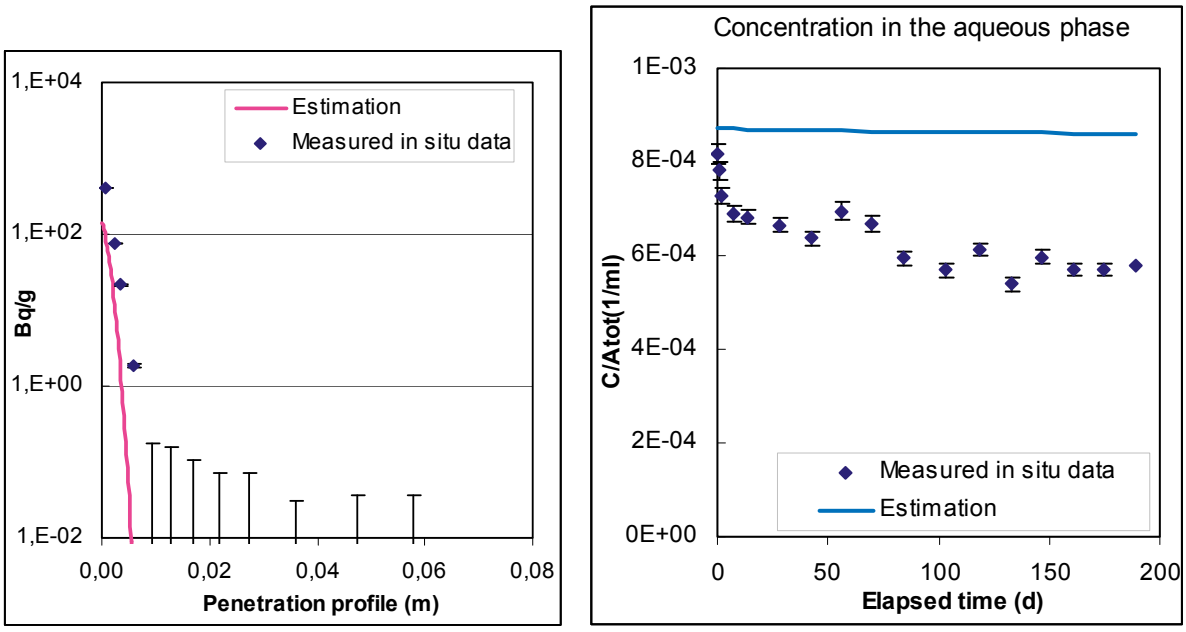

Figure Case 2. *Tracer: Ba-133. Core: D14.*

Cs-137

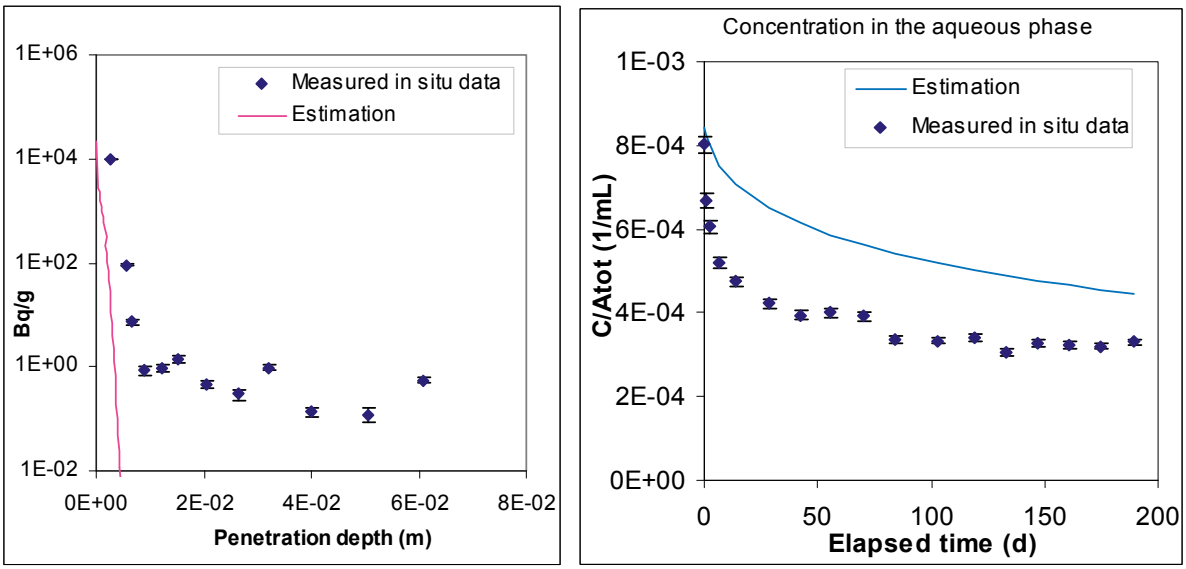

Figure Case 2. *Tracer: Cs-137. Core: A1.*

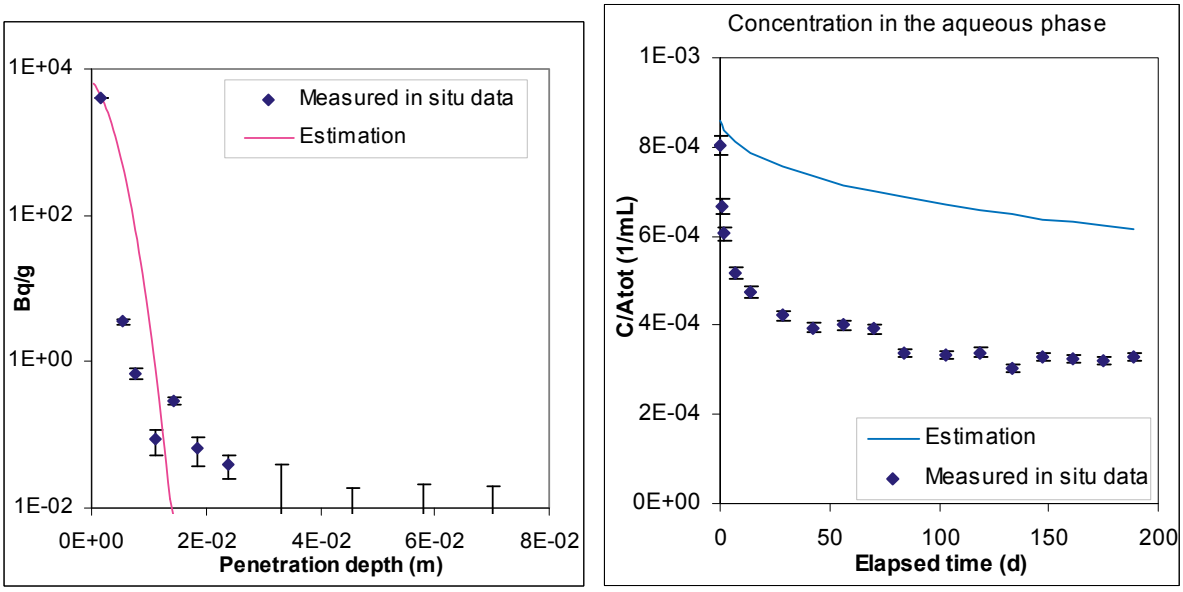

Figure Case 2. *Tracer: Cs-137. Core: A5.*

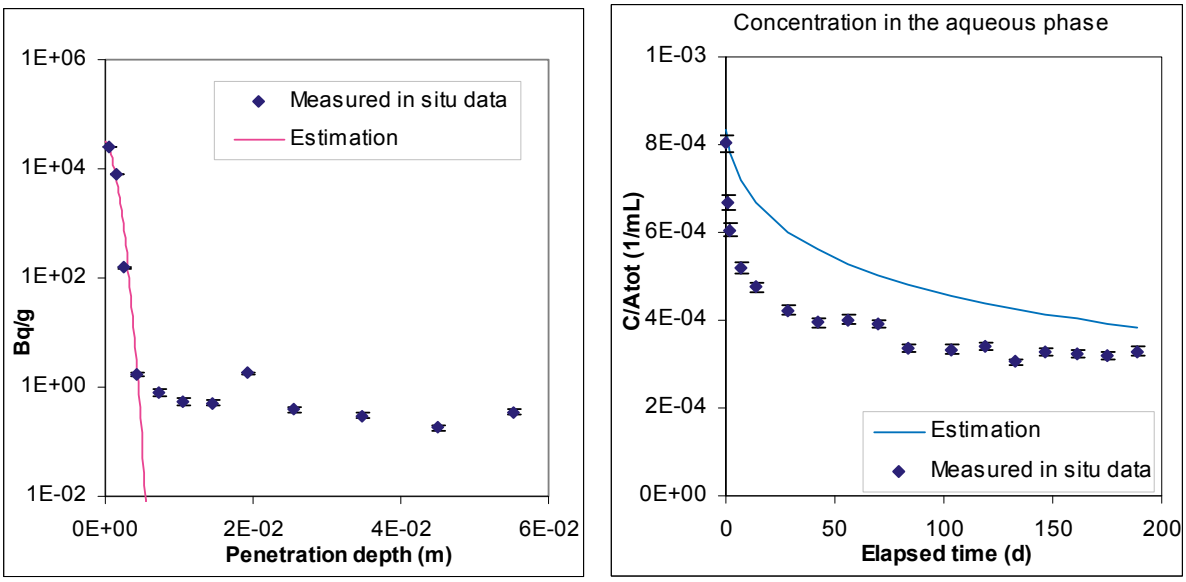

Figure Case 2. *Tracer: Cs-137. Core: A6.*

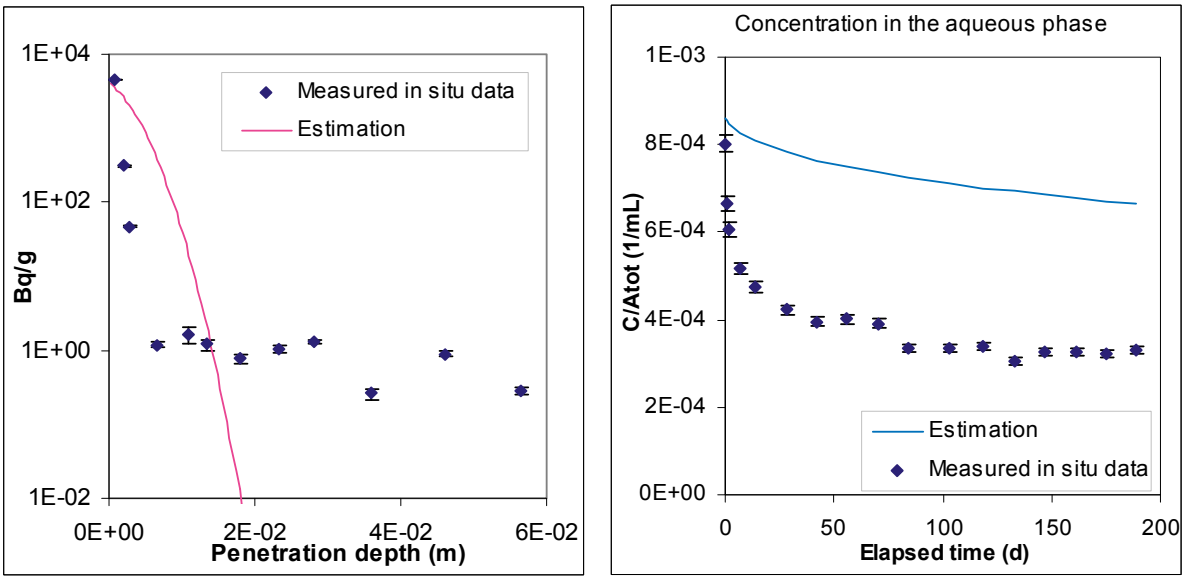

Figure Case 2. *Tracer: Cs-137. Core: A8.*

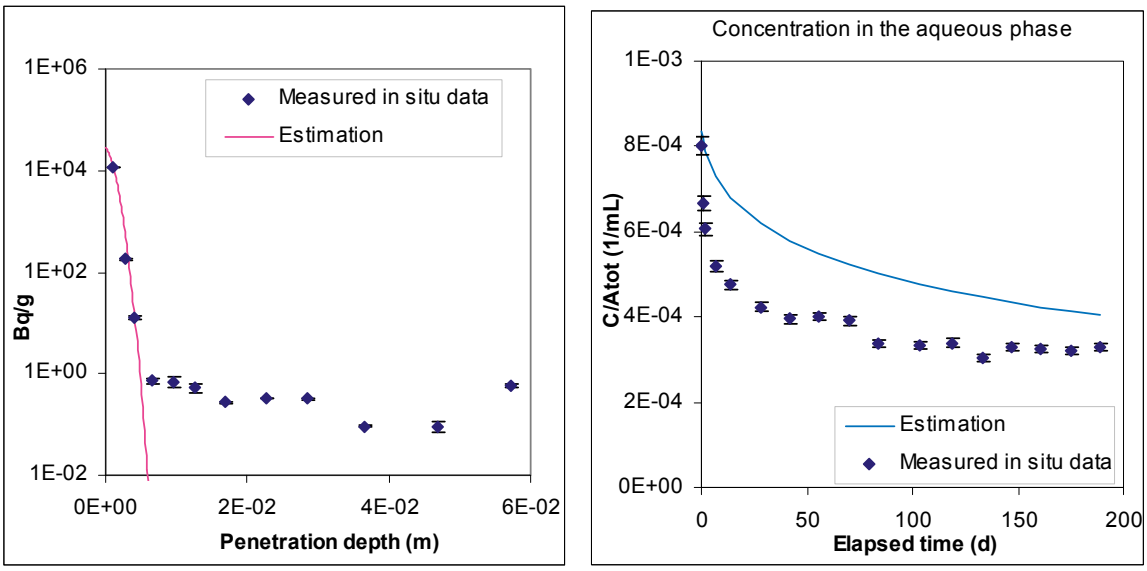

Figure Case 2. *Tracer: Cs-137. Core: A9.*

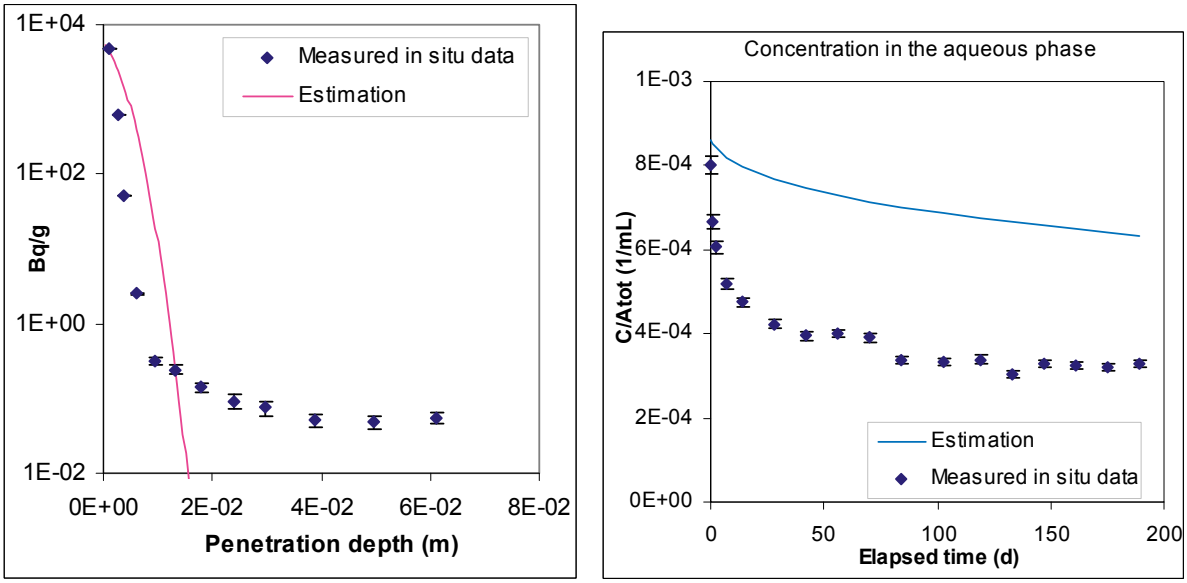

Figure Case 2. *Tracer: Cs-137. Core: A10.*

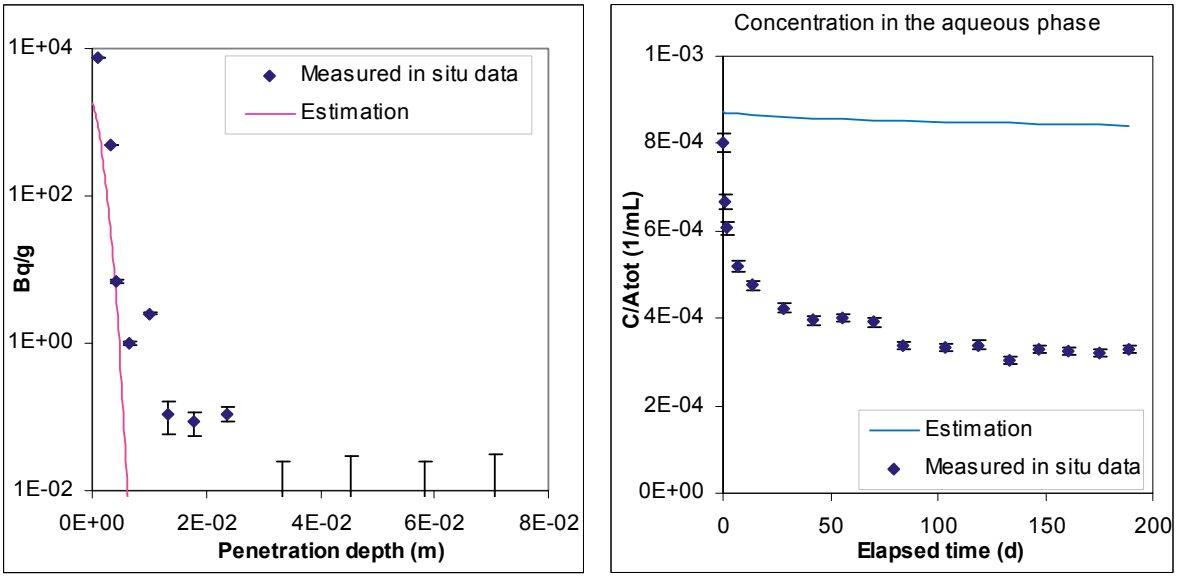

Figure Case 2. *Tracer: Cs-137. Core: A12.*

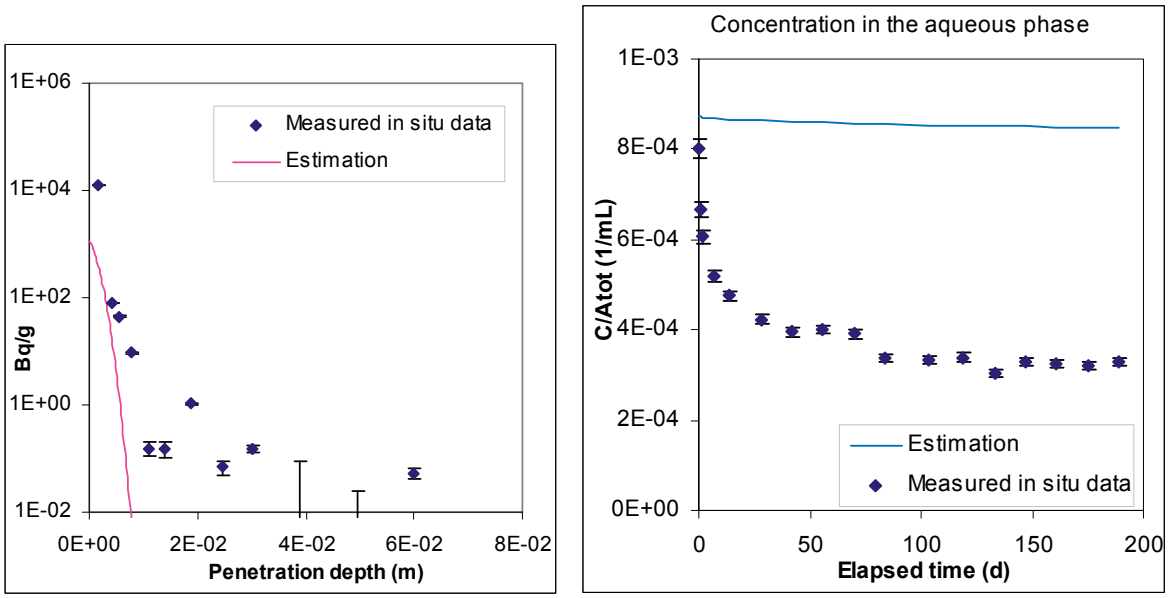

Figure Case 2. *Tracer: Cs-137. Core: A15.*

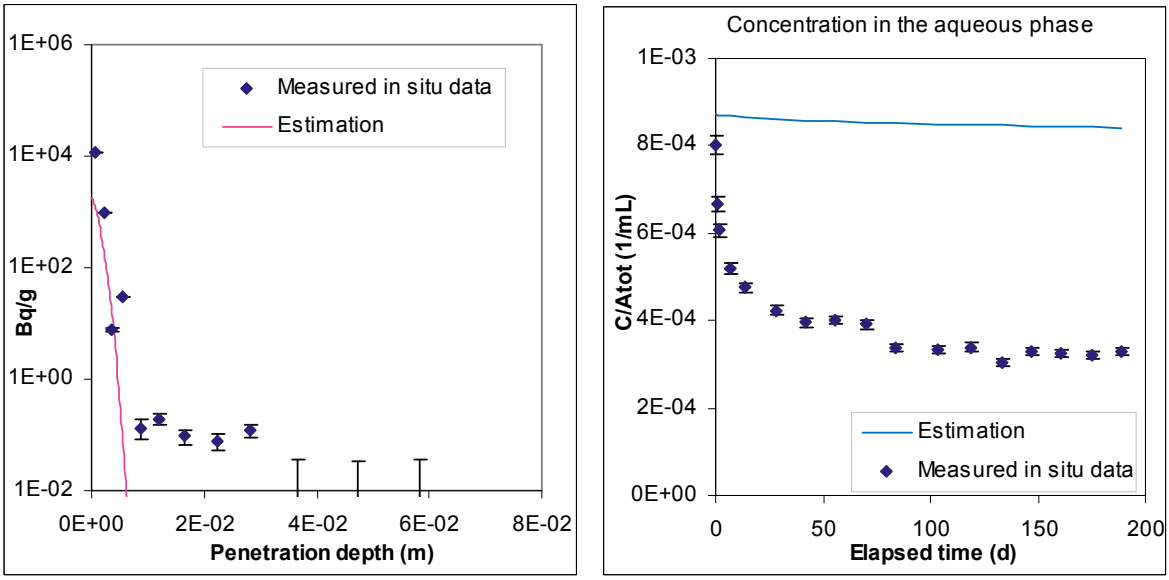

Figure Case 2. *Tracer: Cs-137. Core: A16.*

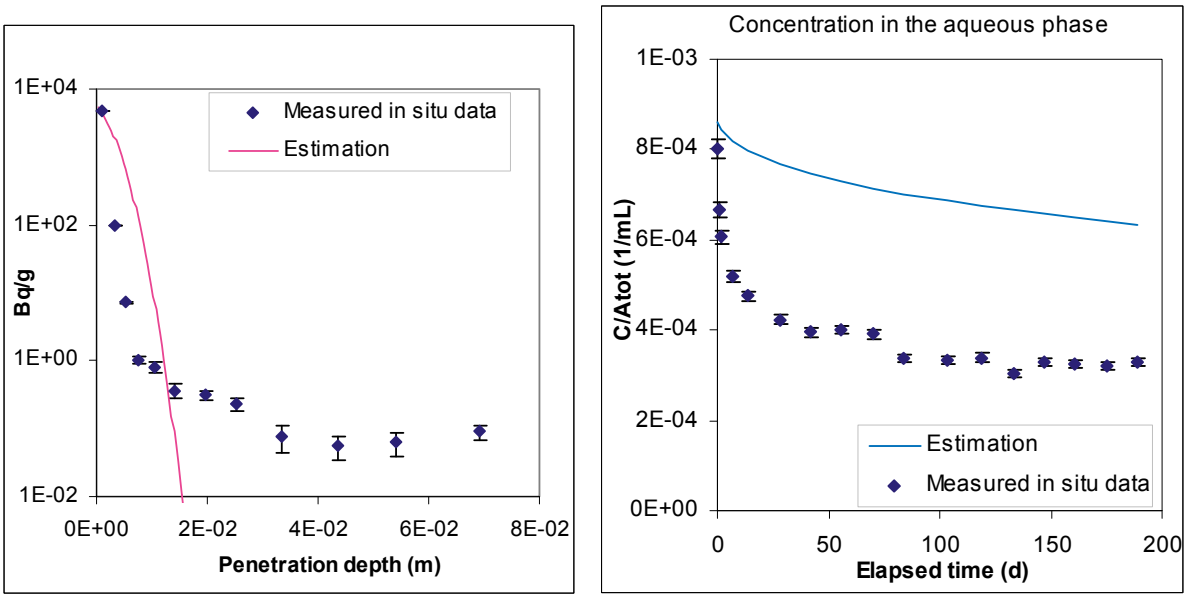

Figure Case 2. *Tracer: Cs-137. Core: A17.*

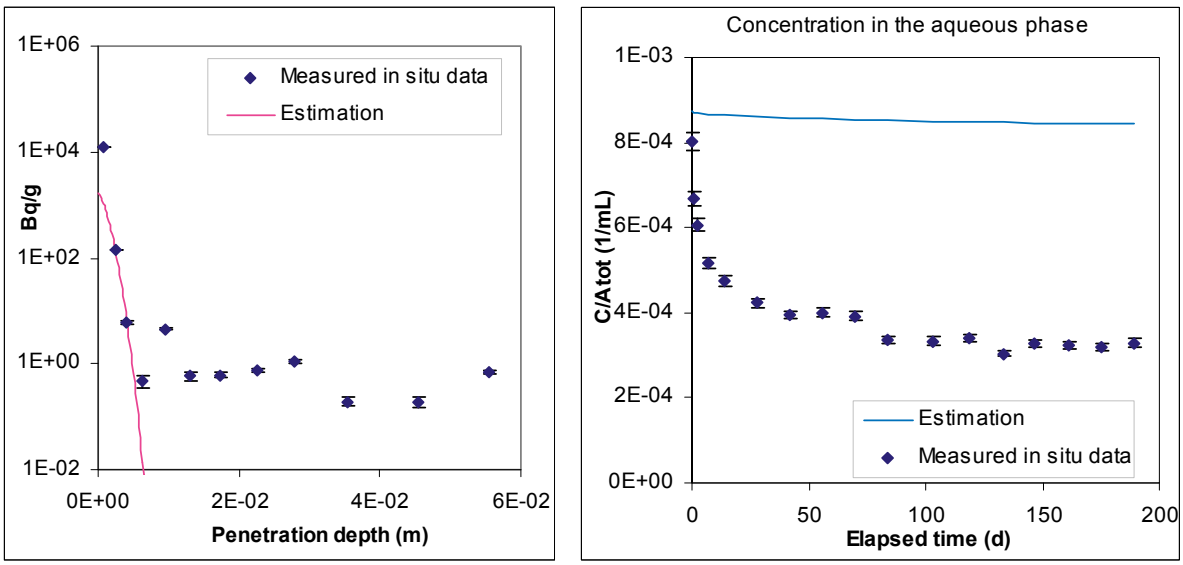

Figure Case 2. *Tracer: Cs-137. Core: D1.*

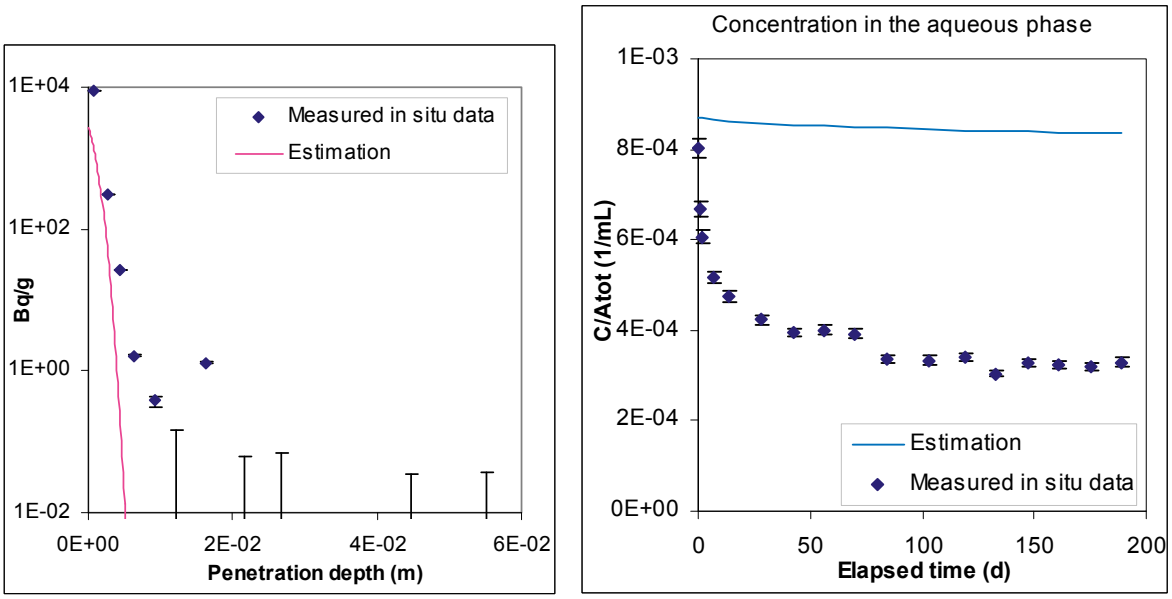

Figure Case 2. *Tracer: Cs-137. Core: D5.*

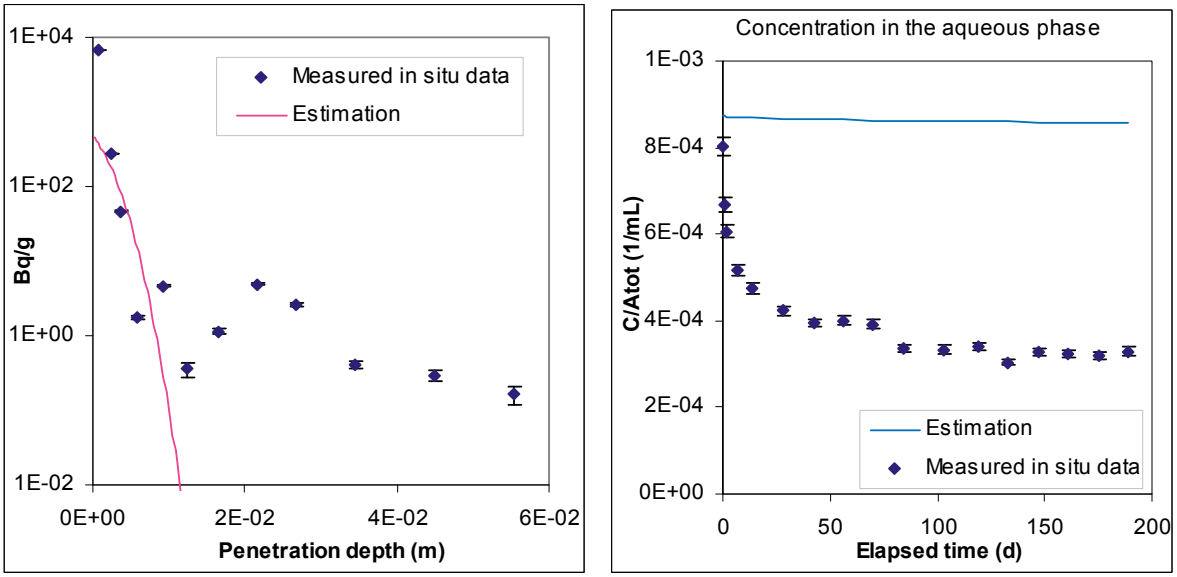

Figure Case 2. *Tracer: Cs-137. Core: D6.*

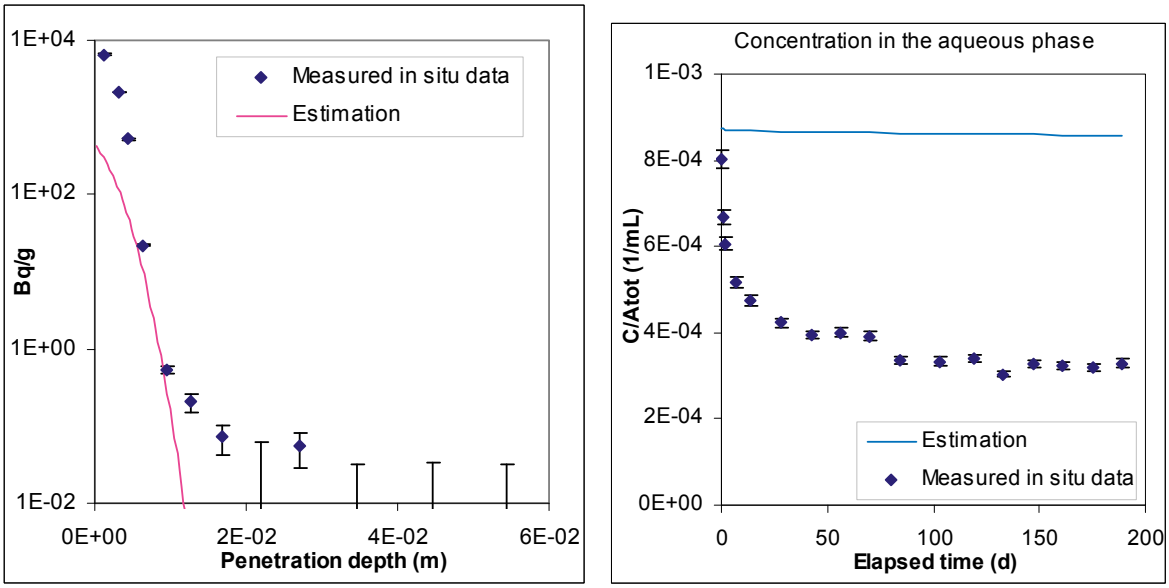

Figure Case 2. *Tracer: Cs-137. Core: D7.*

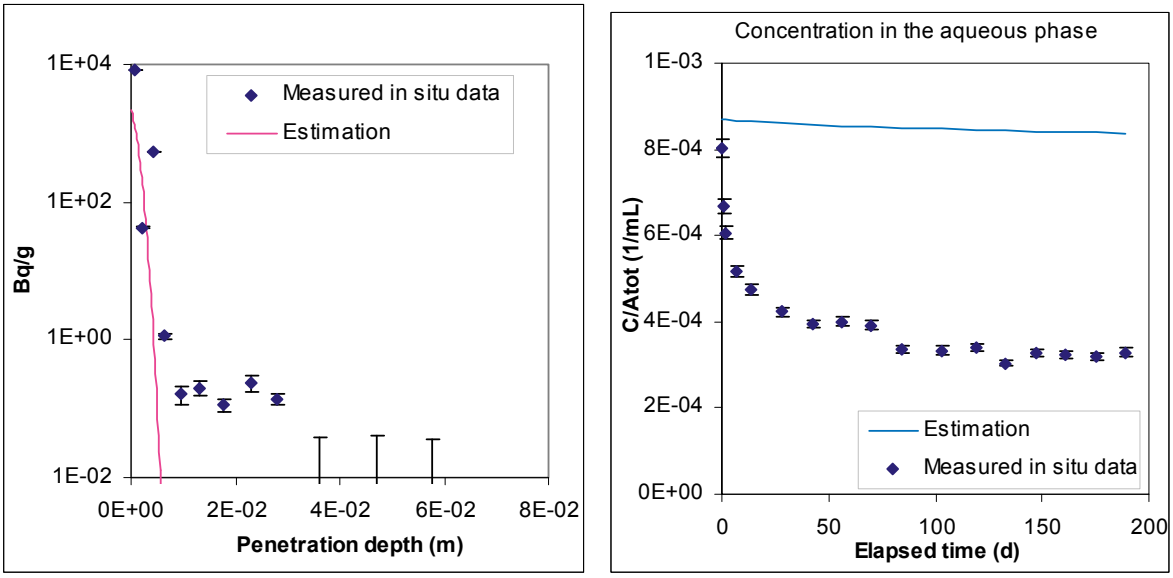

Figure Case 2. *Tracer: Cs-137. Core: D8.*

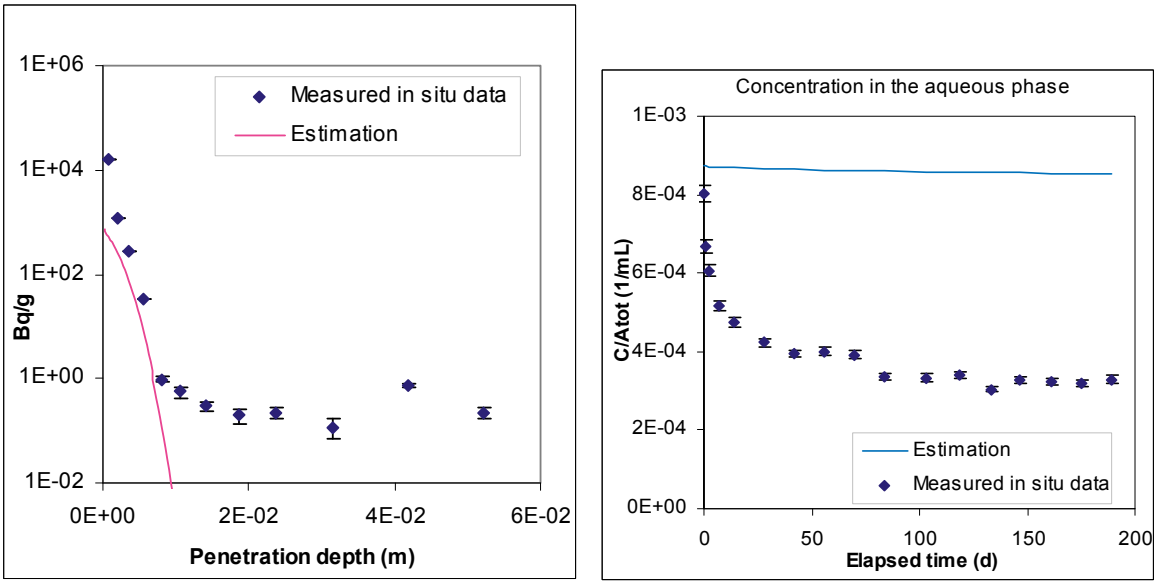

Figure Case 2. *Tracer: Cs-137. Core: D12.*

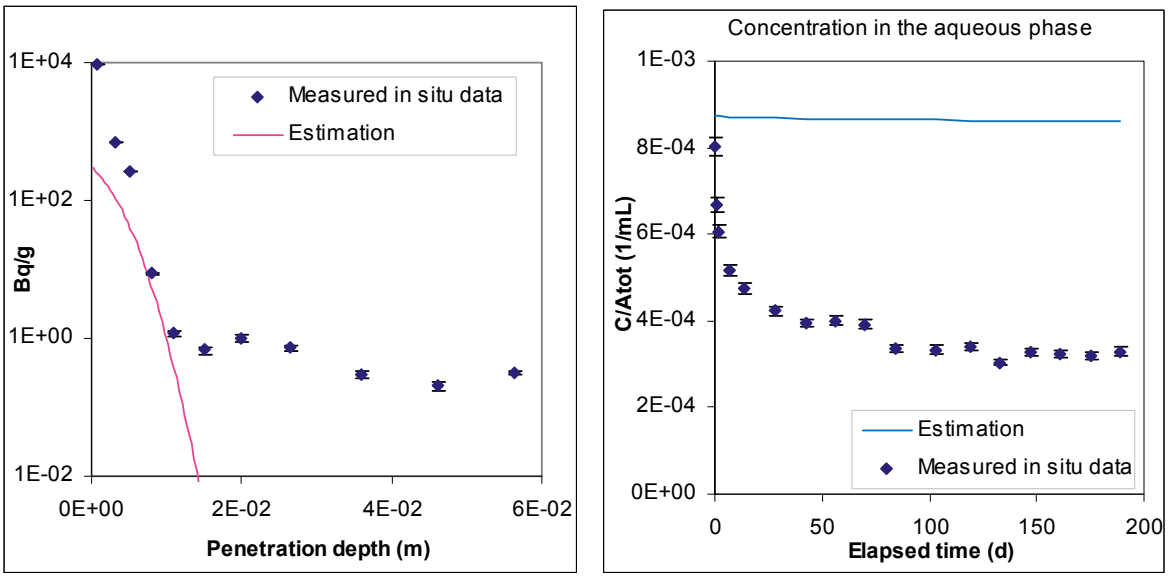

Figure Case 2. *Tracer: Cs-137. Core: D13.*

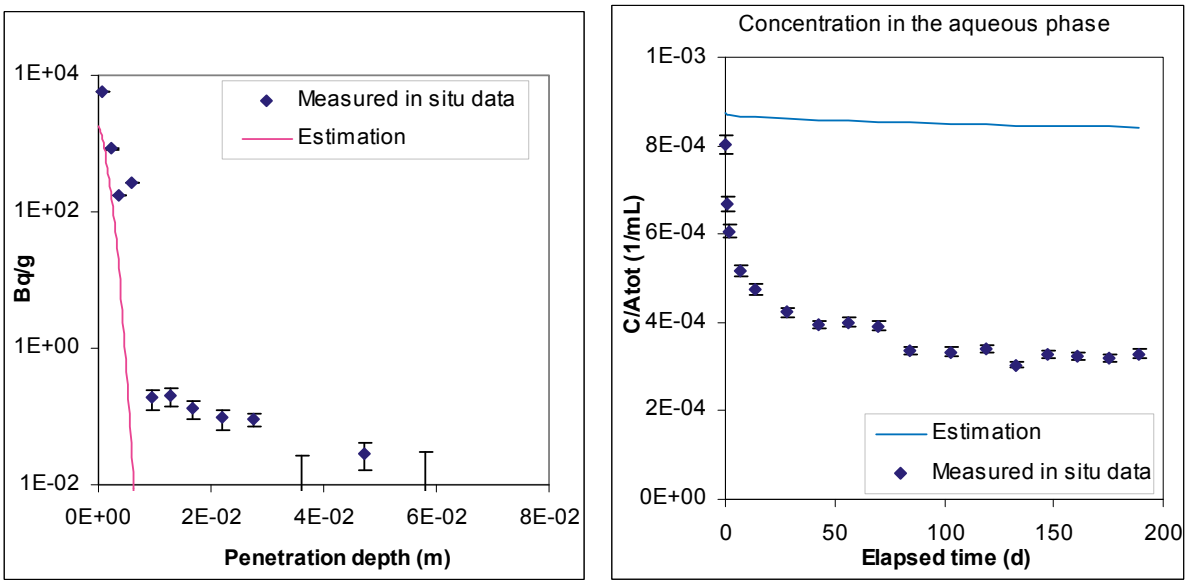

Figure Case 2. *Tracer: Cs-137. Core: D14.*

Na-22

A1

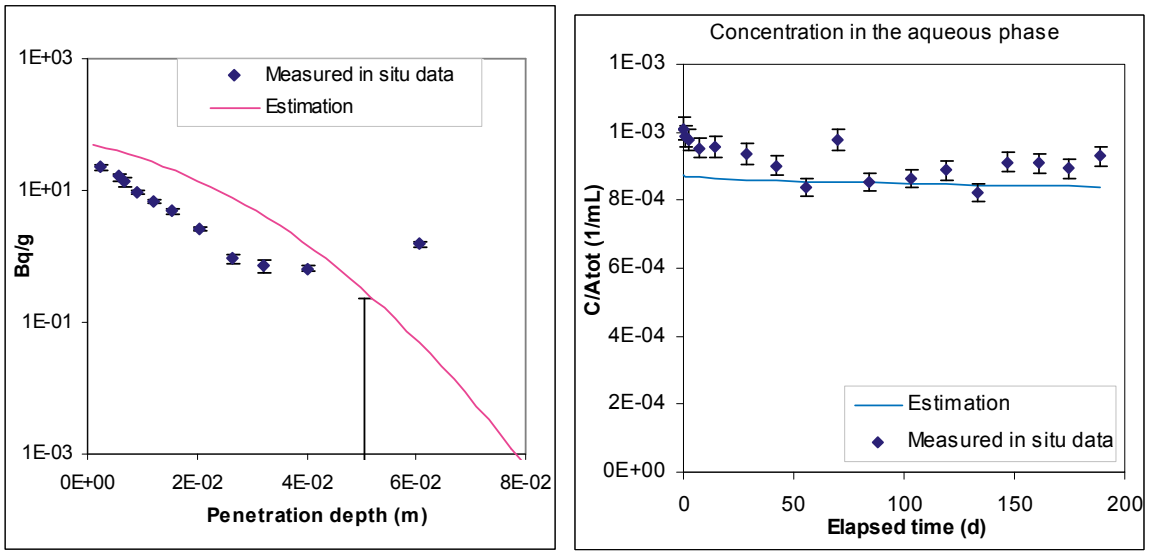

Figure Case 2. *Tracer: Na-22. Core: A1.*

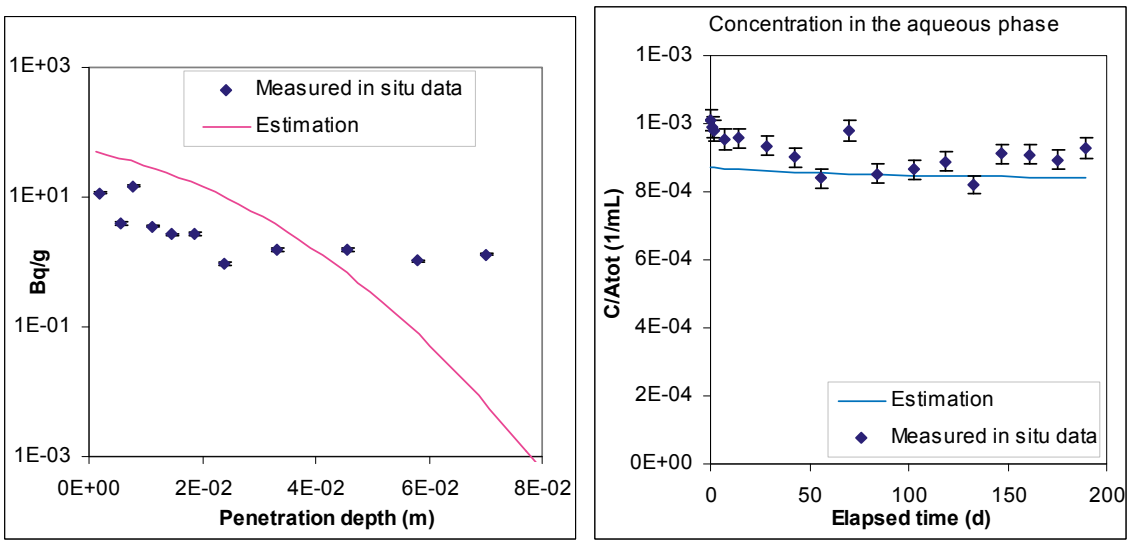

Figure Case 2. *Tracer: Na-22. Core: A5.*

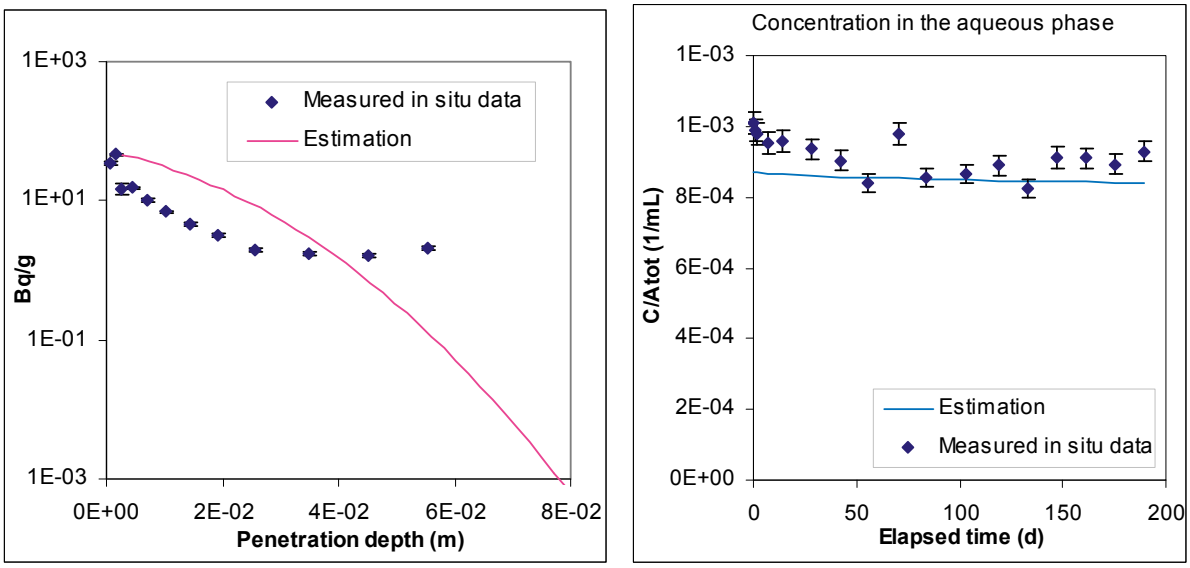

Figure Case 2. *Tracer: Na-22. Core: A6.*

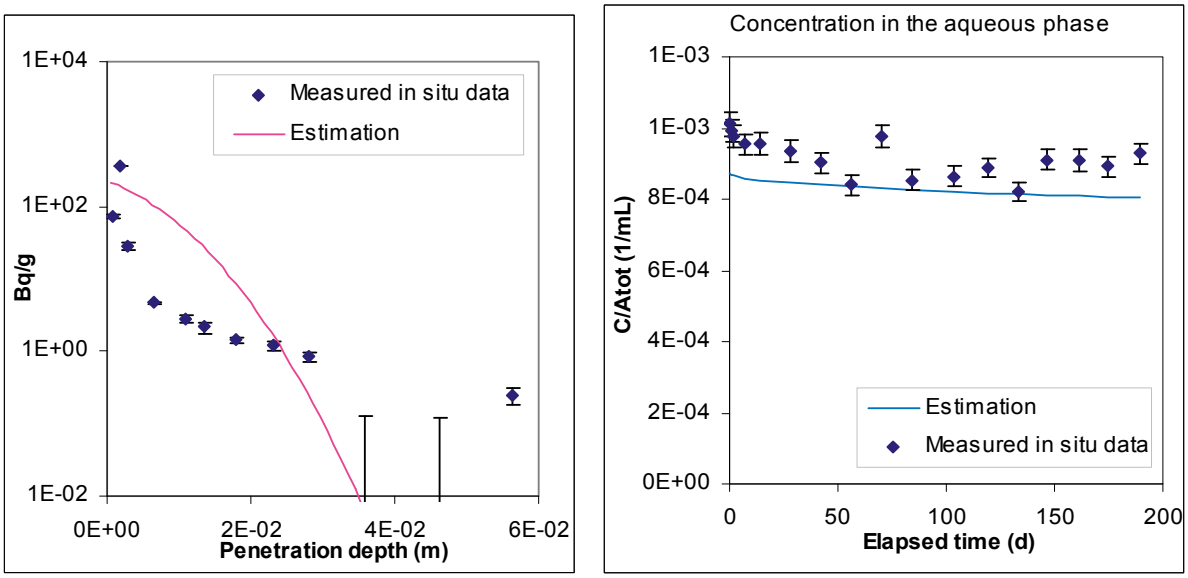

Figure Case 2. *Tracer: Na-22. Core: A8.*

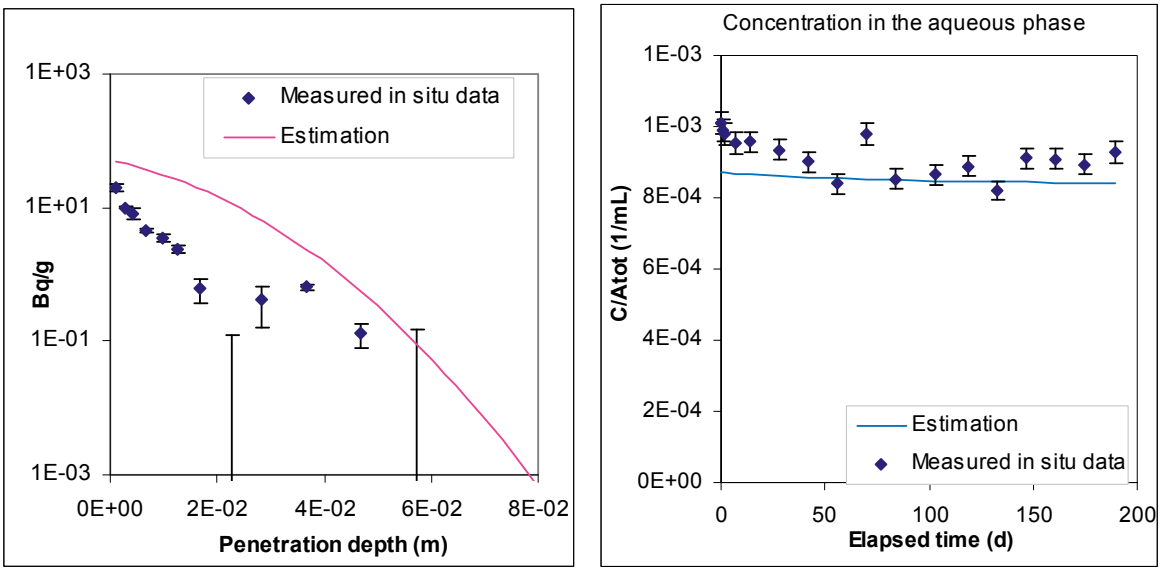

Figure Case 2. *Tracer: Na-22. Core: A9.*

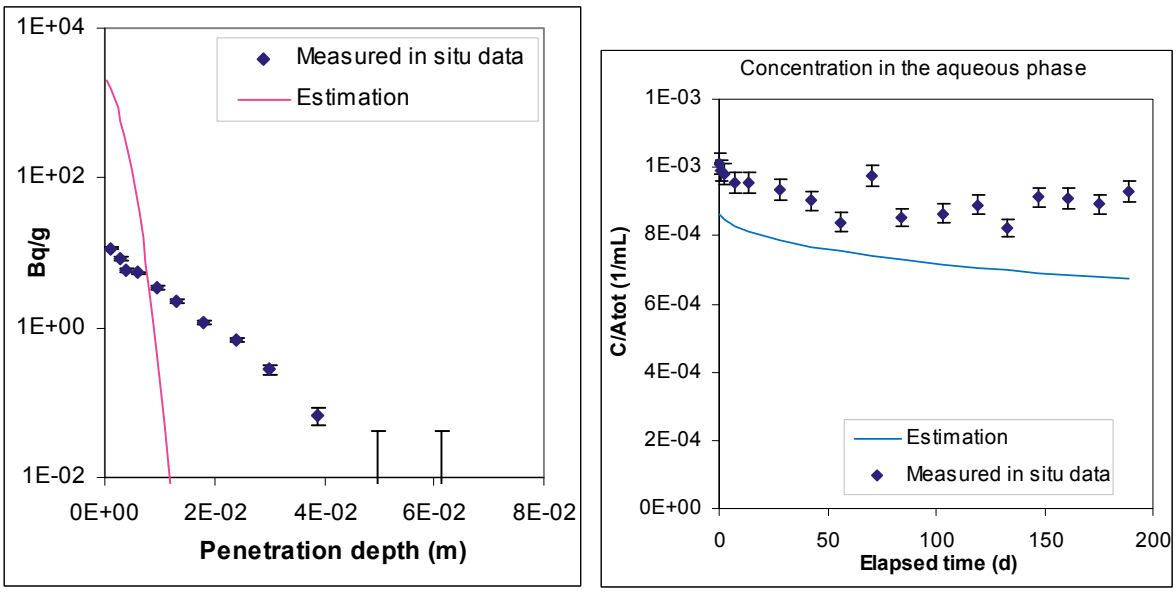

Figure Case 2. *Tracer: Na-22. Core: A10.*

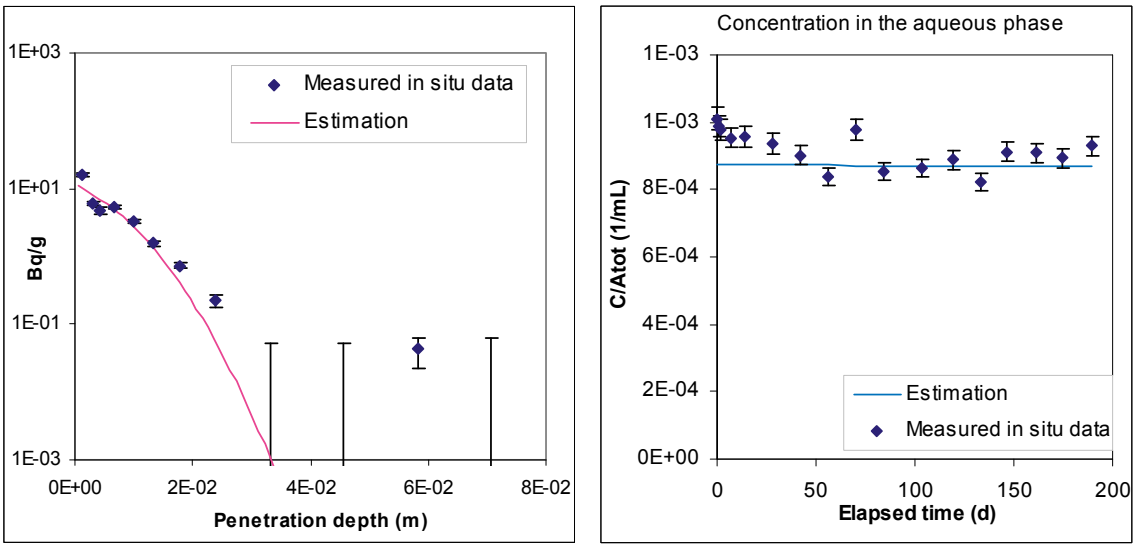

Figure Case 2. *Tracer: Na-22. Core: A12.*

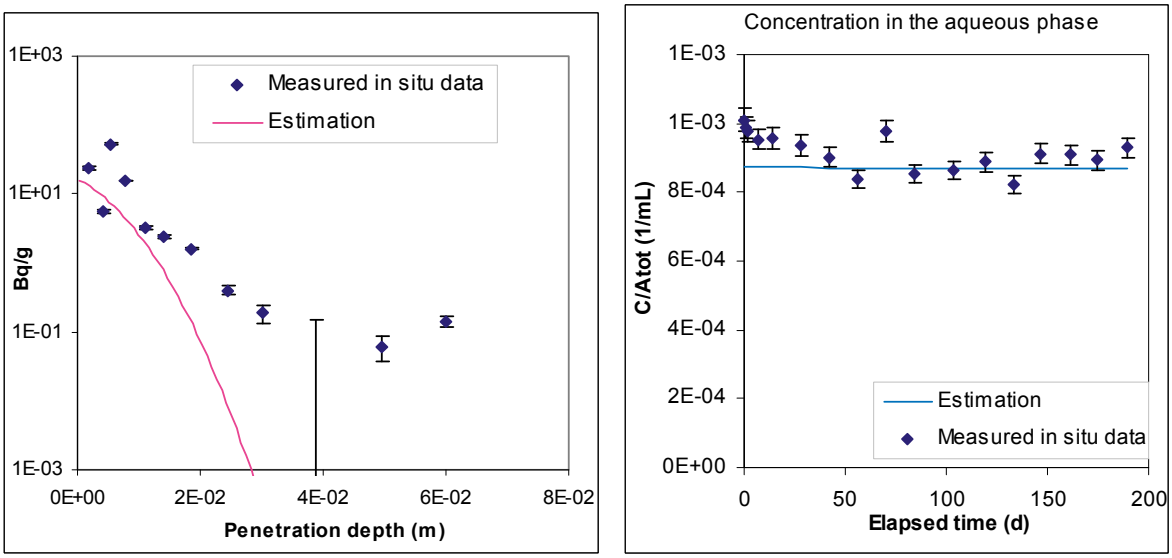

Figure Case 2. *Tracer: Na-22. Core: A15.*

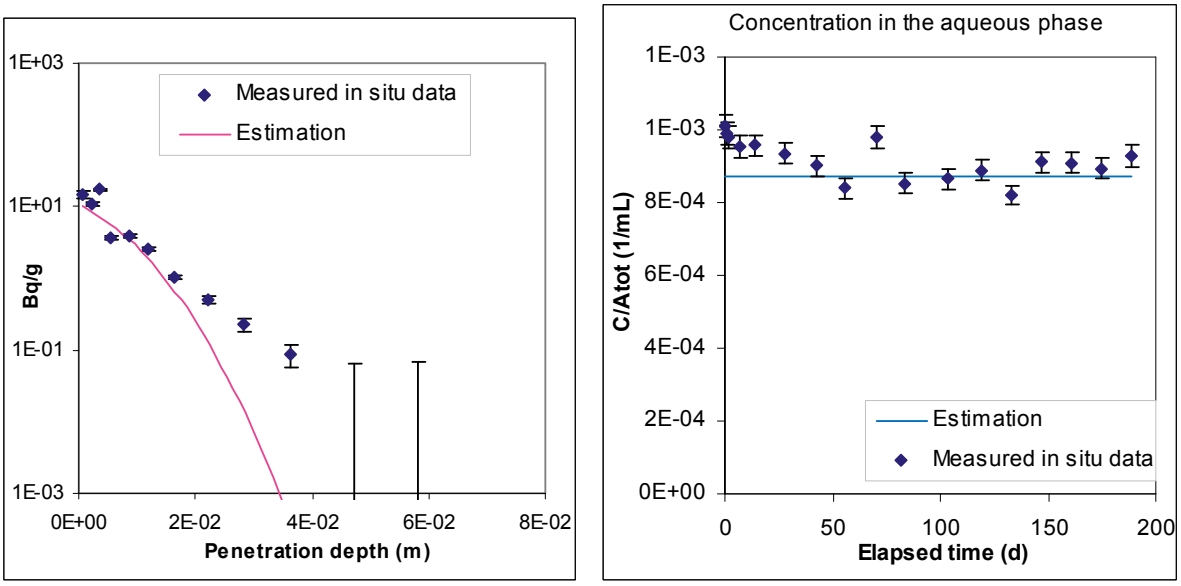

Figure Case 2. *Tracer: Na-22. Core: A16.*

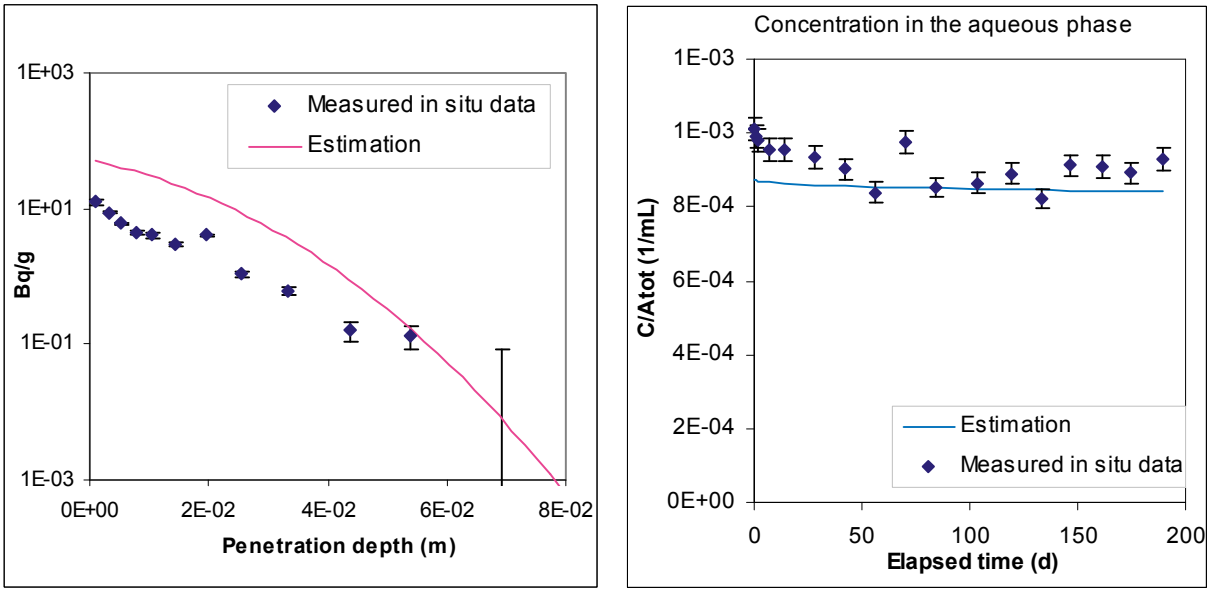

Figure Case 2. *Tracer: Na-22. Core: A17.*

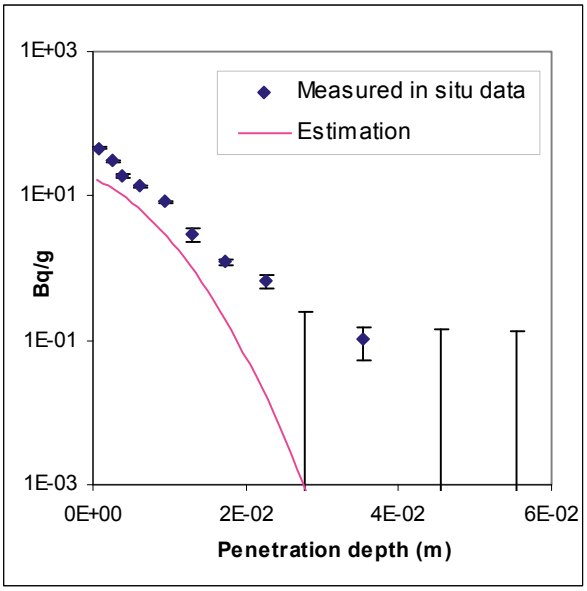

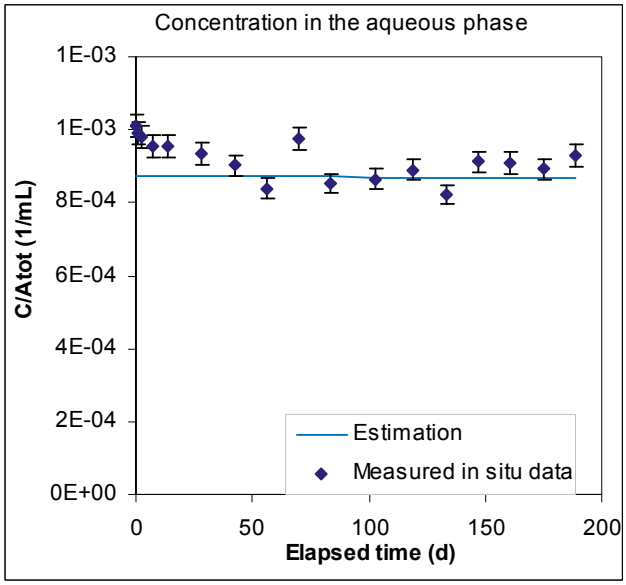

Figure Case 2. *Tracer: Na-22. Core: D1.*

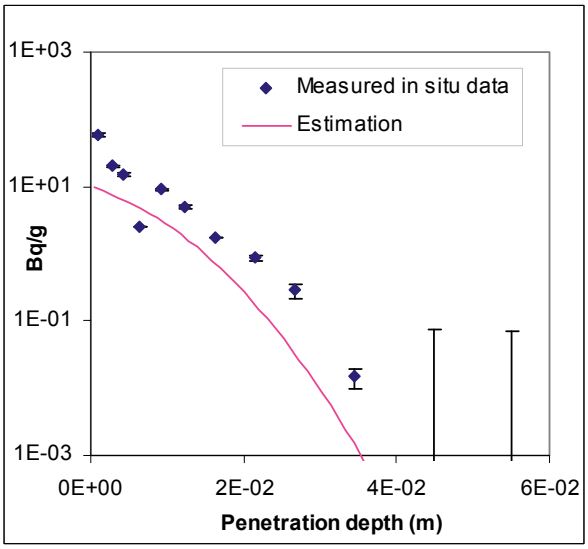

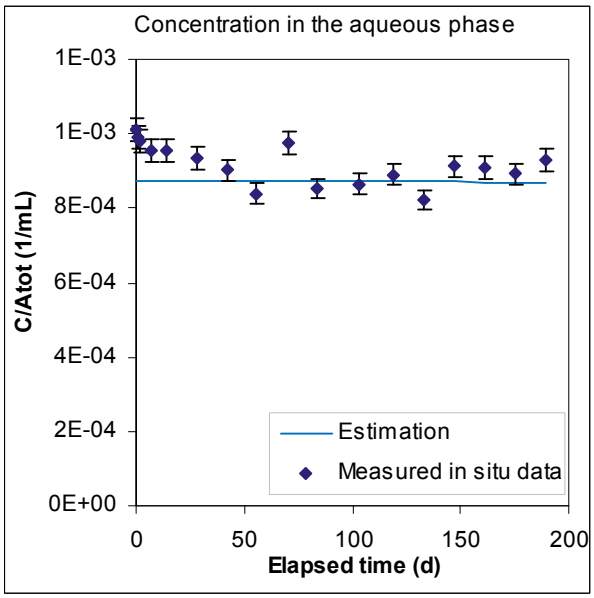

Figure Case 2. *Tracer: Na-22. Core: D5.*

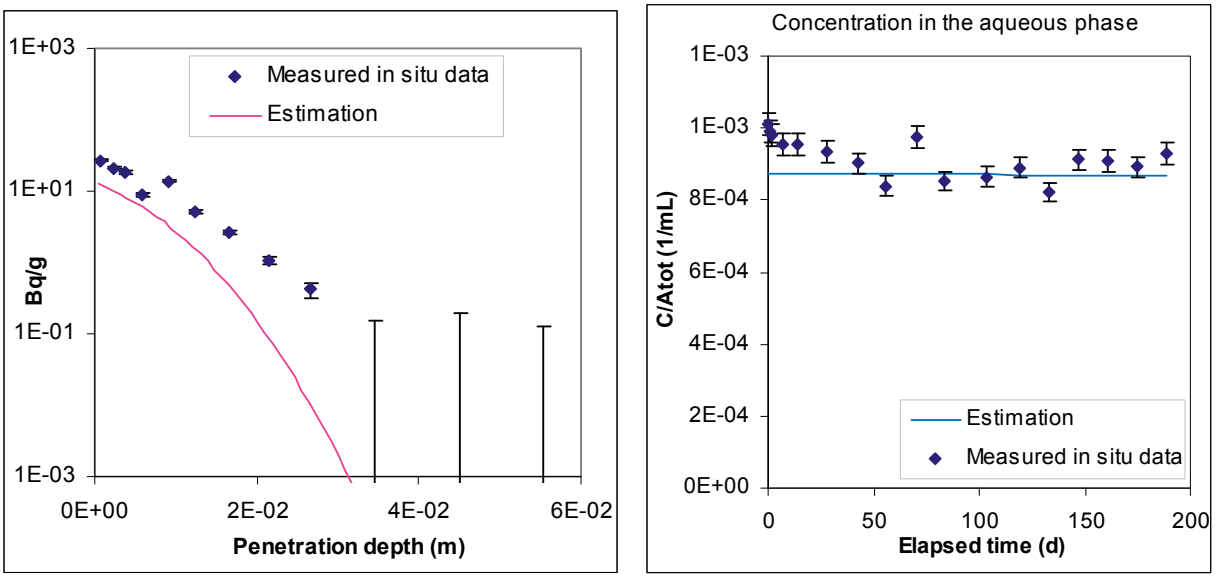

Figure Case 2. *Tracer: Na-22. Core: D6.*

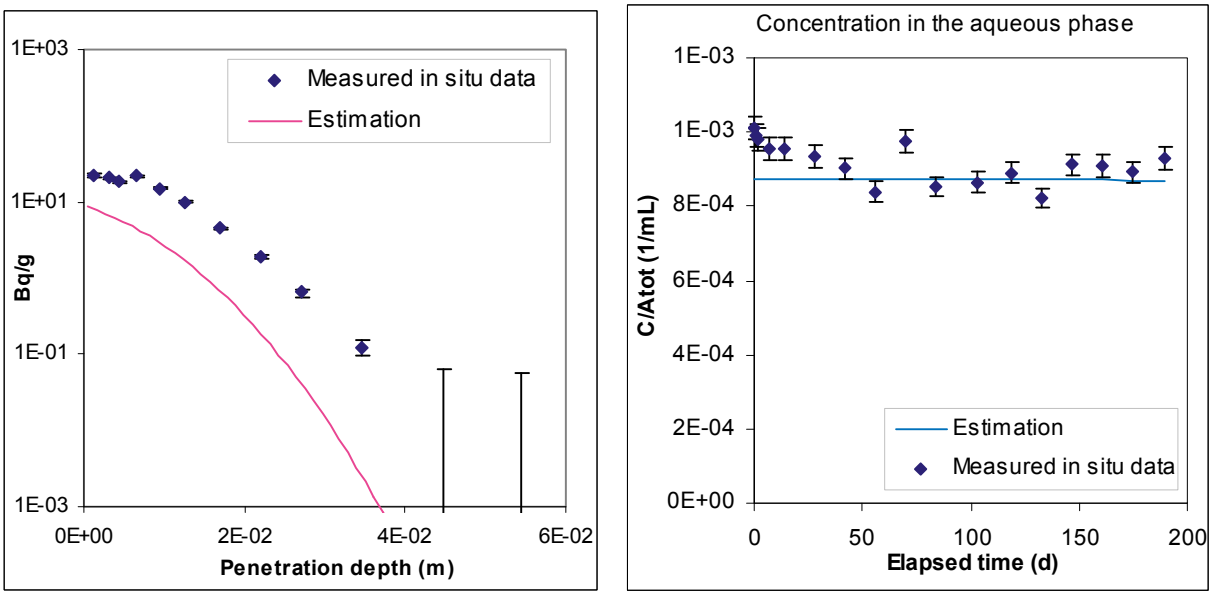

Figure Case 2. *Tracer: Na-22. Core: D7.*

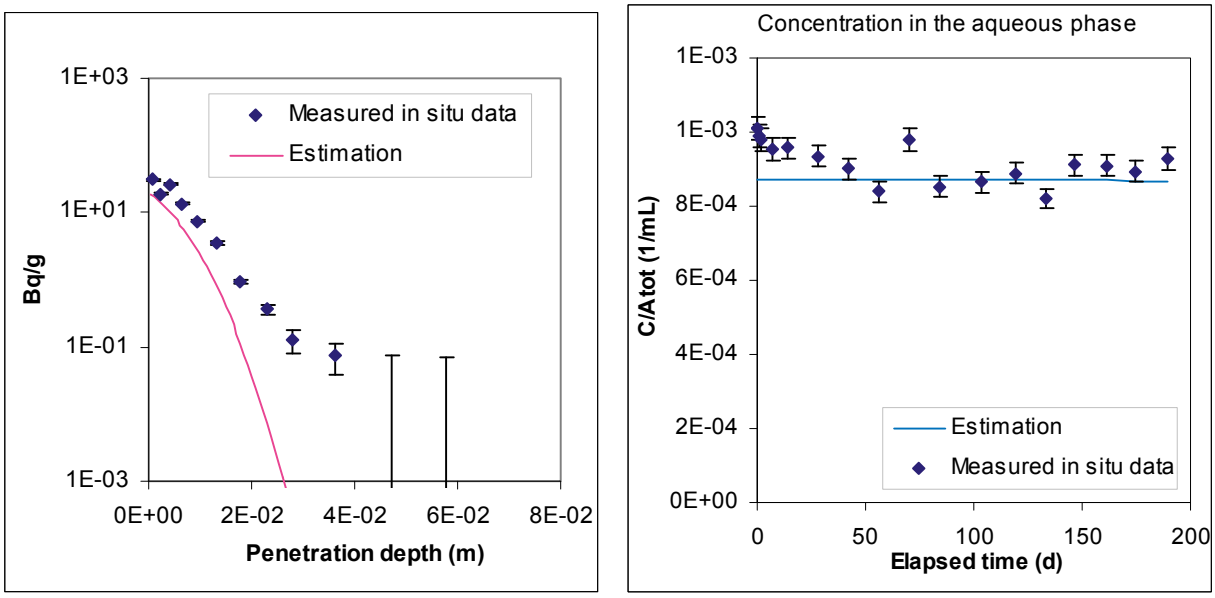

Figure Case 2. *Tracer: Na-22. Core: D8.*

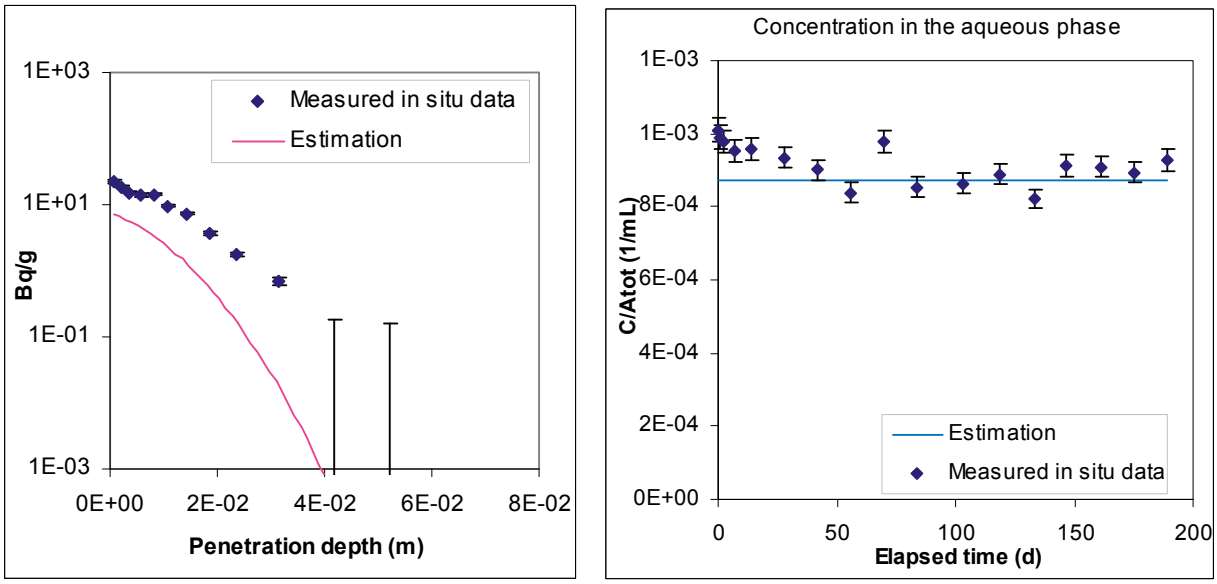

Figure Case 2. *Tracer: Na-22. Core: D12.*

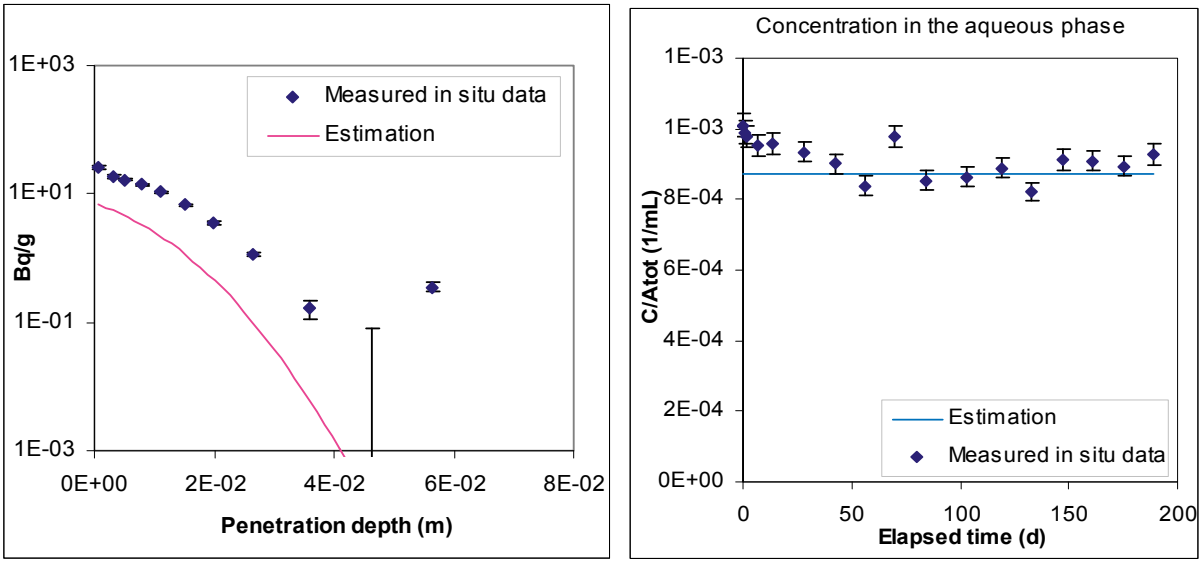

Figure Case 2. *Tracer: Na-22. Core: D13.*

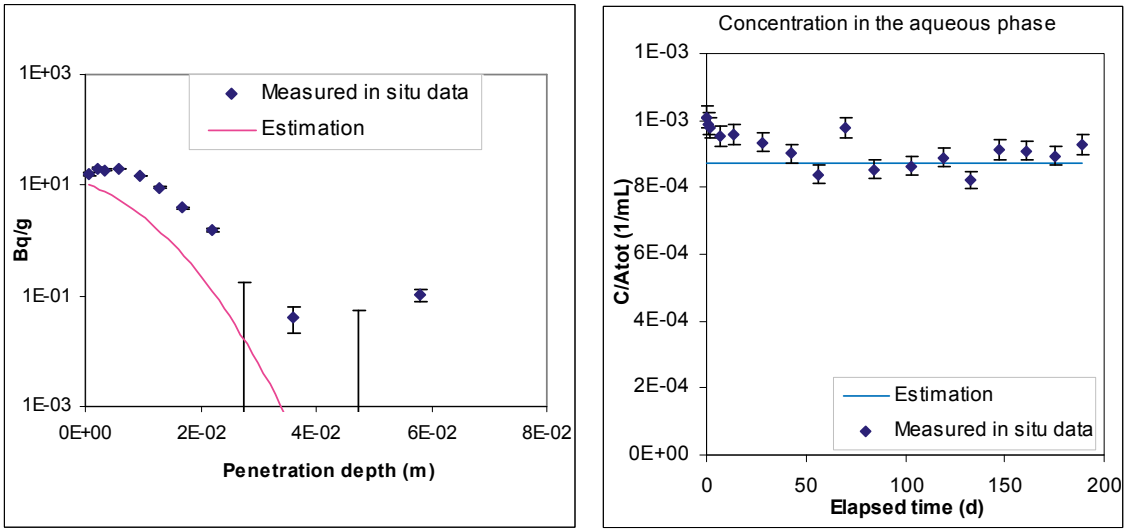

Figure Case 2. *Tracer: Na-22. Core: D14.*

Ni-63

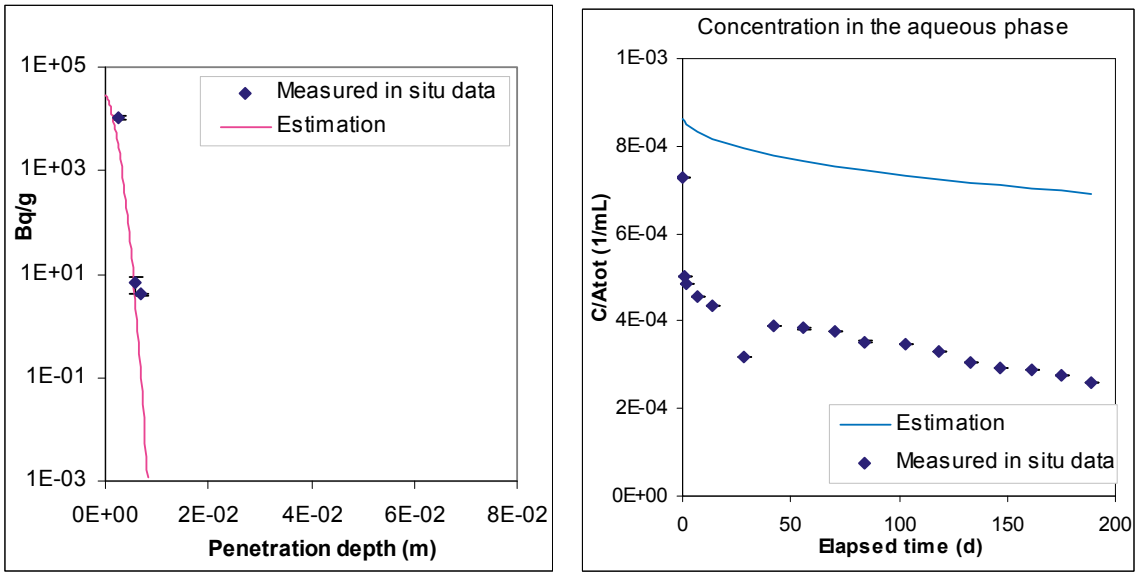

Figure Case 2. *Tracer: Ni-63. Core: A1.*

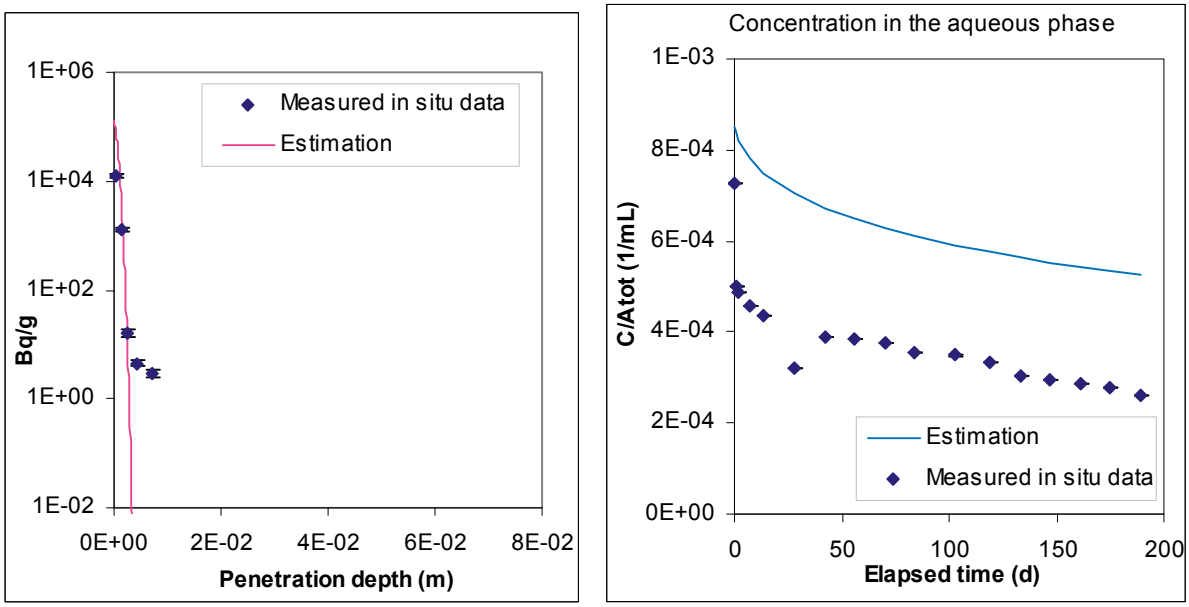

Figure Case 2. *Tracer: Ni-63. Core: A6.*

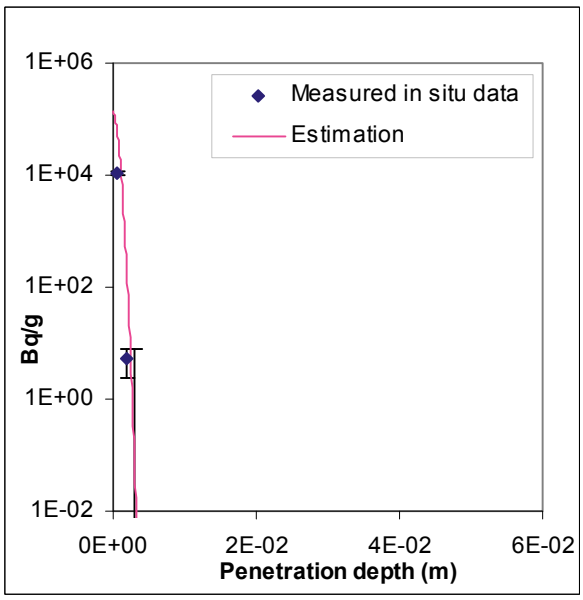

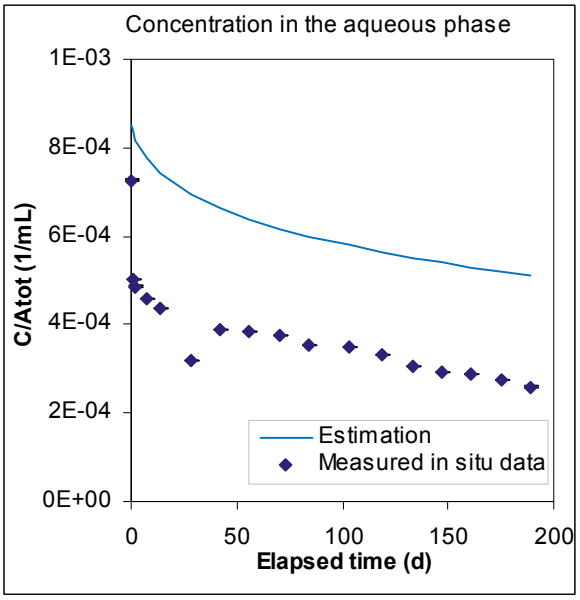

Figure Case 2. *Tracer:Ni-63. Core: A8.*

Ni-A9

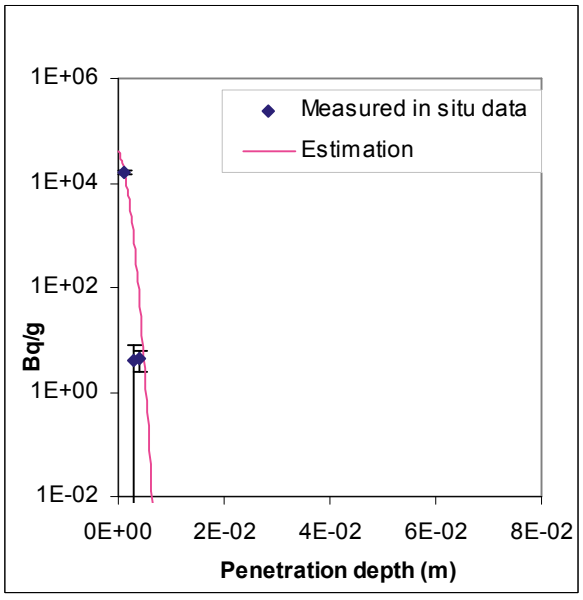

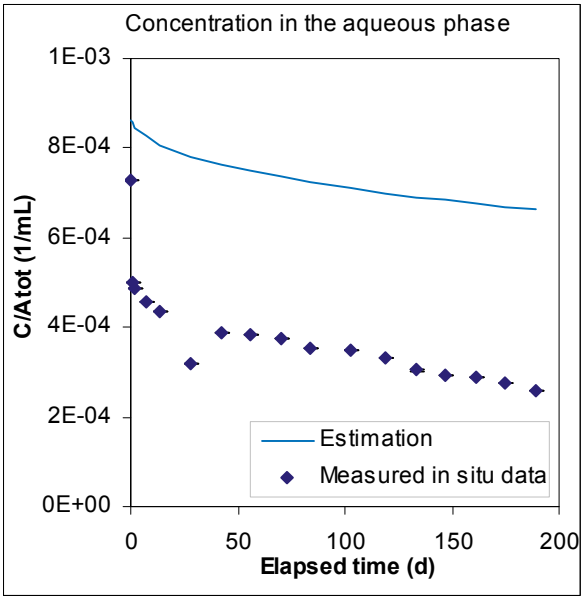

Figure Case 2. *Tracer: Ni-63. Core: A9.*

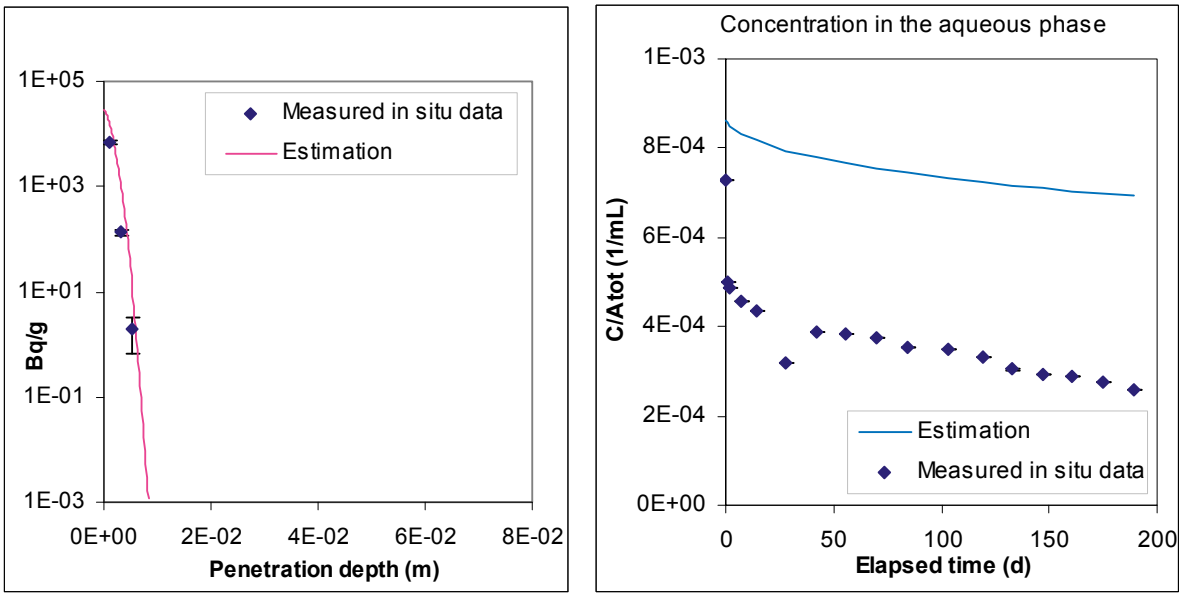

Figure Case 2. *Tracer: Ni-63. Core: A17.*

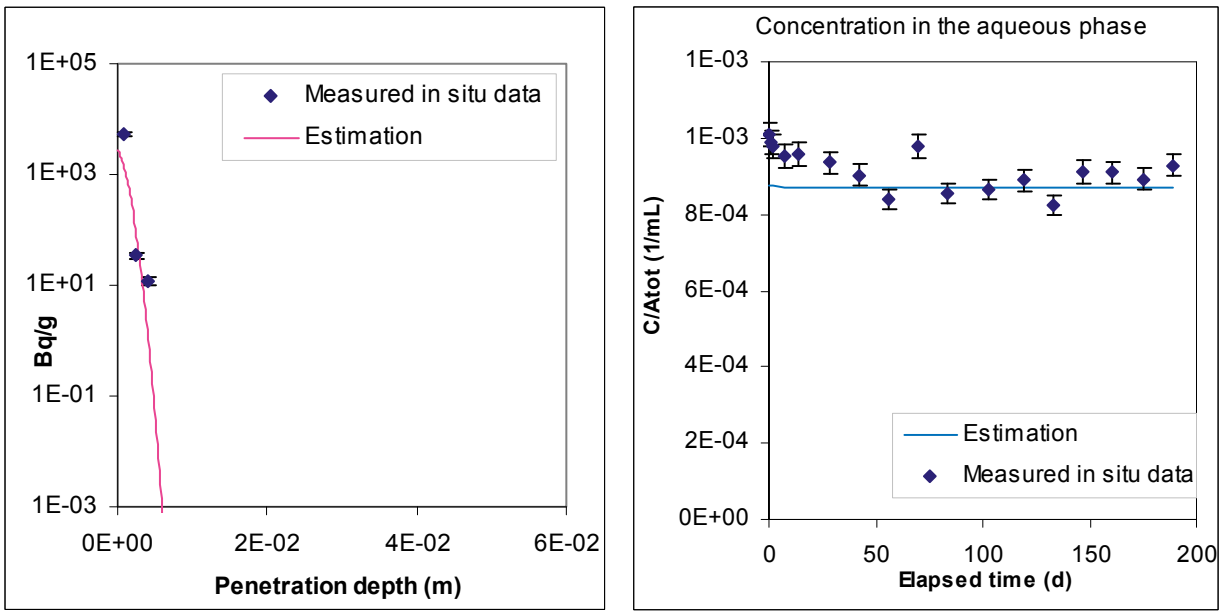

Figure Case 2. *Tracer: Ni-63. Core: D1.*

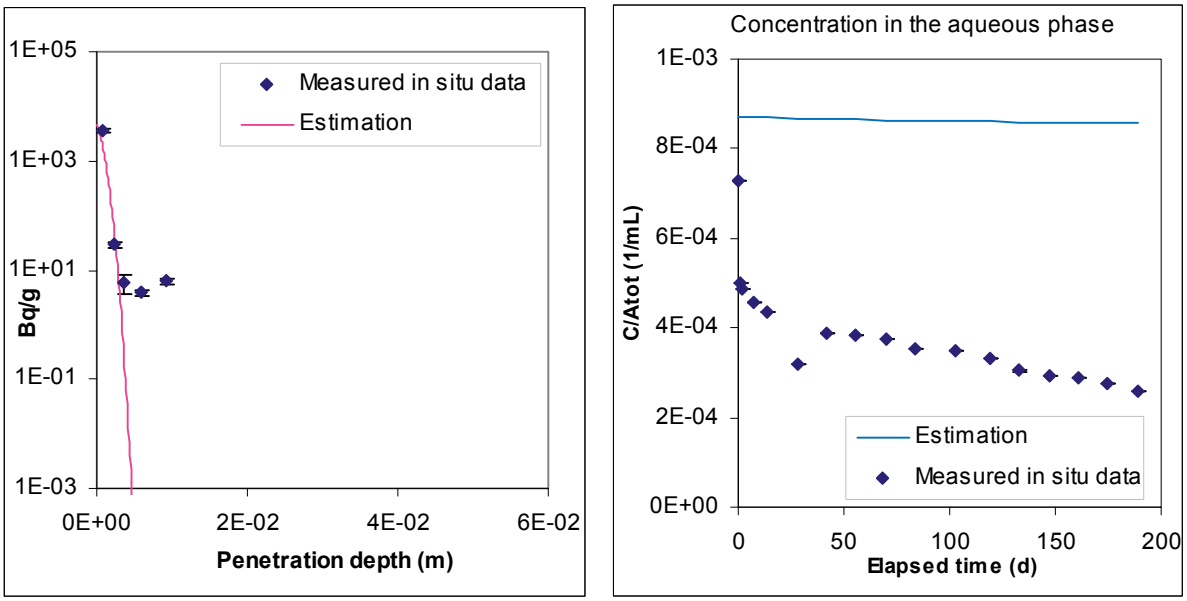

Figure Case 2. *Tracer: Ni-63. Core: D6.*

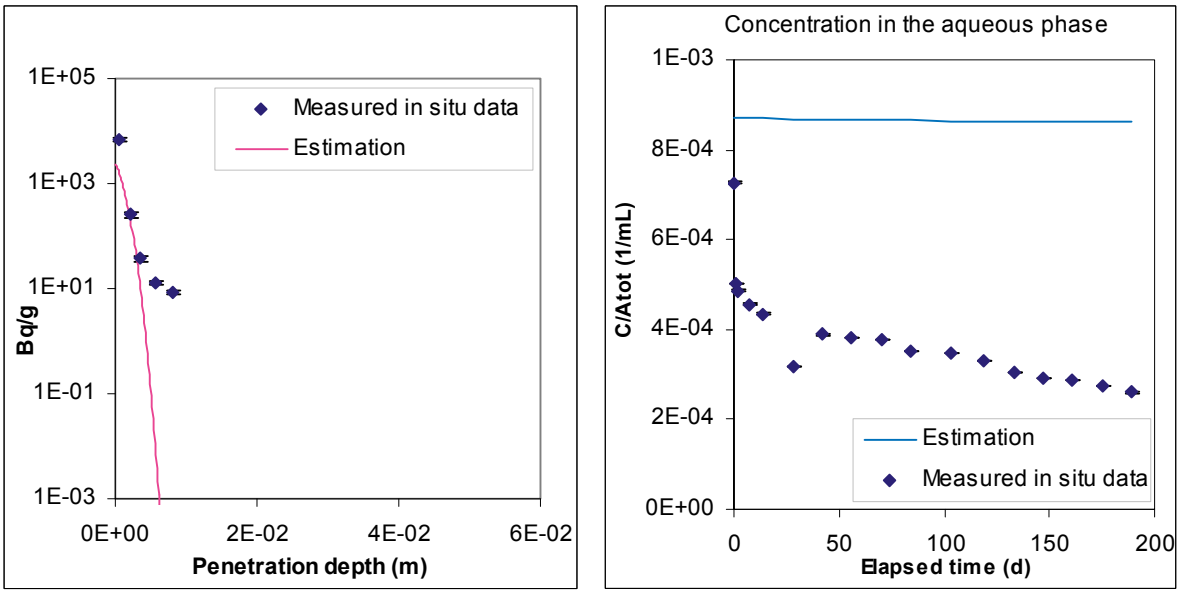

Figure Case 2. *Tracer: Ni-63. Core: D12.*

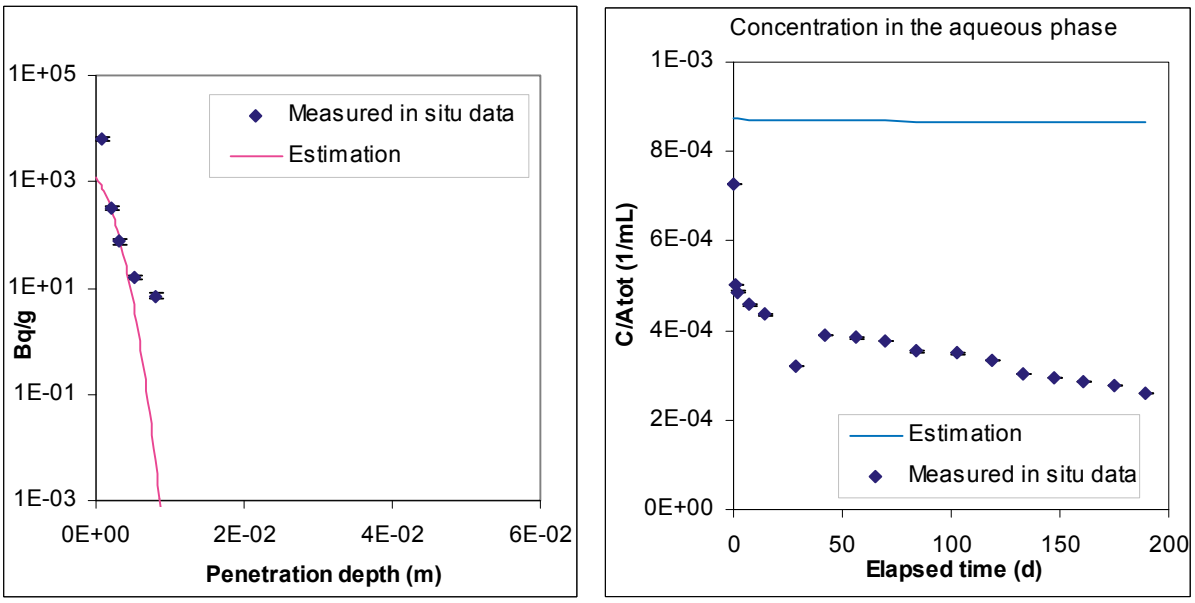

Figure Case 2. *Tracer: Ni-63. Core: D13.*

The Figures below present the estimated K_d's when F_f and ε were held constant in the calculation (Case 2). In addition to the modelled K_d's, K_d values determined from batch experiments are presented. These K_d's are given as intervals with a maximum and a minimum.

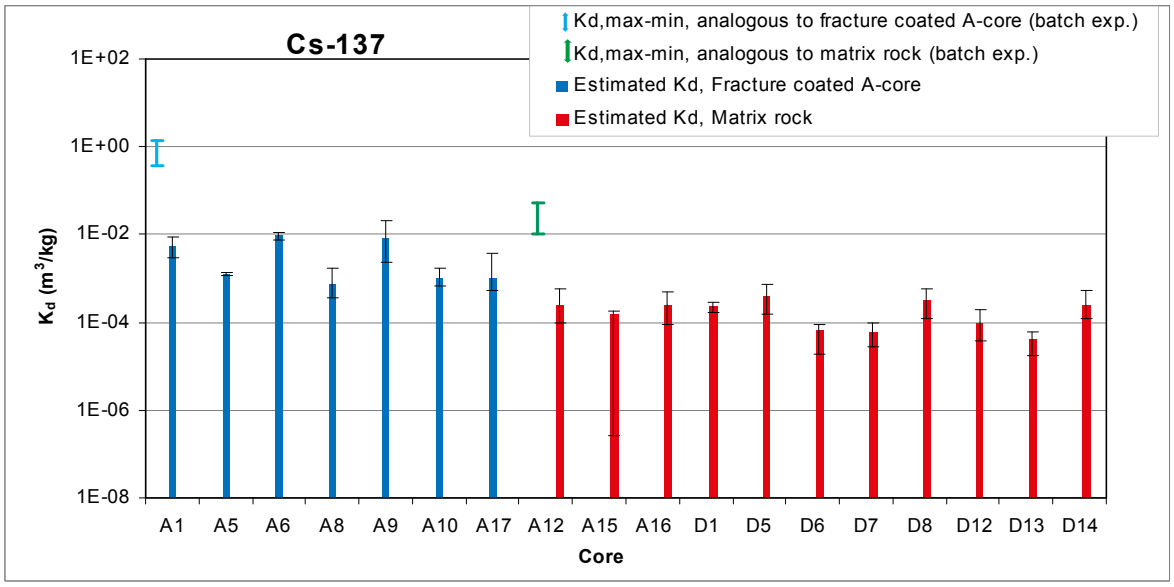

Figure Case 2. *Estimated K_d vs K_d from batch laboratory data. F_f was held constant in the calculation.*

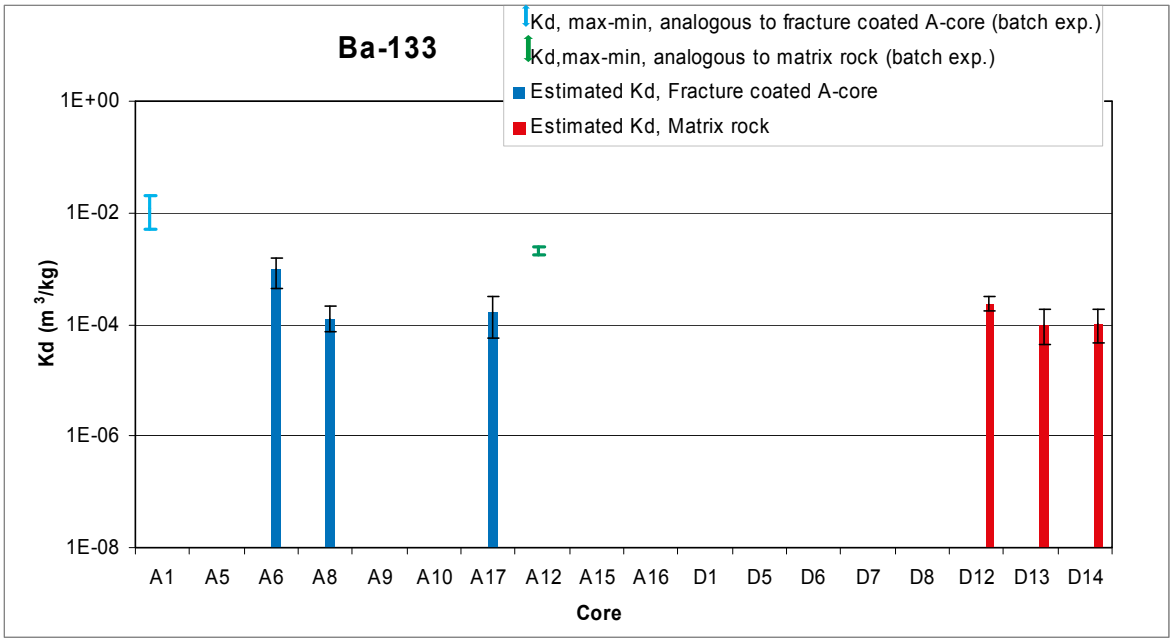

Figure Case 2. *Estimated K_d vs K_d from batch laboratory data. F_f was held constant in the calculation.*

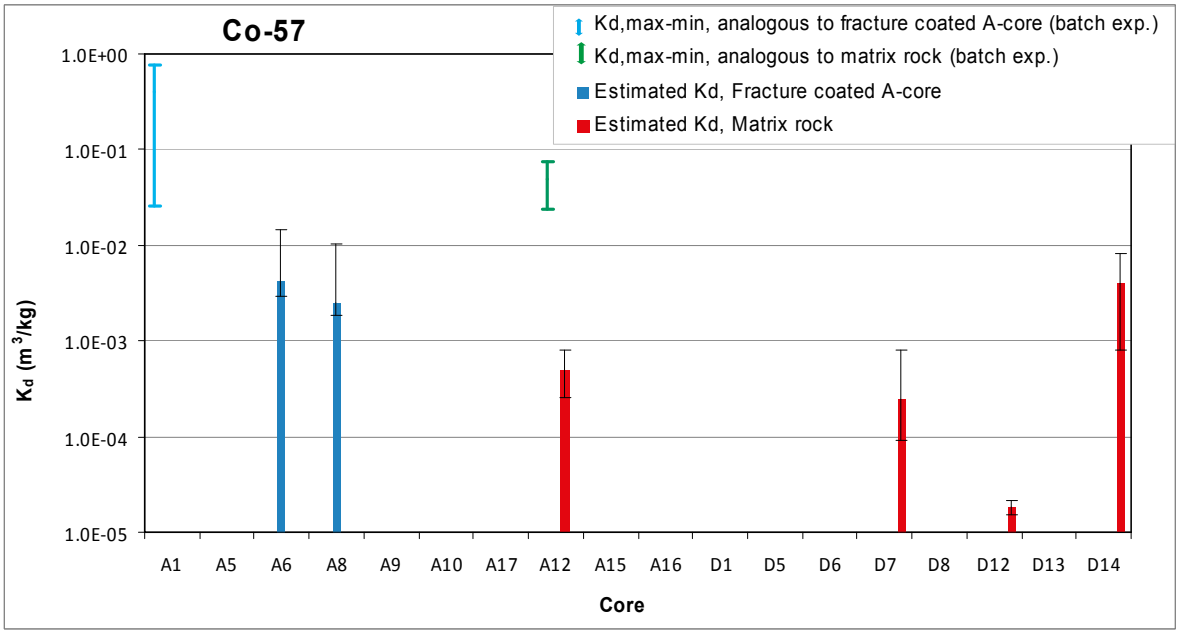

Figure Case 2. *Estimated K_d vs K_d from batch laboratory data. F_f was held constant in the calculation.*

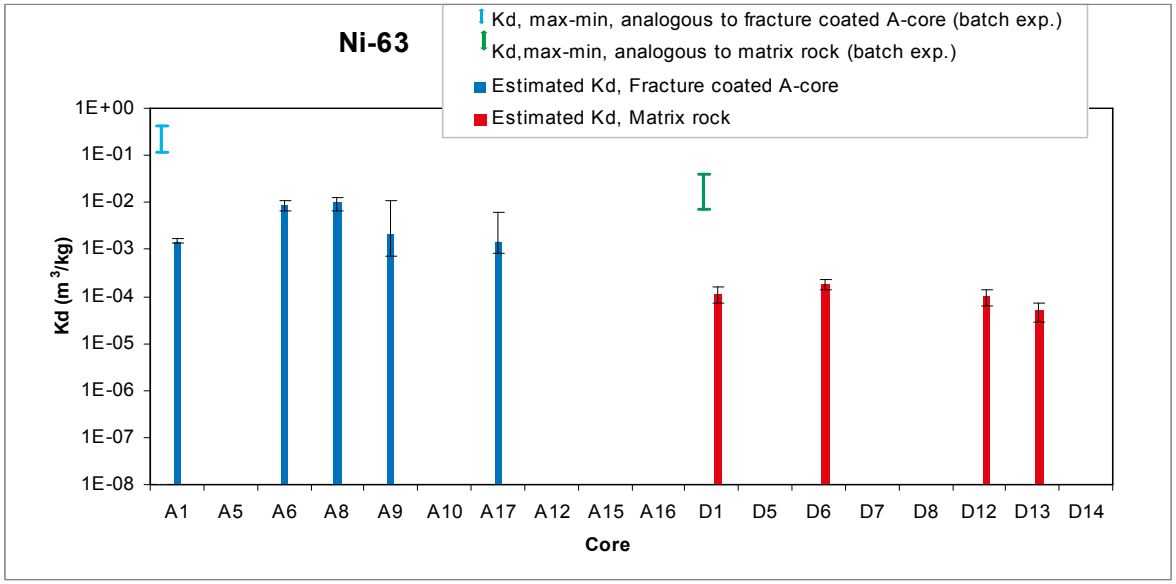

Figure Case 2. *Estimated K_d vs K_a from batch laboratory data. F_f was held constant in the calculation.*

Case 3

Na-22

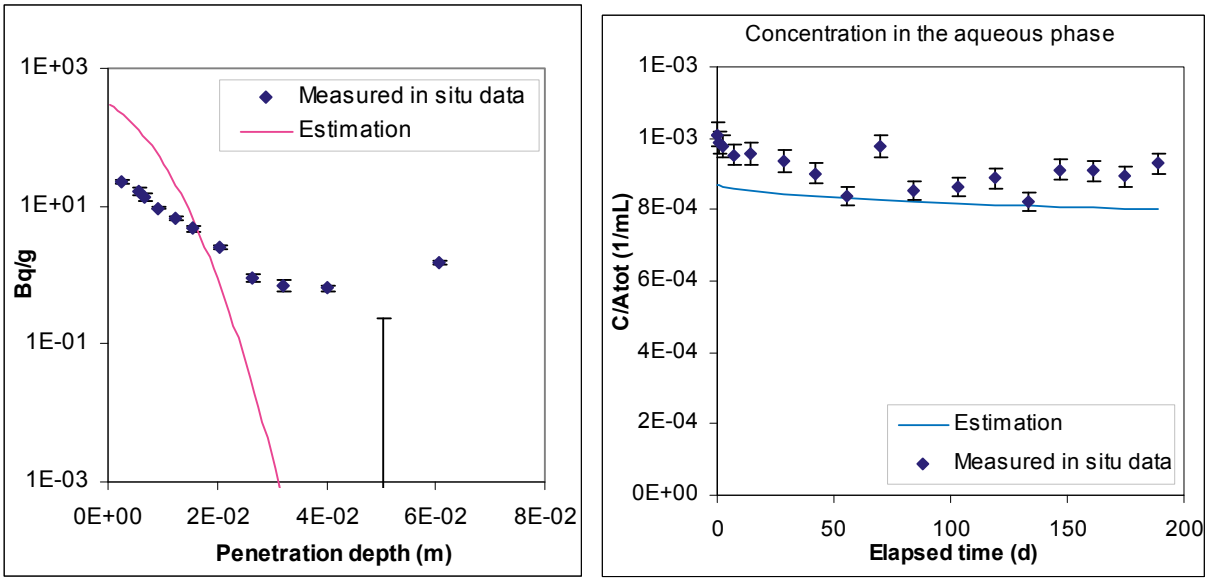

Figure Case 3. *Tracer: Na-22. Core: A1.*

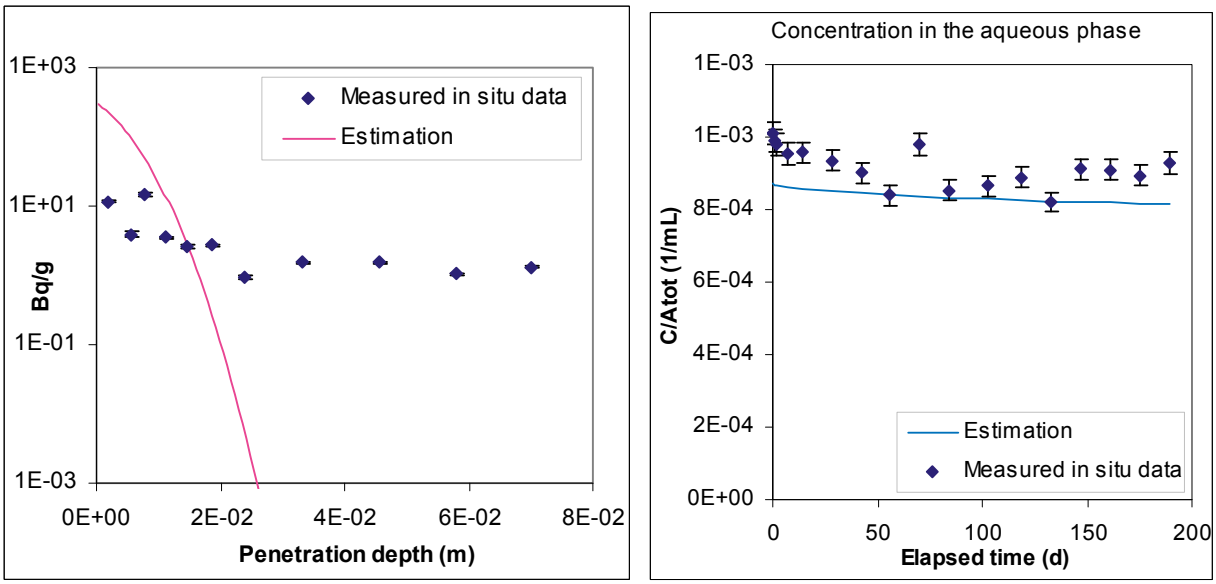

Figure Case 3. *Tracer: Na-22. Core:A5.*

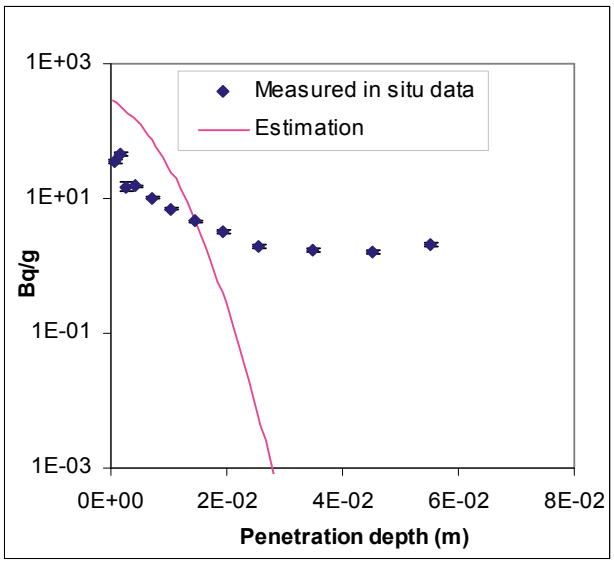

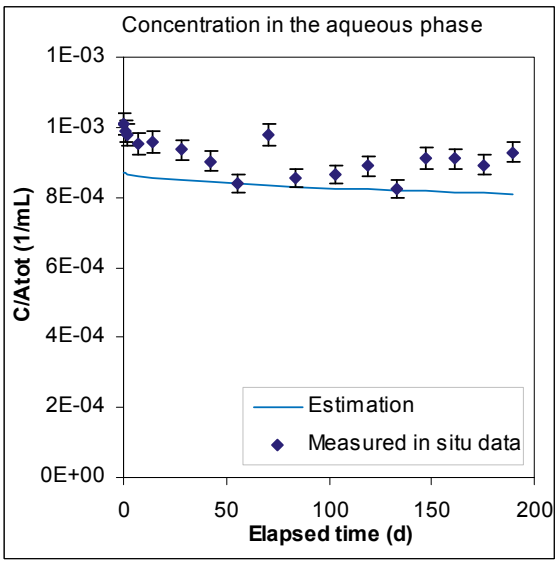

Figure Case 3. *Tracer: Na-22. Core: A6.*

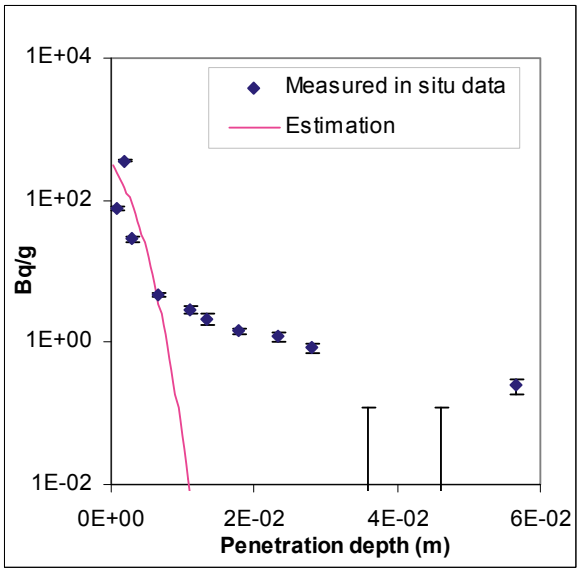

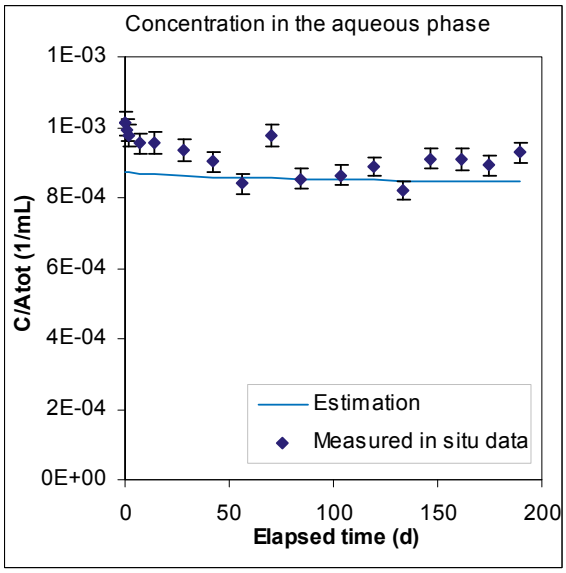

Figure Case 3. *Tracer: Na-22. Core: A8.*

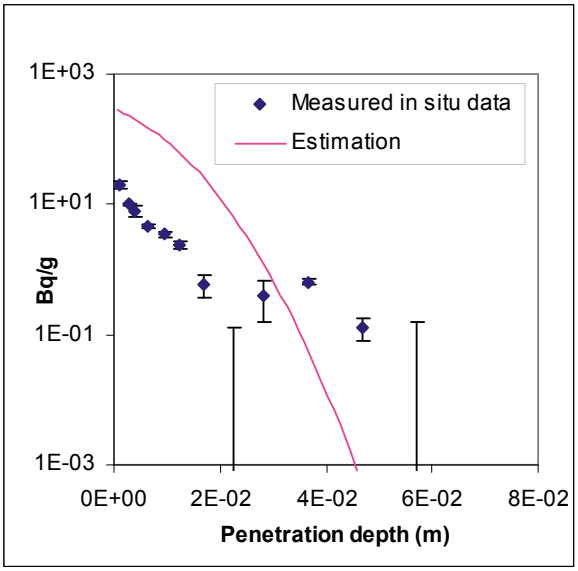

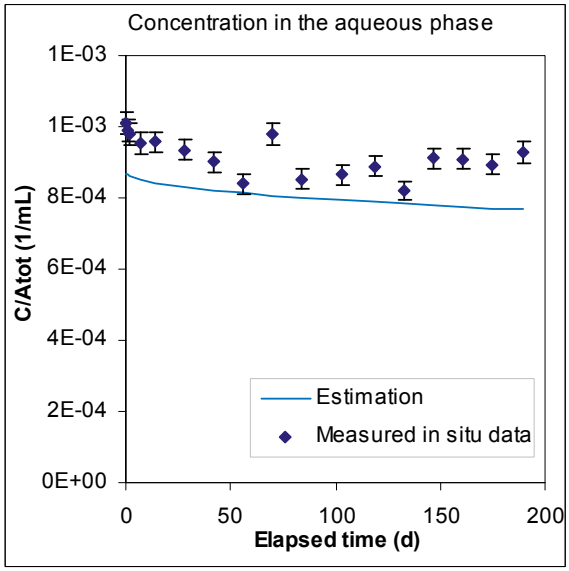

Figure Case 3. *Tracer: Na-22. Core: A9.*

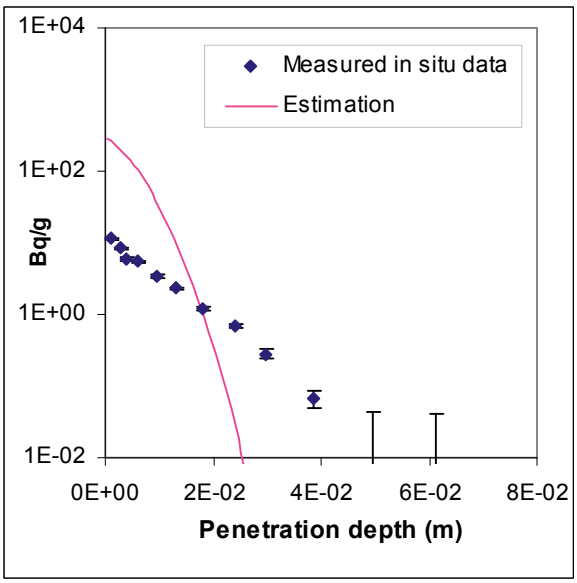

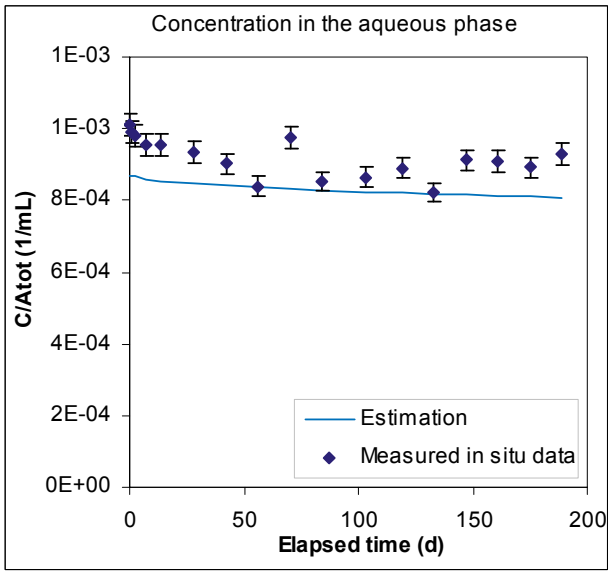

Figure Case 3. *Tracer: Na-22. Core: A10.*

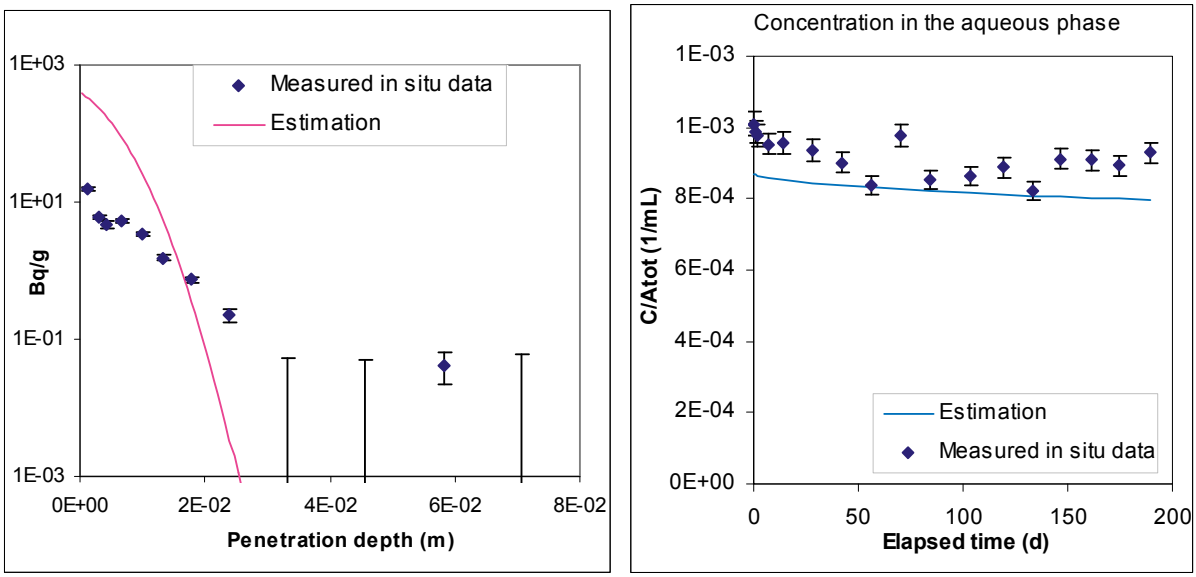

Figure Case 3. *Tracer: Na-22. Core: A12.*

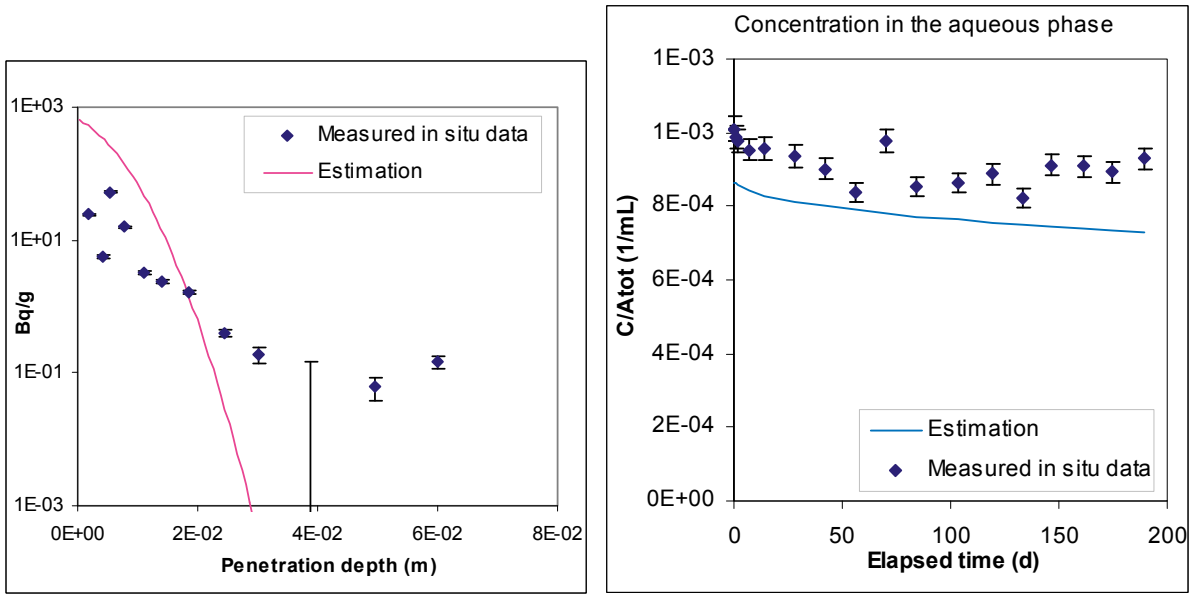

Figure Case 3. *Tracer: Na-22. Core: A15.*

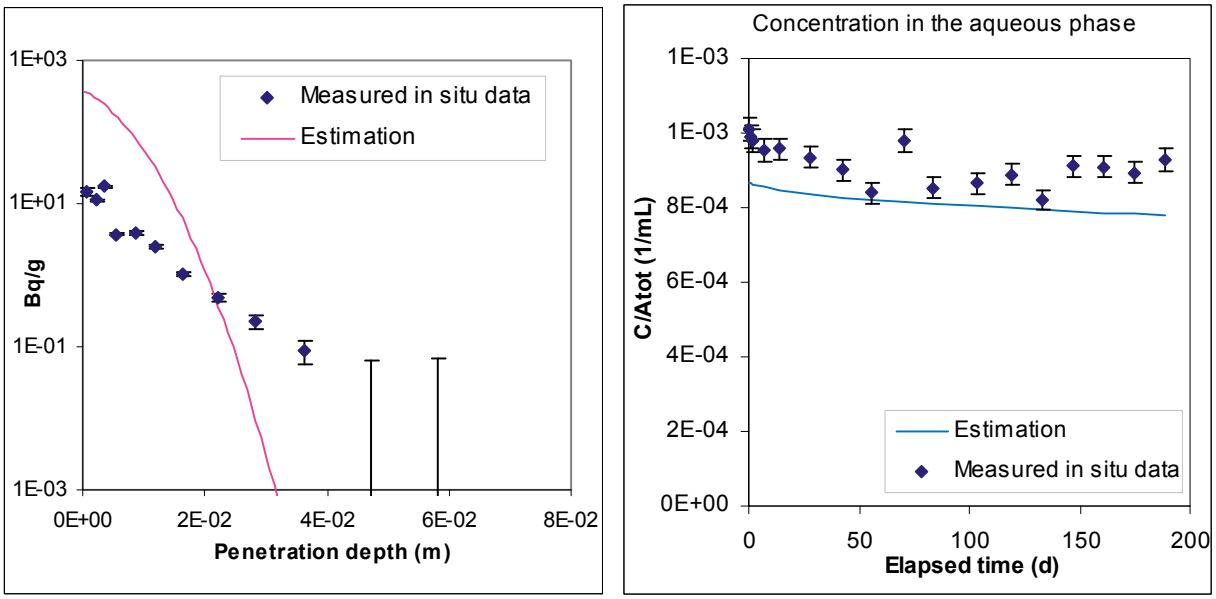

Figure Case 3. *Tracer: Na-22. Core: A16.*

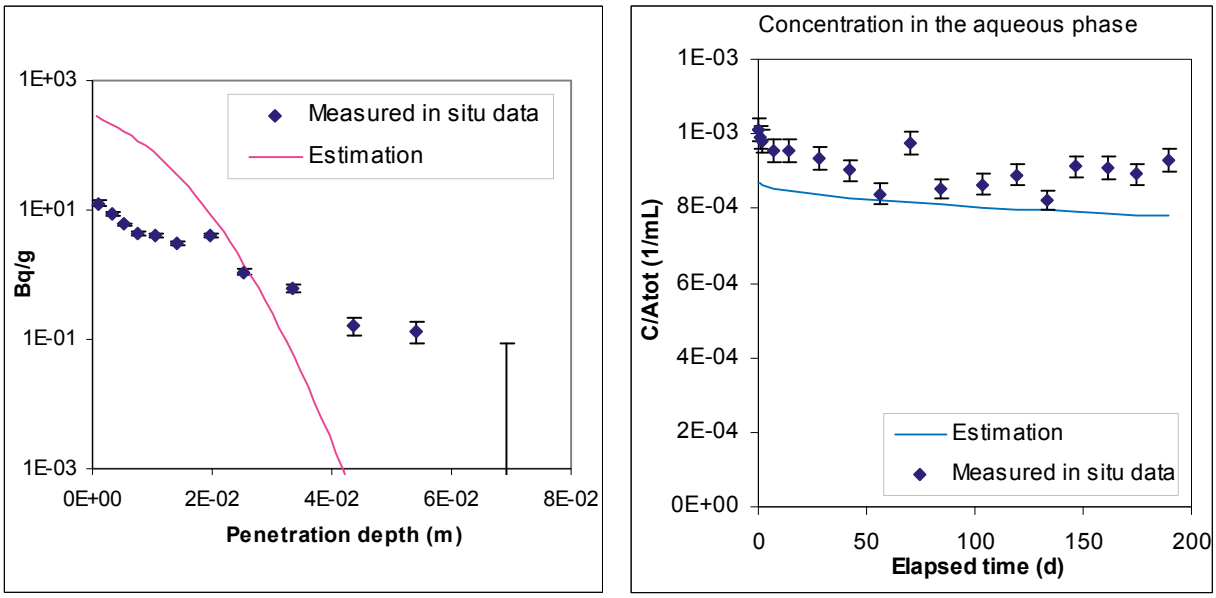

Figure Case 3. *Tracer: Na-22. Core: A17.*

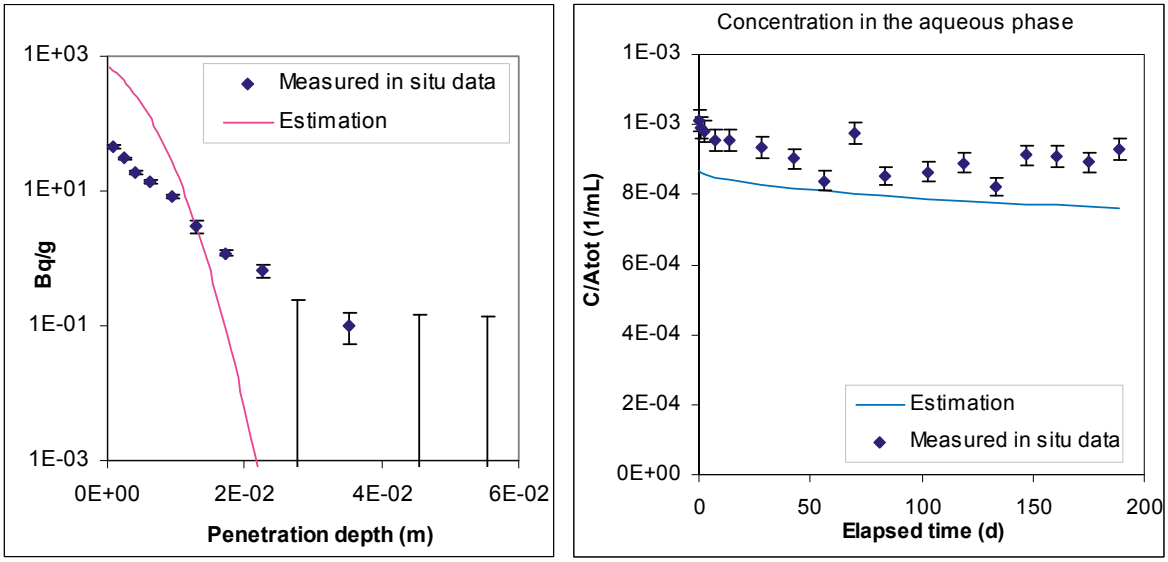

Figure Case 3. *Tracer: Na-22. Core: D1.*

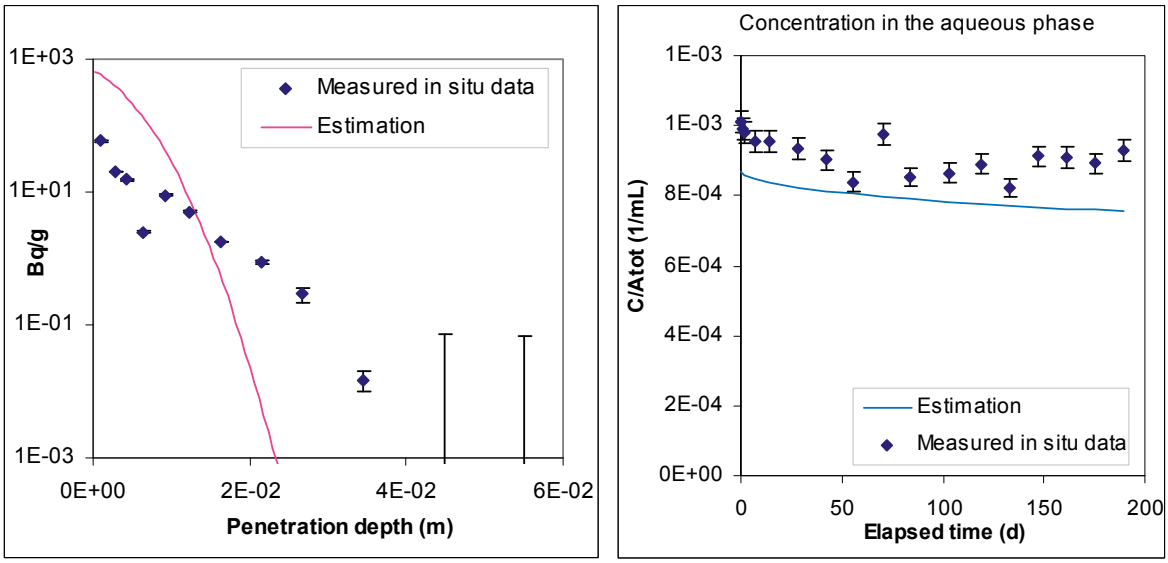

Figure Case 3. *Tracer: Na-22. Core: D5.*

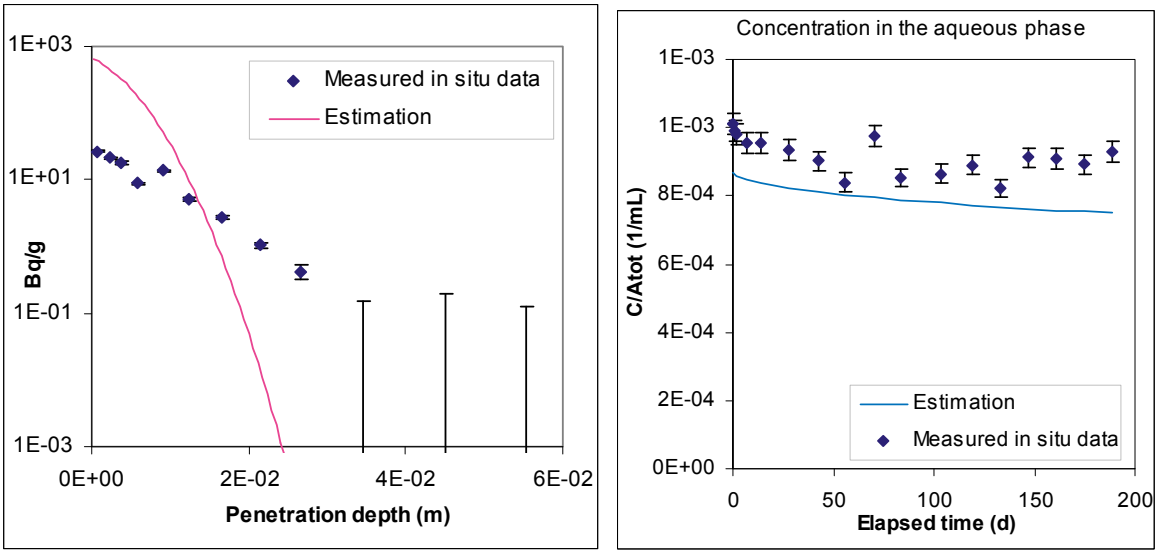

Figure Case 3. *Tracer: Na-22. Core: D6.*

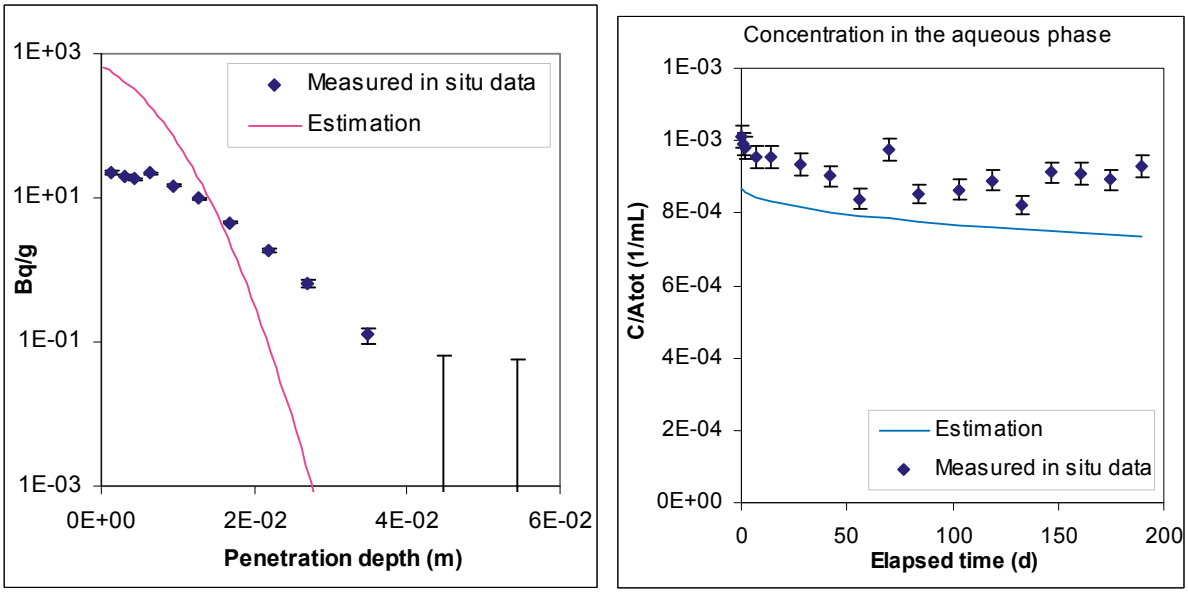

Figure Case 3. *Tracer: Na-22. Core: D7.*

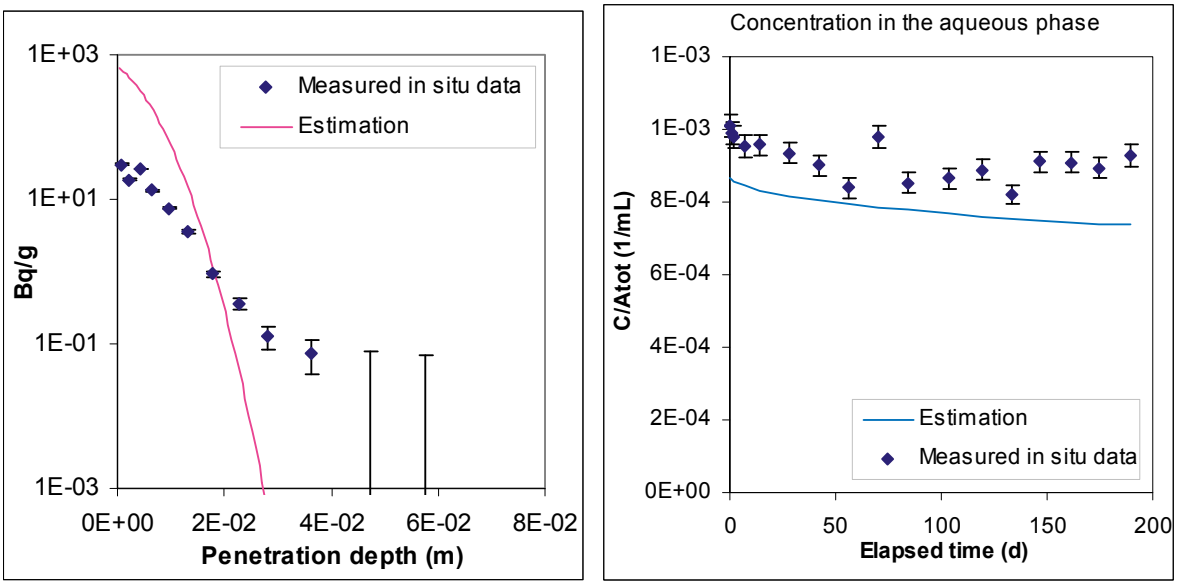

Figure Case 3. *Tracer: Na-22. Core: D8.*

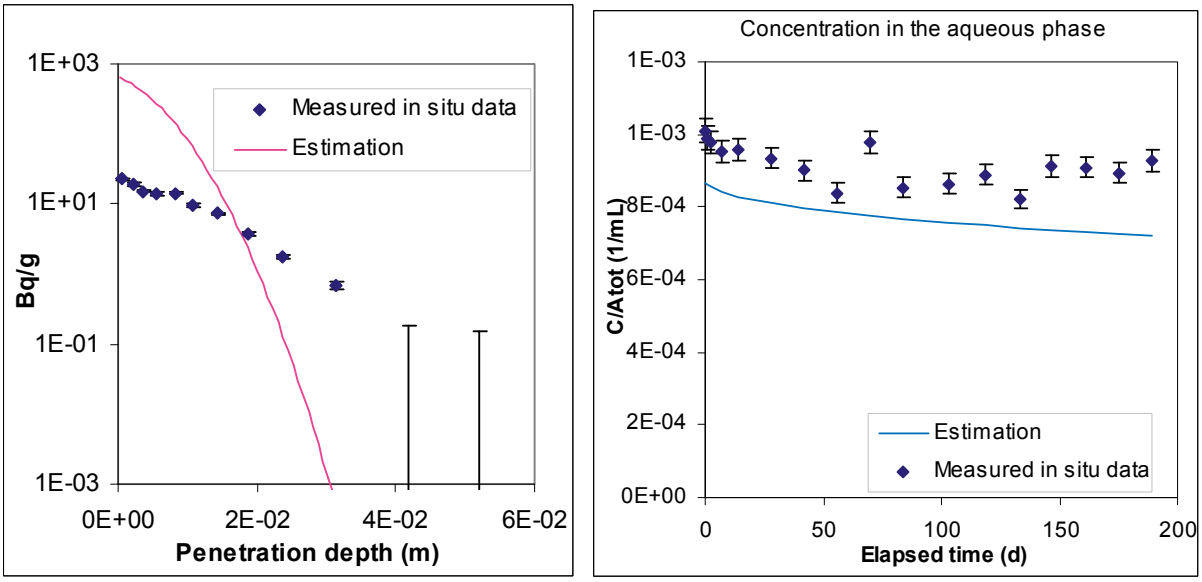

Figure Case 3. *Tracer: Na-22. Core: D12.*

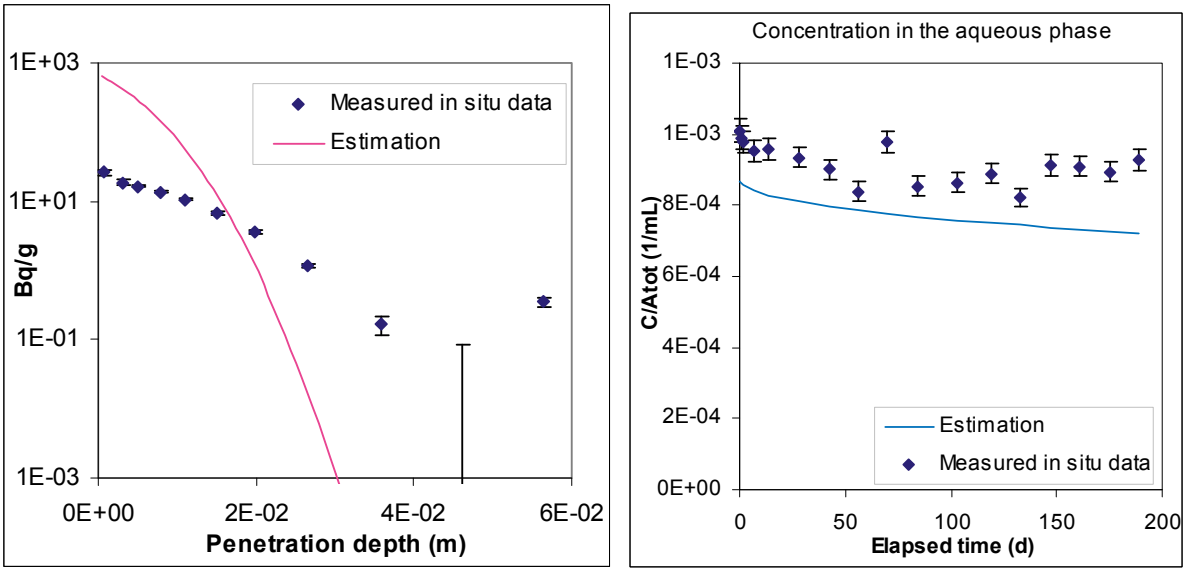

Figure Case 3. *Tracer: Na-22. Core: D13.*

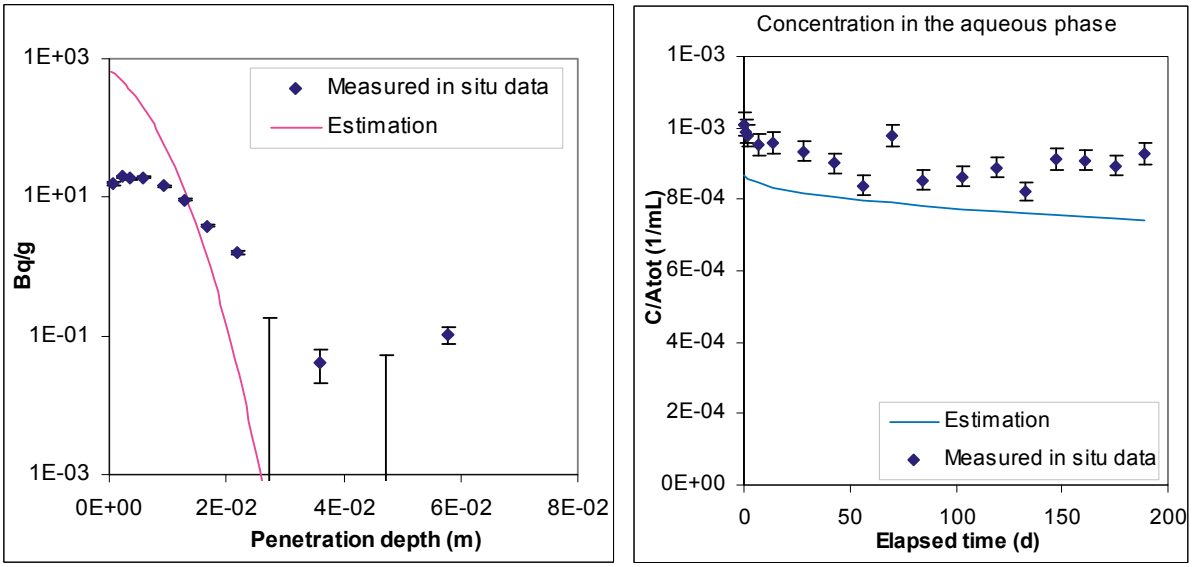

Figure Case 3. *Tracer: Na-22. Core: D14.*

Ba-133

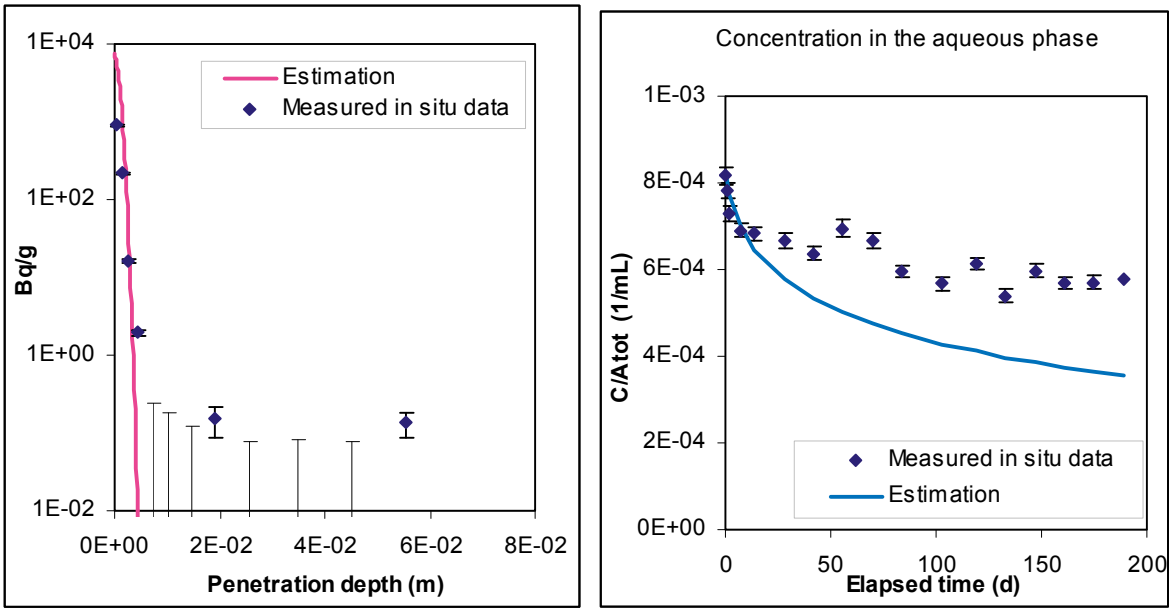

Figure Case 3. *Tracer: Ba-133. Core: A6.*

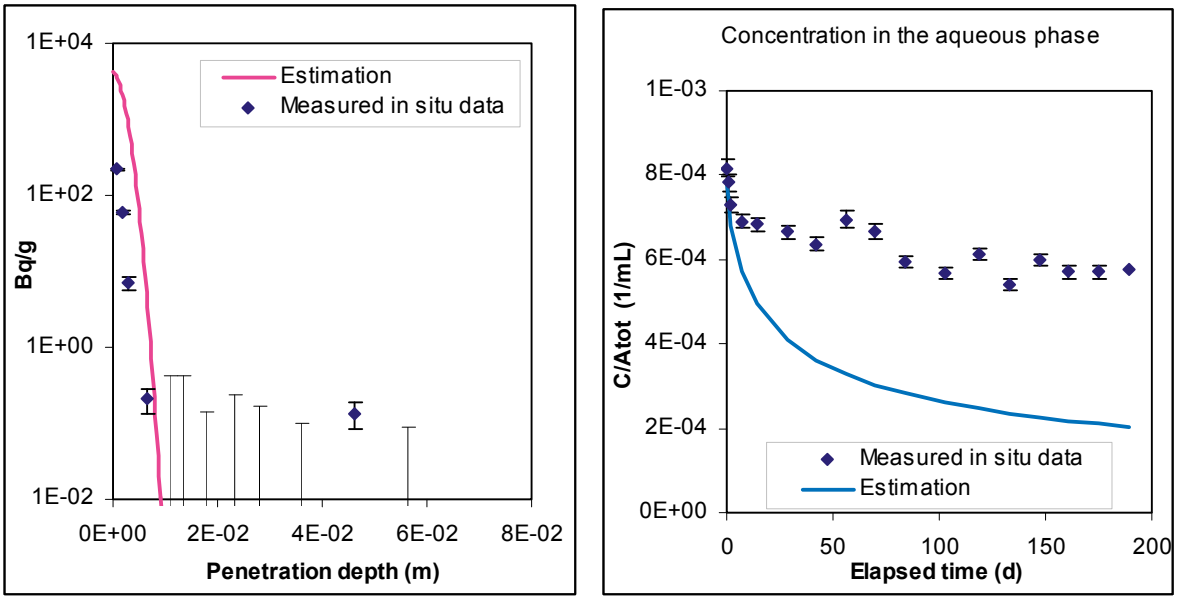

Figure Case 3. *Tracer: Ba-133. Core: A8.*

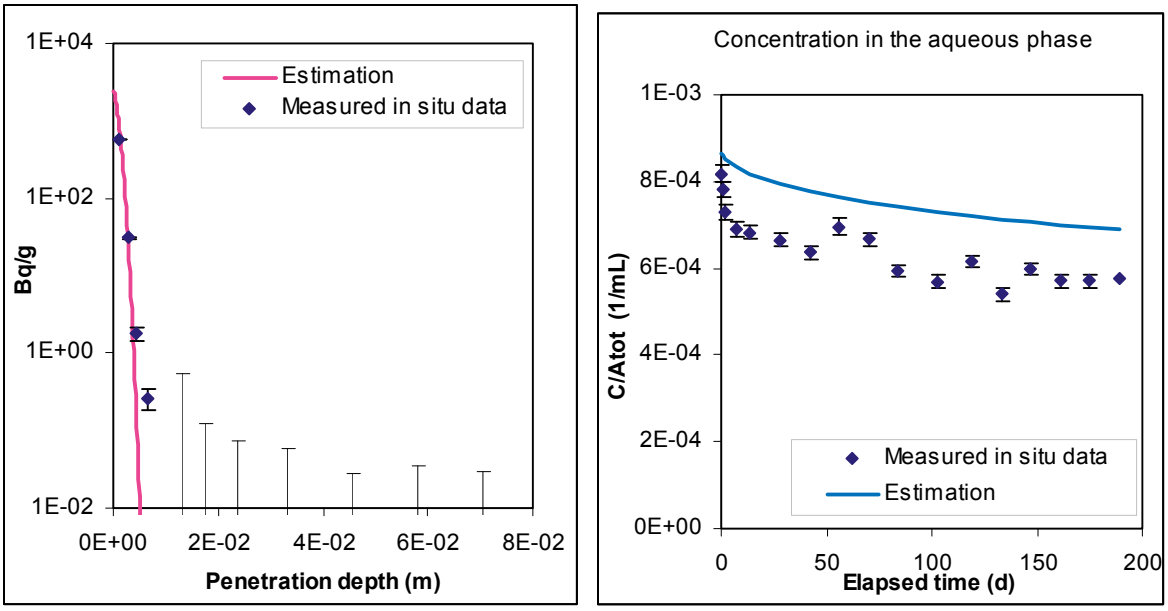

Figure Case 3. *Tracer: Ba-133. Core: A12.*

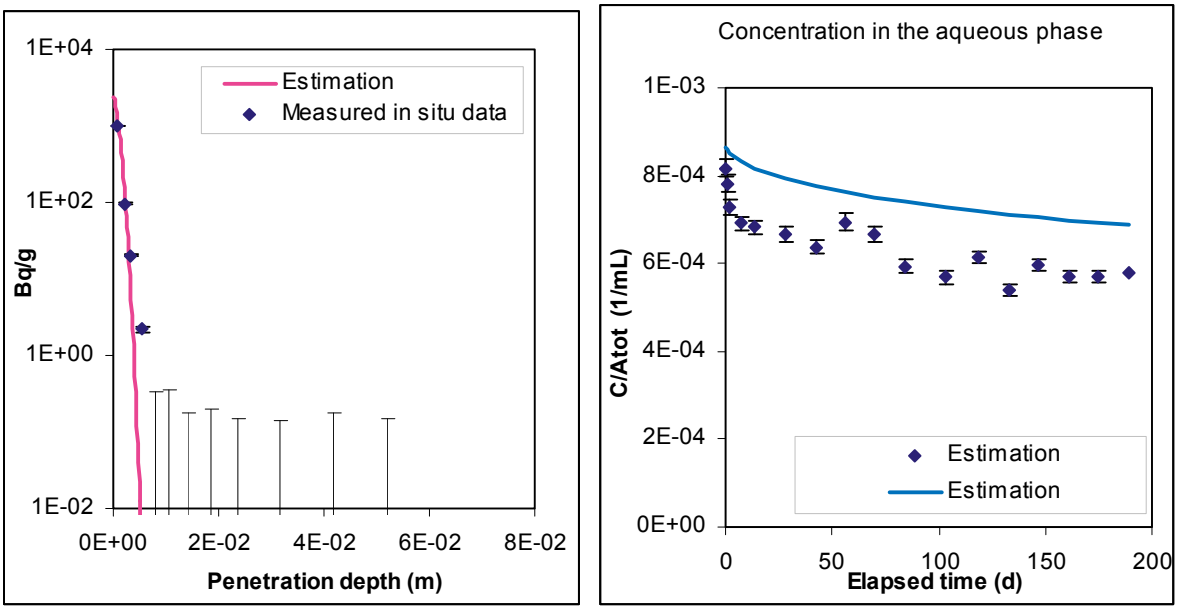

Figure Case 3. *Tracer: Ba-133. Core: D12.*

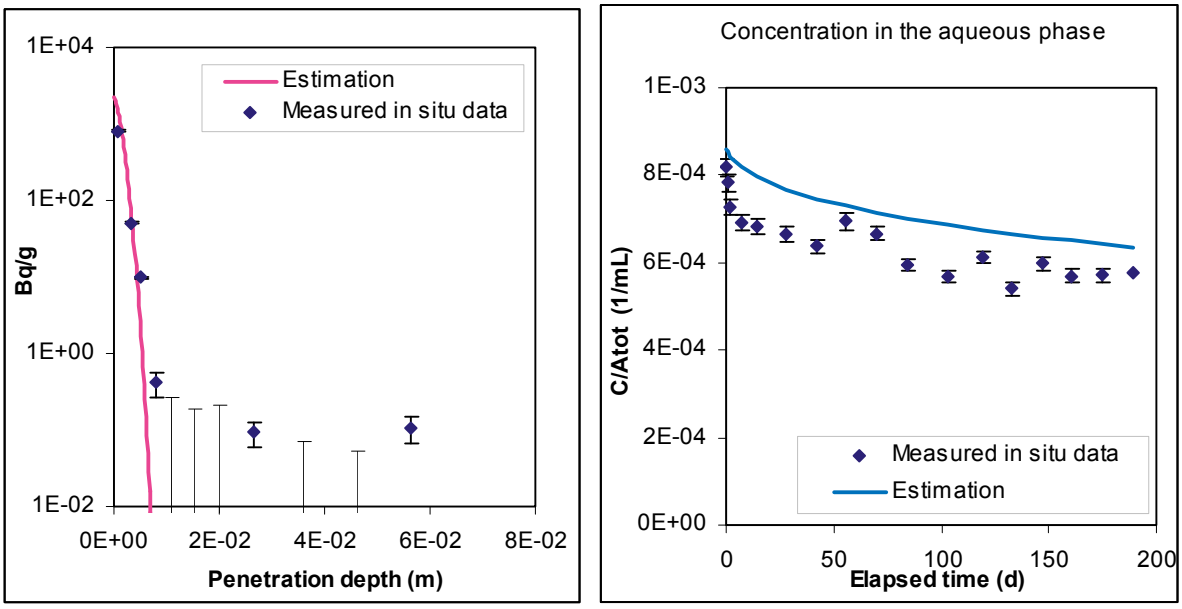

Figure Case 3. *Tracer: Ba-133. Core: D13.*

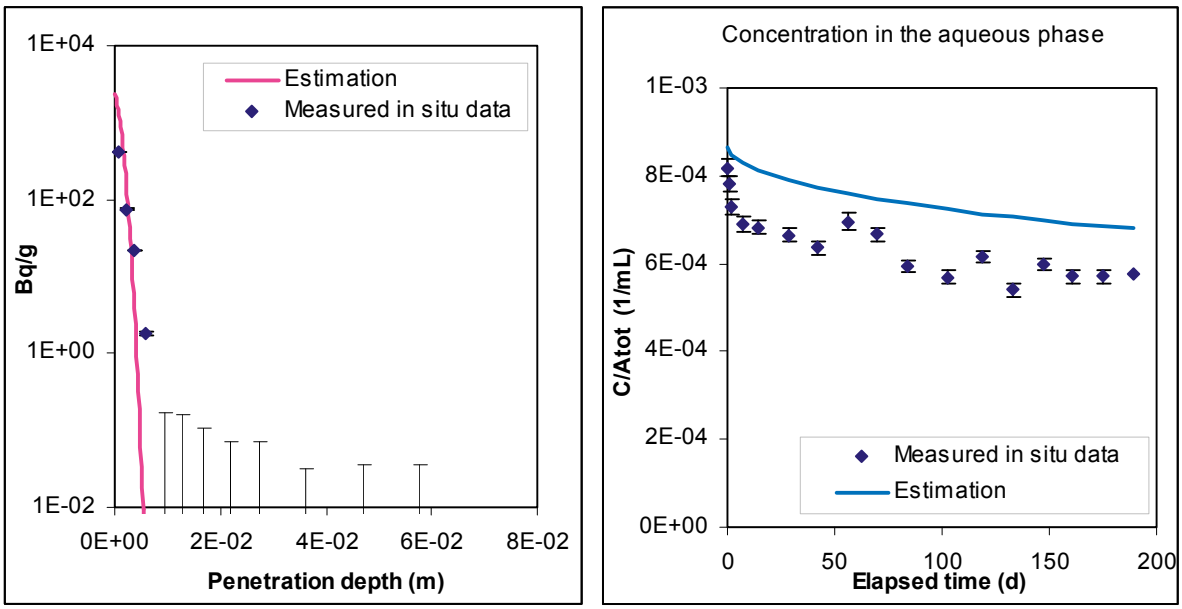

Figure Case 3. *Tracer: Ba-133. Core: D14.*

Ni-63

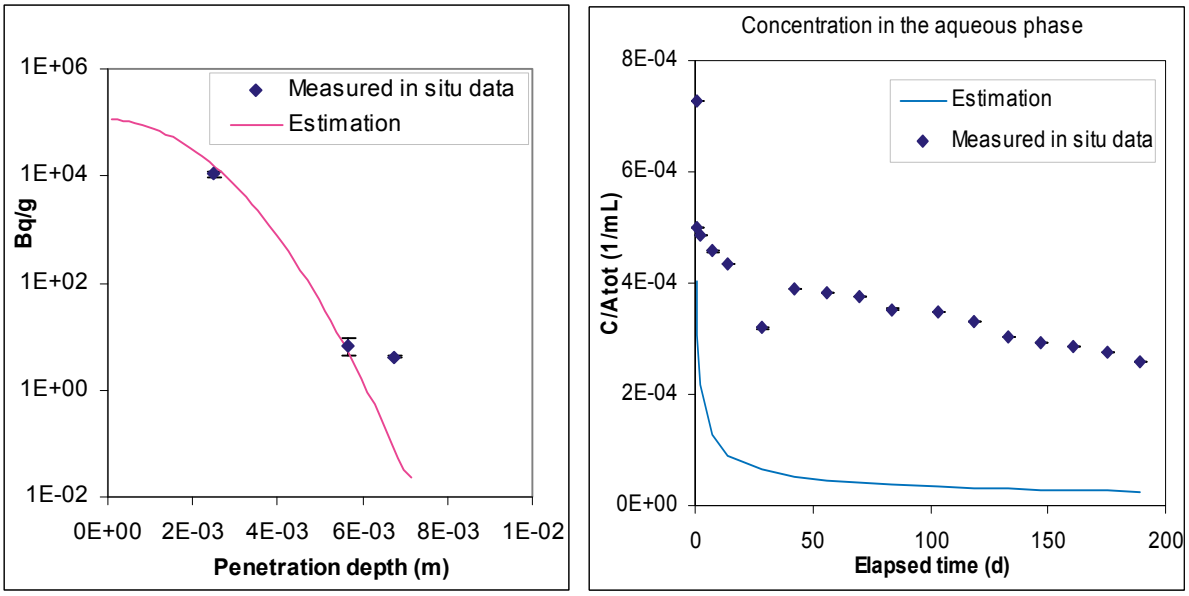

Figure Case 3. *Tracer: Ni-63. Core: A1.*

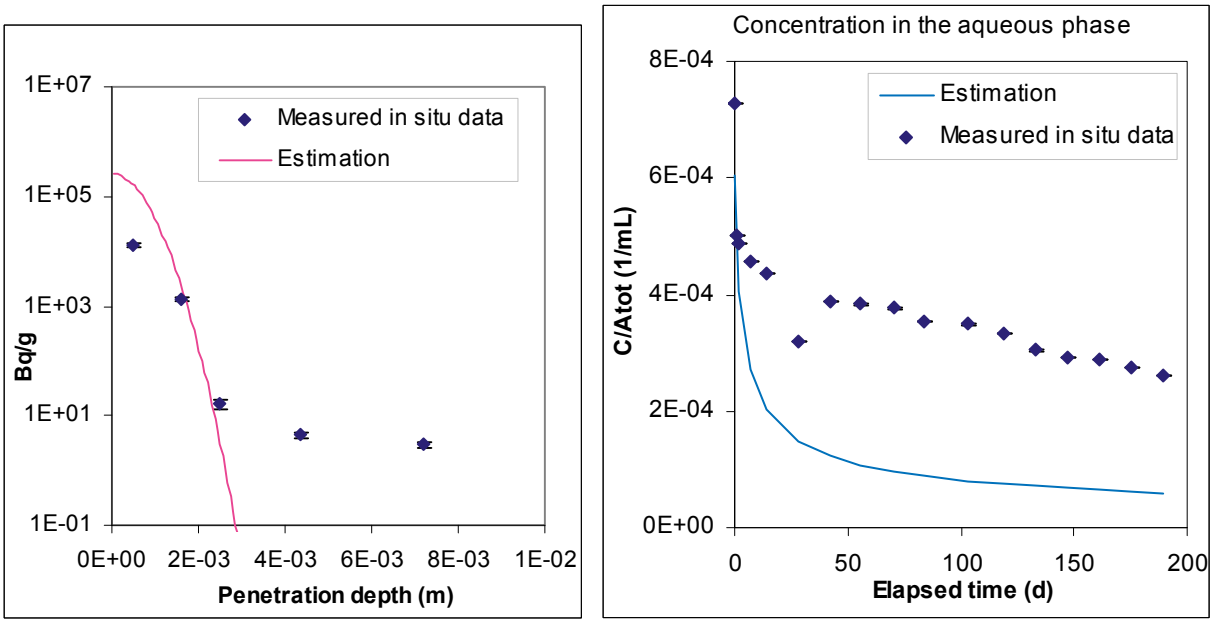

Figure Case 3. *Tracer: Ni-63. Core: A6.*

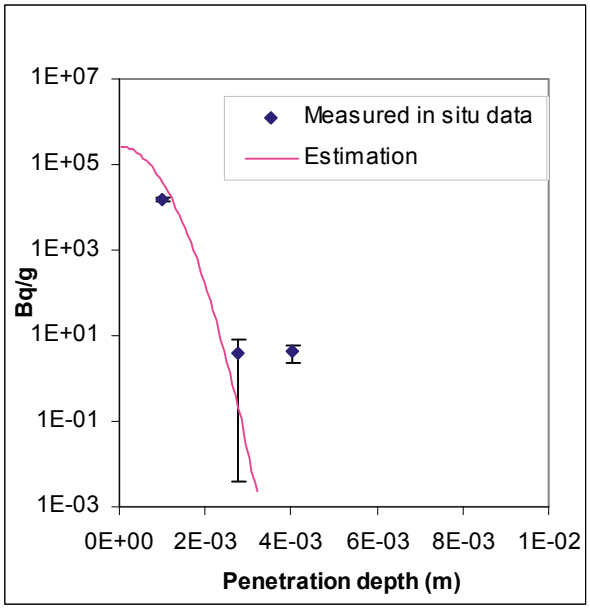

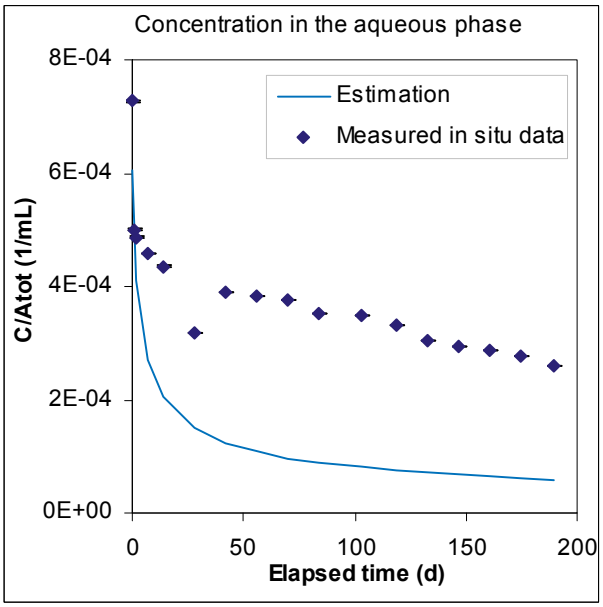

Figure Case 3. *Tracer: Ni-63. Core: A9.*

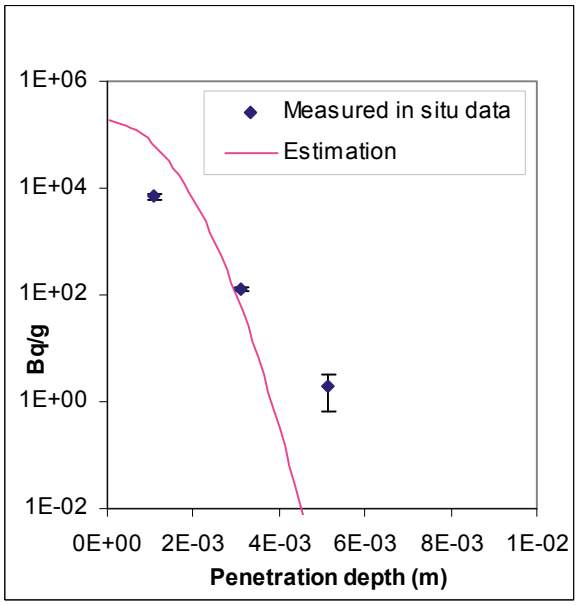

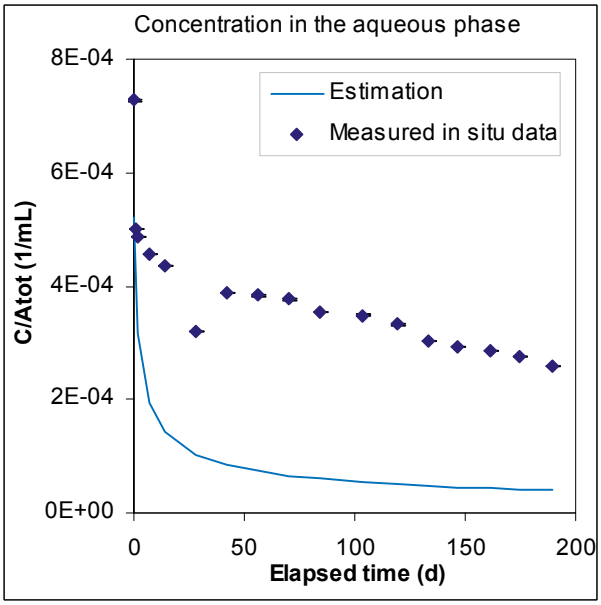

Figure Case 3. *Tracer: Ni-63. Core: A17.*

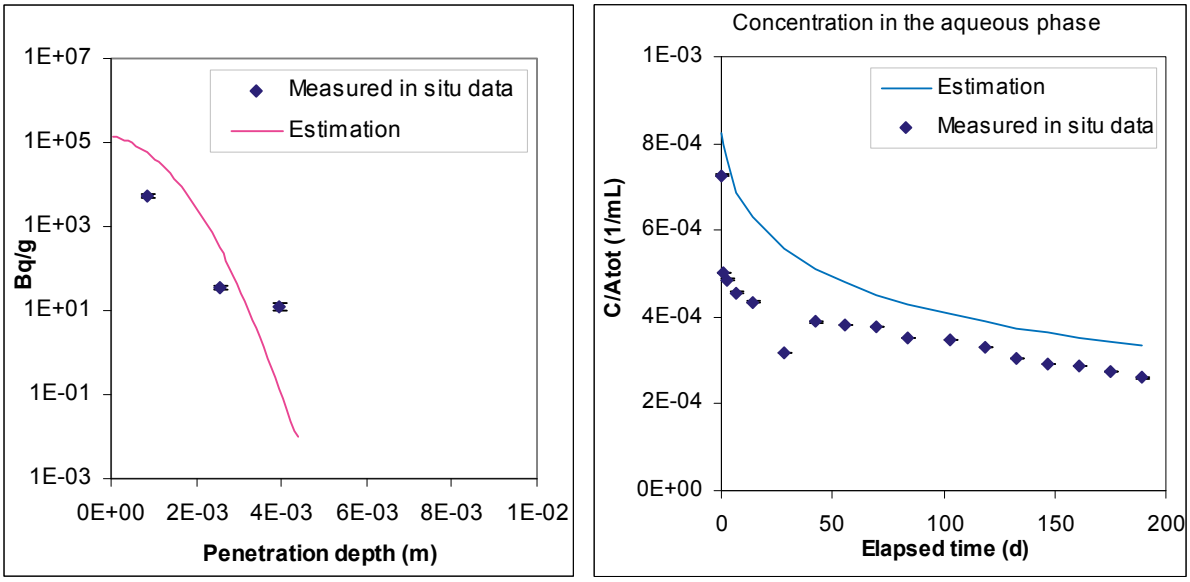

Figure Case 3. *Tracer: Ni-63. Core: D1.*

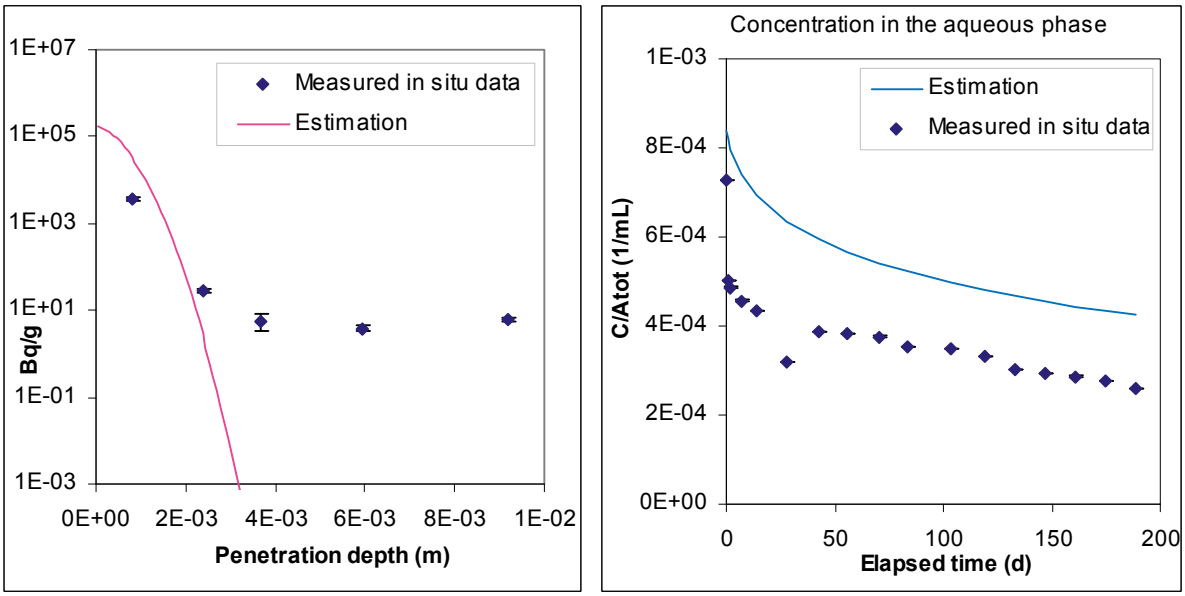

Figure Case 3. *Tracer: Ni-63. Core: D6.*

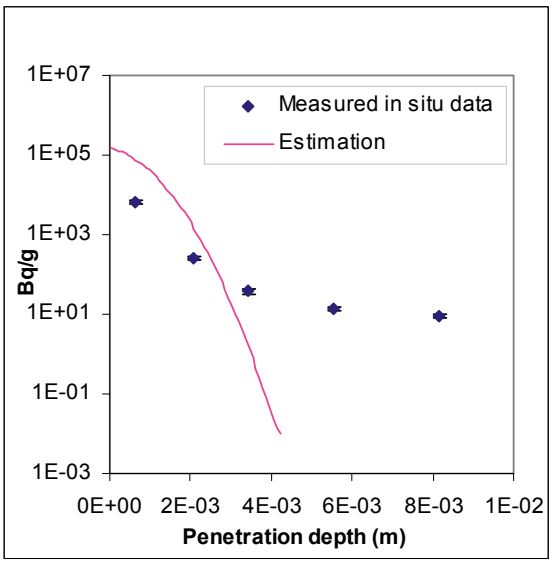

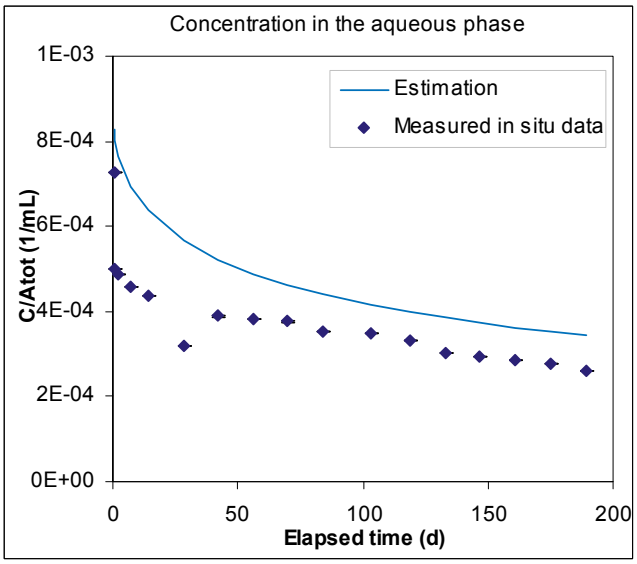

Figure Case 3. *Tracer: Ni-63. Core: D12.*

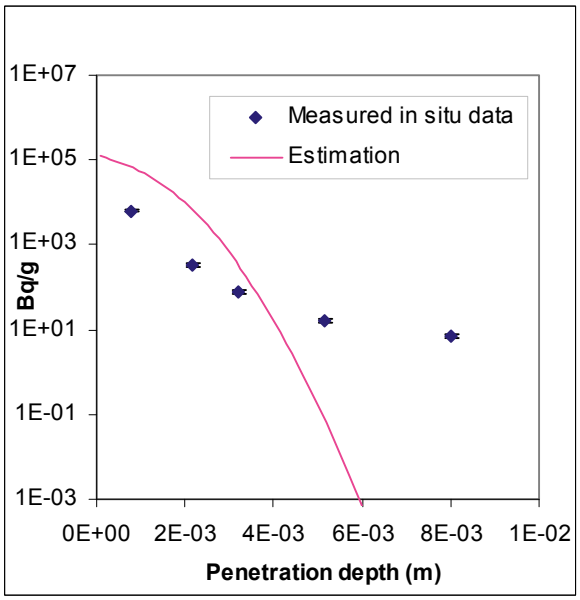

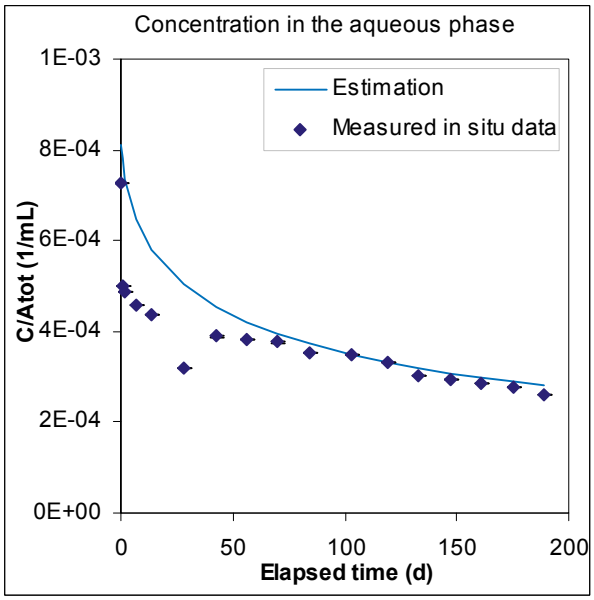

Figure Case 3. *Tracer: Ni-63. Core: D13.*

Cs-137

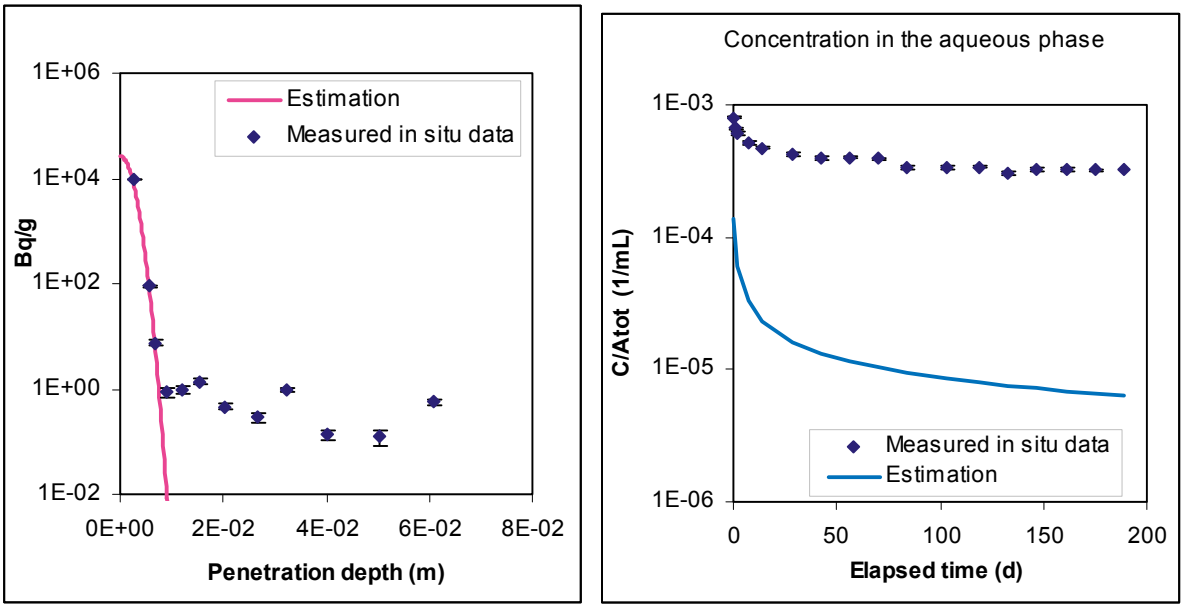

Figure Case 3. *Tracer: Cs-137. Core: A1.*

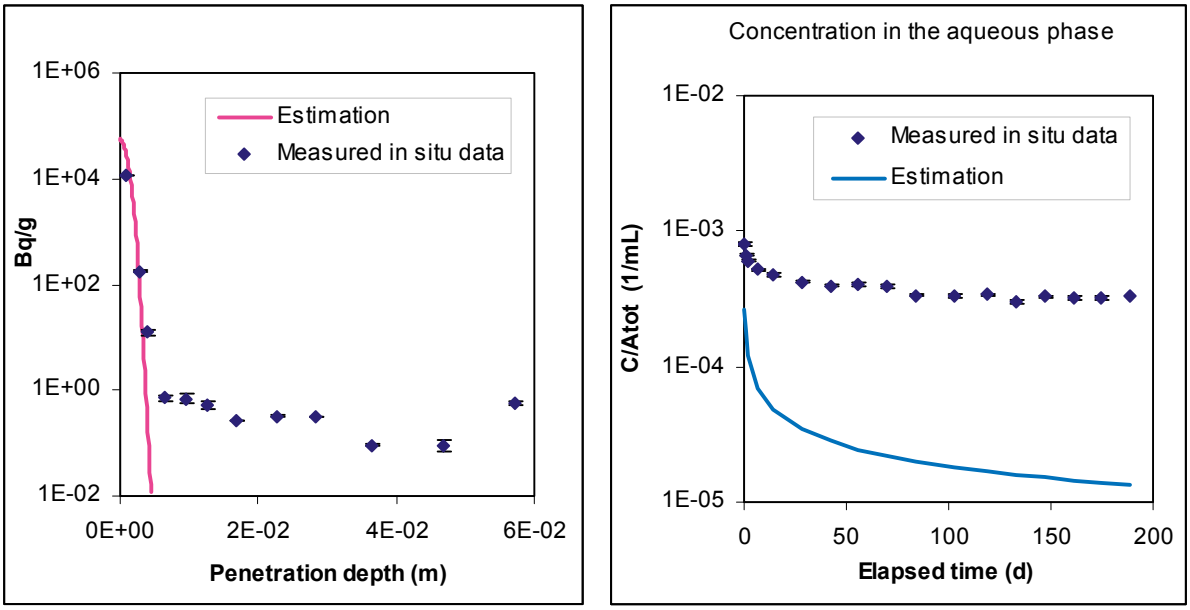

Figure Case 3. *Tracer: Cs-137. Core: A9.*

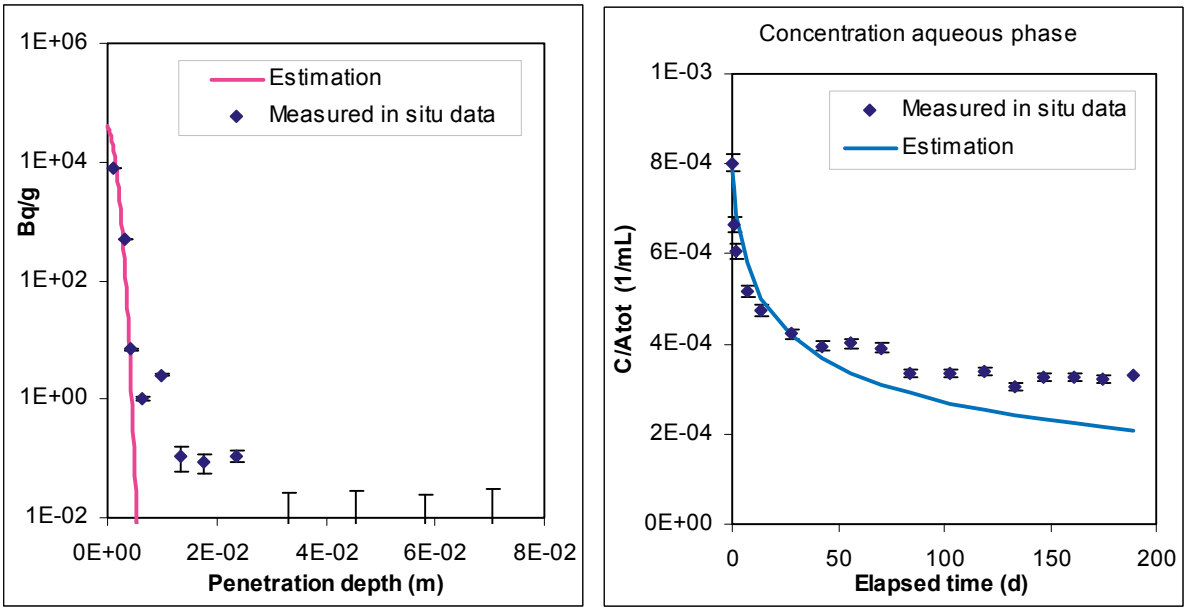

Figure Case 3. *Tracer: Cs-137. Core: A12.*

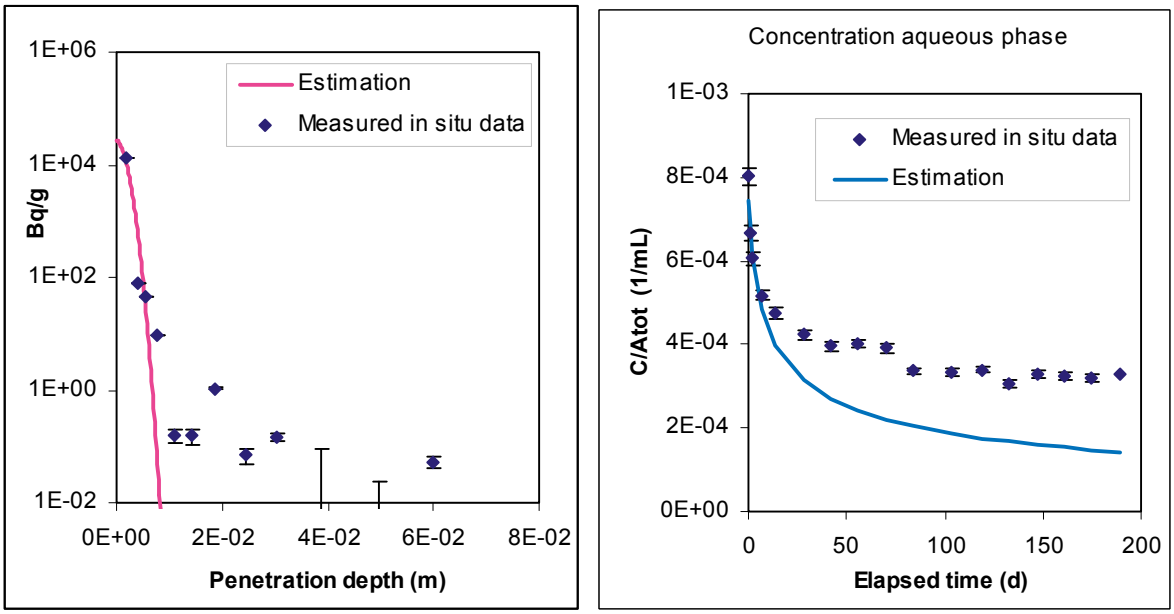

Figure Case 3. *Tracer: Cs-137. Core: A15.*

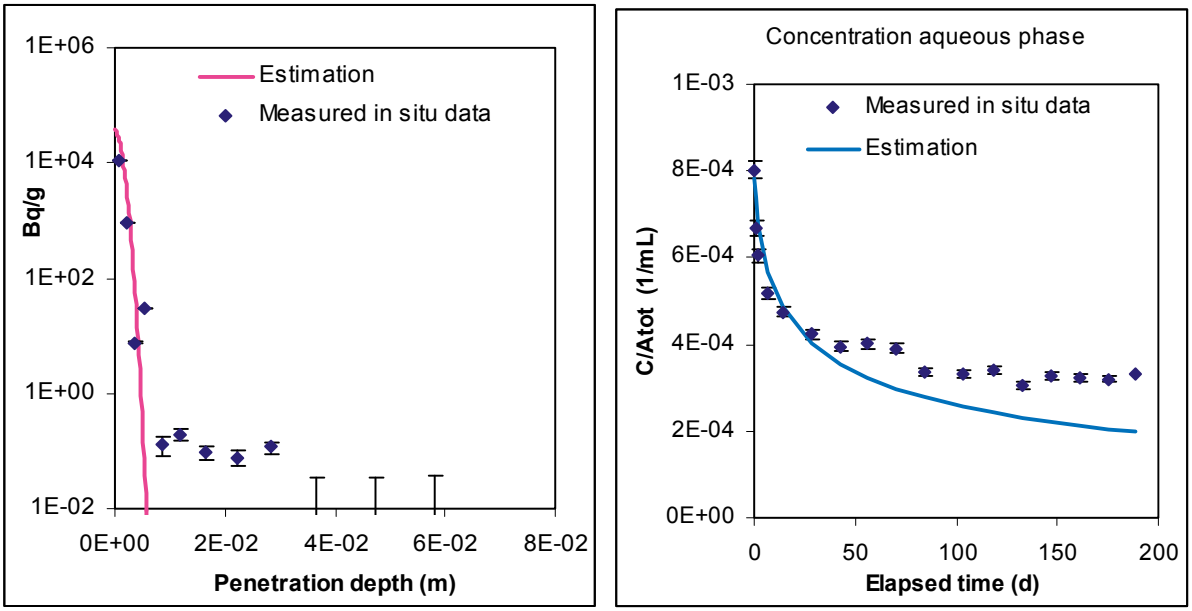

Figure Case 3. *Tracer: Cs-137. Core: A16.*

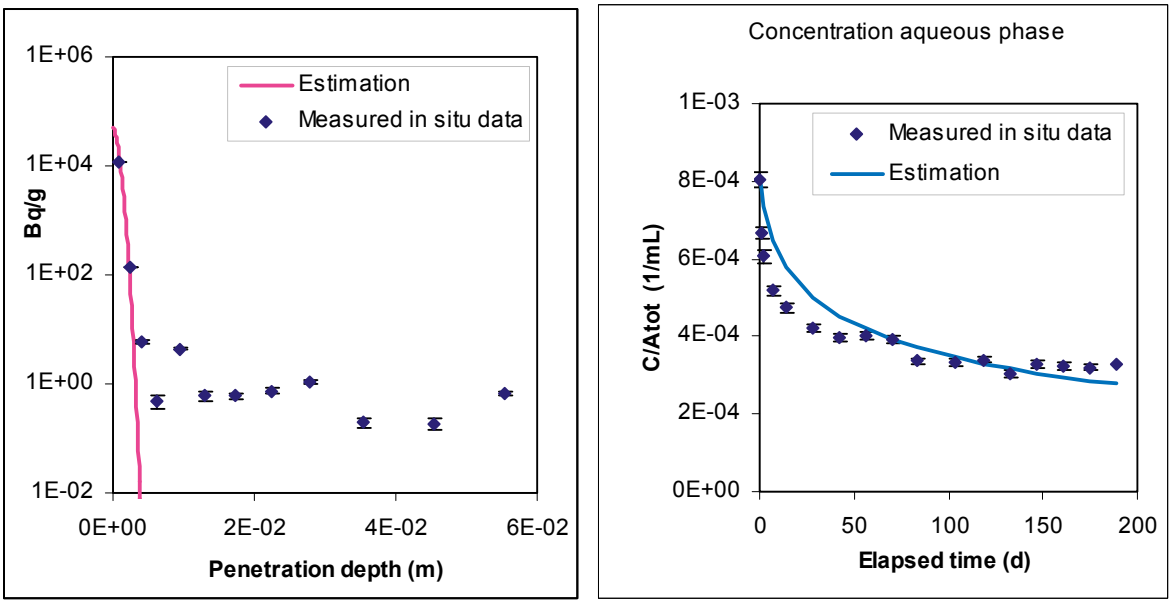

Figure Case 3. *Tracer: Cs-137. Core: D1.*

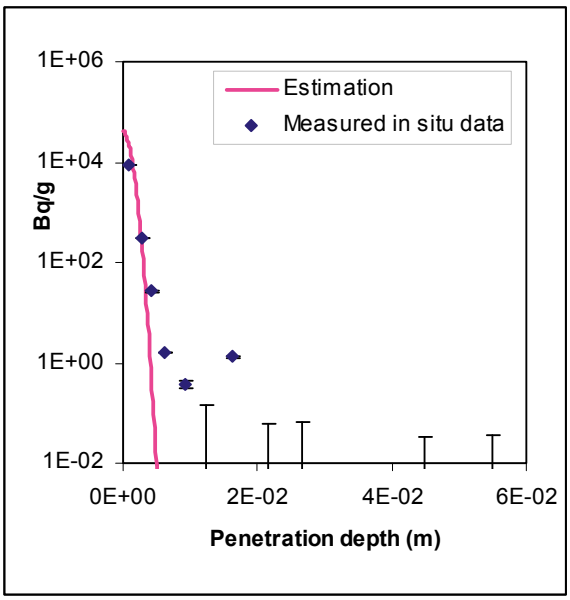

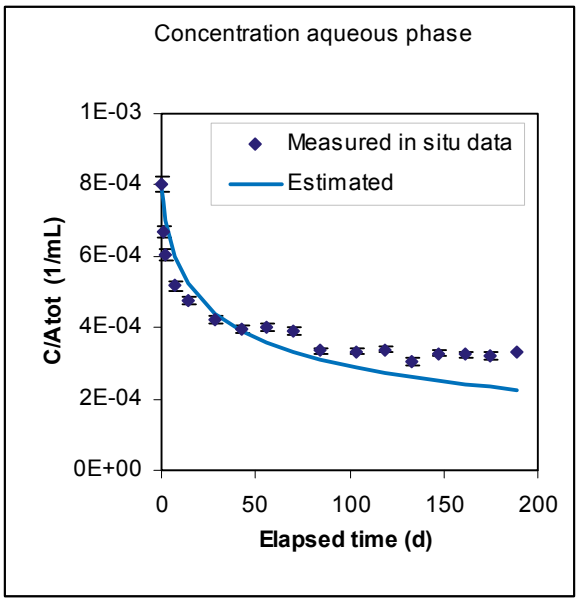

Figure Case 3. *Tracer: Cs-137. Core: D5.*

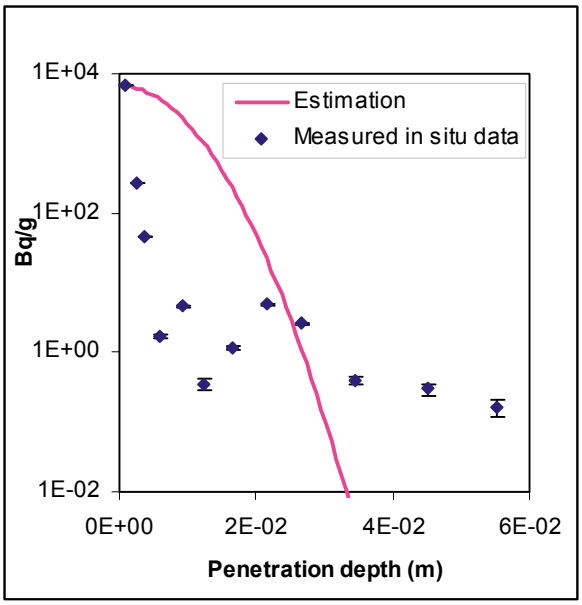

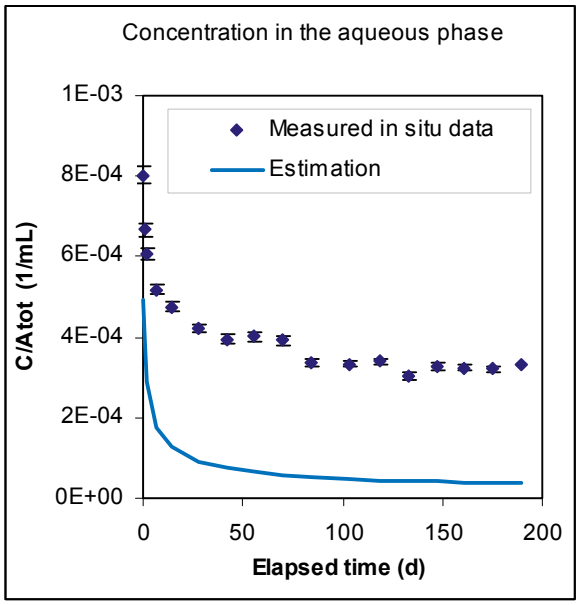

Figure Case 3. *Tracer: Cs-137. Core: D6.*

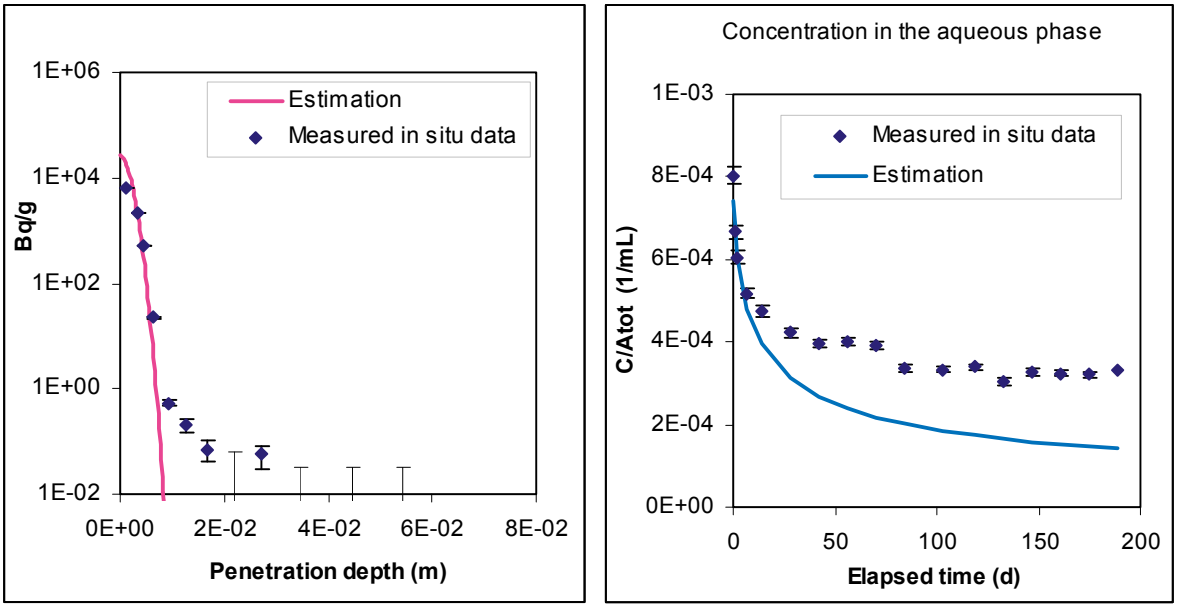

Figure Case 3. *Tracer: Cs-137. Core: D7.*

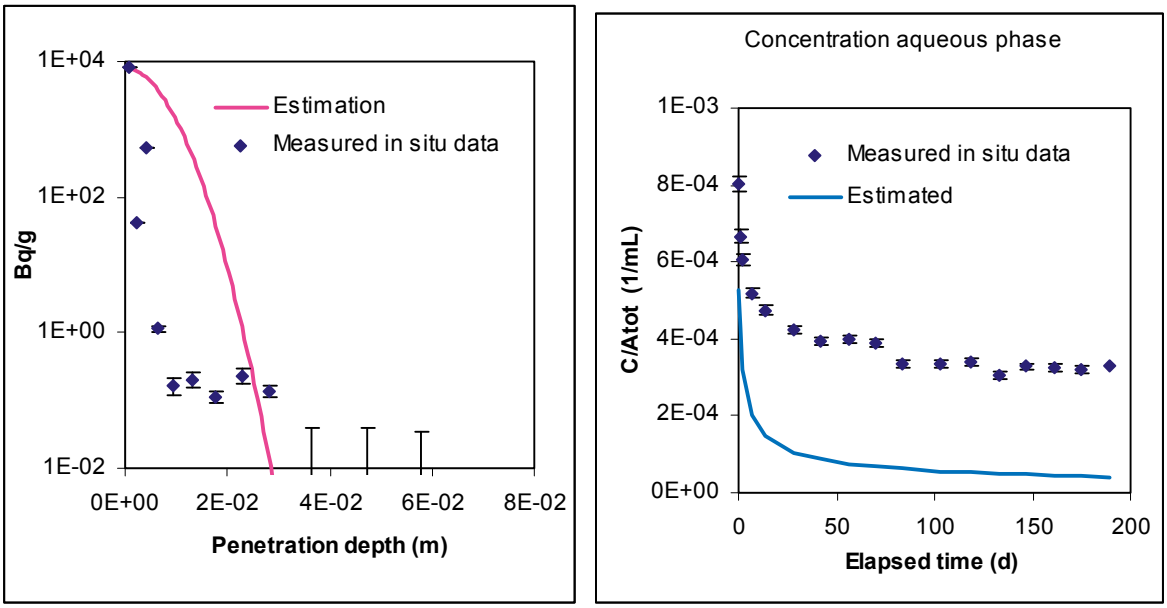

Figure Case 3. *Tracer: Cs-137. Core: D8.*

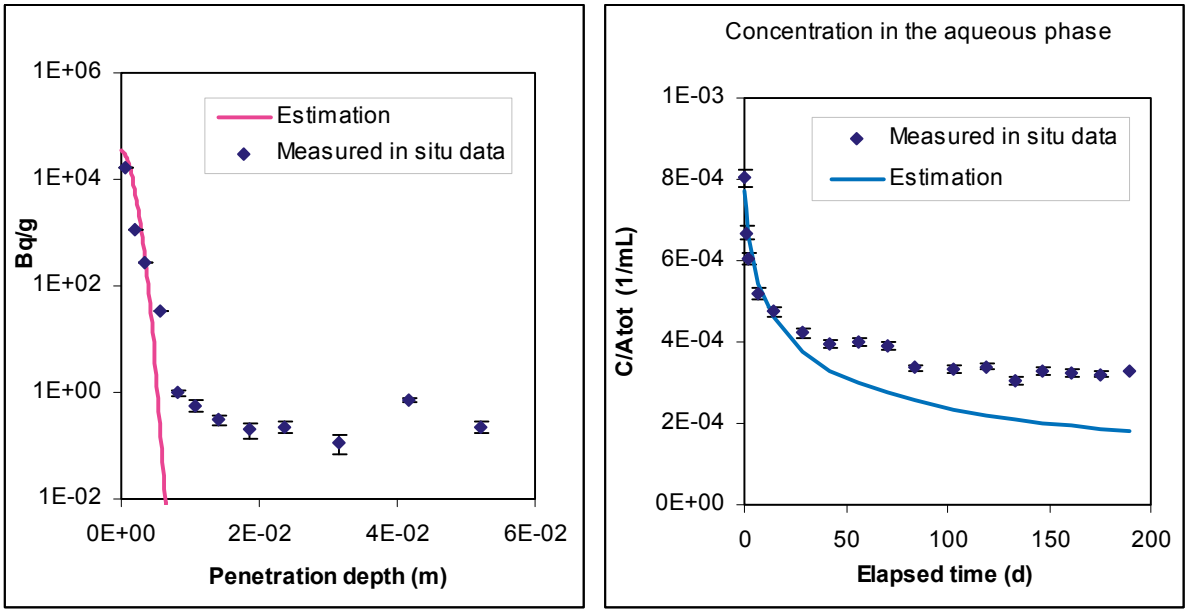

Figure Case 3. *Tracer: Cs-137. Core: D12.*

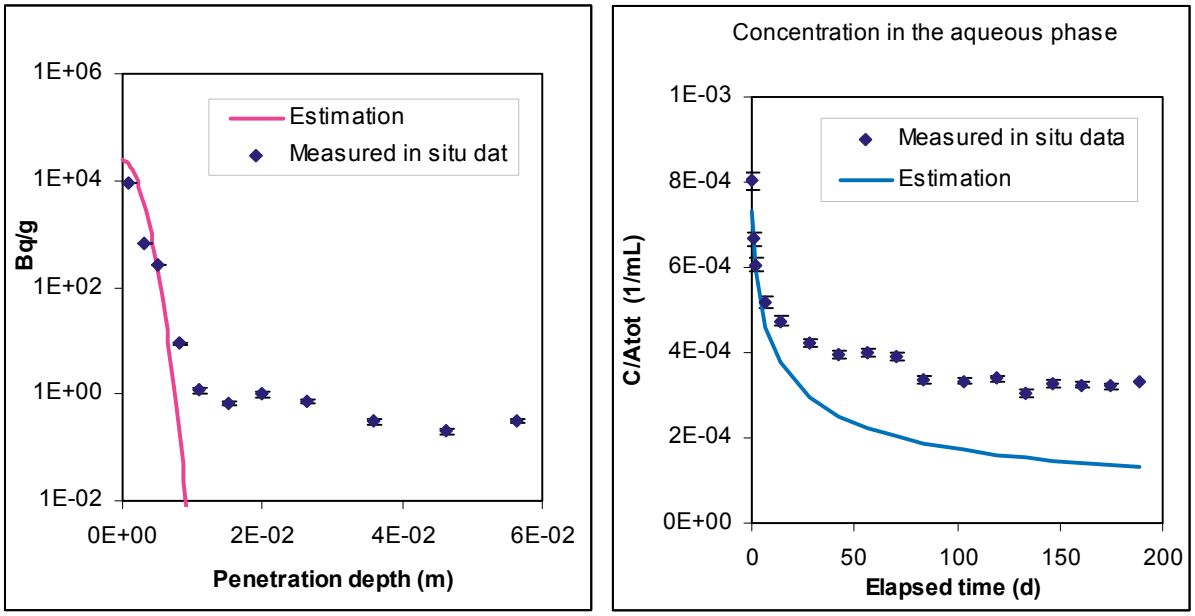

Figure Case 3. *Tracer: Cs-137. Core: D13.*

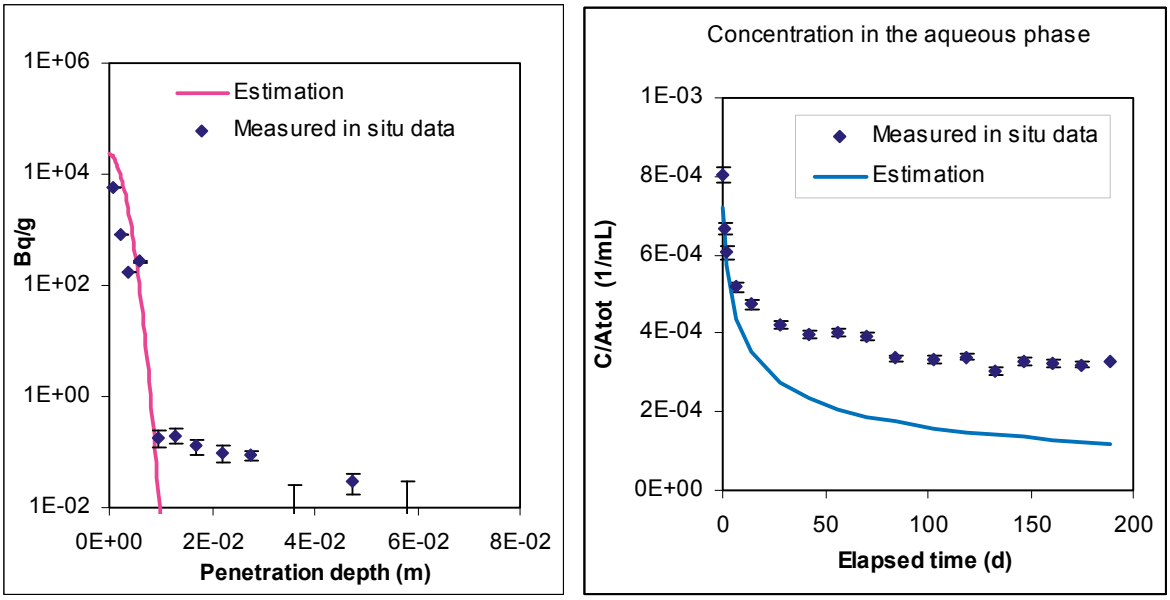

Figure Case 3. *Tracer: Cs-137. Core: D14.*

Co-57

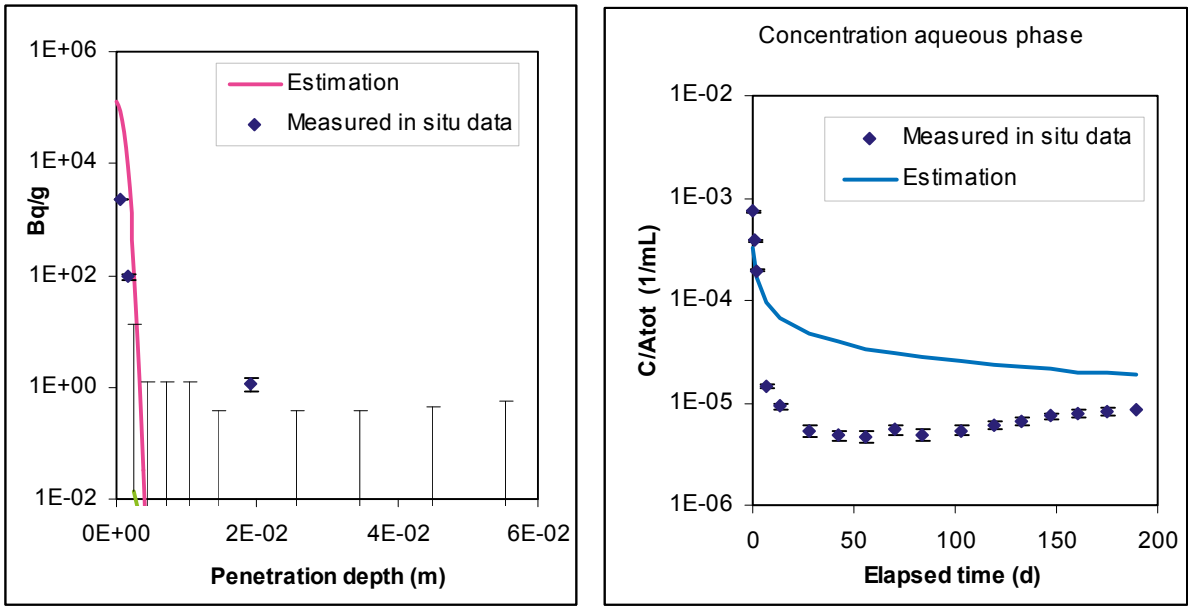

Figure Case 3. *Tracer: Co-57. Core: A6.*

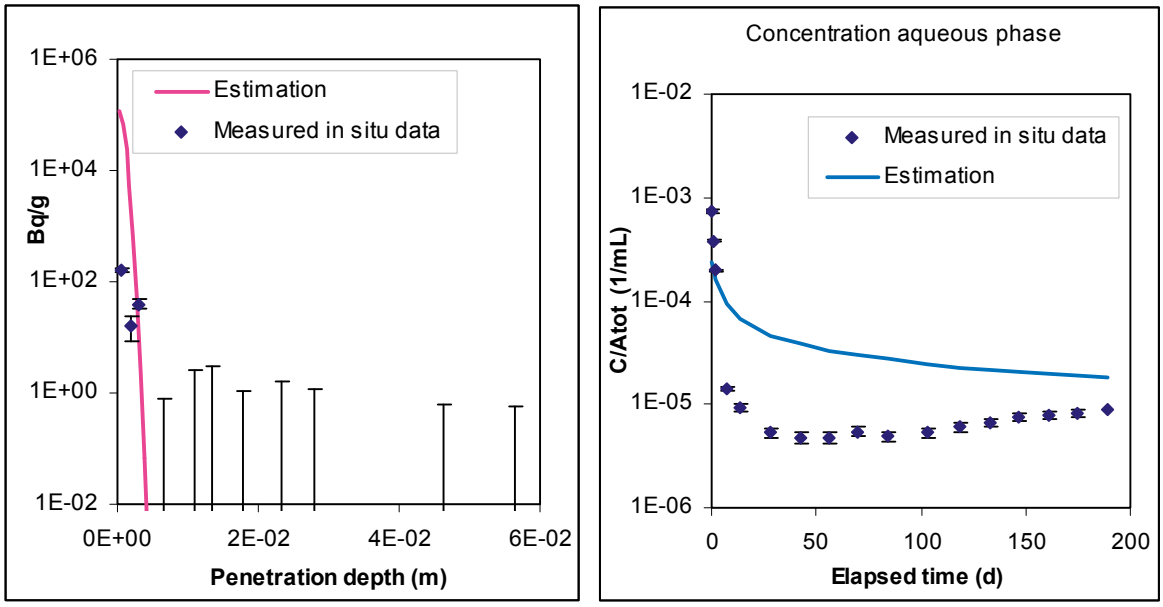

Figure Case 3. *Tracer: Co-57. Core: A8.*

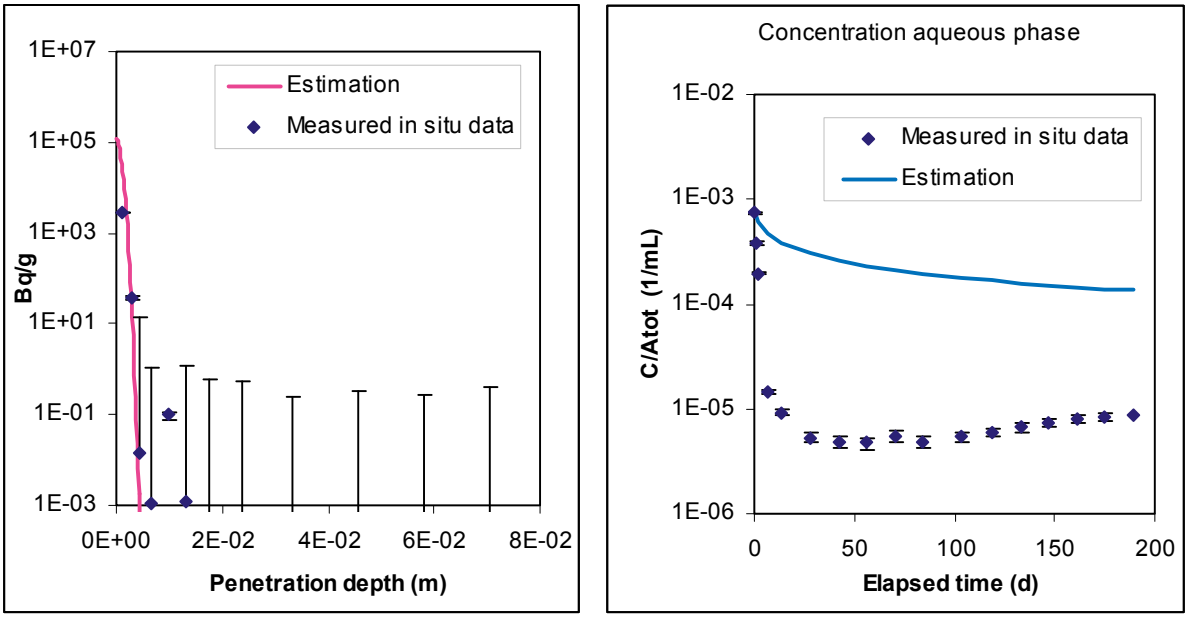

Figure Case 3. *Tracer: Co-57. Core: A12.*

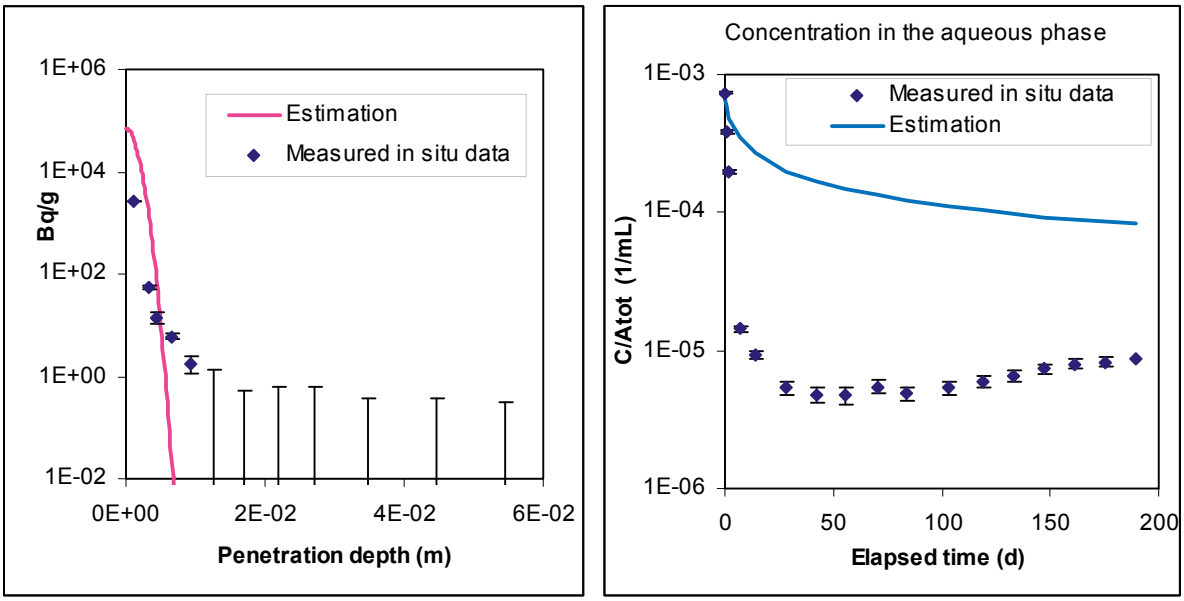

Figure Case 3. *Tracer: Co-57. Core: D7.*

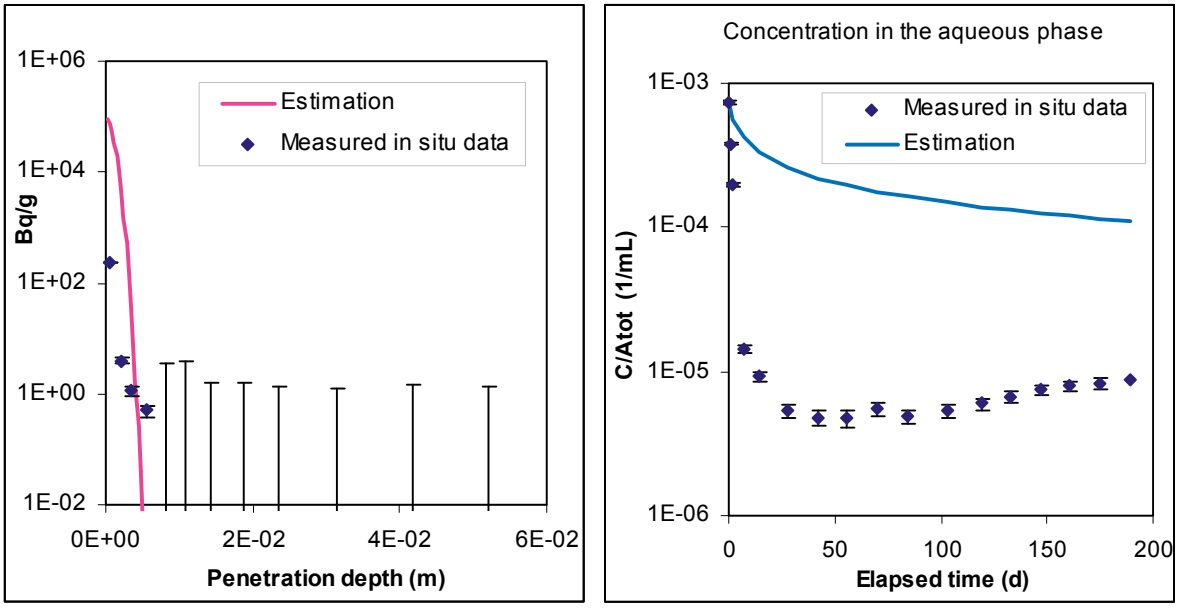

Figure Case 3. *Tracer: Co-57. Core: D12.*

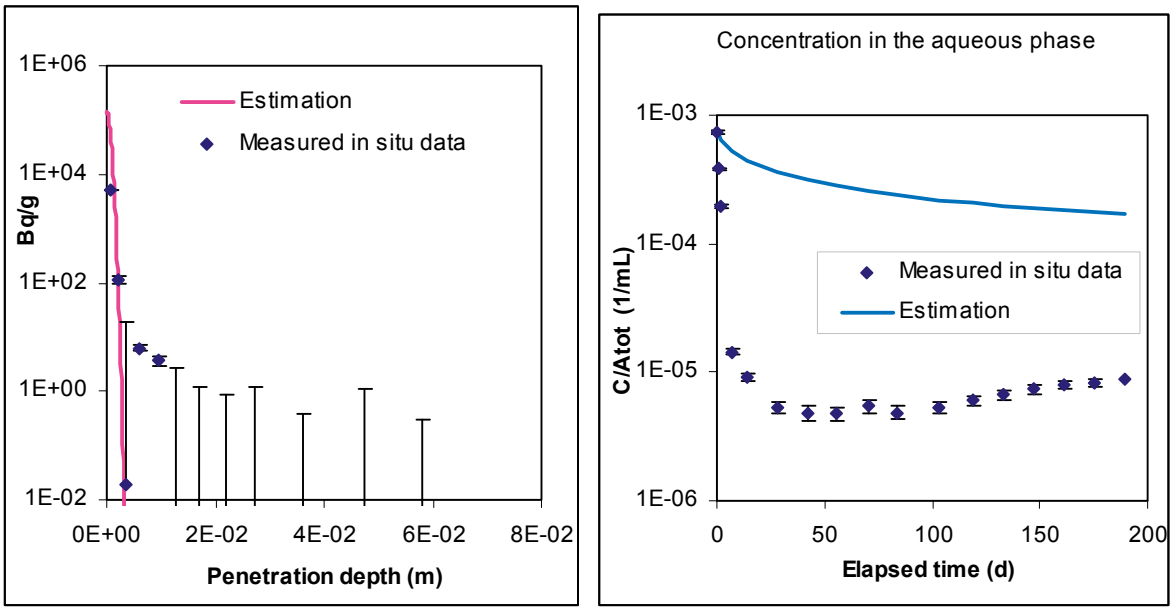

Figure Case 3. *Tracer: Co-57. Core: D14.*

Cd-109

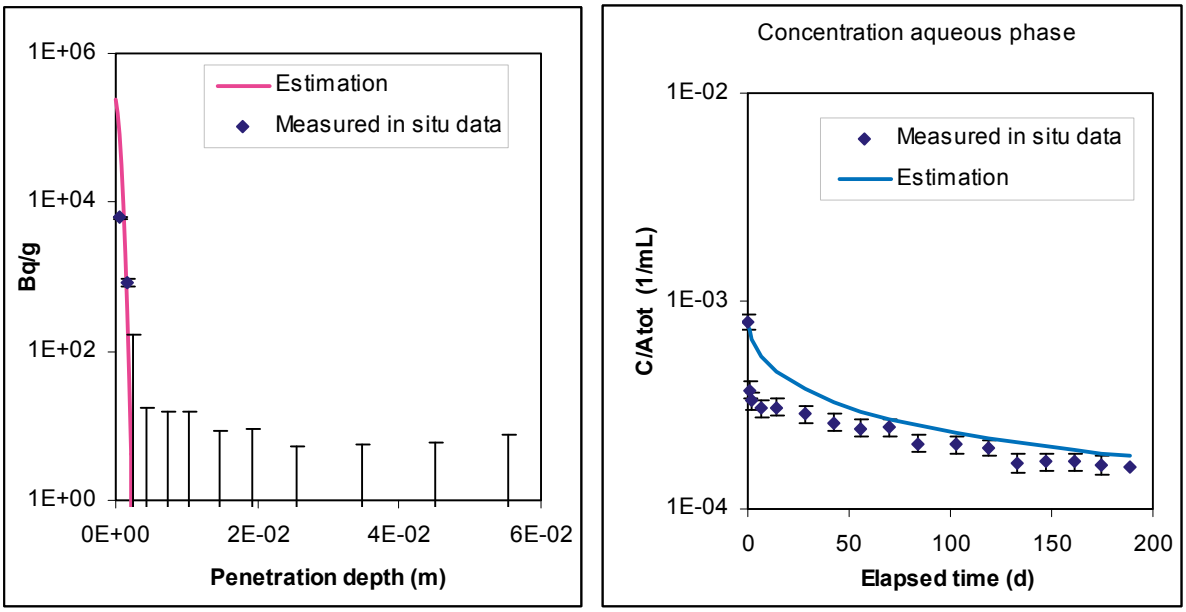

Figure Case 3. *Tracer: Cd-109. Core: A6.*

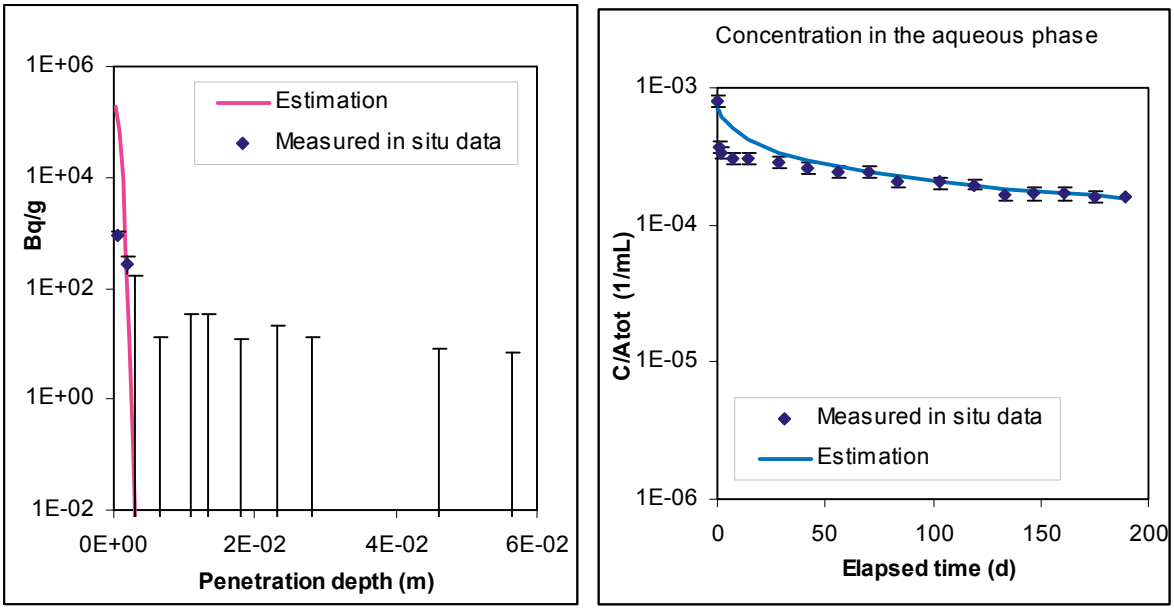

Figure Case 3. *Tracer: Cd-109. Core: A8.*

Case 4

Na-22

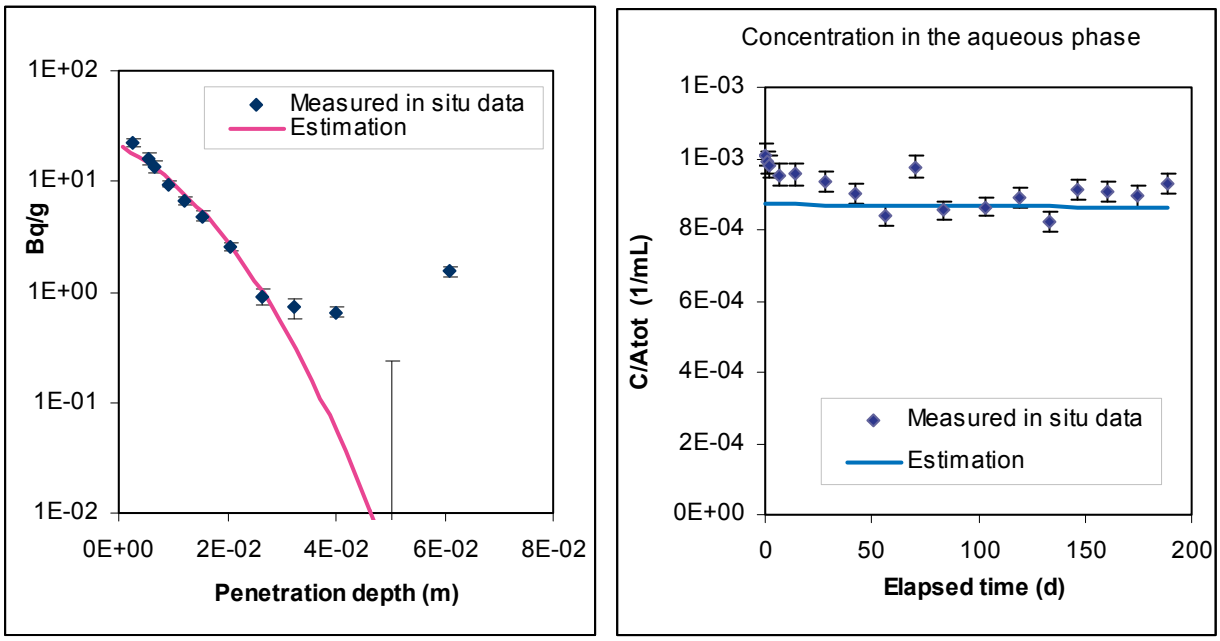

Figure Case 4. *Tracer: Na-22. Core: A1.*

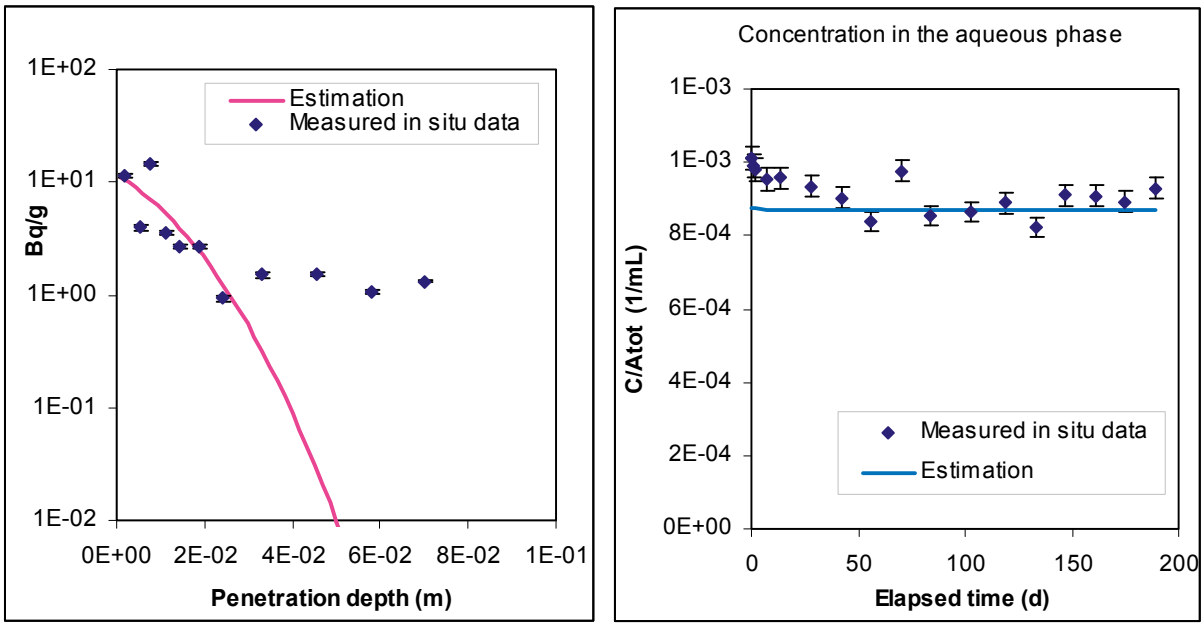

Figure Case 4. *Tracer: Na-22. Core: A5.*

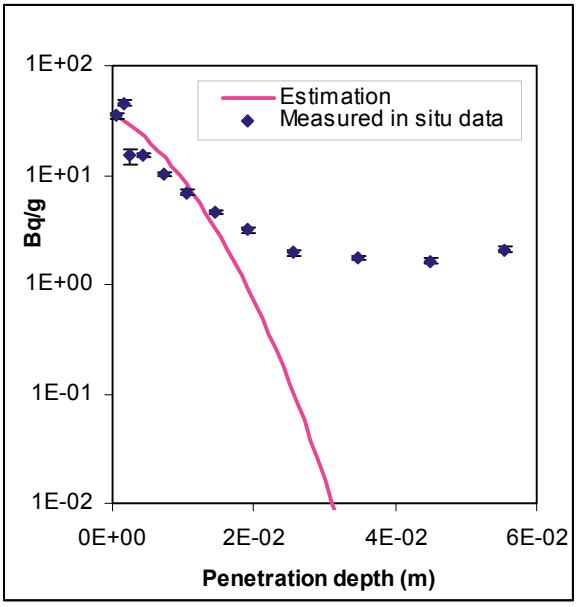

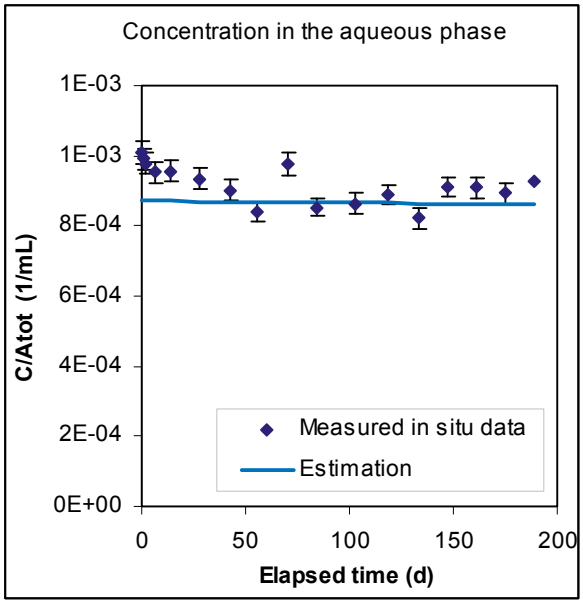

Figure Case 4. *Tracer: Na-22. Core: A6.*

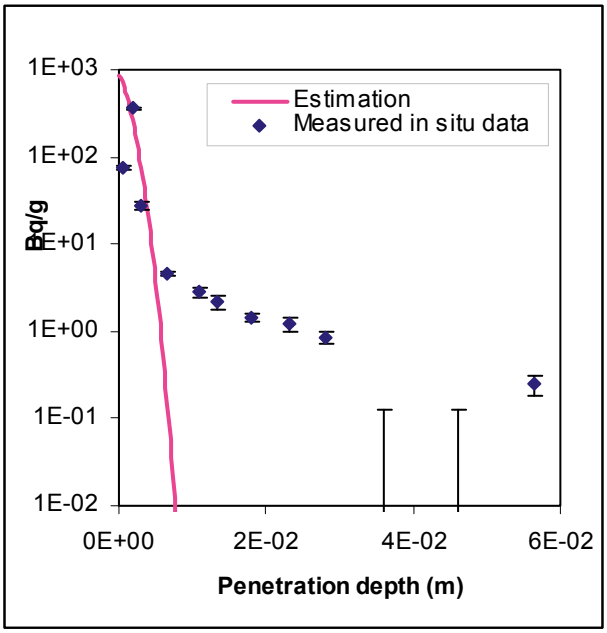

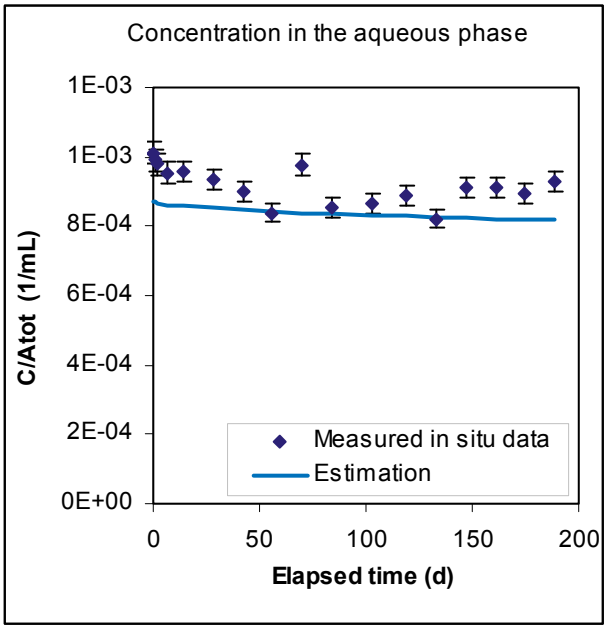

Figure Case 4. *Tracer: Na-22. Core: A8.*

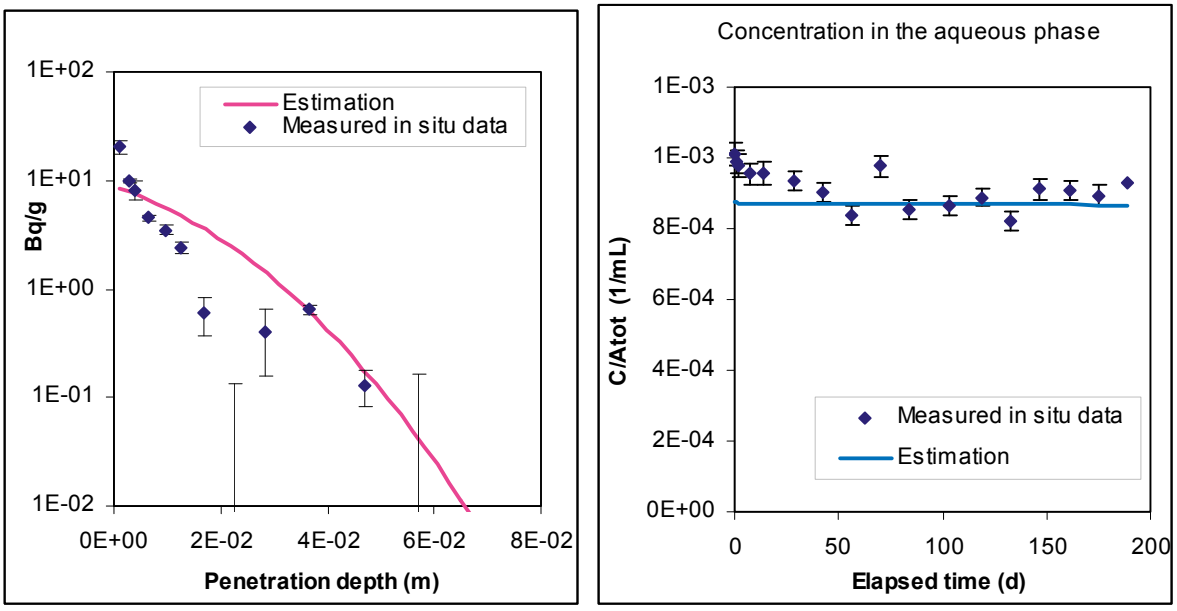

Figure Case 4. *Tracer: Na-22. Core: A9.*

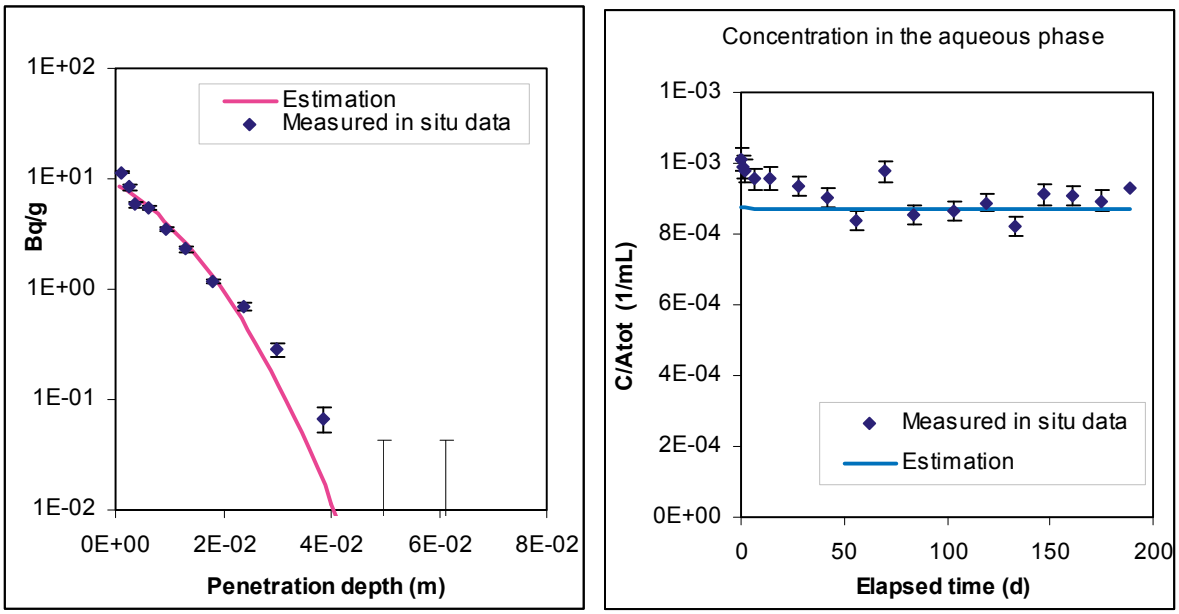

Figure Case 4. *Tracer: Na-22. Core: A10.*

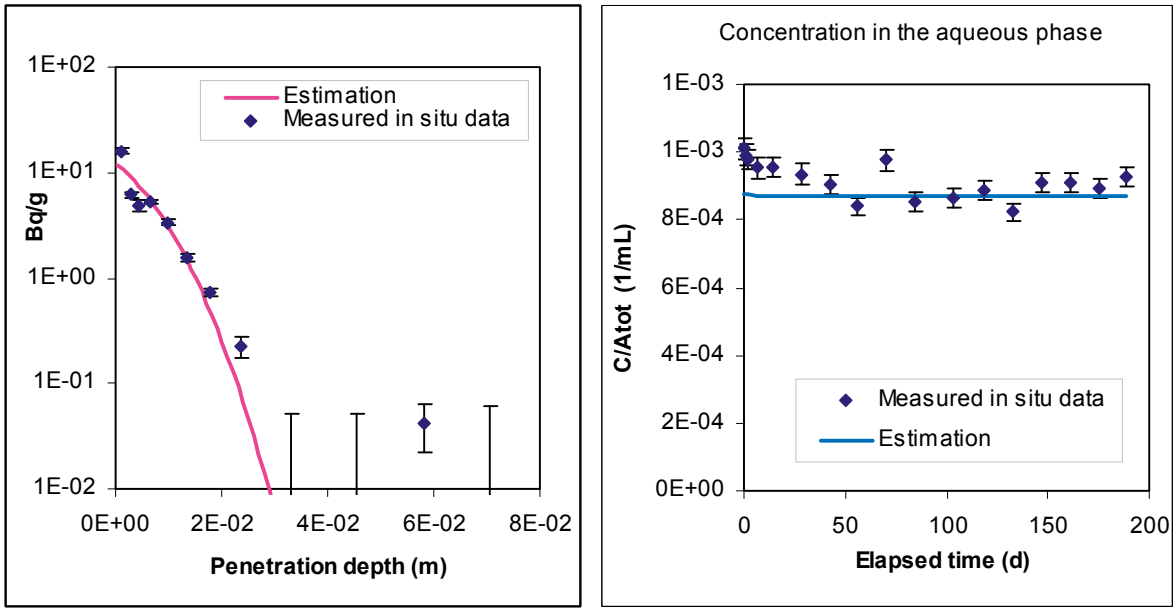

Figure Case 4. *Tracer: Na-22. Core: A12.*

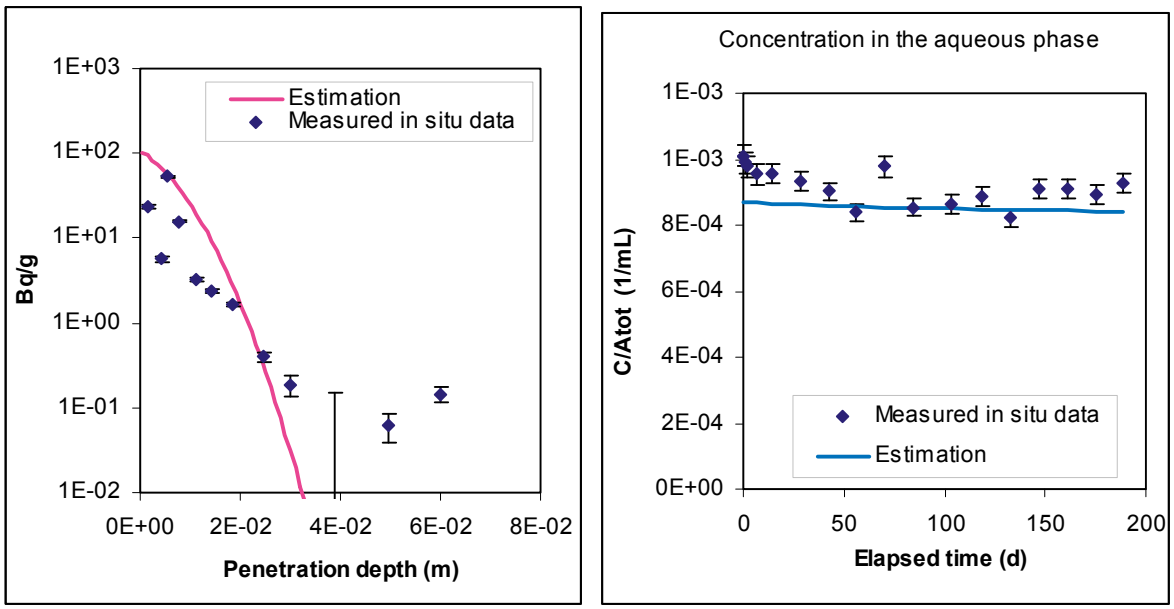

Figure Case 4. *Tracer: Na-22. Core: A15.*

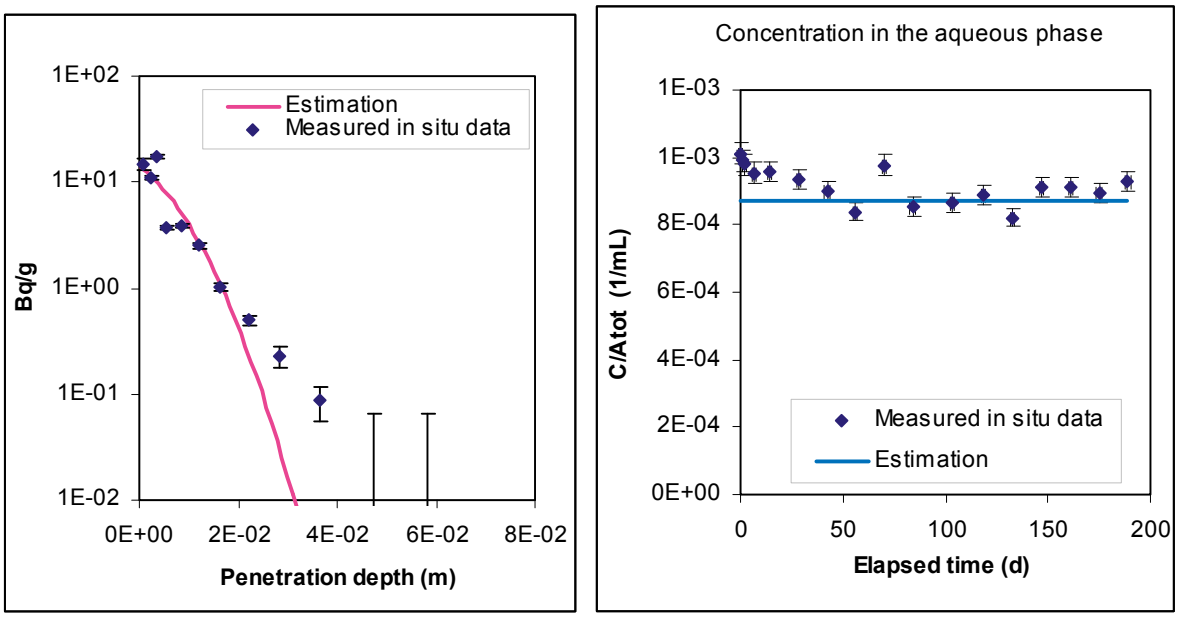

Figure Case 4. *Tracer: Na-22. Core: A16.*

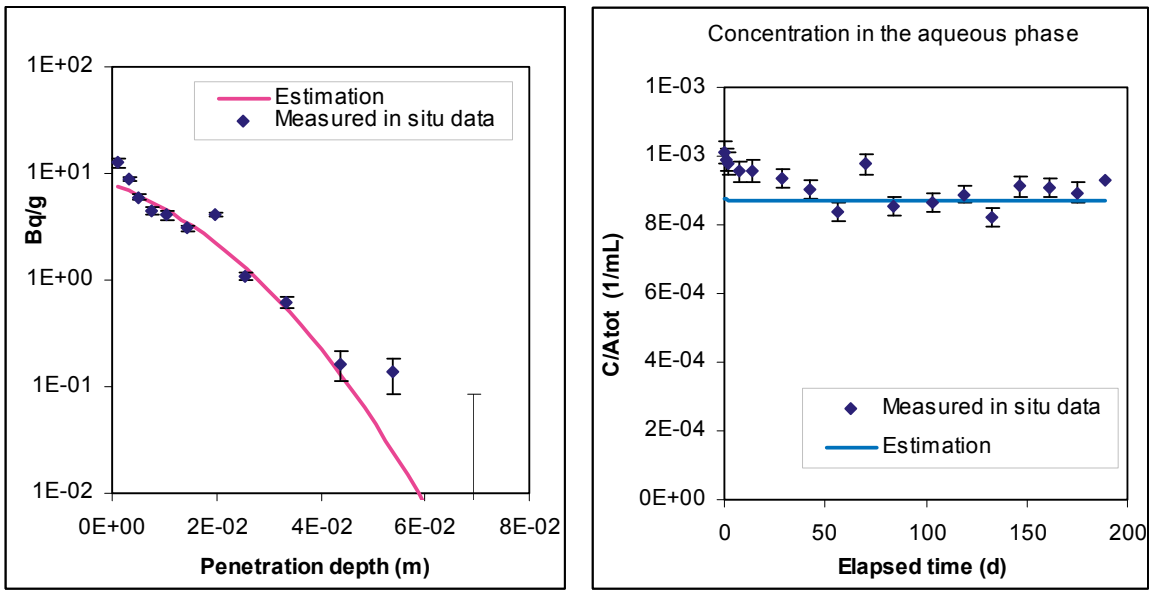

Figure Case 4. *Tracer: Na-22. Core: A17.*

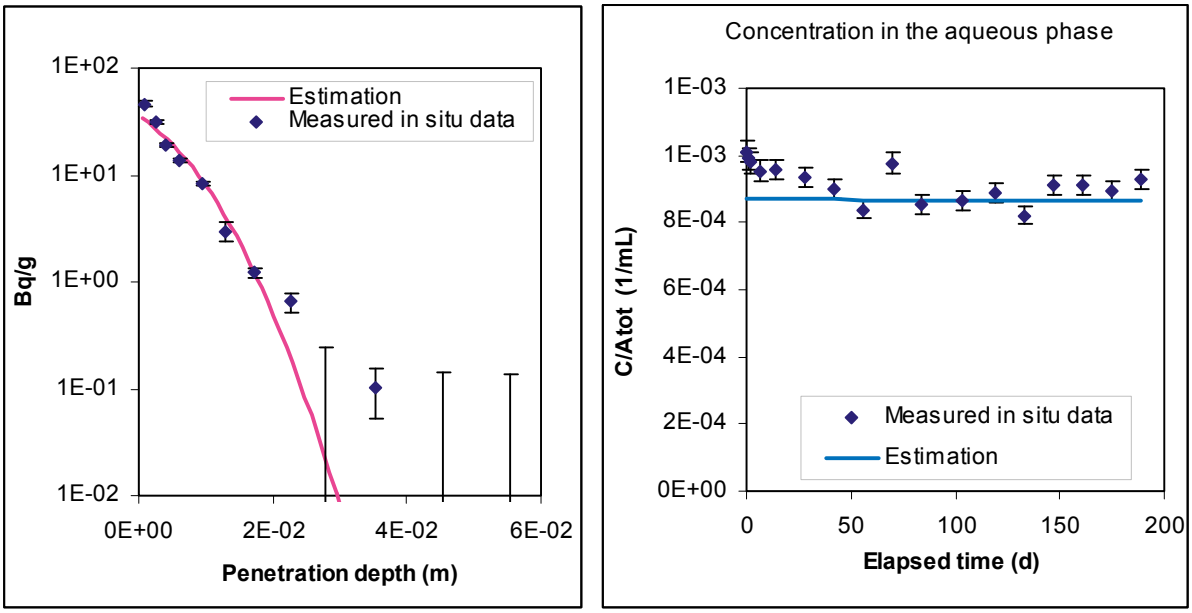

Figure Case 4. *Tracer: Na-22. Core: D1.*

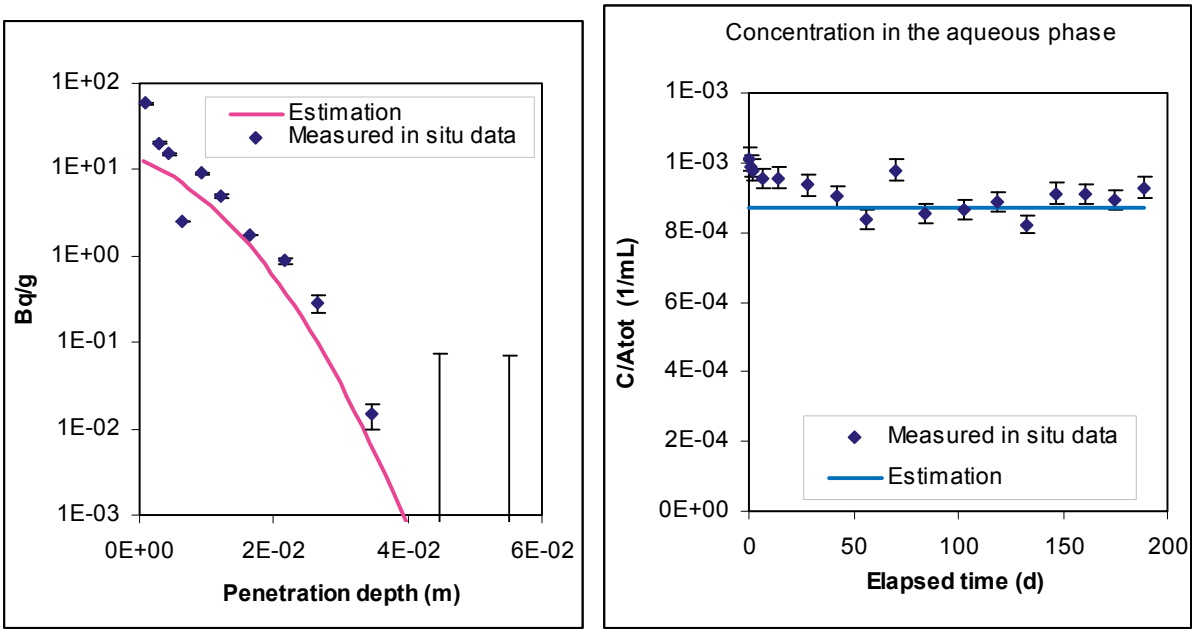

Figure Case 4. *Tracer: Na-22. Core: D5.*

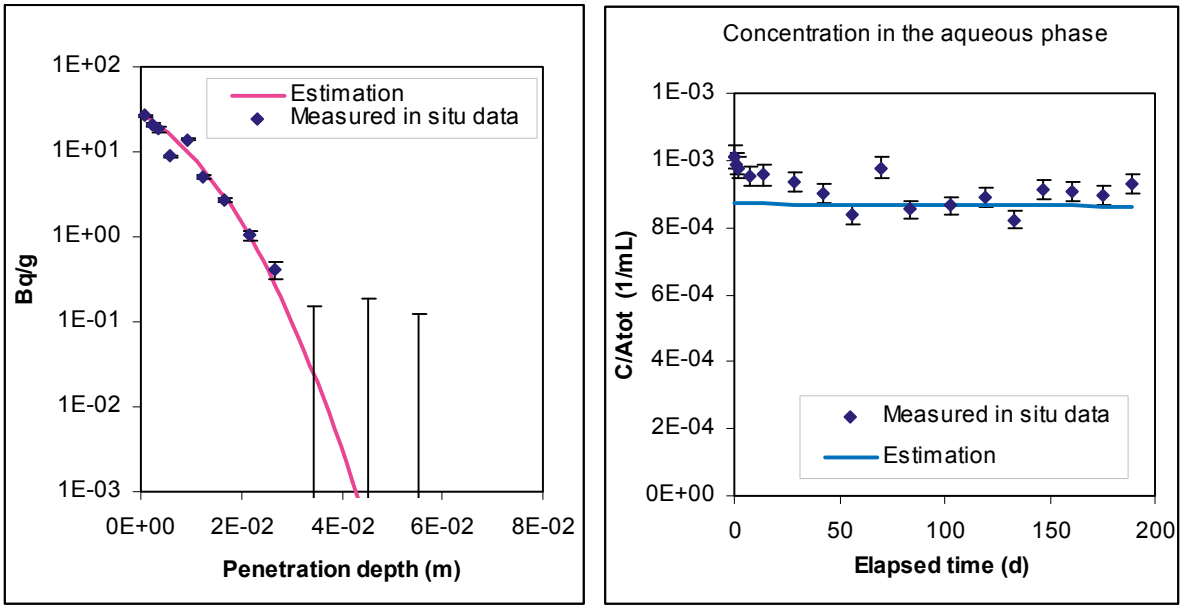

Figure Case 4. *Tracer: Na-22. Core: D6.*

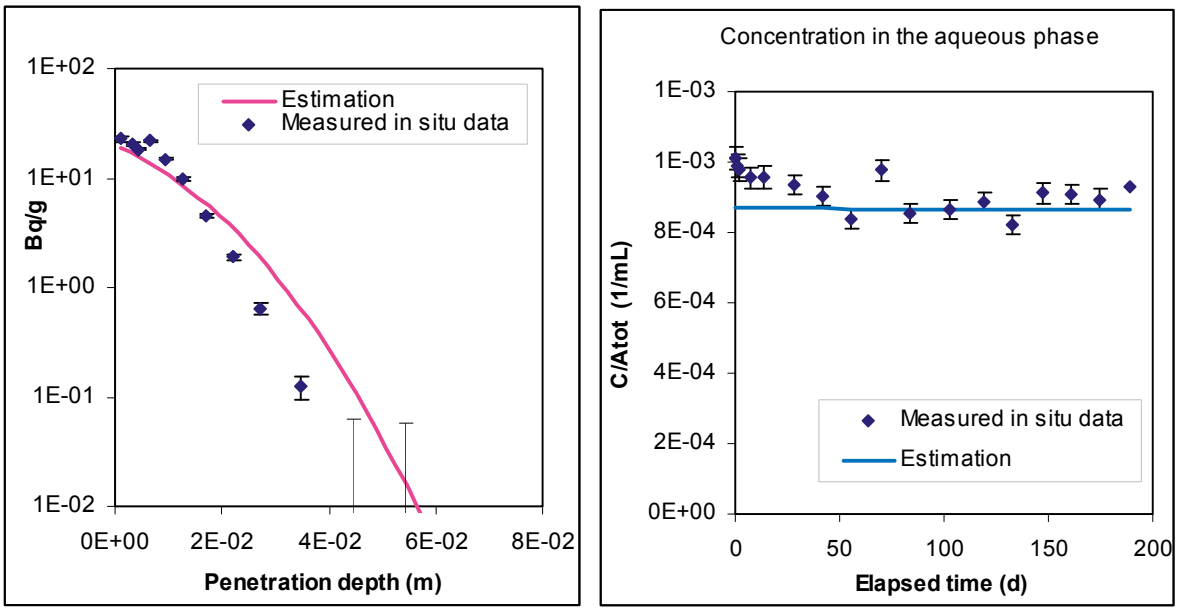

Figure Case 4. *Tracer: Na-22. Core: D7.*

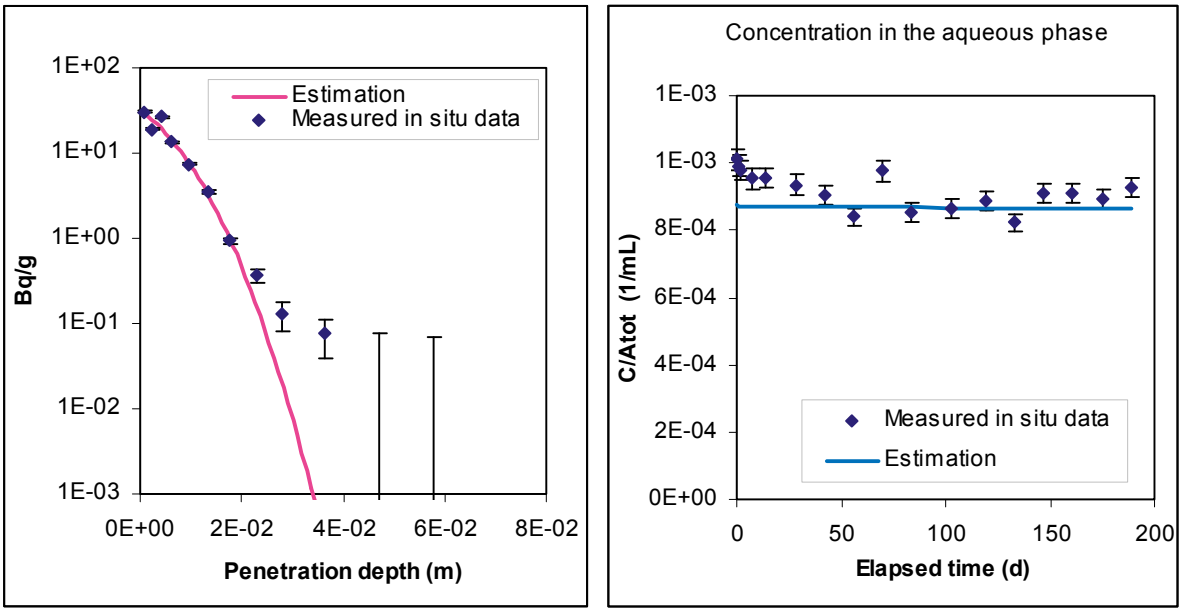

Figure Case 4. *Tracer: Na-22. Core: D8.*

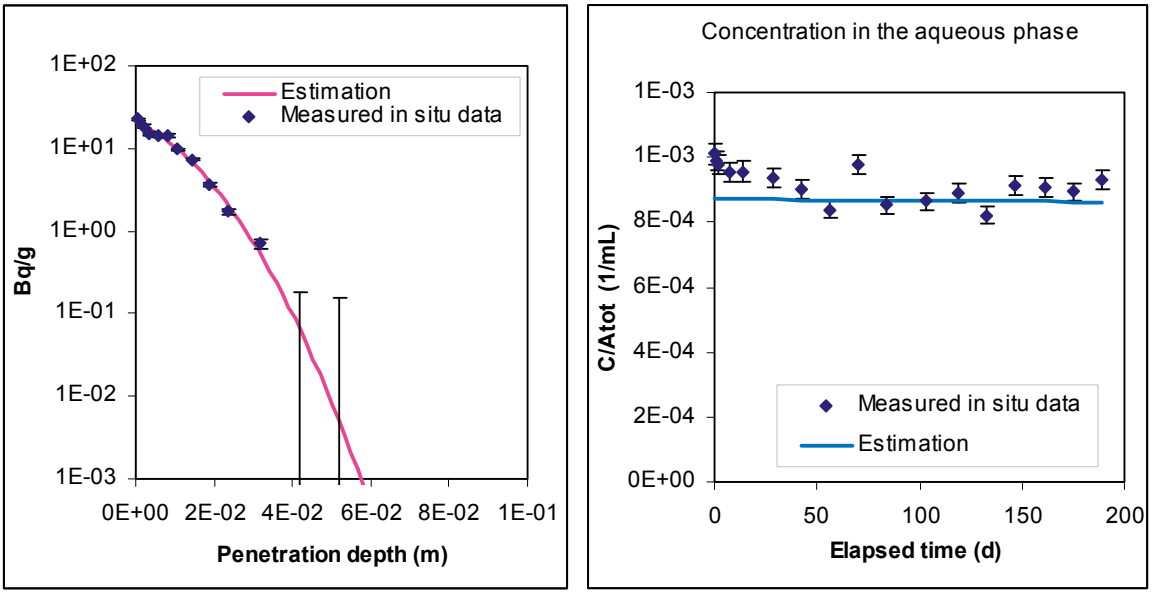

Figure Case 4. *Tracer: Na-22. Core: D12.*

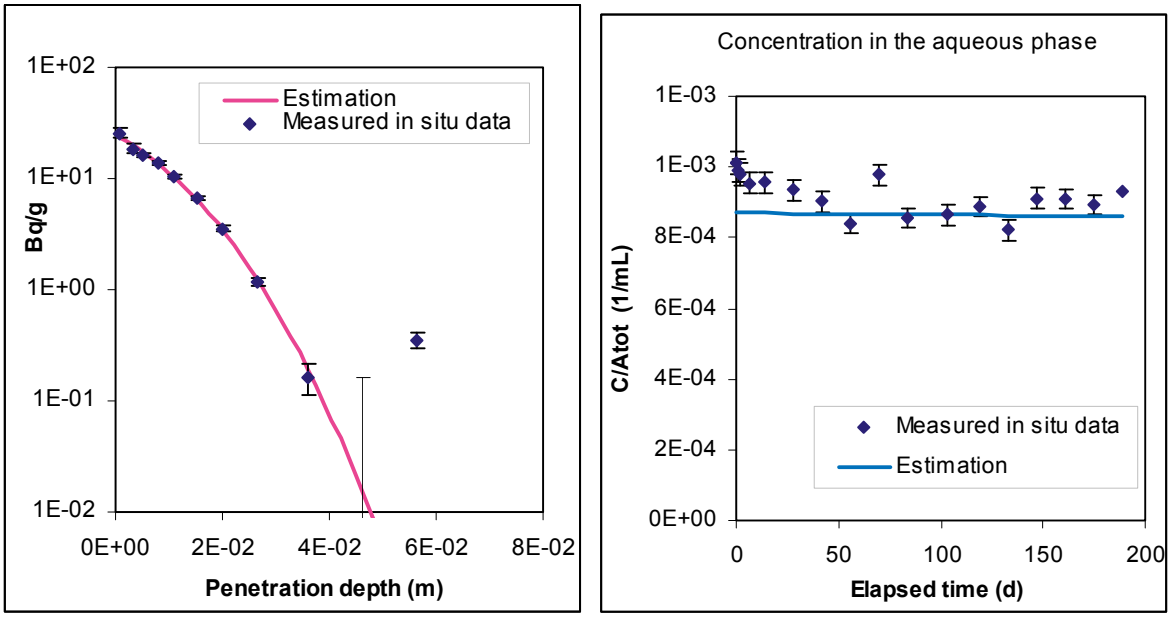

Figure Case 4. *Tracer: Na-22. Core: D13.*

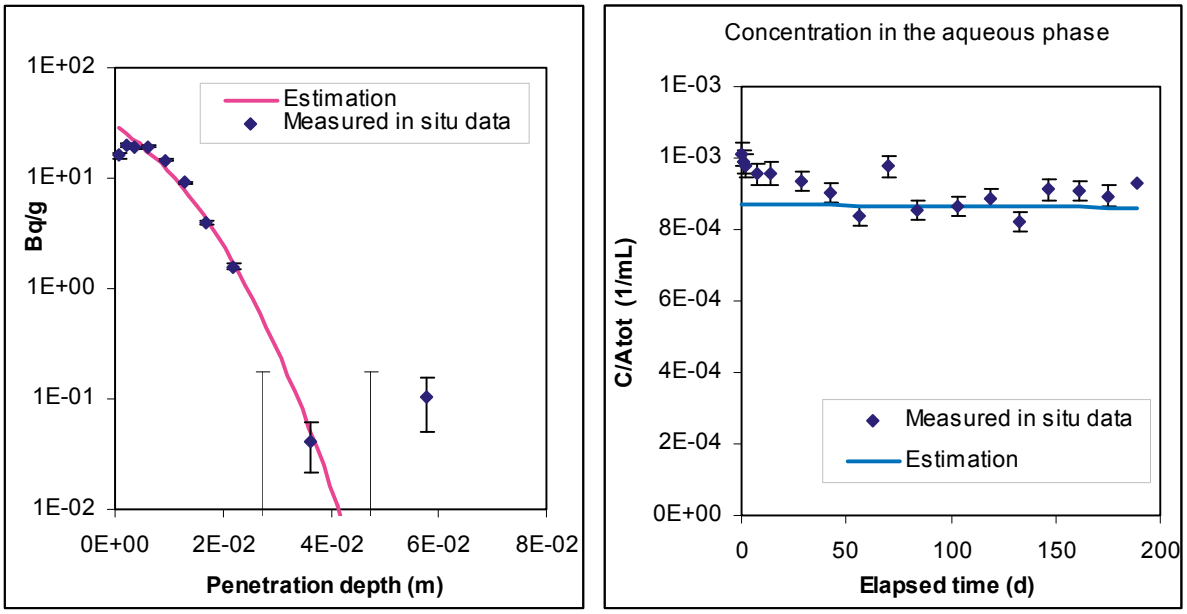

Figure Case 4. *Tracer: Na-22. Core: D14.*

Ni-63

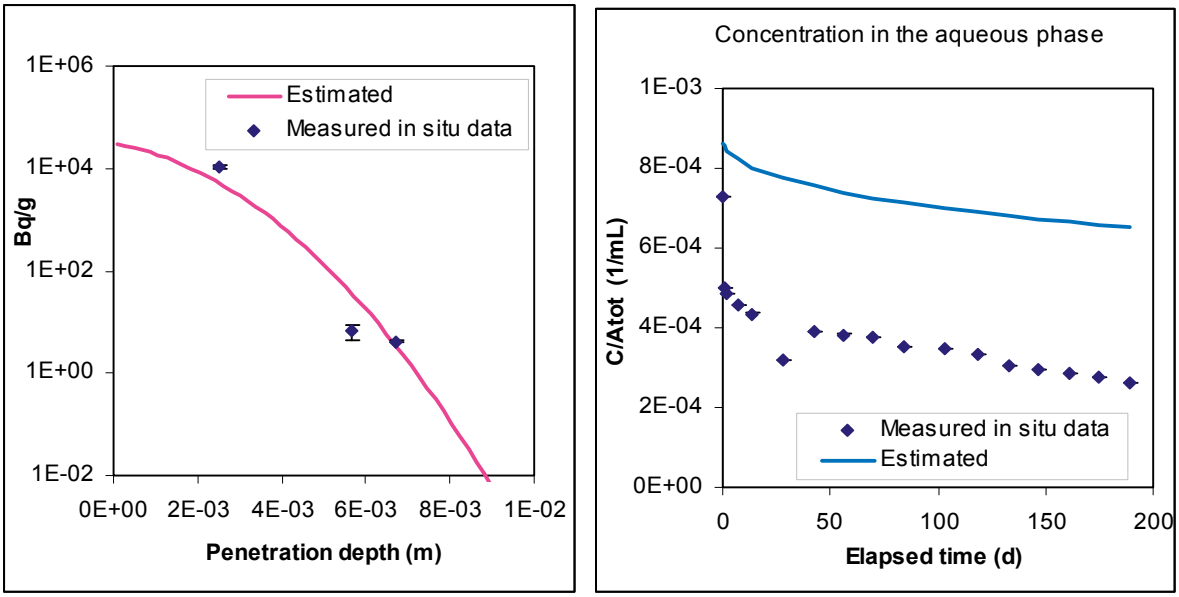

Figure Case 4. *Tracer: Ni-63. Core: A1.*

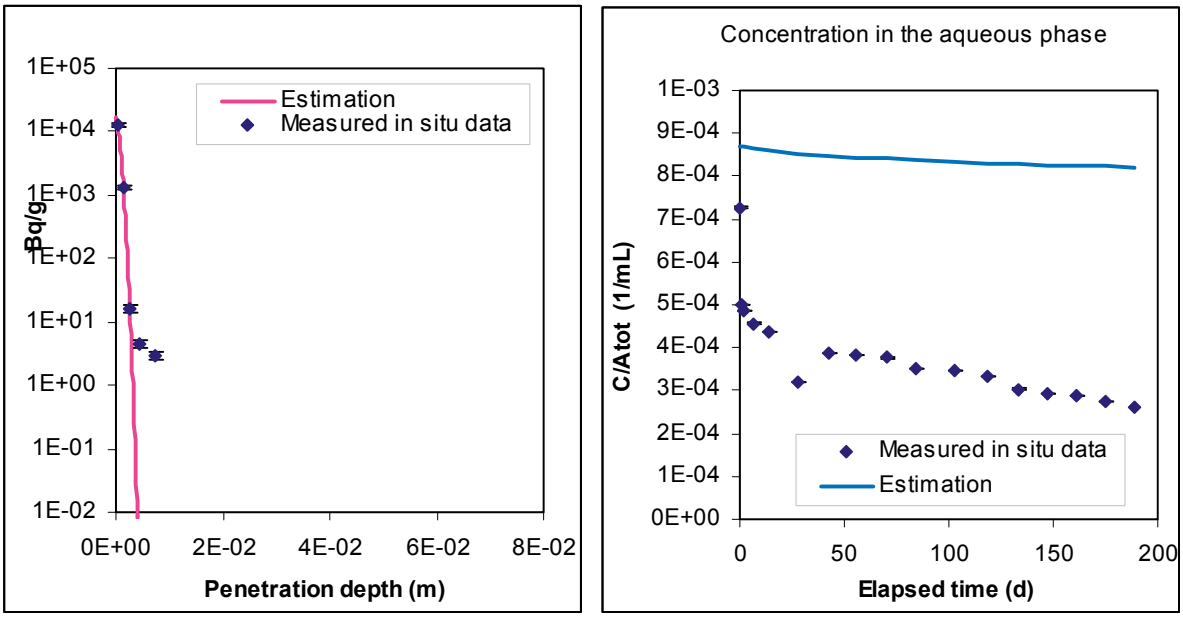

Figure Case 4. *Tracer: Ni-63. Core: A6.*

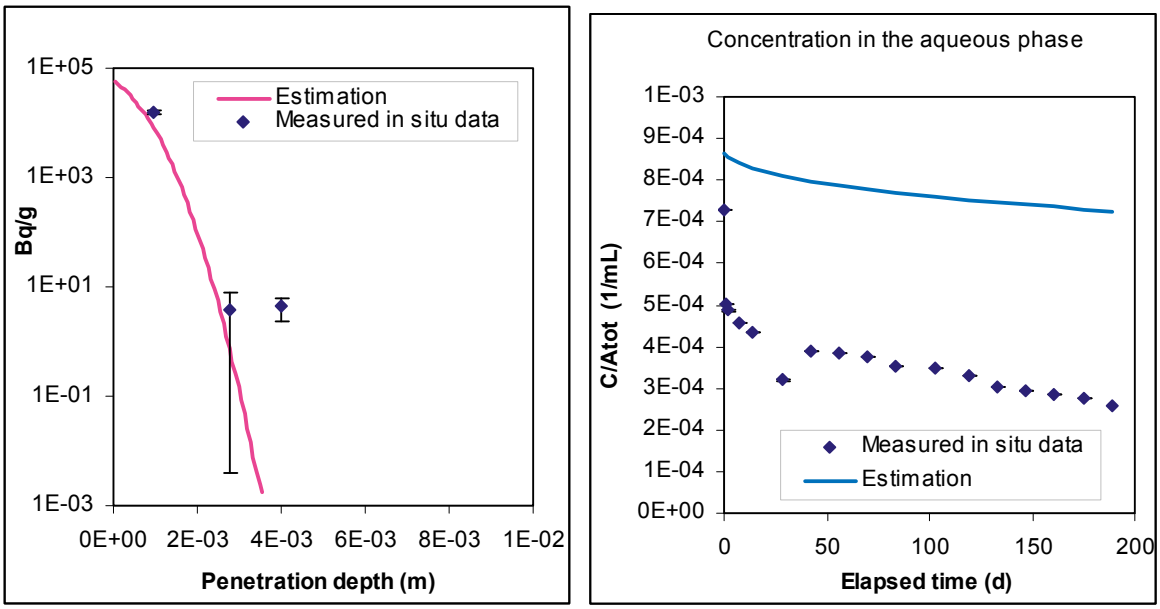

Figure Case 4. *Tracer: Ni-63. Core: A9.*

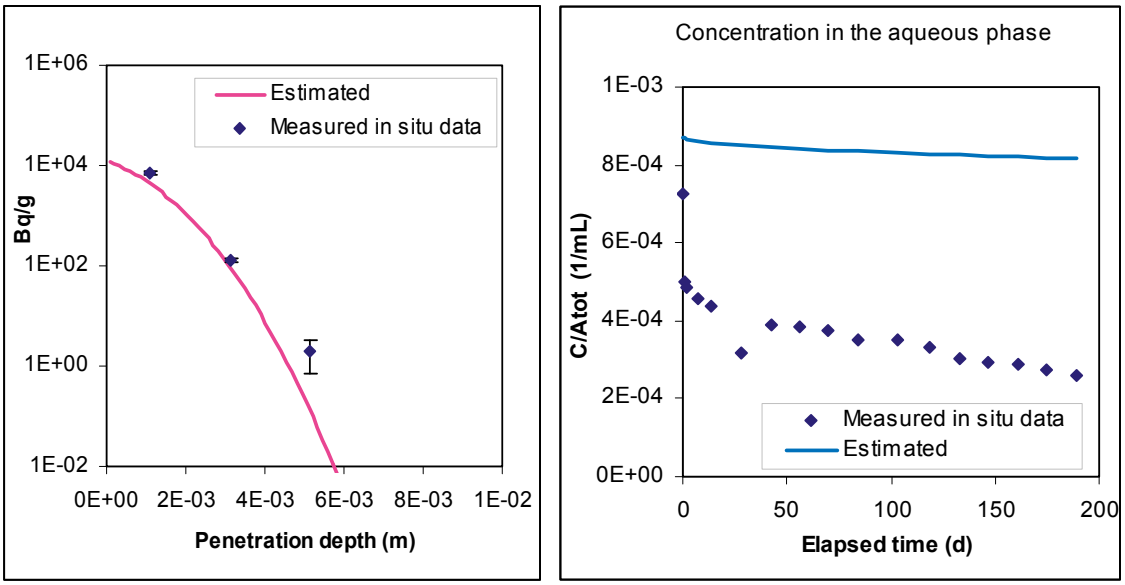

Figure Case 4. *Tracer: Ni-63. Core: A17.*

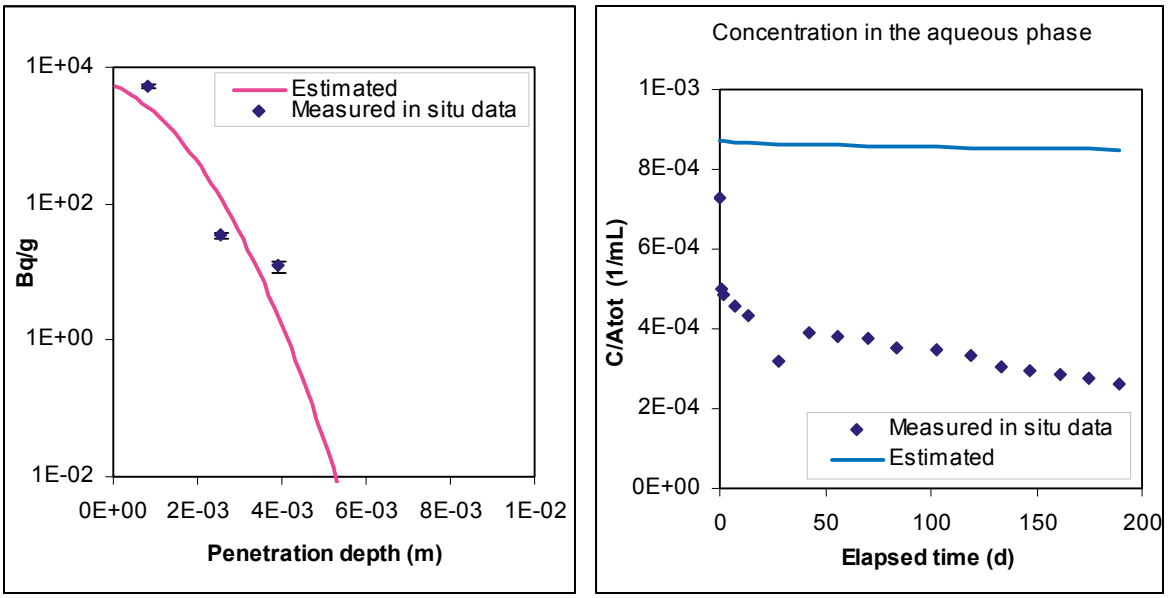

Figure Case 4. *Tracer: Ni-63. Core: D1.*

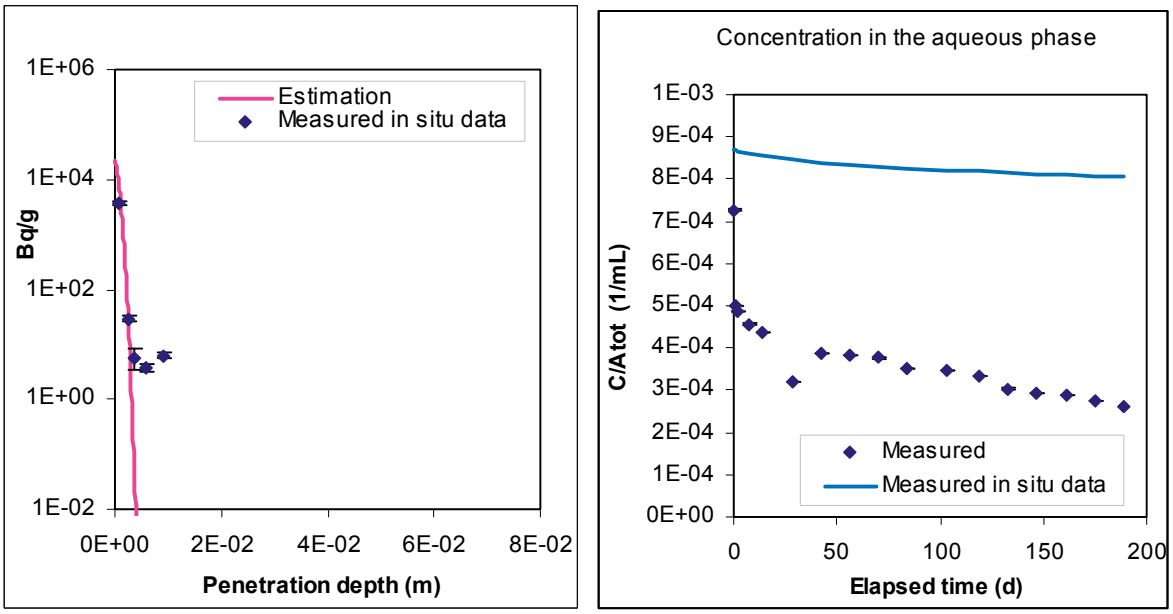

Figure Case 4. *Tracer: Ni-63. Core: D6.*

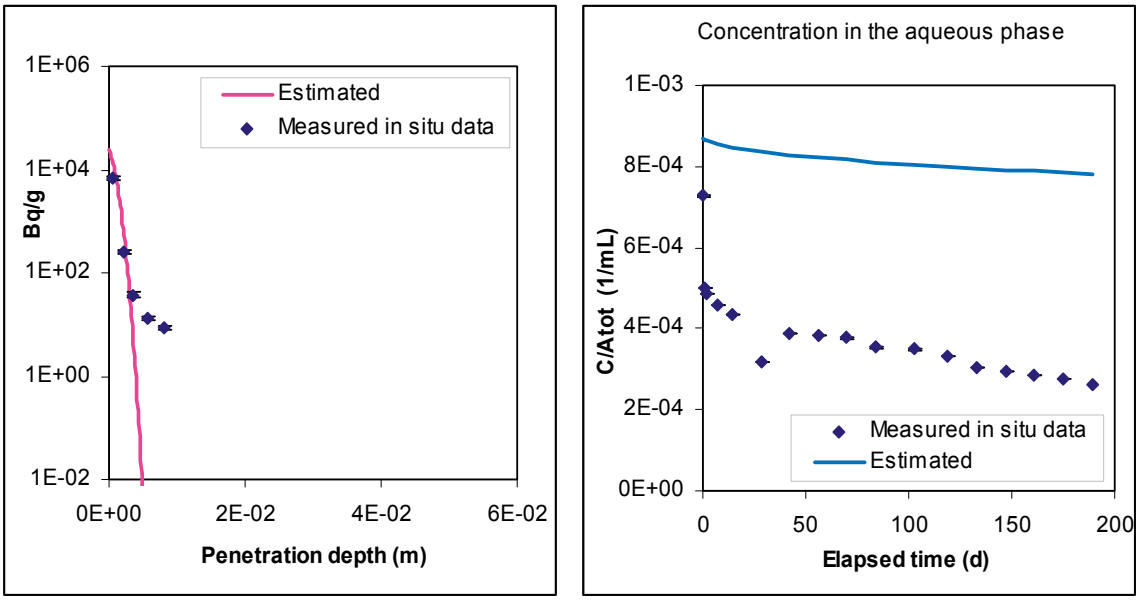

Figure Case 4. *Tracer: Ni-63. Core: D12.*

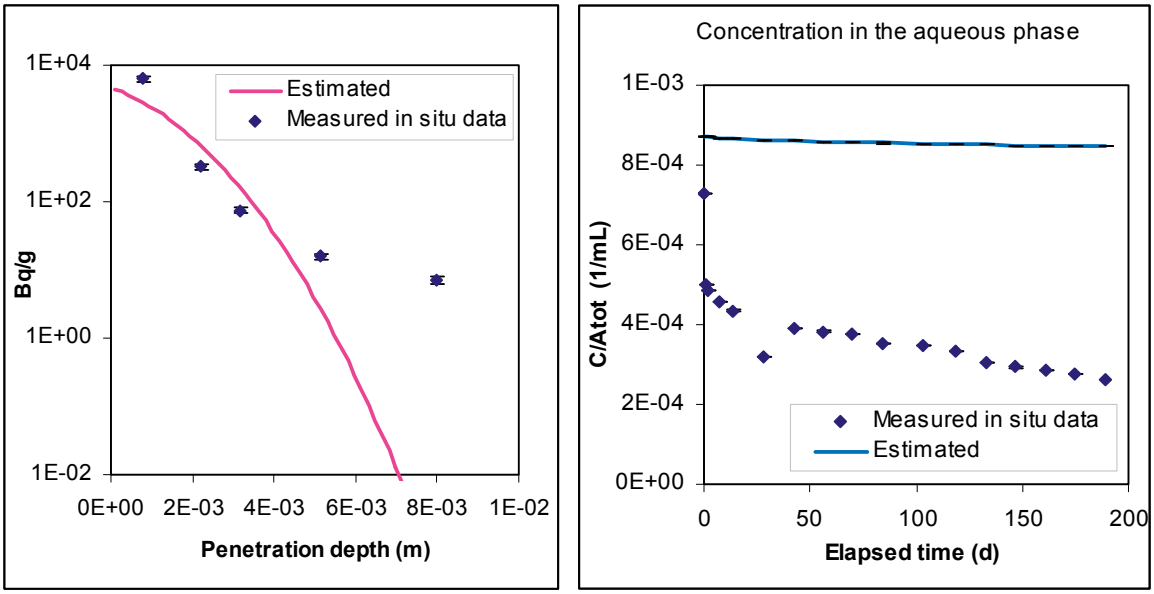

Figure Case 4. *Tracer: Ni-63. Core: D13.*

Ba-133

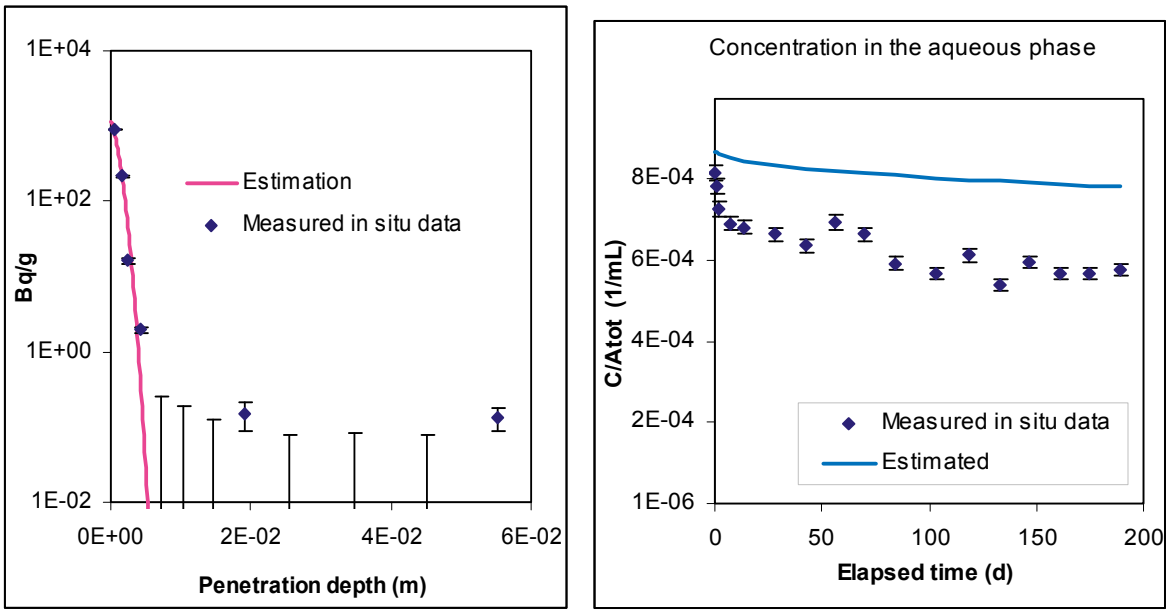

Figure Case 4. *Tracer: Ba-133. Core: A6.*

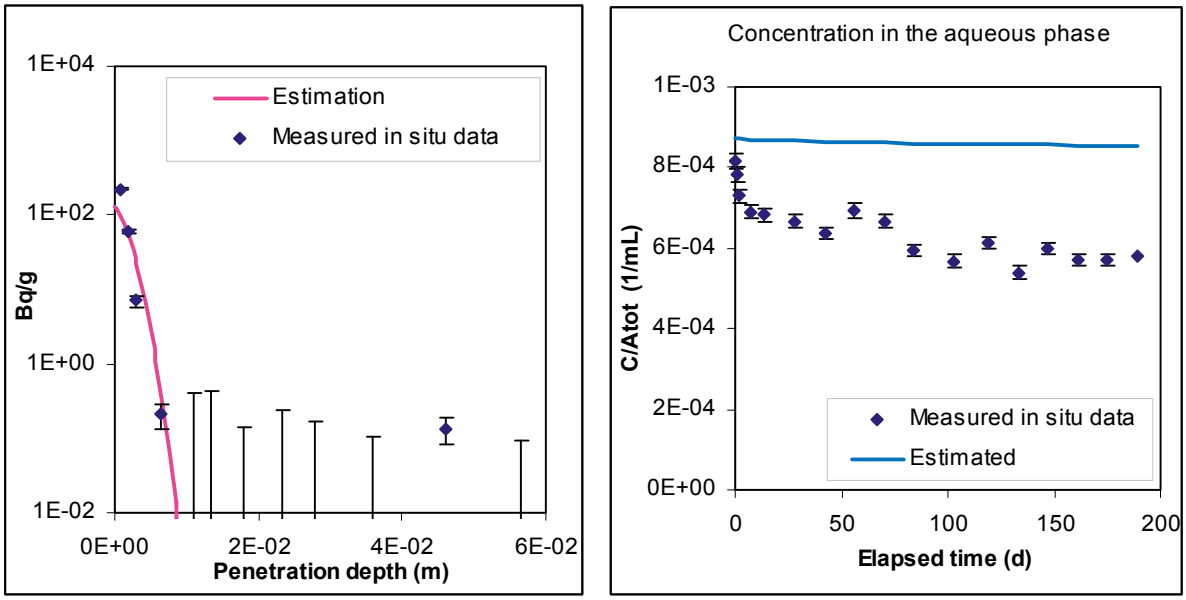

Figure Case 4. *Tracer: Ba-133. Core: A8.*

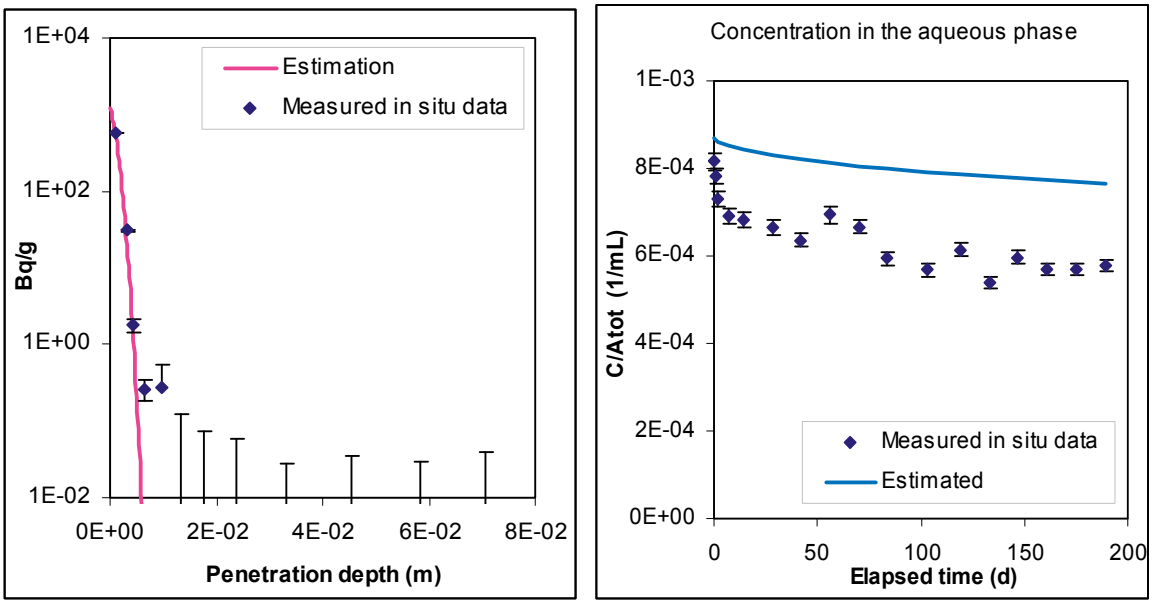

Figure Case 4. *Tracer: Ba-133. Core: A12.*

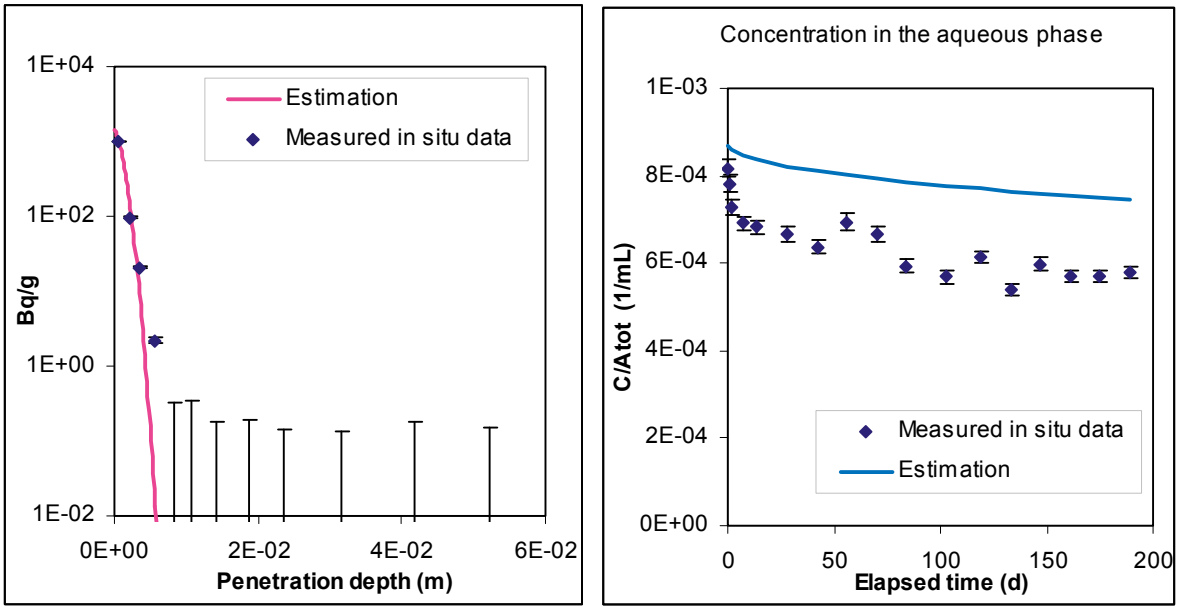

Figure Case 4. *Tracer: Ba-133. Core: D12.*

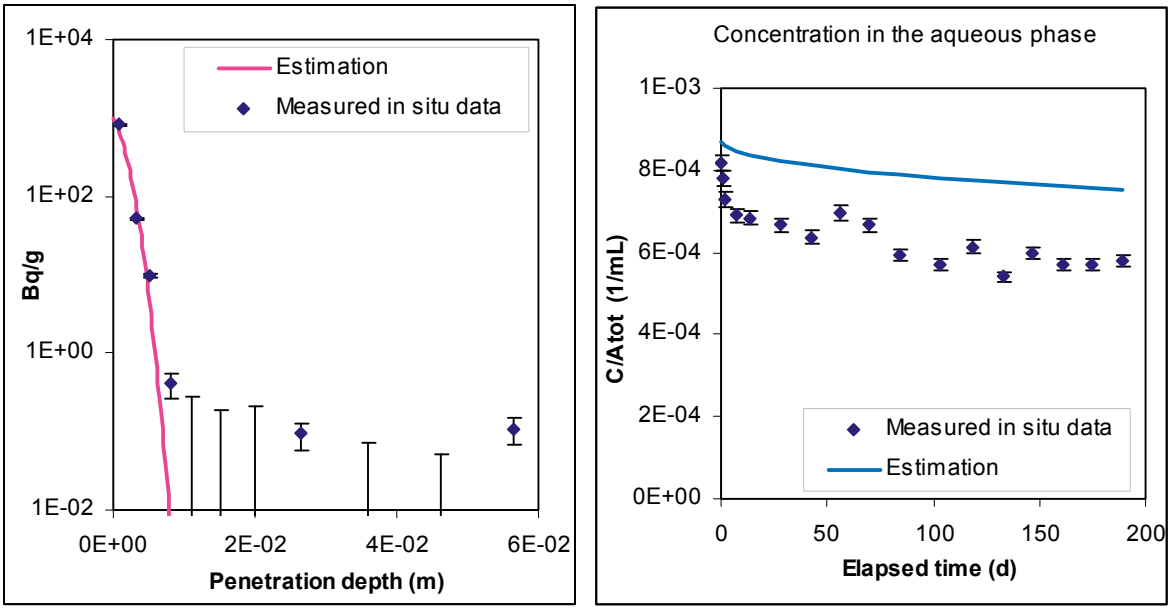

Figure Case 4. *Tracer: Ba-133. Core: D13.*

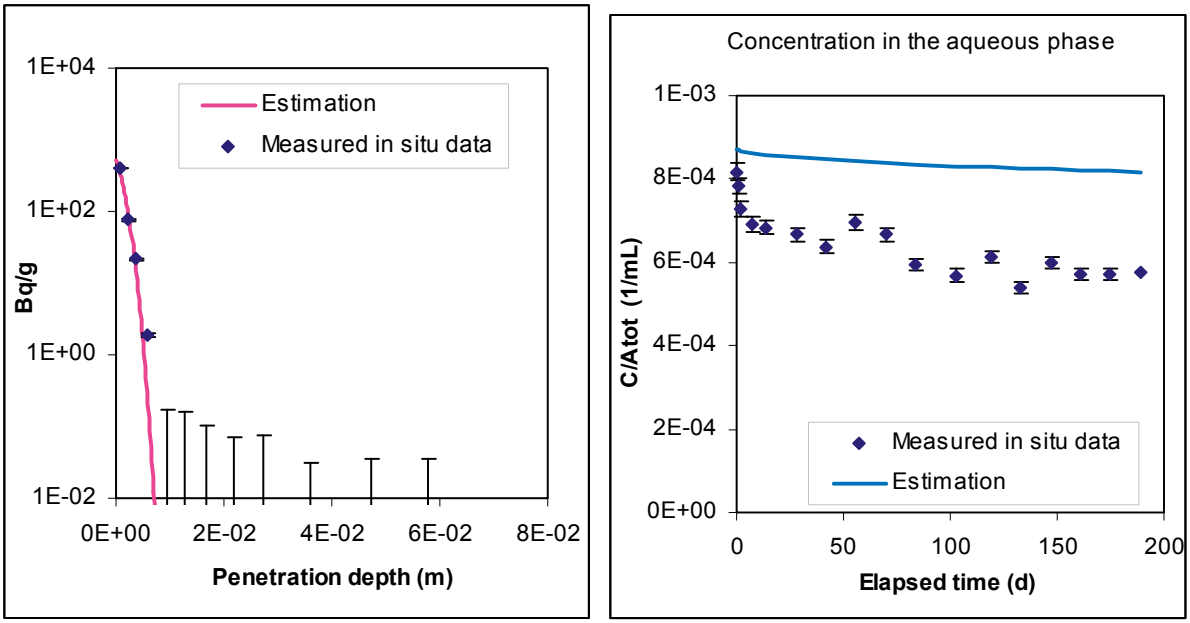

Figure Case 4. *Tracer: Ba-133. Core: D14.*

Cs-137

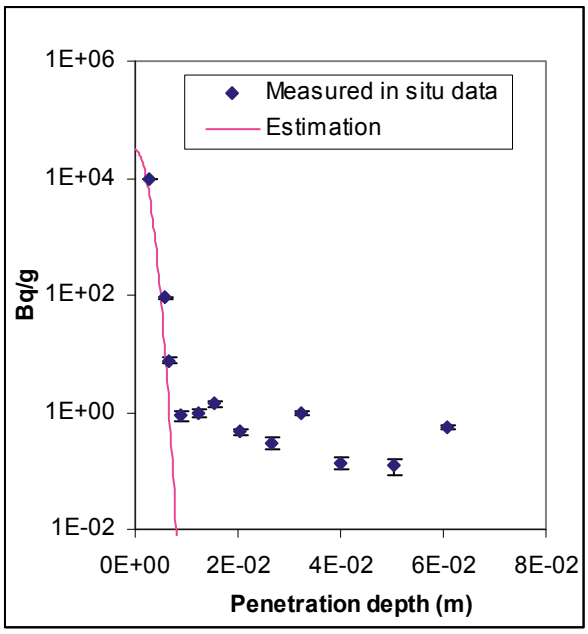

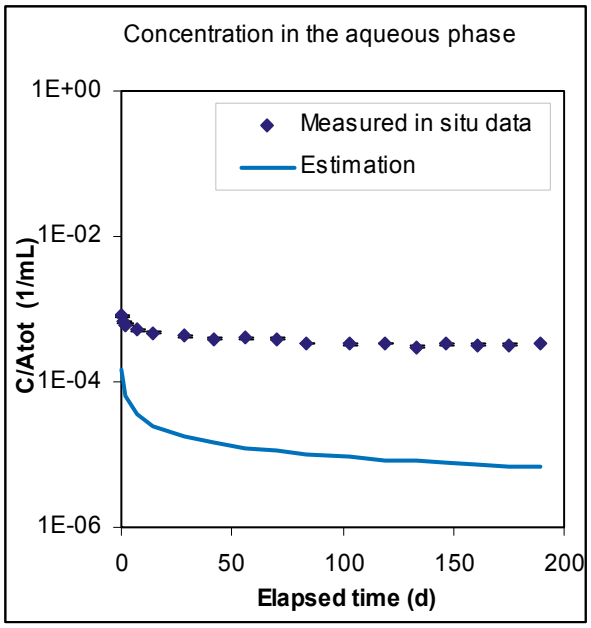

Figure Case 4. *Tracer: Cs-137. Core: A1.*

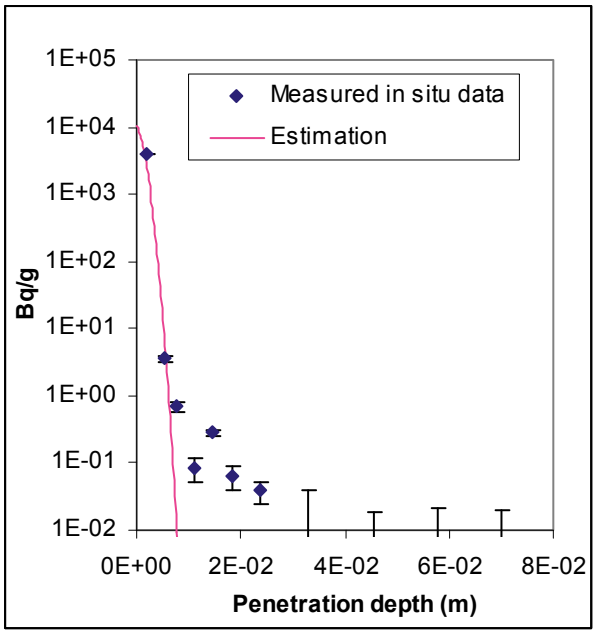

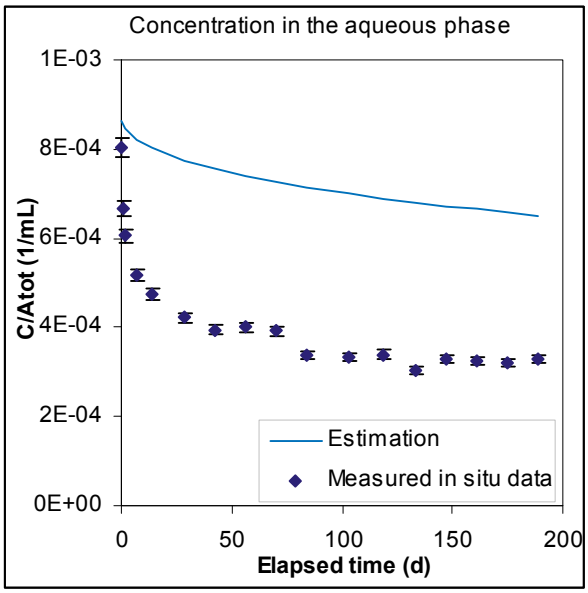

Figure Case 4. *Tracer: Cs-137. Core: A5.*

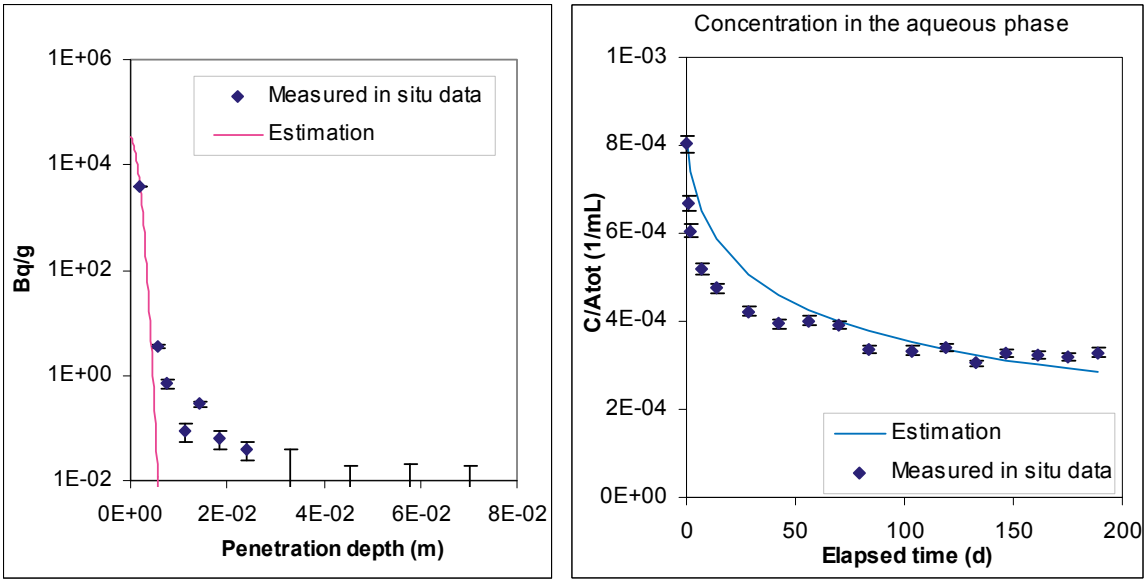

Figure Case 4. *Tracer: Cs-137. Core: A6.*

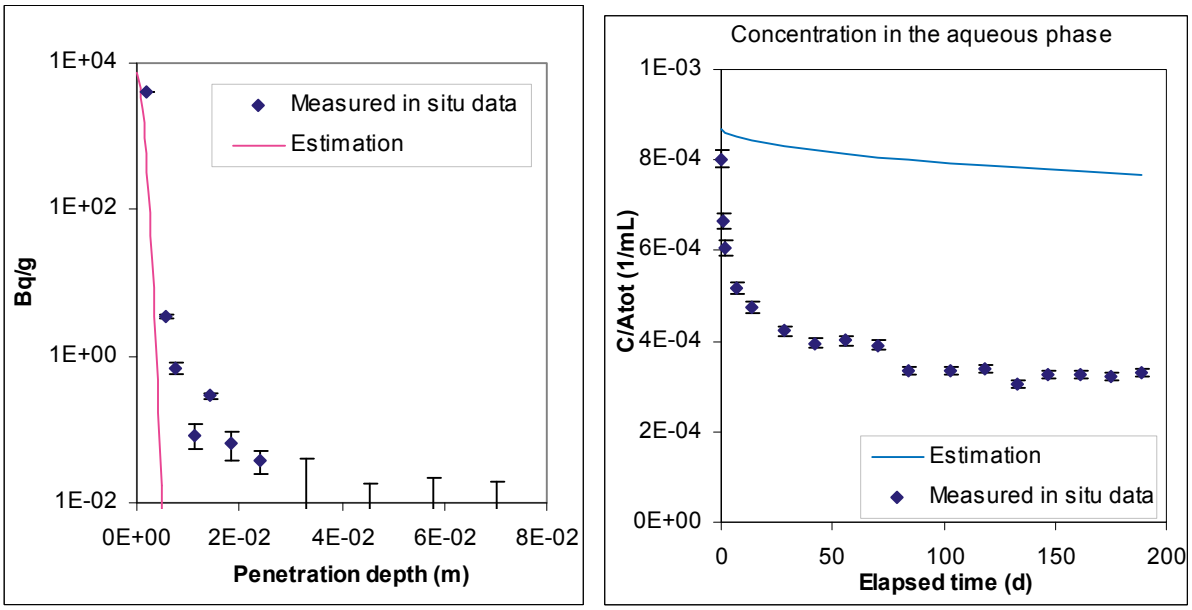

Figure Case 4. *Tracer: Cs-137. Core: A8.*

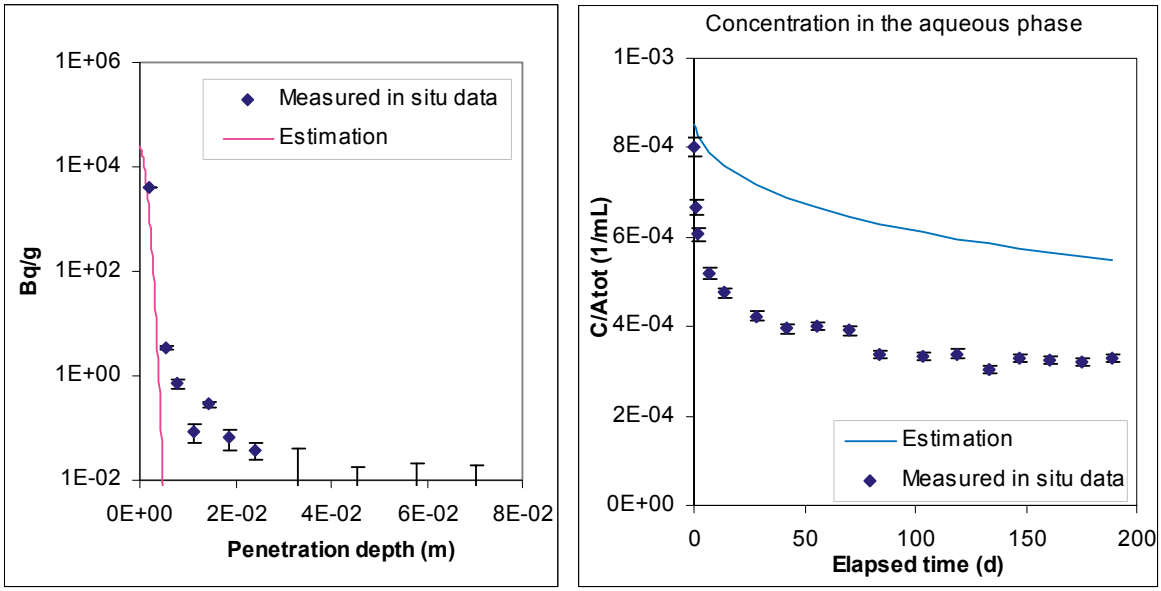

Figure Case 4. *Tracer: Cs-137. Core: A9.*

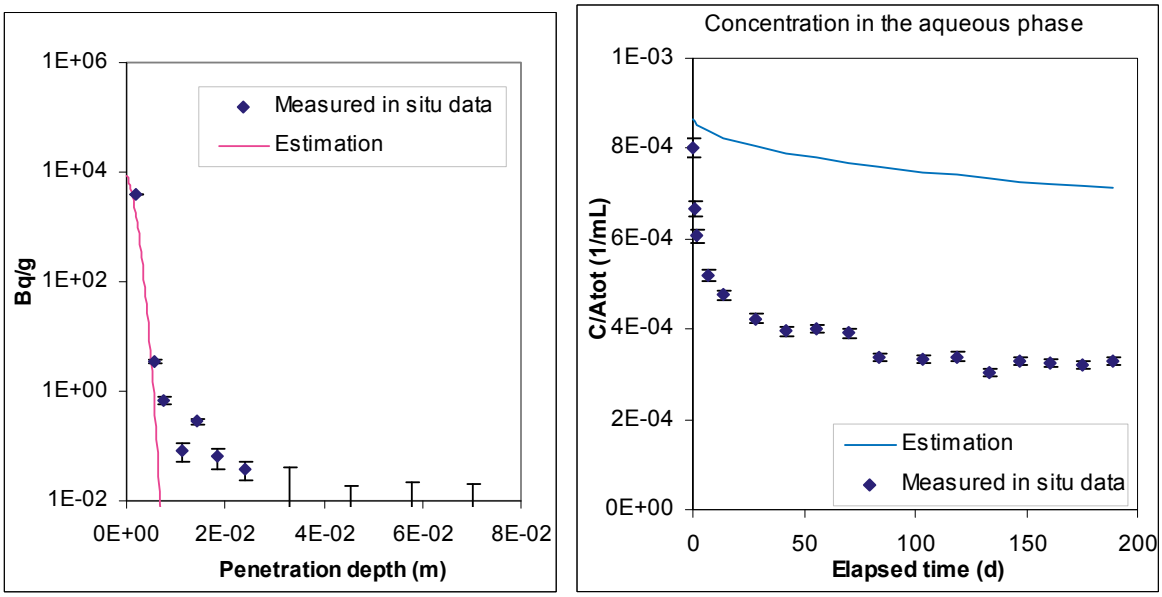

Figure Case 4. *Tracer: Cs-137. Core: A10.*

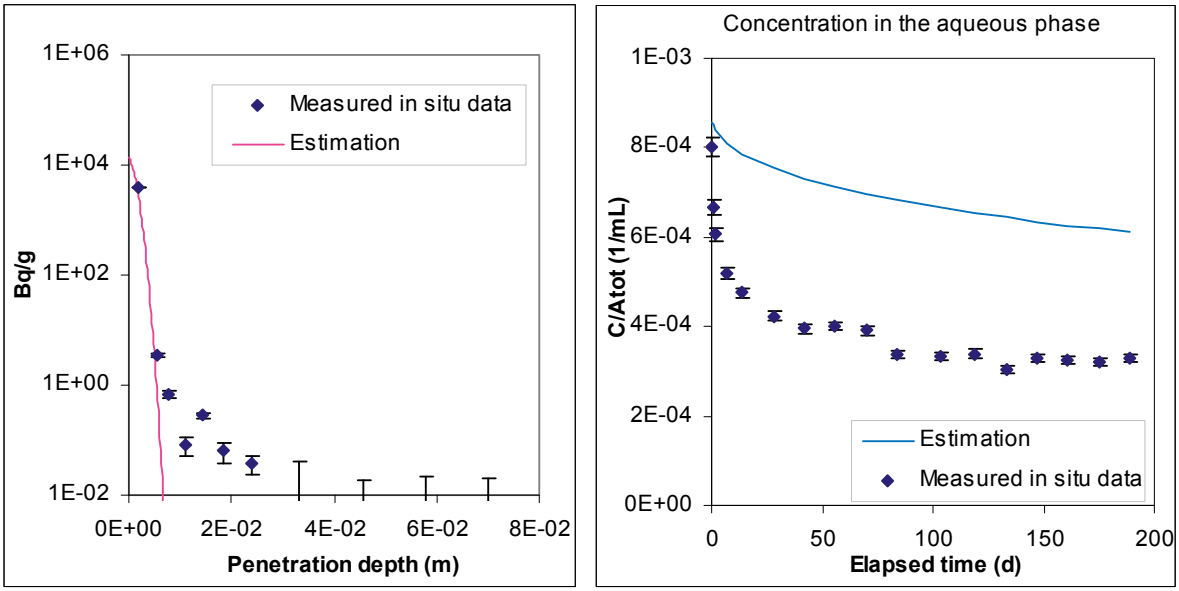

Figure Case 4. *Tracer: Cs-137. Core: A12.*

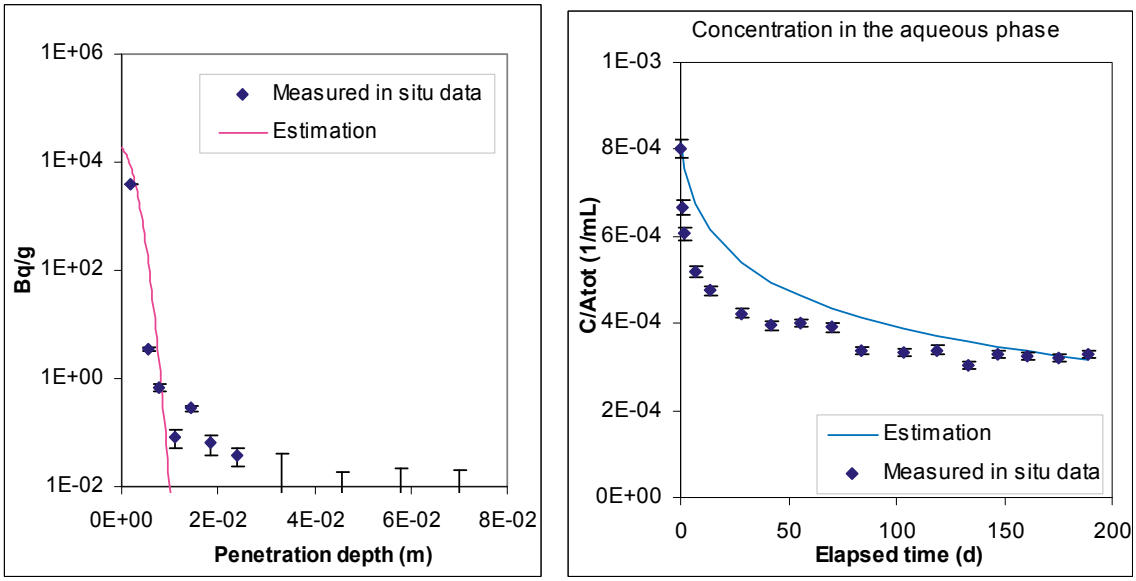

Figure Case 4. *Tracer: Cs-137. Core: A15.*

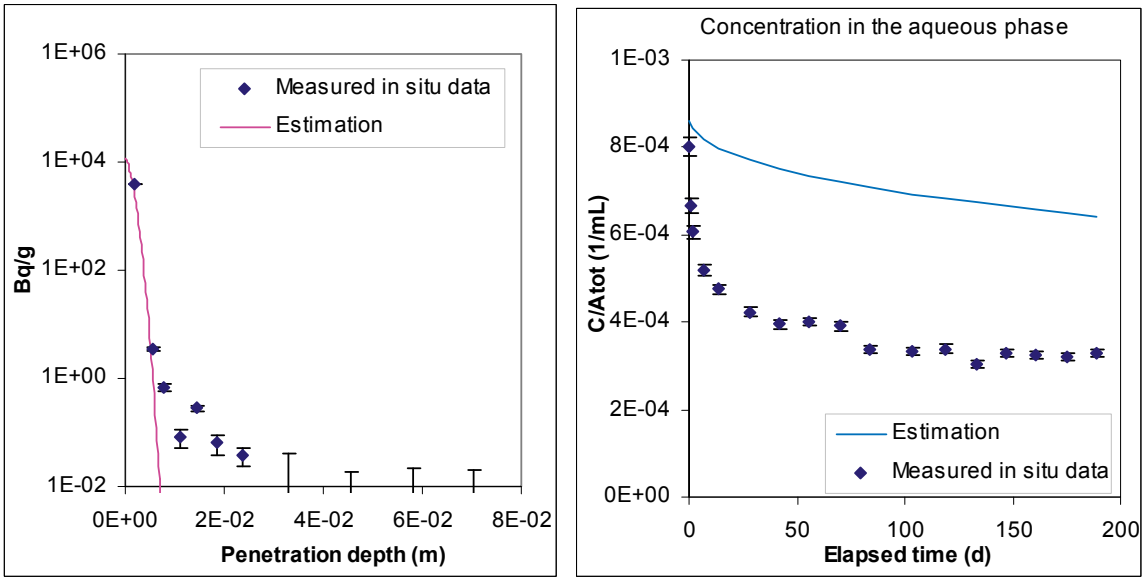

Figure Case 4. *Tracer: Cs-137. Core: A16.*

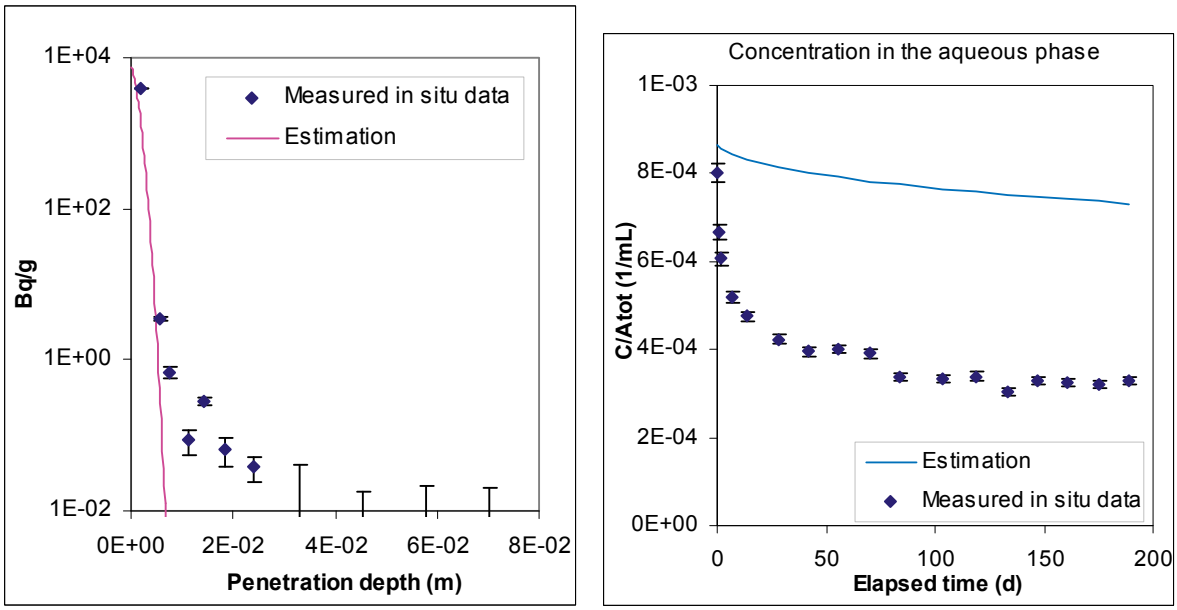

Figure Case 4. *Tracer: Cs-137. Core: A17.*

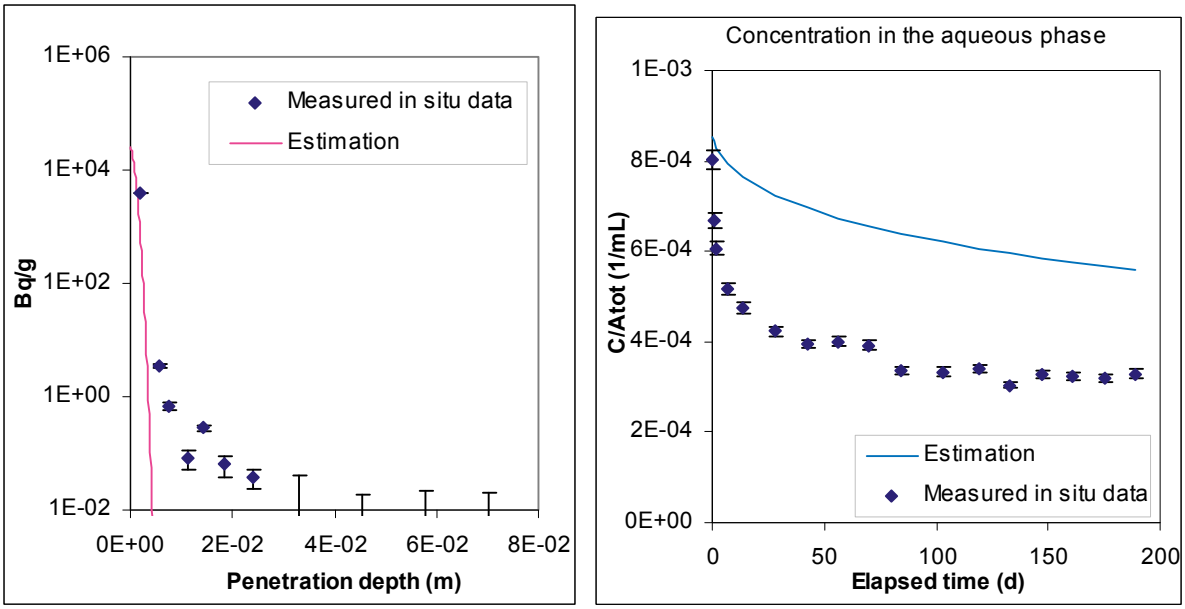

Figure Case 4. *Tracer: Cs-137. Core: D1.*

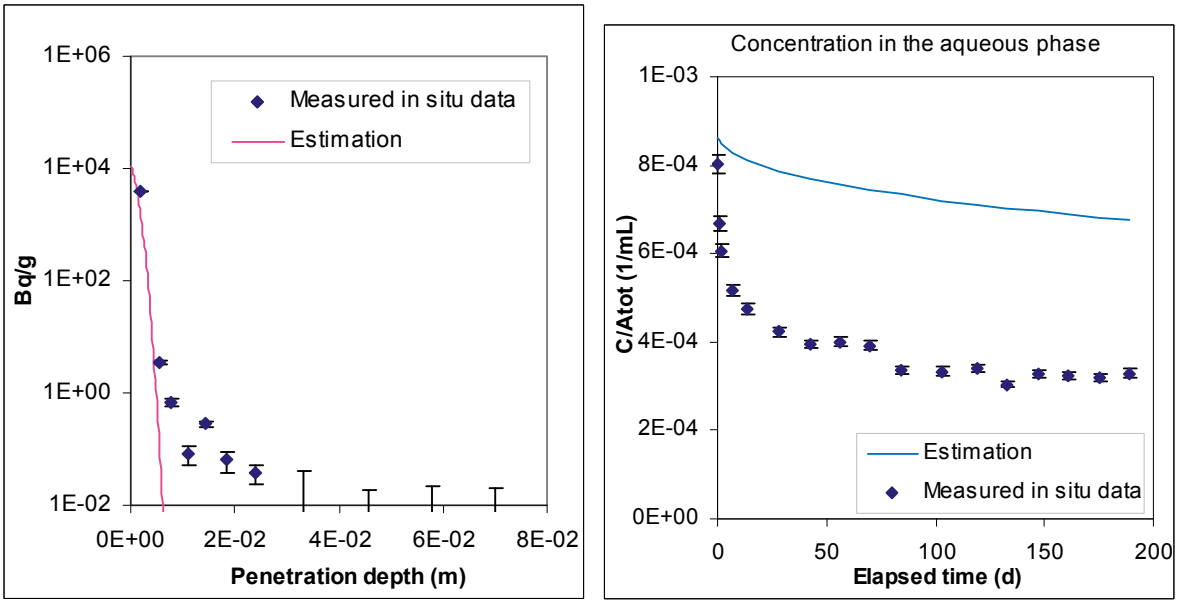

Figure Case 4. *Tracer: Cs-137. Core: D5.*

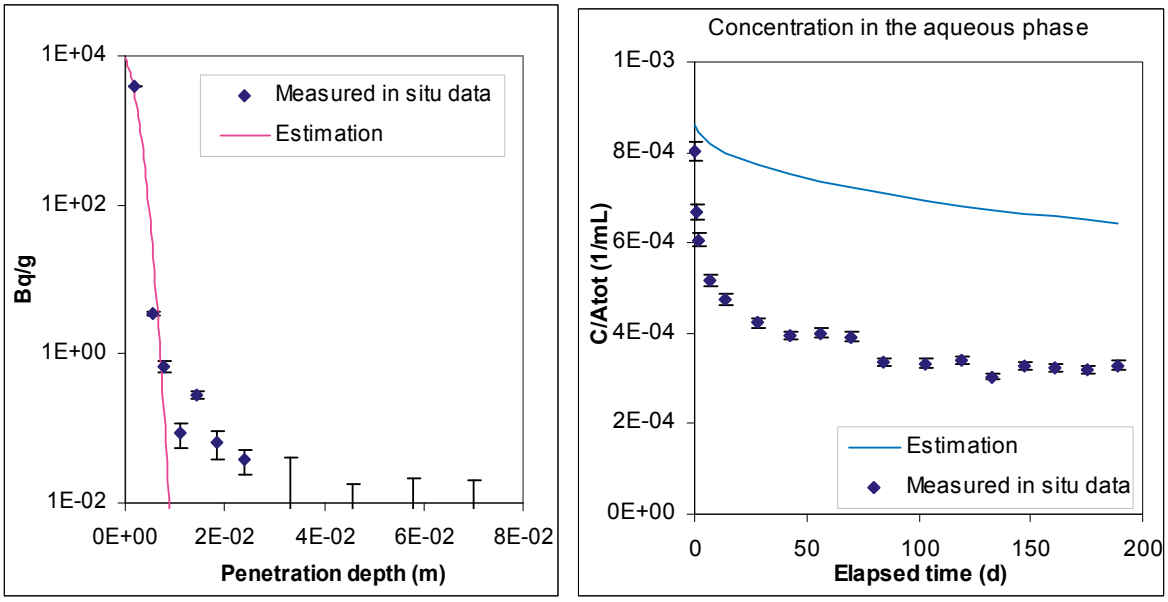

Figure Case 4. *Tracer: Cs-137. Core: D6.*

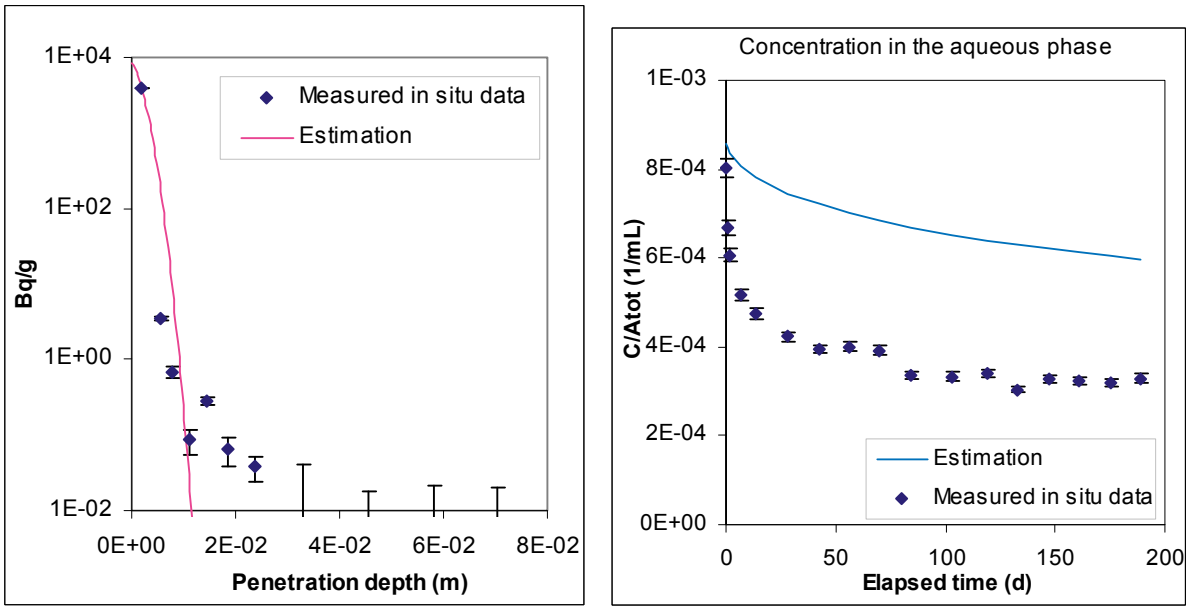

Figure Case 4. *Tracer: Cs-137. Core: D7.*

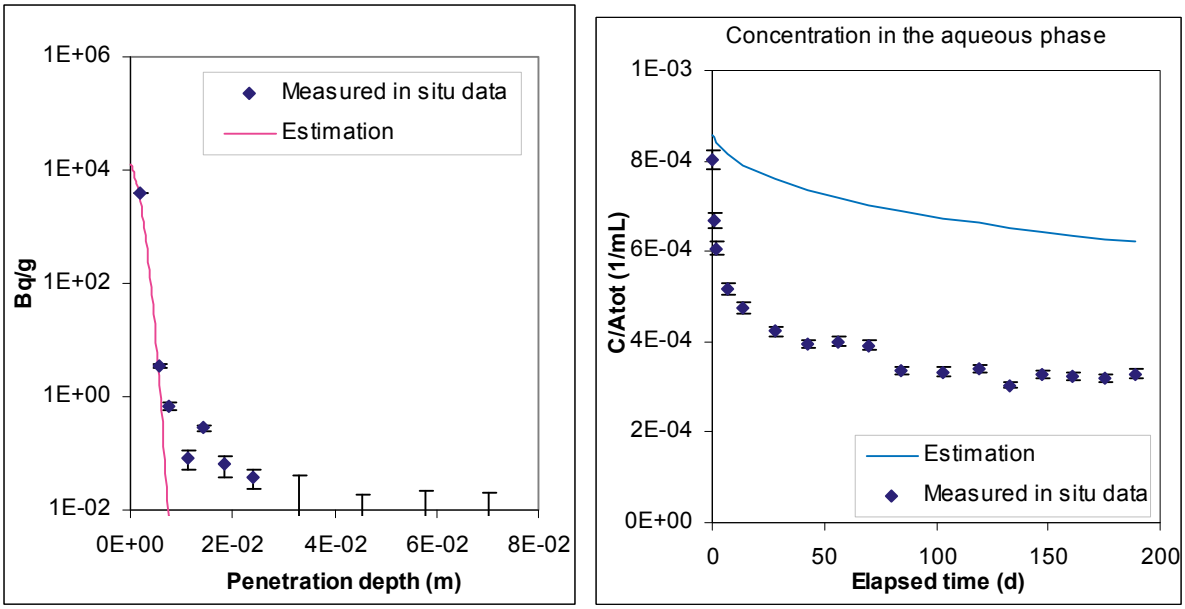

Figure Case 4. *Tracer: Cs-137. Core: D8.*

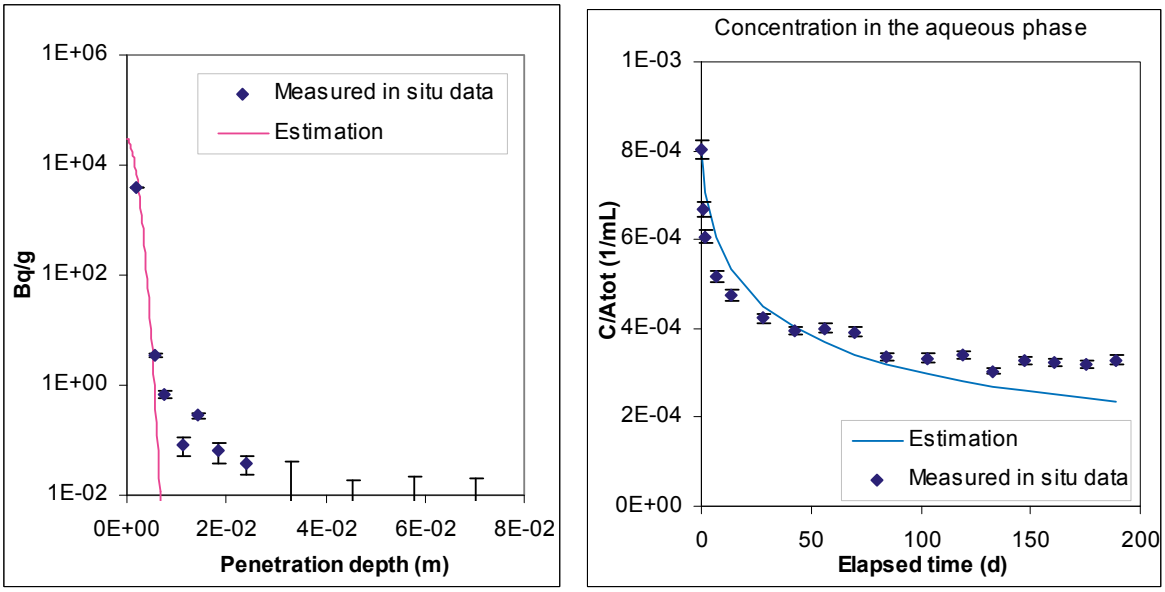

Figure Case 4. *Tracer: Cs-137. Core: D12.*

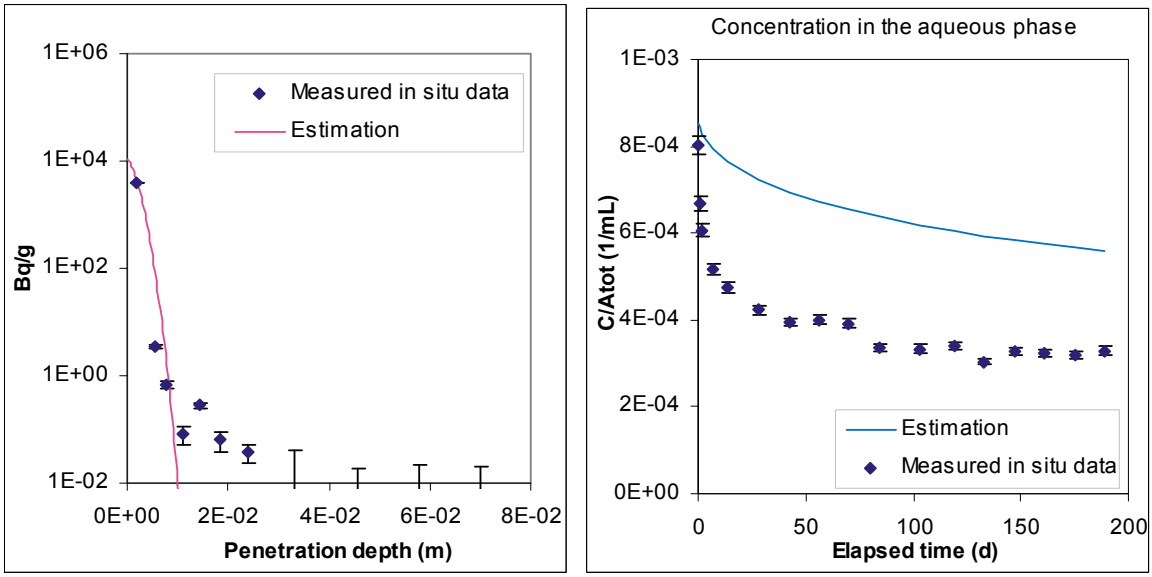

Figure Case 4. *Tracer: Cs-137. Core: D13.*

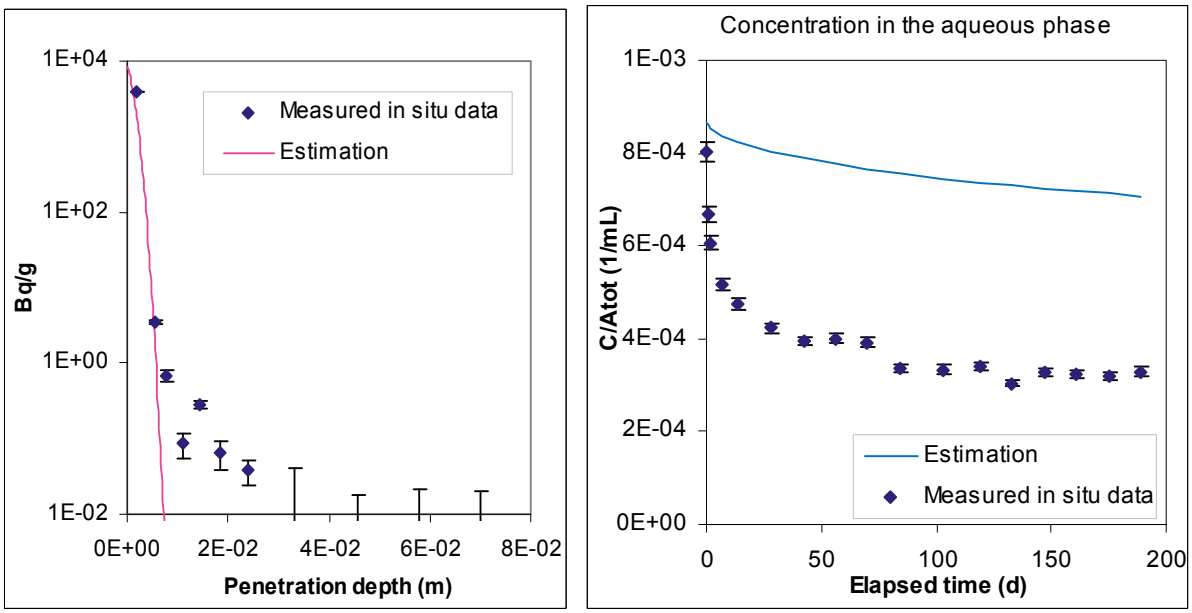

Figure Case 4. *Tracer: Cs-137. Core: D14.*

Co-57

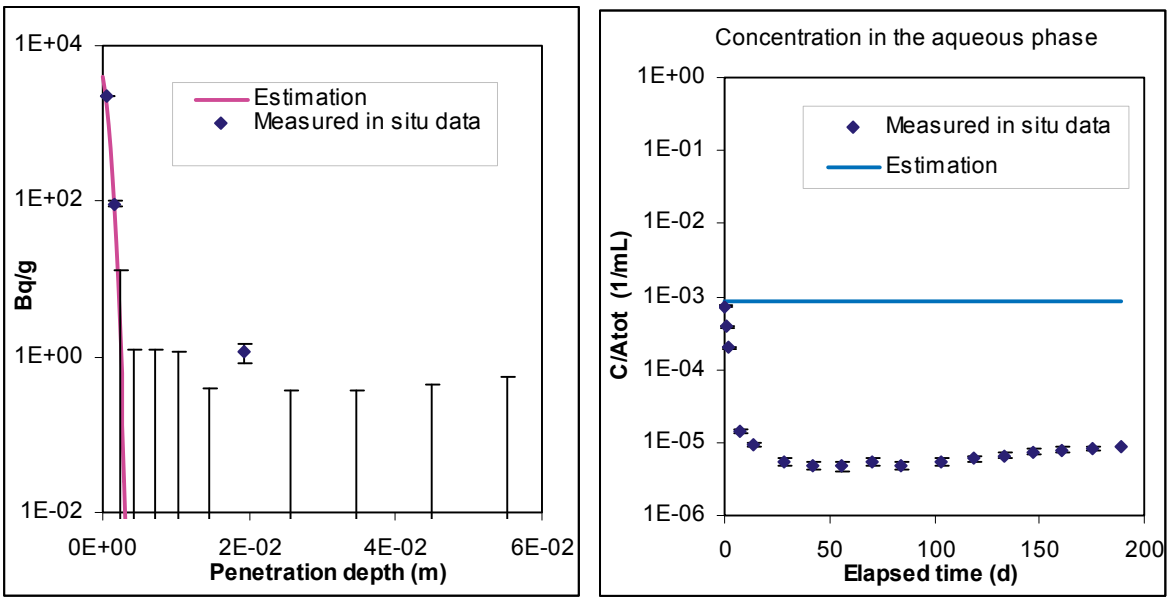

Figure Case 4. *Tracer: Co-57. Core: A6.*

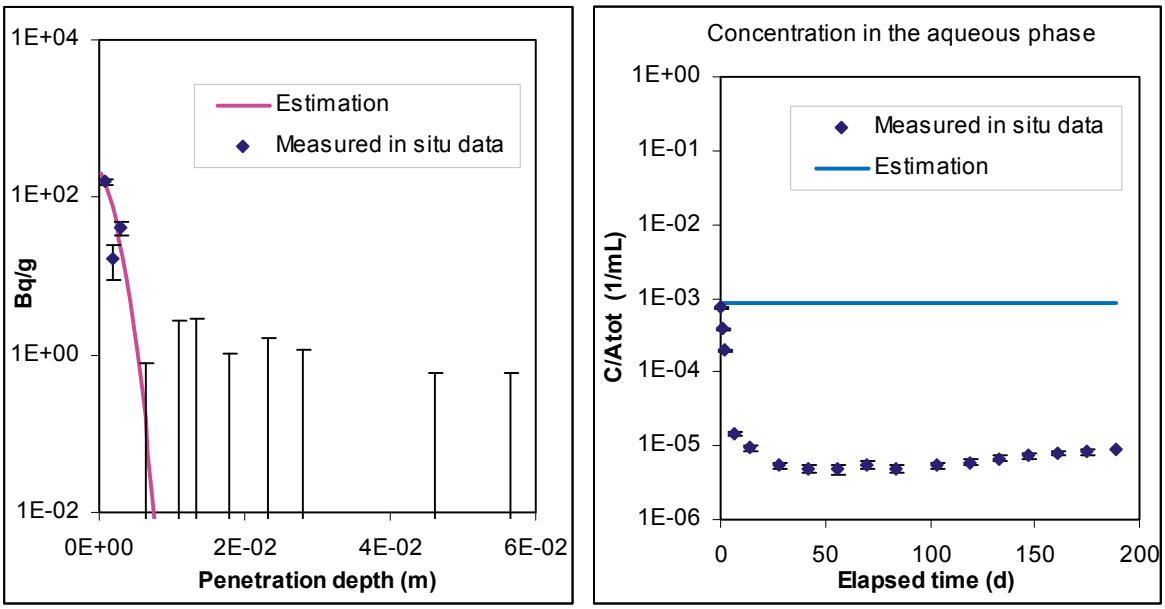

Figure Case 4. *Tracer: Co-57. Core: A8.*

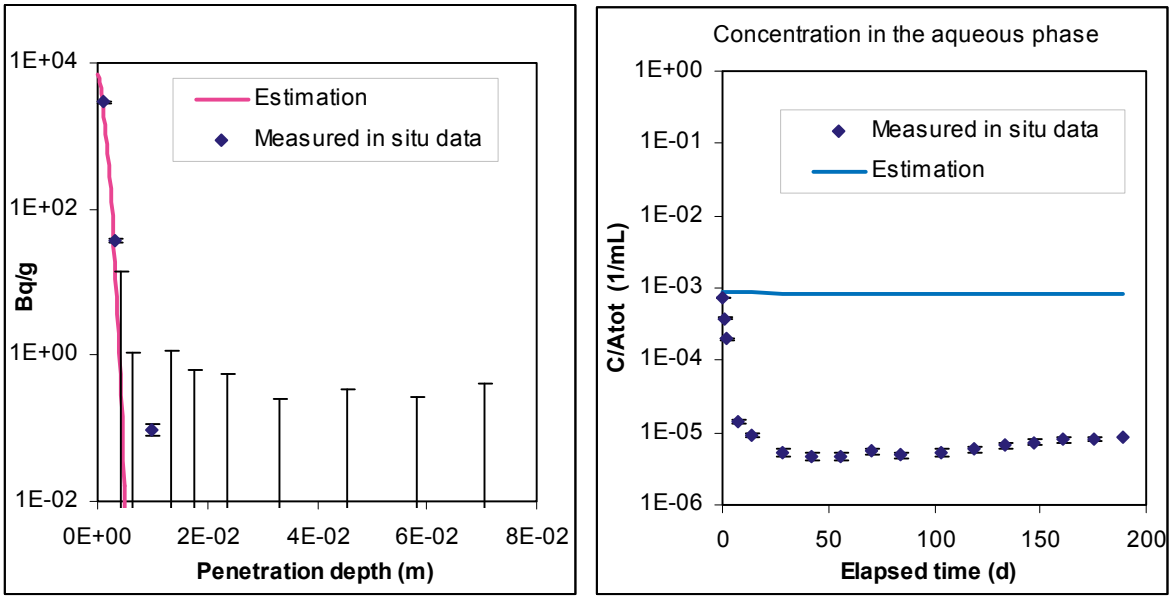

Figure Case 4. *Tracer: Co-57. Core: A12.*

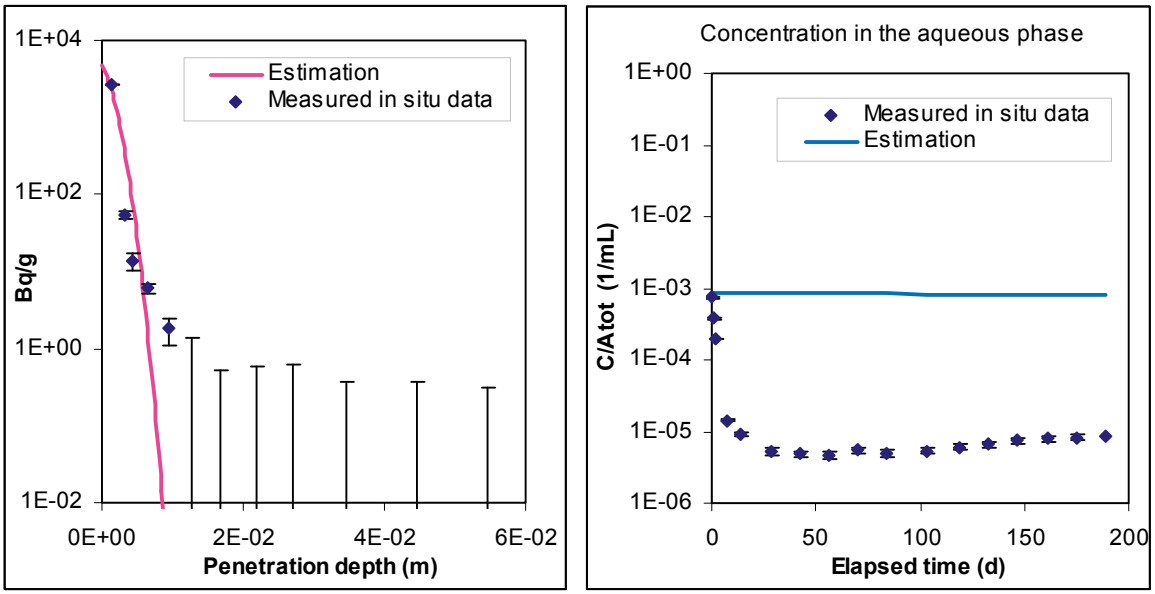

Figure Case 4. *Tracer: Co-57. Core: D7.*

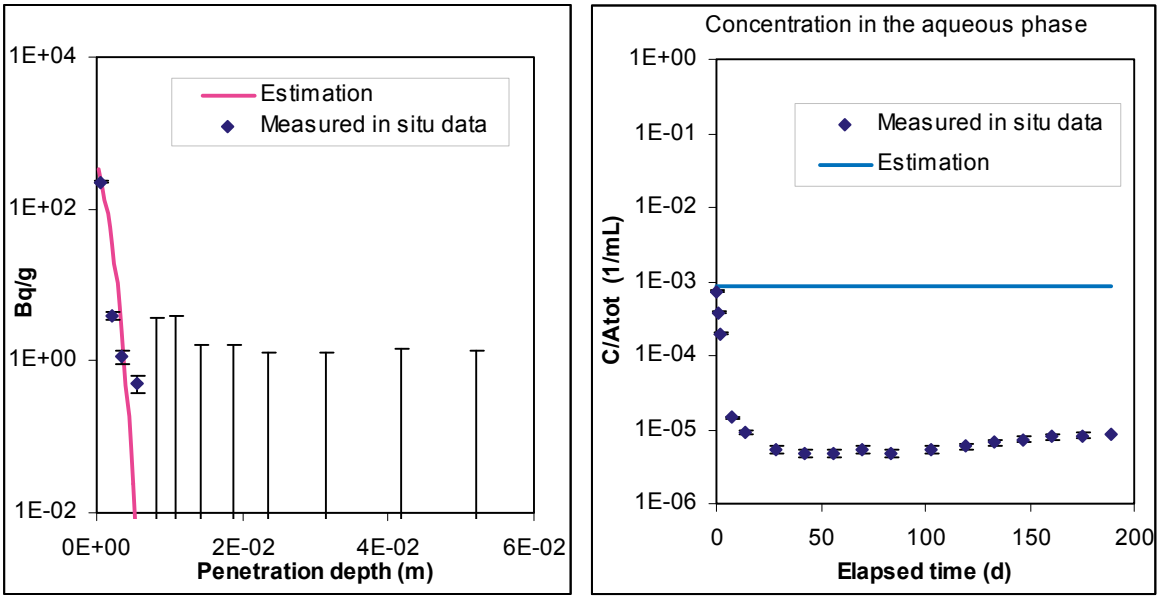

Figure Case 4. *Tracer: Co-57. Core: D12.*

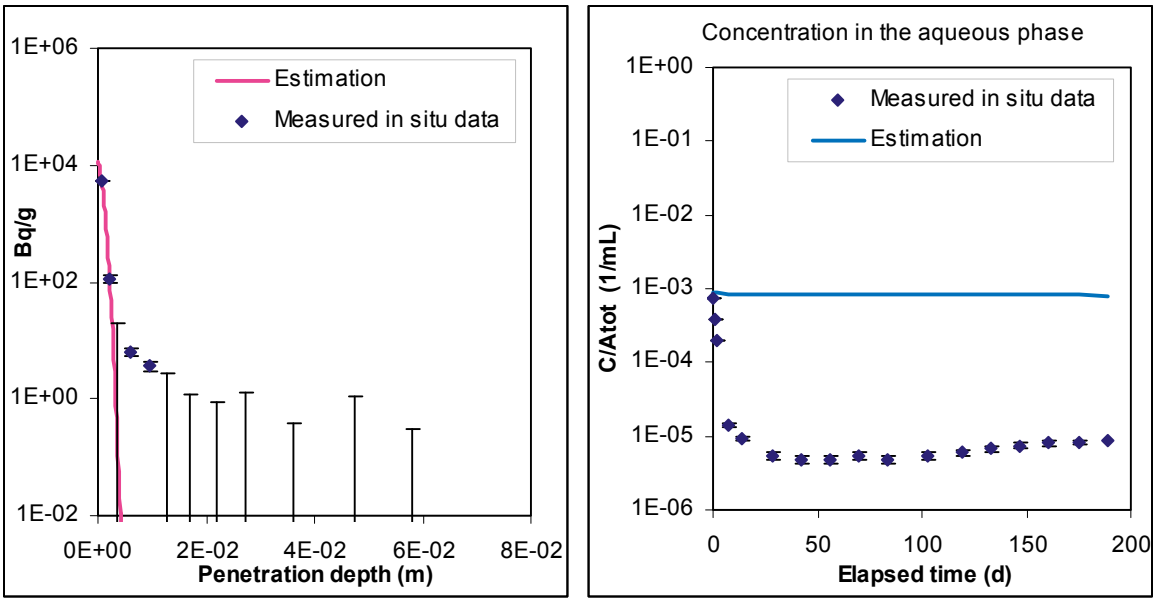

Figure Case 4. *Tracer: Co-57. Core: D14.*

Cd-109

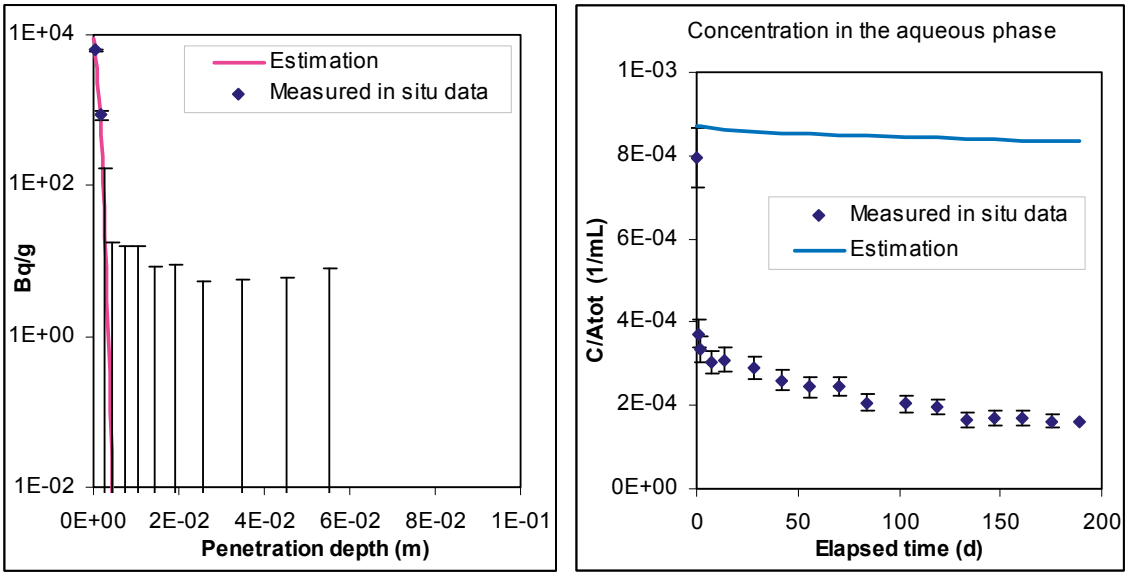

Figure Case 4. *Tracer: Cd-109. Core: A6.*

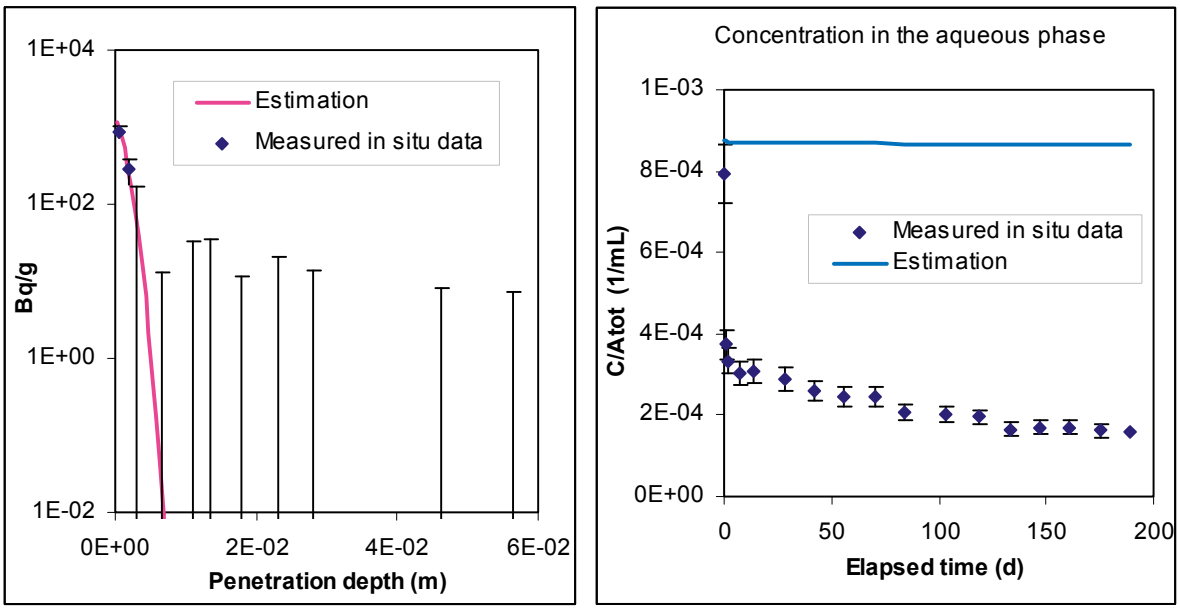

Figure Case 4. *Tracer: Cd-109. Core: A8.*

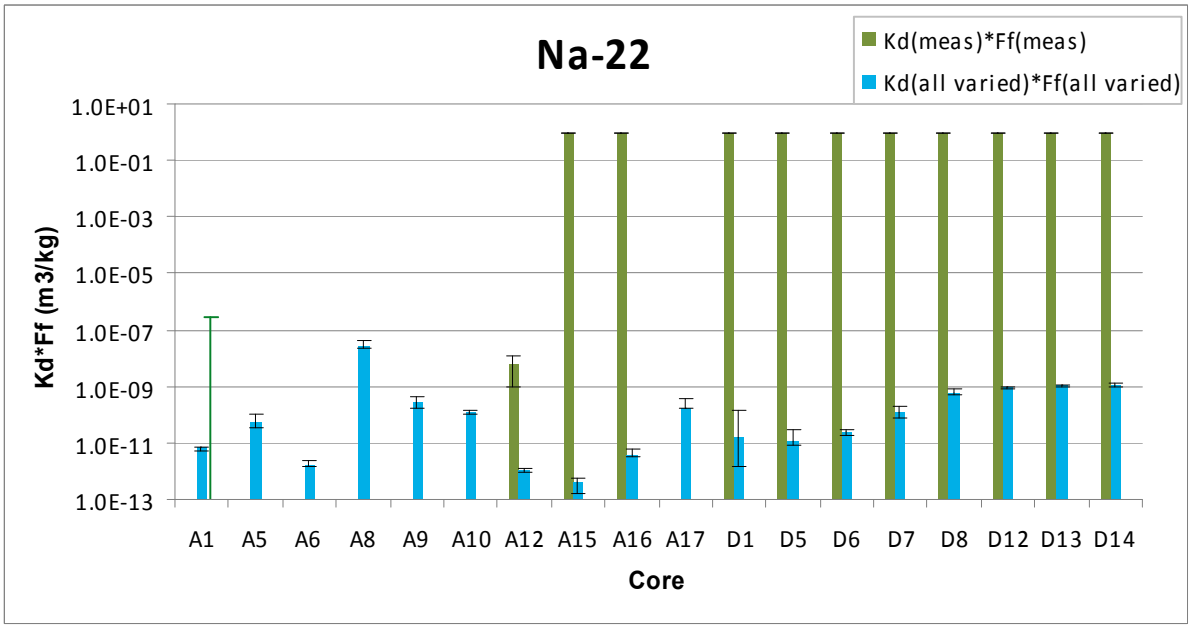

Figure Case 4. *The product K_d*F_f (m^3/kg) obtained from the estimation calculation where the parameters (K_d, F_f and ε) all were fitted to the penetration curve. For the fracture coated A-cores only a highest value could be obtained from measured data. This is indicated in the figure with only a thin green error bar. Hence, no colored staple bars is given.*

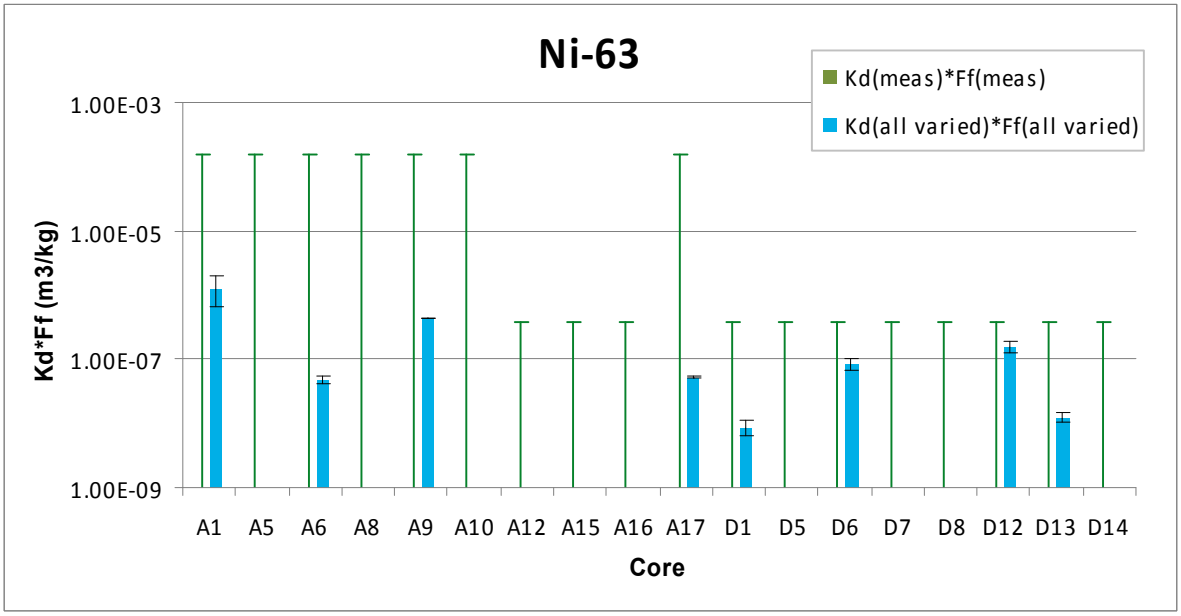

Figure Case 4. *The product K_d*F_f (m^3/kg) obtained from the estimation calculation where the parameters (K_d, F_f and ε) all were fitted to the penetration curve. For both the fracture coated A-cores and the matrix rock only a highest value could be obtained from measured data. This is indicated in the figure with only a thin green error bar for both materials. Hence, no colored staple barrs are given.*

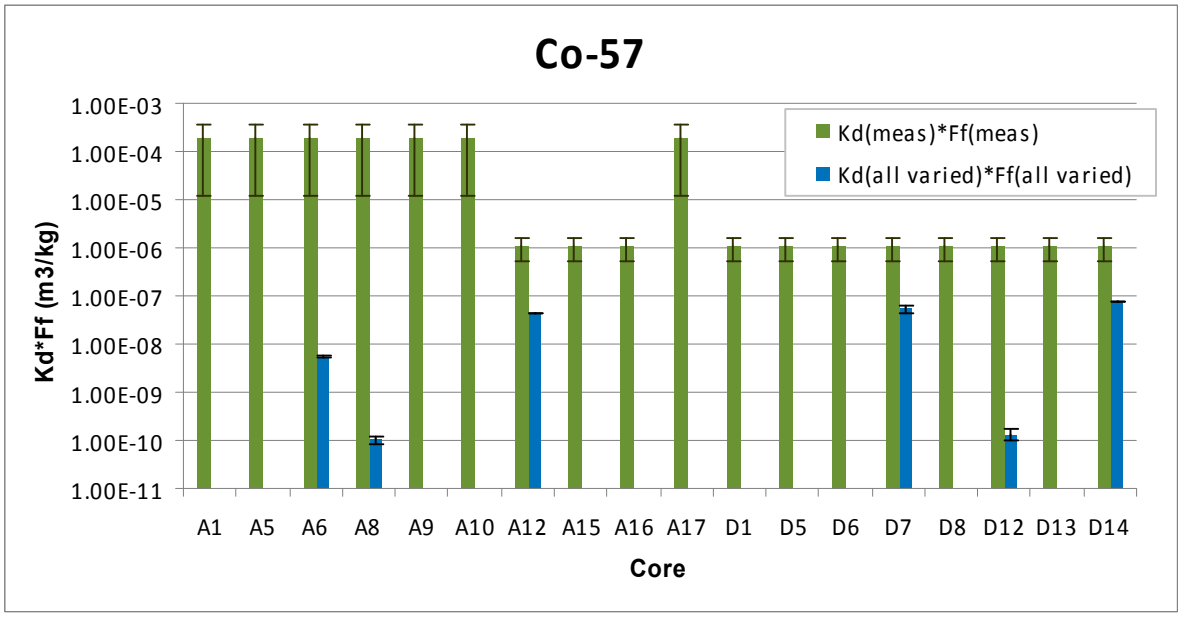

Figure Case 4. *The product K_d*F_f (m^3/kg) obtained from the estimation calculation where the parameters (K_d, F_f and ε) all were fitted to the penetration curve.*

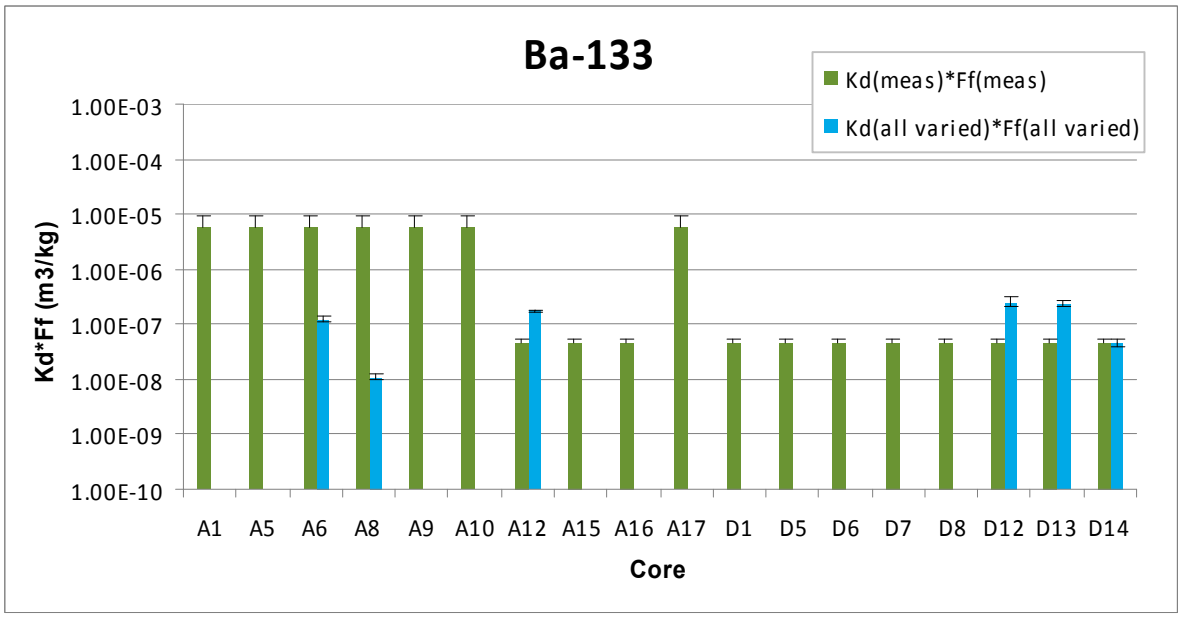

Figure Case 4. *The product K_d*F_f (m^3/kg) obtained from the estimation calculation where all parameters (K_d, F_f and ε) were fitted to the penetration curve.*

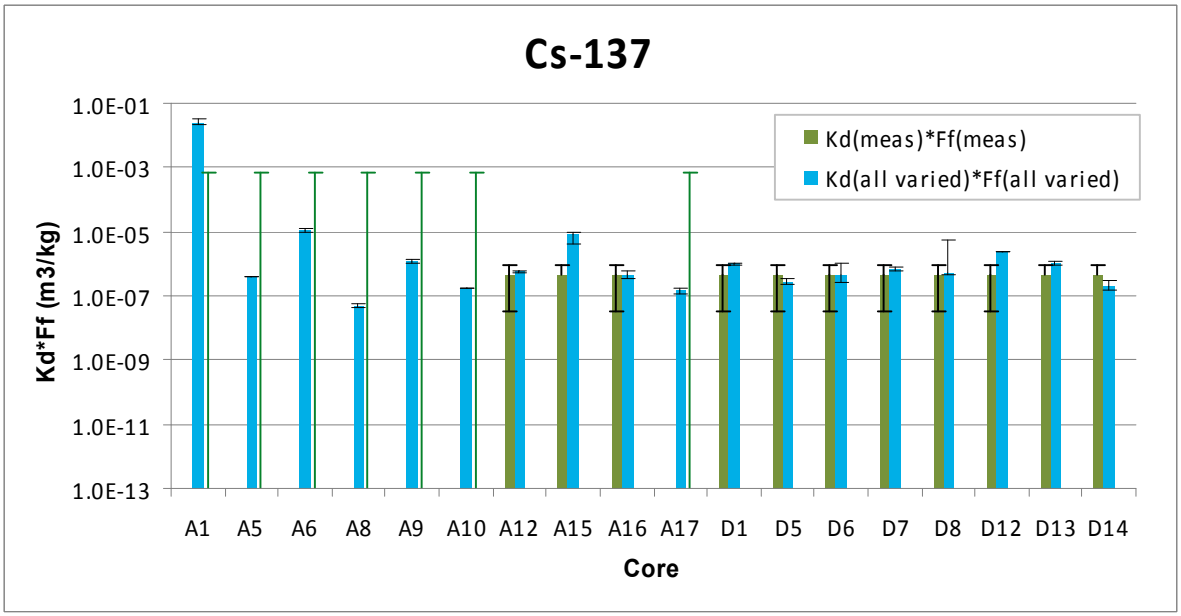

Figure Case 4. *The product K_d*F_f (m^3/kg) obtained from the estimation calculation where all parameters (K_d, F_f and ε) were fitted to the penetration curve. For the fracture coated A-cores only a highest value could be obtained from measured data. This is indicated in the figure with only a thin green error bar. Hence, no colored staple bars are given.*

Case 5

Results from modelling of Case 5 are presented in diagrams below. The object of Case 5 was to vary all the parameters K_d (m^3/kg), F_f and ε simultaneously in the diffusion model. As in data, both measured *in situ* penetration profile data and *in situ* aqueous concentration-time data were used. Figures 1 to 6 present the estimation results for Ni for the cores A1, A6, A8, D1, D12 and D13.

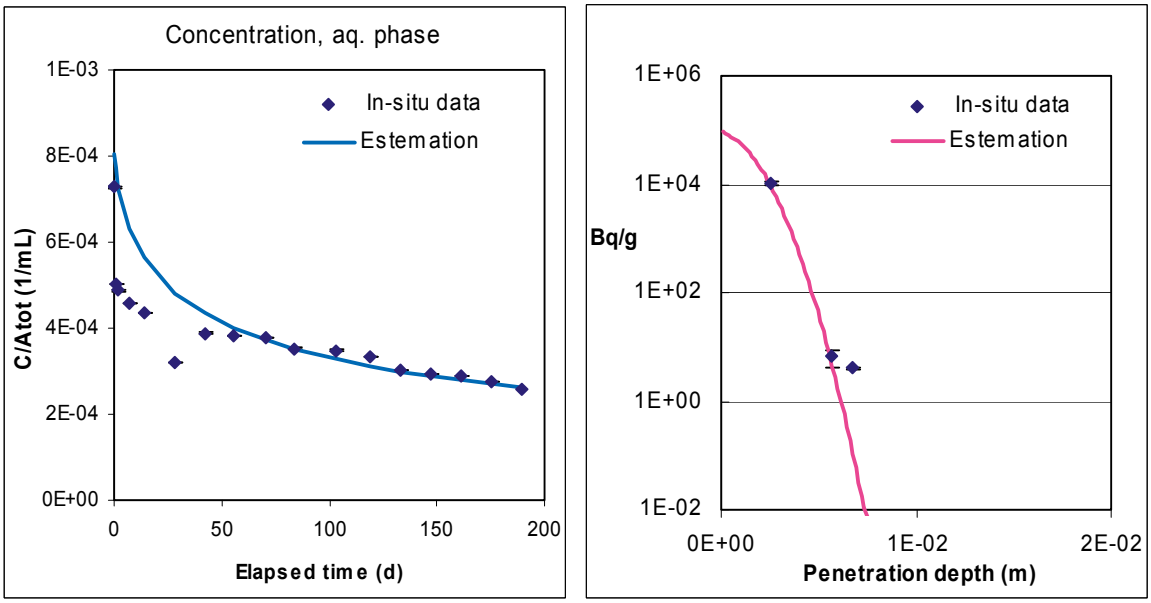

Figure 1. *Estimation of K_d, F_f and ε using both penetration profile and aqueous concentration-time data in the fitting procedure. Tracer: Ni. Core: A1.*

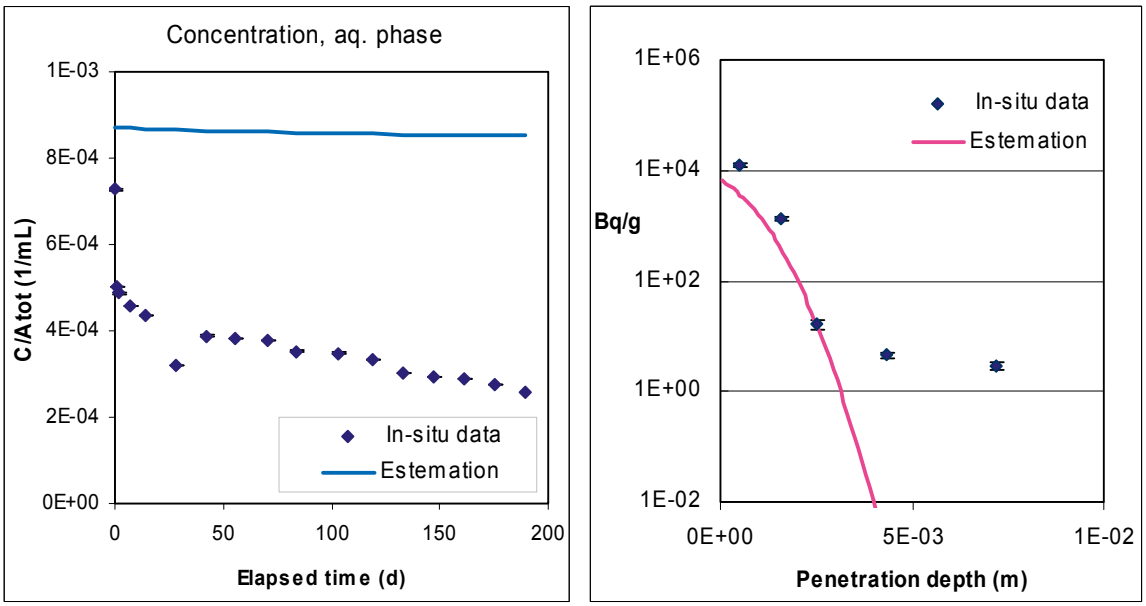

Figure 2. *Estimation of K_d, F_f and ε using both penetration profile and aqueous concentration-time data in the fitting procedure. Tracer: Ni. Core: A6.*

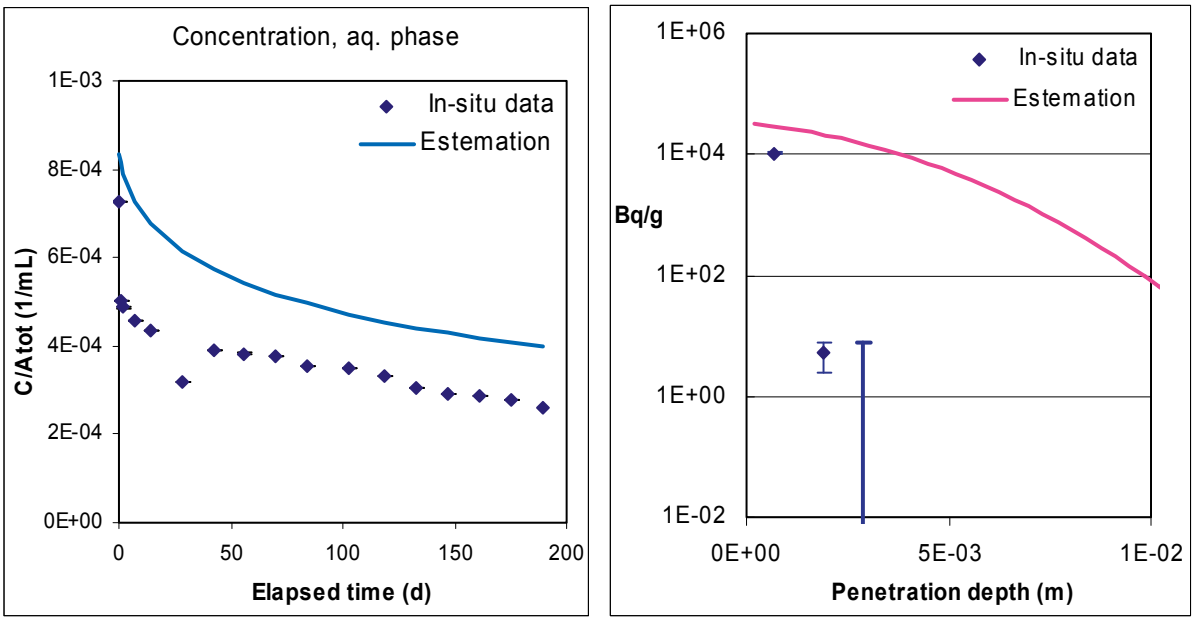

Figure 3. *Estimation of K_d, F_f and ε using both penetration profile and aqueous concentration-time data in the fitting procedure. In the penetration profile diagram (right), at approximately 2.5 mm, the measured data point is presented by an error bars, corresponding to the detection limit. Tracer: Ni. Core: A8.*

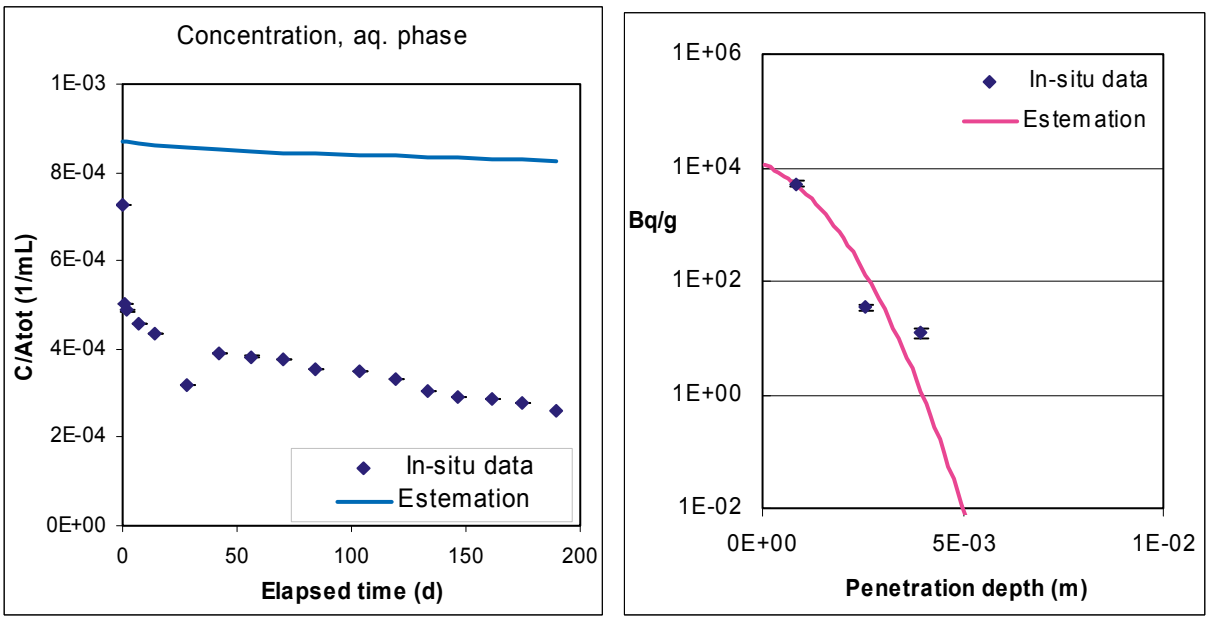

Figure 4. *Estimation of K_d, F_f and ε using both penetration profile and aqueous concentration-time data in the fitting procedure. Tracer: Ni. Core: D1.*

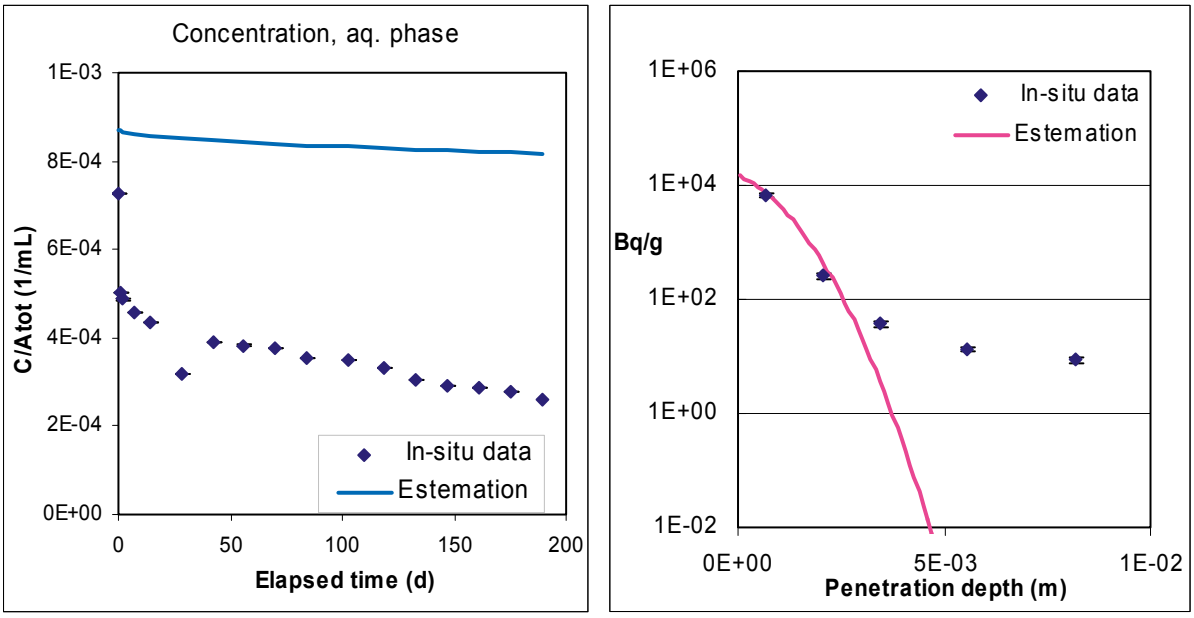

Figure 5. *Estimation of K_d, F_f and ε using both penetration profile and aqueous concentration-time data in the fitting procedure. Tracer: Ni. Core: D12.*

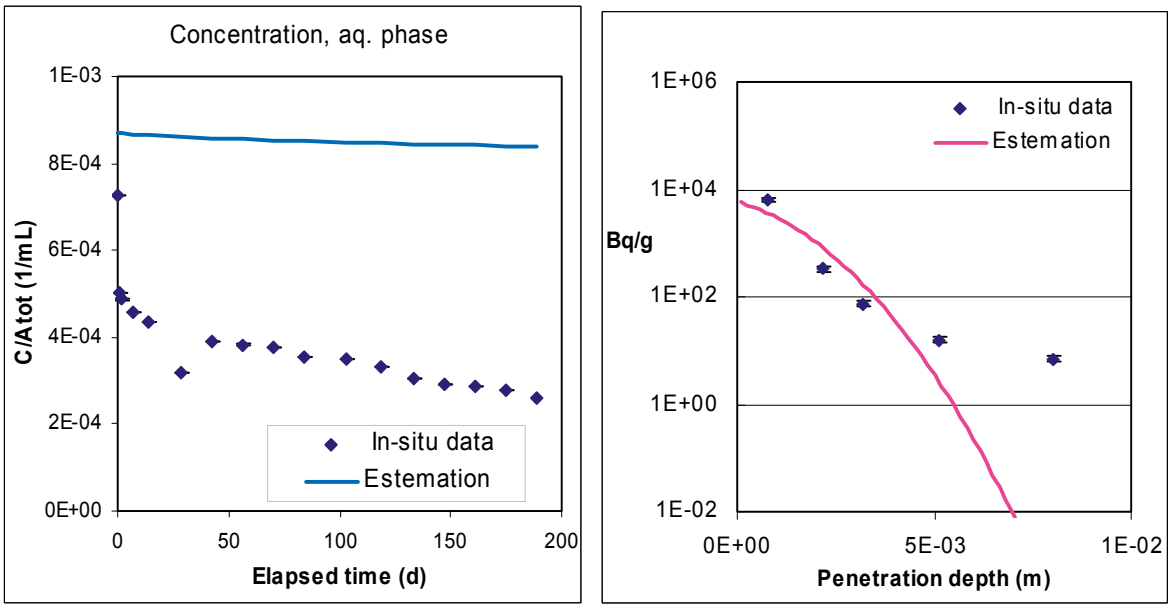

Figure 6. *Estimation of K_d, F_f and ε using both penetration profile and aqueous concentration-time data in the fitting procedure. Tracer: Ni. Core: D13.*

Similarly, Figures 7 to 12 present the estimation results made for Cs for the cores A1, A6, A8, D1, D12 and D13.

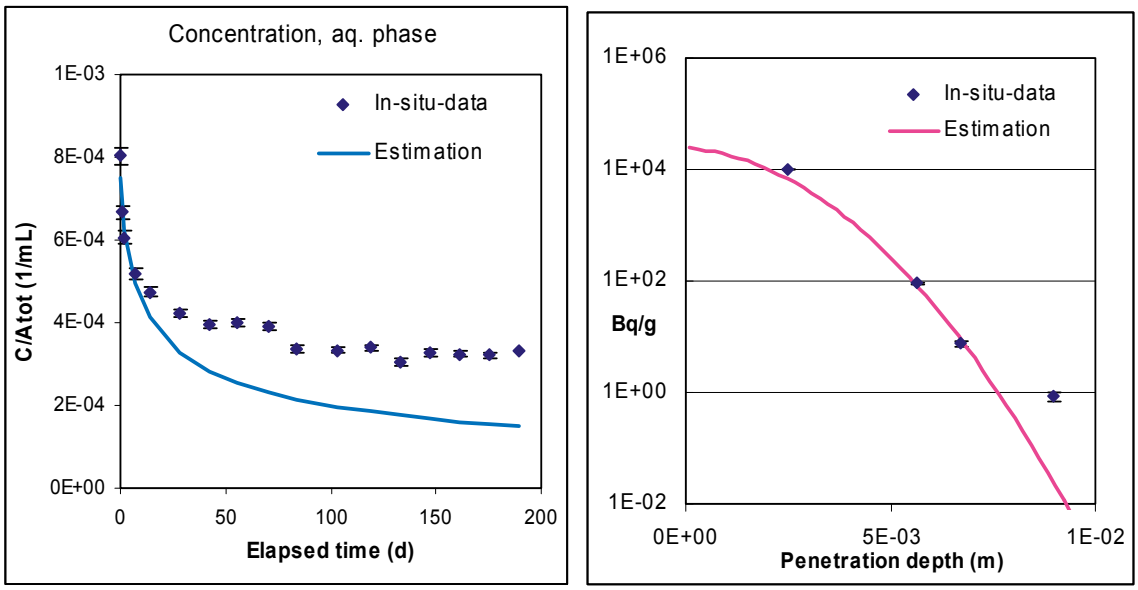

Figure 7. *Estimation of K_d, F_f and ε using both penetration profile and aqueous concentration-time data in the fitting procedure. Tracer: Cs. Core: A1.*

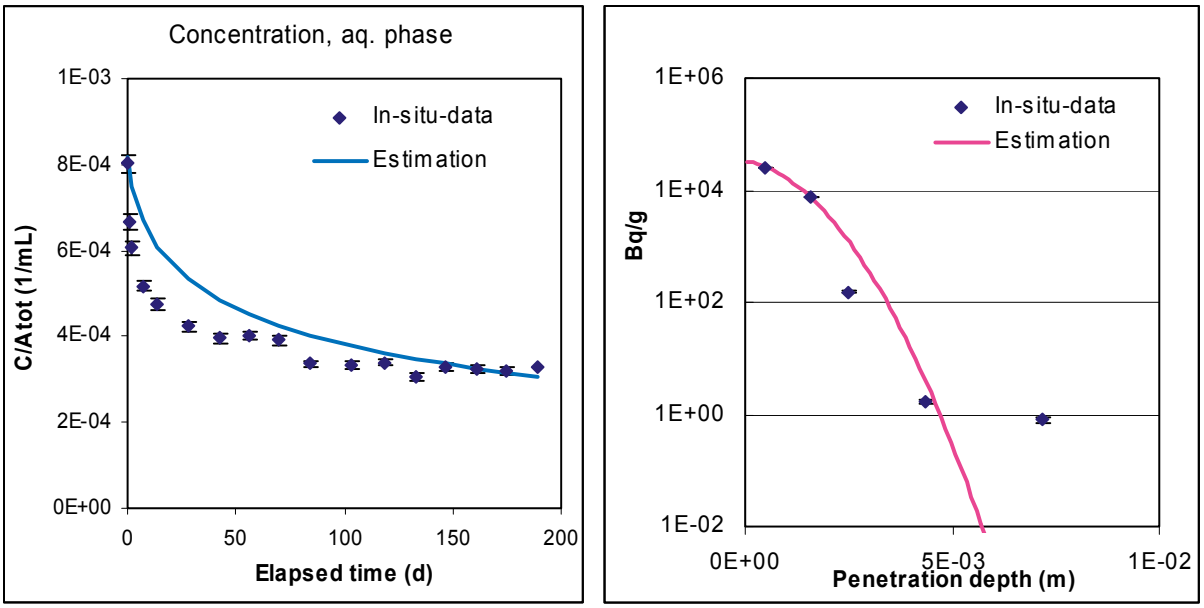

Figure 8. *Estimation of K_d, F_f and ε using both penetration profile and aqueous concentration-time data in the fitting procedure. Tracer: Cs. Core: A6.*

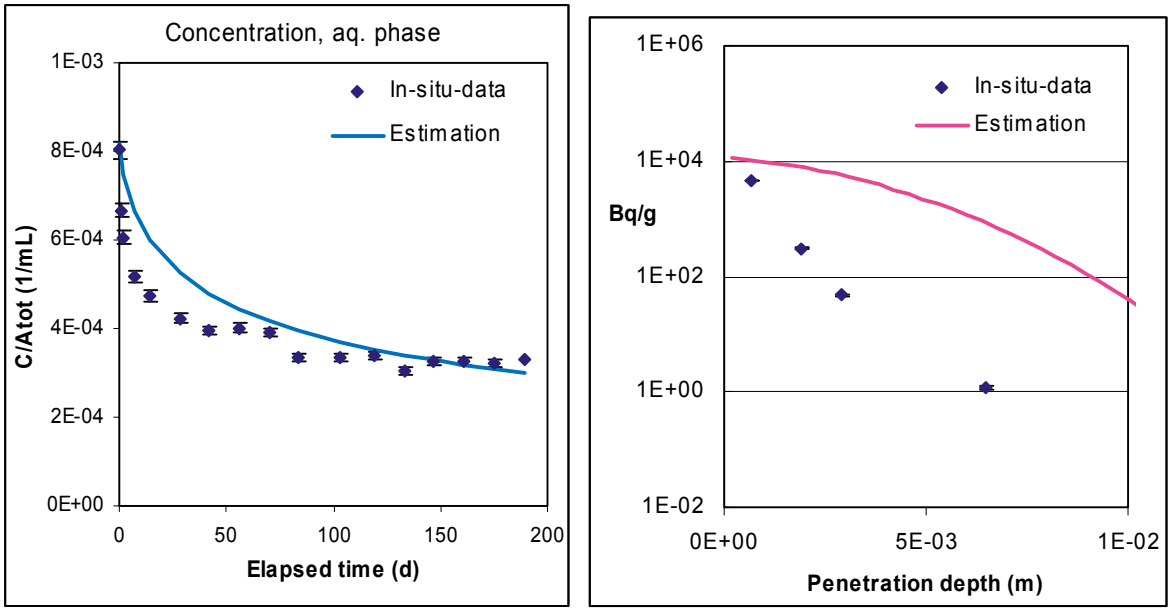

Figure 9. *Estimation of K_d, F_f and ε using both penetration profile and aqueous concentration-time data in the fitting procedure. Tracer: Cs. Core: A8.*

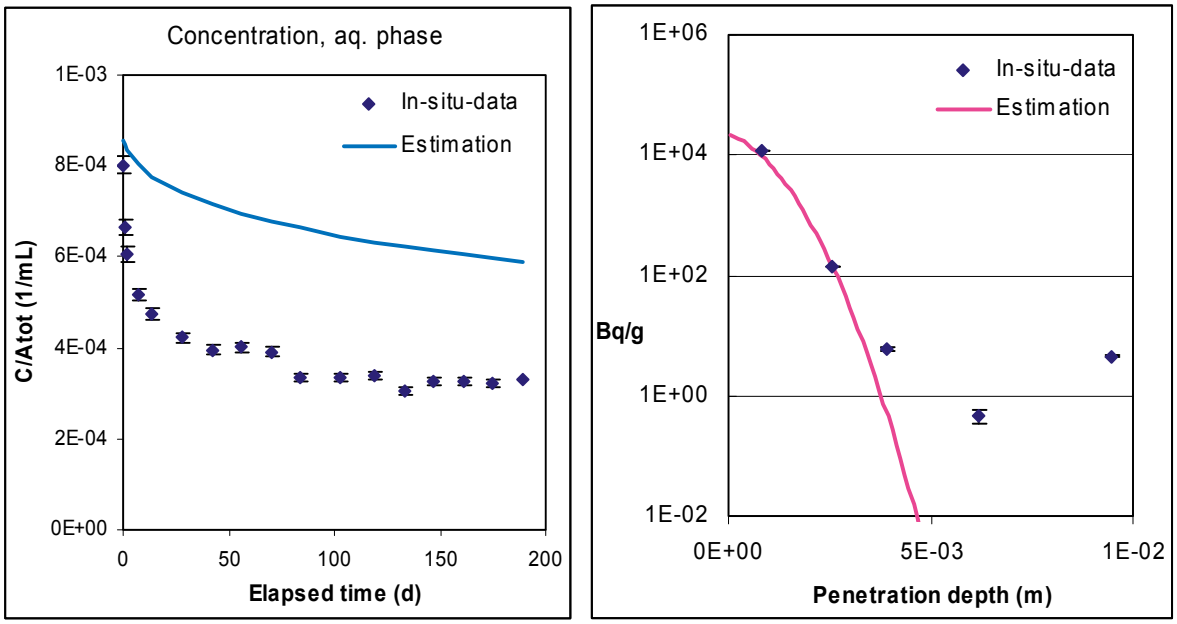

Figure 10. *Estimation of K_d, F_f and ε using both penetration profile and aqueous concentration-time data in the fitting procedure. Tracer: Cs. Core: D1.*

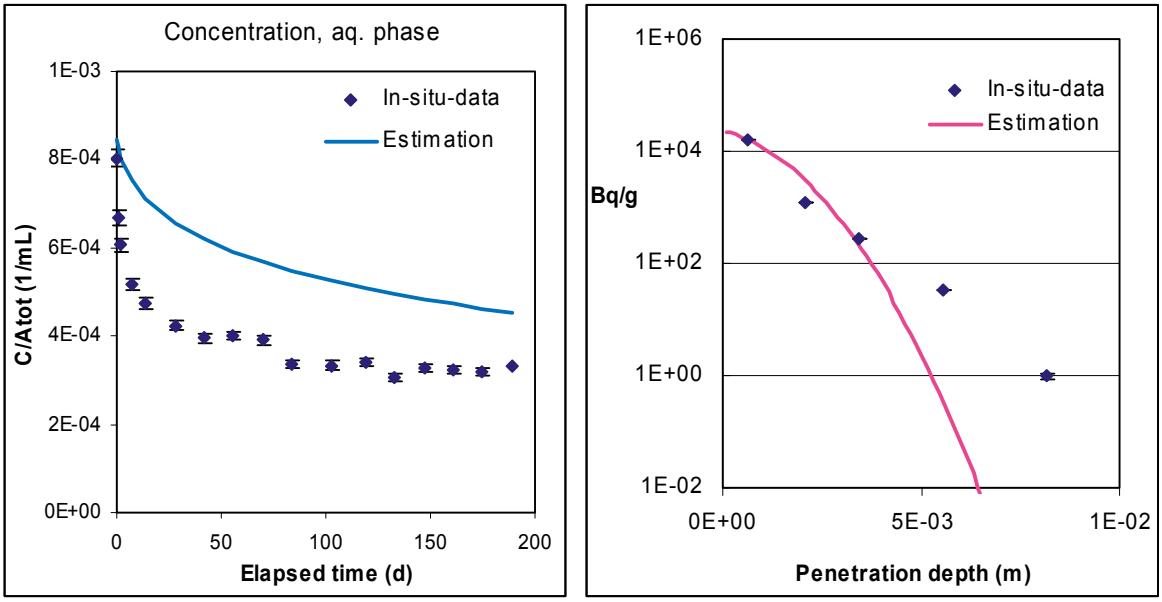

Figure 11. *Estimation of K_d, F_f and ε using both penetration profile and aqueous concentration-time data in the fitting procedure. Tracer: Cs. Core: D12.*

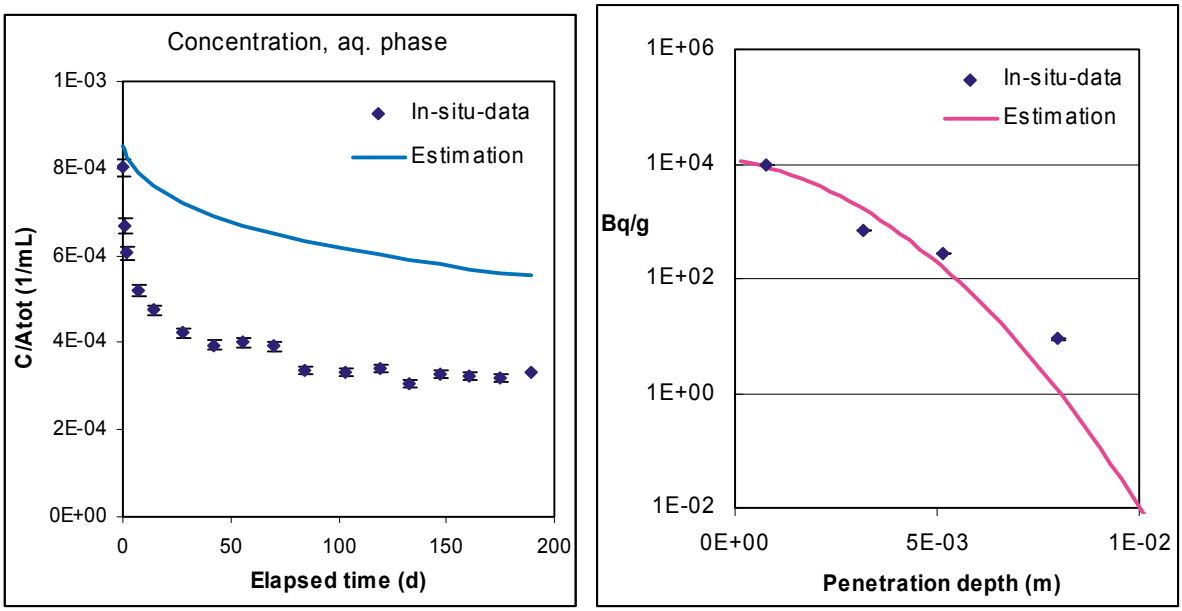

Figure 12. *Estimation of K_d, F_f and ε using both penetration profile and aqueous concentration-time data in the fitting procedure. Tracer: Cs. Core: D13.*

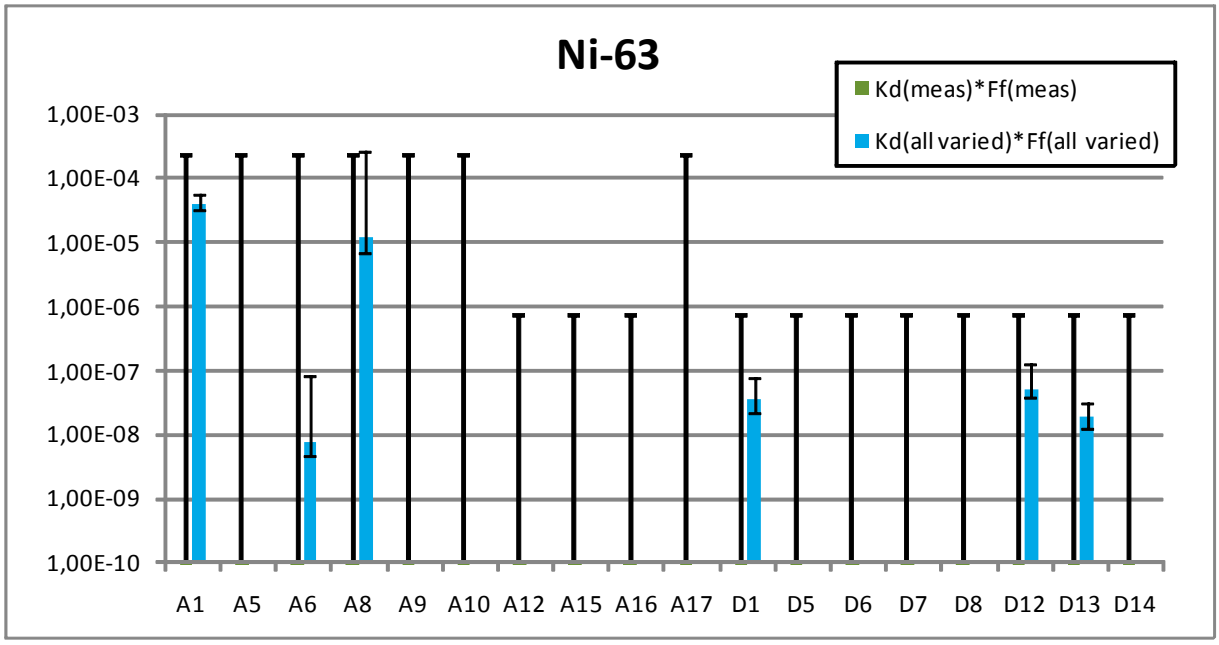

Figure Case 5. *The product K_d*F_f (m^3/kg) obtained from the estimation calculation where all parameters (K_d, F_f and ε) were fitted to both the penetration profile curve and the aqueous concentration-time data. For both the fracture coated A-cores and the matrix rock only a highest value could be obtained from measured data. This is indicated in the figure with only black error bars for both materials. Hence, no colored staple bars are given in these cases.*

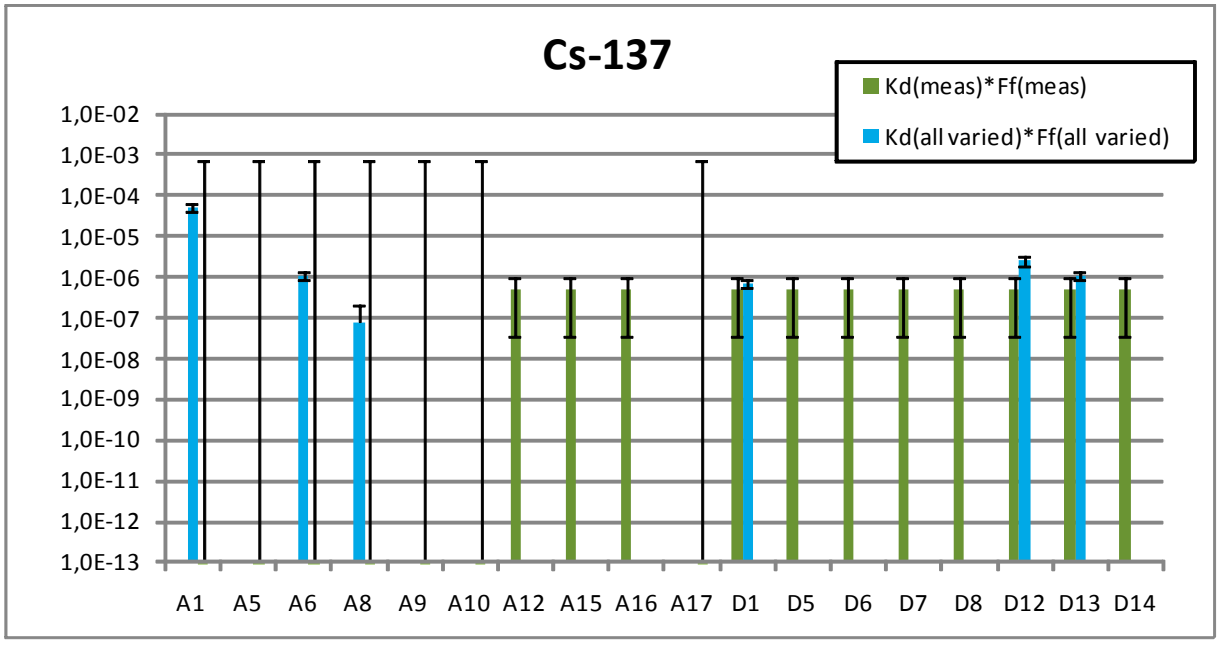

Figure Case 5. *The product K_d*F_f (m^3/kg) obtained from the estimation calculation where all parameters (K_d, F_f and ε) were fitted to both the penetration profile curve and the aqueous concentration-time data. For the fracture coated A-cores only a highest value could be obtained from measured data. This is indicated in the figure with black error bars. Hence, no colored staple bars are given.*

Appendix 10

Modelling data

Table Case 2. Estimated K_d (m^3/kg) obtained from the best fit to the *in situ* penetration profile data. The formation factor, F_f, and the porosity, ε, were held constant during the calculations.

Core	Na-22			Ni-63			Ba-133			Cs-137		
	K_d (m^3/kg)	+	–	K_d (m^3/kg)	+	–	K_d (m^3/kg)	+	–	K_d (m^3/kg)	+	–
A1	<1.4E–05			1.5E–03	2.0E–04	1.8E–04				5.6E–03	3.4E–03	2.7E–03
A5	<1.7E–05			No data						1.2E–03	8.4E–05	7.7E–05
A6	<9.7E–06			8.8E–03	2.6E–03	2.2E–03	9.5E–04	5.5E–04	5.2E–04	9.4E–03	2.1E–03	1.7E–03
A8	7.0E–05	2.9E–04	6.2E–05	9.8E–03	2.8E–03	3.0E–03	1.3E–04	9.0E–05	5.3E–05	7.1E–04	1.0E–03	3.3E–04
A9	<1.3E–05			2.2E–03	8.6E–03	1.5E–03				8.0E–03	1.3E–02	5.5E–03
A10	1.0E–03	3.4E–04	1.1E–04	No data						1.0E–03	7.7E–04	3.2E–04
A12	3.4E–06	7.8E–07	1.0E–06	No data			1.6E–04	1.5E–04	1.0E–04	2.5E–04	3.5E–04	1.5E–04
A15	5.2E–06	4.8E–06	3.6E–06	No data						1.6E–04	2.9E–05	1.6E–04
A16	3.0E–06	1.4E–06	1.3E–06	No data						2.5E–04	2.5E–04	1.6E–04
A17	<2.2E–05			1.5E–03	4.6E–03	6.7E–04				1.0E–03	2.8E–03	4.8E–04
D1	5.6E–06	4.2E–06	2.5E–06	1.1E–04	4.7E–05	4.4E–05				2.3E–04	5.1E–05	7.2E–05
D5	2.8E–06	2.2E–06	2.0E–06	No data						3.8E–04	3.8E–04	2.2E–04
D6	4.0E–06	3.0E–06	2.2E–06	1.9E–04	4.6E–05	4.8E–05				6.3E–05	2.9E–05	4.5E–05
D7	2.5E–06	3.3E–06	1.8E–06	No data						5.9E–05	3.5E–05	3.2E–05
D8	6.4E–06	3.6E–06	2.8E–06	No data						3.1E–04	2.9E–04	1.9E–04
D12	2.0E–06	2.3E–06	1.5E–06	1.0E–04	3.9E–05	4.0E–05	2.3E–04	2.1E–04	1.4E–04	1.0E–04	8.9E–05	6.3E–05
D13	1.8E–06	2.4E–06	1.5E–06	4.9E–05	2.5E–05	2.1E–05	9.9E–05	9.8E–05	6.4E–05	4.0E–05	2.1E–05	2.2E–05
D14	3.2E–06	3.2E–06	2.2E–06	No data			1.0E–04	8.6E–05	5.5E–05	2.5E–04	2.9E–04	1.3E–04

Table Case 2. Estimated K_d (m^3/kg) obtained from the best fit to the penetration profile data. The formation factor, F_f, and the porosity, ε, were held constant during the calculation. (Continued.)

Core	Co-57			Cd-109			Gd-153		
	K_d (m^3/kg)	+	–	K_d (m^3/kg)	+	–	K_d (m^3/kg)	+	–
A1									
A5									
A6	4.2E–03	1.0E–02	1.3E–03	3.0E–03	4.7E–03	1.0E–03	1.6E–05	1.2E–05	1.1E–05
A8	2.6E–03	7.7E–03	6.9E–04	3.2E–03	1.5E–02	1.3E–03			
A9									
A10									
A12	4.9E–04	3.1E–04	2.3E–04				2.7E–03	2.6E–04	2.3E–04
A15									
A16									
A17									
D1									
D5									
D6									
D7	2.5E–04	5.6E–04	1.6E–04						
D8									
D12	1.8E–05	3.3E–06	2.8E–06						
D13									
D14	4.0E–03	4.3E–03	3.2E–03						

Table Case 3. F_f **and ε obtained from the best fit to the *in situ* penetration profile data.** K_d **(m³/kg) was held constant during the calculation. The porosity, ε, is only given for Na as the ε term is negligible compared to the** $K_d\rho$ **term for all the other tracers. See Section 2.9.1, Equation (2.2) for further details.**

Core	Na-22				Ni-63			Ba-133			Cs-137		
	F_f	+	–	ε	F_f	+	–	F_f	+	–	F_f	+	–
A1	4.0E–04	2.0E–04	1.6E–04	< 2E–01	3.7E–02	1.6E–02	8.5E–03				6.3E–02	1.5E–02	9.7E–03
A5	2.7E–04	2.8E–04	7.9E–05	< 1E–01	No data								
A6	3.1E–04	3.1E–04	1.1E–04	< 1E–01	6.4E–03	2.4E–03	1.6E–03	1.1E–03	3.4E–04	2.2E–04			
A8	6.0E–05	6.4E–05	2.6E–05	< 4E–01				4.9E–03	2.9E–03	1.3E–03			
A9	9.2E–04	1.1E–03	3.3E–04	< 2E–01	6.3E–03	9.9E–01	3.0E–03				1.4E–02	3.9E–02	5.2E–03
A10	3.2E–04	6.3E–04	1.4E–04	< 2E–01	No data								
A12	3.4E–04	4.3E–04	1.3E–04	< 3E–01	No data			2.9E–04	1.1E–04	6.5E–05	1.0E–03	7.6E–04	2.0E–04
A15	7.5E–04	6.0E–04	2.4E–04	< 2E–01	No data						2.5E–03	7.9E–04	4.8E–04
A16	5.2E–04	1.2E–03	2.2E–04	< 4E–01	No data						1.2E–03	7.8E–04	3.3E–04
A17	6.9E–04	1.4E–03	2.9E–04	< 2E–01	1.4E–02	5.5E–03	3.1E–03						
D1	4.2E–04	7.1E–04	1.9E–04	< 3E–01	1.4E–03	8.5E–04	3.9E–04				5.2E–04	4.5E–04	1.6E–04
D5	4.9E–04	5.5E–04	1.8E–04	< 3E–01							8.7E–04	4.8E–04	2.4E–04
D6	5.3E–04	1.1E–03	2.2E–04	< 3E–01	8.8E–04	5.5E–04	2.5E–04				4.3E–02	3.7E–02	1.8E–02
D7	6.9E–04	7.6E–04	2.5E–04	< 3E–01	No data						2.5E–03	9.3E–04	5.2E–04
D8	6.7E–04	5.0E–04	2.1E–04	< 2E–01	No data						3.1E–02	5.4E–02	2.1E–02
D12	8.4E–04	1.5E–03	3.4E–04	< 3E–01	1.2E–03	6.7E–04	2.9E–04	3.0E–04	1.6E–04	7.9E–05	1.5E–03	4.1E–03	5.4E–04
D13	8.3E–04	8.7E–04	3.0E–04	< 3E–01	2.2E–03	1.0E–03	5.3E–04	5.5E–04	2.7E–04	1.4E–04	3.0E–03	2.3E–03	9.0E–04
D14	6.1E–04	7.3E–04	2.4E–04	< 3E–01	No data			3.3E–04	2.8E–04	1.1E–04	3.5E–03	8.9E–04	6.7E–04

Table Case 3. F_f and ε obtained from the best fit to the *in situ* penetration profile data. K_d (m^3/kg) was held constant during the calculation. The porosity, ε, is only given for Na as the ε term is negligible compared to the $K_d\rho$ term for all the other tracers. See Section 2.9.1, Equation (2.2) for further details. (Continued.)

Core	Co-57			Cd-109		
	F_f	+	–	F_f	+	–
A1						
A5						
A6	2.7E–02	1.1E–02	2.5E–02	1.6E–03	5.4E–03	9.5E–04
A8	2.8E–02	3.8E–02	1.6E–02	2.2E–03	4.9E–03	1.0E–03
A9						
A10						
A12	3.8E–03	1.4E–03	8.0E–04			
A15						
A16						
A17						
D1						
D5						
D6						
D7	1.1E–02	4.6E–03	2.5E–03			
D8						
D12	5.7E–03	5.2E–03	1.9E–03			
D13						
D14	2.4E–03	8.7E–04	5.1E–04			

Table Case 4. Estimated K_d (m³/kg), F_f and ε obtained from the best fit to the *in situ* penetration profile data. The porosity, ε, is only given for Na as the ε term is negligible compared to the $K_d\rho$ term for all the other tracers. See Section 2.9.1, Equation (2.2) for further details.

Core	Na-22								
	$\varepsilon + K_d\rho$	+	–	F_f	+	–	K_d (m³/kg)	+	–
A1	2.07E–02	4.58E–03	2.21E–03	1.0E–04	5.5E–06	1.9E–05	7.65E–06	1.70E–06	8.17E–07
A5	1.14E–02	3.09E–04	4.10E–03	7.0E–05	4.7E–05	2.7E–05	4.23E–06	1.15E–07	1.52E–06
A6	3.53E–02	7.94E–03	1.09E–02	7.2E–05	1.9E–05	1.1E–05	1.31E–05	2.94E–06	4.04E–06
A8	9.53E–01	3.55E–01	5.96E–01	7.8E–05	4.8E–05	1.6E–05	3.53E–04	1.31E–04	2.21E–04
A9	8.76E–03	3.99E–03	1.96E–03	9.6E–05	4.8E–05	4.3E–05	2.94E–06	1.34E–06	6.57E–07
A10	8.75E–03	1.88E–03	1.11E–03	3.7E–05	7.9E–06	4.9E–06	3.24E–06	1.48E–06	7.24E–07
A12	1.20E–02	1.77E–03	3.59E–03	2.5E–05	7.2E–06	2.9E–06	3.24E–06	6.97E–07	4.11E–07
A15	9.94E–02	8.22E–02	8.65E–02	2.0E–04	7.6E–05	1.2E–04	4.45E–06	6.57E–07	1.33E–06
A16	1.39E–02	3.74E–03	5.18E–03	3.2E–05	1.9E–05	6.0E–06	3.68E–05	3.04E–05	3.20E–05
A17	7.91E–03	3.10E–03	1.94E–03	7.1E–05	7.7E–05	9.2E–06	5.14E–06	1.38E–06	1.92E–06
D1	3.45E–02	2.02E–02	7.09E–03	6.4E–05	5.7E–04	5.7E–05	2.93E–06	1.15E–06	7.20E–07
D5	1.30E–02	9.87E–03	7.67E–03	3.5E–05	4.8E–05	1.1E–05	1.28E–05	7.47E–06	2.63E–06
D6	2.66E–02	5.69E–03	6.07E–03	7.9E–05	2.0E–05	1.7E–05	4.83E–06	3.66E–06	2.84E–06
D7	1.94E–02	3.67E–02	2.28E–03	1.4E–04	9.4E–05	5.0E–05	9.84E–06	2.11E–06	2.25E–06
D8	3.12E–02	5.87E–03	4.34E–03	5.6E–05	1.4E–05	7.5E–06	7.18E–06	1.36E–05	8.45E–07
D12	2.17E–02	2.28E–03	1.70E–03	1.2E–04	9.4E–06	1.2E–05	1.15E–05	2.18E–06	1.61E–06
D13	2.45E–02	1.36E–03	7.55E–04	1.2E–04	2.2E–06	7.2E–06	8.02E–06	8.44E–07	6.30E–07
D14	2.91E–02	4.47E–03	5.71E–03	1.1E–04	2.6E–05	1.3E–05	9.06E–06	5.02E–07	2.80E–07

Table Case 4. Estimated K_d (m^3/kg), F_f and ε obtained from the best fit to the *in situ* penetration profile data. The porosity, ε, is only given for Na as the ε term is negligible compared to the $K_d\rho$ term for all the other tracers. See Section 2.9.1, Equation (2.2) for further details. (Continued.)

Core	Ni-63						Ba-133					
	K_d (m^3/kg)	+	–	F_f	+	–	K_d (m^3/kg)	+	–	F_f	+	–
A1	1.7E–03	3.2E–03	1.7E–03	7.1E–04	4.9E–04	3.1E–04						
A5	No data											
A6	7.3E–04	1.8E–04	6.5E–05	6.5E–05	7.4E–06	7.3E–06	8.9E–04	1.9E–04	4.0E–05	1.4E–04	1.4E–05	1.3E–05
A8	No data						9.4E–05	1.1E–05	3.2E–05	5.1E–05	1.9E–05	5.1E–06
A9	2.7E–03	5.2E–06	5.8E–05	1.6E–04	2.4E–06	3.4E–07						
A10	No data											
A12	No data						9.3E–04	9.1E–06	6.3E–06	1.9E–04	6.9E–07	2.3E–06
A15	No data											
A16	No data											
A17	5.1E–04	4.4E–05	3.8E–05	1.0E–04	8.8E–06	4.2E–06						
D1	2.0E–04	8.6E–05	7.1E–05	4.1E–05	1.3E–05	9.1E–06						
D5	No data											
D6	1.0E–03	2.3E–04	3.7E–04	8.4E–05	2.2E–05	1.7E–05						
D7	No data											
D8	No data											
D12	1.1E–03	2.3E–04	3.7E–04	1.4E–04	3.2E–05	2.6E–05	1.2E–03	2.1E–04	1.8E–04	2.2E–04	4.9E–05	3.5E–05
D13	1.9E–04	4.5E–05	5.2E–05	6.2E–05	1.4E–05	9.3E–06	8.0E–04	2.3E–04	5.9E–05	2.9E–04	4.2E–05	4.1E–05
D14	No data						3.8E–04	1.0E–04	2.9E–05	1.2E–04	1.8E–05	1.3E–05

Table Case 4. Estimated K_d (m³/kg), F_f and ε obtained from the best fit to the *in situ* penetration profile data. The porosity, ε, is only given for Na as the ε term is negligible compared to the $K_d\rho$ term for all the other tracers. See Section 2.9.1, Equation (2.2) for further details. (Continued.)

Core	Cs-137						Co-57					
	K_d (m³/kg)	+	–	F_f	+	–	K_d (m³/kg)	+	–	F_f	+	–
A1	4.4E–01	8.3E–02	8.5E–02	5.9E–02	1.3E–02	9.4E–03						
A5	1.9E–03	3.1E–05	3.0E–05	2.1E–04	4.1E–06	4.0E–06						
A6	1.4E–02	1.8E–03	3.2E–03	7.5E–04	1.3E–04	1.0E–04	2.9E–04	4.2E–06	4.2E–06	1.9E–05	3.9E–07	3.7E–07
A8	8.5E–04	1.9E–04	1.8E–04	5.6E–05	8.9E–06	6.9E–06	1.5E–05	3.6E–06	2.7E–06	7.2E–06	1.3E–06	1.3E–06
A9	5.2E–03	6.3E–04	4.2E–04	2.1E–04	4.8E–05	8.6E–06						
A10	1.4E–03	8.4E–05	3.2E–05	1.3E–04	4.2E–06	5.2E–06						
A12	2.5E–03	1.3E–04	1.2E–04	2.3E–04	1.8E–05	4.1E–06	5.2E–04	4.6E–06	4.5E–06	8.1E–05	8.1E–07	8.0E–07
A15	6.8E–03	7.9E–03	1.2E–03	1.2E–03	3.4E–04	5.3E–04						
A16	2.2E–03	8.7E–04	5.5E–04	2.0E–04	5.9E–05	4.2E–05						
A17	1.3E–03	5.6E–04	1.1E–04	1.1E–04	1.8E–05	1.8E–05						
D1	5.6E–03	5.5E–04	3.6E–04	1.8E–04	1.8E–05	1.1E–05						
D5	2.0E–03	4.2E–04	4.2E–04	1.3E–04	5.6E–05	1.0E–05						
D6	1.7E–03	4.9E–04	3.8E–04	2.5E–04	3.4E–04	9.3E–05						
D7	1.7E–03	7.4E–04	1.3E–04	4.3E–04	5.3E–05	5.3E–05	3.4E–04	4.6E–05	2.6E–05	1.6E–04	2.5E–05	3.0E–05
D8	2.4E–03	3.1E–04	1.4E–03	2.4E–04	2.1E–03	2.9E–05						
D12	1.5E–02	1.8E–03	1.5E–03	1.1E–03	1.5E–04	1.1E–04	2.4E–05	3.0E–06	2.7E–06	5.6E–06	1.9E–06	1.2E–06
D13	2.3E–03	4.7E–04	4.4E–04	4.4E–04	8.9E–05	6.5E–05						
D14	1.4E–03	3.2E–04	4.8E–04	1.4E–04	6.3E–05	2.4E–05	8.6E–04	6.9E–07	4.9E–07	8.5E–05	6.6E–08	1.0E–07

Table Case 4. Estimated K_d (m^3/kg), F_f and ε obtained from the best fit to the *in situ* penetration profile data. The porosity, ε, is only given for Na as the ε term is negligible compared to the $K_d\rho$ term for all the other tracers. See Section 2.9.1, Equation (2.2) for further details. (Continued.)

Core	Cd-109					
	K_d (m^3/kg)	+	–	F_f	+	–
A1						
A5						
A6	4.8E–04			5.3E–05		
A8	4.3E–05			1.9E–05		
A9						
A10						
A12						
A15						
A16						
A17						
D1						
D5						
D6						
D7						
D8						
D12						
D13						
D14						

Table Case 5. Estimated K_d (m³/kg) and F_f obtained from the best fit to the *in situ* penetration profile data and the aqueous concentration time measured data.

Core	Ni-63						Cs-137					
	K_d (m³/kg)	+	–	F_f	+	–	K_d (m³/kg)	+	–	F_f	+	–
A1	1.3E–02	3.8E–03	3.7E–03	3.2E–03	1.3E–03	7.0E–04	1.8E–02	4.2E–03	3.9E–03	2.6E–03	7.0E–04	4.6E–04
A5												
A6	2.8E–04	2.5E–04	2.1E–04	2.7E–05	2.7E–04	9.7E–06	2.4E–03	5.2E–04	4.9E–04	4.5E–04	9.9E–05	7.1E–05
A8	2.9E–03	8.6E–03	2.2E–03	4.1E–03	8.6E–02	1.8E–03	4.4E–03	5.0E–03	9.0E–04	2.1E–03	9.3E–04	6.6E–04
A9												
A10												
A12												
A15												
A16												
A17												
D1	4.9E–04	3.4E–04	3.6E–04	7.2E–05	8.0E–05	2.7E–05	4.1E–03	2.5E–03	3.4E–04	1.7E–04	3.7E–05	3.1E–05
D5												
D6												
D7												
D8												
D12	6.5E–04	2.6E–04	5.5E–04	8.1E–05	1.1E–04	2.0E–05	5.9E–03	1.5E–03	1.4E–03	4.3E–04	1.4E–04	9.4E–05
D13	2.5E–04	1.5E–04	1.5E–04	7.5E–05	5.3E–05	2.4E–05	2.4E–03	5.2E–04	4.9E–04	4.5E–04	9.9E–05	7.1E–05
D14												

Appendix 11

Reference sample cores

In addition to the 18 drill cores, which were known to have been in contact with the aqueous solution containing the radionuclide mixture, 3 additional drill cores where collected and they should be regarded as blank samples since they were collected outside the isolated area with rock contact to the tracer solution. These cores were denoted A19, A20 and A21, respectively. Two of these drill cores, A20 and A21, have been measured and small amounts of ^{137}Cs and ^{133}Ba have been detected. The core A20 was further sawn into thinner slices (se Section 2.2). The measured spectra showed that the radionuclides can be found at different length along the core, see e.g. Figure A11-1. Samples of A20 were also object for ^{36}Cl determination and no activity could be found (Table A11-1). This does, however, not exclude that ^{36}Cl is present at low concentrations, which is limited by the possible dynamic range of analyzing this radionuclide. The drill core of A19 was chosen for determination of porosity and has thus not yet been analyzed with regard to radionuclide content.

Table A11-1. Results from LSC measurements of ^{36}Cl in crushed and leached A20 samples.

Sample	^{36}Cl Bq/g
A20.1	< 0.1
A20.2	< 0.2
A20.3	< 0.7
A20.4	< 0.2
A20.5	< 0.2
A20.6	< 0.2
A20.7	< 0.1
A20.8	< 0.1
A20.9	< 0.07
A20.10	< 0.07
A20.11	< 0.07
A20.12	< 0.07
A20.13	< 0.06
A20.14	< 0.06

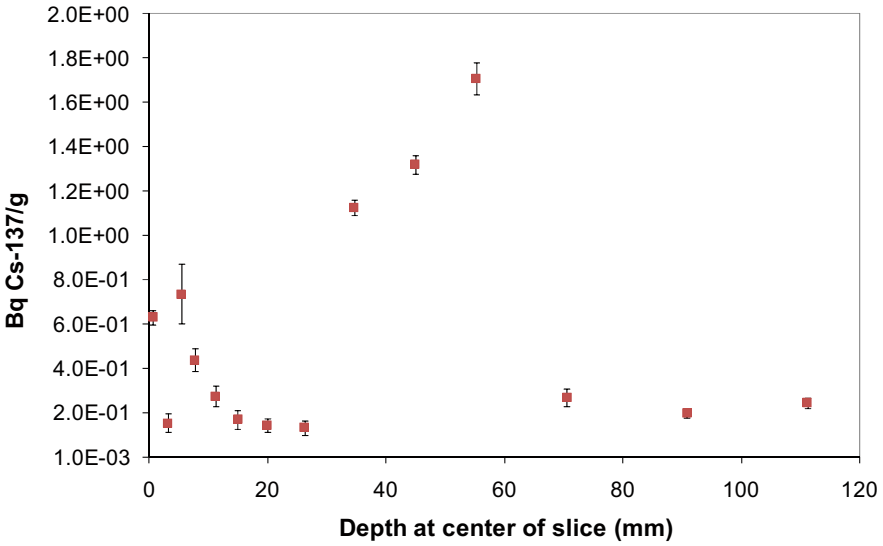

Figure A11–1. *Cs–137 activity distribution measured by γ–spectrometry in slices of the drill core A20.*

The fact that small amounts of radionuclides can be found in A20 and A21 can have several explanations. It may be contamination of the cores, even though these cores were collected outside the surface exposed to aqueous phase containing the radionuclides. One should keep in mind that the rock surface exposed to the radionuclides contained in the order of 1–10 kBq/g, whereas the samples from the A20 drill core only contained about 1 Bq/g. A very small fraction of the radionuclides from the surface exposed to radionuclides is sufficient to explain the observed activities in the A20 and A21 core.
A radioactive contamination of the detector system or the sample containers was excluded by two independent measurements of samples from A20.